2013

Proceedings of the 2013 Coal Operators' Conference

Naj Aziz
University of Wollongong, naj@uow.edu.au

Bob Kininmonth

Jan Nemcik
University of Wollongong, jnemcik@uow.edu.au

Ting Ren
University of Wollongong, tren@uow.edu.au

John Hoelle
Anglo Coal Australia

PROCEEDINGS OF THE 2013 COAL OPERATORS' CONFERENCE

UNIVERSITY OF WOLLONGONG, NSW

14 - 15 FEBRUARY 2013

ORGANISERS

UNIVERSITY OF WOLLONGONG - MINING ENGINEERING
AUSTRALASIAN INSTITUTE OF MINING AND METALLURGY- ILLAWARRA BRANCH
MINE MANAGERS ASSOCIATION OF AUSTRALIA

PRINTED IN AUSTRALIA BY
The University Of Wollongong Printery

ISBN: 978 1 921522 83 3

All papers in these proceedings are peer reviewed

Published on line: http://ro.uow.edu.au/coal
and Via: http://research.uow.edu.au/coal

EDITORIAL BOARD

ORGANISING COMMITTEE

REVIEWERS

The organising committee would like to thank the following referees for technically reviewing the papers included in these proceedings

SPONSORS

The mining engineering group of the University of Wollongong, the Illawarra Branch of The AusIMM and the Mine Managers Association of Australia gratefully acknowledge the financial assistance of the following organisations which have sponsored the COAL2013 Conference:

Diamond Sponsors

bhpbilliton resourcing the future
Illawarra Coal

Peabody ENERGY

AMC CONSULTANTS

Gold Sponsors

MINOVA

AIR LIQUIDE

DSI

The University Of Queensland AUSTRALIA

SMI MISHC Minerals Industry Safety & Health Centre

University of Wollongong Centre for Infrastructure Protection and Mining Safety

Silver Sponsors

AngloAmerican

GeoGAS

JM AUS Jennmar Australia

xstrata coal

Endress+Hauser People for Process Automation

FOREWORD

On behalf of the organising committee I welcome you to the 13th Coal Operators Conference (Coal2013). The conference series, held annually at the University of Wollongong, become a well recognised entity with diverse interests on coal mining operations. As a unique Australian coal mining forum, it is very humbling to see broader paper contributions and participation in the conference, from both surface and underground operators. It is particularly pleasing to have more papers from surface mining operations; therefore, I welcome Dr John Hoelle to the editorial panel with responsibility on surface mining. Of course our conference is also enriched by international participation from various coal producing countries. Primarily the conference will remain focused in serving the interests of the Australia coal mining industry, as initially planned. More papers, reporting on new ideas and innovations, are being presented in the conference, and the number of quality papers is increasing year by year. This demonstrates the importance and credibility of the conference. Also, more companies are supporting the conference in the form of sponsorship or exhibiting their products. Industry support in the form of sponsorship is vital for the viability of the conference and therefore much appreciated.

Coal Operators' Conference online holds 431 records, which have been downloaded a total of 265 500 by January 2013. This access is not confined to Australia alone, other countries making frequent access include USA, China, UK, Germany and Iran. More than 130 countries have accessed the conference publications since the papers went online in 2008. I would therefore, like to take this opportunity of extending a special thanks to Michael Organ, Manager - Repository Services of the UOW Library for his help in organising and uploading all past conference papers on the University websites http://ro.uow.edu.au/coal as well as providing all the statistics necessary for the benefit of the conference.

Special thanks to the paper reviewers; the editorial team members, Bob Kininmonth, Jan Nemcik Ting Ren and John Hoelle; Zhongwei Wang for typesetting the conference proceedings; Peter Vrahas of Eventico for his conference general management and efficient administration of the conference website; The University of Wollongong printery staff Tristan Dus for designing the conference proceedings cover page, Maria O'Hearn for printing the conference proceedings.

All papers are independently peer reviewed and edited to maintain the highest quality.

Professor Naj Aziz
Conference chairman and convenor

TABLE OF CONTENTS

COALLOG: THE STANDARD FOR COLLECTION RECORDING STORAGE AND TRANSFER OF GEOLOGICAL AND GEOTECHNICAL DATA FOR THE AUSTRALIAN COAL INDUSTRY

John Simmons[1], Paul Maconochie[2], Brett Larkin[3] and David Green[4]

ABSTRACT: A standard has been developed to improve and upgrade the collection and coding of geotechnical data as part of geological exploration activity. CoalLog was developed by industry-based geoscientists and geotechnical specialists in response to outdated terminologies, non-translatable data coding, and con-conformances with relevant Australian and international standards for geotechnical investigation, testing, and reporting. The new standard will allow the industry to use geotechnical information efficiently and accurately, thereby minimising potential legal liabilities associated with non-conformance to recognised standards that are already in-place in the non-coal geotechnical sector. Adoption of this standard will also promote opportunities for a wider range of geotechnical specialists to provide services to the coal industry.

WHAT IS COALLOG

CoalLog (Larkin and Green, 2012) is the geological exploration information coding system that has rationalised and updated a wide variety of previous systems across the Australian coal industry. Several decades previously a standard GEODAS dictionary of geological terms had been introduced when computerised data management commenced. GEODAS codes were as abbreviated as possible in order to compress both quantitative data (e.g. depth and moisture content), and qualitative data (e.g. unambiguous visual-tactile description of a lithological unit), into the then-available punched-card line record length limit of 80 ASCII characters. The industry quickly adopted GEODAS, but competing and business interests were equally quick to customise the generic codes and formats. By 2010 many such enhancements had become unique to specific sites and organisational IT systems, but the resulting data sets were incompatible, non-transferrable, and deficient in clarity and meaning.

Modern geological data management systems provide complex functionality to access and manipulate information across a wide variety of information content, file specifications, and platforms. These systems continue to provide immense benefit to the industry and the advent of CoalLog will enhance this value. While there have also been significant improvements in drilling and geophysical logging capabilities, the fundamental processes of geological exploration have not changed. Rig geologists must use visual-tactile skills to observe and describe geological features accurately and quickly. Direct computerised field data entry is now becoming the norm, and the rig geologist must generate code accurately and quickly.

Most rig geologists are early-career professionals, usually working as contractors, who have to use the different "flavours" of data coding systems used by their range of clients. Most rig geologists have no exposure to geotechnical terminology and knowledge through either their original education or subsequent workplace mentoring by supervisors who have had equally minimal exposure.

Current geological data coding systems may be perceived to satisfy most of the industry's more organisation-specific immediate needs but several shortcomings lead to the development of CoalLog. Accuracy and meaning of coded information is no better, and perhaps systematically worse, than in the earliest days of GEODAS when there was more time and opportunity to check meanings and correct coding errors. The standard of visual-tactile description of geotechnical parameters is often so inadequate for due diligence purposes that the costs of original data collection are almost totally wasted. Transfer and checking of data from older exploration records for prospective areas can be computationally difficult and mind-numbingly tedious and frustrating to highly skilled individuals. All such shortcomings represent real costs to the business interests of the owners and operators involved.

[1] *Principal, Sherwood Geotechnical and Research Services,< john.simmons@sgrs.com.au> Tel+61 (0)7 5471 2640*
[2] *Principal, GeoTek Solutions Pty Ltd*
[3] *Director, GeoCheck Pty Ltd*
[4] *Principal, Green Exploration and Mining Services*

This situation has been recognised for some time, and the need for rationalisation was apparent from any multi-party viewpoint. CoalLog was developed though a process of consensus involving geological data, geotechnical, geophysical log data transfer, and geological data base management experts who originally convened at an invitational meeting in Brisbane in 2010. ACARP support was obtained in 2011 to provide documentation and an information roll-out which occurred in Singleton, Moranbah, Emerald, and Brisbane in February 2012. The Australian Institute of Mining and Metallurgy agreed to provide the web-hosting services.

CoalLog is therefore an industry-generated initiative, lead by competent, experienced, and recognised technical specialists across the coal mining industry, supported by ACARP and AusIMM, and continuing to be managed and enhanced by industry-recognised volunteer specialists. CoalLog is effectively owned and supported by the Australian coal mining industry.

CoalLog features a standard dictionary with a flexible method of implementation where the base content can be transferred electronically without loss of meaning. The structure of the coding process has been intentionally designed to allow flexibility for additional details required for implementation with particular platforms and organisations.

HOW COALLOG IS MANAGED

CoalLog is managed by consensus through a committee process. This has the advantage of decisions not being controlled or dictated by any individual or organisation, but the disadvantages of time taken to consider, approve, and implement any changes. The perceived concern of decisions being dominated by a particular party or viewpoint has not arisen to date, reflecting the commitment of individual professionals to technically sound but workable solutions that are acceptable to the interests of all the industry operators that are represented.

The CoalLog management process is best understood in terms of its evolution to date. This started with many discussions over a period of years during both commercially-sensitive work activities and open meetings of industry-based geologists, geotechnical and geophysics specialists, and personnel specialising in databases and modelling. Activities of the Bowen Basin Geologists Group, an ad-hoc organisation of persons interested in the geology of the Bowen Basin and sponsored by the Coal Geology Group of the Geological Society of Australia, provided regular opportunities in Queensland. Similar discussions and conversations took place within the New South Wales coal geology community. The June 2010 meeting in Brisbane invited representatives of all potentially interested parties, and volunteers were appointed to four sub-committees dealing with geology, geotechnical, geophysics, and database matters. Each of these sub-committees continues to meet as required to consider both its own direct subject matter as well as any multi-subject matters arising. Currently all CoalLog activities are coordinated and facilitated by two of the authors (Larkin and Green).

Most of the CoalLog sub-committee members and conveners are involved in Australian Coal Association Research Program (ACARP) activities in some manner. Once it became clear that the professional peer consensus process could deliver the CoalLog goals, ACARP support was obtained for preparation of a manual and workshops in early 2012 and ongoing AusIMM sponsorship was obtained for the CoalLog website. Further ACARP support has been requested for improvements to the manual and provision of training in the art and practice of geotechnical core logging.

Time devoted to CoalLog activities is fundamentally an in-kind contribution by the individuals concerned and the organisations they represent. Notwithstanding the highly competitive nature of industry-based organisations, the peer-regulated and industry-supported nature of CoalLog is robust and capable of providing continuation of leadership and productive outcomes as the contributions of individuals change over time.

WHY STANDARDISATION IS SO IMPORTANT

Generational succession is rapidly overtaking the individuals who implemented and nurtured computerised data collection from its earliest beginnings. Historical reasons for changes to coding for particular geological or geotechnical subjects have been forgotten, and computational limitations or personal conventions are rapidly becoming outdated or meaningless.

Corporate and statutory governance purposes generally requires due diligence studies and reporting in compliance with the JORC standard (JORC, 2004). Manipulation and transfer of complex data sets generates formatting, coding, and output requirements where incompatibility issues have consumed an increasing proportion of the time and costs of specialists. CoalLog is designed to remove such demands, and has been recognised by the New South Wales government as meeting its requirements for statutory reporting in paperless format. A similar outcome is under discussion in Queensland.

JORC-compliant reporting is based on levels of technical assessment. Business finance and insurance is based on the accuracy and clarity of information disclosure. Specifically, geotechnical parameters are assessed from both geological and geotechnical data, and an "economically mineable resource" (JORC, 2004 Para. 28) implies that mining is possible "under reasonable financial assumptions" based on due consideration of geotechnical matters. Geotechnical assessment is in turn based on recognised measures of risks from ground-related hazards. If forecasts are significantly in error because of coding errors or misinterpretation of information, or if damages result from failures involving inadequate geotechnical assessment, the resulting costs may have legal liabilities affecting both organisations and individual professionals. Litigation includes focus on compliance with recognised standards and tests of reasonable judgement.

CoalLog therefore has two forms of implied legal status. It has to be as unambiguous and accurate as possible to all parties, but the attribute descriptions and meanings that are used must also be as compliant as possible with recognised Australian or international standards. Consideration of relevant geotechnical codes was a significant aspect of CoalLog development.

PRACTICALITIES OF GEOTECHNICAL DATA COLLECTION

Exploration for coal is primarily based on drillholes supported by geophysical traverses, but can include mapping of exposures in small pits or full-scale mine excavations. Near-surface, weathered, or non-coal bearing units do not include coal of economic significance but are usually zones of critical geotechnical and project significance. Casing is required particularly when drilling through weak near-surface materials that may also be water-sensitive.

Logging of all subsurface materials requires rapid and accurate descriptions based on visual-tactile observations. Soils may be described geologically as unconsolidated sediment, which is a term totally unrelated to geotechnical meaning or characteristics. The CoalLog codes were therefore designed to support unambiguous geotechnical as well as geological description. Most exploration drilling is by open-hole or chip-hole methods where logging is based on collection and description of cuttings, hopefully with due allowance for fall-in and flush lag-time. Such logging may be inadequate for JORC-standard reporting that involves geotechnical assessments unless additional information can be measured by testing or inferred from accurate description. CoalLog has been designed to minimise errors and under-reporting of near-surface geotechnical data particularly where casing has been used.

Cored drillholes provide maximum geological and geotechnical information. Cutting and retrieval of core causes damage through vibration, stress relief, and cutting fluid erosion, while surface exposure will result in irreversible deterioration if the core is allowed to dry. All of these factors affect what is observed and must be kept in mind by the rig geologist, particularly when wireline coring may recover core faster than the rate at which observations can be recorded. The CoalLog core description process provides for quickly and accurately recording a basic level of key geotechnical data. CoalLog also provides an alternative and more detailed core description process that follows the same protocols but allows for more detail to be coded where the purpose of the drillhole is primarily geotechnical.

Coal cores require particularly detailed geological description and sampling because of product processing and quality considerations. In contrast, coal may be merely another rock material in terms of both open-cut and underground mining assessments that are focussed on rock mass and rock structure strength and deformation responses. An innovation of CoalLog is the recording of depth intervals as rock mass units, as distinct from lithological units. An alluvial floodplain overbank facies, for example, may consist of several tens of metres of a repeated sequence of laminated siltstones and sandstones including thin to thick sandstone bands. Full lithological detail would require complex description, but CoalLog allows such an interval to be described alternatively as a single rock mass unit having essentially uniform geotechnical parameters, thus enabling vital field time to be focussed on defect descriptions and sampling.

Many descriptions may be updated or changed based on quantitative laboratory techniques ranging from microscopy to tests of physical and chemical parameters. This may occur at a later time in a very different place, and involve other personnel who may have no knowledge of the actual field conditions or contact with the field geologist. Typical examples are the mean and range of particle sizes for soil or sedimentary rock, or a strength indicator of the material such as the UCS for rock or the plasticity for a cohesive soil. Over the decades of GEODAS enhancements, the meaning of many strength-related codes has been so diluted as to be uninterpretable. CoalLog has therefore been structured with a common standard based on updated geotechnical coding, but in such a manner that a particular organisation may still utilise its "legacy" codes.

Calculations of individual rock defect strength, rock mass strength, and even ground support requirements can now be made almost automatically using freeware or customised geotechnical software. In developing CoalLog, careful attention was therefore paid to facilitate observation and coding of geotechnical data in a reliable manner to facilitate subsequent calculations.

COMPLIANCE WITH STANDARDS AND GOOD PRACTICE

Coal mining is driven by business considerations, for which geotechnical considerations provide fundamental risk controls. Mining operations may result in potentially fatal consequences for hazards where the associated risks are not effectively controlled. If geotechnical advice and design actions are inadequate because of content dilution or loss of meaning, then there may be associated liabilities which are most likely to be discovered and determined though adversarial and expensive litigation. Insurance cover for coal mining activities is complex and dependent on the acceptability to the insurer of the operator's risk management processes. This means that business value is determined ultimately by the reliability of the information upon which critical decisions are made. From a legal perspective, inadequate data and design assessments are matters of negligence, whereas non-compliance with accepted standards may be a matter of negligence or, in the case of deliberate non-compliance, even professional misconduct.

In Australia all geotechnical information is expected to comply as far as possible with the site investigation standard AS 1726 (1993), which references both descriptive and test result information from related geotechnical testing standards particularly AS 1289 (2000) but also AS 1141 and AS 4133. AS 1289 has particular significance for description of grainsize ranges, where geological description of grainsize has historically followed very different measurement protocols, and descriptions of material strength, where many different scales have been used historically by a diverse range of interest groups.

For compliance with AS 1726, CoalLog adopted a particle size terminology that is essentially logarithmic in its subdivisions, but which is based on the accepted world-wide standards and practice of the geotechnical community. Fortunately, in the coal industry where sedimentary rocks are of greatest interest, it was readily possible to merge accepted size-related geological terms (silt, sand, gravel, pebble, cobble etc) with the AS 1726 geotechnical format, and in the process provide a single consistent and measurable reference for geologists at the cost of minor adaptation to the CoalLog codes.

Also in accordance with AS 1726, CoalLog description of weathering (oxygenated and therefore ground surface-related chemical and physical change processes) is separated from and not based upon assessment of strength which has to be described separately. CoalLog also provides separately for description of alteration, which may result in observationally similar features to weathering, but is attributable to geochemical and physical changes that are not related to near-surface processes. Based on observations, the qualifying codes for alteration follow the same pattern as for weathering.

In AS 1289 there is an overlap between measures invoked in the description of hard cohesive soils and extremely low strength rocks. Provided a reasoned observation is made, this overlap has no geotechnical significance. Reasoned observations that are familiar to geotechnical specialists but less familiar to geologists can also be made for both cohesive and cohesionless soils.

However, AS 1726 uses the Point Load Strength Index as a descriptive measure of rock material strength, whereas in current geotechnical practice the more fundamental measure of Uniaxial Compressive Strength (UCS) is favoured. Coal measures rocks have been the subject of a number of UCS-based descriptive scales with significance for various mining activities and ground support requirements (e.g. BS 5930:1999; Anon, 1977). Aspects of some of these scales have been captured and then diluted in legacy versions of GEODAS codes, to the extent that pre-CoalLog rock strength

descriptions are geotechnically unreliable unless supported by laboratory test data. The UCS-based CoalLog scale for rock material strength, which diverges from AS 1726, deliberately adopted clear and meaningful classes relevant to coal mining practice, together with meaningful visual-tactile methods for field description purposes. The UCS ranges for the CoalLog strength codes are illustrated in Figure 1 which also shows alternatives which were not adopted for various reasons described above.

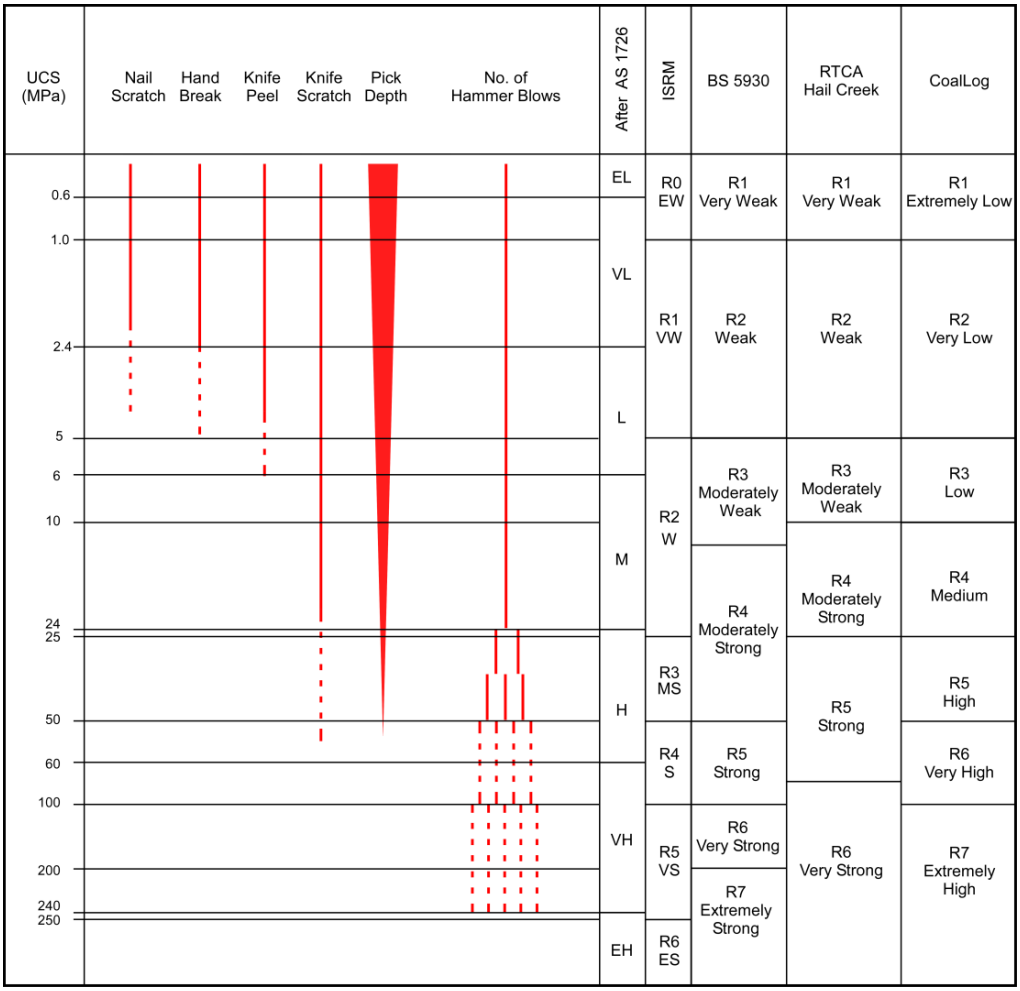

Figure 1 - CoalLog visual-tactile descriptive scale for UCS-based strength classification

Rock defect shear strength requires data based on detailed observation of surface shape, roughness, infill, and wall material. Several geotechnical models for defect strength may be used in later assessments provided that adequate detail is logged. CoalLog provides for a standard level of defect detail, which is recorded on the standard coding pro-forma and which allows only for simplified geotechnical interpretation. An alternative, detailed geotechnical pro-forma can be selected which allows for observation parameters such as roughness and JCS in a format for more specialised later assessment. CoalLog allows either the standard or the detailed pro-forma to be used for a particular corehole, but not both.

The particle-size and strength descriptions represent a significant change from past practices, for some, and are considered essential to comply with application of existing standards and good practice. Best geotechnical practice also requires unambiguous separation of observation and interpretation, which is more difficult for geologists since the recognition and description of interpreted environments and processes is an essential skill. Separation of weathering or alteration and strength observations is necessary best-practice for which both geologists and geotechnical specialists should be mindful. Codes for strength observations were specifically designed in CoalLog to maximise meaningful observation-based description, and are being considered as part of the current revision of AS 1726.

BASE DEPTH AND THE DILEMMA OF CORE LOSS

Previous GEODAS coding based on depth intervals has been replaced in CoalLog by data records described by base depth and thickness. This allows more flexibility for describing different types of depth-related attribute ranging from rock mass unit to lithological unit and zero-thickness horizon. Since almost all field data entry is now computerised, this also allows for powerful self-correction and prompting for missing or incomplete descriptions.

Base depth also allows for computerised handing of actual depths and thicknesses in cases of drillhole deviation from verticality and non-vertical drilling. Full core orientation is the exception rather than the practice in coal exploration, although verticality is often routinely measured when the hole is surveyed geophysically. A protocol is required for measurement of base depth but the protocol is not specified in the CoalLog standard. Best-practice is to fit obviously rotated fragments in the splits and then mark a reference line at which base depth is measured. The rig geologist remains responsible for reconciling measured base depths against drillers' depth records, and post-processing enables marker depths to be adjusted based on geophysical reconciliation.

The sole function of CoalLog codes is to describe attributes with respect to base depth. The angular orientation of features with respect to the core axis can be measured in the field. CoalLog coding is based on a simple premise: angles are measured as departures from a plane perpendicular to the core axis at any base depth. This facilitates automated post-processing of actual drilled depths and orientation relative to drillhole axis, and includes the additional codes that are recorded for fully oriented coring.

Core loss remains a dilemma. There are many reasons for losses, all related to the mechanical performance of the drilling string and the locally damaging effects of the drilling process on the material being penetrated. Sometimes unrecovered stubs are retrieved in the next run and sometimes drilling and flushing removes entire sections of weak material. Driller "feel" and drill rig operating parameters may provide additional clues that can be recorded as comments. In some cases reconciliation with geophysical records is sufficient to allocate core losses accurately in terms of base depth and thickness. CoalLog provides a single code to represent the base depth and thickness of a core loss interval, and further correction and interpretation is then a matter for post-processing based on the skill of and drilling observations by the rig geologist.

RECONCILIATION WITH GEOPHYSICS

Routine geophysical logging is an essential component for post-processing data from open-hole or chip-hole drilling, which is otherwise limited to observations of cuttings that are aggregated over usually 1m depth intervals. Geophysical data sets are normally transferred and post-processed for geological and geotechnical purposes using standard LAS formatted files which are base-depth records of measurements from the tools that are deployed. LAS files also include header records which explain the format of the data records. There is no current standard for the names of various tools and the format of headers. While this is not an impediment for use of CoalLog, further development of the standard is under way to implement a standard for LAS file headers and data record handling that is fully compatible with the CoalLog drillhole header formats and data management standards.

FUTURE DEVELOPMENTS

Vendors of field logging software have been quick to recognise and adopt CoalLog. It is expected that industry implementation will take some time, and that individual organisations will have to make decisions as to how and when CoalLog can be adopted based on their own interests and logistical considerations.

The CoalLog standard is subject to active management. Since its original release in 2011 some minor corrections and amendments have been considered and adopted where appropriate. Further development is expected with respect to data transfer standards and handling of geophysical LAS files. It is expected that Queensland will inevitably follow New South Wales in adopting a policy for submission of statutory data and reporting in fully electronic format based on the CoalLog standard.

The recent upsurge in coal exploration and project evaluation demonstrated that the industry faces a critical shortage of geotechnical resources. Partly this can be attributable to business cycles and generational change, but part is also related to the almost exclusive "ownership" of geotechnical data gathering activity by rig geologists who often lack the necessary training and understanding to be able to observe and describe geotechnical attributes accurately. Within the wider geotechnical community is a considerable resource of specialists who have been under-utilised in coal exploration geotechnical

activities. The advent of CoalLog has provided a platform for logging using geotechnical standards that already exist outside of the coal exploration industry. The CoalLog standard may yet be further developed for adoption and integration into general geotechnical logging methodology and software standards.

REFERENCES

Anon, 1977. The description of rock masses for engineering purposes, *Quarterly Journal of Engineering Geology,* 10:355-388.

Australasian Joint Ore Reserves Committee (JORC), 2004. The 2004 Australasian code for reporting exploration results, mineral resources and ore reserves (The JORC Code). Available from: <http//:www.jorc.org/jorc_code.asp> [Accessed: 2 November 2012].

British Standards Institution, 1999. BS 5930:1999 The code of practice for site investigations.

Larkin and Green, 2012. CoalLog borehole data standard for the Australian coal industry. ACARP Project C21003. Available from <http//:www.ausimm.com.au/content/default.aspx?ID=451> [Accessed: 2 November 2012].

Standards Australia, 1993. AS 1726-1993 Geotechnical site investigations.

Standards Australia, 1999. AS 1141.0-1999 Methods for sampling and testing aggregates. Part 0: List of Methods.

Standards Australia, 2000. AS 1289.0-2000 Methods of testing for geotechnical purposes Part 0: general requirements and list of methods.

Standards Australia, 2005. AS 4133.0-2005 Methods of testing rocks for engineering purposes Part 0: general requirements and list of methods.

GEOTECHNICAL ROOF CLASSIFICATION FOR AN UNDERGROUND COAL MINE FROM BOREHOLE DATA

William Lawrence[1], Jason Emery[2] and Ismet Canbulat[2]

ABSTRACT: It is standard and critical practice in the majority of geotechnical engineering applications to use a rock mass classification system to evaluate the condition of rock in mine planning and operations. The use of geotechnical classification schemes for rock mass characterisation in underground coal mines is well established. Several rock mass classification systems have been developed and used in civil engineering design and for underground mining operations. In the past, these rock mass classification systems were modified and used in the coal mining industry to quantify descriptive geological information for use in coal mine design and roof support selection. To facilitate geotechnical evaluations, mining companies in the Bowen Basin of central Queensland put considerable effort into obtaining geomechanical data from surface exploration boreholes and borecore. The advance or innovation in the proposed method is not in doing the characterisations, but the method of evaluating the required parameters from available borehole geophysics and geomechanical test data. Evaluating radial point-load strength from geophysical correlations is dependent on collating a large comprehensive database of actual point-load test data across the range of lithological types.

INTRODUCTION

Effective and pre-emptive strata control in an underground coal mine is aided by an adequate definition of the geotechnical environment. Major components of the geotechnical environment are the lithological and geomechanical characteristics of the immediate roof. The geomechanics classification systems Rock Mass Rating (RMR) and the Norwegian Geotechnical Institute (NGI) Q-system are the most commonly used in civil and hard rock mining around the world. Both of these systems incorporate Rock Quality Designation (RQD) and are based on actual case histories. The RMR and Q systems have evolved over time to better reflect the perceived influence of various rock mass factors on excavation stability. The introduced modifications have arguably enhanced the applicability of these classification systems, but there are still areas of potential confusion.

The use of geotechnical classification schemes for rock mass characterisation of the immediate roof in underground coal mines is also well established. Simple single-parameter classifications may be derived directly from borehole geophysics. Both well-established and more complex multi-parameter classifications require additional direct testing of borecore or exposed roof strata to provide data for the calculation. Borehole geophysical data is obtained from all surface exploration holes; however, not all boreholes are cored. Where core is available and tested, there is usually insufficient data for each required immediate roof lithological unit; therefore, a method to derive multi-parameter geotechnical roof classifications using borehole geophysics correlated to rock-mass geomechanical properties is required.

Mining companies in the Bowen Basin of central Queensland, including Anglo American Metallurgical Coal's (AAMC) Capcoal operations, place considerable effort into obtaining geomechanical data from surface exploration boreholes. As well as standard geophysical data, core samples are routinely processed and geomechanically tested in laboratories. Point-load tests are conducted on available core in the field by exploration geologists; however, there are often more roof units present than can be tested in an appropriate time frame. Anglo American, through its Capcoal operations, has an extensive exploration database. All available data was not being effectively collated and used for mine design purposes, in particular borecore geomechanical data. A project was instigated to primarily provide geotechnical classification of the immediate roof for the Grasstree longwall mine. This objective required a database of correlated geomechanical properties.

[1] *Geowork Engineering*
[2] *Anglo American Metallurgical Coal, jason.emery@angloamerican.com, 0407589080*

GRASSTREE MINE

The Grasstree Mine is a longwall mine producing high quality coking coal as part of the German Creek complex, operating approximately 30 km west of Middlemount in the Bowen Basin (Figure 1). Underground development commenced in November 2003, eventually forming an extension to the adjacent Southern Colliery when the two mines were joined in 2005.

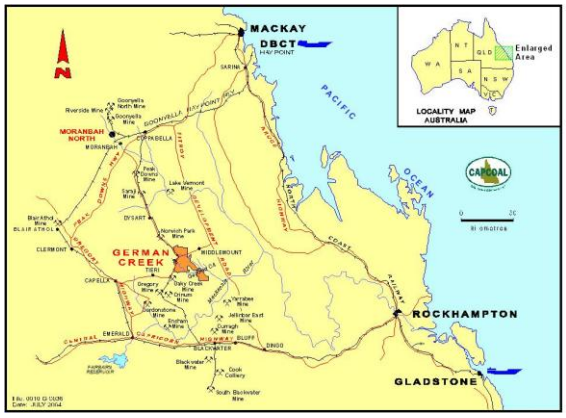

Figure 1 - German Creek mines complex, Queensland

Gateroads and main headings are developed with wide-head continuous miners, mining conventionally and supporting roof and rib with on-board drilling rigs. Grasstree longwall blocks are designed with three heading gate roads, two of which are utilised for ventilation due to the high gas content in the goaf, whereas the remaining heading is utilised for goaf sealing of the previous longwall block.

Longwall panels are currently being developed in the 800 series on the southern side of the main headings. Current depth of mining operations range from 270-385 m in the 800 s series. Future longwall mining on the 900 s side is planned to follow on after the completion of LW807 with maximum depth to reach 450 m.

GEOTECHNICAL ROOF CLASSIFICATION FOR COAL MINES

Numerous geotechnical rock classification schemes are utilised in the Bowen Basin coal mines. Most notable is the Coal Mine Roof Rating, CMRR (Mark and Molinda, 2005), an established coal industry standard. CMRR requires both intact compressive strength and discontinuity geomechanical data for each lithological unit of a mining horizon, typically equivalent to the length of installed support. Uniaxial compressive strength (UCS) (Payne, 2008), is used at several mines, and experience has shown that it can be a relatively good predictor of strata conditions. UCS is typically derived from a correlation to sonic velocity (transit time) from geophysical logs or from laboratory testing. An extension of UCS is the Roof Strength Index (RSI) (Gordon and Tembo, 2005), which incorporates depth of cover. RSI can be correlated to installed support, but is likely to be restricted to depth ranges and may not be sensitive to extremes of low strength. A recent and promising method under development is the Geophysical Strata Rating (GSR) (Hatherly, *et al.*, 2008), which estimates rock-mass competency by an analysis of geophysical logging data. Currently, this system is also being evaluated by AAMC.

Database

As well as evaluating the immediate roof competency, the existing Grasstree geomechanical database is being updated with data from every hole assessed. Primarily, the roof classification project required the calculation of CMRR across current and proposed mining areas at Grasstree. Data points are acquired and collated from surface exploration holes with available electronic geophysical logs, i.e. sonic transit time. Slake durability, UCS, axial and radial point load data and fracture spacing. Sonic Transit Time (STT) or Sonic Velocity (SV) is evaluated for each rock sample to allow correlations between parameters to be developed. The geomechanical database should also have the capability to incorporate other CMRR data, e.g. information from underground exposures and borecore from underground drilling. CMRR has to be readily calculated for various roof horizons. The database needs to be able to calculate UCS and RSI for various roof horizons.

Coal Mine Roof Rating (CMRR)

Mark (1990) integrated CMRR into support design programs like the USBM's Analysis of Longwall Pillar Stability (ALPS) program in the calculations of safety factors for given coal pillar sizes based on applied loads and pillar strength. It is also integrated into a similar design methodology in Australia by Colwell (1998) to determine the appropriate pillar sizes and required secondary support in tailgates. This design methodology is called the Analysis of Longwall Tailgate Serviceability (ALTS). In both cases, statistical analysis from case histories of CMRR values have been used in conjunction with existing pillar design formulae to develop a relationship (called Stability Factor) between the pillar Factor of Safety and CMRR.

Base unit CMRR is calculated from two components using the standard National Institute for Occupation Safety and Health (NIOSH) formulations (Mark and Molinda, 2005). One component uses UCS to characterise material strength. The second component characterises the strength and effect of discontinuities, and uses Radial Point Load Data (RPLD). Additional adjustments can be made to the base CMRR, including a strong bed adjustment, a multiple discontinuity adjustment and a surcharge deduction. Fracture Spacing (FS) and Axial Point Load Data (APLD) are also being collated, and may be correlated or incorporated in the future. UCS, axial and radial PLD and FS are available from the exploration database. No adjustments are made for water, as this should be done on a site-specific basis if water is present. Roof joints are usually not identified by standard borehole geophysics, and again may need to be considered on a site-specific basis. The advance or innovation in the method to calculate CMRR is to derive representative RPLD when explicit tests are not conducted.

CMRR is calculated for distinct individual lithological units. Units are chosen from assessment of geophysical logs (sonic and gamma). Units such as weak mudstone or strong sandstone may be as thin as 0.2 m. Composite roof CMRR can be readily calculated for any roof horizon. Typically, the roof bolt horizon is chosen, in this case 1.7 m (assuming 0.1 m of the standard 1.8 m is protruding from the roof). The composite CMRR is calculated from the cut-roof horizon; it is not calculated from top of seam (ToS). A standard excavation height of 2.8 m from base of seam (BoS) is used to calculate anticipated cut roof horizon.

The current Grasstree UCS to STT correlation is shown in Figure 2, and comprises about 300 data points. The average unit STT is used to calculate the unit UCS. The discontinuity CMRR component could be calculated for each hole using that hole's data, but this would only be possible for cored holes. In addition, RPLD and FS may not be taken for each individual lithological unit, which means that a composite CMRR may not be possible even with cored holes. In the Bowen Basin, discontinuity strength and stiffness broadly varies with lithology, in particular clay content. Infill and faulting also define discontinuity characteristics. Weaker discontinuity strength is evident in siltstones and mudstones and siltstone interbeds. Choosing representative RPLD for each lithology could be possible, but would not represent the likely strength variability within standard lithological units.

The new approach taken is to define a RPLD-to-STT correlation, similar to UCS. Unlike UCS, where an average unit STT is used, for RPLD a maximum STT (minimum SV) is used that corresponds to the low strength "spikes" (Figure 3). The sonic geophysics tool does not have the resolution of a lamination; the low strength spikes are assumed representative of the weakest partings. This method may not be ideal, but there is no other available parameter that could be used instead of STT. The current RPLD-to-STT correlation is shown in Figure 4, and currently comprises about 200 data points. With a larger database and analysis, it may be possible to derive an alternate RPLD correlation to unit UCS, and include parameters such as clay content (gamma) and signal spikiness.

Unlike the unit average value of STT to derive UCS, there is an issue about what RPLD correlation to use. As an example, refer to representative borehole geophysics shown in Figure 5. The average Unit A STT is about 75 µs/ft, with a lower-bound STT of about 80 µs/ft. The average Unit B STT is about 74 µs/ft with a lower-bound STT of about 77 µs/ft. If the average (black) correlation of Figure 4 is used to derive radial point-load strengths, the resultant unit CMRRs are 46 and 52 for Unit A and B, respectively. However, the average correlation of Figure 4 does not consider the presence of weak laminations, which will predominantly affect roof integrity in a laminated stone roof such as Grasstree given the relatively high ratios of horizontal to vertical stress (2:1) in the Bowen Basin.

From the wide data spread there are considerable data points with minimal radial Is50, indicating occasional weak laminations even in a relatively strong unit. Using the red or lower-bound correlation gives unit CMRRs of 40 and 41 for Unit A and B, respectively. While weak laminations do occur in stronger strata units they are not pervasive, and their effects do not predominate considering relatively

high material strength. The green or proposed correlation is midway between, and gives unit CMRRs of 42 and 46 for Unit A and B, respectively. Other correlations and justifications may be possible. If the green correlation is used, the red and black correlations then provide limits of uncertainty that may be used in a risk-based assessment, if required. The CMRR with strong bed adjustment assessment for a portion of Grasstree workings is shown in Figure 6. The assessment is done for the primary support roof horizon, i.e. 0 m to 1.7 m above cut roof horizon.

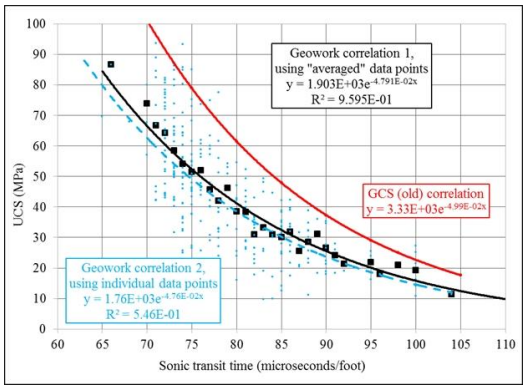

Figure 2 - The current UCS and STT correlation at Grasstree Mine

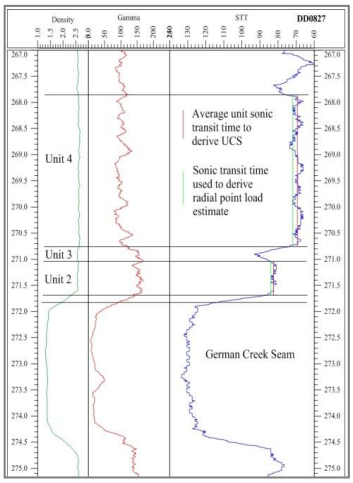

Figure 3 - Geophysical log showing roof units and STT used to derive UCS and RPL

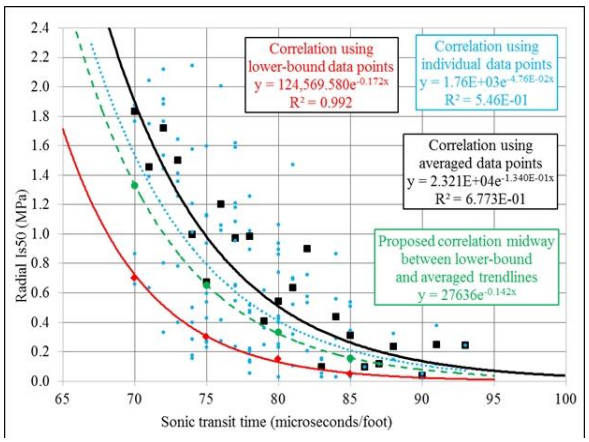

Figure 4 - RPL and STT Correlation at Grasstree Mine

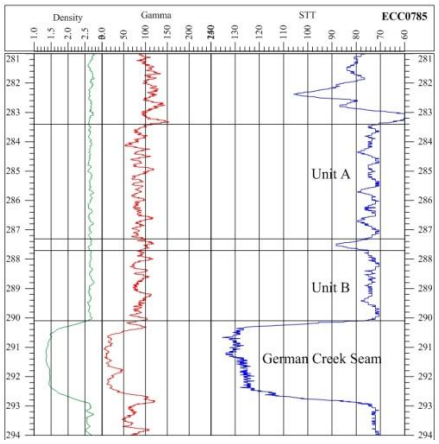

Figure 5 - Example sonic trace

UCS and RSI

UCS is calculated for each lithological unit using the correlation shown in Figure 2. RSI is defined as the UCS (MPa) divided by the in-situ vertical stress (MPa) (Gordon and Tembo, 2005) and is unitless. Vertical stress may be calculated from depth of cover. The UCS and RSI assessments for a portion of the Grasstree workings are shown in Figures 7 and 8, respectively.

CONCLUSIONS

Characterisation of the rock mass across proposed workings is a critical component of mine planning. The advance or innovation outlined above is not in doing the characterisations, which are standard industry assessments, but in the method of evaluating required data from available borehole geophysics. Based on underground observations the utilisation of this technique, specifically the use of low strength spikes in STT to estimate RPLD data, is deemed appropriate for Grasstree Mine. It is acknowledged that this technique is likely limited to a laminated stone roof for which it has been developed. Evaluating radial point-load strength for a lithological unit from geophysical correlations is dependent on first collating a

large comprehensive database of actual point-load test data, across the range of lithological types, whilst also having abundant geophysical data. It is appreciated that different and improved methods of calculated geomechanical data from borehole geophysics may be proposed and developed.

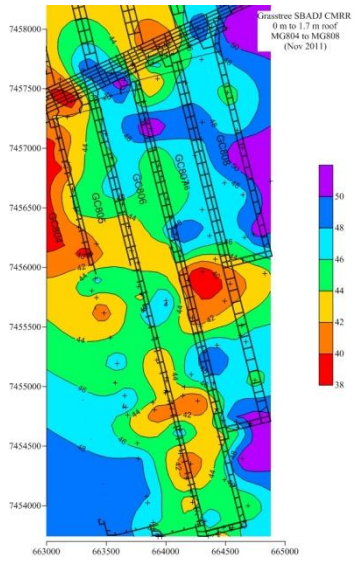

Figure 6 - CMRR MG804 to MG808

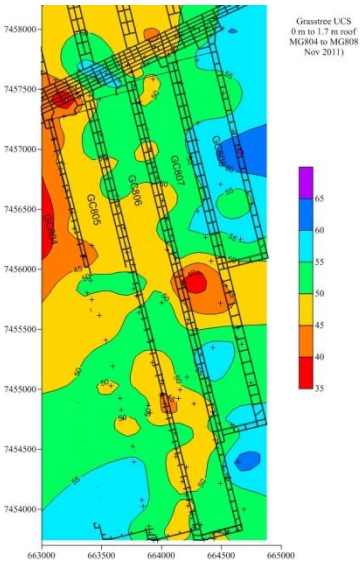

Figure 7 - UCS MG804 to MG808

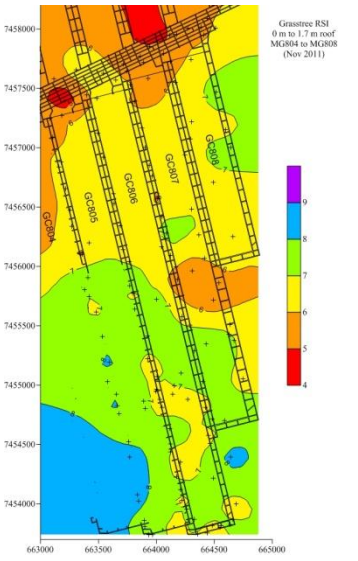

Figure 8 - RSI MG804 to MG808

ACKNOWLEDGEMENTS

The authors acknowledge Anglo American, Capcoal Management and exploration personnel for data access and presentation of outcomes. The principal author acknowledges the support, encouragement and advice provided by the other authors.

REFERENCES

Colwell, M, 1998. Calibration of ALPS to Australian mining conditions. End of Grant Report, *ACARP Project C6036*.

Gordon, N and Tembo, E, 2005. The roof strength index - a simple index to one possible mode of roof collapse, *Bowen Basin Symposium, Yeppon*. 347-352.

Hatherly, P, Medhurst, T and MacGregor, S, 2008. Geophysical strata rating. *Australian Coal Association Research Program Project C15019 Report*. CRCMining, 52.

Mark, C and Molinda, G M, 2005. The coal mine roof rating - a decade of experience *International Journal of Coal Geology*. 64. 85-103.

Payne, D A, 2008. Crinum Mine: 15 Longwalls, 40 Million Tonnes, 45 Roof Falls - What did we learn?" In *Proceedings of the 8th Underground Coal Operators' Conference*, (eds: N Aziz and J Nemcik), University of Wollongong. pp 22-43. http://ro.uow.edu.au/coal/2/.

Mark, C, 1990. Pillar design methods for longwall mining. *Bureau of Mines Information Circular IC 9247*.

GEOTECHNICAL MODELLING BASED ON GEOPHYSICAL LOGGING DATA

Peter Hatherly[1],Terry Medhurst[2] and Binzhong Zhou[3]

ABSTRACT: Computer modelling of coal seams and their properties is standard geological practice for both underground and open cut mining. It is based on correlations of coal seams made between boreholes and the interpolation of relevant coal seam properties on the basis of the inferred coal seam boundaries. In the case of geotechnical studies, this same approach is not followed because there are insufficient geotechnical test results to form a basis for modelling and the geological models do not typically create boundaries for interburden rock types. Instead, geotechnical models tend to be based on coal seam geological models with test results shown as point data in the interburden intervals. This situation can be improved if geophysical logging data are used as the basis for geotechnical modelling. Appropriately analysed, these logs provide continuous measurements of lithological and geotechnical properties. In the case of natural gamma data, an analysis to show the variations in clay content allows sandstones to be separated from finer grained siltstones. If geophysical strata rating values are determined from the geophysical logs, they provide a measure of rock quality. From these analyses, 3D models showing interburden properties as well as boundaries of the relevant rock types can be created and used as a basis for mine design and control of geotechnical hazards.

INTRODUCTION

In both underground and open cut coal mines, there is a need for on-going developments in technologies which allow management of risk and the maintenance of high levels of productivity. In this paper an approach to the characterisation and modelling of rock masses using conventional borehole geophysical logs is described.

At many coal mines, geophysical logs, primarily natural gamma, density and sonic logs are obtained in most exploration boreholes. These geophysical logs provide objective measurements of rock properties which are at great detail. Two useful rock properties that can then be derived are the clay content, which indicates basic stratigraphic variations between rock types such as sandstone and siltstone, and the Geophysical Strata Rating (GSR), which is a measure of rock quality.

Within a borehole, the geophysical logs are usually acquired at cm intervals. These more than adequately sample the vertical variations in the geology. Provided also, that the exploration boreholes are spaced at intervals which adequately sample the lateral variations in the geology (typically at spacings of a few hundreds of metres), the geophysical results can be modelled in 2D and 3D to provide a view of the lithological and geotechnical properties of the strata that are present.

GEOPHYSICAL LOG ANALYSIS

Through ACARP funded research, an approach to the analysis of geophysical logs that allows robust estimates of the porosity, clay content and rock quality within a borehole has been developed. The porosity is best determined using density logging results and clay content can be determined from a natural gamma log or from neutron porosity or resistivity logs, provided the density porosity is also available. In the case of the rock quality, the GSR provides a measure which is based on depth corrected sonic logging data and the values of the clay content and porosity obtained from the other logs. Hatherly *et al*. (2009, 2010) provide more detailed accounts of the approach to geophysical log analysis and the basis of the GSR. An example of the results that can be obtained are shown in Figures 1 and 2.

Figure 1 shows a suite of geophysical logs from a borehole at an open cut mine and their geological interpretation. Two coal seams are present. These can be readily identified as the intervals where there are low densities, low natural gamma responses and low sonic velocities. The boundaries of the coal

[1] *Coalbed Geoscience, geophys@bigpond.net.au, Tel: 04 1746 3832*
[2] *PDR Engineers, tmedhurst@pdrengineers.com.au, Tel: +61 7 4051 5599*
[3] *CSIRO Advanced Coal Technology*

seams can be accurately picked from the density log. Values of about 1.95 t/m^3 typically represent the upper density limit for a coal seam.

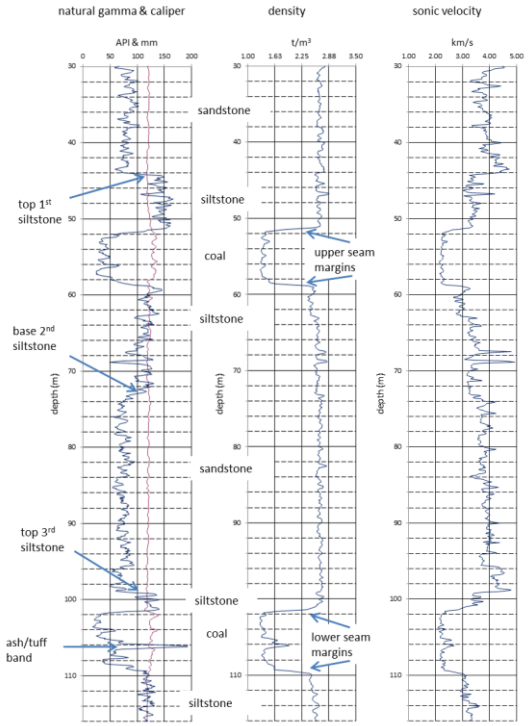

Figure 1 - Example of geophysical logs obtained from an exploration borehole. These logs allow identification of the major rock types present - coal, sandstone and siltstone. A tuff band is also present in the lower coal seam.

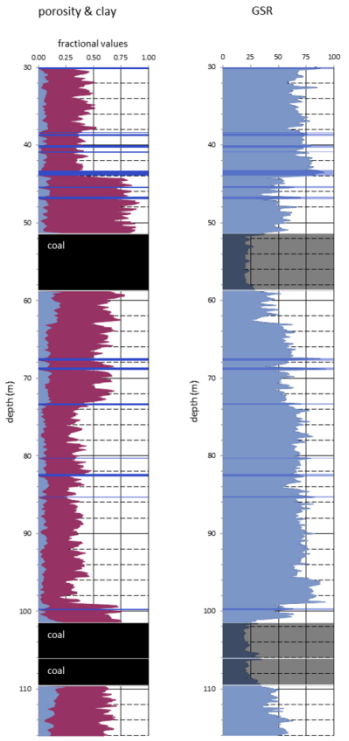

Figure 2 - Interpretation of the geophysical logs from Figure 1. On the left, the porosity is shown in blue and the clay content is shown in red. The clay content is lower in the sandstone than in the siltstone. GSR values are higher in the sandstone than in the siltstone.

Both coal seams are bounded by layers of siltstone. Siltstones typically have higher natural gamma signatures than coal and sandstones. The boundaries between coal and siltstone, and siltstone and sandstone can be sharp or gradational, but in the case of the data shown in Figure 1, the siltstone boundaries are reasonably sharp. The regions with relatively low natural gamma signatures represent sandstone. The actual value may depend on whether the sandstone is quartz rich or more lithic. In the case of lithic sandstones, the individual rock grains can be clay rich and create a situation where the natural gamma response is higher. Another feature of the natural gamma log in Figure 1 is the spike that occurs in the lower coal seam. This spike is due to a tuff band in the coal seam.

The sonic log values show the expected behaviour. As demonstrated by McNally (1990) and Ward (1998), sonic velocities can be empirically related to UCS. In Figure 1, the coal seams have the lowest sonic velocities and are weakest, the siltstone layers identified on the natural gamma logs have intermediate sonic velocities and intermediate strength. The sandstones have the highest velocities and are strongest. Occasional sharp spikes in sonic velocity and density are due to siderite bands.

Figure 2 shows the interpretation of these logs. The porosity and clay contents are derived from the density and natural gamma logs. The GSR values are derived using the procedure described in Hatherly *et al.* (2009 and 2010). The main features in the porosity and clay interpretations are the higher proportions of clay in the siltstone units and the higher porosities in the siltstones at the base of each of the coal seams. These higher porosities are possibly indicating that the siltstones beneath the seams are carbonaceous and, as a consequence, the overall density is lower. As far as the GSR determinations are concerned, the coal has a GSR of about 20, the siltstones have GSR values in the range 40 to 55 and the sandstones have GSR values of about 55 to 80.

MODELLING

Given the detailed information on rock properties that can be obtained from the geophysical logs, interpolation of the data between holes allows development of 2D and 3D models of the subsurface. However, it is first necessary to provide guidance as to how the various layers are linked between the holes. If this is not done, a result such as that shown in Figure 3 might be obtained. Here, a 2D section which passes close to 4 boreholes (including the borehole used for Figures 1 and 2) is shown. The section line is in the dip direction and it is clear that the interpolation has not been able to link the geology between the holes.

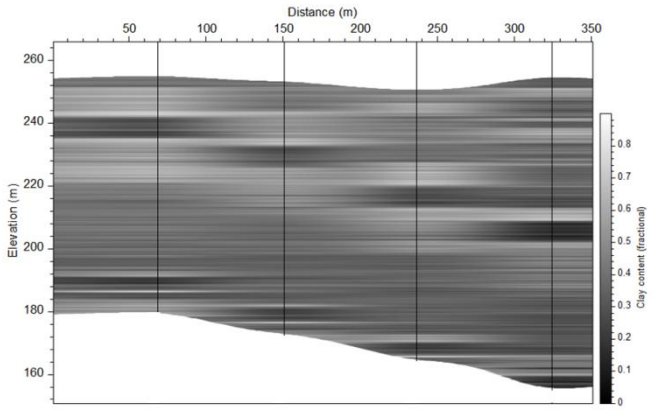

Figure 3 - A model of the clay content determined without any guidance as to how the layers present in the four boreholes should be correlated. In this section, the coal seams should be dipping from left to right. Without guidance, the coal seams show step-like structures which are clearly incorrect.

As shown in Figure 1, the layering and the positions of the boundaries can be established through an examination of the geophysical logs. If the position of the main boundaries is determined in each hole and then interpolated between boreholes, these can be used to provide guidance for the modelling.

Figures 4 and 5 illustrate the process. In Figure 4, the layer boundaries were picked in each hole and then interpolated between the holes. Each boundary was established independently. They can then be used

to constrain the interpolation of the geophysical parameters between holes. In this 2nd stage of the process, only the data from between the boundaries in each of the boreholes is used when interpolating values for that layer between holes.

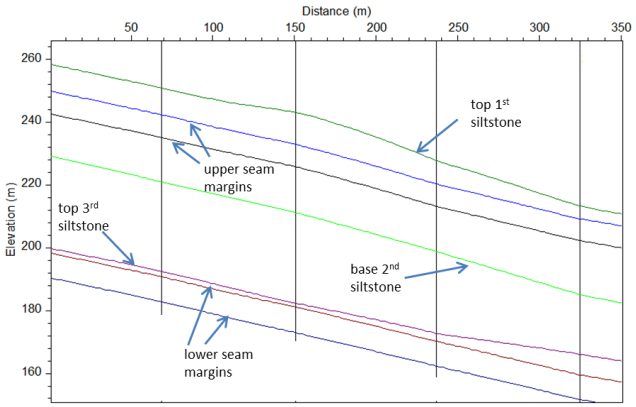

Figure 4 - Layer boundaries determined from geophysical logs from the four boreholes and interpolated between the holes. Once positions of the boundaries are established, they can be used to guide the interpolation of the geophysical data between holes.

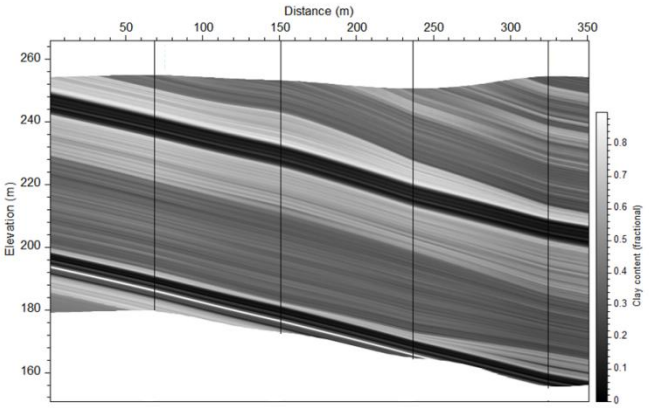

Figure 5 - A model of clay content for the same section as Figure 3 but with the layer boundaries of Figure 4 used to guide the interpolation of the clay contents determined in each borehole

Figure 5 shows the resulting model for the clay content. In contrast to Figure 3, the layering is continuous and it can be seen that the values of the clay content assigned to each layer is properly representative of the layers. Furthermore, within the layers, subtle variations in the clay content are propagated between holes. Given that the geophysical data is being honoured at the boreholes, this indicates that within many rock units, there are numerous consistent geophysical features present in adjacent boreholes. The lateral variability in the rock units can thus be explored in considerable detail.

When the GSR is modelled along the same section line, the results shown in Figure 6 are obtained. As shown in Figure 2, the coal seams have low GSR values, the siltstones have the intermediate values and the sandstones have the highest values. As with the model of the clay content, subtle features in the rock quality are also propagated between holes.

Figures 4, 5 and 6 all show results in 2D section view. If the modelling is conducted in 3D, sections can be created along arbitrary lines and data can be examined in plan view. Plan views can be particularly useful if values are taken parallel to a horizon of interest, as might be the case where there is interest in the rock properties at a certain interval within the roof or floor strata of a coal seam.

An example of a result in plan view is shown in Figure 7. This shows average GSR values for a 6 m interval immediately above the lower coal shown in the previous figures. Also shown on Figure 7 is the position of the profile line for the 2D sections. It can be see that the region of lower GSR on the right of

Figure 7 coincides with the region to the right of Figure 6 where the siltstone overlying the lower coal seam is thicker. Plan views therefore provide an indication of the lateral extent of the units of interest.

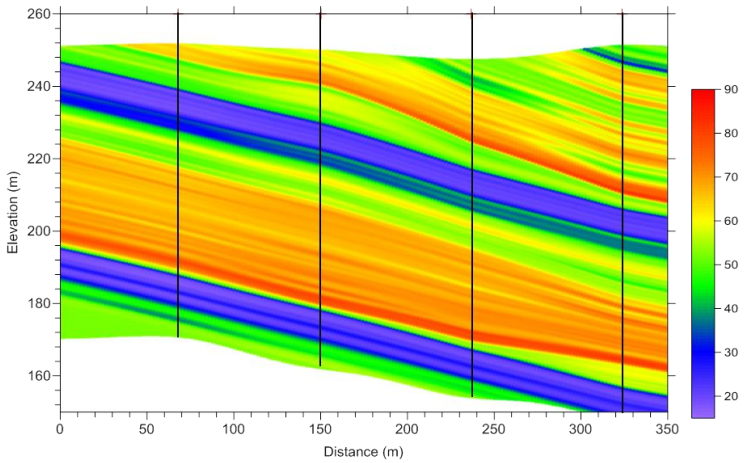

Figure 6 - The GSR model for the same section as Figure 5. Again the layer boundaries of Figure 4 have been used to guide the interpolation of the GSR data between holes.

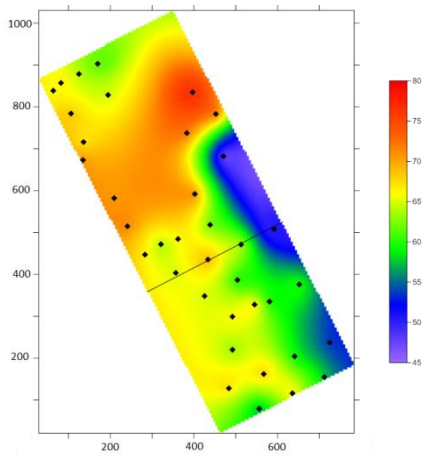

Figure 7 - GSR data in plan view, taken from a 3D model which covers the region of the section line in Figures 3 to 6. The GSR values shown here are averaged over a 6m interval, immediately above the lower coal seam. The section line for Figures 3 to 6 is shown by the thin line. Diamonds indicate borehole locations. The region where the siltstone forms the main part of this interval has lower average GSR values. The region where sandstones predominate has the higher values.

DISCUSSIONS

The approach to geotechnical evaluation described in this paper has the advantage of being based on objective geophysical logging measurements. It also draws on the extensive database provided by exploration drilling programs and the geophysical logging that is undertaken in those holes. Once established, the models of GSR and other petrophysical parameters provide a context for geotechnical observations from core testing, logging and monitoring. They facilitate the development of good geotechnical understanding.

Applications that exist in both open cut and underground mining include:

- Highwall design and the understanding of highwall failure.
- Blast design.
- Predicting and understanding floor heave.
- Longwall caving behaviour.

- Determining roadway support requirements.
- Preparation of hazard plans.

More industry-wide experience is required for these applications to develop. Research is working towards developing tools that allow direct quantitative use of the approach in specific mine design problems. It is hoped that in future years, 3D geotechnical modelling will become just as much a part of the mining process as geological modelling is today.

CONCLUSIONS

Australian coal mining is accustomed to conducting geophysical logging in exploration boreholes. As aresult, a very large database of geophysical logs is available at most mines. Through a quantitative analysis of these logs and determination of GSR values, it is possible to create 3D models of the subsurface which contain detailed information about the occurrence and properties of the strata that are present. These models allow an unprecedented view of geotechnical conditions and have numerous applications in both open cut and underground mining.

REFERENCES

Hatherly, P, Medhurst, T, Ye, G and Payne, D, 2009. Geotechnical evaluation of roof conditions at Crinum Mine based on geophysical log interpretation. In *Proceedings of 9th Coal Operators' Conference*, AusIMM Illawarra Branch, the University of Wollongong, pp16-22. (Eds: N Aziz and J Nemcik). http://ro.uow.edu.au/coal/67/.

Hatherly, P, Medhurst, T and Zhou, B, 2010. The geological strata rating and its derivation from geophysical logs and seismic reflection data. In *Proceedings of 37th Symposium on the Geology of the Sydney Basin*.

McNally, G H, 1990. The prediction of geotechnical rock properties from sonic and neutron logs, *Exploration Geophysics*, 21: 65-71.

Ward, B, 1998. German Creek Mines, rock strength from sonic velocity logs. *Internal report*, Capricorn Coal Management Pty. Ltd.

DEVELOPMENT OF A METHOD FOR LAYOUT SELECTION USING ANALYTICAL HIERARCHY PROCESS

Shaima Abdalla[1], Mehmet S Kizil[1] and Ismet Canbulat[2]

ABSTRACT: One of the most critical and complicated steps in mine planning is the selection of a suitable layout based on geological, geographical, geotechnical and economical parameters. These parameters influence the choice of different layouts of coal mine workings and normally examined on the basis of experience gained in the coalfields. The wide ranging combinations of geological, geotechnical and mining conditions make the selection of the optimum design and layout for a particular situation a difficult task. Variations in these parameters result in multiple feasible mine layouts; where each layout entails some inherent problems and the optimal layout is the one that offers the lowest problems. These variations in designs result in complex multi-decision situations that cannot be solved by a simple technique. This paper develops a method based on an analytical hierarchy process to select the most viable panel orientation for longwall operation. A back analysis of this technique was conducted at a mine located in central Queensland. The geological and geotechnical aspects of the mine resulted in variations in the recommended panel orientations. Three different mine layouts with variable geological and geotechnical impacts were evaluated and the optimum mine layout was determined. This paper also challenged the viability of the obtained results by performing a consistency check at every critical stage of the project.

INTRODUCTION

The selection of mine layout is one of the most critical and problematic phase in mine planning stage. Subsequent operating factors such as ground support requirements, equipment selection and ventilation are entirely influenced by the mine layout. The ultimate goal of mine layout selection is maximising the company's profit and resource recovery while providing a safe environment for the miners by selecting a suitable layout with the fewest problems among the feasible alternatives. Analytical Hierarchy Process (AHP) is a multi-criteria decision method that uses hierarchical structures to solve complicated, unstructured decision problems, especially in situations where there are important qualitative aspects that must be considered in conjunction with various measurable quantitative factors (Shahriar, *et al.*, 2007). The AHP is still being applied in numerous and diverse fields such as software selection, project selection and measuring business performance; however, it has not been applied widely in the Australian mining industry, particularly in mine layout selection. Unlike the traditional approaches utilised for layout selection, AHP makes it possible to select the best layout in a more scientific, semi-quantitative manner that preserves integrity and objectivity (Ataei, *et al.*, 2008). AHP models are transparent and easy to comprehend and apply. The AHP models are unique in their identification of multiple attributes where minimal data is required, and minimal time is consumed (Ataei, *et al.*, 2008).

Analytical Hierarchy Process theory

The AHP methodology was first developed by Saaty (Saaty, 1990). The AHP is a tool that is used to combine qualitative and quantitative factors in the selection of a process. It is based on mathematical framework formed by matrix and vector algebra that can easily be performed in Microsoft® Excel. The mathematical framework starts with a pairwise comparison of the relative weight or dominancy of each criterion over another (Musingwini and Minnitt, 2008). To make the comparisons, scaling of numbers is required to indicate the weight and the dominancy of a particular element over another element with respect to the criterion to which they are compared. This scale is used to express the evaluator's preference of criterion over another by assigning numbers that ranges from 1 for equally importance to 9 for extreme importance (Yavuz, *et al.*, 2007). The relative weight of each pair of criteria, C_i over C_j is denoted by v_{ij} such that $v_{ij} = \frac{1}{v_{ji}}$ for $i \neq j$ and $v_{ii} = 1$, for all i. These weights form a square matrix A, of order n; corresponding to the number of criteria. This matrix is referred to as, reciprocal matrix because of the weight of one criterion over another and is equal to the weight of the second criterion over the first one

[1] *The University of Queensland, School of Mechanical and Mining Engineering, Brisbane QLD 4072; Contact: Mehmet Kizil, m.kizil@uq.edu.au, Tel: 07 3365 4499*
[2] *Anglo American Pty. Ltd. Brisbane, QLD 4000*

(Musingwini and Minnitt, 2008). After the construction of the pairwise comparison matrix, Saaty (1990) proposed an eigenvector (priority vector) approach for the estimation of the overall weights of criteria from a matrix of the pairwise comparisons. The eigenvector has an intuitive interpretation in which it is an averaging of all possible ways of thinking about a given set of alternatives (Ekipman, 2003). The eigenvector, *w* is established such that $Aw = \lambda w$, where λ is the corresponding eigenvalue of matrix A (Musingwini and Minnitt, 2008).

The final stage of the AHP model is the evaluation of the pairwise comparison matrix for consistency. The matrix is consistent if the relative importance is cardinal and/or ordinal consistent. For example, for cardinal consistent matrix, if criterion C_2 is twice as important as criterion C_1 and criterion C_3 is three time as important as C_2, then it follows that criterion C_3 should be six times as important as C_1. For consistent ordinal matrix, if C_1 is preferred to C_2 and C_2 is preferred to C_3, then C_1 should be preferred to C_3 (Musingwini and Minnitt, 2008). However, this consistency is rarely achieved since AHP deals with human judgements which are characteristically inconsistent. Therefore AHP provides a way of measuring the degree of inconsistency in judgements as well as the method to reduce this measure, if it is deemed to be too high (Saaty, 2003).

Identification of main factors related to longwall layout selection

There is large number of geological, geotechnical and coal quality factors that have an impact on longwall layout selection. Large numbers of factors (criteria) are not desired while conducting the pairwise comparison. Large number of factors would lead to computational difficulties and it is considered as a time-consuming process which may result in an unrealistic outcome. Therefore, 14 geological, geotechnical and coal quality factors were identified by a team of experts as the main factors for longwall layout selection;

- Depth of cover;
- Seam inclination;
- Coal quality;
- Gas make;
- Roof and floor strata;
- Geological structures;
- *In situ* stress;
- Multiple seam mining;
- Surface restrictions;
- Surface subsidence;
- Access to reserve;
- Reserve losses due to layout;
- Seam thickness; and
- Roof cavability.

CONSTRUCTION OF AN AHP MODEL

Pairwise comparison of identified factors

From the identified factors, a 14×14 matrix was constructed using the above critical factors. The number scale proposed by Saaty (1990) was utilised in rating each pair of factors to quantify the dominancy of a factor over the other. Therefore, in order to obtain these ratings a workshop was held which involved experts in the longwall mine planning and design process from different functional areas and questionnaire were posed such as; what is the relative importance of factor *i* (matrix row) as opposed to factor *j* (matrix column)? The use of verbal scale instead of numerical scale in the AHP model is to enable the decision-maker to incorporate subjectivity, experience and knowledge in an intuitive and natural way (Ataei, *et al.*, 2008). Due to the dependency of the assigned rates on the location of the proposed mine,

central Queensland, was selected to be the region of interest and the rates of the pairwise comparisons were assigned accordingly.

As can be seen in Table 1, *in situ* stress was rated as highly important compared to the other factors, while surface restrictions and surface subsidence were rated as least important due to minimal restrictions on the surface.

Relative priorities

The estimation of the relative priorities of the identified factors in the pairwise comparison matrix was achieved through the estimation of the eigenvector (priority vector). There are several methods that are available for estimating eigenvector. The computation of the eigenvector of a matrix can be accurately performed using Matlab® software. However this software is not user-friendly; therefore it requires competent user of the softwares. Also, calculated results in Matlab® involve risks associated with human errors encountered during data input; therefore, errors-checking is a difficult task as data input process is required to be repeated for multiple of times to reduce this risk.

Table 1 - Pairwise comparison matrix of the identified factors

	Depth of Cover	Seam Inclination	Coal Quality	Gas Make	Roof and Floor Strata	Geological Structures	In-situ Stress	Multiple Seam Mining	Surface Restrictions	Surface Subsidence	Access to reserve	Reserve losses due to the layout	Seam Thickness	Roof Cavability
Depth of Cover	1.00	7.00	0.13	1.00	1.00	3.00	0.11	7.00	8.00	8.00	1.00	0.33	2.00	2.00
Seam Inclination	0.14	1.00	0.11	0.13	0.13	0.33	0.11	1.00	0.25	1.00	0.14	0.11	0.14	0.13
Coal Quality	8.00	9.00	1.00	9.00	0.50	3.00	1.00	8.00	5.00	8.00	4.00	3.00	6.00	6.00
Gas Make	1.00	8.00	0.11	1.00	0.17	0.33	0.11	5.00	0.25	6.00	0.14	0.14	0.33	0.20
Roof and Floor Strata	1.00	8.00	2.00	6.00	1.00	6.00	0.50	6.00	8.00	8.00	4.00	1.00	1.00	1.00
Geological Structure	0.33	3.00	0.33	3.00	0.17	1.00	0.25	7.00	8.00	9.00	0.50	1.00	1.00	1.00
In-situ Stress	9.00	9.00	1.00	9.00	2.00	4.00	1.00	9.00	9.00	9.00	7.00	3.00	8.00	5.00
Multiple Seam Mining	0.14	1.00	0.13	0.20	0.17	0.14	0.11	1.00	5.00	6.00	0.33	0.14	0.13	0.17
Surface Restrictions	0.13	4.00	0.20	4.00	0.13	0.13	0.11	0.20	1.00	1.00	0.20	0.13	0.14	0.14
Surface Subsidence	0.13	1.00	0.13	0.17	0.13	0.11	0.11	0.17	1.00	1.00	0.13	0.11	0.13	0.13
Access to Reserve	1.00	7.00	0.25	7.00	0.25	2.00	0.14	3.00	5.00	7.69	1.00	0.33	5.00	2.00
Reserve Losses (due to the layout)	3.00	9.00	0.33	7.00	1.00	1.00	0.33	7.00	8.00	9.00	3.00	1.00	7.00	5.00
Seam Thickness	0.50	7.00	0.17	3.00	1.00	1.00	0.13	8.00	7.00	8.00	0.20	0.14	1.00	0.50
Roof Cavability	0.50	8.00	0.17	5.00	1.00	1.00	0.20	6.00	7.00	8.00	0.50	0.20	2.00	1.00
Sum	25.87	82.00	6.05	55.49	8.63	23.05	4.22	68.37	72.5	89.69	22.15	10.64	33.87	24.26

Microsoft® Excel has therefore been used to estimate the eigenvector by implementing an approximation method that is based on normalisation (Kardi, 2006). The process of normalisation for a given reciprocal square matrix ($n \times n$) includes the following steps:

1. Summation of each column of the reciprocal matrix.
2. Division of each element of the matrix with the sum of its own column, this is called normalisation of relative weight, where the sum of each new column is one (1).
3. The normalised principal eigenvector can be estimated by averaging across the rows.

The application of the normalisation process on the identified factors' matrix is shown in Table 2. The eigenvector of the pairwise comparison matrix has also been calculated using Matlab® to confirm the validity of the results obtained by the approximation method. The approximation method results were very close to those calculated using Matlab®, with only 0 to 5% deviation. Therefore the use of the approximation method through the normalisation process was considered acceptable.

As can be seen in Table 2, *in situ* stress was calculated to have the highest calculated priority (20%) as it has been considered as highly important against other identified factors in the pairwise comparison. On

the other hand, surface restrictions, seam inclination and surface subsidence were calculated to have the lowest priorities (1 to 2%). These factors were considered with low dominancy or priority due to the fact that the mine in consideration is located in central Queensland, where there are lower restrictions on surface impact compared to other regions. It is highly important to note that the given the rates and the calculated priorities of these factors are subject to alteration if other regions were considered. For example, if a mine in New South Wales was considered, surface restrictions and surface subsidence would be expected to be given higher ranking and hence higher priorities as it has higher restrictions on surface impact.

Consistency measure

When dealing with tangibles, pairwise comparison judgment matrix may be perfectly consistent but irrelevant and far off the mark of the true values (Saaty, 2003). Therefore, a small degree of inconsistency may be considered as good practice and forced consistency without the knowledge of the precise values may lead to an undesired compulsion. Inconsistency of a matrix indicates the contradiction in preference of a pairwise comparison to another. It is important to note that the AHP does not require the decision-makers to be consistent but, rather, it provides a measure of inconsistency as well as a method to reduce this measure if it is deemed to be too high (Ekipman, 2003). Saaty (1990) stated that AHP estimates consistency by determining the principal (maximum) eigenvalue, λ_{max}.

Table 2 - Normalised matrix of the identified factors

	Depth of Cover	Seam Inclination	Coal Quality	Gas Make	Roof and Floor Strata	Geological Structures	In-situ Stress	Multiple Seam Mining	Surface Restrictions	Surface Subsidence	Access to Reserve	Reserve losses (due to the layout)	Seam Thickness	Roof Cavability	Sum	Priority Vector
Depth of Cover	0.04	0.09	0.02	0.02	0.12	0.13	0.03	0.10	0.11	0.09	0.05	0.03	0.06	0.08	0.96	7%
Seam Inclination	0.01	0.01	0.02	0.00	0.01	0.01	0.03	0.01	0.00	0.01	0.01	0.01	0.00	0.01	0.15	1%
Coal Quality	0.31	0.11	0.17	0.16	0.06	0.13	0.24	0.12	0.07	0.09	0.18	0.28	0.18	0.25	2.33	17%
Gas Make	0.04	0.10	0.02	0.02	0.02	0.01	0.03	0.07	0.00	0.07	0.01	0.01	0.01	0.01	0.41	3%
Roof and Floor Strata	0.04	0.10	0.33	0.11	0.12	0.26	0.12	0.09	0.11	0.09	0.18	0.09	0.03	0.04	1.70	12%
Geological Anomalies	0.01	0.04	0.06	0.05	0.02	0.04	0.06	0.10	0.11	0.10	0.02	0.09	0.03	0.04	0.78	6%
In-situ Stress	0.35	0.11	0.17	0.16	0.23	0.17	0.24	0.13	0.12	0.10	0.32	0.28	0.24	0.21	2.82	20%
Multiple Seam Mining	0.01	0.01	0.02	0.00	0.02	0.01	0.03	0.01	0.07	0.07	0.02	0.01	0.00	0.01	0.28	2%
Surface Restrictions	0.00	0.05	0.03	0.07	0.01	0.01	0.03	0.00	0.01	0.01	0.01	0.01	0.00	0.01	0.26	2%
Surface Subsidence	0.00	0.01	0.02	0.00	0.01	0.00	0.03	0.00	0.01	0.01	0.01	0.01	0.00	0.01	0.14	1%
Access to Rreserve	0.04	0.09	0.04	0.13	0.03	0.09	0.03	0.04	0.07	0.09	0.05	0.03	0.15	0.08	0.95	7%
Reserve Losses (due to the layout)	0.12	0.11	0.06	0.13	0.12	0.04	0.08	0.10	0.11	0.10	0.14	0.09	0.21	0.21	1.60	11%
Seam Thickness	0.02	0.09	0.03	0.05	0.12	0.04	0.03	0.12	0.10	0.09	0.01	0.01	0.03	0.02	0.75	5%
Roof Cavability	0.02	0.10	0.03	0.09	0.12	0.04	0.05	0.09	0.10	0.09	0.02	0.02	0.06	0.04	0.86	6%
Sum	1.00	1.00	1.00	1.00	1.00	1.00	1.00	1.00	1.00	1.00	1.00	1.00	1.00	1.00	14.00	100%

The principal eigenvalue was obtained from the summation of products between each element of the eigenvector (priority vector) and the sum of the columns of the pairwise comparison matrix (Kardi, 2006). The principal eigenvalue of the pairwise comparison matrix for the identified factors was estimated to be 18.13. A consistency Index (CI) was then calculated from λ_{max} to measure the deviation from consistency using the relationship defined by Equation 1.

$$CI = \frac{\lambda_{max} - n}{n-1} \quad (1)$$

Using Equation 1 and the estimated principal eigenvalue, the value of CI was estimated to be 0.32. For a perfectly consistent matrix, $\lambda_{max} = n$; where n is the number of identified factors; and hence a CI value of zero is expected. Since the calculated CI value is greater than zero, inconsistency was expected in the pairwise comparison matrix.

In order to measure the level of inconsistency of a matrix, the Consistency Ratio (CR) was required to be calculated. As a general rule, a CR of 0.10 or less is considered acceptable (Saaty, 1990). The CR is

calculated by assessing the value of CI against judgements that are made by experts and completely at random. Saaty (1990) simulated large sample of random matrices of increasing order and calculated their corresponding CIs which are Random Indices (RI). For matrices of order between 1 and 15, Saaty established the corresponding RI. The CR was calculated by dividing the CI (0.32) by its corresponding RI (1.57), to give a value of 0.2. The calculated CR was clearly higher than the acceptable ratio of 0.1, which made the pairwise comparison matrix inconsistent. Therefore, a revision and reconsideration on the subjective judgements was required.

AHP MODEL VALIDATION

Methodology

Consistent matrices are essential because when dealing with intangibles, human judgments are usually inconsistent, and if the decision-maker is able to improve inconsistency to near consistency, then that could improve the validity of the priorities of a decision (Saaty, 2003). This can be done through the revision of all the data entries in the pairwise comparison matrix and reconsideration of the entries that cause the inconsistency. However, this process can be time consuming as the size of the matrix increases, considering the size of the matrix within this paper is 14×14.

Several alternatives, mostly based on various optimisation techniques, have been proposed to help improve consistency. Saaty (2003) proposed a method based on perturbation theory to find the most inconsistent judgment in the matrix. This method could be followed by the determination of the range of values to which that judgment can be changed and whereby the inconsistency could be improved and then asking the decision-maker to consider changing the judgment to a plausible value in that range (Benítez, *et al.*, 2011). This paper utilised this method in an iterative manner to assist the decision-maker to detect and adjust inconsistencies and to represent more acceptable judgements (Li and Ma, 2007).

The first step in Saaty perturbation theory is the detection of the matrix entry that is causing the inconsistency. Inconsistency detection is based on the fact that:

$$\sum_{\substack{i=1,j=1 \\ i\neq j}}^{n} a_{ij}\frac{w_j}{w_i} = \lambda_{\max} \qquad (2)$$

Where w_i and w_j are the eigenvector entry that corresponds to the matrix entry a_{ij}.

This relationship suggests that examination is required for the entry a_{ij} for which $a_{ij}\frac{w_j}{w_i}$ is the largest, and determine if this entry can reasonably be made smaller. This is because the entry with the largest $a_{ij}\frac{w_j}{w_i}$ value indicates that it has the largest impact on the inconsistency. The reduction of this entry is preferable as such a change will result in a new comparison matrix with smaller eigenvalue and hence more consistency.

The second step in this method is to estimate the most consistent value for the matrix entry. Harker (1987) has shown that the most consistent value for the entry a_{ij} can be estimated by:

1. Replacing the entries $a_{ij}$and its reciprocal, a_{ji}, by zeros, and the two corresponding diagonal entries by two;
2. Calculating the new eigenvector, w'; and
3. Estimating the new (consistent) value of the entry a_{ij} by considering $a_{ij}{}' = \frac{w_{i'}}{w_{j'}}$, where $a_{ij}{}'$ is the consistent value of entry a_{ij}, and $w_i{}'$ and $w_j{}'$ are the entries of the new calculated eigenvector that correspond to the entry a_{ij}.

Results

Implementing Saaty's method, the pair; multiple seam mining and surface restrictions; was identified to have the largest $a_{ij}\frac{w_j}{w_i}$ value. Proceeding with Saaty's method, the most consistent value was estimated. However, another workshop was required to validate the estimated value, as simply substituting the most

consistent value into the matrix creates a forced consistency situation which is undesirable. The pair had an initial value of 5, but applying Saaty's method; a new value of 1 was estimated for the pair. In order to validate the new estimated value, another workshop was held with the same experts, deciding on a value of 2. From the substitution of the new value of the entry and the estimation of the new priority vector, a new CR of 0.19 was estimated.

The application of Saaty's method has resulted in a 5% reduction of the CR; however, this reduction was considered insufficient to achieve the desired consistency. Therefore, multiple iterations were performed with the subsequent largest inconsistent judgements. The identified new values for the inconsistent pairs were substituted into the original pairwise comparison matrix as highlighted in Table 3 and the new priority vector was estimated. From the modified pairwise comparison matrix and the new estimated priority vector, a new CR was estimated to be 0.13. The estimated value of the CR was still above the acceptable consistency limit (0.1); however this degree of inconsistency was still considered as acceptable since forced consistency is undesired.

CASE STUDY: MINE A

Overview

The second stage of the AHP is the construction of pairwise comparisons between various alternatives (mine layouts) under each criterion (factor). In order to complete this stage, a mine at the feasibility stage, Mine A, located in central Queensland was used as a case study. Longwall mining was selected to be utilised for coal extraction. The geological and geotechnical aspects of the mine resulted in variations in the recommended panel orientations. This paper has evaluated three different panel orientations with variable geological, geotechnical and coal quality impacts.

Table 3 - Modified pairwise comparison matrix and priority vector of the identified factors

	Depth of Cover	Seam Inclination	Coal Quality	Gas Make	Roof and Floor Strata	Geological Structures	In-situ Stress	Multiple Seam Mining	Surface Restrictions	Surface Subsidence	Access to Reserve	Reserve losses (due to the layout)	Seam Thickness	Roof Cavability	Priority Vector
Depth of Cover	1.00	7.00	0.13	1.00	1.00	1.00	0.11	5.00	5.00	8.00	1.00	0.33	2.00	1.00	6%
Seam Inclination	0.14	1.00	0.11	0.13	0.13	0.33	0.11	0.25	0.25	1.00	0.14	0.11	0.14	0.13	1%
Coal Quality	8.00	9.00	1.00	9.00	0.50	3.00	1.00	8.00	5.00	8.00	4.00	2.00	4.00	6.00	17%
Gas Make	1.00	8.00	0.11	1.00	0.17	0.33	0.11	5.00	0.25	6.00	0.14	0.14	0.33	0.20	3%
Roof and Floor Strata	1.00	8.00	2.00	6.00	1.00	2.00	0.50	6.00	8.00	8.00	3.00	1.00	1.00	1.00	11%
Geological structure	1.00	3.00	0.33	3.00	0.50	1.00	0.25	5.00	6.00	9.00	0.50	0.50	1.00	1.00	6%
In-situ Stress	9.00	9.00	1.00	9.00	2.00	4.00	1.00	9.00	9.00	9.00	7.00	3.00	5.00	5.00	21%
Multiple Seam Mining	0.20	4.00	0.13	0.20	0.17	0.20	0.11	1.00	2.00	2.00	0.33	0.14	0.13	0.17	2%
Surface Restrictions	0.20	4.00	0.20	4.00	0.13	0.17	0.11	0.50	1.00	1.00	0.20	0.13	0.14	0.14	2%
Surface Subsidence	0.13	1.00	0.13	0.17	0.13	0.11	0.11	0.50	1.00	1.00	0.13	0.11	0.13	0.13	1%
Access to Reserve	1.00	7.00	0.25	7.00	0.33	2.00	0.14	3.00	5.00	7.69	1.00	0.33	1.00	2.00	7%
Reserve Losses (due to the layout)	3.00	9.00	0.50	7.00	1.00	2.00	0.33	7.00	8.00	9.00	3.00	1.00	4.00	1.00	11%
Seam Thickness	0.50	7.00	0.17	3.00	1.00	1.00	0.13	8.00	7.00	8.00	0.20	0.14	1.00	0.50	6%
Roof Cavability	1.00	8.00	0.17	5.00	1.00	1.00	0.20	6.00	7.00	8.00	0.50	1.00	2.00	1.00	7%

Geological and geotechnical conditions

Due to the sensitivity associated with the data collected from Mine A, only general trends of the geological, geotechnical and coal quality data were provided in this paper.

Overall the *in situ* horizontal stress is oriented at N30E. There is only one major normal fault with a dyke oriented at EW direction. The fault has a throw of 6 m down to the north. Surface restrictions are represented by a projected railway line and a creek running across the expected mining activity area as shown in Figure 1. Other geological, geotechnical and coal quality aspects vary in the easterly direction, as shown in Table 4.

Table 4 - Geological, geotechnical and coal quality trend

Factor	Unit	East	West
Depth of cover	m	250.00	550.00
Rank		1.20	1.45
Volatiles	%	25.00	19.00
Gas make	m^3/t	7.00	12 to 13
Seam Thickness	m	5.00	6.50

Other factors such as multiple seam mining, roof and floor strata and roof cavability were considered to have the same conditions within the active mining areas.

Proposed mine layouts

Figures 1, 2 and 3 represent the three proposed layouts against the horizontal stress, major fault and other surface features.

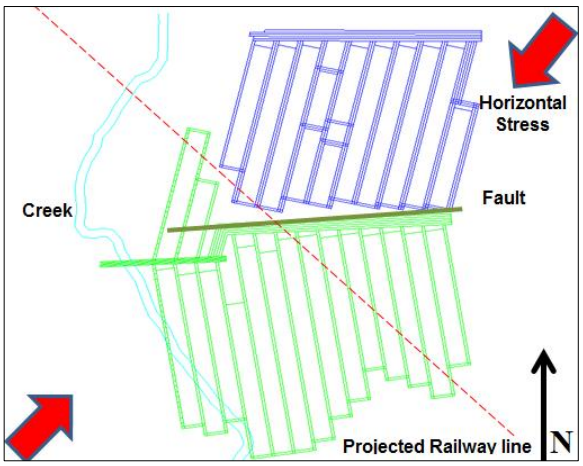

Figure 1 - First proposed mine layout

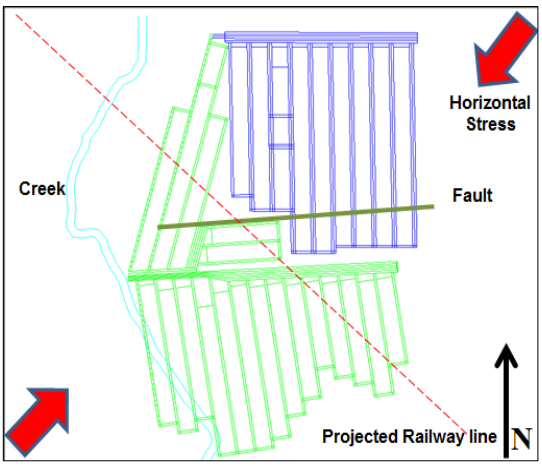

Figure 2 - Second proposed mine layout

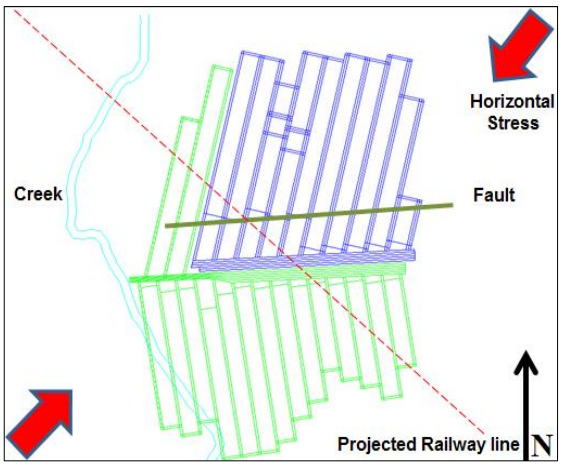

Figure 3 - Third proposed mine layout

Layouts comparisons

The three proposed different longwall layouts have different mining directions, panel orientations and panel configurations. These variations in layout were expected to have various geological, geotechnical and coal quality impacts, such as:

- In terms of coal quality, layout 2 was more preferable than layouts 1 and 3 as it provided a consistent coal quality per panel compared to the other two layouts.

- Considering the longwall panel length of the three layouts, layout 3 has the greatest panel length than other layouts. Therefore, layout 3 would require more complex gas drainage and hence least preferable compared to other layouts.
- Considering the location of the major fault, layout 1 was strongly more preferable than layouts 2 and 3 as the fault was avoided in layout 1, whereas it cut through the longwall panels in the layouts 2 and 3.
- All the layouts have different panel orientations to the *in situ* horizontal stress; therefore, various impacts with respect to stability of the layouts were expected. Layouts 1 and 2 are proposed to retreat from South to North, in which the stress notch is minimal and potentially notch only in the tailgate, which will be supported. On the other hand, layout 3 is proposed to retreat from North to South, in this case there may be maingate stress notch, which is undesirable as the conveyor belt will be placed in the gateroad. Also layout 1 has potentially lower stress notch on the tailgate than layout 2, since layout 1 is aligned more with the *in situ* horizontal stress. Therefore, from the horizontal stress notching point of view layout 1 was considered as most preferable, while layout 2 was more preferable than layout 3.
- The only surface restrictions are represented by the railway line and the creek. Layout 1 was considered to be more preferable than the other two layouts. This because larger sections of the railway line are above the mining activity area in the other two layouts compared to layout 1.
- Considering the access to reserve, access to layout 3 can be established relatively quickly and at lower cost from the existing workings of the mine. Whereas layouts 1 and 2 will require conveyor drift, man and material vertical shaft. Therefore, layout 3 was considered strongly more preferable than layouts 1 and 2.
- Due to the various panels configuration between all the layouts, layout 3 was considered to have the least reserve losses compared to layout 1 and 2. Also layout 1 has also lower losses than layout 2.
- Impacts with respect to the other factors such as depth of cover, seam inclination, roof and floor strata, multiple seam mining, surface subsidence, seam thickness and roof cavability were considered to be similar for all the layouts. All the layouts were therefore considered equally important with respect to these factors.

Pairwise comparisons of the proposed layouts

The second phase of the AHP is the construction of layouts pairwise comparison matrices and the assignation of rates for the alternatives (layouts) with respect to each criterion (factor). This was performed through the construction of a workshop with the same experts where questionnaires were posed to compare alternative *i* against alternative *j* with respect to a particular criteria. This comparison was performed using the same number scale proposed by Saaty (1990). The eigenvector (priority vector), the principle eigenvalue ($\lambda_{\max}$) and the consistency ratio (CR) were calculated in the same manner as the pairwise comparison of the identified factors as shown in Tables 5 to 12.

The three layouts had an equal importance with respect to other factors such as seam inclination, roof and floor strata, multiple seam mining, surface subsidence, seam thickness and roof cavability. Therefore, the pairwise comparison matrix and the estimated priority vector for these factors were expected to be identical to the pairwise comparison matrix and the estimated priority vector of the three layouts with respect to depth of cover as shown in Table 5.

Overall priorities and the optimum mine layout

The final stage of the AHP model is the estimation of the overall composite weight of each layout based on the estimated priority vector of both identified factors and layouts. Table 13, shows the priority vector of the identified factors, the priority vector of the layouts with respect to each identified factor and the estimated overall weight of the layouts. The overall weight has been estimated by the summation of the product between the priority value of an identified factor and its corresponding priority value of a particular layout.

Table 5 - Pairwise comparison of the three layouts with respect to depth of cover

Depth of Cover

Reciprocal matrix

Layouts	1	2	3
1	1.00	1.00	1.00
2	1.00	1.00	1.00
3	1.00	1.00	1.00
Sum	3.00	3.00	3.00

Normalised Matrix

Layouts	1	2	3	Sum	Priority Vector
1	0.33	0.33	0.33	1.00	0.33
2	0.33	0.33	0.33	1.00	0.33
3	0.33	0.33	0.33	1.00	0.33
Sum	1.00	1.00	1.00	3.00	1.00

n =	3
Lambda Max.	3.00
Consistency Index (CI)	0.00
Consistency Ratio (CR)	0.00%

Table 6 - Pairwise comparison of the three layouts with respect to coal quality

Coal Quality

Reciprocal matrix

Layouts	1	2	3
1	1.00	0.50	1.00
2	2.00	1.00	2.00
3	1.00	0.50	1.00
Sum	4.00	2.00	4.00

Normalised Matrix

Layouts	1	2	3	Sum	Priority Vector
1	0.25	0.25	0.25	0.75	0.25
2	0.50	0.50	0.50	1.50	0.50
3	0.25	0.25	0.25	0.75	0.25
Sum	1.00	1.00	1.00	3.00	1.00

n =	3
Lambda Max.	3.00
Consistency Index (CI)	0.00
Consistency Ratio (CR)	0.00%

Table 7 - Pairwise comparison of the three layouts with respect to gas make

Gas Make

Reciprocal matrix

Layouts	1	2	3
1	1.00	1.00	2.00
2	1.00	1.00	2.00
3	0.50	0.50	1.00
Sum	2.50	2.50	5.00

Normalised Matrix

Layouts	1	2	3	Sum	Priority Vector
1	0.40	0.40	0.40	1.20	0.40
2	0.40	0.40	0.40	1.20	0.40
3	0.20	0.20	0.20	0.60	0.20
Sum	1.00	1.00	1.00	3.00	1.00

n =	3
Lambda Max.	3.00
Consistency Index (CI)	0.00
Consistency Ratio (CR)	0.00%

Table 8 - Pairwise comparison of the three layouts with respect to geological structures

Geological Structure

Reciprocal matrix

Layouts	1	2	3
1	1.00	2.00	5.00
2	0.50	1.00	3.00
3	0.20	0.33	1.00
Sum	1.70	3.33	9.00

Normalised Matrix

Layouts	1	2	3	Sum	Priority Vector
1	0.59	0.60	0.56	1.74	0.58
2	0.29	0.30	0.33	0.93	0.31
3	0.12	0.10	0.11	0.33	0.11
Sum	1.00	1.00	1.00	3.00	1.00

n =	3
Lambda Max.	3.00
Consistency Index (CI)	0.00
Consistency Ratio (CR)	0.42%

Table 9 - Pairwise comparison of the three layouts with respect to *in situ* stress

In-situ (Horizontal) Stress

Reciprocal matrix

Layouts	1	2	3
1	1.00	3.00	7.00
2	0.33	1.00	5.00
3	0.14	0.20	1.00
Sum	1.48	4.20	13.00

Normalised Matrix

Layouts	1	2	3	Sum	Priority Vector
1	0.68	0.71	0.54	1.93	0.64
2	0.23	0.24	0.38	0.85	0.28
3	0.10	0.05	0.08	0.22	0.07
Sum	1.00	1.00	1.00	3.00	1.00

n =	3
Lambda Max.	3.10
Consistency Index (CI)	0.05
Consistency Ratio (CR)	8.34%

Table 10 - Pairwise comparison of the three layouts with respect to surface restrictions

Surface Restrictions

Reciprocal matrix

Layouts	1	2	3
1	1.00	3.00	3.00
2	0.33	1.00	1.00
3	0.33	1.00	1.00
Sum	1.67	5.00	5.00

Normalised Matrix

Layouts	1	2	3	Sum	Priority Vector
1	0.60	0.60	0.60	1.80	0.60
2	0.20	0.20	0.20	0.60	0.20
3	0.20	0.20	0.20	0.60	0.20
Sum	1.00	1.00	1.00	3.00	1.00

n =	3
Lambda Max.	3.00
Consistency Index (CI)	0.00
Consistency Ratio (CR)	0.00%

From Table 13, it is evident that layout 1 is the optimum mine layout with a weight of 0.38; followed by layouts 2 and 3 with equal weight of 0.31. These results were expected as layout 1 had higher priority than the other two layouts with respect to *in situ* stress, which also had the highest priority against other factors.

Table 11 - Pairwise comparison of the three layouts with respect to access to reserve

Access to Reserve

Reciprocal matrix

Layouts	1	2	3
1	1.00	1.00	0.20
2	1.00	1.00	0.20
3	5.00	5.00	1.00
Sum	7.00	7.00	1.40

Normalised Matrix

Layouts	1	2	3	Sum	Priority Vector
1	0.14	0.14	0.14	0.43	0.14
2	0.14	0.14	0.14	0.43	0.14
3	0.71	0.71	0.71	2.14	0.71
Sum	1.00	1.00	1.00	3.00	1.00

n =	3
Lambda Max.	3.00
Consistency Index (CI)	0.00
Consistency Ratio (CR)	0.00%

Table 12 - Pairwise comparison of the three layouts with respect to reserve losses

Reserve losses due to the layout

Reciprocal matrix

Layouts	1	2	3
1	1.00	2.00	0.25
2	0.50	1.00	0.25
3	4.00	4.00	1.00
Sum	5.50	7.00	1.50

Normalised Matrix

Layouts	1	2	3	Sum	Priority Vector
1	0.18	0.29	0.17	0.63	0.21
2	0.09	0.14	0.17	0.40	0.13
3	0.73	0.57	0.67	1.97	0.66
Sum	1.00	1.00	1.00	3.00	1.00

n =	3
Lambda Max.	3.08
Consistency Index (CI)	0.04
Consistency Ratio (CR)	6.87%

Table 13 - Overall priorities and the overall composite weight of the layouts

Factors	Factors Priorities	Layout Priorities		
		1	2	3
Depth of cover	0.06	0.33	0.33	0.33
Seam inclination	0.01	0.33	0.33	0.33
Coal quality	0.17	0.25	0.5	0.25
Gas make	0.03	0.4	0.4	0.2
Roof and floor strata	0.11	0.33	0.33	0.33
Geological structures	0.06	0.58	0.31	0.11
In situ stress	0.21	0.64	0.28	0.07
Multiple seam mining	0.02	0.33	0.33	0.33
Surface restrictions	0.02	0.60	0.20	0.20
Surface subsidence	0.01	0.33	0.33	0.33
Access to reserve	0.07	0.14	0.14	0.71
Reserve losses due to the layout	0.11	0.21	0.13	0.66
Seam thickness	0.06	0.33	0.33	0.33
Roof cavability	0.07	0.33	0.33	0.33
Composite weight		0.38	0.31	0.31

Overall consistency measure

It is still essential to estimate the overall consistency of the hierarchy as this will give an indication on the validity of the AHP results. The overall consistency of the hierarchy was estimated by dividing the sum of the weighted CI by the sum of the weighted RI. The overall consistency of the AHP has been estimated to be 0.1, which indicates that the results are consistent and valid.

CONCLUSIONS

This paper summarised development of a method for layout selection using the AHP. Due to the broadness of the proposed study, the scope was directed to the development of a method for longwall layout selection in the central Queensland region. The geological, geotechnical and the coal quality aspects that influence the selection of panel orientation were identified.

These inter-relationships between the factors and the dependency of a factor on the other indicated the necessity of AHP as a decision-making tool. From the identified factors, an AHP model has been created. A pairwise comparison matrix has been constructed for the identified factors, where *in situ* stress has been identified as the most important factor with priority of 0.21 for the selection of a longwall layout. On the other hand, surface subsidence and surface restrictions have been identified as the least important as there are limited restrictions on surface in central Queensland compared to other regions.

A longwall mine at the prefeasibility stage, located in central Queensland, was assessed using the methodology developed. Three proposed layouts were compared with respect to each identified factor and their priorities were calculated. The results from the pairwise comparisons of the identified factors and the layouts were then combined and further evaluated to select the optimum mine layout.

The results of each stage in the AHP model were validated through the estimation of the consistency. For inconsistent matrices, a method has been implemented to improve the consistency of the judgements and transform the inconsistent matrix to a near consistent one.

The results revealed that the AHP model developed in this paper can be used as a basis for implementing longwall layout selection. If new critical factors and hence new criteria emerge to satisfy decision-makers need, then they can be included in the AHP model to select the optimum layout. Unlike the traditional approaches to layout selection, the AHP method requires less data and reduces the time consumed in the decision-making process.

ACKNOWLEDGEMENTS

The authors wish to thank the following persons for their support and guidance, who have given up their time to aid at every stage of the project:

- Anna Mills, specialist geotechnical engineer at Anglo American, who assisted in the data collection process.
- Andrew Laws who greatly assisted in providing invaluable geological data for the project.
- Anglo American Metallurgical Coal for providing access to the data and permission to publish this paper.
- Lastly, thanks to Dr Phillip Isaac, lecturer in the School of Mathematics and Physics at the University of Queensland, who also gave up his time to aid with data validation process and providence of support and guidance when progress stalled.

REFERENCES

Ataei, M, Janshidi, M, Sereshki, F and Jalali, S, 2008. Mining method selection by AHP Approach, *The Journal of The Southern African Institute of Mining and Metallurgy,* 108(12):741-750.

Benítez, J, Delgado-Galván, X, Izquierdo, J and Pérez-García, R, 2011. Achieving matrix consistency in AHP through linearization, *Applied Mathematical Modelling,* 35:4449-4457.

Ekipman, A, 2003. A decision support system for optimal equipment selection in open pit mining: analytical hierarchy process, *Istanbul University, Mining Engineering Department*, 16(2):1-11.

Harker, P, 1987. Derivatives of the perron root of a positive reciprocal matrix: with applications to the analytic hierarchy process, *Applied Mathematics and Computation*, 22:217-232.

Kardi, T, 2006. Analytic hierarchy process (AHP) tutorial. [online]. Available from: http://people.revoledu.com/kardi/tutorial/AHP/ [Accessed: 10 March 2012].

Li, H and Ma, L, 2007. Detecting and adjusting ordinal and cardinal inconsistencies through a graphical and optimal approach in AHP models, *Computers and Operations Research,* 34 (3):780-798.

Musingwini, C, and Minnitt, A, 2008. Ranking the efficiency of selected platinum mining methods using the analytic hierarchy process (AHP), in *Proceedings third International Platinum in Transformation,* pp 319-327 (The Southern African Institute of Mining and Metallurgy: *Witwatersrand*).

Saaty, T, 1990. How to make a decision: the analytic hierarchy process, *European Journal of Operational Research,* 48(1):9-26.

Saaty, T, 2003. Decision-making with the AHP: why is the principal eigenvector necessary, *European Journal of Operational Research,* 145: 85-91.

Shahriar, K, Bakhtavar, E, Saeedi, G and Akbarpour, S, 2007. A new numerical method and AHP for mining method selection, in *Proceedings Fourth International Symposium High Performance Mine Production*, pp 289-306 (AACHEN International Mining Symposia).

Yavuz, M, Iphar, M and Once, G, 2007. The optimum support design selection by using AHP method for the main haulage road, *Journal of Tunnelling and Underground Space Technology*, 23:111-119.

A HOLISTIC EXAMINATION OF THE GEOTECHNICAL DESIGN OF LONGWALL SHIELDS AND ASSOCIATED MINING RISKS

Russell Frith

ABSTRACT: This paper examines the design of longwall shields, focusing on those geotechnical aspects that are critical to either their success or failure during longwall extraction. The driver for the paper is the recognition that in many instances, longwall shields are assessed and designed along similar lines to that of roadway ground support systems, namely according to typical or normal geotechnical conditions. However the paper will contend that for longwall shields, this is inappropriate as unlike roadway ground support systems, longwall shields cannot be supplemented with additional or secondary support in localised areas of adverse geotechnical conditions. In other words, the longwall shield needs to be designed according to what are judged to be worst case or adverse geotechnical conditions, the outcome being that a well-designed shield will be significantly over-rated for the majority of its working life. However it will be argued that the additional capital cost of such shield design can be readily justified as a prudent risk-based outcome that is essential to minimising future business risks due to strata instability on the longwall face. Shield geometry is discussed including such relevant factors as leg angle, inclination of the top caving shield, canopy ratio, operating height range and tip to face distance, these all being well established longwall shield design considerations and most importantly, areas whereby inadequate design can render a longwall shield highly ineffective. The issue of tip to face distance is considered in detail, in particular the extent by which it is an important geotechnical design consideration. The critical importance of maximising set to yield ratio within practical operating limits is discussed. Overall the aim of the paper is to provide industry with a set of suggested guidelines for future use when designing longwall shields and hopefully to initiate discussion on a subject that unlike roadway ground support design is not well covered in its entirety in the published technical literature.

INTRODUCTION

Few in industry would argue that most longwall faces work well for the majority of the time. It is the exception rather than the rule that the longwall is unstable with large cavities hindering production and requiring both remediation and recovery. That is not to say that some longwall faces are not more prone to strata instability than others and certainly, when major roof cavities do form the operational difficulties and costs involved in the recovery are substantial.

This paper does not address in detail the various geotechnical drivers for strata instability on the longwall face, for example:

- depth of cover, panel width and general face loading conditions;
- extraction height and the propensity for face spall;
- the contribution of the chain pillar to face stability for sub-critical panels;
- periodic weighting of the near-seam overburden;
- the influence of chain pillar cut-throughs in causing surges in face loading;
- the competence of the immediate roof strata;
- traversing major geological structures such as faults and dykes;
- the alignment of joints with respect to the longwall face.

These have all been covered in detail in other publications (e.g. Frith and McKavanagh, 2000; Frith, 2005) and are well established based on both research studies by various groups and the investigation of numerous longwall roof falls.

Principal Geotechnical Engineer, Mine Advice Pty Ltd, rfrith@idl.net.au, Tel: +61(0)409056514

On the assumption that all of these geotechnical parameters are used and considered as part of a longwall feasibility process and a longwall panel layout is established, once mining commences the mine operator has only two controls available to prevent instability on the longwall face – the longwall shields and face operations. Good longwall operational practice (e.g. keeping the face straight, setting of shields and maintenance) has been the subject of significant industry interest via the regular column "*Wills on Walls*" in the "Australian Longwalls" journal, whereby one of the industries authorities on the subject, Nick Wills, provides an informative and at times, amusing commentary on the subject.

Unless longwall shields are well-designed in the first place, best-practice operational controls may not be sufficient to prevent face instability. For example, if the shield legs are leaking significantly or a minor roof cavity (which can always occur) has resulted in the excavation height being greater than the operating range of the shields, the potential for instability on the face may be far greater than what can be achieved by operational controls such as "keeping going".

Therefore, the focus of this paper is to consider the design of the longwall shields in a more holistic manner in order to assist mining companies make informed choices when procuring face equipment, thus maximising the likelihood that operational controls will be effective during mining.

CURRENT STATE OF THE ART

Establishing the current state of the art is actually difficult, as the amount of published literature or industry guidelines on the complete subject of longwall shield design is essentially nil. Many papers discuss longwall instability case histories or report research studies on their *in situ* performance, but none (that could be found) actually address the issue of how to go about designing a longwall shield in a known set of geological and geotechnical circumstances. Given the critical importance of the longwall shields to the economic performance of a longwall face, this is a surprising state of affairs and one that perhaps the industry might wish to address.

What appears to occur with the shield design process is that:

(a) the mining company undertakes a feasibility study and decides that it will invest upwards of A$1 billion in a longwall mine;

(b) the longwall OEM's are provided with a series of design parameters (e.g. shield width, yield load rating, set:yield ratio, operating height range.);

(c) the individual OEM's then each prepare a face/shield design to allow the mining company to make an informed decision as to which OEM will be contracted to provide the equipment.

From experience of having been involved in these processes in the past, common focus areas are (i) fatigue design and testing of the shields, (ii) building the shields to the design specification and (iii) commercial terms. Certainly there would be many examples of highly rated, structurally well-designed longwall shields in the industry that have performed far below expectation in terms of longwall face stability. Accepting that the geotechnical environment is a significant driver of face instability, the question that has to be asked is whether there are other elements of shield design that are critical to its supporting effectiveness that therefore should also be evaluated as part of the procurement process?

GENERAL CONCEPTS

As a starting point, it is suggested that longwall shields offer the highest level of roof control when they meet the following six design requirements:

(i) they are able to be set to the roof along all or most of their canopy length.

(ii) the leg loads are applied to the roof as close to the face as possible, albeit within practical mining considerations.

(iii) the tip to face distance is as small as possible, noting that the tip to face distance is defined by the closest position to the face that the canopy is first in contact with the roof not simply by the canopy tip itself.

(iv) the yield rating of the shield is as high as possible, the higher the better in terms of roof control on the longwall face.

(v) the set:yield ratio is as high as possible, this leading to improved levels of direct or active reinforcement to the immediate roof of the longwall face.

(vi) the leg hydraulics are not impaired by fluid leaks that would allow leg loads and stiffness to drop during the mining cycle.

However it is immediately obvious that some of these shield design requirements lead to compromises with other longwall design aspects. For example:

- the location of the shield legs with respect to the longwall face is limited by the presence of the AFC and a forward walkway, both having width requirements if they are to meet other longwall design outcomes (e.g. AFC conveying capacity and front walkway ergonomics).
- even if the canopy tip could be set against the roof at the face, risks associated with the shearer drums colliding with the canopy preclude that as a practical proposition.
- yield loads are limited by such issues as capital cost and shield weight in terms of transporting them underground using rubber-tyred vehicles.

Recognising that such compromises exist, the design of longwall shields should seek to reach the best overall balance such that none of the required design outcomes are unduly poor, the final question then being how they are likely to perform within the geotechnical environment of the longwall face under consideration.

The shield design aspects considered as part of this paper are:

(i) shield width

(ii) tip to face distance

(iii) canopy ratio

(iv) planned working height range in relation to the maximum operating height

(v) inclination of the top caving shield within the planned operating height range

(vi) floor bearing pressures

(vii) yield load rating

(viii) set:yield ratio

(ix) flipper arrangement

(x) inclination of legs towards the face

Each will now be considered individually by reference to the conceptual mechanistic model of the longwall face and shield that was first published by Frith (2005) and is reproduced herein as Figure 1.

Shield width

Shield widths have increased during the past 20 years from 1.5 m, to 1.75 m and currently 2 m wide shields are becoming more common. This evolution has been driven largely by operational efficiency considerations such as reducing the face production constraint due to shield Lower-Advance-Reset (LAR) cycle times, reducing the number of shields and AFC pans to be moved during face relocations (the move to wider longwall faces has simply exacerbated this requirement), less components on the longwall face requiring maintenance or that can fail.

It is also true to say that as individual shields get wider, higher load capacities can be achieved (without increasing leg pressures markedly) as increased leg diameters that are directly proportional to the increased shield width, act to increase the shield load rating by the leg diameter squared. The load rating of the current 2 m wide Moranbah North longwall shields (875 t/m) could not have been achieved within a 1.75 m wide shield without significantly increasing leg pressures.

The major downside of increasing shield width (and shield loading as a direct consequence), is that the shields become very heavy and potentially difficult to move around the mine. The 2 m wide, 1750 t rated Moranbah North shields weigh in the order of 60 t each, such that purpose built LHD's. needed to be designed and developed to allow their transport within the mine.

Therefore, shield width is clearly a compromise decision between having the option of increasing the effective load rating of the shield in terms of t/m of face (as has proven to be very effective at Moranbah North - Martin, *et al.*, 2012), against the practicalities of moving them within the mine.

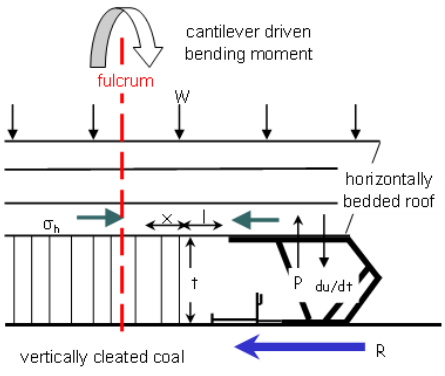

W - abutment loading
t - extraction height
l - tip to face distance prior to spall
x - increase in tip to face distance due to spall
σ_h - horizontal stress due to strata bending
du/dt - rate of powered support/roof convergence
P - powered support loading
R - rate of face retreat

Figure 1 - Simplified mechanistic model of a longwall face

Tip to face distance

Tip to face distance is undoubtedly the simplest concept in relation to roof stability on the longwall face, it being directly analogous to roadway width. It represents the unsupported span between the face and the tip of the shields from where roof instability emanates. Few longwall operators would disagree that maintaining the tip to face distance as low as possible has a positive impact on roof stability on the longwall face.

The actual tip to face distance in place at any point within the mining process will be governed by a number of independent factors:

(i) the minimum tip to face distance as determined by the face equipment and method of working (see "l" in Figure 1) which is commonly found to be in the order of 500 mm;

(ii) an increased tip to face distance due to face spall effects (see "x" in Figure 1);

(iii) an increased tip to face distance caused by the tip of the shields not being set to the roof – this can have a number of different causes such as the cutting of steps in the roof (Figure 2) and whether two or four leg shields are being used (Figure 3).

Figure 2 - Illustration of the impact of "steps" in the roof on effective tip to face distance

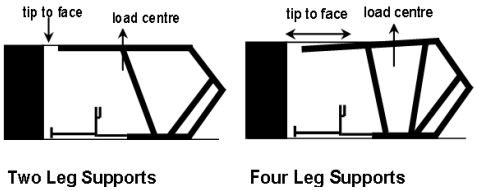

Figure 3 - Illustration of different setting characteristics of two and four leg shields on tip to face distance and load centre

It is usual for the tip to face distance to be analysed and optimised by reference to the position of the shields and face before the cut is taken. The tip location in relation to the face relates to the shields being back from the AFC and the cut yet to be taken. A theoretical tip to face of approximately 500 mm is consistent with current well-designed longwall shields operating in the Australian coal industry and cannot be reduced further, primarily due to shearer collision concerns. In other words, operational rather than geotechnical considerations are the limiting factors in this regard.

In reality the tip to face distance during longwall extraction will only fleetingly if ever be as low as 500 mm. The influence of face spall can be very significant at times (e.g. under peak face loading conditions or in proximity to a major geological structure) and the author has observed face spall of several metres in conjunction with major instability on the face has been observed rendering any arguments about whether the tip to face distance should be 450 mm or 500 mm for roof control reasons as essentially meaningless.

Even though the method of face working can be changed to reduce the tip to face figure under extreme face loading conditions by an amount determined by the web depth (e.g. double chocking when working Uni Di IFS which can only be used when significant face spall is occurring anyway), tip to face distances of 1 m to 2 m with the shields behind the AFC waiting for the AFC to be advanced (so that double-chocking can again take place) are an inevitable outcome during mining under high face loading conditions, particularly in thick seam environments.

The designed tip to face distance as is shown on OEM face cross-sections is no more than a practical minimum value rather than what is likely to be the case during mining. Accepting that the tip to face distance prior to the cut should be minimised, it should not be done at the expense of front walkway utility, AFC width or canopy ratio (see next section) due to the potentially overriding influence of face spall. It is assessed to be of little overall value to compromise the overall face geometry to minimise tip to face before the cut, only to eventually realise that it makes little or no difference to the maximum values that inevitably occur during mining when the potential for roof instability is logically also at a maximum.

Canopy ratio

Canopy ratio is basically the ratio between the canopy length ahead of the legs divided by the canopy length behind the legs (A/B in Figure 4). The importance of the canopy ratio is to provide a balanced canopy whereby its centre of mass is reasonably close to the location of the legs. This ensures that the canopy tip doesn't have a significant tendency to drop away from the roof, which will either tend to reduce tip loading of the shield if it stays in contact with the roof or increase the tip to face distance if it doesn't, neither of these outcomes are beneficial in terms of roof control.

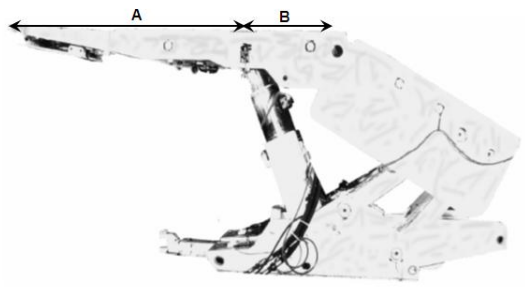

Figure 4 - Shield side profile showing the definition of canopy ratio (A/B)

There does not appear to be any design values for canopy ratio that are backed by fundamental shield design research, optimum values commonly used are between two and three, with values closer to two

being preferred. Obviously, a better canopy balance could be achieved by making the length of the canopy behind the legs (B) longer, although this simply adds weight and hence cost to the shields. It also tends to reduce the shield Support Load Density (SLD) (in t/m^2), which whilst being a commonly used parameter is not a particularly useful means of assessing shield design. This is because maximising SLD (by reducing the distance B behind the legs) will almost certainly lead to the canopy becoming less balanced via an increased canopy ratio, which is counter-productive in terms of roof control.

The other obvious outcome when considering canopy ratio is that lengthening the canopy to reduce tip to face distance for strata control reasons is also potentially counter-productive, as it will tend to increase the canopy ratio thus making the canopy less balanced.

Certainly a combination of reducing tip to face distance by making the canopy longer ahead of the legs (A) and also increasing the shield SLD by reducing the canopy length behind the legs (B) is a recipe for disaster in terms of canopy ratio and shield effectiveness. It is noted at least one set of relatively recently procured shields in the Australian coal industry that have been designed with exactly this concept in mind and significant consequences in terms of roof control on the longwall face have seemingly eventuated.

Planned operating height range in relation to the maximum operating height

It is important that when a shield is working at the upper end of its designated operating height range, there is still an amount of leg travel to allow the shield to be correctly set to the roof should either the cut inadvertently be taken too high or a small roof cavity forms ahead of the shields. Having the ability to set the shield to the roof for a distance above the designated planned maximum working height is a prudent shield design consideration, as once the shield cannot be correctly set to the roof, the threat of major roof instability occurring increases significantly.

Again there are no industry accepted design guidelines in this regard, the amount of extra operating height above the planned maximum working height being a risk mitigation measure to be decided upon by the mine itself. However as a general rule, it is considered that two criteria should be applied:

(i) the higher the general likelihood of roof instability occurring on the longwall face for geotechnical reasons, the greater the additional operating height, over and above the planned maximum working height, should be; and

(ii) the higher the maximum planned working height, the greater the additional operating height should be - this relates to the argument that the severity of major roof falls on the face increases in line with the face operating height.

Building-in increased operating height into the shields results in additional capital cost and will also make the shields slightly heavier. However when this is compared against the consequences of production or reserve losses associated with (a) unplanned roof falls on the face or (b) having to reduce the face working height to ensure that a sufficient amount of leg travel is available to accommodate small cavities and/or cut roof horizon variations, such additional costs and shield weight are surely prudent compromises to make.

Inclination of the top caving shield within the planned operating height range

It is a fundamental requirement of shield design that the inclination of the top caving shield is never less than about 30 degrees to the horizontal. The reason is that broken goaf material should always slide off the top caving shield so that when the shield is being reset to the roof, the available leg load is applied to the roof above the canopy (where it assists roof stability) rather than through the top caving shield where it has no useful purpose other than to raise broken goaf material during the shield setting process. These two scenarios are illustrated schematically in Figures 5(a) and 5(b).

Frith and Stewart (1994) undertook shear tests between steel and rock and found that the limiting angle of friction was in the order of 26° to 27°. Therefore a top caving shield inclination of no less than 30° would logically have a very high likelihood of the resulting broken goaf material sliding off and not directly loading the shield.

(a) goaf load slides off the top caving shield - leg load applied to roof

(b) goaf load direct loads top caving shield - leg load applied to goaf

Figure 5 - Schematic illustrations of how the Inclination of the top caving shield influences leg load distribution

Whilst not published, several examples are known in Australia and overseas of longwall shields being worked very close to the bottom of their operating range with top caving shield inclination angles of substantially less than 20°. Face roof control difficulties have commonly occurred under this scenario.

Maintaining the inclination of the top caving shield at > 30° throughout the operating height range increases in difficulty as the operating height range is increased. The higher the operating range, the longer the top caving shield needs to be in order to provide enough shield reach, therefore the lower its inclination at the bottom of the operating height range will be (all other factors being equal).

The conclusion reached is that whilst providing for a large operating height range may have theoretical benefits, particularly when the seam thickness in a given mine varies significantly, there are potential major roof control downsides when operating such longwall shields at the bottom of their operating range due to the top caving shield having a very shallow inclination angle. This has been observed on several occasions as being a major controlling factor in on-going strata control difficulties on the longwall face.

Floor bearing pressures

Whilst there are no publications discussing this issue in detail with respect to longwall shields, there are known examples (albeit not published) of major longwall collapses occurring either fully or partly due to the presence of very soft floor beneath the shields causing a dramatic reduction in shield loading to the roof. It is a fundamental design requirement that any form of standing support (including longwall shields) should be able to be set against both the roof and floor without either undergoing compressive failure.

Whether a longwall shield will fail the floor beneath and so effectively "sink" into it, is essentially a bearing failure type mechanism. Therefore it is appropriate to consider it in this manner. Based on available information, the peak vertical stress acting through the shield pontoons and into the floor is typically around 8 MPa, this being applied at or very close to the toe of the base.

The bearing capacity of any strata unit beneath the shields is a function of (a) the load being applied, (b) the width of the footing (in this case the shield base) and (c) the strength and thickness of the floor material. There are many different methods of analysis that could be used in this regard. Seedsman (2012) provides the following equation for use when considering the stability of the floor beneath a coal pillar:

Bearing Capacity = UCS / 2 (4.14 + W / 2 / h)

where:

W = pillar width;
h = unit thickness with an Unconfined Compressive Strength (UCS).

Using this equation with a peak applied stress of say 8 MPa, a UCS can be determined that would represent the limiting equilibrium condition for the first 1 m of floor beneath the shields in terms of whether a bearing failure would occur or not. On the assumption that a pontoon is in the order of 700 mm wide (this representing the minimum footing dimension expected for a 1.75 m shield), it is found that for the first 1 m of floor beneath the base, the limiting equilibrium UCS is 3.6 MPa. For values lower than this floor failure is likely, for values above this, floor failure becomes less likely. The above equation can be used to consider floor stability for different sections of strata beneath the shields, different maximum floor

pressures and different pontoon widths. However the analysis presented indicates that the typical UCS of the first 1 m of floor needs to be below 4 MPa before the issue of floor failure compromising shield effectiveness becomes a significant possibility.

It is noted that this analysis has not considered the extent by which the shields may tend to "plough" the floor material ahead of the pontoons as they are advanced. This relates to such considerations as the effectiveness of base lifting rams to lift the toe of the base clear of the floor and also whether the shields are being advanced up-dip or down-dip, the specifics of which are outside the scope of this report.

Yield load rating

The yield load rating of longwall shields in terms of their supporting effectiveness is simply covered by the statement "*the bigger the better*". The justification for this statement is that the load rating design of a longwall shield cannot and should not be likened to that of roadway ground support whereby support levels can be modified during mining according to the actual conditions encountered. With a longwall face the only available roof support is that contained within the shield, therefore it should be specified based on worst-case face loading and strata conditions. The problem from a design perspective is that those worst case loading and strata conditions are almost certainly undefined; hence it is not possible to then design the shields on that basis.

As a result the shield needs to carry the highest "practical" level of available load so that on those infrequent occasions when it is required, it is available for use. If longwall shields are designed according to background or typical face loading conditions and so potentially down-rated for either cost or weight savings, the impact upon face stability and hence, production levels could be many times more significant than any capital or shield weight benefits.

Does this then mean that all mines should simply default to the 2 m wide, 1750 t Moranbah North shields described by Martin *et al.* (2012)? The answer is "of course not" as these shields were clearly designed and procured based on both a history of major roof control difficulties at the mine and concern over the increasing cover depths. In other words there were a number of geotechnical reasons as to why these shields were necessary in the first place.

The point being made is that the design of the yield load rating of longwall shields should not be based on a detailed technical assessment of typical or normal geotechnical conditions (by whatever means), but a risk-based assessment of both the general background conditions (to provide overall context as to the stability of the longwall face in general terms) in combination with the potential for locally adverse strata conditions where the roof fall potential is significantly elevated. How this may be done is not considered further in this particular technical paper.

Set:Yield ratio

The history of shield development over the past 50 to 60 years, all points to the concept that as well as the yield load rating being "*the bigger the* better", the set:yield ratio should be "*the higher the better*". The justification for this is that the longwall shield is essentially a reinforcing device for the immediate roof of the longwall face and in the same way that roof bolts and tendons reinforce the roof of a mine roadway, it acts to "*clamp together*" what is typically a stratified strata sequence immediately above the shield.

It is argued that the initial driver for guttering type failure of the immediate roof ahead of the shields is bending of the immediate roof strata around the face (see Figure 1). Whilst the shield is rarely ever able to prevent such bending, it can act to minimise it. Therefore it makes no sense to allow such bending of the roof to compress the shield and so develop load in the legs. It is far better to apply such load actively back to the roof and so limit the overall level of shield closure and hence roof bending about the face, this then contributing positively to roof stability ahead of the shields. It may also be the case that by setting the shields to the highest possible or practical level and so reducing roof to floor closure, this acts to reduce face spall, which is again a positive aspect in terms of roof stability ahead of the shields.

Trueman *et al.* (2008) made the suggestion that under certain face loading conditions, it may be preferable to set the shields to only 60% rather than say 90% of their yield loading. The following quote is taken from that paper:

"*Where periodic weighting is high enough to result in periodic shield overload, it may be better for set pressures to be nearer 60% of yield than 90% (with shields of support density of 100 t per square meter or*

greater before the cut). This relates to the effect of time. If the support is set to 60% of yield then it will take much longer to the first yield event and for the same cycle time, there will be fewer yields. Fewer yields will result in less convergence and subsequent roof degradation and it will be easier to mine through the periods of support overload. If a shield periodically has an inadequate capacity for the conditions, the authors have seen no evidence that very high setting loads will stabilise the roof. The belief that very high set pressures are beneficial may have arisen when support capacities were less and set pressures close to the yield value were necessary for the set pressure to be adequate".

The underlying logic behind this statement seems to be that leg yield events allow increased rates of roof convergence, in which case the statement potentially makes sense. However in all of the shield convergence monitoring studies across the coal industry reported by Frith and Stewart (1994), not once was the rate of shield closure seen to increase due to the legs going into yield. The rate may have remained constant after going into yield (which makes sense) but certainly it never accelerated. Therefore the idea that reducing the set pressures (assuming it could be done on an as-needs basis), thus allowing greater shield convergence to simply reduce the number of subsequent yield cycles, may not be well- founded and certainly goes against the entire history of the development of longwall shields.

Fortunately, Trueman *et al.* (2011) make the following statement:

"*Operational controls can nevertheless be effective in minimising roof control issues in the presence of high level periodic weighting leading to support overload. Specific attention to achieving the highest set pressure practicable without compromising the attitude of the support canopy can reduce the extent of cavities and associated delays in many instances*".

It is possible to agree with this later statement because it appears that there is no obvious dissention to the universal concept of maximising the set:yield ratio of shields in order to increase their supporting effectiveness.

Flipper arrangement

The flipper at the tip of a shield serves two distinct purposes:

(i) it allows some measure of direct support to the upper coal face which has both roof stability and also safety benefits, and

(ii) in the event that significant amounts of face spall occur, it can be used to offer confinement to the exposed roof ahead of the tips.

Both are legitimate functions although as discussed by Payne 2008, in order to function as a roof support ahead of the tips, the flipper needs to be double-articulated. Otherwise the situation shown in Figure 6 will eventuate whereby the flipper can only act to control the face and not the roof when the face has spalled.

Figure 6 - Inability of single articulated flippers to secure the face or roof due to previous face Spall (Payne, 2008)

The available load capacity of a flipper arrangement is generally small, however in terms of acting to control a buckling/guttering type failure mechanism in the tip to face area, roadway roof support knowledge shows that relatively small vertical loads can prevent buckling under much higher levels of horizontal stress (Colwell and Frith, 2010). Therefore despite a low load rating, a flipper that can be positively set to the roof offers potential roof control advantages.

However the limitations of a flipper are two-fold, namely:

(i) that like a shield, at some point it needs to be retracted from the roof during which time if it were preventing roof buckling, such failure could then occur resulting in a small roof cavity which immediately then acts to reduce over shield supporting effectiveness.

(ii) its reach is limited ahead of the tip, therefore as the amount of face spall increases, its overall effectiveness in terms of roof control decreases.

Overall, a double-articulated flipper is a useful addition to a longwall shield, particularly in high seams with friable roof. However it only assists roof control and will not usually prevent large scale roof collapses that are driven by excessive face loading and associated face spall. It is certainly not a substitute for a well-designed and proportioned longwall panel layout and highly rated and well-designed longwall shield.

Inclination of legs towards the face

The inclination of the shield legs has been a general shield design consideration since Peng (1990) first published the concept of an "active horizontal force" assisting roof stability ahead of the shield tips (see Figure 7).

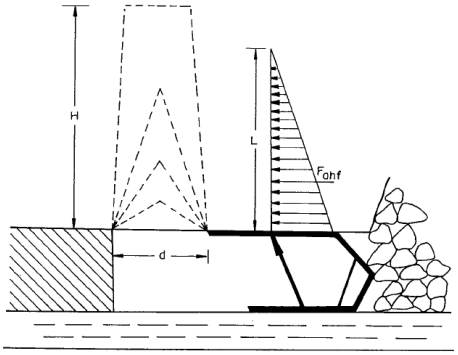

Figure 7 - Active horizontal force concept (Peng, 1990)

It is considered that the active horizontal force concept has little or no practical impact on shield effectiveness because:

(i) the active horizontal force is limited by friction between the canopy and roof (which is why Frith and Stewart (1994) undertook shear tests between steel and rock;

(ii) accepting that roof stability on a longwall face decreases as the face height increases, an increasing face height results in the legs becoming more vertical, therefore any active horizontal force decreases as a direct consequence. In other words, when it would be most required it is least able to be generated; and

(iii) the model shown in Figure 1 has the immediate roof ahead of the shields initially failing due to horizontal stress driven buckling, the horizontal stress being generated due to bending of the roof strata. Therefore adding active horizontal force into this area due to the design of the shields can hardly be beneficial to roof stability in the tip to face distance.

As shown in Figure 3, the primary reason why two leg shields result in far better roof control than four leg shields (which was the context behind the development of the active horizontal force concept) is that they are more effective at (a) setting the canopy tip to the roof and (b) keeping the total leg load as close to the face as possible.

The primary concern with leg inclination is assessed to be to ensure that it does not result in a significant reduction in vertical force being applied to the roof. On the basis that the vertical force applied is equivalent to the leg load multiplied by the cosine of the leg inclination angle (to the vertical), a leg inclination of 20° only results in a 6% reduction in the vertical component as compared to the absolute leg loading. When it is remembered that the maximum leg inclination occurs with the shield at the lower end of its operating range, such a reduction is judged to be insignificant in terms of the overall roof instability threat.

As a general shield design concept, leg inclination should be maintained at no more than 20° to the vertical throughout the defined operating height range.

CONCLUSIONS

The objective of the paper has been to demonstrate that over and above geotechnical and panel layout design considerations, the effectiveness of a longwall shield is subject to a series of compromises that need to be well thought through as part of a shield design process.

It is hoped that following the publication of this paper, tip to face distance as illustrated on an OEM cross-section of the shield and face will never again be considered as a strata control concern. It solely relates to shearer collision concerns which change as a function of extraction height. This is not to say that tip to face distance is not a relevant strata control consideration simply that it should be evaluated based on face loading and face stability issues as well as how the shield sets to the roof. These subject areas are far more informative and relevant than simply an OEM cross-section of the shield and face.

The two most important aspects of this paper relate to canopy ratio and the inclination of the top caving shield during mining. Both are judged to be fundamental aspects of shield design that should never be compromised as part of improving the SLD of the shield or extending its upper operating height. Having a balanced canopy with all or most of the available leg loading acting through it is fundamental to the effectiveness of a longwall shield.

On a positive note, with all of the relevant shield design considerations to-hand and a good appreciation of the various geotechnical drivers of face line instability, there is no reason why a well proportioned longwall shield cannot be developed that provides the maximum possible reinforcing effectiveness within the known geometrical face constraints. This then gives the longwall operators the best possible chance of managing the mining conditions during operations through good operational practices. Given the critical role of operational controls, in the context of longwall shield design, this is the best possible outcome that can be achieved.

REFERENCES

Colwell, M and Frith, R, 2010. AMCMRR - An analytical model for coal mine roof reinforcement. In *Proceedings of 10th Coal Operators Conference*, University of Wollongong, pp 73-83. http://ro.uow.edu.au/coal/302/.

Frith, R C and Stewart, A M, 1994. Optimisation of powered support performance in relation to strata loading and engineering criteria. End of Grant Report, NERDDC Project 1445.

Frith, R and McKavanagh, B, 2000. Optimisation of longwall mining layouts under massive strata conditions and management of the associated safety and ground control problems. End of Grant Report, *ACARP Project C7019*.

Frith, R C, 2005. Half a career trying to understand why the roof along the longwall face falls in from time to time? In *Proceedings 24th International conference on ground control in mining*, West Virginia.

Martin, K, Kizil, M and Canbulat, I, 2012. Analysing the effectiveness of the 1750 tonne shields at Moranbah North Mine. In *Proceedings of 12th Coal Operators Conference*, University of Wollongong, pp 32-42. http://ro.uow.edu.au/coal/388/.

Payne, D, 2008. Crinum Mine, 15 years, 40 million tonnes, 45 toof falls - what did we learn? In *Proceedings of Coal 2008*, Aus.I.M.M. and University of Wollongong, pp 22-43. http://ro.uow.edu.au/coal/2/.

Peng, S S, 1990. Design of active horizontal force for shield supports for controlling roof falls, *The Mining Engineer*, 149(345):457-461.

Seedsman, R, 2012. The strength of the pillar-floor system. In *Proceedings of 12th Coal Operators Conference*, University of Wollongong, pp 24-31. http://ro.uow.edu.au/coal/387/.

Trueman, R, Lyman, G and Cocker, A, 2008. Managing roof control problems on a longwall face. In *Proceedings of The Coal Operators Conference*, University of Wollongong, pp 10-21. http://ro.uow.edu.au/coal/1/.

Trueman, R, Thomas, R and Hoyer, D, 2011. Understanding the causes of roof control problems on a longwall face from shield monitoring data - a case study. In *Proceedings of 11th Coal Operators Conference*, University of Wollongong. pp 40-47. http://ro.uow.edu.au/coal/338/.

MONITORING LONGWALL WEIGHTING AT AUSTAR MINE USING MICROSEISMIC SYSTEMS AND STRESSMETERS

Baotang Shen[1], Xun Luo[1], Adrian Moodie[2] and Gregory McKay[2]

ABSTRACT: Cyclic weighting is a major hazard for longwall operations in many deep mines with strong roof strata. Significant cyclic weighting events had been experienced at Austar Mine, resulting in production delays. Early warning of imminent weighting events by means of geotechnical monitoring will help to minimise the risk associated and to develop preventative solutions.

This paper describes a study undertaken by CSIRO and Austar Mine in which an integrated stress and microseismic monitoring system was trialled to detect strata responses to the mining processes. The main objectives of this study were to understand the caving mechanics and develop an effective early warning system for roof weighting management.

The field monitoring results clearly demonstrated the effectiveness of using both stress and seismic signatures to infer longwall caving and weighting events. Stress changes recorded by stressmeters in shallow surface strata and underground roadway roofs showed a strong correlation with the chock pressure increase at the longwall face. The same phenomenon had also been observed from the recorded microseismic events.

In order to develop an automated early warning system for longwall weighting, a trigger index method, which integrates the warning signs from different sensors, was developed and tested against the mine weighting observations and chock pressure data. A remarkably good agreement was achieved. For a limited number of cases examined, the warning signs from the monitoring system mostly occurred at least several hours before the roof weighting events and the major increase in chock pressure. This has demonstrated that the integrated stress and microseismic monitoring system, together with the analysis method developed, is capable of providing sufficient early warning for imminent underground weighting events.

INTRODUCTION

Cyclic weighting is a phenomenon of roof strata break-up, causing dynamic loading on the longwall support system. It is a major hazard for longwall mining operations as it can damage longwall chocks and cause production losses. This phenomenon is more pronounced in deep mines with strong roof strata. Early warning of imminent weighting events by means of geotechnical monitoring will help to minimise the associated risk and lead to development of preventative solutions.

Austar Mine is the first mine in Australia to successfully implement the Longwall Top Coal Caving (LTCC) mining method. The mine is extracting the Greta Seam of 6 m thickness at a depth of approximately 520 m. The main overburden unit is the Branxton Formation which is massive and strong (fine to medium sandstone/silty sandstone/pebbly bands). Significant cyclic weighting had been experienced when Panels A3 and A4 were mined, resulting in significant production delays. It had been observed that, where the top coal (2 m) was not extracted in the central part of the panel, the severity of cyclic weighting appeared to have been reduced. However, the reason for this weighting reduction is not yet understood. To better manage and prevent the damaging cyclic weightings, it is essential to understand which strata units contribute to the loading cycles. It is also necessary to investigate the impact on the weighting frequency and severity of leaving top coal unextracted. Microseismic monitoring and stressmeter monitoring are considered to be feasible methods for characterising and forecasting longwall weighting events.

Microseismic monitoring is an efficient technology for locating rock fracturing events inside a rock mass which is being stressed. The event occurrence and locations can be used to infer the location of high stress regimes and rock fracturing characteristics in the overburden strata associated with longwall mining. Rock fracturing events may be considered as the precursors of a weighting event because the

[1] *CSIRO Earth Science and Resource Engineering, PO Box 883, Kenmore, QLD 4069, Australia, +61 73327 4560*
[2] *Austar Coal Mine Pty Ltd, Locked Bag 806, Cessnock, NSW 2325 Australia*

rock fracturing could break up roof beams that may later create excessive load on the longwall support system. In a CSIRO study at Southern Colliery in Queensland, 60% of roof weighting events had microseismic precursors (Guo, *et al.*, 2000).

Stress sensors installed in overburden strata have demonstrated in previous studies the ability to detect caving events occurring behind the longwall face at a distance of at least 800 m from the sensors (Shen, *et al.*, 2008). Using sensitive stressmeters (such as the vibrating wire stressmeter), a small stress change in the roof strata, caused by beam breakage and caving, can be detected at a distant location.

This paper describes a study undertaken by CSIRO and Austar Mine in late 2011 and early 2012 in which an integrated stress and microseismic monitoring system was trialled to detect strata responses to the mining processes at Longwall Panel A5, Austar Mine. The main objectives of this study were to:

- Obtain the key microseismic and stress signatures associated with longwall weighting events;
- Understand the mechanisms of cyclic weighting at Austar Mine through the microseismic and stress measurement data sets;
- Investigate the feasibility of using microseismic and stress monitoring techniques for weighting event forecast; and
- Investigate the ability of partial or no-cave-zones to assist in the management of the cyclic weighting event.

MONITORING DESIGN AND SYSTEM INSTALLATION

An integrated monitoring system was used for monitoring Longwall Panel A5 at Austar Mine. The system is composed of four independent sub-systems, including a surface and an underground stressmeter system and a surface and an underground microseismic system (Figure 1). Each system has its own data logging unit which records stress and microseimic data continuously. Their results, however, can be correlated during data analysis.

Microseismic network

The microseismic monitoring network includes a ground surface array and an underground array. The ground surface array consists of four triaxial geophones which were grouted (using non-shrinking grout) in four 15 m deep boreholes. The lateral spacing of the geophones is about 180-250 m. Seismic signals monitored by the geophones were transmitted through cables to the monitoring station located in the middle of the array.

The underground array consists of three triaxial geophones installed at three cut-throughs near the travel road. Two of the geophones were installed in 5 m long vertical roof holes and the other geophone was installed in a coal pillar right below a ground surface geophone. The underground geophones were connected through cables to a 12 channel microseismic data acquisition unit that was located near the Mains.

The ground surface and underground geophone arrays form an ideal configuration for event detection and location. Manual data downloading was conducted for both of the units once every 4-7 d (depending on battery charged level).

Stress monitoring systems

The surface stressmeter system consists of one biaxial stressmeter and two uniaxial stressmeters which were installed in three shallow boreholes (15 m deep), together with a data logging system. The three holes are approximately 100 m apart along the centreline of Longwall Panel A5. The logging system was located next to the seismic logging station. It was powered by a battery and a solar panel.

The underground stress monitoring system consisted of six uniaxial stressmeters which were installed in the roof at three locations next to the geophones (Figure 1). At each location, two roof boreholes (depth = 5 m and 8 m) were drilled at a spacing of approximately 1 m, and the stressmeters were installed at the ends of the roof holes. All the underground stressmeters were connected through cables to safety

barriers before a data logger that was located in the underground monitoring station near the Mains. The stress data were recorded every five minutes.

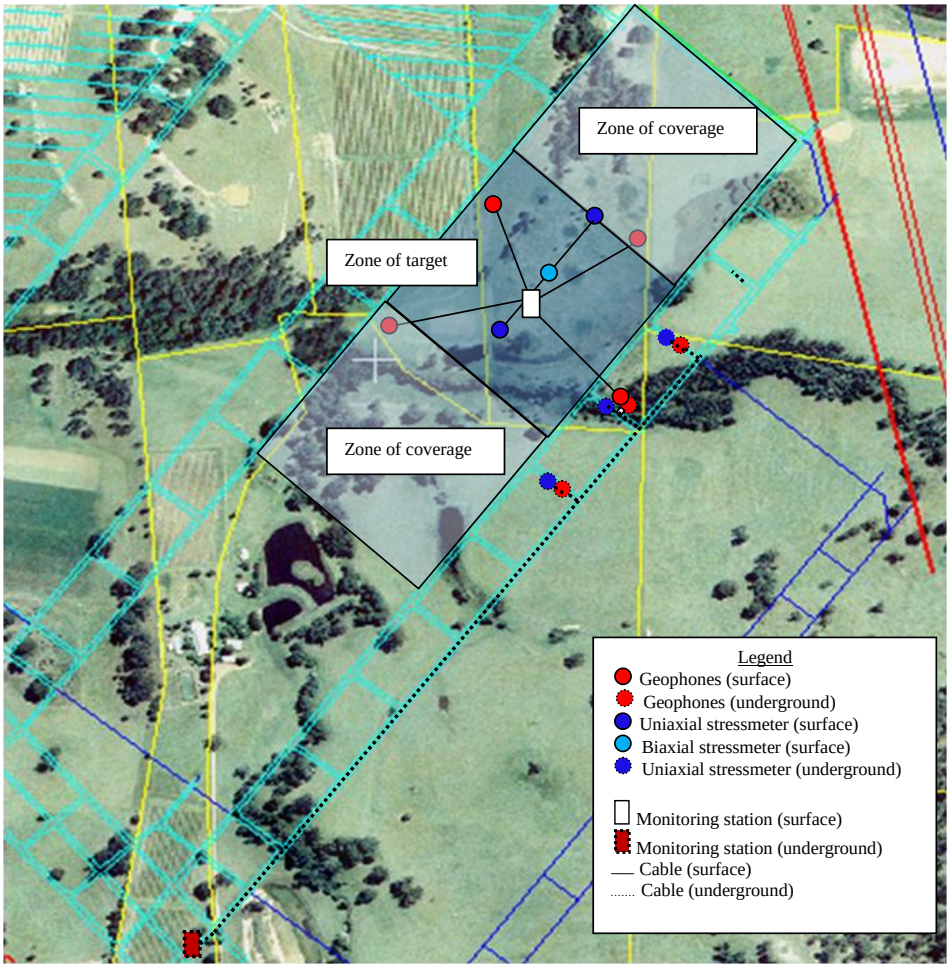

Figure 1 - Locations for geophones and stressmeters in a monitoring trial at Panel A5, Austar Mine

Field installation

All surface stressmeters and geophones were installed during the 12th -13th July 2011 (Figure 2). All stressmeters were orientated in the direction along the centreline of the panel. The two uniaxial stressmeters measures the horizontal stress changes in the mining direction whereas the biaxial stressmeter measures the stress changes in both mining and face directions.

The underground stressmeters and geophones were installed during the 13th -17th June 2011. At each of the three cut-throughs (9CT, 8CT and 7CT), two stressmeters were installed with one oriented parallel to the cut-throughs and the other at a 45° angle pointing at the longwall start-up.

The geophones were installed at the top end of 5 m vertical boreholes in the roof. They were grouted in the boreholes in order to achieve good coupling between the geophones and the rock. Judging from the monitoring results, however, it is suspected that the grout might not have fully covered the geophones at the borehole top ends, possibly due to leakage of the grout. This poor coupling led to data quality below expectation.

Mining of Longwall Panel A5 commenced on the 11th July 2011 and it advanced at an average speed of about 40 m per week.

(a) Surface stressmeter system **(b) Surface microseismic system**
Figure 2 - Installation of surface stressmeter and microseismic systems

MONITORING RESULTS

The monitoring program lasted for approximately six months until the longwall face had advanced to outside the targeted zone. During mining, the top coal of 2 m thickness was left in the goaf for the first 320 m longwall to control weighting. The operation reverted to a full face caving afterward.

Stress monitoring results

The horizontal stress changes in shallow strata at the three monitoring locations are shown in Figure 3. It is noted that the horizontal stress in the shallow strata was generally reducing as the longwall face approached and passed the monitoring locations.

Figure 4 shows the monitored horizontal stress changes in the immediate roof strata at the three underground locations. The underground stressmeters were installed in the immediate roof in the three cut-throughs, 7CT, 8CT and 9CT. Stressmeters 7CTA, 8CTA and 9CTA were installed to measure the horizontal stress change orientated at 45 degree toward the longwall start-up, whereas 7CTB, 8CTB and 9CTB were measuring the stress change in the direction parallel to the cut-through (or longwall face direction). The distance between the three cut-throughs and the longwall start-up was approximately 360 m, 260 m and 160 m respectively.

It was observed that the horizontal stresses in the 45 degree direction to the longwall face (8CTA and 7CTA) increased as the longwall face passed the monitoring locations. Stresses parallel to cut-throughs (8CTB and 7CTB) decreased after the longwall face passed. Horizontal stresses at 9CT (A and B) showed a different trend, both decreasing as the longwall face passed, possibly due to the complex effect of initial caving and 3D geometry as 9 CT is close to the longwall start-up and full caving might not have been developed as the face passed this location.

The results shown in Figures 3 and 4 do not show clear signs of longwall caving events. The surface monitoring results give apparently smooth stress change with time. The underground results showed a few steep changes as the sensors are closer to the face locations and might have been affected by the localised pillar/roof fracturing. However, if the monitored stress changes are plotted in the form of "stress rate", clear signs of sharp changes can be seen from the monitoring results, see Figure 5. The stress rate used in this analysis is calculated over a 15 min duration (three data readings with an interval of five minutes) using the equation below

$$S_{rate}(MPa/day) = \frac{S(t_0+15min)-S(t_0)}{0.0105} \quad (1)$$

where S_{rate} is the stress rate (MPa/d); S (t_0) and S (t_0+15min) are the monitored stress changes at time t_0 and t_0+15min, respectively.

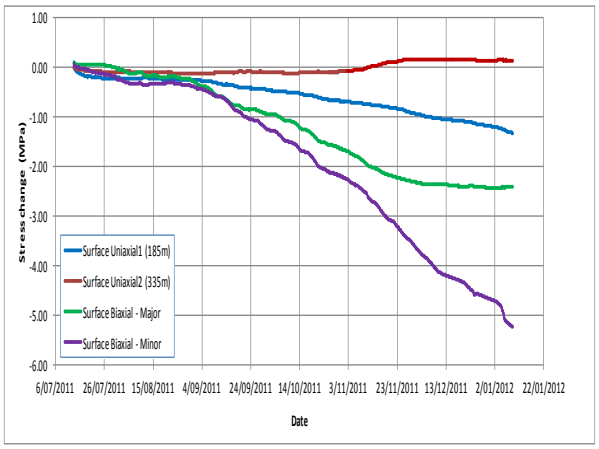

Figure 3 - Horizontal stress changes in shallow strata and monitored by two uniaxial stressmeters (red and blue curves) and one biaxial stressmeter

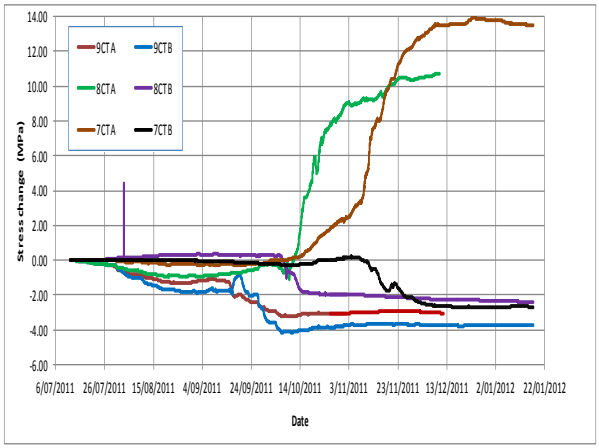

Figure 4 - Horizontal stress changes in the immediate roof strata in three cut-throughs at a respective distance of 160 m, 260 m and 360 m from the longwall start-up

Figure 5 shows an example of the correspondent stress change curve and stress rate plot for the surface biaxial stressmeter. There are numerous clear spike-like changes in the stress rate plot which reflect sudden stress changes although their magnitudes are still very small (e.g. 0.2 MPa/d). Also noted from the stress rate plot is that periodic stress changes occurred with a seven days cycle. A detailed examination showed that the stable period corresponds to the weekends when the longwall mining operation was stopped for maintenance. The monitoring results appear to reflect the mining activities very well.

Microseismic monitoring results

The advantages of using microseismic monitoring at Austar Mine are that this technology can reliably detect seismic events generated by rock fracturing near the longwall face and provide accurate locations of the rock fractures for ground stability analysis. In addition, the techniques can also provide the occurrence time and magnitude of an individual seismic event. The event counts and magnitude levels can be used as indicators for impending roof weighting analysis.

More than 15 000 seismic events were recorded during this monitoring period. Most of the events were weak and only recorded by one or some geophones. It was expected that significant roof weighting events should not be controlled by small events but strong ones. Therefore, only strong events that triggered most of the geophones and have the maximum waveform amplitude (ground vibration velocity) greater than 10^{-1} mm/s were analysed and located.

The seismicity (number of microseismic events against a specified time period) of the strong events is plotted in Figure 6 for the surface systems. Similar results were obtained from the underground system. The strongest event occurred on 26/09/2011 with the waveform amplitude of 90 mm/s. There is a general trend that the seismic event magnitude increased gradually until 26/09/2011 when the largest event occurred. This is followed by a relative quiet period of about 25 d before the seismic activities increased again.

The locations of the strong events in plan view are shown in Figure 7. The majority of the events are located within the longwall panel being mined and with a concentration towards the tailgate side. A number of events occurred in the adjacent panel that had already been mined. Few events were located in the adjacent panel that had not been mined.

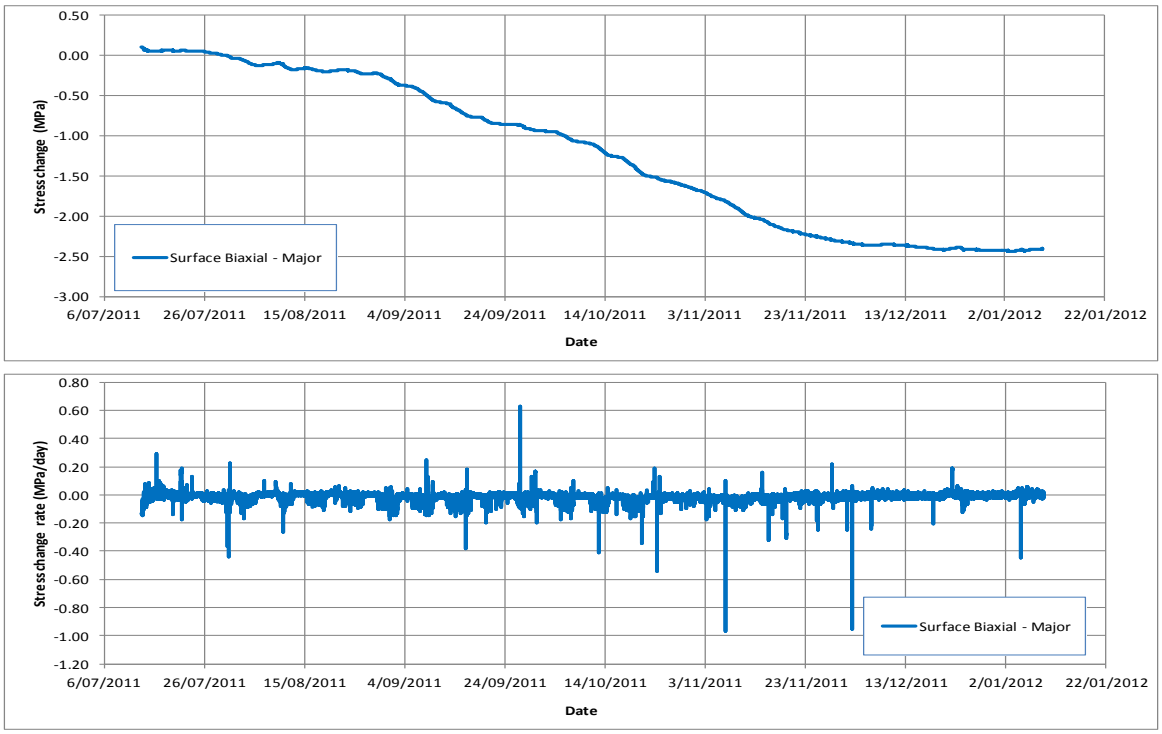

Figure 5 - Comparison of monitored stress change and stress rate, major stress from surface biaxial stressmeter

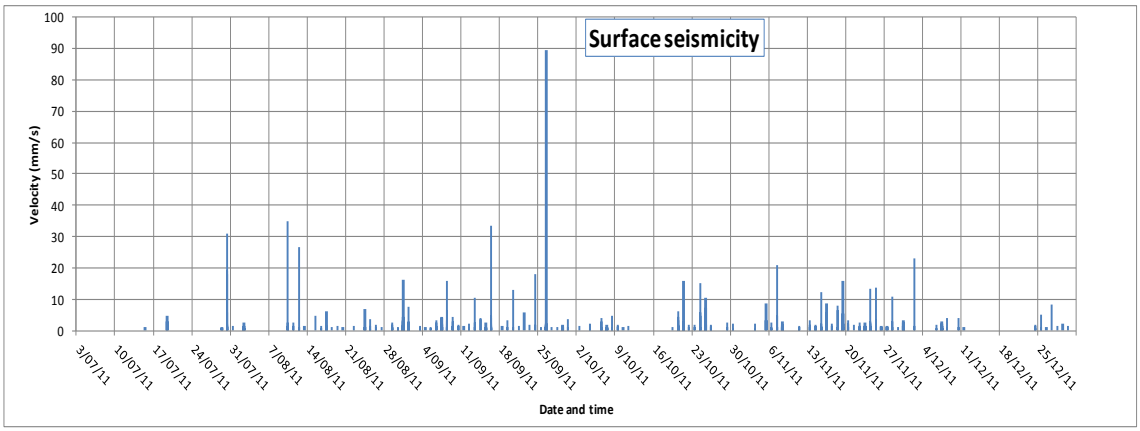

Figure 6 - The amplitude and occurrence of strong seismic events recorded by the surface microseismic monitoring system

A summary of located event distribution vs. depth is shown in Figure 8. It is evident that more than 90% of the events are located in the roof. A concentration of seismic events occurred about 30-150 m above the coal seam, in sandstone/siltshale, or the Branxton Formation which is massive and strong.

DETERMINATION OF CAVING PRECURSORS

Visual examinations of the stress rate plots (e.g. Figure 5) and seismic plots (e.g. Figure 6) can identify events that could be associated with major caving. If the stress rate or seismicity is consistently low for a period of time and then followed by a sudden change like a spike, it often indicates a fracturing event. However, it is important that the level of the background noise due to the instrument itself and normal mining operations is filtered out during this process. Otherwise too many false alarms could result.

One simple way to do so is setting a uniform threshold level above the background noise, and when the spike in stress rate and/or the seismicity energy is over the threshold level, a trigger is considered. This simple method however has a major shortcoming particularly for the underground monitoring systems. When the longwall face is far away from the monitoring location, the recorded stress rate or seismicity is

relatively low, and the threshold level is unlikely to be triggered. In contrast, when the longwall face is getting closer to the monitoring location, the stress rate and seismicity can be much higher and even the background noise may trigger the threshold level. It is important to recognise that the real telltale sign for a major fracturing event is not the absolute value of the stress rate or seismicity recorded by the monitoring instruments. Rather, it is the sudden out-of-trend spike that reflects rock fracturing and failure events.

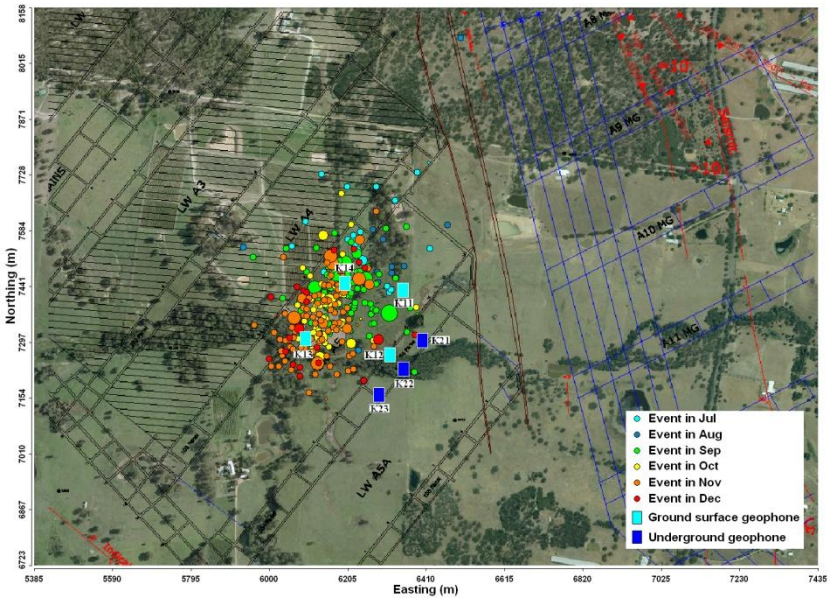

Figure 7 - Plan view of the strong events recorded by the ground surface stations, from July to December 2011

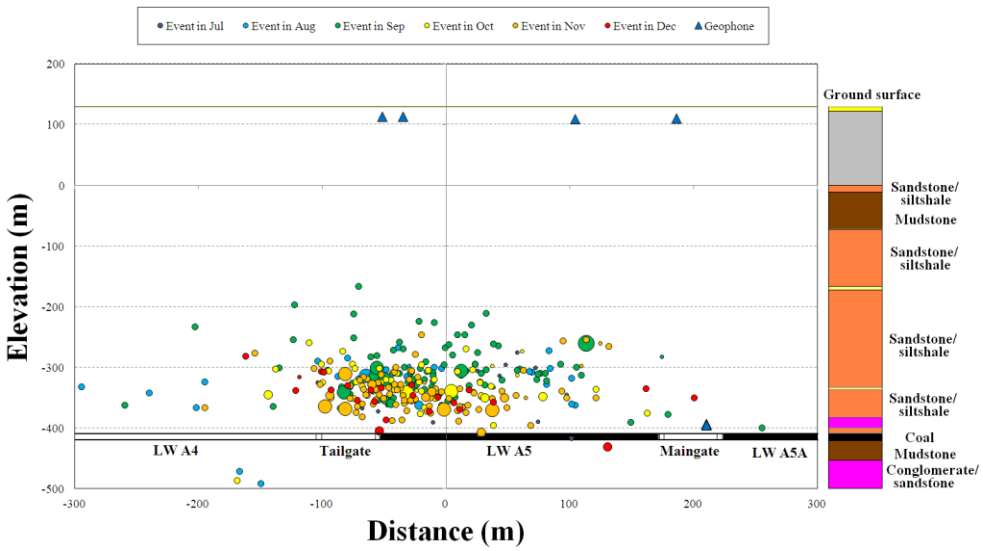

Figure 8 - Vertical cross-section of the strong events recorded from July to December 2011

Based on the above consideration, an intelligent method for detecting precursors of longwall caving events has been developed. This method uses the mean value and standard deviation of the signals (including noises) within a given period as the baseline. If the stress rate or seismicity is low, the standard deviation will be low. When they change suddenly, the immediate stress rate or seismicity will be high but the standard deviation remains low because it uses the data over a past period. In this case, the stress rate or seismicity becomes greater than the standard deviation multiplied by a factor, a caving precursor is then detected.

This method using standard deviation as a measure will minimise false alarms, in particular, immediately after a major caving event. It is also effective to minimise the effect from the varying distance between the longwall face and the sensors. A stronger signal is often detected when the longwall face is closer to the

sensor. However, this does not mean that the caving is more likely to occur. Details of this method can be found in Shen *et al.*, (2012).

Four monitoring systems were installed at Panel A5, including two for surface and underground stressmeters, and two for surface and underground microseismicity. The stressmeter systems have a number of stressmeters whose results are analysed independently. The microseismic systems also have several sensors but each of the two surface and underground systems are analysed as a system, and only those events triggering all the surface or underground geophones are considered.

A caving event may or may not trigger all the four systems and its sensors depending on its strength and magnitude. A method to quantify the strength of a precursor is developed based on the number of systems and sensors being successfully triggered by the event. This method uses a "Combined Trigger Index" for the four systems with triggering value ($T_{trigger}$) defined as:

$$T_{trigger} = T_{stress\_su} + T_{stress\_ug} + T_{seis\_su} + T_{seis\_ug} \quad (2)$$

where T_{stress_su} and T_{stress_ug} are the trigger index of the surface and underground stress monitoring system, respectively, whose value is in the range of (0 - 1.0) and is determined by the number of stressmeters triggered. T_{seis_su} and T_{seis_ug} are trigger index for the correspondent surface and underground seismic monitoring system.

The Combined Trigger Index method was tested against the monitoring data in Panel A5. Figure 9 shows the resultant Combined Trigger Index ($T_{trigger}$) over a period from July 2011 to January 2012. Also shown in the figure are the chock pressure data and the longwall chainage data. The red clusters in the chock pressure plot indicate high chock pressure, and possibly longwall weighting events. Some red clusters that have a constant value for a few days may not be real weighting events as they mostly occurred when the chainage stopped and longwall face was not advancing.

The figure demonstrates a good correlation between the high trigger index event ($T_{trigger} \geq 1.0$) and high chock pressure (red clusters). Notably, the index showed the first major trigger ($T_{trigger}=2.0$) on 30/07/2011 1:55 p.m. while a major chock pressure increase occurred between 30/07/2011 and 2/08/2011. This event could be the initial caving after the longwall face had advanced by 70 m.

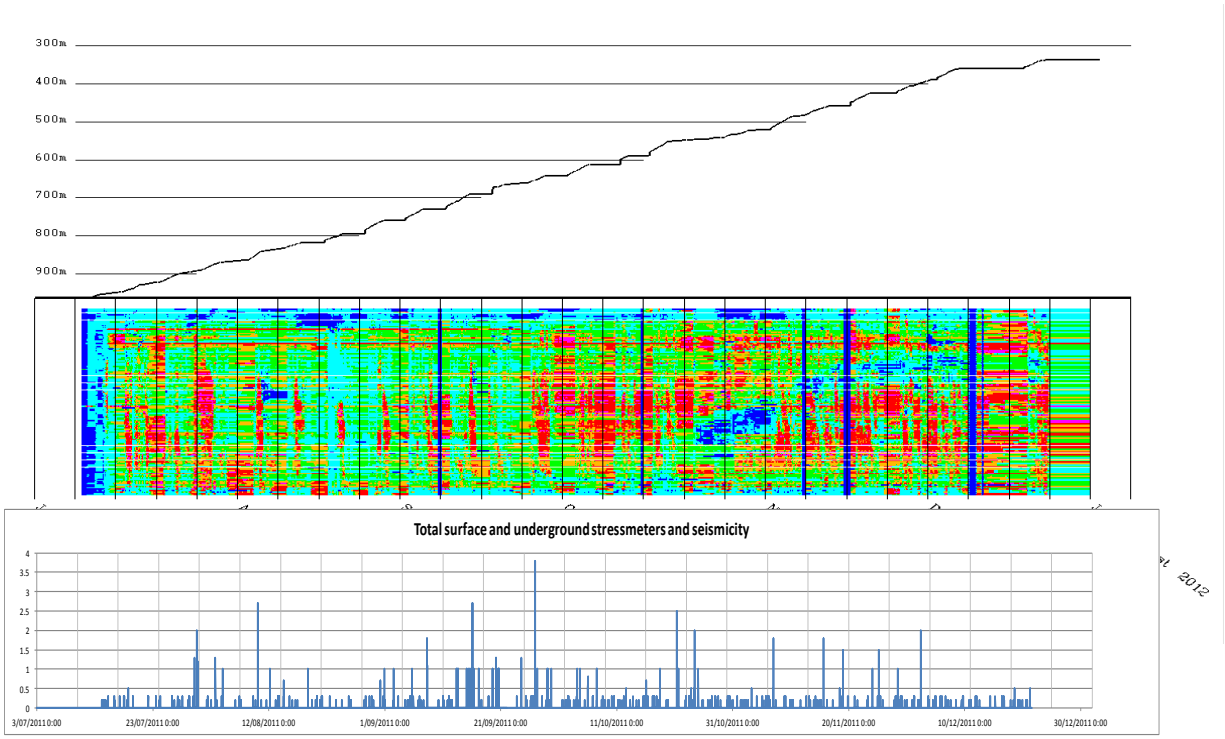

Figure 9 - Trigger index compared with chock pressure and longwall chainage at Panel A5, Austar Mine

Also detected by the trigger index are a major caving event on 16/09/2011 ($T_{trigger}$=2.4) and the strongest caving event on 26/09/2011 (Ttrigger=3.8).

An attempt has been made to correlate the mining observation records and the chock pressure (LVA) data with the triggers derived from the monitoring data. The two most severe weighting events occurred on 10/08/2011 8:00 am. and 16/09/2011 5:25 am. based on the mining records. The monitoring system was triggered at 10/08/2011 1:00 am. (trigger level = 2.7 out of 4.0) and 16/09/2011 2:40 am. (trigger level = 2.7 out of 4.0). These represent a successful early warning for the two major events by about 7 hours and 2.75 hours respectively prior to the actual events.

Comparing the monitoring triggers with all the major and minor weighting events recorded during mining operations, a rate for successful early warning of 8 out of 13 (i.e. 62%) is obtained. The rate of missed warning is 5 out of 13 (38%), and the rate of false alarm is 3 out of 13 real events (23%). The above results are based on both the surface and underground stressmeter and microseismic results, using a pre-set trigger level of 1.0 out of maximum 4.0.

The underground stressmeter and microseismic systems were effective until 7 November 2011 when some sensors and cables were damaged by pillar failures and roof falls. If we only consider the effective monitoring duration before this date and use the results from underground systems only, the resultant rate for successful early warning is 10 out of 12 (i.e. 83%). The rate of missed warning is 2 out of 12 (17%), and the rate of false alarm is 3 out of 12 real events (25%). A pre-set trigger level of 0.5 out of maximum 2.0 is used.

The successful warning triggers occurred mostly hours or days before the increase in chock pressure. It is therefore possible to use this monitoring technique and the trigger index method to forecast an imminent longwall loading event.

CONCLUSIONS

An integrated stress and seismicity monitoring system was trialed at Panel A5 at Austar Mine to detect and forecast longwall weighting events. The integrated monitoring system is composed of four independent sub-systems, including a surface and an underground stressmeter system; and a surface and an underground microseismic system.

The monitoring results have demonstrated that this experiment had been successful in detecting both stress and seismic signatures associated with caving and longwall weighting events. Both the stress changes recorded by stressmeters installed in shallow surface strata and underground roadway roofs showed a strong correlation with the chock pressure increases at the longwall face. The same phenomenon had been observed from the recorded microseismic events.

In order to develop an automated early warning method for longwall weighting, a trigger index method, which integrates the warning signs from all the four systems, was developed and tested against the mine weighting observations and chock pressure data. A good agreement had been observed. For all the weighting events observed, a rate of successful warning of up to 83% was achieved at Panel A5 using this trigger index method. The warning signs from the monitoring system mostly occurred at least several hours before the underground weighting events and the major increase in chock pressure. This demonstrates that the integrated stress and microseismic monitoring system, together with the analysis method developed, is capable of providing sufficient early warning for imminent underground weighting events.

No clear difference in the monitoring results was observed when the longwall operation changed from partial top coal caving to full face top coal caving.

Future development will focus on updating the integrated monitoring system to a wireless and fully automated system which can be easily used for early warning of longwall weighting.

ACKNOWLEDGEMENTS

The work presented in this paper was sponsored by Austar and CSIRO. The stressmeters were installed by Gavin Langerak of GEL Instrumentations Pty Ltd. We would also like to thank our CSIRO colleague

Shivakumar Karekal, Joey Duan, Brett Poulsen, Qingdong Qu, Zak Jecny for their help in instrumentation, data processing and numerical modelling.

REFERENCES

Guo, H, Luo, X, Zhou, B, Poulsen, B, Kelly, M, Craig, S, Adhikary, D, LeBlanc, S G, Caris, C, Yago, J, King, A, Ross, J and Coulthard, M, 2000. *Southern Colliery LW704 geotechnical study, CSIRO Report 759*, p200.

Shen, B, King, A and Guo, H, 2008. Displacement, stress and seismicity in roadway roofs during mining induced failure. *International Journal of Rock Mechanics and Mining Sciences.* 45:672-688.

Shen, B, Luo, X, Karekal, S and Duan, J, 2012. Monitoring longwall weighting at Austar mine using microseismic systems and stressmeters. *CSIRO Earth Science and Resource Engineering Report EP123936*.

PREDICTION OF DAMAGED ZONE IN LONGWALL WORKING PANELS

Hamid Mohammadi[1], Hossein Jalalifar[2] and Mohammad Ali Ebrahimi[3]

ABSTRACT: In longwall mining, the instability of roadways can affect the mine safety, production rate and consequently the economic condition of mine. Therefore their stability analysis is one the most important technical problems in underground mining. The stability analysis and the design of support systems have to be investigated from two points of view; 1) the pressure and displacements of damaged zone around gate roadways due to the construction process and stress redistribution and 2) the working loading due to coal seam extraction and overburden caving that extends the damaged zone size. The aim of this research is the calculation of working effect on the damaged zone around gate roadway considering geomechincal properties of medium and the geometric characteristic of the roads and working. Therefore, a method has been obtained to calculate the total damaged zone area and working influence coefficient using geometric concepts and mathematical relations, then a design algorithm has been suggested based on the obtained method.

INTRODUCTION

One of the objectives in coal mining is high productivity while considering the safety conditions. The stability of the roadways plays an important role in the success of longwall mining and their efficiency. Analysis of the redistribution of ground stresses around underground openings is one of the most important problems. During the roadway construction, the amount and orientation of the *in situ* stress field will change and is concentrated depending upon the *in situ* stress ratio. This stress concentration damages the *in situ* rock mass through initiation and propagation of cracks. Hence, construction of any underground opening creates a zone of disturbed rocks; around or within this zone there may exist a zone of damaged rocks (Whittaker and Singh, 1981; Unal, *et al*., 2001; Toran, *et al*., 2002; RafiqulIslam, *et al*., 2009; Sagong and Lee, 2005). The displacement which may lead to convergence and damage to the roadway is caused by redistribution of field stresses around the excavation as well as attainment of equilibrium by the disturbed rock mass. The convergence and damage to the roadway reduces the efficiency of the ventilation, speed and reliability of the transport system of men and material as well as the removal of the coal. The groadways, which have experienced high deformation require repair and noted that repair work not only costs money but also time which, in turn, dramatically decreases the efficiency (Juarez-Ferreras, *et al*., 2008; Yavuz, 2004; Lawrence, 2009).

The exact mechanism of damage is complicated, because a lot of factors influence it. With attention to previous studies, it can be shown that the stability analysis and the support design of roadways have to be investigated from two points of view; 1) the properties of the damaged zone around a roadway due to the construction process and stresses redistribution such as pressure and displacements and 2) the loading due to coal seam extraction and caving of working overburden that extend the damaged zone size (Juarez-Ferreras, *et al*., 2008; Yavuz, 2004; Lawrence, 2009).

The main purpose of this study is the calculation of the effect on the damaged zone around roadway considering geomechincal properties of the medium and the geometric characteristic of the roadway. The is divided into two parts;

1) Calculation of damaged zone properties due to a) the excavation of the roadway and redistribution of stresses (without working effect) and b) effects of coal seam extraction on the roadway (working effect).

2) Determination of influence coefficient of longwall working and suggestions for a design algorithm. The method that will be used to calculate of the effect of longwall working is based on the geometrical mechanism concept.

[1] *Mining Engineering Department, Shahid Bahonar University of Kerman, Iran. E-mail: mohammadi_79@yahoo.com, +983412112764*
[2] *Mining and Petroleum Engineering Department, Shahid Bahonar University of Kerman, Iran. E-mail: jalalifar@yahoo.com*
[3] *Mining Engineering Department, Shahid Bahonar University of Kerman, Iran. E-mail: maebrahimi@uk.ac.ir*

CALCULATION OF DAMAGED ZONE PROPERTIES WITHOUT WORKING EFFECT

Different methods have been presented to calculate of damaged zone around roadways (Biron and Arioglu, 1983; Pariseau, 2007). There are different methods such as *in situ* measurement, laboratory physical simulation and numerical modeling to determine damaged zone properties. The *in situ* tests provide helpful and reliable results, but they are time consuming and expensive. Thus several researchers have proposed empirical methods for estimating the damaged zone properties. One of these methods is the arch theory. As shown in figure 1, according to this method, due to roadway excavation, redistribution of thr stress field and resistance condition of medium, a natural arch is created above the roadway, as within this arch, the resistance properties of material has reduced roadway, thus along this natural arch, the rocks may loosen and separate from the above part of the overburden (Pariseau, 2007).

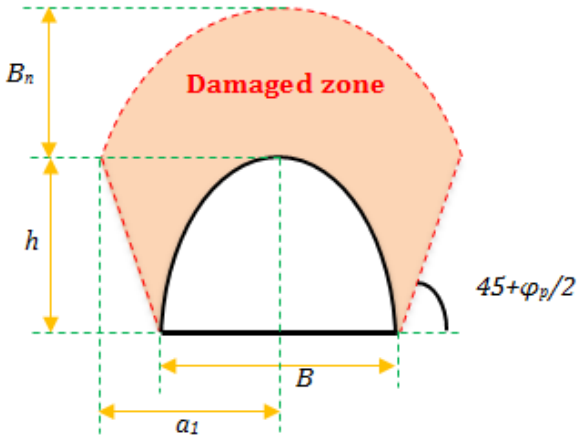

Figure 1 - Damaged zone above roadway

Based on instrumentation and monitoring results, Janas suggested an empirical relation for calculating of damaged zone height as follows (Snuparek and Konecny, 2010; Janas, 1990):

$$B_n = K_n B^{0.4} u^{0.6} \quad (1)$$

Also he obtained the following relation to calculate the damaged zone displacements (Janas, 1990).

$$u = 0.1B\left(e^{\frac{1.5H-q}{45\sigma_R}} - 1\right) \quad (2)$$

Where, H is overburden thickness of the roadway; B is roadway width, σ_R is average compressive strength of the strata of above the roadway; q is bearing capacity of support system (to calculate of maximum displacement, q must be considered equal 0); K_n is the coefficient characterizing the relationship between the damaged zone displacement (u) and roadway width (B) that is calculated based on the *in situ* measurements. For t→∞, the maximum of damaged zone height of is calculated by the following relation (Snuparek and Konecny, 2010; Janas, *et al.*, 2009).

$$B_n = 2B\left(e^{0.03\frac{H}{\sigma_R}} - 1\right)^{0.6} \quad (3)$$

Investigation of working effect on LDZ of gate roadway

According to the mechanism of the longwall mining method, due to coal seam extraction, after advancing of support system, a null space in working is created. Thus the immediate roof, a part of working roof between goaf and support systems is unsupported and hence is allowed to collapse and cave-in some distance behind the support system or in the goaf area. The downward movements of the roof strata will cause the disturbed roof strata and hence a caving zone with height of H_c is created. Therefore, the overburden pressure above the caving zone will be redirected towards the front abutment and the two

adjacent neighbouring solid sections where the roadways, the intervening barrier pillar and the adjacent un-mined solid sections are located. So the influence of redistribution of stress fields on the face ahead and the roadways must be considered in galleries design using a proper method such as numerical modelling, physical modelling, analytical solution and empirical methods (Yavuz, 2004; Lawrence, 2009; Snuparek and Konecny, 2010).

Calculation of height of caving zone

Many researchers have investigated the behaviour of the working roof, the process of the gradual upward movement and height of the caving zone (Chuen, 1979; Singh and Kendorski, 1981; Peng and Chiang, 1984; Fawcett, *et al*., 1986; Zhou, 1991). There are several methods to determine the height of caving zone such as *in situ* measurement, laboratory physical simulation, numerical modelling, and mathematical modelling (Majdi, *et al*., 2012). Based on the results of these methods, several empirical relations have been presented that their most important are mentioned in Table 1.

Table 1 - The most important empirical relation to calculate caving zone height

Relation	Overburden condition	Rock property constants			Remarks	References
		C	b	a		
$H_C = \frac{100h_s}{(a.h_s + b)}$	Weak	3100	5.00	-	-	Chuen, 1979
	Medium	1.6	3.6	-		
	Strong	1.2	2.00	-		
$H_C = 56(h_s)^{1/2}$	General relation	-	-	-	$0.0 \le h_s \le 3.5$	Singh and Kendorski, 1981
$H_C = \frac{h_s}{b-1}$	Without subsidence	-	-	-	-	Peng and Chiang, 1984
$H_C = aW - b$	-	0.83	11.00	-	-	Fawcett, *et al.*, 1986
$H_C = \frac{100h_s}{[(a.h_s + b) \pm c]}$	Hard rock	0.640	16.00	8.20	Modified by Peng &Chiang 1984	Zhou, 1991
	Medium	1.433	19.00	7.20		
	Soft rock	1.890	32.00	4.90		
	Weathered	2.134	63.00	3.90		

Also, in 2012, five mathematical models to calculate of damaged zone height have been presented. One of the models is an arithmatic model. According to this model, the tensile failure occurs at two extreme ends of the panel perpendicular to the advancing direction. Hence the width of the caving zone is equal to the extracted panel width (working length). The suggested relation by this model is nonlinear, as the other models and Peng model are it sub model. In this research, the arithmetic model is used to calculate caving zone height as follows (Majdi, *et al*., 2012).

$$H_c = \frac{h_s(h_s + 3d)}{2d} \quad (4)$$

Where, d is the expansion factor of broken rock and h_s is coal seam thickness.

Quantitative calculation of working effect on damaged zone

Due to the advancing coalface, creating a caving zone above the workings and the redistribution of stress field, an additional load is applied to the coal pillars and roadway. Based on the results of several coal mines and numerical modelling, Snuparek and Konency showed the additional load on the galleries during the creation of the caving zone can be deduced from a schematic concept of the mechanism, causing the additional load according to Figure 2. According to Figure 3, the additional loading relates to part of triangule ABC t located outside of parabolic. Also some of parameters such as pillar width, the height of the caving zone and caving angle have an influence on the value of the additional loading (Snuparek and Konecny, 2010).

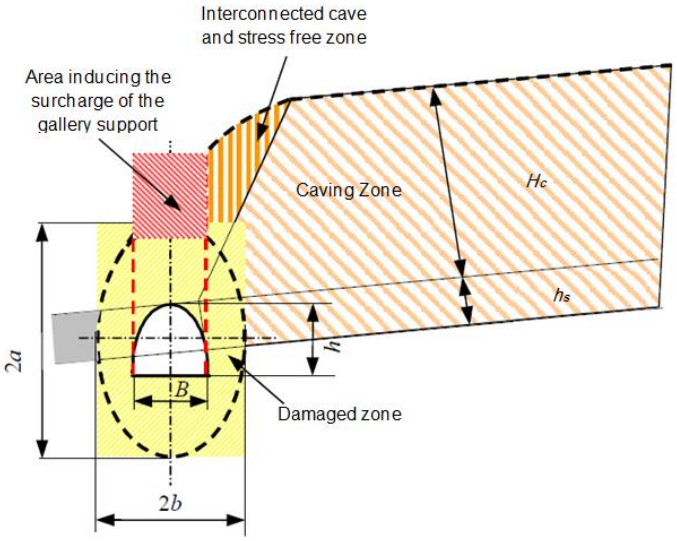

Figure 2- influence of longwall working on roadway damaged zone (Snuparek and Konecny, 2010)

For determining the area of triangle ABC and the parabolic area (damaged zone area due to roadway construction), must be calculated caving angle (φ_0), damaged zone width above the roadway ($2a_1$) and the height of triangle ABC (X) from following relations.

$$\phi_0 = \tan^{-1}\frac{H_C}{W} \tag{5}$$

$$\alpha_1 = \tan^{-1}\frac{H_C}{\frac{H_C}{\tan\phi_0} + B + h\tan\left(45 - \frac{\phi_p}{2}\right)} \tag{6}$$

$$2a_1 = B + 2h\tan\left(45 - \frac{\phi_p}{2}\right) \tag{7}$$

$$X = 2a_1\tan\alpha_1 \tag{8}$$

Thus the areas of triangle ABC and parabolic arch are calculated by Eq. (9) and Eq. (10) respectively.

$$S_{\Delta} = a_1 X \tag{9}$$

$$S_{Par} = \frac{4a_1 B_n}{3} \tag{10}$$

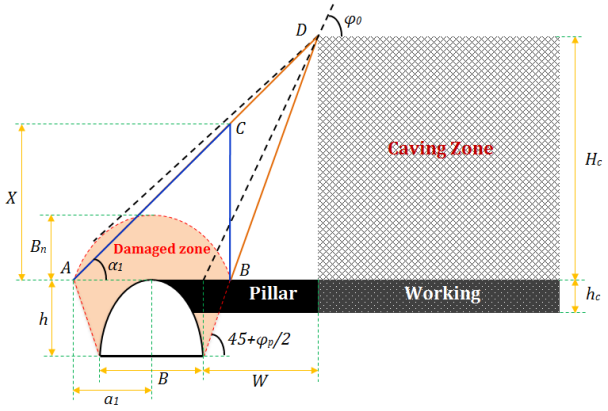

Figure 3 - Working effect on damaged zone based on the geometric concept

Also, in this paper, based on the mathematical calculations and for 3 states, equations of total area f damaged zone (S_T) and the area of additional loading (S_a) are obtained as shown in Table 2.

Table 2 - Relation of total area of damaged zone and additional loading area

Total area of damaged zone	Area of additional loading	conditions
$S_T = S_{Par} + S_a = S_\Delta$	$S_a = a_1 X - \frac{4a_1 B_n}{3}$	$X > 2B_n$
$S_T = S_{Par} + S_a$	$S_a = \frac{a_1 X}{2} - \frac{a_1 B_n}{6}$	$X = 2B_n$
$S_T = S_{Par} + S_a$	$S_a = a_1 X - a_1^{\,2} \sin 2\alpha_1$	$X < 2B_n$

For designing the support system of roadways, the increment value of damaged zone area due to mining operation must be considered. Thus it has been considered in the process of calculation of support system. Eq. (11) shows the support pressure without the effect of working (in damaged zone, the cohesion of broken rocks is decreased extremely, so it can be considered equal to zero) (Snuparek and Konecny, 2010).

$$P = \frac{\frac{\gamma B}{2} - c}{K \tan \phi_p} \left(1 - e^{-K \tan \phi_p \frac{2B_n}{B}} \right) \tag{11}$$

According to Eq. (11), the support system depends on the height of the damaged zone (B_n), thus for determining new support pressure (P_E) (with considering of the effect of working and mining operation) it is considered the height of total damaged zone (B_{nE}). B_{nE} is calculated based on Eq. (12).

$$B_{nE} = \frac{3S_T}{4a_1} \tag{12}$$

According to Eq. (13), by substitution of B_{nE} into Eq. (3) an equivalent height of overburden (H_E) is obtained and creates a damaged zone with height of B_{nE} without the effect of working. Eq. (14) is to calculate the influence working coefficient (*G),* which can be used to determine the effect value of working on the roadway with considering pillar width. Also for determining total displacement of roadway under working effect, H_E substitutes into Eq. (2).

$$H_E = \frac{\sigma_R}{0.03} \ln \left(\left(\frac{3S_T}{8Ba_1} \right)^{1.67} + 1 \right) \tag{13}$$

$$G = \frac{H_E}{H} \tag{14}$$

Suggestion of a design algorithm

In roadway stability analysis and in designing a pillar and support system, it is necessary to include two important factors; A) the loading effect due to damaged zone of roadway without working effect and B) additional loading effect due to mining operation of longwall working. Pillar width has a very important role to decrease working effect on roadway. The greater pillar width decreases the working effect, but the economic problems must be considered. In this research, after considering different factors and methods, an algorithm to design and analyse roadways has been suggested (Figure 4). The following matters have been considered; 1) roadway stability with two different conditions; A) without working effect and is with working effect, 2) support system analysis and 3) pillar design.

Validation

In order to validate the proposed method in calculating the working effect coefficient on roadways, one of the longwall workings of Parvade2 coal mine of Tabas in Iran was considered. This working has been developed in C1 coal seam of Parvade2. C1 coal seam, with thickness equal to 1.85 m, contains over 40% of the reserves of Parvade2 coal mine. The hanging wall of C1 consists of argillite and siltstone and the footwall consists of argillite, siltstone and sandstone. Length of working is 100 m and to protect the roadways a pillar with width (w) of 10 m was considered (Javaheri, 2009). Investigation of instrumentation and monitoring results are shown the convergence of roadway is over 50 cm. in this study, based on working properties (Table 3) and suggested algorithm, the stability condition of roadway was investigated and the results have been mentioned in Table 4.

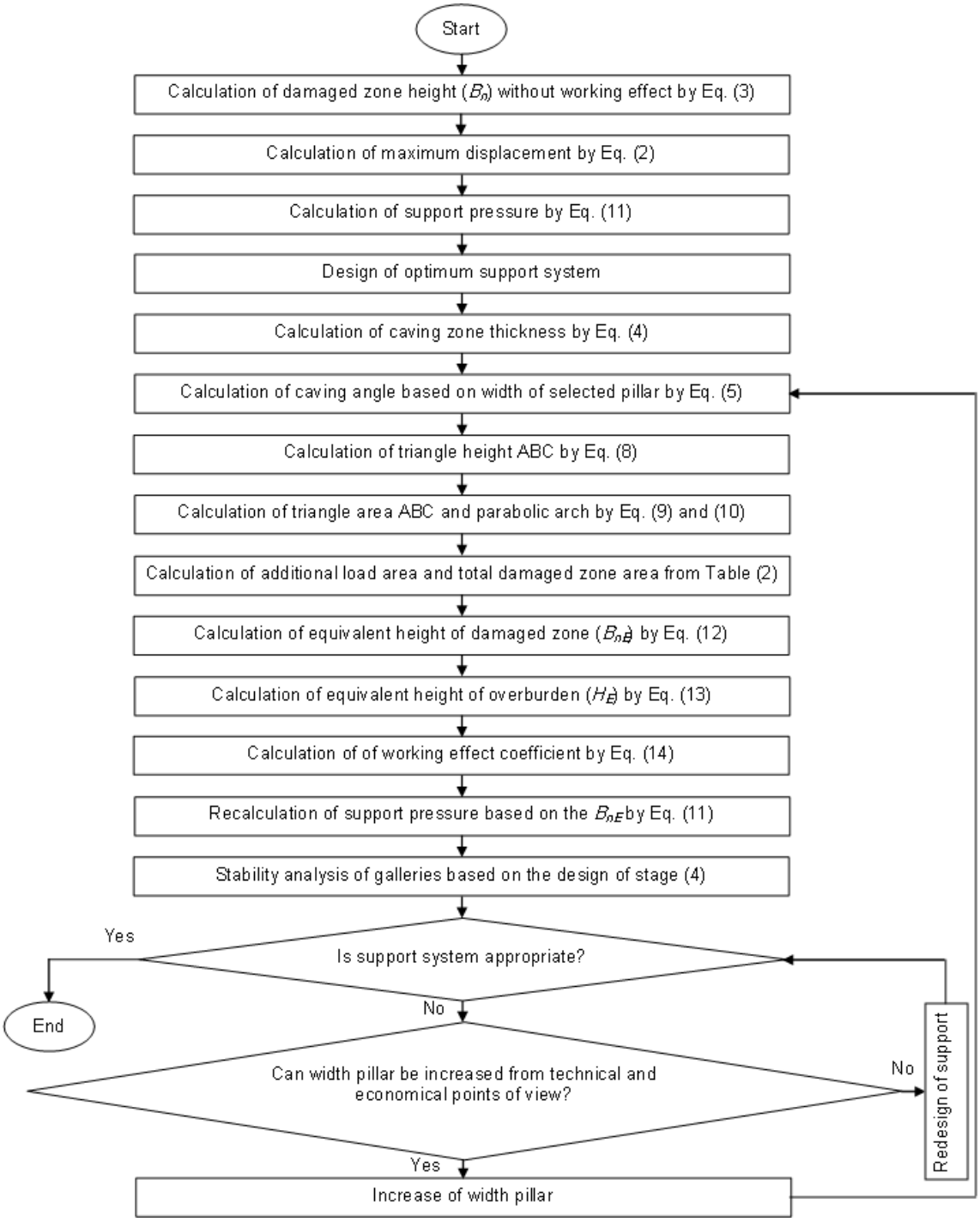

Figure 4 - Suggested algorithm for designing roadway

According to Table 4, the roof displacement of roadway and support pressure without working effect are 22.48 cm and 92.16 kPa respectively. Considering the working effect and pillar width, the roof displacement is increased about 173% (615.1 mm) that conforms with results of instrumentation and monitoring. Also, the support pressure has been increased about 56% (143.86 kPa) and working effect coefficient was obtained as 2.05.

Table 3 - Geomechanical and Geometrical properties of longwall working in Parvade2 coal mine (Javaheri, 2009)

d	γ(t/m^3)	K	c (MPa)	φ_P (deg.)	h (m)	B (m)	σ_R (MPa)	H (m)
0.1	2.2	0.26	0.6	28	2.6	3.6	17	250

Table 4 - Analysis results one of longwall working in Parvade2 coal mine

P_E (KPa)	u_E (cm)	G	H_E (m)	B_{nE} (m)	H_c (m)	P (KPa)	u (cm)	B_n (m)
0.1	2.2	0.26	0.6	28	2.6	3.6	17	250

Sensitivity analysis of pillar width

To investigate of the influence of pillar width in transferring the effect of mining operation on roadways, 32 analyses under various pillar widths were performed and the parameters of support pressure, displacement, caving angle and working effect coefficient were calculated and have been shown in Figure 5. As mentioned, the relationship between pillar width and output parameters are nonlinear. For example, with an incremet of pillar width from 10 m to 3 0 m (three times), the working effect coefficient decreases from 2.05 to 1.18.

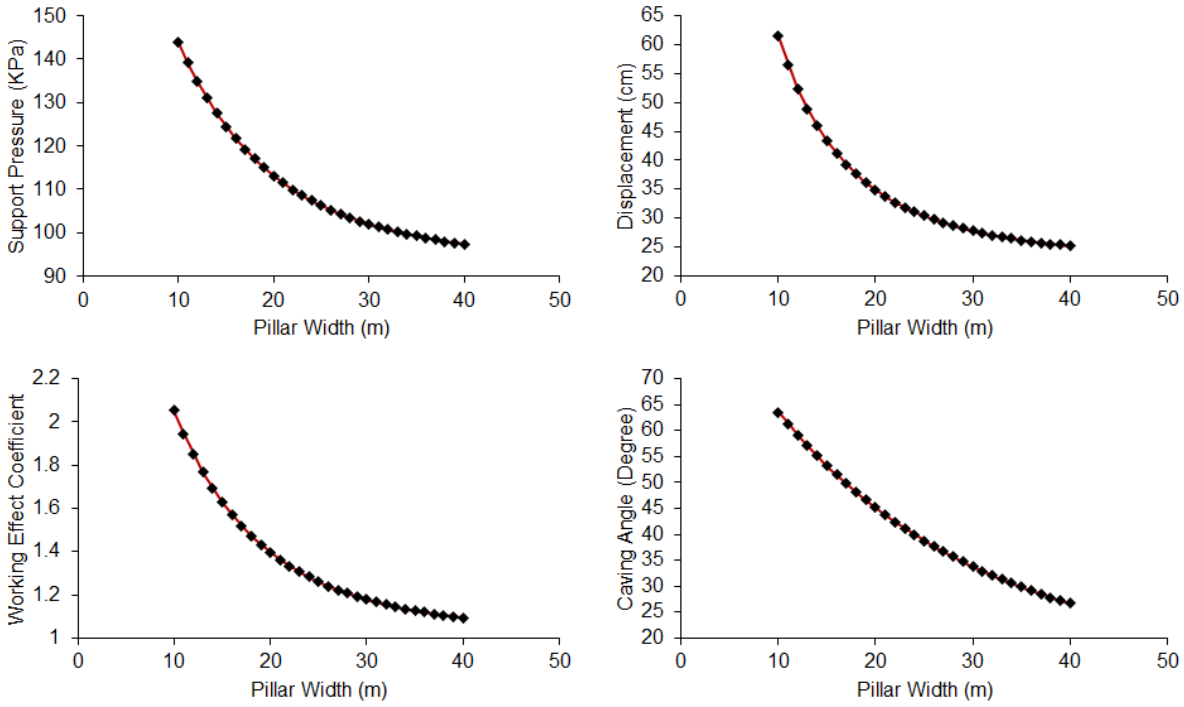

Figure 5 - results of sensitivity analysis of pillar width

RESULTS AND CONCLUSIONS

In this study, the longwall working effect on roadways was investigated and the following results were obtained:

1. Based on the geometric concepts, the mechanism of working effect on roadway damaged zone was investigated and a mathematical method was presented to calculate the additional loading and total damaged zone.

2. To determine the quantity effect of working on roadways, the working effect coefficient was presented.
3. Based on the proposed method, a design algorithm was suggested.
4. To validate the proposed method, one roadways of Parvade2 coal mine of Tabas was investigated and obtained a proper results. Also the working effect was obtained as 2.05.
5. Based on the results of sensitivity analysis of pillar width, it was detected that the relationship between pillar width and parameters of support pressure, displacement, caving angle and working effect coefficient is nonlinear.

REFERENCES

Biron, C and Arioglu, E, 1983. Design of support in mines, John willey and Sons.

Chuen, L T, 1979. Practice and knowledge of coal mining under water bodies, *10th World Mining Congress*, Istanbul.

Fawcett, R J, Hibberd, S and Singh, R N, 1986. Analytic calculations of hydraulic conductivities above longwall coal face, *Int. J. Mine Water, International Mine Water Associations*, pp45-60.

Janas, P, 1990. Dimensioning of roadway supports in conditions of Ostrava-Karvina coalfield, *Proceedings of World Mining Congress*, Novosibirsk. Russia, pp124-129.

Janas, P, Snuparek, R and Krejsa, M, 2009. Probabilistic approach to designing anchor support in mine workings in Ostrava-Karvina coal district, *Tunel*, 4:37-43.

Javaheri, A, 2009. Stress analysis around a lateral gallery; case study: Level III, Parvade 2 coal mine, Tabas, M.Eng thesis, Shahid Bahonar University of Kerman, Iran.

Juarez-Ferreras, R, Gonzalez-Nicieza, C, Menendez-Diaz, A, Alvarez-Vigil, A E and Alvarez-Fernandez, M I, 2008. Measurement and analysis of the roof pressure on hydraulic props in longwall, *International Journal of Coal Geology*, 75:49-62.

Lawrence, W, 2009. A method for the design of longwall gateroad roof support, *International Journal of Rock Mechanics and Mining Sciences*, 46:789-795.

Majdi, A, Hassani, F P and Yousef Nasiri, M, 2012. Prediction of the height of distressed zone above the mined panel roof in longwall coal mining, *International Journal of Coal Geology*, 98:62-72.

Pariseau, W G, 2007. Design analysis in rock mechanics, Taylor and Francis, London.

Peng, S and Chiang, H, 1984. Longwall mining, John Wiley and Sons, Inc., New York, NY., 708 pp.

RafiqulIslam, M D, Hayashi, D and Kamruzzaman, A B M, 2009. Finite element modeling of stress distributions and problems for multi-slice longwall mining in Bangladesh, with special reference to the Barapukuria coal mine, *International Journal of Coal Geology*, 78 (2):91-109.

Sagong, M, and Lee, J S, 2005. A new approach to estimate plastic region near tunnel considering excavation induced damage and *in situ* rock mass condition, Underground Space Use: Analysis of the Past and Lessons for the Future - Erdem and Solak (eds), Taylor andFrancis Group, London, pp205-210.

Singh, M M and Kendorski, F S, 1981. Strata disturbance prediction for mining beneath surface water and waste impoundments, *Proc. 1st Conference on Ground Control in Mining*, pp76-89.

Snuparek, R and Konecny, P, 2010. Stability of roadways in coalmines alias rock mechanics in practice, *Journal of Rock Mechanics and Geotechnical Engineering*, 2 (3):281-288.

Unal, E, Ozkan, L and Cakmakci, G, 2001. Modelling the behaviour of longwall coal mine gate roadways subjected to dynamic loading, *International Journal of Rock Mechanics and Mining Sciences*, 38:181-197.

Toran, J, Rodriguez Diez, R, Rivas Cid, J M, and Casal Barciella, M M, 2002. FEM modeling of roadways driven in a fractured rock mass under a longwall influence, *Computers and Geotechnics*, 29: 411-431.

Whittaker, B N, and Singh, R N, 1981. Stability of longwall mining gate roadways in relation to rib pillar size, *International Journal of Rock Mechanics and Mining Sciences*, 18:331-334.

Yavuz, H, 2004. An estimation method for cover pressure re-establishment distance and pressure distribution in the goaf of longwall coal mines, *International Journal of Rock Mechanics and Mining Sciences*, 41:193-205.

Zhou, Y, 1991. Evaluating the impact of multi-seam mining on recoverable coal reserves in an adjacent seam, Virginia Division of Mineral Resources, Commonwealth of Virginia, Department of Mines, Minerals and Energy, Publication, 104.

ESTIMATION OF ROCK CAVABILITY IN JOINTED ROOF IN LONGWALL MINING

Alireza Jabinpoor[1], Ahmad Jafari[2] and Mehdi Yavari Shahreza[2]

ABSTRACT: Longwall mining is one of the major methods in the coal mining industry. A main concern in this method is roof cavability and caving step or required advance length to make the roof to cave; this is specifically important when roof is relatively hard and caving is controlled by discontinuities within the roof rock. In this research roof caving is studied for different advances and various specifications of discontinuities. A rating method is suggested to characterize the rock mass based on the developed models. A graph has been constructed using the proposed rating system, which can be utilised to predict necessary caving step for the roof.

INTRODUCTION

Caving methods are one of important category of methods which can compete with surface mining from productivity point of view. Among them, longwall mining is one of the major methods in the coal mining industry (Hartman, 2002). A major concern in the longwall method is the cavability of roof in a way to guarantee safety as well as optimum load imposed on the support equipment. To ensure appropriate caving of roof information about cavability of a given rock I needed. Successful caving depends on appropriate planning and stope design (Hardwick, 1965) Rock cavability depends on a number of factors e.g. rock structures *in situ* stresses, induced stresses in the caving area and rock mass classification (Laubscher, 1994; 2000). Thus rock cavability can be predicted base on these parameters. Vast use of caving mining methods has increased the importance of understanding rock cavability aspects in mine design. Prediction of cavability is a complicated task which has been the focus of many researches; most of the attempts have been based on experiences of different mines and data gathered from the field. However, development of numerical methods has shaped another possible approach for solving this problem and developing a different method of prediction.

CAVABILITY PREDICTION

Experimental approach

This approach is based on analysis of experienced obtained from field by different people. Among most popular approaches of this kind are the Mathews and Laubscher methods. They generally apply classification methods to rock and propose a relationship between rock rating and rock hydraulic radius.

Mathews methods: Mathews *et al.,* (1980) proposed his method using data obtained from his studies in open stopes (Suorieni, 2010). He proposed calculation of stability number (N), to be used for cavability prediction, as follows:

$N = Q' \times A \times B \times C$
While $Q' = (RQD/J_n) \times (J_r/J_a)$

The three correction factors A, B and C represent stress factor, joint defect orientation factor and gravity factor respectively and can be determined using graphs proposed by Mathews. Figure 1 shows the cavability of rock depending on stability number and hydraulic radius (ratio of area to perimeter of a rectangular) of opened area. According to Mathews proposal three different zones, i.e. stable zone, potentially unstable zone and potentially caving zone can be distinguished. Later, some attempts were made to improve Mathews proposed method. The latest study (Brown, 2003) has considered additional data from 400 mines, result of which is shown in Figure 2, the same three zones can be seen in this figure. It should be noted that hydraulic radius is characterizing the open area but does not include opening height.

[1] *Graduate Student, School of Mining Engineering, University of Tehran*
[2] *Ass. Professor, School of Mining Engineering, University of Tehran*

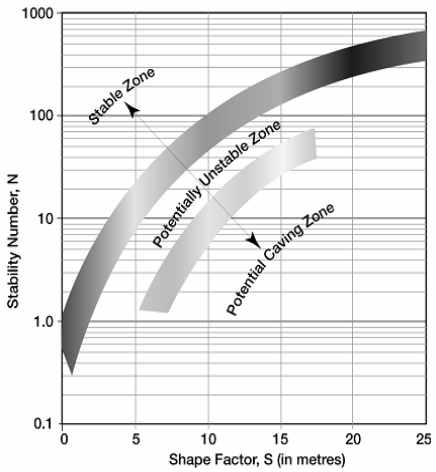

Figure 1 - Rock cavability for different stability number and hydraulic radius (Mathews, *et al*., 1980)

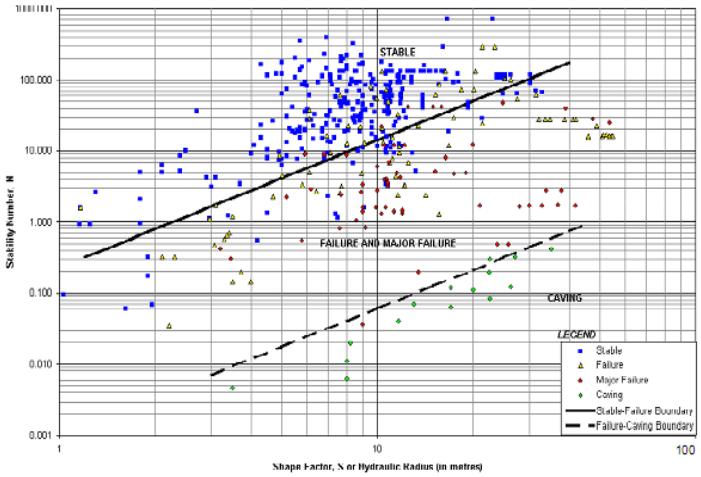

Figure 2 - Corrected rock cavability (Mawdesley, 2002)

Laubscher method: Laubscher (2000) has started a series of investigations in this area since 1977. He first divided the rock mass into five groups based on geomechanical parameters. He then introduced the new approaches based on Mining Rock Mass Rating (MRMR) and *in situ* Rock Mass Rating (IRMR).

MRMR is developed based on RMR by applying four correction factors for weathering, joint orientation, mining induced stresses and blasting. IRMR was later introduced in 2000. One major change was discarding RQD from the classification; Figure 3 shows the final cavability prediction graph proposed by Laubscher which is based on the MRMR value of the rock and the hydraulic radius of the open area. This figure, similar to Mathews method, divides the rock into three categories i.e. stable, caving and transitional zone

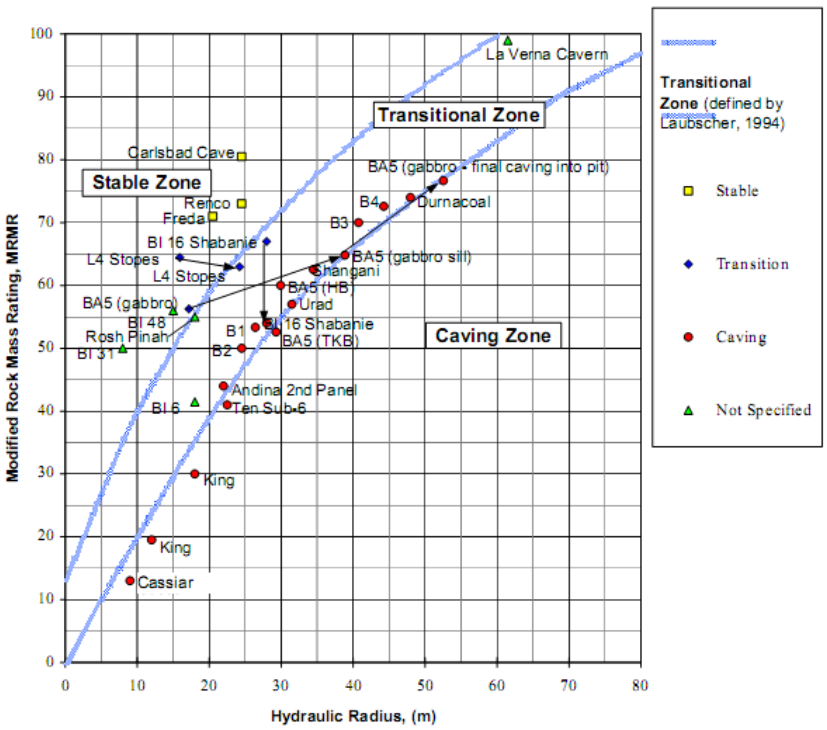

Figure 3 - Rock cavability prediction (Mawdesley, 2002)

Both described methods show that when rock quality is better a higher hydraulic radius is required to force the rock to cave. Higher hydraulic radius can be practically obtained by increasing the minimum span of the area i.e. width of the stope in longwall.

Numerical approach

Numerical approaches use the advantage of applying mathematical relationships between rock elements and blocks and combining them towards problem solution. Tollenear (2008) and Vyanzmensky (2008) have shown application of these methods in characterizing caving procedure.

In general such modelling can be done using continuous or discontinuous simulation. Considering the effect of discontinuities on rock caving especially for harder rocks, the latter method is preferable and used in this research. The code UDEC (Itasca, 2000) is proper available software for such modelling. This code can accommodate large displacement and block rotation which is inevitable for caving simulation.

LONGWALL MODELLING

The modelling was done in two dimensions and a Mohr coulomb failure criterion was used for the rocks. Figure 4 shows the general geometry of the model. Displacement of roof was monitored and cavability was judged based on the amount of displacement for different spans. Cavability is considered to be controlled by two factors, rock displacement and span size. More displacement in smaller span means good cavability and vice versa.

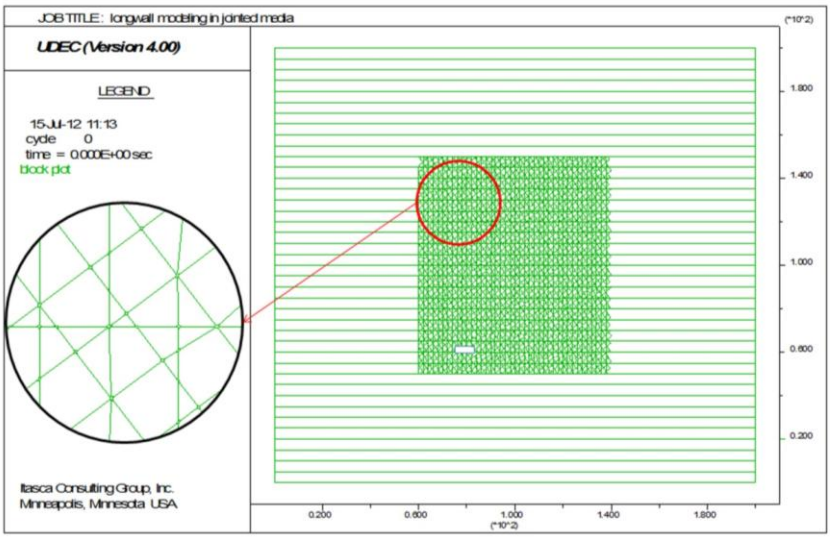

Figure 4 - General geometry of constructed model

The model size is 200 m x 400 m, however to decrease computation time, only the central part was jointed. Comparison with a fully jointed model shows the results are very much similar. The central part of the model is subject to four joint sets. To make the roof cave, the stope was advanced in 2 m steps. As the stope was advanced the displacement of roof was monitored. A vast number of models were tested to evaluate the effect of four major parameters of joints i.e. spacing, dip angle, friction and cohesion. These parameters were found to be the main controlling factors for cavability, details of which are discussed below:

Joint spacing: This parameter indicates block sizes in rock mass which in turn affects the failure and caving of roof. Figure 5a shows the effect of joint spacing on roof displacement which is an indication for cavability. The figure depicts stability increases for larger spacing.

Dip angle: Dip variation is studied for dip magnitude between 20 and 80 degrees; figure 5b shows the results. As can be seen when the dip angle is 45˚, large displacement happens in smaller spans. In general cavability is better for less dipped jointed rock.

Joint friction and cohesion: Shear strength is an important factor affecting displacement, which is controlled by friction angle and cohesion. As can be seen in Figure 5c, by increasing friction angle rock joints become stronger against shearing thus cavability decreases. In other words larger spans are needed for roof to cave. Figure 5d similarly shows the cohesion effect. As is expected an increase in

cohesion, increases shear strength of joints and stability, thus roof may only cave by increasing the opening span.

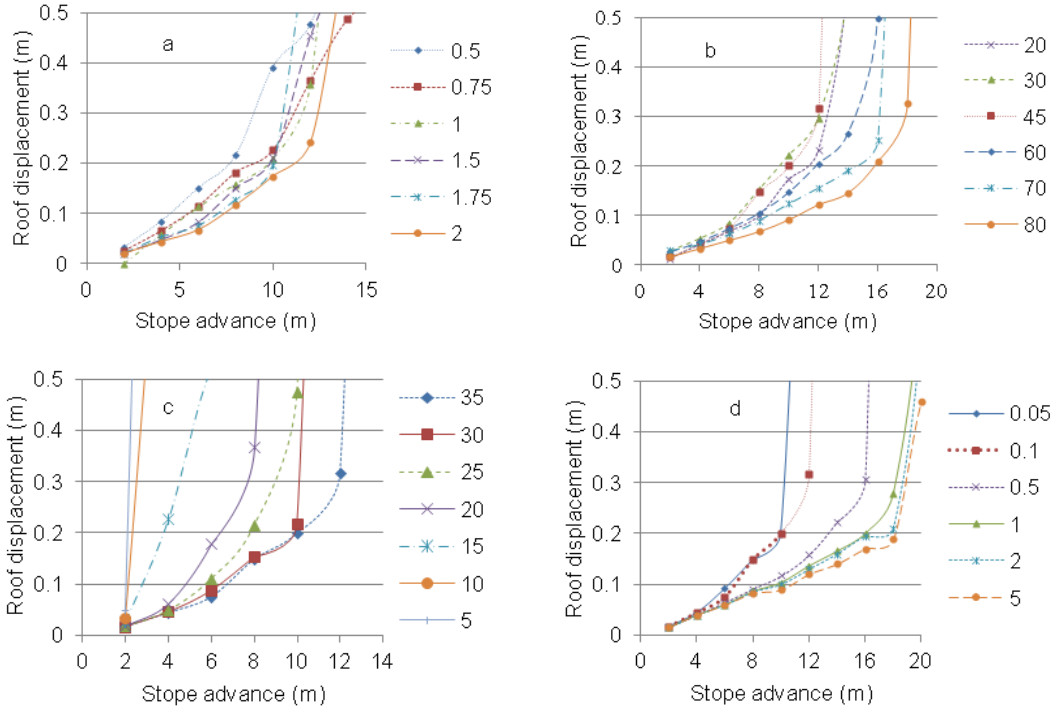

Figure 5 - Effect of a) joint spacing, b) joint dip, c) joint friction, d) joint cohesion, variation on roof displacement

CAVABILITY PREDICTION

Results of the modelling show that displacement and cavability is determined and controlled by different factors. It is necessary to combine these different effects. For this purpose a rating system was employed to allocate different weights to each parameter. Five different rating systems were tested using studied parameters, shown in Table 1; total rating is 100 for each state of rating. First state shows uniform distribution of total rating for different factors while the importance of each factor is different in the other four states of rating. Higher value of total rating indicates more stable rock and less cavability. Tables 2 to 5 show rating distribution for each of the four parameters. Joint spacing is divided into five categories while dip is considered into three.

The ruling dip of the joint sets is considered in the analysis. Joint cohesion is stated as a percentage of rock cohesion and it can be maximum equal to rock cohesion.

Caving is assumed to happen if rock displacement is more than 50 cm while the rock with displacement less than 15 cm is assumed as stable. No judgment is made for the intermediate conditions. Figure 6 shows the produced graph which determines the cavability based on proposed rock rating and opening span. This figure is based on first state of rating mentioned in Table 1. Other rating states result in similar graphs.

Table 1 - Joint parameters under study and allocated rate

Parameter	Rate				
	State 1	State 2	State 3	State 4	State 5
Spacing	25	30	30	40	40
Dip angle	25	25	20	20	25
Friction angle	25	30	30	20	20
Cohesion	25	15	20	20	15
Total rate	100	100	100	100	100

Table 2 - Allocated rate for joint spacing

Class	Spacing (m)	Rate				
		Sate 1	State 2	State 3	State 4	State 5
I	S≥2	25	30	30	40	40
II	1.5<S<2	20	24	24	32	32
III	1<S<1.5	15	18	18	24	24
IV	0.5<S<1	10	12	12	16	16
V	S≤0.5	5	6	6	8	8

Table 3 - Allocated rate for dip angle

Class	Dip (degree)	Rate				
		State 1	State 2	State 3	State 4	State 5
I	50-90	25	25	20	20	25
II	0-40	15	15	10	10	15
III	40-50	5	5	1	1	5

Table 1 - Allocated rate for friction angle

Class	Friction angle (degree)	Rate				
		State 1	State 2	State 3	State 4	State 5
I	≤10	5	1	1	1	1
II	11-20	15	10	10	7	7
III	21-30	20	20	20	14	14
IV	≥31	25	30	30	20	20

Table 5 - Allocated rate for cohesion

Class	Cohesion	Rate				
		Sate 1	State 2	State 3	State 4	State 5
I	$C_j \geq C_j$	25	15	20	20	15
II	$0.7C_r < C_j < C_r$	20	12	16	16	12
III	$0.5C_r < C_j < 0.7C_r$	15	9	12	12	9
IV	$0.3C_r < C_j < 0.5C_r$	10	6	8	8	6
V	$0.1C_r < C_j < 0.3C_r$	5	3	4	4	3
VI	$C_j \leq 0.1C_r$	1	1	1	1	1
C_r = Rock cohesion, C_j = Joint cohesion						

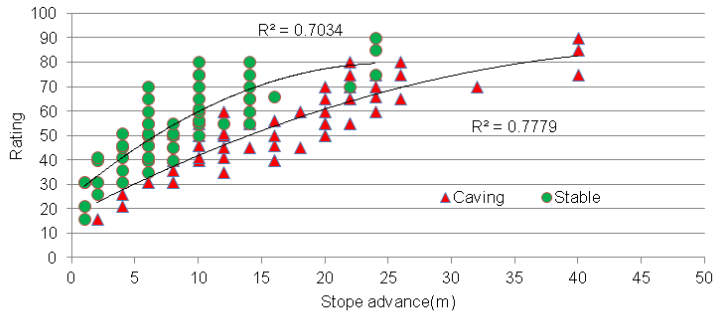

Figure 6 - Cavability prediction by equal rating of four joint parameters

It should be noted that variation of depth and stress state is not considered in these modelling and resulting graph.

When four input parameters (spacing, dip, friction angle and cohesion) were used in rating system third state of the rating, i.e. 30, 20, 30, 20 produced best result, judging by correlation coefficient. Figure 7 shows the final proposed graphs for cavability prediction based on both rating systems. For each rating two spans can be determined which indicate the stable roof and caving conditions. The spans between

these two marginal figures can be considered as transitional. When the span is increased beyond a certain size the effect of roof strength on caving becomes less.

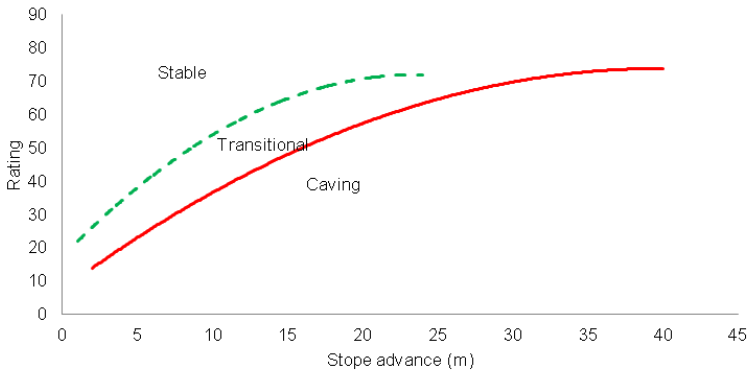

Figure 7 - Proposed graph for cavability prediction

CONCLUSIONS

The longwall method is one of the major coal mining methods in which roof caving is an important issue affecting safety and performance of mining operations. During the mining procedure, when the roof is hard, caving is basically controlled by joints and its properties. It is important to know the minimum span required for caving for different conditions. A series of models were constructed and run to evaluate stability and/or caving of the roof when joint spacing and specification change.

Some graphs were produced based on a proposed rating system. Joint properties, i.e. spacing, dip, friction angle and cohesion were input in the rating system which resulted in a design graph. Based on the proposed graph it is possible to evaluate the required span for caving by knowing the rock rating from the proposed method. This rating system gives a simple means for evaluation of rock cavability.

REFERENCES

Brown, E T, 2003. *Block Caving Geomechanics.* Queensland: Julius Kruttschnitt Mineral Research Centre Isles, 516p.

Hardwick, W R, 1965. Block-caving copper mining methods and costs at the Miami mine. US. Dept. of the Interior, Bureau of Mines. Washington: Miami Copper Company.

Hartman, Howard L, 2002. *Introductory Mining Engineering*, John Wily and sons, 584p.

Laubscher, D H, 1994. Cave mining-the state of the art, *The Journal of The South African Institute of Mining and Metallurgy*, 94:279-293.

Laubscher, D H, 2000. *A practical manual on block caving,* Prepared for International Caving Study, JKMRC and Itasca Consulting Group, Brisbane, 500p.

Mathews, K E, Hoek, E, Wyllie, D C and Stewart, S B V, 1980. *Prediction of stable excavation spans for mining at depths below 1000 meters in hard rock*. Golder Associates Report to Canada Centre for Mining and Energy Technology (CANMET), Department of Energy and Resources, Ottawa, Canada.

Mawdesley, C, 2002. Predicting cave initiation and propagation in block caving mines. PhD thesis (unpublished), University of Queensland, Brisbane.

Suorieni, F T, 2010. The stability graph after three decades in use: Experiences and the way forward. 4, Taylor and Francis, *International Journal of Mining, Reclamation and environment,* 24:307-339.

Tollenaar, R N, 2008. Characterisation of discrete fracture networks and their influence on cavability and fragmentation, MSc thesis (unpublished), University of British Columbia, Canada.

Vyanzmensky, A, 2008. Numerical modelling of surface subsidence associated with block cave mining using a finite element-discrete element approach, PhD thesis, Simon Fraser University, Canada.

ANALYSIS AND DESIGN OF FACEROAD ROOF SUPPORT (ADFRS)

Mark Colwell[1] and Russell Frith[2]

ABSTRACT: This paper summarises the results of a research project whose goal was to provide the Australian coal industry with a longwall installation roadway design methodology that could be utilised by suitably qualified colliery staff. This goal has been achieved and the design methodology (and software package) is referred to as *Analysis and Design of Faceroad Roof Support (ADFRS)*. The intended benefits to underground operations, in the provision of this information and resource, are a safer and more productive workplace. ADFRS now fills the gaping void that existed in the Australian underground coal industry with respect to the geotechnical design and management of longwall installation roadways. In addition to the standard two-pass widening, ADFRS deals with all other aspects of installation roadway design, including faceroad intersections, stables and adjacent maingate and tailgate intersections. ADFRS is based on a sound mechanistic understanding of the roadway development and widening process and the design equations (with strong to very strong correlations) are fully consistent with measured roof behaviour. To the best of the authors' knowledge ADFRS is the first systematic faceroad design technique to be developed for any country's underground coal industry.

INTRODUCTION

The original intent of the project was to develop a roof support design methodology for wide roadways, where a wide roadway is generally considered to be greater than 5.5 m wide and in many cases is the result of widening an existing underground roadway (e.g. a longwall installation roadway). The widening of an existing underground roadway is prescribed as a high risk activity by the NSW Coal Mine Health and Safety Regulation 2006 requiring an approval under the NSW Coal Mine Health and Safety Act 2002 (refer Clause 49, Part 2 - Page 57). It is apparent that our industry fully appreciates that increasing roadway width results in a disproportionate decrease in stability and therefore a significant increase in safety and business risk.

However, during the data collection phase (initial year) of the project it was found that other than for longwall installation roadways, colliery records in relation to other types of wide roadways (e.g. drive head excavations) were generally incomplete (i.e. accurate roof support plans and/or monitoring information was not readily available). Fortunately this was not the case for most longwall installation roadways, particularly those widened in recent years, where quite detailed/accurate records were generally available.

Therefore it was decided to focus the research effort on longwall installation roadways (i.e. faceroads) so that the design methodology would (as best as possible) encompass all aspects of installation roadway design, including faceroad intersections, stables and adjacent maingate and tailgate intersections. Therefore the aim of this project became the development of a roof support design methodology for longwall installation roadways encompassing all aspects of their formation.

BACKGROUND

In relation to other strata control issues, such as coal mine pillar and roof support design (for standard roadway widths), there has been comparatively very little research undertaken in relation to the geotechnical design and management of longwall installation roadways. As a result, in terms of a satisfactory outcome, faceroads within Australia have been quite problematic and by way of example of the 207 cases associated with the two-pass dataset, 40 resulted in an unsatisfactory outcome involving the use of standing support, Polyurethane Resin (PUR) injection and/or high levels of remedial tendon support with two faceroads "lost" and having to be re-driven due to major roof falls. Another 33 of the 207 cases were considered manageable.

[1] *Principal, Colwell Geotechnical Services, markcolwell@bigpond.com*
[2] *Principal, Mine Advice Pty Ltd, russellfrith@mineadvice.com.au*

The authors were also aware of several other faceroads that were abandoned in recent years due to major roof falls however due to a lack of site specific information they could not be included in the database. Nonetheless *a failure rate* of approximately 20% is judged to be unacceptable. The authors' contend the principal reason for such a failure rate is the clear absence of suitable design equations that relate the required levels/type of roof support as a function of the competency (or some valid measure of the competency) of the roof and the horizontal stress acting across the roadway.

Due to the lack of reference material on the topic and to assist in achieving the goal of developing a roof support design methodology for installation roadways that can be effectively utilised at all Australian collieries, a comprehensive review of current practices associated with the design and management of longwall installation roadways was undertaken as a part of the study.

LONGWALL INSTALLATION ROADWAYS - CURRENT PRACTICE AND OUTCOMES

The vast majority of longwall installation roadways in the Australian underground coal industry are developed in two or more "passes" in order to form the final excavation width. For the majority of an installation roadway's length, it would be usual to form up an initial or 1st pass at the standard roadway width used at the mine (typically between 4.8 m and 5.5 m) and then strip out on one side (which can be either side of the roadway) to form the final roadway width of approximately 7.5 m to 12 m depending upon the size and length of the longwall face equipment.

The major advantage of forming up a wide roadway in two or more passes is that it allows the full range of roof conditions along the roadway to be exposed at a standard roadway width prior to stripping. Therefore the actual condition of the roof and the need for secondary tendon support (i.e. longer cables) prior to stripping can be reviewed on an informed basis and secondary support prior to stripping can usually be installed whilst the continuous miner is driving the adjacent bleeder roadway.

In terms of reviewing current practice, formulating/analysing the database and subsequently developing a credible design methodology some measure or statement of acceptable or unacceptable outcomes needs to be available. Furthermore in addressing the issue of success for an installation roadway, it is necessary to consider the operational context in which the safety of mine workers is taken as a mandatory requirement.

In overall risk terms it is clear that as per most other geotechnical design in underground coal mining, the general design requirement is for a suitably conservative level of roof support in the installation roadway while no more than is prudent from a risk-based perspective. Both optimistic under-support and highly cautious over-support carry significant business risks in the context of minimising the production outages between successive longwall panels.

In technical terms success or failure with respect to roof support design will be related to a roof stability outcome, accepting that this will have a consequent effect on mining operations as discussed above. As a roof support design study, the focus is on roof stability outcomes and the necessary operational responses in defining success and failure for longwall installation roadways.

In terms of a satisfactory outcome, ostensibly there really is only one definition, namely that the roof of the installation roadway behaved in such a way that there was no requirement to either trigger the Trigger Action Response Plans (TARP) or undertake remedial roof support measures in order to maintain its serviceability up to the time of longwall shield installation. This does not mean that the roof does not move or that time dependent creep effects do not occur following widening. Simply that the measured outcomes were tolerable in the context of the requirements of the installation roadway. Furthermore with respect to roof movement there are many instances where only the first level of the TARP is triggered and this generally simply requires greater observation/more frequent monitoring rather than the immediate introduction of remedial support.

In addition, from a practical point of view, there are instances where a low (or even moderate level of remedial support in isolated areas along a roadway) is tolerable dependent on the type of roadway and its use. For example a low or moderate level of remedial support in isolated areas along a tailgate (while of course never desirable) may be tolerable and/or have minimal/negligible effect on safety or productivity, as opposed to a belt road where the installation of remedial support about the belt is difficult, will inevitably cause production stoppages and is essentially unacceptable.

With respect to a longwall installation roadway, in this regard it is far more akin to a tailgate than a belt road. The critical issue is that remedial support, if required, is installed to further reinforce and control a roof that is still largely self-supporting and that the roof has not softened to an extent where a roof fall is imminent. Therefore the use of standing support in an installation roadway or remedial cables to "suspend" a softened installation roadway roof would be an unacceptable outcome in terms of a proactive design methodology.

Another important aspect of an installation roadway is the "stand-time" between widening and the setting of the longwall shields. For a very short "stand-time" following widening, significant time dependent creep effects in the roof may be an acceptable outcome if it allows the construction period to be reduced by the use of less roof support. Conversely for a roadway with a stand-time of say six months, any significant long-term creep effects would probably be unacceptable from an operational perspective. Such stand-time considerations will clearly have an impact upon the degree of conservatism used in the overall roof support design.

In terms of an unsatisfactory outcome relating to roof stability, these are varied and carry a significant range in terms of operational consequences:

(i) The need to install unplanned/remedial roof support to arrest unacceptable rates/levels of roof movement following widening, in the context of whether they may lead to unacceptable roof deterioration at some point in the future if left unabated.

(ii) The need to erect standing support in the roadway to arrest what has been predicted to be an imminent roof fall based on either physical roof conditions in the roadway or high measured rates of movement. Usually this cannot be initially achieved with long tendon type roof support due to the time period required to install such support and the capacities needed to control "dead weight roof loads" in a wide roadway. Once set in place though, such standing support will need to be removed, hence significant other remedial support measures (e.g. cable slings, extra long tendons or strata consolidation via resins or grouts i.e. PUR) will be required before this can occur.

(iii) The occurrence of a roof fall is obviously the worst case operational outcome. It will require that either (a) the fall is recovered or (b) a replacement installation roadway is driven. This brings into question issues such as how to recover a major roof fall safely and the need to then back-fill the roof cavity so as to allow longwall shields to be set to the roof, against the time and cost of driving a replacement roadway. The business consequences of a major roof collapse in a longwall installation roadway are always severe.

Clearly the operational consequences involved can vary from relatively minor in the case of (i) if the installation of the extra support does not delay the start-up of the longwall, to major in the case of (iii).

Remembering then that many installation roadways are formed up on the critical path for the start-up of the next longwall and that in itself, an overly conservative roof support system may be an unacceptable mining outcome, risk-based considerations may allow some likelihood that point (i) occurs in a portion of the installation roadway, this being a trade-off between minimising the time required to form the roadway and the downside risks should it not be fully stable following widening. However neither points (ii) or (iii) can be tolerated from either a safety or business consequence perspective, hence the roof support design must be highly reliable in terms of their prevention.

Based on the preceding discussion and in terms of the database, the roadway condition (or section thereof) was assessed both subsequent to 1st pass drivage and after the faceroad was fully widened utilising the following three criteria based categories:

1. Satisfactory - is where the faceroad development went according to plan and while there may be a low level or infrequent triggering of the TARP, essentially no remedial support was required.
2. Manageable - is where the TARP is being triggered on a more frequent basis and/or there is a need for low to isolated moderate levels of remedial tendon roof support.
3. Unsatisfactory - is where a roof fall or faceroad abandonment has occurred, where PUR or standing support is required and/or where significant levels of remedial tendon roof support is required.

THE INDUSTRY REVIEW

The aim of the industry review is to:

1. Construct both a contemporary and historical database of longwall installation roadway (i.e. faceroad) performance and,
2. Utilise this information to determine the significant predictors of faceroad performance.

The data collection phase of the project predominantly took place during 2010 with faceroad information collected from 26 longwall operations involving all the major coalfields. Information associated with 162 faceroads was reviewed in terms of completeness and accuracy for inclusion in the final database. Unfortunately on many occasions it was not possible to fully verify support patterns, levels of roof movement and/or remedial support measures where required. Based on the quality and completeness of the information provided, this resulted in 123 case studies suitable for inclusion in the project database. These 123 case studies have generated:

- 169 standard widening cases ranging in width from 7.5 m to 9.5 m;
- 160 stables (i.e. shearer, maingate and tailgate stables) ranging in width from 7.7 m to 12 m;
- 30 faceroad intersections;
- 64 maingate/tailgate intersections adjacent to the faceroad.

A standard widening case is where after development of the initial roadway (i.e. the 1st pass of the faceroad) there is only one further drivage sequence referred to as the 2nd pass. The standard widening will account for the vast portion of the faceroad; however there are instances associated with a number of the case studies where the roof properties change resulting in variable behaviour and/or requiring variable levels of support along the length of the faceroad generating two or more standard widening cases for the one case study.

With respect to the stables, it was not uncommon that the formation of this section of the faceroad involved three and even up to four passes. In terms of the shearer stables, where a shearer stable was removed from or away from the influence of the maingate/tailgate intersections (i.e. it is not a maingate or tailgate stable) 38 of these 54 faceroad cases were formed by a 1st and 2nd pass sequence. Therefore these 38 shearer stable cases can be readily combined with the 169 standard widening cases in terms of the statistical analyses as they are formed on simply a two pass basis (i.e. 207 two pass cases).

During the site inspections information was collected on factors affecting faceroad performance including geometric details, *in situ* and mining induced stresses, roof and floor properties, as well as the ground support patterns which includes the type, placement, timing and quantity of roof and rib support installed (including remedial support where required). All available monitoring information as well as TARP related information was also collected. Where stress relief roadways were utilised this was noted and the effect on faceroad performance was assessed.

In addition, discussions were held with colliery personnel to ascertain how current faceroad performance compared to past experience. On many occasions this resulted in a detailed description of the gradual development of the faceroad ground support/monitoring/TARP systems currently employed, which allowed for a greater appreciation of some of the difficulties faced by the collieries satisfactorily managing faceroad behaviour. The collection of this information also allowed for a thorough understanding of the current faceroad design techniques employed in the Australian underground coal industry.

Construction of the database

Based on a literature review, the authors' own experience and discussions with colliery personnel, the following are assessed to be dominant factors influencing faceroad behaviour for which data was collected:

1. Structural integrity of the roof and floor;
2. Geometry (i.e. roadway width, height and drivage direction for each pass, cover depth and pillar size where a bleeder or stress relief roadway is driven);

3. The ground support systems employed (roof and rib);
4. *In situ* and mining induced stress;
5. TARP;
6. Stand Time (time in days between final widening and installation of longwall supports).

In addition to collecting information concerning the factors affecting faceroad behaviour, all available monitoring information (i.e. extensometry data) was also collected to assist in assessing faceroad performance (i.e. The Outcome). The database includes the following broad input and/or output categories:

- General
- Roof and floor details (i.e. identification of geotechnical units, rock mass ratings and material properties)
- Geometry
- Roof and rib support hardware and patterns
- Roof support ratings
- *In situ* stress parameters
- Where applicable the additional abutment stress from the previous longwall panel
- Analytical Model for Coal Mine Roof Reinforcement Factor of Safety (AMCMRR FOS) Values in relation to 1st pass drivage - refer Colwell and Frith (2010)
- Measured roof displacements
- 1st pass roadway condition
- Fully widened roadway condition

Rock mass classification systems

In developing a roof support design methodology for longwall installation roadways it was decided to assess/calculate, record and "test" all the readily available Rock Mass Ratings/Classification Systems utilised in the Australian underground coal industry for roof support design as a part of the database analyses. By far the most commonly used index is the Coal Mine Roof Rating (CMRR) which is specific to the primary bolted interval. Via the various ALTS research projects (Colwell, 1998; Colwell, *et al.*, 2003; Colwell and Frith, 2009; Colwell, 2010) it has been clearly demonstrated that the CMRR can be successfully used for roof support design purposes at all Australian collieries.

In addition to the CMRR, at many collieries the average Uniaxial Compressive Strength (UCS) of the roof (over various distances above the roof line) is contoured and at some collieries (e.g. Crinum - Payne, 2008) the average UCS is utilised on a site specific basis to specify levels of roof support. On most occasions the UCS is derived from sonic velocity logs where sonic velocity has been correlated with laboratory UCS values.

Another rock mass classification index which is sometimes utilised is the Roof Strength Index (RSI, refer Stam, *et al.*, 2012). The RSI is once again calculated over various distances above the roof line and is the average UCS divided by the vertical stress (i.e. RSI = Average UCS/σ_V). As yet no industry wide based roof design tool/methodology has been successfully demonstrated in using Average UCS or RSI.

In recent years another rock mass classification index has been proposed namely the Geophysical Strata Rating (GSR) having been developed with the funding support of ACARP. Hatherly, *et al.,* (2009) suggest that the GSR delivers results that are commensurate with CMRR values (or more to the point the Unit Rating values where the Unit Ratings, for the individual rock units, are essentially the "basic building blocks" of the CMRR). It should be noted that a GSR value is actually calculated every 5 cm to 10 cm (dependent on the geophysical logs) along the section of the borehole under review, therefore once the rock unit has been identified an average GSR for the unit is calculated.

Via ACARP Project C17009 (Medhurst, *et al.*, 2010) the GSR was extended to allow for the assessment of coal roof. This is extremely important as in the Australian underground coal industry there is currently and historically an abundance of coal roofs or mine roofs with a significant percentage of coal i.e. Angus Place, Austar, Broadmeadow, Dartbrook, Dendrobium, Elouera, Moranbah North, Newlands, North Goonyella, Springvale, Ulan, United and West Wallsend collieries. All these collieries are contained within the ALTS database and all except Elouera and Dartbrook (which have closed) are contained in the database associated with this project. In terms of coal as a rock unit, it comprises approximately 40% of all the rock types within the ALTS and ADFRS databases (i.e. as compared to sandstones, mudstones, shales etc).

Therefore including the GSR within the analyses associated with this project was considered to be most worthwhile. Also the real test of any rock mass classification index when used for ground support design is the strength of the correlations with respect to ground support levels. This can only be truly ascertained if the index is tested within an industry wide database and the GSR was yet to be tested in this manner. If the GSR can find the same widespread application and acceptance as for example the CMRR has (in terms of roof support design), then our industry could take full advantage of available borehole information (i.e. geotechnical/geophysical logging and geomechanical testing of the core) for geotechnical design and evaluation purposes.

STATISTICAL ANALYSES

The statistical techniques of linear and logistic regression were utilised in examining the database. Linear (or in this instance multiple) regression is routinely used where the dependent variable (i.e. outcome) is continuous rather than categorical. Multiple regression was successfully utilised throughout the various ALTS research projects when assessing the required level of roof support (i.e. PRSUP and GRSUP) in terms of the CMRR and resultant horizontal stress acting across the roof.

The Primary Roof Support (PRSUP) Rating is a measure of the bolting capacity (kN) per square metre of roof normalised to the primary bolted interval and includes all bolt/tendon support that is installed off the continuous miner or mobile bolter as part of development. The GRSUP Rating incorporates all bolt and longer tendon roof support installed within the roof of a roadway into a single rating, regardless of when the roof support is installed. This includes all roof bolts, longer tendons, cables and trusses.

The GRSUP is calculated in a similar manner to that of the PRSUP; in fact if no additional support is installed within the roof subsequent to that installed off the continuous miner or mobile bolter then GRSUP will equal PRSUP. For further information in calculating PRSUP and GRSUP the interested reader is referred to Colwell and Frith (2009) and Colwell and Frith (2012).

In relation to similar multiple regression analyses associated with the various ALTS projects all unsatisfactory cases are removed from the dataset, such that the resultant outcome (PRSUP and GRSUP) is based solely on satisfactory cases (e.g. belt road design) or in other instances where remedial action is more tolerable (i.e. productivity risk is lower) a combined satisfactory/manageable dataset is utilised. Similar analyses where conducted in relation to the various faceroad datasets combining the satisfactory and manageable cases.

A limitation of ordinary linear regression models is the requirement that the outcome is continuous rather than categorical. But many interesting dependent variables/outcomes are categorical - patients may live or die, people may pass or fail exams, coal rib lines may collapse or be stable, faceroad performance is satisfactory or unsatisfactory and so on. A range of statistical techniques have been developed for analysing data with categorical dependent variables, including discriminant analysis, probit analysis, log-linear regression and logistic regression.

Logistic regression allows for the classification of cases or observations into two (or more) populations based on an outcome, which is referred to as the dependent variable. Logistic regression is able to distinguish which parameters (referred to as the independent variables) are significant predictors of a particular outcome and to then rank and quantify the relative importance of these independent variables on said outcome.

Furthermore logistic regression can determine the most appropriate equation (in relation to those independent variables analysed) to act as a *boundary of separation* between the two populations in terms of the outcome. Within this study that equation is referred to as the *Discriminant Equation,* which can then

be used to predict the outcome based on the significant predictors. The statistical software package SPSS was used in relation to these analyses. The statistical component of Microsoft® Excel was utilised for the linear/multiple regression analyses and simple statistical analyses in terms of mean, standard deviation etc.

Linear (Multiple) regression analyses - two pass dataset

Due to space constraints associated with a conference paper it is only the two-pass dataset analyses that are presented herein. The interested reader is referred to Colwell and Frith (2012) for a full description of all database analyses including the maingate/tailgate stables, stables formed utilising a three or even four pass process and maingate/tailgate intersections adjacent to the faceroad.

The two pass (formation) faceroad dataset comprises 207 cases; with 134 considered satisfactory, 33 manageable and 40 assessed as unsatisfactory. With respect to the linear regression analyses only the satisfactory and manageable cases are combined in terms of assessing appropriate levels of roof support. Based on the definition of a manageable case (i.e. "it is where the TARP is being triggered on a more frequent basis and/or there is a need for low to isolated moderate levels of remedial tendon roof support"), it is considered appropriate to include such cases as the outcome will represent an appropriate level of support where a properly considered TARP is in place.

The research associated with the ALTS 2006 project (Colwell and Frith, 2009; Colwell, 2010) clearly indicated that the principal geotechnical drivers which, in combination, essentially dictate the level of roof support required to maintain a stable roof both on development and during longwall extraction are the structural integrity of the immediate roof (as measured by the CMRR) and the resultant stress acting across the roof (σ_R).

With respect to an installation roadway the resultant horizontal stress acting across the roof (i.e. normal to the direction of drivage) is taken to be σ_R-Dev and is estimated by utilising the ratios of the major and minor horizontal stress to the vertical stress (i.e. σ_H:σ_v and σ_h:σ_v respectively) and the angle of σ_H to the direction of drivage while taking into account the stress ratios which best represent the roof section being reviewed.

The initial series of linear regression analyses reviewed total roof support levels in terms of the fully widened section of faceroad under review. In terms of a rock mass classification index the roof support analyses associated with the various ALTS research projects utilised the CMRR as a measure of the structural integrity of the roof and therefore the analyses essentially relate to the primary bolted interval and this is predominantly why the GRSUP calculation is normalised to the bolted interval. With respect to this dataset the primary bolt length ranged from 1.8 m to 2.4 m with an average length of 2.0 m.

In terms of this project it was recognised that for a fully widened faceroad (as compared to a standard roadway width of 4.5 m to 5.5 m) a greater distance into the roof should be reviewed. Therefore in addition to assessing the CMRR (being specific to the bolted interval) for this series of analyses set distances of 2 m, 3 m and 5 m into roof were also reviewed using average values for UR, GSR, RSI, UCS and load bearing capacity (P, MPa). The estimate for σ_R-Dev was also revised in terms of the distance and rock types within the section of roof under review. In keeping with the rationale of normalising the calculation of the GRSUP to the bolted interval (i.e. distance over which the CMRR is calculated), for the greater distances of 3 m and 5 m any longer cables were be normalised to those respective distances.

In terms of 167 combined satisfactory/manageable cases associated with the two pass (formation) faceroad dataset. It was clear from these analyses that the Average UR is by far the superior rock mass classification index with respect to the r^2 value (i.e. strength of correlation in terms of the regression equation).

The analyses also indicate it is beneficial to utilise a roof section greater than the primary bolted interval in assessing the total level of roof support required to maintain satisfactory/manageable faceroad behaviour. The strongest relationship is for GRSUP as a function of Average UR and σ_R-Dev calculated over a roof section 5 m above roofline. Based on the multiple regression analyses the following relationship was found:

$$\text{GRSUP Total}_{5m} = 490.37 \times e^{-0.0427 \text{ Average UR5m}} \times e^{0.0345\ \sigma\text{R-Dev}} \quad (1)$$

The above relationship is illustrated in Figure 1.

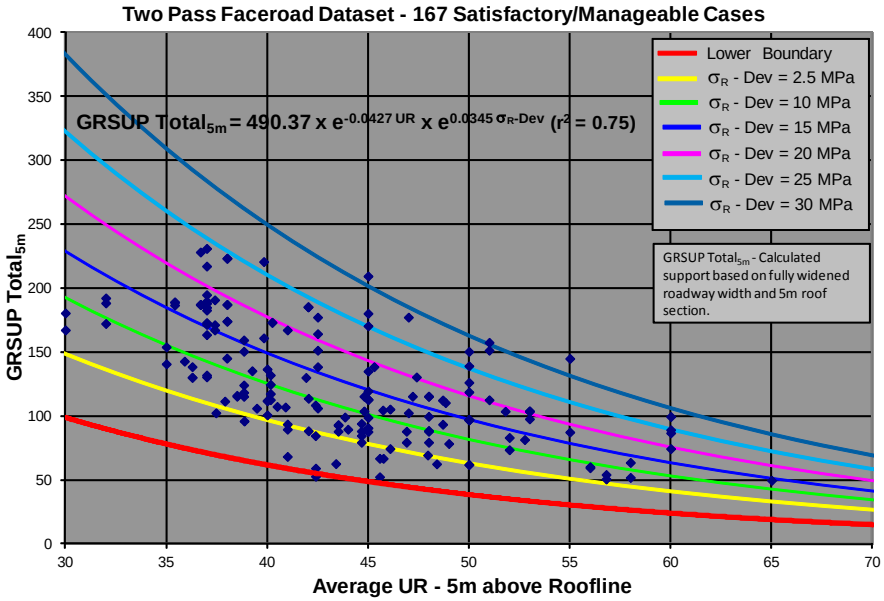

Figure 1 - GRSUP $Total_{5m}$ v's average UR and σ_R-Dev - two pass dataset

Another important aspect in relation to faceroad roof support design is to determine the appropriate level of roof support to install within the 1st pass drivage prior to widening. It was decided to plot GRSUP calculated over a 5 m roof section for both 1st pass and with respect to the fully widened roadway width (i.e. GRSUP $Total_{5m}$).

Figure 2 indicates that approximately 65% of the total roof support capacity installed within the fully widened faceroad (as measured by GRSUP 1st $Pass^*_{5m}$ with respect to GRSUP $Total_{5m}$) is installed within the 1st pass drivage prior to widening to achieve a satisfactory/manageable outcome. The statistical analyses associated with the combined 167 satisfactory/manageable cases clearly indicate that a viable design methodology for longwall installation roadways can be developed.

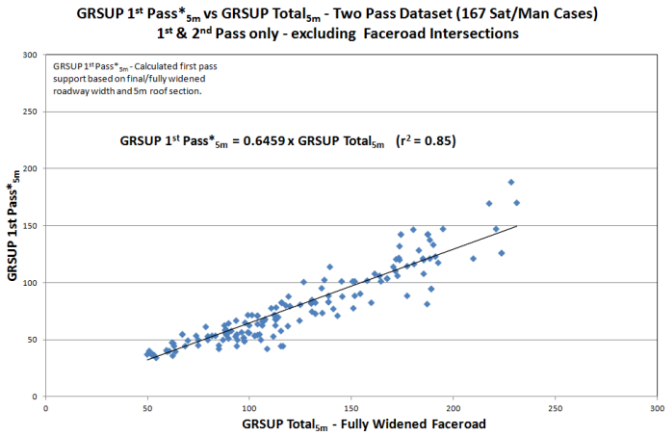

Figure 2 - GRSUP 1st $Pass^*_{5m}$ v's GRSUP $Total_{5m}$ - two pass dataset

Logistic regression analyses - two pass dataset

To undertake binomial logistic regression with a multinominal outcome (i.e. satisfactory, manageable and unsatisfactory), it was decided to eliminate the manageable cases (i.e. 33 cases) and compare the satisfactory cases (i.e. 134 cases) to the unsatisfactory cases (40 cases) thereby providing a dichotomous outcome. Therefore the resultant *Discriminant Equation* would potentially represent a design equation approximating a manageable outcome (i.e. effectively a *boundary of separation* between the two populations).

The uneven nature of the outcome (i.e. 134 satisfactory cases v's 40 unsatisfactory cases) limits the ability of most statistical techniques to discern an unbiased result. With respect to logistic regression a significantly greater weighting would be given to the satisfactory cases in terms of the resultant *Discriminant Equation*, which could potentially result in a design equation or methodology that does not adequately address the more difficult conditions.

However a facility exists within SPSS to weight cases and in this instance it was decided to weight the unsatisfactory cases by a factor of 3. This results in a simulated database (for analysis) of 134 satisfactory and 120 unsatisfactory cases. Numerous statistical analyses were performed on the two-pass data set. The interested reader is referred to Table 7.2 of Colwell and Frith (2012) which contains a sample of the various parameters utilised during these analyses (many more were assessed) and details the range as well as mean and standard deviation.

The two best predictors of the final outcome were the AMCMRR FOS values calculated in relation to the 1st pass against both buckling and compressive yielding of the roof material over a distance of 5m above the roof line and in relation to the 1st pass roadway width. When utilising an AMCMRR FOS value associated with the 1st pass drivage for the purpose of this study i.e. as an index/predictor of the fully widened roadway outcome to assist with the design process, it is considered far more practical in terms of the eventual design methodology to simply use one or the other index rather than both.

From a statistical point of view there was essentially no difference in relation to which FOS value was utilised, however from a geotechnical point of view the FOS calculated in relation to compressive yielding of the roof material is considered more appropriate as it limits the mechanical advantage applied within the load balance calculation by the yield strength of the rock units over the 5 m interval. The resultant *Discriminant Equation* incorporating AMCMRR $FOS_{5m\text{-}yield}$ is:

$$z = 3.339\ FOS_{5m\text{-}yield} - 4.745 \qquad (2)$$

The value z is referred to as the predicted log odds value. When z is less than zero one would predict/classify the case as unsatisfactory and when greater than zero the case would be predicted as satisfactory. Equation 2 successfully classified 105 of 120 weighted unsatisfactory cases (therefore in actual fact 35 of 40 unsatisfactory cases or 87.5% correct) and 107 of the 134 satisfactory cases (79.9% correct) for an overall classification success rate of 81.6%. Equation 2 can be rearranged so that the design variable $FOS_{5m\text{-}yield}$ relating to a manageable outcome can be calculated i.e. $FOS_{5m\text{-}yield}$ = 4.745/3.339 = 1.421

The above findings essentially indicate that if on the 1st pass $FOS_{5m\text{-}yield} > 1.421$ then it is more likely that the longwall installation roadway will be manageable following widening, however when $FOS_{5m\text{-}yield}$ = 1.421 this also means there is 50:50 chance of the outcome (i.e. fully widened roadway performance) being satisfactory or unsatisfactory.

It is extremely important to recognise that in this way $FOS_{5m\text{-}yield}$ associated with the 1st pass drivage is being used as a predictor of the eventual outcome and not as a Factor of Safety. To emphasise this point; in developing the design methodology $FOS_{5m\text{-}yield}$ is not referred to as a Factor of Safety, it is referred to as the 1st Pass Reinforcement Index or $RF_{5m\text{-}yield}$.

Further analyses were undertaken specifically relating $RF_{5m\text{-}yield}$ to other roof performance indices. For example Figure 3 plots the Surge (mm, being defined as the initial increase in vertical roof displacement post-widening) against $RF_{5m\text{-}yield}$, Figure 4 plots the Creep Rate (mm/d being defined as the vertical roof displacement rate subsequent to the initial Surge) against $RF_{5m\text{-}yield}$, while Figure 5 plots Height of Softening (HOS), which is defined as the distance into the roof where the measured displacement first exceeds 1mm, against $RF_{5m\text{-}yield}$.

With respect to Figure 4 it should be noted that in relation to the unsatisfactory cases there were two instances where there were falls and as such the creep rate was extremely high! In addition there were two other cases where creep rates of 8.33 and 18.44 mm/d were recorded requiring the use of standing support to avert a fall. So as not to overly increase the y-axis (and lose the visual detail for creep rates of < 0.5 mm/d), these four cases have been given a nominal creep rate of 2.5 mm/d.

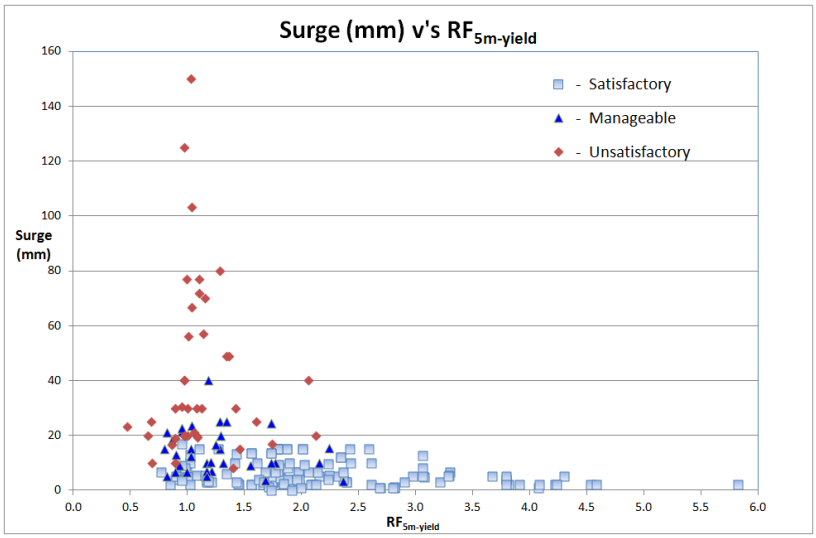

Figure 3 - Surge (mm) v's $RF_{5m\text{-}Yield}$

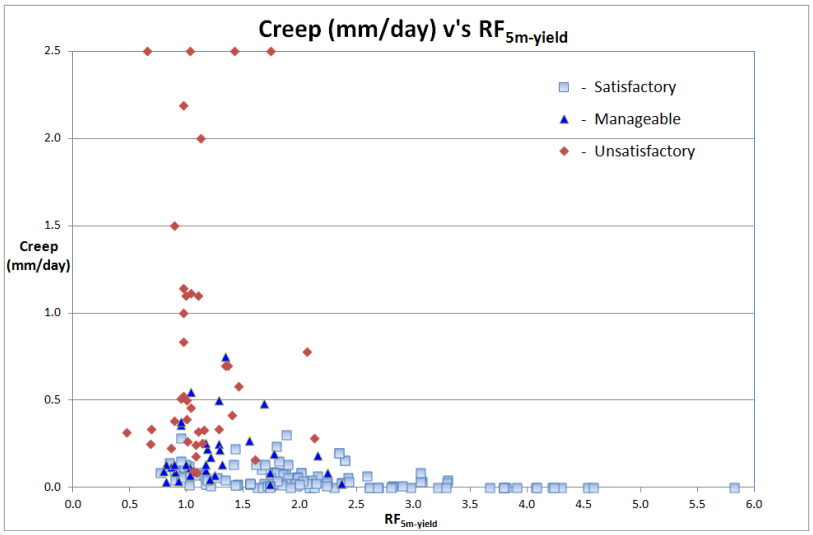

Figure 4 - Creep Rate (mm/d) v's $RF_{5m\text{-}Yield}$

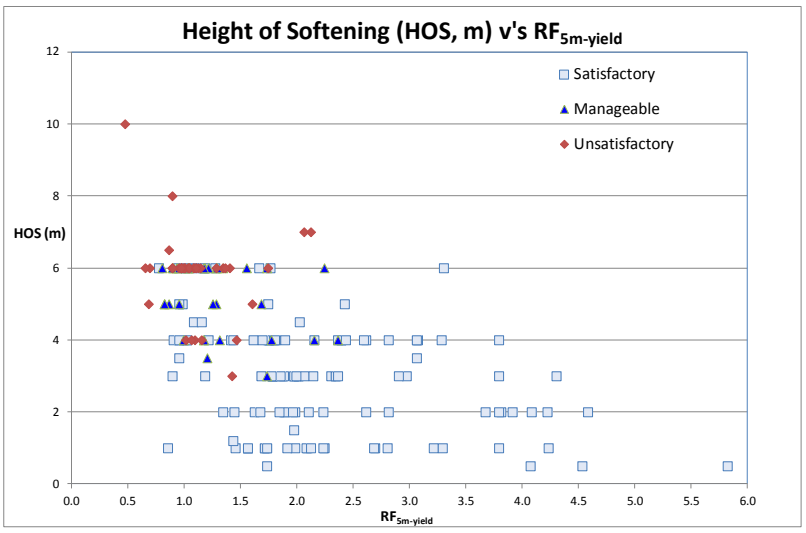

Figure 5 - Height of Softening (HOS, m) v's $RF_{5m\text{-}Yield}$

DISCUSSIONS

The linear (multiple) regression analyses clearly demonstrate that the principal geotechnical drivers which, in combination, essentially dictate the level of roof support required to maintain a stable roof are the structural integrity of the immediate roof and the resultant stress acting across the roof. This being totally consistent with previous research associated with the development of ALTS (Colwell and Frith, 2009) and essentially consistent with the findings of Thomas (2010).

The strength of the relationship between GRSUP $Total_{5m}$ as a function of the Average UR (over the first 5 m of roof) and σ_R-Dev (i.e. equation 1 and as depicted in Figure 1) would be considered strong to very strong with a correlation (i.e. r^2 value) of 0.75.

The logistic regression analyses in conjunction with the very simple mean and standard deviation analyses (reported in Table 7.2 of Colwell and Frith, 2012) as well as plotting $RF_{5m\text{-}yield}$ against other roof performance indices (refer Figures 3, 4 and 5) illustrate that the 1st Pass Reinforcement Index, $RF_{5m\text{-}yield}$ can be effectively utilised as a part of the design process.

Furthermore in relation to the level of reinforcement required with the 1st pass drivage prior to widening, Figure 2 very strongly indicates that approximately 65% of the total roof support capacity installed within the fully widened faceroad (as measured by GRSUP 1st $Pass^*_{5m}$ with respect to GRSUP $Total_{5m}$) should be installed within the 1st pass drivage prior to widening to achieve a satisfactory/manageable outcome. Furthermore it was found that on average 64.5% was utilised with respect to the satisfactory cases and 61.9% in terms of the manageable cases, while there was a significant drop to 54.2% in relation to the unsatisfactory cases.

All of this information, in addition to the very strong relationships that already exist within ALTS (so as to achieve satisfactory standard width roadway conditions while accounting for variances in the structural integrity of the roof and applied stress), indicated that a robust design methodology for installation roadways would be developed. This proved to be the case resulting in ADFRS (Colwell and Frith, 2012).

CONCLUSIONS

In relation to other strata control issues, such as coal mine pillar and roof support design (for standard roadway widths), there has been comparatively very little research undertaken in relation to the geotechnical design and management of longwall installation roadways. As a result, in terms of a satisfactory outcome, faceroads within Australia have been quite problematic and by way of example of the 207 cases associated with the two-pass dataset, 40 resulted in an unsatisfactory outcome involving the use of standing support, PUR and/or high levels of remedial tendon support with two faceroads "lost" and having to be re-driven due to major roof falls.

The authors were also aware of several other faceroads that were abandoned in recent years due to major roof falls however due to a lack of site specific information unfortunately they could not be included in the database. Nonetheless *a failure rate* of approximately 20% is judged to be unacceptable. The authors' contend the principal reason for such a failure rate is the clear absence of suitable design equations that relate the required levels/type of roof support as a function of the competency (or some valid measure of the competency) of the roof and the horizontal stress acting across the roof.

Thomas' (2010) findings in a way essentially represented our industry's state of empirical knowledge prior to this study. The strength of the relationships found by Thomas (2010) when plotting his roof support indices (RDI and SRDI) against a "*measure of the roof's propensity to buckle"* (being the SSR - Stress Strength Ratio) would, for geotechnical design, be considered weak to moderate at best with r^2 values of 0.499 and 0.325 respectively and reinforced the need for suitable design equations with strong correlations around which can be engineered a credible design methodology.

The design methodology resulting from this study is called *ADFRS* and now fills the gaping void that existed in the Australian underground coal industry with respect to the geotechnical design and management of longwall installation roadways. ADFRS is based on a sound mechanistic understanding of the roadway development and widening process and the design equations (with strong to very strong correlations) are fully consistent with measured roof behaviour.

Over the last two decades (particularly subsequent to the findings associated with the Moura disaster in 1994, i.e. Windridge, 1995), many aspects of strata management have evolved, such that risk management has become the *"core"* of the strata management process at most Australian collieries. This is borne out with the advent of strata management plans, roadway and longwall hazard plans and in relation to ground support, the categorisation of various zones as a part of the mine manager's support rules.

The ADFRS Design Methodology has been formulated to complement the mine site risk management approach to strata control/management. However because there are factors affecting longwall installation roadway behaviour that are either specific to or more pronounced at an individual colliery, it is imperative that the ADFRS design recommendations, resulting in the formulation of a ground support design strategy, be assessed within the framework of a properly facilitated mine site risk assessment and that a properly considered TARP is in place prior to any development taking place.

REFERENCES

Coal Mine Health and Safety Regulation, 2006. Under the Coal Mine Health and Safety Act 2002. 2006. Published in Gazette No 189 of 22 December 2006, page 11553.

Colwell, M G, 1998. Chain pillar design - calibration of ALPS. Final Report - ACARP Project C6036, 67p.

Colwell, M G, 2010. Pillar design procedures and research methodologies - can there or should there be a unified approach? In *Proceedings of the 2nd Australasian Ground Control in Mining Conference: Ground Control in Mining: Technology and Practice*: Sydney 23 - 24 November 2010, pp 67-77.

Colwell, M G, Hill, D J and Frith, R C, 2003. ALTS II - A longwall gateroad design methodology for Australian collieries. In *Proceedings of the 1st Australasian Ground Control in Mining Conference*: Ground Control in Mining: Technology and Practice: Sydney 10 - 13 November 2003, pp 123-135

Colwell, M G and Frith, R, 2009. ALTS 2009 - A 10 year journey. In *Proceedings of the 9th Underground Coal Operator's Conference*, Wollongong NSW, pp. 37-53. http://ro.uow.edu.au/coal/70/.

Colwell, M and Frith, R, 2010. AMCMRR - An analytical model for coal mine roof reinforcement. In *Proceedings of the 29th Conference on Ground Control in Mining*. Morgantown West Virginia University, pp 38 - 45. http://icgcm.conferenceacademy.com/papers/detail.aspx?subdomain=ICGCM&iid=279.

Colwell, M and Frith, R, 2012. Analysis and design of faceroad roof support (ADFRS) - a roof support design methodology for longwall installation roadways. *Final Report - ACARP Project C19008*, 153p.

Hatherly, P, Zhou, B, Peters, T and Urosevic, M, 2009. Detailed geological characterisation from seismic data. *Final Report - ACARP Project C15018*, 39p.

Medhurst, T, Hatherly, P, Zhou, B and Ye, G, 2010. Application of the geophysical strata rating in production settings. *Final Report - ACARP Project C17009*, 46p.

Payne, D, 2008. Crinum Mine - 15 Longwalls in Weak Roof, What did we Learn? In *Proceedings of the 8th Underground Coal Operator's Conference*, Wollongong NSW, pp. 22-43. http://ro.uow.edu.au/coal/2/.

Stam, S, Guy, G and Gordon, N, 2012. Back analysis of roof classification and roof support systems at Kestrel North. In *Proceedings of the 12th Coal Operator's Conference*, Wollongong NSW, pp 43-52. http://ro.uow.edu.au/coal/389/.

Thomas, R, 2010. The design and management of wide roadways in Australian coal mines. In *Proceedings of the 29th Conference on Ground Control in Mining*. Morgantown West Virginia University, pp 283–293. http://icgcm.conferenceacademy.com/papers/detail.aspx?subdomain=ICGCM&iid=325.

Windridge, F W, 1995. Wardens Inquiry Conducted pursuant to Section 74 of "The Coal Mining Act 1925". Report on an Accident at Moura No 2 Underground Mine on Sunday, 7 August 1994.

MANAGEMENT OF SUBSIDENCE AT THE TASMAN AND ABEL MINES - ISSUES AND OUTCOMES

Steve Ditton[1] and Tony Sutherland[2]

ABSTRACT: Tasman and Abel Mines are underground pillar extraction coal mines located to the west of Newcastle, NSW. Tasman mine extracts coal from the Fassifern Seam in the Upper Newcastle Coal Measures and Abel Mine operates in the Upper Donaldson Seam to the north in the Tomago Coal Measures. Each mine apply a range of partial to total pillar extraction techniques depending on allowable impact limits to a broad range of sensitive surface features such as cliff lines, Schedule 2 creeks, Hunter Water lines, public recreation areas and walking tracks, broadcasting and 132/330 kV transmission towers, highly significant aboriginal heritage sites and an operating cattle agistment business. This paper will discuss the mine management responses required to deal with delayed softening of claystone floors, optic fibre cable relocation, irregular surface cracking and how surface and subsurface monitoring techniques were applied to validate subsidence predictions and modify mine design layouts to meet the required performance measures.

INTRODUCTION

This paper discusses the management of mine subsidence control issues and impact outcomes from the development application stage through to the implementation of the Subsidence Management Plans (SMP) at the Tasman and Abel underground coal mines. Both mines are underground bord and pillar mines owned and operated by Donaldson Coal Pty Ltd (a subsidiary of Yancoal Australia Group). The mines are located 20 km west of Newcastle, NSW (Figure 1).

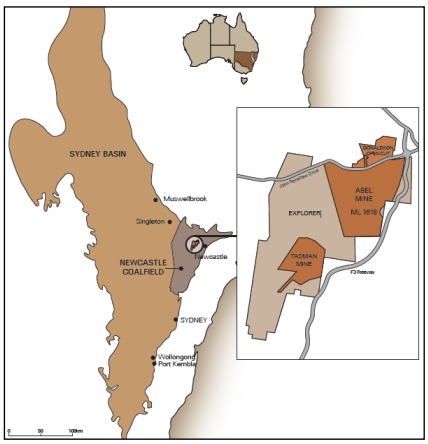

Figure 1 - Location of Abel and Tasman mines

Tasman mine was granted development consent by the Department of Planning in 2004. The mine commenced in 2006 and secondary extraction began in the Fassifern Seam in 2008. The 975 000 t/a consent limit Run Of Mine (ROM) coal is transported by road 20 km to Bloomfield coal preparation plant for processing and subsequent rail transport to the port of Newcastle for export. The Duncan Method of partial pillar extraction commenced in October 2008 with ten out of 14 pillar extraction panels extracted successfully using this technique. Abel mine received project approval in 2007 and is approved to mine up to 4.5 Mtpa. Abel mines the Upper Donaldson seam using predominantly total pillar extraction techniques below semi-developed rural land in the Black Hill area.

The overall successes of both projects have been reviewed in regards to (i) the planned mining layouts and actual extraction layouts approved by the Department of Trade and Investment, Regional

[1] *Principal Geotechnical Engineer - Ditton Geotechnical Services Pty Ltd, Australia, Email: steve.dgs@westnet.com.au, Phone: 0249209798*
[2] *Technical Services Manager Underground Operations - Donaldson Coal Pty Ltd, Australia, Tony.Sutherland@gcl.com.au, M:0407 239 820*

Infrastructure and Services (DTIRIS), and (ii) the achievement of impact limits defined within the performance measure constraints provided in the project approval. The influence of geological hazards (structure and wind blast), latent soft floor conditions, surface topography and stakeholder issues on the mining layouts is discussed.

TASMAN MINE

Geological conditions

The Fassifern coal seam working thickness is typically 2.2 m to 2.5 m. Seam floor consists of 4 m of coal interbedded with moisture sensitive claystone/carbonaceous shale units. The upper roof is characterised by regular massively-bedded units including a consistent unit of conglomerate greater than 20 m in thickness (Teralba Conglomerate). The immediate seam roof is 0.5 m to 1.4 m of shale overlain by two distinct roof types either side of a NW-SE trending transition zone across the centre of the deposit. On the northeast side of the transition zone the shale is overlain by 1.5 m to 2 m of coal, overlain by 6 m to 10 m of sandy claystone (Awaba Tuff). While on the southwest side of the transition zone, the shale is overlain by 0.1 m to 0.4 m of coal, overlain by 10 m to 15 m of sandstone and conglomerate. In addition, Several NW-SE and NE-SW striking normal faults/dykes traverse the site.

Surface conditions

The Sugarloaf Range is characterised by steep topography, cliffs and forest (Figure 2). The steep slopes range from 18^{o}-35^{o} and generally exist below 5-30 m high sandstone/conglomerate cliff lines and Sugarloaf Recreation Area and walking tracks. Man-made features on the site include three broadcasting towers, AAPT Optical Fibre Cable (OFC) and Telstra copper cabling, four TransGrid tension towers, Ausgrid 11 kV power line, public access road and several highly significant Aboriginal Archaeological sites. The proximity and visibility of the cliff-lines of the Sugarloaf Range State Conservation Area to Newcastle resulted in strict mine approval conditions regarding subsidence outcomes. Under the Tasman Development Consent, there is to be no impact on the high level cliff lines as a result of subsidence.

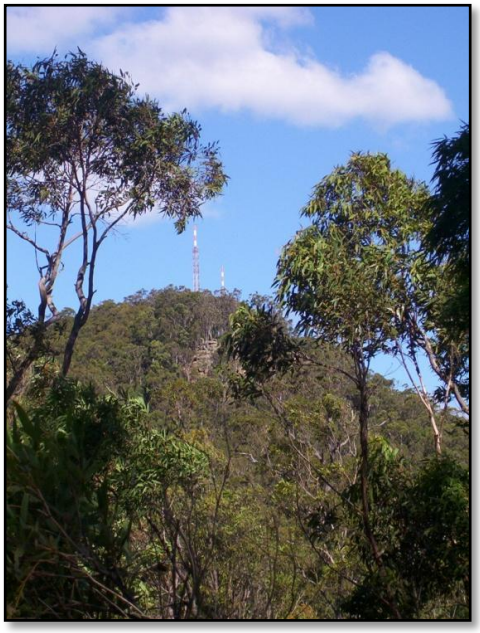

Figure 2 - Cliff lines and Broadcasting towers on the Western side of the Tasman mining lease

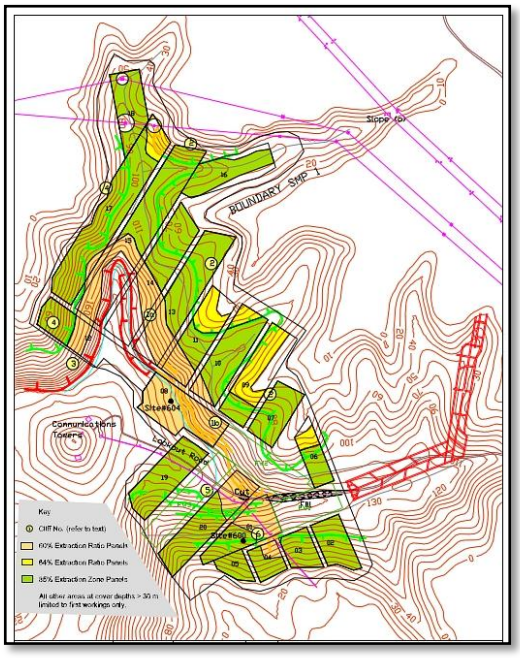

Figure 3 - Subsidence control zones for proposed Tasman mine plan in SMP application

Mine design constraints and proposed mining geometry

The performance criterion for subsidence impact set by DTIRIS was "negligible impact (i.e. no cracking) to the surface below areas with public access".

Level 1 to 4 subsidence control zones were developed for mine planning purposes (Figure 3) in increasing order of subsidence controls required for the existing surface features:

Level 1 - (Green) no mining constraints (total extraction allowed);

Level 2 - (Yellow) subsidence < 150 mm along shallow cover below ephemeral creeks, steep slopes and minor cliffs; Aboriginal Heritage sites; Optical fibre cable.

Level 3 - (Red) subsidence < 100 mm below Sugarloaf area, TransGrid Towers (tension).

Level 4 - (White) Subsidence < 3 mm and horizontal displacements < 20 mm at the Mount Sugarloaf Communication Towers (NBN, TransGrid and Broadcast Australia).

Level 1 areas were considered suitable for total pillar extraction (S_{max} = 60% Mining Height or 1.2-1.3 m). Level 2 and 3 areas required partial pillar extraction techniques that could also support abutment loading from Level 1 areas. Level 2 and 3 had similar subsidence constraints however, remnant pillar FoS ranged from 1.6 to > 2.11 respectively and required squat pillar geometries (i.e. w/h >5) for strain hardening response in yield. Maximum spans between remnant pillars of 27 m and cover depth > 55 m was assessed to avoid plug failures to the surface. First workings were allowed where > 30m of cover existed to minimise the likelihood of plug failures.

Subsidence predictions for the Modified Duncan Method were based on calibrated analytical models of roof-pillar-floor systems and the Voussoir beam analogue presented in Das (1998) and Diedrichs and Kaiser (1999).

Mining conditions encountered and subsidence response

The mining layout has evolved as subsidence data and mining experience was obtained during the course of the panels being mined.

The first panel in Level 1 area (1-North) was a total extraction panel with 106 m x 122 m spans and 60-120 m of cover (Figure 4). The panel was located to the east of the transition zone and subsequently had Awaba Tuff in the immediate roof. There was some initial concern raised by DTIRIS that the Awaba Tuff would fail (despite exploration bore core showing UCS values >40 MPa) requiring coring and testing of the immediate roof before second workings could commence. During mining, the Teralba conglomerate spanned between ribs and Awaba Tuff did not cave up to the Northern Seam (approximately 15 m above) as anticipated. At the completion of Panel 1 the potential for windblast was acknowledged as minimal subsidence was seen on the surface (i.e. S_{max} < 60 mm). This triggered the change in mining method to conventional partial pillar extraction and then the Modified Duncan system (Sutherland and McTyer, 2010).

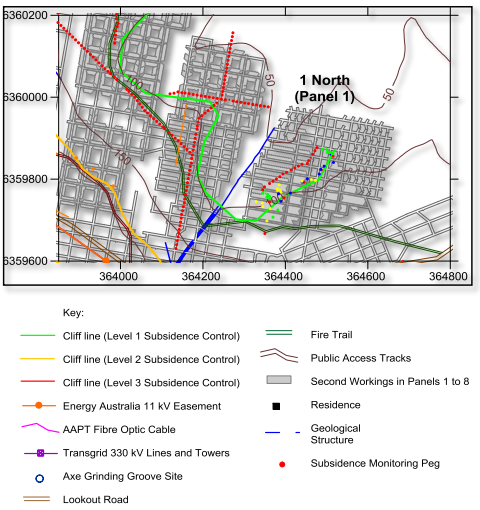

Figure 4 - 1-North total extraction panel in Level 1 area (with subsidence pegs and cover contours)

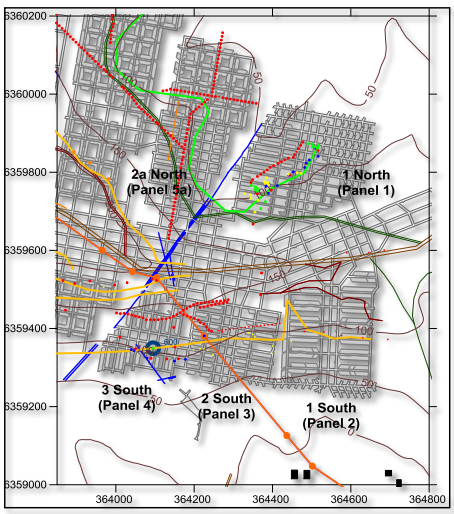

Figure 5 - 1, 2 and 3-South partial extraction panels in Level 2 area (with subsidence pegs and cover contours)

The next four panels (1-3 South and 2a-North) were located in Level 2 areas (below cliffs, power line, public access track and archaeological sites) and mined using single and double sided lifting partial pillar extraction. The maximum subsidence was < 150 mm for these panels, with tilts < 3 mm/m and strains < 1.5 mm/m. However, extraction ratios were marginal at ~60% (Figure 5).

The Modified Duncan (MD) partial extraction system was developed to maximise the number of extraction tonnes for each metre of panel development (Figure 6). Subsidence was expected to be < 150 mm for the cover depth range provided the FoS was > 1.6. The MD Pillar extraction method achieved greater extraction ratios (70-80%) with minimum remnant pillar width of 18 m (w/h >7.5) set by Continuous Miner (CM) length at cover depths < 110 m. Remnant pillars stripped on 4-sides were proposed to be increased up to widths of 27 m as cover depth and subsidence level controls increased below Mount Sugarloaf.

Floor heave and rib spall started to occur in the deeper panels on first workings to west of the transition line (light blue hatching in Figure 6). Claystone beds, 0.1 m to 0.4 m thick exist between moderate to high strength carbonaceous shales units in the first 4 m of floor. It was assessed that the claystone units in the first 1.2 m of floor had softened from 2-3 MPa to 0.15-1 MPa, based on underpass exposures, floor core and windy borer tests (Figure 7). Laboratory tests (Atterberg limits, moisture content and slake durability) indicate the claystone is highly sensitive to moisture and has similar plasticity/smectite minerology of Awaba Tuff in the floor of Cooranbong and Awaba collieries.

No deterioration of Awaba tuff in the roof has occurred in any of the partial extraction panels, with moderate strength tuff continuing to span 16 m to 27 m between remnant pillars above Panels 1-4 east of the transition.

First workings pillar stresses of 5-8 MPa in 3-North and 4-South Panels resulted in floor heave of 300 mm to 500 mm and rib spall up to 400 mm on one to four sides. Subsidence was measured at < 50 mm in heaved areas. Second workings were completed and subsidence was still < 150 mm for pillar stress between 8 and 19 MPa.

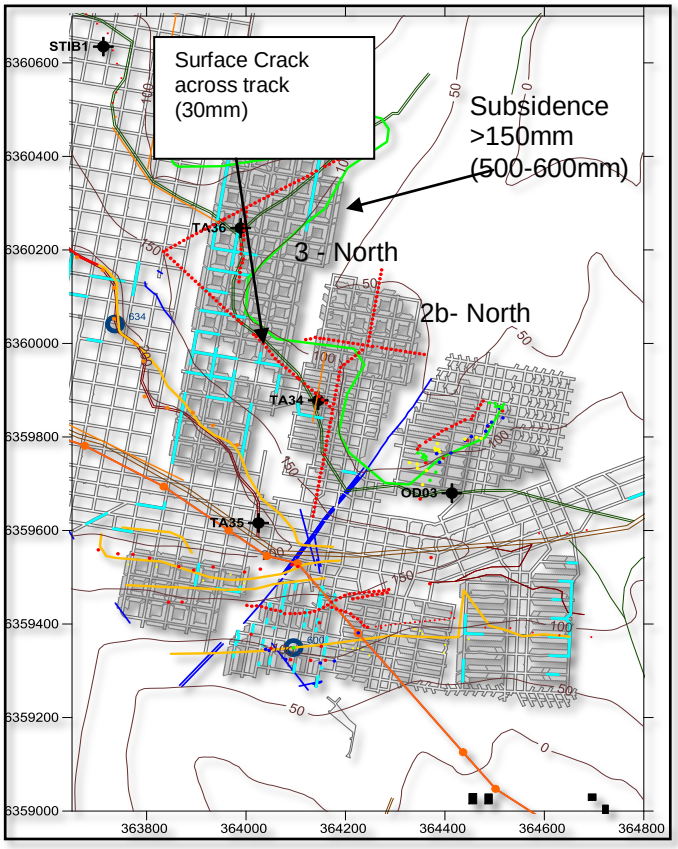

Figure 6 - Modified Duncan panels (2b-North, 3 North & 4 South) to west of transition zone and cover contours

3-North Panel was in a Level 1 Control area with 110 m of cover. The panel was commenced as a 4-heading 203 m wide panel and widened to 5-headings or 250 m where cover depths ranged from 60 m to 110 m. Over-wet floor conditions resulted in grubbing and belt road relocation. Subsidence was measured at 120 mm (12 months after extraction was completed) and 300 mm at 18 months after completion. Remnant pillar stress was 16 to 19 MPa based on Full Tributary Area Loading. Two years since panel completion, subsidence reached 521 mm (Figure 8) and subsidence development rates had slowed to < 5 mm/week from a peak of 12 mm/week. A surface crack of 30 mm width developed above the rib line and across a public access path after subsidence was >300 mm. No remediation was considered necessary and no slope instability or other impacts have occurred to-date above the panel.

Groundwater flows also increased in shallow areas of North-East and 4-West Panel (H=60 m to 110 m), which resulted in excessive floor heave and panel abandonment where grubbing failed to control affected roadways. 4-West Panel is in a Level-1 Control Area and has also developed subsidence > 150 mm six months after panel completion.

The subsidence increases observed above 3-North and 4-West panels are considered to be indicative of claystone floor unit softening that has resulted in pillar punching and lateral squeezing failures within the first 1.5 m of floor strata (Figure 9). The development of the 'time-dependant' subsidence behaviour (Figure 10) appears to have been driven by (i) pillar load increases from yielding conglomerate spans and (ii) reduction of floor strength due to softening of exposed claystone units and lateral strata confinement above 27 m wide roadways between remnant pillars. Marino and Choi (1999) discuss a similar mechanism in US bord and pillar mines after mine water ponding occurs for a period of time above moisture sensitive claystone).

The two-layered floor strength formula for lateral 'squeezing' failures below square pillars by Brown and Meyerhoff, (1969**)** was applied as follows:

$q_u = N'_{square} \times UCS_1/2 = [0.33(w/t) + 5.14]\ UCS_1/2$

where, N'_{square} = Modified bearing capacity coefficient for a square footing;
w = proposed stripped widths
UCS_1= weak claystone strength = 2 MPa (unsoftened) and 1 MPa (softened)

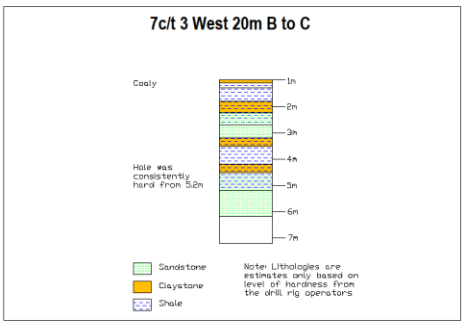

Figure 7 - Claystone units in first 4.5 m of floor

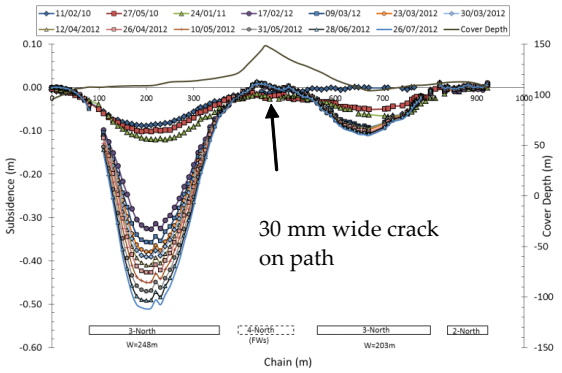

Figure 8 - Delayed subsidence above 3-North in Level 1 Area

Figure 9 - Moderate floor heave in 3-North panel (outbye)

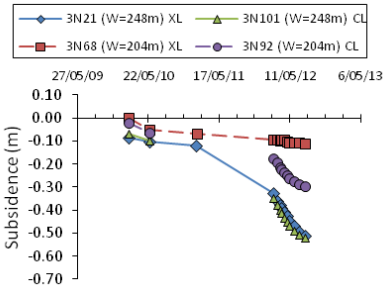

Figure 10 - Subsidence development above 3-North panel

The response to the floor softening was to reduce the remnant and barrier pillar stress in the last three panels within the Level 2 and 3 Control Zones as follows:

- Panel spans limited to 4-headings or 185.5 m to maintain spanning capability of Teralba Conglomerate.
- Pillar loads were estimated two ways (i) 0.8 x Full Tributary Area (FTA) loading on remnants and Effective Double Abutment (DA) loading on Inter Panel Barriers and (ii) FTA on all pillars.
- Increase remnant pillar widths by limiting stripping to single or double sided under worst case loading.
- Inter panel barrier pillars are not to be stripped to provide load sharing redundancy if remnant pillar floor yields.
- Minimum softened floor FoS of 2 in Level 3 Areas and 1.5 in Level 2 Areas.
- Maximum pillar stress of 9 MPa in Level 3 Areas and 12 MPa in Level 2 Areas.
- Bearing capacity of softened floor assessed to range from 16 to 18 MPa for FoS Calculation.
- Effective floor stiffness after softening reduced from 1.5 GPa to 0.7 GPa to estimate subsidence when floor FoS>1.5. Floor stiffness reduces to 0.15 GPa through back analysis when lateral squeezing occurs.

In regard to Level 3 subsidence control beneath the TransGrid towers, after several Modified Duncan panels were completed (and before the softened floor event in 3-North), confidence in the subsidence control method was high. It was considered unnecessary to modify the panels beneath the TransGrid towers or OFC if maximum subsidence was < 150 mm, tilts < 3 mm/m and tensile strains < 1.5 mm/m. The approach was initially accepted by TransGrid and Telstra.

As the TransGrid tower were tension towers, DTIRIS required that at least four first workings pillars with 39.5 m widths be left beneath each tower in partial pillar extraction panels (Figure 11). This decision was probably the correct one in light of the subsequent softening event above 3-North and 4-West Panels. To-date, the TransGrid Towers have performed well, with < 50 mm of subsidence and strains < 1 mm/m (Figure 12) measured under pillar stresses of 2 - 5 MPa.

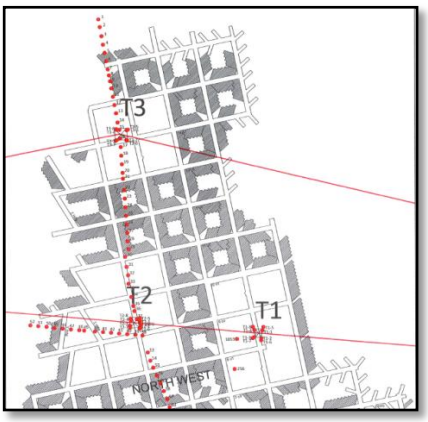

Figure 11 - North West panel extraction under the TransGrid towers

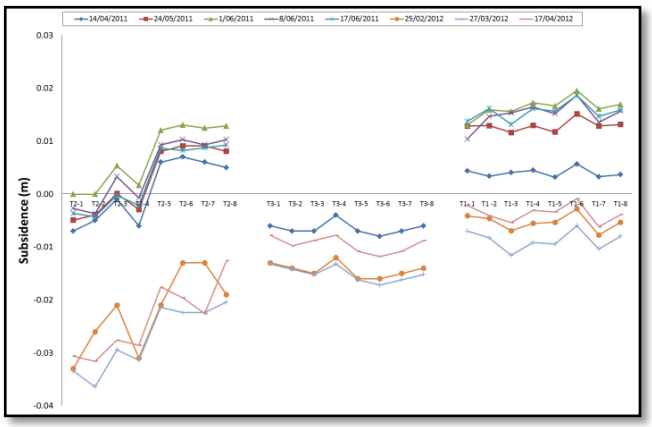

Figure 12 - TransGrid tower subsidence above NE/NW

Review of mine planning and subsidence

In hindsight, the over confidence in the Modified Duncan method was due to the focus on the Awaba Tuff and massive, spanning conglomerate in the roof, and the belief in the robustness of the pillar design by all parties involved. The floor heave and subsequent rib spall was generally ignored as subsidence above the first seven panels did not indicate any anomalous subsidence behaviour immediately after panel completion.

The proposed partial pillar extraction panels beneath the towers had remnant pillars with pillar stress 7.5-9.5 MPa and were unlikely to have resulted in the same magnitude of subsidence that has occurred above 3-North. To-date subsidence and strain below the OFC has been < 150 mm and < 1.5 mm/m with no signal losses incurred (Figures 13 and 14).

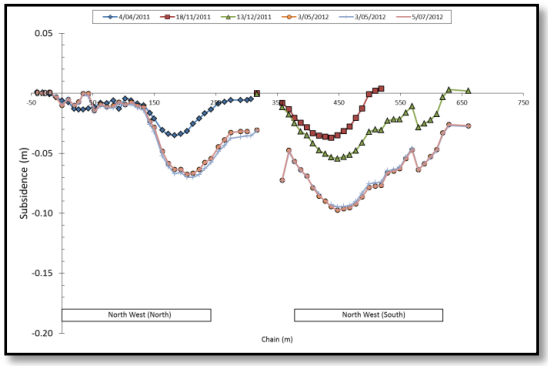

Figure 13 - OFC subsidence above NW panel

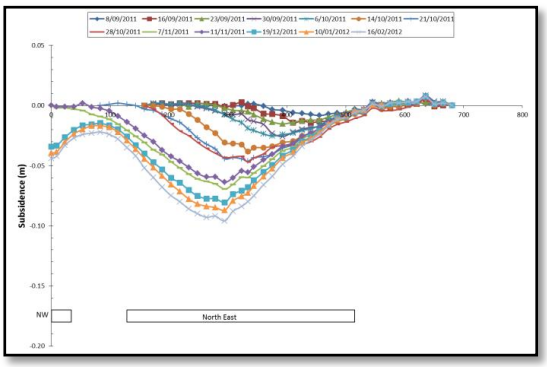

Figure 14 - OFC subsidence above NE panel

Subsidence exceedance response

The ramifications of the softening claystone floor in the shallower areas of the mine has resulted in significant adjustments required below the Level 2 and 3 Control areas beneath Sugarloaf Mountain (steep slopes, cliff lines and public recreation areas) where cover depth ranges from 150 m to 230 m.

Mining outcomes

Review of the potential softening and strength loss of the claystone units in the first three to four metre below the floor has required the remnant pillar stress in Level 3 Areas to be reduced to 8 MPa with a FoS of two against lateral squeezing failure of claystone beds. Level 2 Areas pillar stresses were reduced to 10-12 MPa with a FoS of 1.5.

The bearing strength for the multi-layered floor was estimated to range from 16 to 18 MPa with measured claystone unit thicknesses of 0.31 m to 0.44 m and softened UCS strengths of 1 MPa. This has significantly reduced the extraction ratios with only single sided stripped allowed beneath the Level 3 areas. The 39.5 m wide inter panel barriers between the 150 m wide panels have also been limited to first workings with no stripping allowed (see Figure 15).

A comparison between the originally proposed and approved SMP Panel remnant pillar FoS, pillar w/h and extraction ratios using the Modified Duncan Method are summarised in Table 1.

Table 1 - Tasman proposed v. approved mining outcomes using Modified Duncan method

Subsidence Control Area	Remnant Pillar Extraction Ratio (%)		Remnant Pillar Stress (MPa)		Remnant Pillar FoS		Remnant Pillar Floor FoS	
	Proposed	Approved	Proposed	Approved	Proposed*	Approved	Proposed^	Approved
1	75 - 85	75 - 85	9 - 19	9 - 19	1.27-3.51	1.20-2.54	0.64-1.95	0.64-1.95
2	69 - 78	57 - 75	12 - 18	8.3 - 9.8	1.60-1.90	2.57-3.10	1.11-1.81	1.51-1.79
3	64 - 69	46 - 48	12 - 16	8.4 - 8.6	2.14-2.24	4.54-4.78	1.15-1.25	2.06-2.12

* - 0.4 m of rib spall included. ^ - Based on softened floor conditions.

Far-field effects at the broadcasting towers have not been detected outside the proposed buffer zone defined by a 45^{o} Angle of Draw. Far Field Displacement (FFD) monitoring is conducted at the NBN tower after the completion of each panel. Post processing GPS has been utilised to provide the best possible accuracy on horizontal movements. Numerical modelling of yielded partial pillar and total pillar extraction panels (worst-case scenario) by DgS, 2007 indicated that far-field effects are likely to be < measureable survey tolerances.

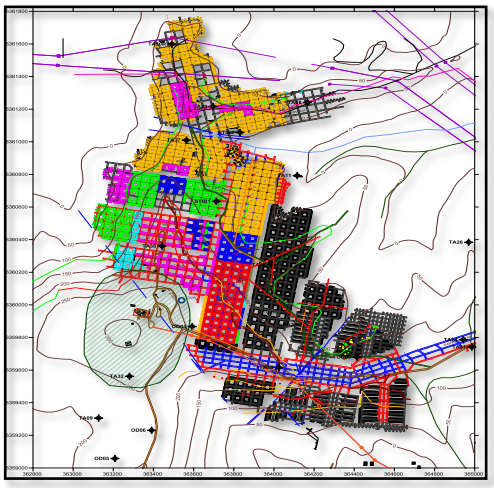

Figure15 - Final approved Tasman Mine layout

ABEL MINE

Mining at Abel has taken place in the first two SMP areas under a combination of land owned by Black Hill Land Pty Limited, the Catholic Diocese of Maitland - Newcastle, a narrow strip traversing the area owned by Hunter Water Corporation and ten private rural residential land holdings. A Boral Asphalt plant exists in the north eastern corner of the site. The current application seeks approval to mine coal by the pillar extraction method from the Upper Donaldson Seam at depths of cover ranging generally from 50 to 150 m.

Geological conditions

The Upper Donaldson Seam mined at Abel ranges in thickness from 1.6 m to 3.8 m. The mining height on first workings is typically 2.5 m with additional coal taken where possible when lifting off. The overburden comprises medium bedded sandstone and siltstone with a moderate strength mine workings coal roof and non-moisture sensitive carbonaceous shale floor. Several N-S striking faults exist within the mining area that were a significant hazard in regards to underground strata control.

Surface conditions

The surface conditions in the SMP Areas 1 and 2 include mild to moderate slopes (2^{o}-15^{o}), Schedule 2 Viney Creek and its tributaries, Optus OFC and Telstra copper cabling, One TransGrid tension tower and several TransGrid suspension towers (Figure 16) - the towers were already fitted with cruciform footings in the early 1980's in anticipation of future underground mining). There are also three significant Aboriginal Archaeological sites, Ausgrid 132 kV and rural 11 kV power lines and private access roads. Previous land use was a Steggles Chicken Battery Farm with several clay-capped areas of contaminated fill located around the site.

Figure 16 - Cruciform footings installed under the TransGrid 330 kV suspension towers in the early 1980's

Current land use is predominately cattle agistment with three rental properties (Catholic Diocese Land). The stakeholder requested protection for a cattle loading ramp and yard, with remediation of fences, access roads and water supply lines in a timely manner. A commercial/industrial subdivision is proposed after 2013 by Black Hill Land Pty Ltd. A primary or secondary school was initially proposed by the Catholic Diocese during the EA stage, however, no development application for it has been presented to Council at this stage.

Mine design constraints and proposed mining geometry

Under the project approval, effective subsidence (deemed to be 95% of predicted) as a result of secondary extraction had to be completed by June 2013. Therefore, the majority of panel extraction in SMP Area 1 and 2 had to be completed prior to this date. The potential for subsidence development due to standing pillar instability beyond this date was also required to be minimised.

Surface constraints to mining included Viney Creek and the TransGrid tension tower, both of which needed to be protected from subsidence impacts using an appropriate buffer zone.

Under the Project Approval, mining is limited to first workings under all Principal residences & commercial structures (Boral Asphalt Plant) above the mining areas.

All subsidence impacts were to be remediated to the satisfaction of the stakeholder unless an alternative compensation agreement was negotiated prior to subsidence development. Total extraction panels were proposed outside subsidence control buffers to Viney Creek, TransGrid tension tower and principal residences.

The extraction panels in SMP Areas 1 and 2 were originally all total extraction panels with widths of 120 m (Panel 1) and 160 m (Panels 2 to 26) with 25 m wide barrier pillars (Figure 17).

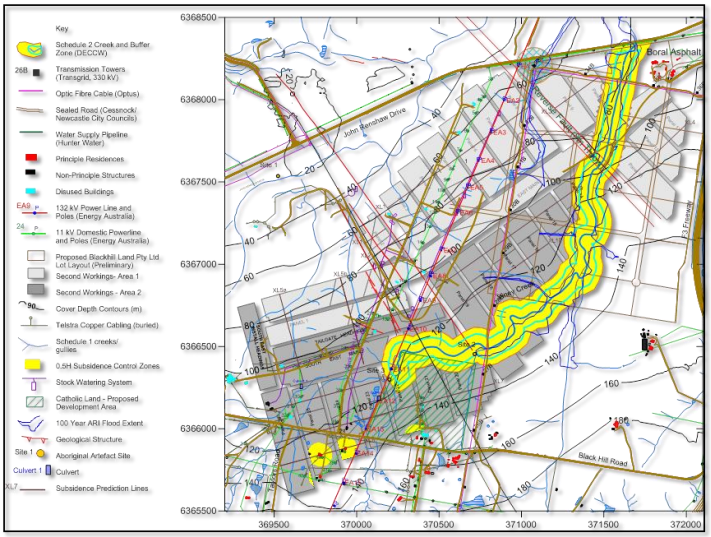

Figure 17 - Proposed SMP area 1 and 2 panels at the Abel Mine

Review of subsidence predictions and impacts

Subsidence predictions were estimated based on ACARP, 2003 empirical Longwall model and an effective mining height (i.e. assumed mining height x extraction ratio). Measured subsidence has ranged from 0.82 to 1.25 m with original predicted subsidence values from 0.87 to 1.76 m for assumed mining heights of 2.0 to 3.2 m and an extraction ratio of 95%. The predicted subsidence was significantly higher in places due to differences in assumed mining heights and the sizes of stooks left to control roof adjacent to the fault structure.

Revised predictions were subsequently based on data from the first four panels and revised from 0.92 to 1.31 m for mining heights of 2.35 to 3.0 m and extraction ratio of 85% (to allow for bulking of goaf/stooks). Tilts and strains were generally within predictions with maximum measured tilts ranging from 23 to 63 mm/m, tensile strain from 4 to 23 mm/m and compressive strain from 2 to 17 mm/m.

Cracking was predicted to range between 40 - 260 mm above panels where cover depths were < 80 m (i.e. W/H > 2) and < 150 mm for cover depths > 80 m. Measured crack widths (bold represent exceedances) above Panels 1 to 4 were 180 mm, 50 mm, 260 mm and 300 mm respectively for cover depths of 100 m, 75 m, 55 m and 55 m. The distribution of cracking was erratic in places, however, and could be explained by biased strain distribution towards the high side of sloping ground and the presence of compacted clay fill. The direction of mining or goaf development may also have contributed (Figures 18 and 19). The exceedances represented < 5% of all measured crack widths.

Subsidence mitigation works that were agreed to before mining were carried out in a timely manner. The works included:

- Ripping and regrading cracked ground, drainage earthworks along gravel access road and out of channel ponded areas.
- Extraction panels were set back from cattle ramp and race and temporary fences installed above cracked areas so as not to injure livestock or disrupt cattle agistment while repair works to fences were carried out (wire strands broke or sagged).
- Loss of clearance to ground above sagging 415 kV powerlines were repaired by Ausgrid.
- Timely repairs to damaged buried water supply pipes used to water cattle.

The surveying program also used Feno survey markers to minimise injury potential to the cattle.

Figure 18 - Typical tension crack above total extraction panels with cover depths of 60-80 m

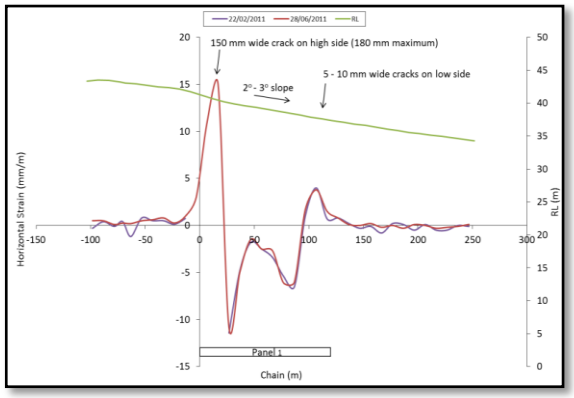

Figure 19 - Strain profile bias towards high side of gentle slope for Panel 1 (100 m of cover)

Deep borehole extensometers and multi-vibrating wire piezometers were placed over the panel centres and chain pillars respectively of Panels 1 and 2 and successfully identified heights of fracturing (A Zone) and constrained or strata dilation (B Zone) zone thickness for cover depths of 76 m and 95 m (Table 2). Shallow slotted standpipe measurements confirmed shallow groundwater levels had been lowered due to strata dilation. Further monitoring data required to assess if leakages occurring directly to the workings from B Zones.

Table 2 - Measured fracture and dilated zones above total extraction panels 1 and 2

Panel No.	Width W (m)	Cover H (m)	Effective Mining Height T_e (T) (m)	Fractured Zone (A Zone)			Constrained Zone (B Zone)		
				Thickness (m)	Anchor Displ. (mm)	Vertical Strain (mm/m)	Thickness* (m)	Anchor Displ. (m)	Vertical Strain (mm/m)
Panel 1	120	95 - 99	2.55 (2.6)	45 ($18T_e$)	734-1351	120	40 ($15T_e$)	14-33	0-3
Panel 2	150	73 - 76	1.88 (2.5)	46 ($24T_e$)	78-298+	11	20 ($11T_e$)	-13- -18	-1-0

e =extraction ratio for panel at instrument location. * - Constrained zone thickness extends from A to <10 m below surface.

The extensometer and piezometer data for Panel 2 is shown in Figures 20 and 21.

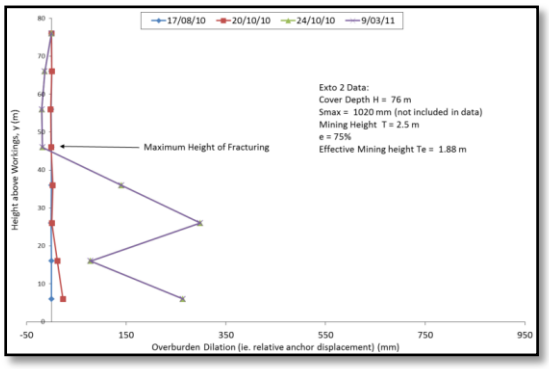

Figure 20 - Borehole extensometer for panel 2

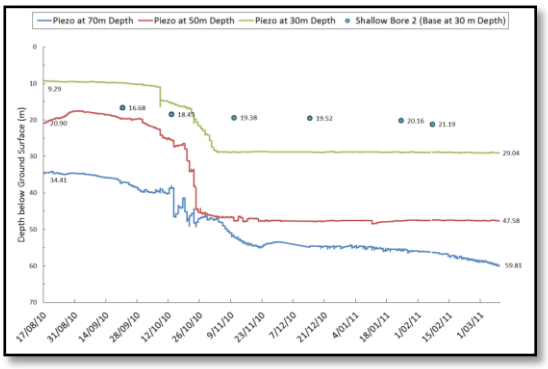

Figure 21 - Piezometer and standpipe for panel 2

Three panels were changed from total extraction to partial pillar (Modified Duncan) extraction panels in the south-western area of the SMP Area 2 to meet the practical subsidence completion deadline (Figure 22). The proposed panels will be developed on a 3 and 5-heading layout with 50 m and 45 m centre-centre square pillar spacing respectively and 5.5 m wide headings and cut-throughs. The mining height has been assumed to equal the seam thickness and ranges from 2.85 m to 3.3 m for pillar stability assessment and subsidence prediction purposes.

The panels will typically have final mined widths (W) of 118 m and 211 m with cover depths (H) ranging between 100 and 130 m. The panels will have *super-critical* to *critical* W/H ratios of 1.91 to 0.94, indicating the maximum pillar loads will be close to or equal to full tributary area magnitudes.

The pillars will then be 'stripped' or reduced in width along four sides on retreat, leaving square remnant pillars with factors of safety (FoS) > 2.11 (under the assumed design loading conditions) and w/h ratios >7.

The roof between the remnant pillars is expected to cave readily and the floor comprises moisture insensitive shales and sandstone of moderate strength. The pillar stress will range from 9.7 to 11.6 MPa with maximum subsidence expected to be < 150 mm. The remnants will also have strain hardening properties that will limit subsidence to < 300 mm in the unlikely event that they go into yield. The potential for significant impact to future surface features or developments is very low.

Mining outcomes

The mining outcomes for SMP Areas 1 and 2 for Abel are summarised below:

- The proposed panels east of a large reverse fault had to be abandoned due to the cost of mining through the structure.
- Panels have been extracted with minimal subsidence effect (any mitigation work conduced as per the various Property/Infrastructure Management Plans).
- No injuries to cattle were reported.
- No loss of creek or surface water flows. Surface to seam connection not detected below total extraction panels with cover depths ranging from 73 to 99 m. Fracture heights ranged from 18 to 24 x Effective Mining Height.
- No impact to TransGrid Tension or suspension towers. Tilt meters were installed for real time monitoring and Infrastructure Management plans were prepared in consultation with TransGrid and approved by DTIRIS.
- Mitigation works have restored the function of infrastructure (power lines, roads and buried water supply system).
- Optus optic fibre cable was relocated with assistance from MSB around the extraction areas of SMP Areas 1 and 2.
- Existing residences were not undermined by total or partial pillar workings due to mine layout adjustment.

- Consultation with the local community has been extensive with SMP Area Stakeholder days held and regular updates to the Abel Mine Community Consultative Committee.
- Three panels have been changed to the Modified Duncan Method to meet the June 2013 subsidence development completion deadline. The extraction ratio for the partial extraction panels will range from 72% to 75%.
- The proposed panel locations and extraction ratios of > 95% were achieved, with Panels 1 and 2 requiring additional stooks at several locations to support structure affected roof. The extraction ratios were reduced to between 83% and 93% where additional stook support was required.

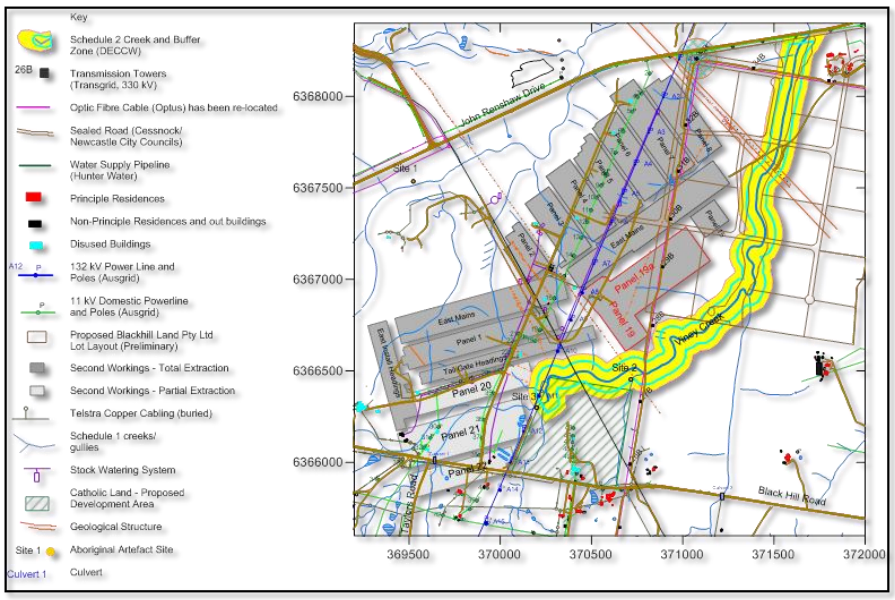

Figure 22 - Final approved Abel Mine SMP area 1 and 2 mining layout

CONCLUSIONS

Overall, it is assessed that maximising the extraction ratios in non-sensitive areas and reviewing subsidence responses at the Abel and Tasman Mines and has enabled good mine design efficiency outcomes to be achieved despite significant mining constraints in highly sensitive areas. Negligible impact to steep surface topography, infrastructure and public safety has also been achieved.

The Modified Duncan Method of partial pillar extraction has been used successfully at the Tasman mine where the control of surface subsidence is a critical mining constraint. The method has allowed a high degree of flexibility in regards to adjusting mining layouts in response to latent floor heave conditions. The deterioration of the floor occurred after higher than normal groundwater inflows were encountered during mine development in the shallower areas of the mine.

Total pillar extraction mining at relatively shallow depths (60 m to 130 m) at the Abel Mine has also allowed a high degree of flexibility to mine plan layouts where a range of surface subsidence constraints and hazardous underground geological conditions exist. The Modified Duncan method of partial pillar extraction has also recently been approved to meet Stakeholder expectations in regards to subsidence development at the Mine. Other factors, such as communicating impact expectations with stakeholders can be a difficult and on-going process, despite reasonable impact predictions being provided beforehand. The thorough monitoring of subsidence effects and review of impacts allow timely (and transparent) explanations to be made when problems arise, which is important for fair and productive outcomes to be achieved.

ACKNOWLEDGEMENTS

Contributions made by Matthew Wright, John Krick and Grant Lord of Donaldson Coal Technical Services Department, and Kevin Price of Brunskill Pty Ltd, are appreciated.

REFERENCES

Ditton, S and Frith, R C, 2003. Review of industry subsidence data in relation to the impact of significant variations in overburden lithology and initial assessment of sub-surface fracturing on groundwater, ACARP Project No. C10023, Strata Engineering Report No. 00-181-ACR/1 (Sep).

Brown and Meyerhof, 1969. Experimental study of bearing capacity in layered clays. In *Proceedings of 7th International Conference on Soil Mechanics and Foundation Engineering*, Mexico.

Das, 1998. Principles of geotechnical engineering (4th Edition), Das, B.M., PWS Publishing Company Inc.

Diedrichs and Kaiser, 1999. Stability of large excavations in laminated hard rock masses: the voussoir analogue revisited. *International Journal of Rock Mechanics and Mining Sciences,* 36.

DgS, 2007. Far-field displacement predictions for the NBN and broadcast Australia towers due to the proposed pillar extraction panels at the Tasman Mine. Ditton Geotechnical Services Report No. TAS-003/1(29.08.07).

Marino, G G and Choi, S, 1999. Softening effects on bearing capacity of mine floors. *Journal of Geotechnical and Geoenvironmental Engineering*, Dec, 1999.

Sutherland, T and McTyer, K, 2011. The Duncan method of partial pillar extraction at Tasman Mine, In *proceedings 11th Underground Coal operators Conference*, Wollongong, February 10/11 2011, ISBN 978-1-921522-16 -1 (Eds: N Aziz, B Kinninmonth, J Nemcik and T Ren), pp 8-15. http://ro.uow.edu.au/coal/334/.

APPLICATION OF ADVANCED INSAR TECHNIQUES FOR THE MEASUREMENT OF VERTICAL AND HORIZONTAL GROUND MOTION IN LONGWALL MININGS

Javier Duro, David Albiol, Oscar Mora and Blanca Payàs

ABSTRACT: Synthetic aperture radar interferometry technology detects ground motion with millimetric precision. The measurements are taken remotely from space and represent a very efficient tool for ground motion measurement even in large and remote areas where land-based measurement techniques are inconvenient and costly. Furthermore and due to the availability of archive radar images, InSAR technology is the only technology able to provide measurements of ground deformations that occurred in the past. Past data allow the establishment of early baselines before any coal production starts and before any subsidence induced by previous production activities. This allows the total levels of subsidence to be identified and allows mine decision-makers to determine the vulnerable zones that could be affected by subsidence. Results of a recent ground motion study on a longwall mine in the Southern Coalfields of NSW, Australia are discussed. The results were obtained using an advanced differential interferometric chain, Stable Point Network, (SPN) which is capable of processing radar images at millimetric precision and very high density of measurements. The paper aims to compare the advanced InSAR retrieved motion with surveying data and to show that InSAR can retrieve the vertical and the horizontal motion that can be present in this type of mining.

INTRODUCTION

Radar satellites continuously orbit the earth on a fixed polar orbiting track, taking more or less 100 min to complete one full orbit. Since the earth is rotating below the satellite, its path successively moves around the globe, meaning that over time satellites build up complete images of the whole globe. The satellite can revisit the same location after a few hours to 46 d on a regular basis, depending on the mission. Space borne Synthetic Aperture Radar (SAR) sensors are active systems on board satellites that acquire during day and night and operate in the microwave domain (cm to dm wavelength) providing global acquisitions almost independent from the meteorological conditions. These radar satellites provide high resolution images which have a wide range of applications and are suitable for operational monitoring tasks.

SAR interferometry (InSAR) is one of the main applications of radar imagery because it fully exploits the geometric precision of the SAR systems (in the order of the sensor wavelength, few millimetres). These radar satellite images, unlike optical satellite images, provide an accurate measurement of the distance between the satellite and the ground. The principle of interferometry is based on the superposition of waves from two images in order to detect differences in distance measured in wavelength fractions (Massonnet and Feigl, 1998).

For ground motion monitoring projects several satellite images taken at different times are compared. By means of the analysis of the evolution of the distance between the sensor and the ground of the different acquisitions, information regarding the topographical relief and ground deformation can be extracted, see Figure 1. These two main components are superimposed in the interferometric signal jointly with other unwelcome contributions, the most critical one being the one due to the variations in the state of the atmosphere during the image acquisition. It is important to properly filter these unwanted variations in order to avoid possible errors when interpreting the InSAR data. Altamira Information owns an InSAR processing technique, Stable Point Network (SPN), which estimates and compensates all these undesired phase components, allowing the achievement of millimetric precision in the measurements of ground motions.

SPN offers very high density of measurements (~600 point/km^2) over wide areas (tens of kilometres), which allows the identification of the perimeter of those areas with motion and the gradients of the ground deformations. For these reasons the application of this technology in longwall mining is very suitable and

Altamira-Information, javier.duro@altamira-information.com, M: 04 1836 8917

it can complement local and *in situ* surveying techniques, particularly over the areas surrounding the longwall panels where smooth gradients of motions can be expected to occur.

SPN TECHNOLOGY

The Stable Point Network (SPN) (Arnaud, *et al.*, 2003) is an advanced differential interferometric software developed by Altamira Information in order to process large stacks of radar images to achieve millimetric ground motion measurements. This technique requires a minimum number of images to identify the points that are electromagnetically stable during the period of study. This selection process is a crucial step as the precise measurements of ground deformations will be primarily achieved in these electromagnetically stable points.

The basis of the SPN technique is the separation of the different components from the interferometric phase ($\emptyset_{INTERF}$): the topographic component ($\emptyset_{TOPO}$), the movement component, ($\emptyset_{MOV}$), the atmospheric contribution ($\emptyset_{APS}$) and the noise component ($\emptyset_{NOISE}$).

$$\emptyset_{INTERF} = \emptyset_{TOPO} + \emptyset_{MOV} + \emptyset_{APS} + \emptyset_{NOISE} \quad (1)$$

The topographic component can be mainly compensated from an external Digital Elevation Model (DEM). Consequently, assuming that $\emptyset_{NOISE}$ and $\emptyset_{APS}$ are known, using equation 1 the phase contribution due to ground deformation $\emptyset_{MOV}$ can be obtained.

Several satellite images covering a series of dates are acquired to properly retrieve the phase contribution related to the ground motion. This large stack of data allows the generation of time series which show the space-time evolution of the deformations (see Figure 1 and Duro, *et al.*, 2003).

The application of SPN is very suitable for longwall panel monitoring as it can cover wide areas at a very high resolution and with millimetric precisions allowing to perfectly define the perimeter and the gradients of the ground deformations over the mined panels and the surroundings. The availability of archive SAR data also offers a unique opportunity to look into the past and to perform historical studies and continuing afterwards with ongoing monitoring to quantify deformation at the land surface.

By using a combination of classical interferometry and SPN, millimetric and centimetric movements can be monitored. Results are provided in GIS format and can be received and analysed by the mine managers and by the owners of surface infrastructure remotely without the need for site visits (Espinosa and Mora, 2012).

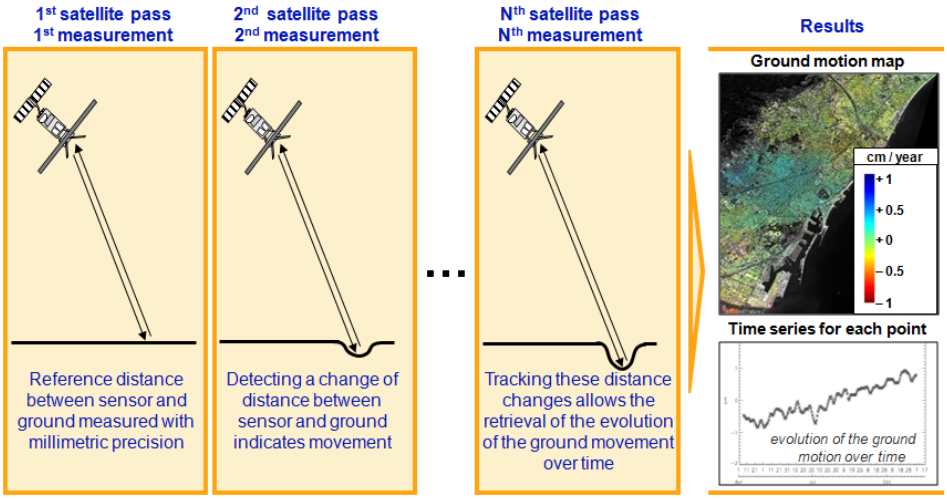

Figure 1 - Performance of InSAR technology to measure the ground deformation from the comparison of the evolution of the distance between the sensor and the ground in repeated satellite passes. On the right side there is an example of the two main outputs: ground deformation maps and vector files with the time series for each measurement point.

INSAR SAMPLING GEOMETRY IN LONGWALL MINING DEFORMATION AREAS

Satellites follow polar orbits (approximately ±14º with respect to the North) at a right look direction offering ascending and descending acquisitions from the west and the east side respectively (see Figure 2). Furthermore, space-borne SAR sensors have an oblique geometry of observation, which determines the measurement direction of observation; this is called the Line of Sight (LOS) of the sensor. The LOS of the satellites is rarely direct above, i.e. vertical, and is typically varying from 18º up to 50º with respect to the vertical direction. As shown in Figure 3, depending on the orientation of the true motion vector, the ascending or descending view will measure (sample) different magnitudes of the real motion. In any case, purely vertical or horizontal motions are measured in InSAR LOS with a significant magnitude (left and right case Figure 3). The acquisition geometry of the satellite can be selected in conjunction with the direction of the expected ground motion to get an optimum sampling.

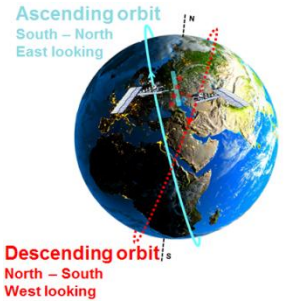

Figure 2 - Illustration example of the two possible acquisition geometries, ascending and descending flights

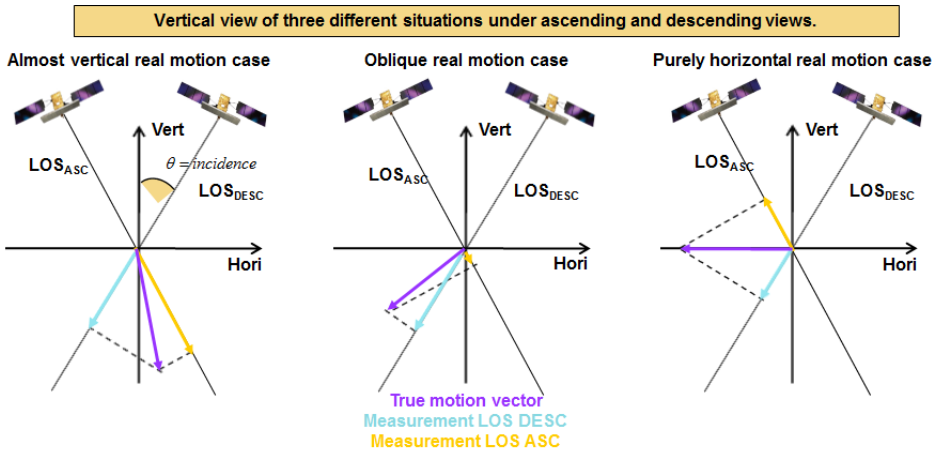

Figure 3 - Illustration example of the detected magnitude in LOS direction in function of different orientations of the true motion vector for ascending and descending views

InSAR techniques measure the ground motions in the LOS of the acquisitions. Consequently, when aiming at decomposing the measured LOS motion into the vertical and horizontal components, i.e. eastings and northings, using InSAR techniques, it will be necessary to combine ascending and descending views of the same motion. However, even if only one acquisition mode is available, it is still possible to obtain the vertical and the horizontal components of the observed movement, but only if external information, such as monitored GPS data, modelling or assumptions about the expected motion is available.

The majority of the sagging subsidence that is seen on the surface occurs over the centre of a mined panel and far less subsidence is seen at and beyond the edges of the panel. Where several panels are mined in a series with chain pillars left between the panels, the observed maximum subsidence, over this series of panels, generally increases after the extraction of each further panel. The horizontal component of mining induced subsidence, in flat terrain and under conventional conditions, increases from zero at the initial pegs that are remote from the edges of the mined panels and to a maximum value near the point of maximum tilt near the edge of the panel.

The magnitude of mining-induced horizontal movements and the directions of these horizontal movements are controlled by a complex interaction of multiple factors, including the magnitude of the vertical subsidence, the presence and proximity of previously extracted panels, the depth of cover, the location of the peg relative to the current and previously extracted voids, the steepness and profiles of the surface topography, the seam dip, the direction of mining in relation to the surface and the seam slope, the geology and thicknesses of the various strata layers, and the magnitude and direction of the *in situ* horizontal compressive stresses.

The acknowledgement of the nature of the observed ground deformations could be used as a priory assumption for the motion decomposition when using one InSAR acquisition mode. As shown in Figure 4, depending on the location of the measurement points with respect to the excavation areas within the active longwalls, the measurement motion can be re-projected to obtain a more accurate interpretation and magnitude. Hence, if the measurement point is close to the centre of an active longwall panel it can be assumed that the main component of the true motion will be in the vertical direction (motion from B to B' in Figure 4). However if the measurement point is in the surroundings it can be assumed that the principal component of the real motion is in the horizontal direction (motion from C to C' in Figure 4). As shown in Figure 4, the resulting re-projected vertical and horizontal vectors (from one mode InSAR LOS measurement) overlay the true motion vector, indicating that the final re-projected magnitude is exactly the same as the original one. Nevertheless in the transition areas (motion from A to A' in Figure 4), where the true motion vector is not purely dominated by the vertical or the horizontal component, the re-projected LOS measurement will present some discrepancies with respect to real magnitude.

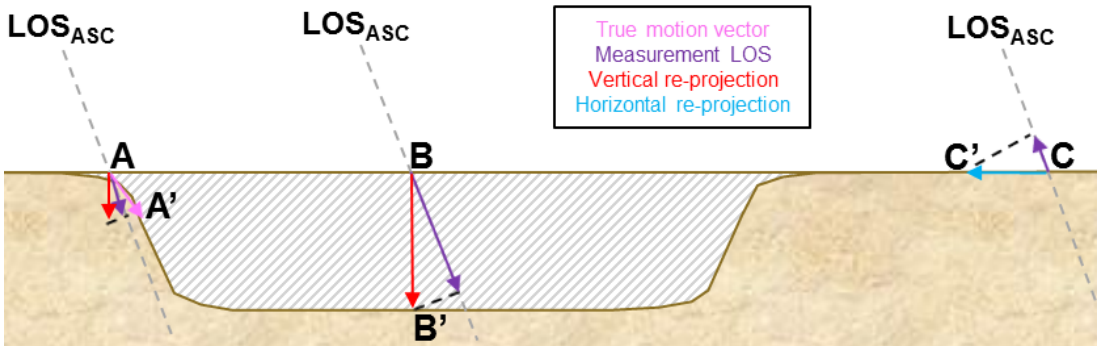

Figure 4 - Illustration of three examples of the detected magnitude in LOS direction and the resulting re-projected vectors in vertical direction (red) and in horizontal direction (blue)

REAL CASE APPLICATION

The case study that is presented in this section was performed using archive past data of the ALOS satellite. This satellite was launched by the Japanese Aerospace Exploration Agency (JAXA) in January 2006 and was operating until 2011. Among other sensors on board, it contains a Phased Array type L-band Synthetic Aperture Radar (PALSAR) which provides resolution images of 4.5 m x 5 m with the fine beam single polarisation mode with a maximum interferometric revisit time of 46 d. A total of 25 ALOS images were acquired between December 2006 and January 2011 over the operating area and its surroundings. The main objectives of this InSAR project were to quantify the subsidence magnitude range and to determine the extent of the subsidence area.

The SPN processing was very successful over this area retrieving a very high measurement point density (800 points/km^2) and with precisions of 4 mm. The produced ground deformation map has a uniform distribution of the measurement points through the whole area of interest minimising as much as possible the local areas without measurements. In particular, areas without points are over the rivers (water covered areas), crop fields and over the centre of the active longwall panels.

It is important to bear in mind that the critical factor in determining whether a measurement point can be used is whether the ground surface remains invariant during the period of study. In agricultural and highly vegetated areas, seasonal changes occur which could cause a reduction of the measurement point density over those areas.

As it can be seen in Figure 5, different rates of subsidence at the surroundings of the longwall panels are detected. These rates can be directly linked with the extraction activities taking place in the underground

mine, and thus help to obtain parameters for further planning, helping to anticipate areas that will be vulnerable in the future, or to corroborate and complement the *in situ* measurements and the modelling.

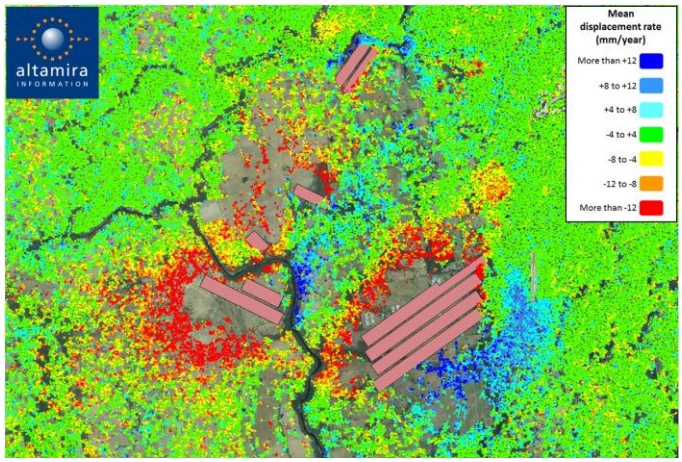

Figure 5 - Mean velocity map in the LOS direction obtained over the area of interest superposed to the longwalls schema

InSAR detected motion compared to ground data

Longwall mining activities present a special behaviour regarding induced ground deformation phenomena. This occurs because the longwall face advances with time generating a strong movement pattern in the area that surrounds the activity. As it can be seen in the spatial profiles in Figure 6 and Figure 7, the centres of the active longwall panels are affected by strong movement (approximately more than 50 cm of accumulated deformation) and cannot therefore be measured by using SPN alone because it exceeds the detection limits (Massonnet and Feigl, 1998). In these cases complementary InSAR techniques (other than SPN) can be applied to measure such abrupt ground motions which occur in the centre of the longwall panels. However, this type of processing is outside the scope of this paper. The comparison between the measured displacements in the LOS direction and ground data shows that movements are underestimated in the areas where there is an important vertical component.

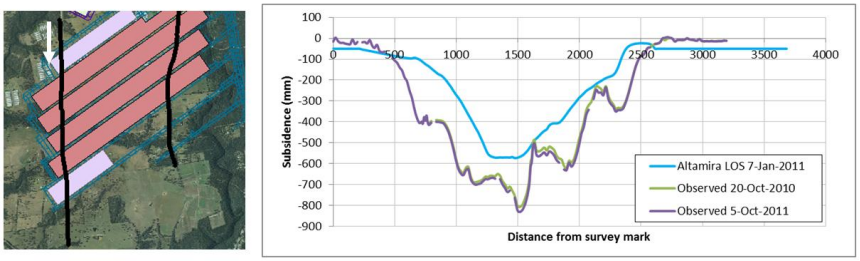

Figure 6- Section views of the ground measured total subsidence compared with satellite subsidence measured in the LOS direction

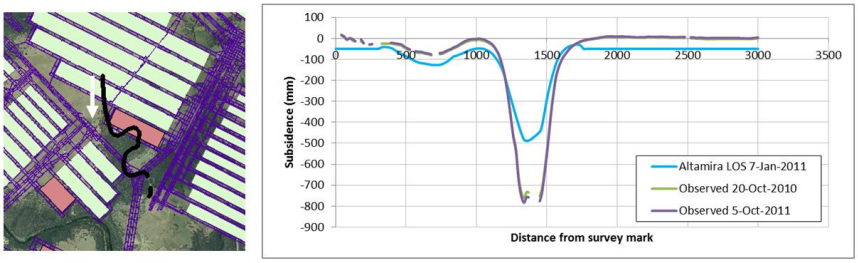

Figure 7 - Section view of the ground measured total subsidence compared with satellite subsidence measured in the LOS direction

InSAR vertically re-projected motion compared to ground data

The LOS measurements have been re-projected into the vertical axis for those areas closer to the centre of the active longwall. This re-projection has been performed taking into consideration that the principal component of the true motion is mainly vertical. As a consequence, the final magnitude is adjusted for each measurement point in accordance with the local angle, which determines the conversion factor (approximately $1/\cos\theta_{incid}$). The direction is set according to the satellite ascending view ground observation geometry given by this archive data.

Figure 8 and Figure 9 show the comparison of ground data with the vertically re-projected InSAR measurements. As can be observed the section profiles of the re-projected InSAR data are similar to the ones obtained by the ground surveys. This comparison confirms the hypothesis of the vertical re-projection over those areas.

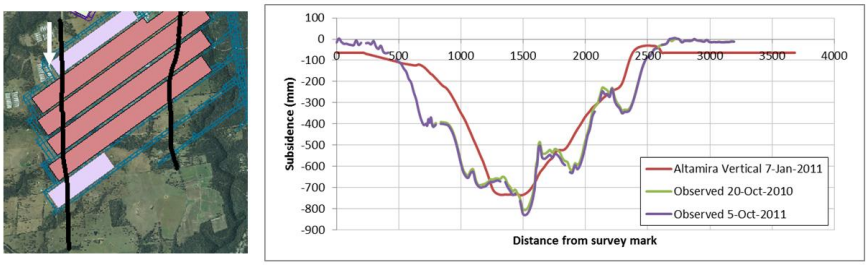

Figure 8 - Section view of the ground measured total subsidence compared with satellite measured motion re-projected to vertical direction

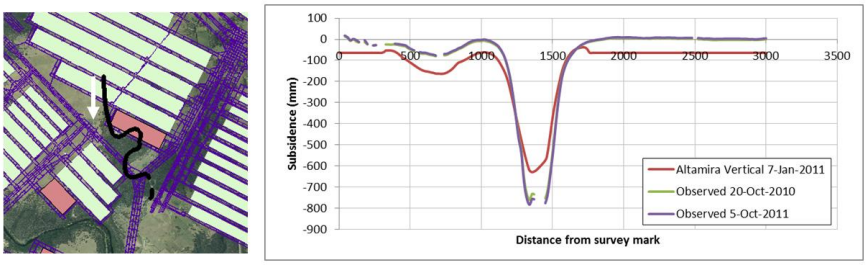

Figure 9 - Section view of the ground measured total subsidence compared with satellite measured motion re-projected to vertical direction

InSAR horizontally re-projected motion

The LOS measurements at the surroundings of the longwall panels are re-projected into the horizontal axis considering the acquisition geometry of the ALOS data. The main assumption made is that the ground motion over these areas has a dominant component which is in the horizontal direction due to mine activities.

As was the case for the vertical re-projection, the final magnitude is adjusted for each measurement point in function of the local angle, which determines the conversion factor (approximately $1/\sin\theta_{incid}$). The direction is set according to the satellite ascending view ground observation geometry given by this archive data.

An example of an area obtained after performing horizontal re-projection is shown in Figure 10. As can be observed, the perimeter of the ground deformation can be precisely defined thanks to the very high density of measurement points. As discussed in the previous section, the re-projection is valid assuming that the true motion vector is predominantly horizontal. In addition, the magnitude and sign of the horizontally projected values are adapted depending on the local acquisition geometry. It is important to remark that this assumption may not be valid for all the areas, like for instance at the boundaries of the creeks where the topography of the river banks can originate changes in the direction of the ground motions.

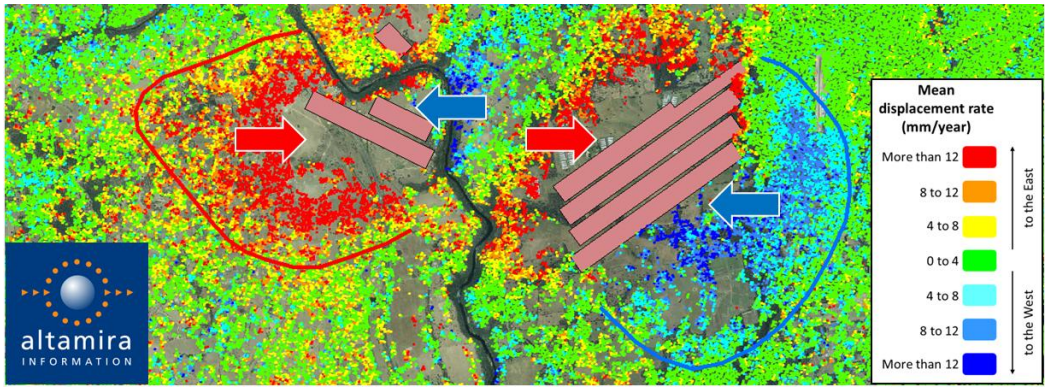

Figure 10 - Horizontal mean deformation rate map over the surroundings of the active longwalls area. The perimeter of ground deformation is marked with the red and blue lines, and the movement direction is indicated with the blue and red arrows

This assumption over the mine far field areas is useful for InSAR motion interpretation. As observed in Figure 10 the areas on the western side of the longwalls move towards the east and the areas on the west side move towards the west at a rate of 10 mm/year. The re-projection also adjusts the magnitude of the measured motion allowing a more accurate analysis of the impact of such deformations. Further studies are ongoing to enhance and validate this approach.

CONCLUSIONS

The application of satellite interferometric techniques is oriented to management measures as these techniques allow identifying and monitoring large areas experiencing different magnitudes and intensities of motion. InSAR measurements provide support in the evaluation of the existing subsidence mechanisms and are effective risk management tools used in mines worldwide to activate mitigation measures when required.

This paper shows an approach to understand and better interpret the measured InSAR motions in longwall mining areas, and in particular how the measurements of vertical and horizontal motions are possible using only one acquisition. This paper also goes a step further proposing the application of different motion direction assumptions based on the location of the measurement points with respect to the active longwalls. In the areas close to the longwall centre improved InSAR measurements are obtained taking into account that the principal component of the ground motion is in the vertical direction. Finally a qualitative comparison of InSAR data with surveying data shows that the correlation between both measurements significantly increases with the re-projection when the assumption is met.

In the same way, the InSAR measurements at the surrounding of the active long wall panels are horizontally re-projected knowing that the ground deformation there has a horizontal dominant component. The results show that the horizontally re-projected InSAR measurements allow defining and mapping the extension of the areas affected by mining-induced horizontal movements and a better definition of the spatial gradients over each single ground structure.

In the presented case study, due to the fact that one satellite mode has been used, external data (modelling, surveying, knowledge of the nature of the ground motion) have been mandatory to identify the areas with predominantly horizontal and vertical motion where the re-projection is properly done. The discussed results demonstrate the suitability and the potentiality of InSAR technology to complement and under certain conditions even supplement other *in situ* surveying techniques for a better characterisation and understanding of the mine induced ground deformations.

The presented case study has been performed using archive data from a low resolution satellite with limited quantity of images and precision, nevertheless the results already show the extreme potential of the technology.

Altamira's InSAR processing techniques adapted for longall mines demonstrate several distinctive parameters that define this remote sensing methodology as a very promising, effective and cost saving surveying technique, the most important ones being:

- High density of measurements points that allows to precisely set the boundaries of the ground deformation and to map the different shapes and magnitudes affecting each zone (hundreds of points in km^2 in this case which can be improved to thousands of points in km^2 when using High Resolution sensors).
- High precision of measurements (4 mm in this case, improved to 2 mm when using High Resolution sensors) that places SPN interferometry as one of the most precise surveying technologies.
- Pixel size (40 m in this case and 3 m in High Resolution sensors) allowing an excellent sampling of the results.

Nowadays, with the current radar satellite constellations it is possible to program an intense data acquisition that, either with one or with two modes, will assure gathering vertical and horizontal motion vectors with maximum precision and accuracy.

ACKNOWLEDGEMENTS

The assistance of Don Kay and Bronwyn Maher of Mine Subsidence Engineering Consultants Pty Ltd (MSEC) who assisted in the preparation of plots in this paper and provided editorial assistance on this paper, particularly in respect of coal mining subsidence issues and their generous assistance is gratefully acknowledged.

REFERENCES

Massonnet, D and Feigl, K L, 1998. Radar interferometry and its application to changes in the Earth's surface, in *Rev. Geophys.*, 36(4):441-500. doi:10.1029/97RG03139.

Arnaud, A, Adam, N, Hanssen, R, Inglada, J, Duro, J, Closa, J and Eineder, M, 2003. ASAR ERS interferometric phase continuity, in *Proceedings Geoscience and Remote Sensing Symposium 2003*, IEEE International, 2:1133-1135.

Duro, J, Adam, N, Arnaud, A, Closa, J and Inglada, J, 2003. High resolution differential interferometry using time series of ERS and ENVISAT SAR data, in *Proceedings FRINGE Symposium*, ESA-ESRIN, p.72.1.

Espinosa, A and Mora, O, 2012. Tecnologías InSAR en El Teniente Rajo Sur, Revista Minería Chilena, Marzo 2012, n 369, p51.

TECTONIC STRESS ENVIRONMENT OF COAL-ROCK DYNAMIC HAZARD IN KAILUAN MINING AREA, CHINA

Jun Han[1,2], Bin Liang[3], Hongwei Zhang[1], Zhijie Zhu[1], Hai Rong[1] and Zhaoyu Gao[1]

ABSTRACT: Using HI (Hollow Inclusion) method, the *in-situ* stress of Kailuan mining area was measured in the field. The characteristics of the *in-situ* stress field and the relationship to regional structures are analysed systematically. Then the relationship between *in-situ* stress field coal-rock dynamic hazard, include coal and gas outburst, rockburst and water inrush, is analysed. Studies show that *in-situ* stress field in Kailuan mining area is a high stress zone of Earth dynamical field, with the horizontal tectonic stress being dominant. The magnitude and azimuth of the stress regime is controlled by Kaiping syncline. *In-situ* stress is the highest in Kaiping synclinal axis section, and as far away from the axis, the stress decreases gradually. The orientation of the maximum principal stress is approximate perpendicular to the axis of Kaiping syncline. The tectonic stress field also controls coal structure, gas content, coal permeability and other parameters. In the Kailuan mining area, coal and gas outburst and rock burst occurred in synclinal axis section of Kaiping syncline where *in-situ* stress is the highest, whilst water inrush occurred in the wing of Kaiping syncline where *in-situ* stress is the lowest. Coal-rock dynamic hazard in Kailuan mining area has almost identical tectonic stress environment.

INTRODUCTION

Coal-rock dynamic hazard, including coal and gas outburst, rockburst and water inrush, is an serious threat to the safety in mining and underground engineering. Although many scholars have different opinions about the occurrence mechanism of these hazards, the idea that the hazard is a mechanical process of coal and rock mass deformation and failure, energy accumulation and release is commonly accepted by all scholars (Skochinski, 1954; Cook, 1965; Huoduote, 1966; Zhou, *et al.*, 1991; Zhang, *et al.*, 1991; Yin, *et al.*, 1997; Qi, *et al.*, 1997; Li, *et al.*, 2005).The failure modes and energy release characteristics of coal and rock depend on two conditions, one is the physical and mechanical properties of coal and rock mass, the other is external boundary and loading conditions. In order to study the mechanism of coal - rock dynamic hazard, the physical and mechanical properties, structural features and tectonic stress environment of coal and rock related could be analysed to understand the mechanism and controlling conditions of coal-rock dynamic hazard. Kailuan mining area had been mined for 130 years, and during this period, coal and gas outburst, rockburst and water inrush occurred frequently in mining. Jiang, *et al.* (2005), Liu, *et al.* (2006), Qi, *et al.* (2006), Meng, *et al.* (2009) and Wang (2011) had respectively studied the geological factors of coal and gas outburst, rockburst and water inrush in Kailuan mining area. In this study, the authors investigated the coal-rock dynamic hazard of Kailuan mining area according to geological background, structure characteristic and *in-situ* stress field. The relationship between coal-rock dynamic hazard and tectonic stress field of Kailuan mining area was discussed in detail.

AN OVERVIEW OF COAL-ROCK DYNAMIC HAZARD IN KAILUAN MINING AREA

Kailuan mining area is located in the east of Hebei Province with a mining area of 670 km^2. Coal seam exists in the four groups of Permo-Carboniferous Period. From top to bottom, the groups are Lower Permian Tangjiazhuang Group, Damiaozhuang Group, the Upper Carboniferous Zhaogezhuang Group and Kaiping Group. Damiaozhuang includes 4 to 6 coal seams, 5^{th} coal, 8^{th} coal and 9^{th} coal are the major mining seams. Zhaogehuang Group includes 3 to 5 coal seams, 12^{th} coal is major mining seam. At present, there are ten mines in Kailuan mining area, with an annual coal production of nearly 30 million tons. Among these coal mines, Majiagou is a coal and gas outburst prone mine, whilst Zhao Gezhuang mine is coal and gas outburst and rockburst mine, Tang shang mine has rockburst hazard risk, and Fangezhuang and Donghuantuo mine are water inrush mines (Figure 1). Majiagou Mine is located in the northwest of Kaiping syncline, formation dip is more than 45°. Coal and gas outburst has occurred more

[1] *College of Mining, Liaoning Technical University, China, hanj_lntu@163.com, Tel: +86 4183350473*
[2] *Kailuan Group, Tangshan 063000, China*
[3] *Department of Mechanics and Engineering Sciences, Liaoning Technical University, China*

than 55 times since it started mining operation. The first outburst occurred in the 9th coal seam in September 9th, 1964. The most severe outburst involved 370 t coals and 7500 m^3 gas. The 9th coal and 12th coal are the main working seams with gas outburst prone hazard.

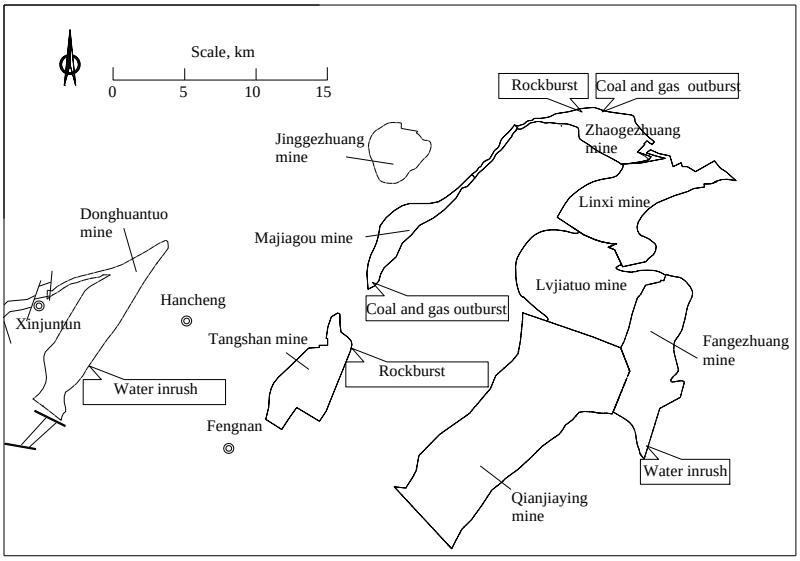

Figure 1 - Coal mine of Kailuan mining area

Zhaogezhuang mine is in the northeast edge of Kailuan syncline. The dip of the coal seam in east is about 30°and in west is from incline to steep until overturned. Coal and gas outburst occurred first in 1955. Until today, outburst incident has occurred for nearly 30 times. The most severe coal and gas outburst occurred on September 15th 1973 with the ejection of 100 tons of coal and 3000 m^3 gas emission. The 9th coal and 12th coal are main coal and gas outburst seams. Rockburst first occurred on June 24th 1995. As mining depth extends continuously, the frequency and strength of rockburst increases with it, rockburst has occurred for 23 times. Tangshan mine located in southwest of Kaiping syncline, rockburst has been more and more serious with the increase of mining depth since the first rockburst occurred in June 7th, 1964. Up to now, rockburst has occurred more than 90 times. Rockburst mainly occurred in 5th coal seam and 8th coal seam under 520m depth. Fangezhuang mine located in the southeast of Kaiping syncline. Water inrush had occurred for 49 times. Among these water inrushes, there is 24 times roof water inrush, 18 times floor water inrush, 5 times karst collapse column water inrush, twice fault water inrush. The most severe water inrush made shaft flooded. Water source of inrush in Fangezhuang mine mainly consists of sandstone group fracture confined aquifers between 12th and 14th coal seam. Donghuantuo mine located in the west of Kaiping syncline and its hydrogeology condition is extremely complex, maximum water inflow has reached 62.84 m^3/min during its construction. 11 water inrush incidents have been reported since 2000.

THE STRUCTURE CHARACTERISTICS OF KAILUAN MINING AREA

The Kaiping coal field is a large and compound coal-bearing syncline structure. It is a representative permo-carboniferous system in north China. There are four coal bearing structures, namely, the Kaiping syncline, Chezhoushan syncline, Jinggezhuang syncline and Xigangyao syncline. Both Kaiping syncline and Chezhoushan synclines belong to long axial oblique, in the middle of them is the Beiziyuan concealed anticline (Figure 2). The main structure of Kaiping coal field is an ejective fold and its axial is NE trending. From east to west is Kaiping syncline, Beiziyuan anticline, Jinggezhuang syncline, Gangyao syncline and Chezhoushan syncline. Kaiping syncline is the main structure, and its main axial trending for 30°~60° and as it approaches to the Guye district, the trending gradually turns to east-west almost.

Most folds in the Kaiping coal field are asymmetric, strata dip is great in the north-west wing of syncline and even reverse, the south-east wing is mild, and anticline is opposite (Figure 3, Figure 4).

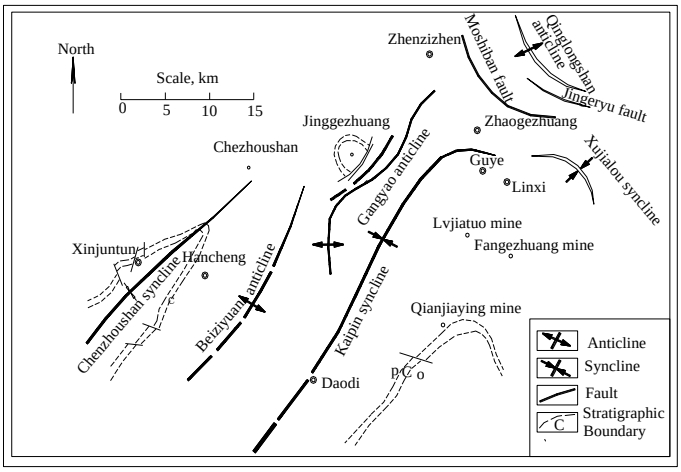

Figure 2 - Sketch of geologic structure in the Kailuan mining area

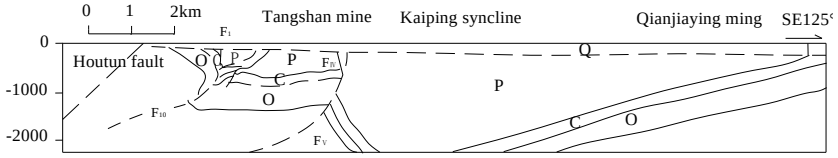

Figure 3 - Profile of Tangshan mine - Kaiping syncline - Qianjiaying mine

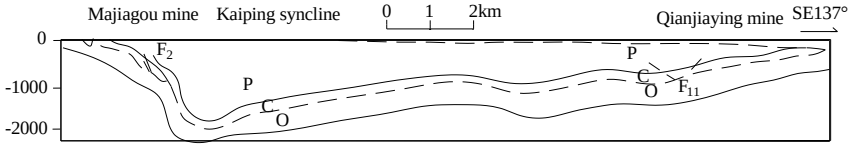

Figure 4 - Profile of Majiagou mine - Kaiping syncline - Qianjiaying mine

IN-SITU STRESS FIELD OF KAILUAN MINING AREA

A large number of *in-situ* stress measurements had been conducted in Kailuan mining area with a hug amount of important raw data. Measurement sites included Jinggezhuang mine, Qianjiaying mine, Fangezhuang mine, Lvjiatuo mine and Donghuantuo mine, Zhaogezhuang mine, Linxi mine and Tangshan mine from 2009 to 2012. Figure 5 shows a comprehensive plot of *in-situ* stress field measurement results in Kailuan mining area.

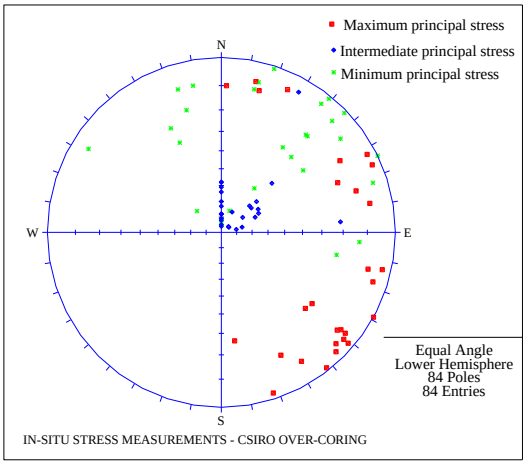

Figure 5 - *In-situ* stress of Kailuan mining area

From the distribution of the maximum principal stress in Kailuan mining area, the highest stress is in Linxi mine which located in the north axis section of Kaiping synclinal. The stress of Qianjiaying mine which located in the south wing of Kaiping synclinal is higher relatively, the stress of Fangezhuang mine which is slightly away from the axis of kaiping syncline is comparatively lower. By examining the distribution characteristics of the *in-situ* stress, it appears that the magnitude of *in-situ* stress of Kailuan mining area is mainly controlled by Kaiping syncline. The site close to the Kaiping syncline axis is the high stress area, with the transition to two wings of syncline, the magnitude of the *in-situ* stress gradually reduces (Figure 6). This observation is in agreement with the theoretical analysis results (Han, *et al.*, 2008).

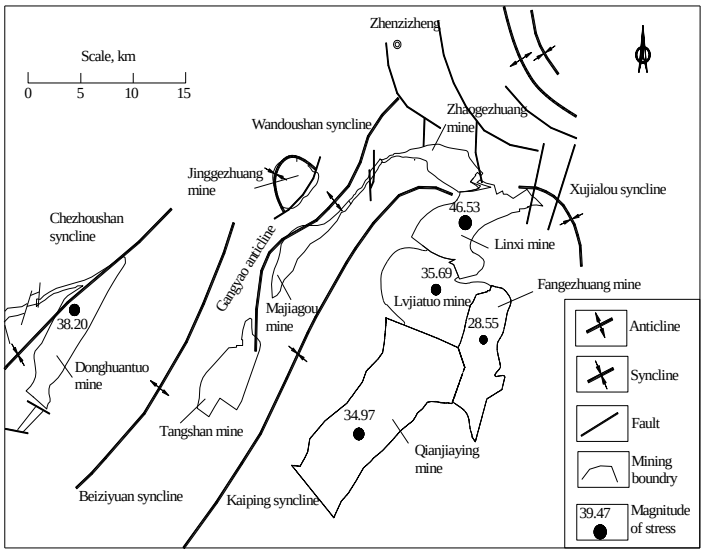

Figure 6 - The max principal stress at -1000 m depth of Kailuan mining area

It is closely related between the azimuth of maximum principal stress and Kaiping syncline axis. The position of maximum principal stress is approximate perpendicular to the Kaiping syncline axis. In the northeast of Kaiping syncline, Zhaogezhuang mine and Linxi mine, the azimuth of maximum principal stress is nearly south-north. In the southwestern of Kaiping syncline, Tangshan mine, Qianjiaying mine, Lvjiatuo mine and Fangezhuang mine, the azimuth of maximum principal stress is north-west. In the area where the Kaiping syncline axis transits from north-east to north-south, the azimuth of maximum principal stress is also gradually transit from north-west to nearly north-south. It reflects that the *in-situ* stress field of Kailuan mining is controlled by Kaiping syncline (Figure 7).

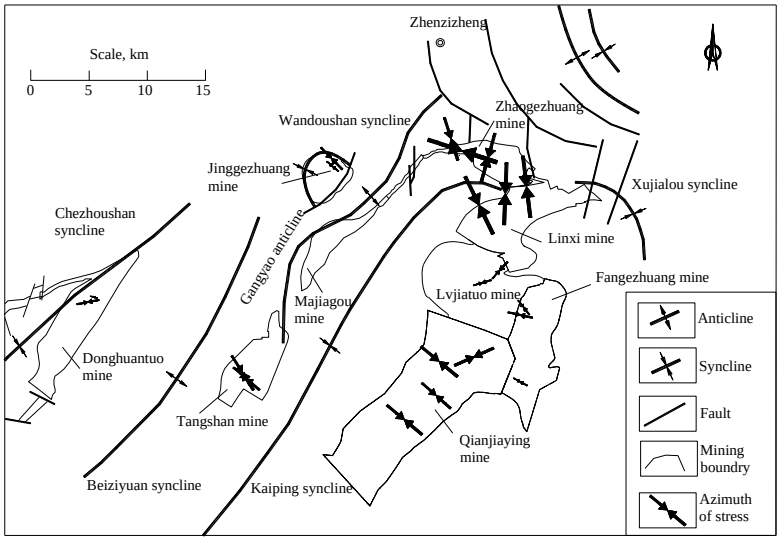

Figure 7 - Azimuth of max principal stress of Kailuan mining area

The general rock engineering indicates the *in-situ* stress in 20~30 MPa as high *in-situ* stress (more than 800 m deep). Because of different rocks have different elasticity modulus, the storage performance of rock is also different, according to GB50218-94(the Chinese Classification standard of rock engineering):

$R_C/\sigma_{Max} < 4$ is extremely high stress, and
$R_C/\sigma_{Max} = 4\text{-}7$ is high stress.

where R_c is UCS (uniaxial compressive strength) of rock; σ_{Max} is maximum principal stress. The relationships between the maximum principal stress and depth in Kailuan mining area is
$\sigma_{Max} = 0.000008\ h^2 + 0.0407\ h + 4.8826$

Thus the mean value of maximum principal stress is 32.32 MPa in - 800 m of Kailuan mining area. If judged by the depth, the *in-situ* stress in Kailuan mining is high stress level because it is more than 30 MPa. The UCS of rock was tested in laboratory. The R_C/σ_{Max} is 0.61 - 2.91, all less than four, therefore the *in-situ* stress of kailuan mining area is in high *in-situ* stress level. In addition, the core disking during the *in-situ* stress measurement of - 1300 m depth in Zhaogezhuang mine is an important indication of high stress.

TECTONIC STRESS ENVIRONMENT OF COAL-ROCK DYNAMIC HAZARD

Tectonic stress environment of coal and gas outburst

The research shows that multilayer flexure rock's stress and strain system depend on the system consisting of the coal seam and roof and floor (Han, *et al.*, 2008). In the syncline structure formation system, the soft coal seam often forms shear action, whilst the surrounding rock has bending effect as a hard layer. Coal's structure under shear action was broken and a lamellar or lay-like tectonic coal was developed (Figure 8). Tectonic coal development degree was correlated with coal seam relative sliding and the state of stress. Tectonic development reduces the strength of coal and the needed energy for triggering coal and gas outburst.

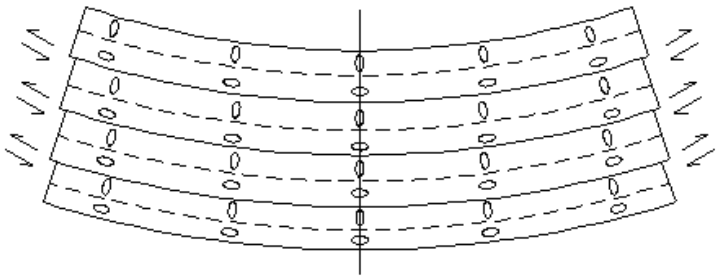

Figure 8 - Relative and unattached strain system in multilayer's bend and glide

The coal seam dip of Kaiping syncline west wing was higher and the slide of coal seam was greater, so tectonic coal exists widely. Especially in the Kaiping syncline west wing where geological structure further damaged the coal seam structure. Majiagou mine and Zhaogezhuang mine are located in the axis of Kaiping syncline west wing nearby, tectonic coal developed and coal permeability is low. Coal's consistence coefficient is 0.14-0.50, the Index (∇p) of initial diffusion rate of coal gas is generally less than 10 mm Hg. In addition, the thick 9^{th} coal (average thickness is 3.47 m, and finally reached 10.00 m), was damaged most seriously in the syncline forming process. Other mines like Qianjiaying mine located in Kaiping syncline's east wing and away from synclinal axis, coal seam dip angle is small and the coal body structure damage slightly.

The gas content of coal seam has distinct characteristics in the wings and axis of Kaiping syncline. In Majiagou mine gas pressure of 9^{th} coal seam was 2.27 MPa and gas content is 15.0 m^3/t. In Zhaogezhuang mine, the highest gas content is near the axis of Kaiping syncline, and the gas content of the 9^{th} coal seam is 8.5 m^3/t, the western average is 7.0 m^3/t, gas pressure is 1.1-1.4 MPa. In Tangshan mine gas content of 9^{th} coal seam is 8 m^3/t. The gas content of Qianjiaying mine, Lvjiatuo mine and Zhaogezhuang mine which are far away from the axis of Kaiping synclinal is very low (gas content is 0.15-1.69 m^3/t) (Figure 9).

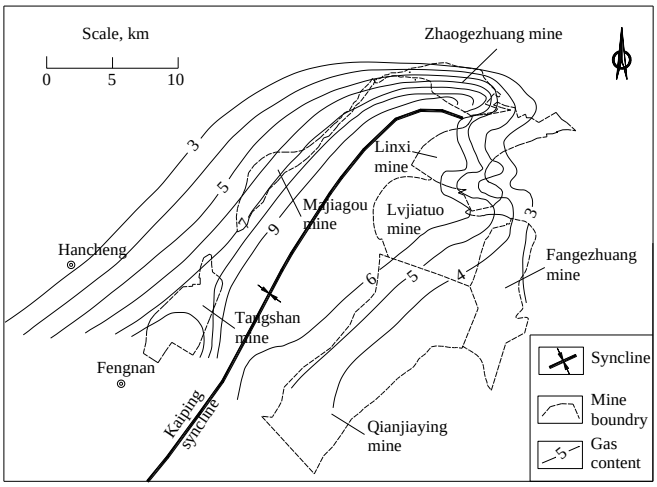

Figure 9 - Gas content of No.9 coal seam in Kailuan mining area

High tectonic stress makes coal seam high gas content and low permeability characteristics in the axis of syncline, and coal's strength is reduced at the same time. Hence the axis section of the syncline has coal and gas outburst danger, and the mines in the wing section of syncline, because of relatively weak tectonic stress.

Tectonic stress environment of rockburst

Rockburst in Laohutai mine, Tianchi mine, Mentougou mine, Fangshan mine and Huating mine showed that the axis section of fold was a rockburst prone zone. The high *in-situ* stress plays a key role in triggering the process of rockburst.

In-situ stress in the Kaiping syncline axis section is higher, which provides a dynamic environment for rockburst. Zhaogezhuang mine and Tangshan mine located in Kaiping syncline axis section, both have higher *in-situ* stress than other mines that are far away from the syncline axis section. In addition, the *in-situ* stress azimuth has a significant effect on rockburst. In Kailuan mining area, because of Kaiping syncline and the maximum principal stress are approximate vertical the mining drivage direction and the maximum principal stress are approximate vertical, this is the roadway under high tectonic stress action. The existence of Kaiping syncline resulted in the heterogeneous characteristics of Kailuan mining area tectonic stress distribute in three-dimensional space. Near the Kaiping synclinal axis section, the tectonic stress enables the rock to accumulate a large number of elastic energy. High i*n-situ* stress provides a dynamic condition and energy source for rockburst.

Tectonic stress environment of water inrush

According to the hydraulic fracturing mechanics principle, during the crack formation, if there is enough fracturing fluid and pressure that can make the crack open and dilated, then fracture will extend along the line of least resistance. The pressure that can extend fracture not only depends on the minimum principal stress, but also the fracture type, size and rock formation property. Theory of water inrush explains as: floor water inrush is the interaction result of the mining pressure and floor confined water pressure, the mining pressure leads to the fracture onset in floor water-resisting layer at certain depth, thus reducing the rock mass strength and the impervious performance, which redistribute the floor stress field. When the rock mass is softened by the confined water that further infiltrates the fracture, this leads to the inductive water fracture continue to expand, till the interaction reduces the minimum principal stress of the floor water-resisting layer rock mass below the confined water pressure, then fracture dilation will occur and induce water inrush. This can be expressed as:

$I=P_w/\sigma_{hmin}$,

where I is water inrush Critical index, P_w is water pressure of floor water-resisting layer rock mass, and σ_{hmin} is minimum principal stress of the floor water-resisting layer rock mass.

If the confined water pressure (P_w) is less than the minimum horizontal principal stress (σ_{hmin}), it will not produce fracturing expansion effect and water inrush. Only confined water pressure (P_w) is more than the minimum horizontal principal stress (σ_{hmin}), there will be fracturing expansion effect and water inrush.

The research of *in-situ* stress stress in Kailuan mining area identified the high stress area close to the Kaiping syncline axis section, the low stress area away from the axis section, and the low *in-situ* stress area in Fangezhuang Donghuantuo mine. Figure 4 showed that at -800m depth, the maximum principal stress reached 44.2 MPa in Linxi mine and 25.0 MPa, 25.33 MPa and 31.7 MPa respectively in Fangezhuang mine and Donghuantuo mine. The minimum principal stress is 6.5-13.9 MPa in Fangezhuang mine and Donghuantuo mine, the minimum principal stress is in a relatively low level. According to water inrush theory, areas with low minimum principal stress will have a high water inrush risk. Thus the mine far from Kaiping syncline axis has more water inrush risk.

CONCLUSIONS

Based on the stress test results in Kailuan mining area, the tectonic stress environment of coal and gas outburst, rockburst, water inrush was analysed. The results show that coal and gas outburst, rockburst, water inrush is mainly controlled by the stress field in Kailuan mining area.

The compression of tectonic stress field in Kailuan mining area led to high gas content and low permeability in the syncline axis section of the coal seams. Combined with low coal mass strength caused by tectonism, the syncline axis section is more prone to coal and gas outburst. Coal mines located in the syncline wing have relatively high permeability, low gas content due to relatively low *in-situ* stress. Thus these coal mines do not have coal and gas outburst conditions.

The Kaiping syncline axis section is an area with high *in-situ* stress, which provides the dynamic conditions for the occurrence of coal- gas outburst and rockburst. As Zhaogezhuang and Tang Shan located Mine are both located near the Kaiping syncline axis section with high *in-situ* stress, they have more serious coal and rock dynamic conditions.

The lower the minimum principal stress, the higher the risk of water inrush, thus coal mines located far away from the syncline axis section will have higher water inrush risk. The water inrush in Fangezhuang mine and Donghuantuo mine is caused by the rupture formed by fault structure relief and mining failure in the low tectonic stress environment.

ACKNOWLEDGMENTS

The work presented in this paper was financially supported from the National Natural Science Foundation of PR China (Grant No. 51104085) and Doctoral Fund of Ministry of Education of China (Grant No. 20102121120007). The authors acknowledge the help of Dr Ting Ren, University of Wollongong, for improving the paper in English.

REFERENCES

Cook, NGW, 1965. The failure of rock. *Int J Rock Mech Min Sci*, 389-403.

Han, J, Zhang, H and Huo, B, 2008. Discussion of coal and gas outburst mechanism of syncline. *Journal of China Coal Society*, 33(8): 908-913 (in Chinese).

Jiang, Y, Liu, W and Zhao, Y, 2005. Study on surrounding rock stability of deep mining in Kailuan mining group. *Chinese Journal of Rock Mechanics and Engineering*, 24(11):1857-1862 (in Chinese).

Jiang, Y, Zhao, Y and He, M, 2007. Investigation on mechanism of coal mine bumps based on microscopic experiments. *Chinese Journal of Rock Mechanics and Engineering*, 26(5): 901-907 (in Chinese).

Li, T, Cai, M and Wang, J, 2005. Discussion on relativity between rockburst and gas in deep exploitation. *Journal of China Coal Society*, 30(5): 562-567 (in Chinese).

Liu, W, Jiang, Y and Shan, X, 2006. Analysis on induced factors of pressure bump occurred in deep mine roadway of Zhaogezhuang mine. *Coal Science and Technology*, 34(11): 60-63 (in Chinese).

Meng, Z, Yi, W and Lan, H, 2009. Water inrush characteristics of Fangezhuang coal mine field in Kailuan and its geological condition analysis of water inrush from coal seam floor. *Chinese Journal of Rock Mechanics and Engineering*, 28(2): 228-237 (in Chinese).

Qi, L, Lin, B and Zhi, X, 2006. Study on the mechanism of coal and gas dynamic phenomenon in Majiagou mine. *China Safety Science Journal*, 16(12): 30-34 (in Chinese).

Qi, Q, Shi, Y and Liu, T, 1997. Mechanism of instability caused by viscous sliding in rockburst. *Journal of China Coal Society*, 22(2): 144-148 (in Chinese).

Skochinski, A A, 1954. Modem concepts on the nature f sudden outbursts of gas and coal and control techniques, *Ugol.* 7:4-10 (in Russian).

Wang, R, 2011. Study on water inrush geomechanical condition and its water inrush risk of coal roof and floor. Ph.D thesis (unpublished), China University of Mining and Technology, Beijing (in Chinese).

Yin, G, Xian, X and Jin, L, 1997. The effect of crustal stresses on rock burst and evaluation of zone prone to rock burst. *Journal of China Coal Society*, 22(2):133-137 (in Chinese).

Zhang, M, Xu, Z and Pan, Y, 1991. A united instability theory on coal (rock) burst and outburst. *Journal of China Coal Society*, 16(4):48-53 (in Chinese).

Zhou, S and He, X, 1990. Rheological hypothesis of coal and methane outburst mechanism. *Journal of China University of Mining and Technology*, 19(2):1-8 (in Chinese).

EXPERIMENTAL APPROACH TO MEASURE STRESS AND STRESS CHANGES IN ROCK AHEAD OF LONGWALL MINING FACES IN CZECH COAL MINES

Kamil Soucek, Petr Konicek, Lubomir Stas, Jiri Ptacek and Petr Waclawik

ABSTRACT: The measurement and monitoring of stress in rock mass are very important tasks in mining geomechanics. With increasing mining depth and worsening of the geological and mining conditions, a suitable method to determine and monitor rock stress and stress changes due to longwall coal mining is needed. Detailed knowledge of the stress state in rock mass is very useful when designing safe mining activity, especially in rockburst areas. The paper presents a brief description of the Compact Conical-ended Borehole Monitoring (CCBM) method for rock stress evaluation and the technical details of this innovative technology. The second part of the contribution evaluates and discusses initial results and experience obtained from the use of CCBM equipment for determination and observation of mining-induced stresses during mining of selected longwall panels in the conditions of the deep coal mines of the Upper Silesian Coal Basin.

INTRODUCTION

Knowledge of the stress state in rock mass is very important in mining geomechanics, especially in rockburst areas. According to the rockburst legislation (OKD, DPB, a. s., 2005) of the Czech Republic, the range of mining-induced stresses in front of longwall faces and their influence on mining conditions needs to be determined.

The problems of rock stress and its determination have been under investigation at the Institute of Geonics for a long time. With increasing mining depth and worsening of the geological and mining conditions, a suitable method to determine and monitor rock stress and stress changes due to longwall coal mining is needed. During the past 20 years, the hydraulic fracturing method was commonly used, but this method does not appear to be fully satisfactory for these purposes because it does not allow determination of all the components of the stress tensor or continuous observation of stress changes. Due to a problem with the long-term stability of the boreholes used, the decision was made to develop a device which enables determination of all three principal stress components. Development of the device described in this paper was based on the experience of Sugawara and Obara from Kumamoto University. They were the first to develop and use the Compact Conical-ended Borehole Overcoring system (CCBO) (Sugawara and Obara, 1999; Obara and Sugawara, 2003). The conical shape of the CCBO probe provides a sufficient number of strain measurements in independent directions in one probe position in the borehole so that all values of the stress tensor can be determined. Two variants of the CCBO probe were developed at the Institute of Geonics - the first variant is equipped with a microprocessor for remote, wireless automatic recording of measured data on the probe's internal memory, and the second one can be connected to a data-logger and power supply via a cable. The latter type CCBM device, was used for long-term monitoring of stress tensor changes (Stas, *et al.*, 2005).

This paper begins with a brief description of the conical ended borehole monitoring method and the technical details of this innovative technology. The second part of the contribution evaluates and discusses results and experience obtained from the use of CCBM equipment for determination and observation of mining-induced stresses during extraction of selected longwall panels in deep coal mines.

MINING PRACTICE FOR DETERMINING THE RANGE AND EXTENT OF MINING-INDUCED STRESSES

According to the rockburst rules (OKD, 2005) of the Czech Republic, the range of mining-induced stresses in front of the longwall face and their influence on mining conditions needs to be determined. Recent mining practice in Czech underground coal mining operations in the Upper Silesian Coal Basin

Institute of Geonics AS CR, v. v. i. kamil.soucek@ugn.cas.cz, +420596979218

has interpreted the range of the induced stress by using the monogram based on physical modelling for approximately 30 years (OKD, 2005). This method of stress range assessment turns out to have ample security. The main input data for determining the range and extent of mining-induced stresses are the depth under the surface and the thickness of the excavated coal seam (see Figure 1). The figure serves as an example for interpretation of the mining-induced stress range in the surroundings of the longwall face mined out of a coal seam of thickness 5 m at a depth of 900 m under the surface. The resulting induced stress range is here 110 m. The disadvantage of this way of determining the induced stresses is the lack of information about their magnitude and course around the longwall block (panel). In general, the induced stress level rapidly increases in the immediate vicinity of the mined out area and then slowly decreases. A similar stress state theoretically manifests itself along the gob (old man). Therefore monitoring the induced stresses in front of the longwall faces using the CCBM probes on trial was started four years ago.

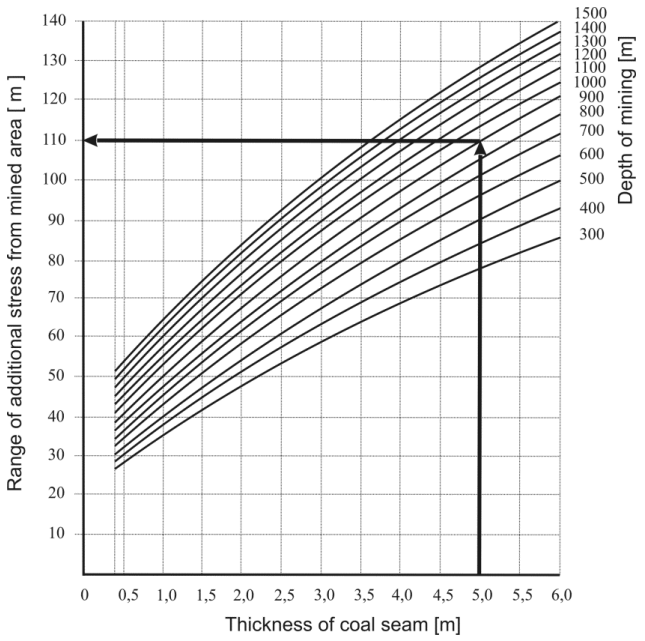

Figure 1 - Monogram for determining mining-induced stresses

FUNDAMENTAL DESCRIPTION OF THE CCBM EQUIPMENT

The CCBM probe is designed for boreholes 76 mm in diameter. The waterproof probe body has a diameter of 55 mm. Six pairs of mutually perpendicular strain gauges are mounted onto the conical tip of the probe with an apical angle of 60° (see Figure 2), at the level where the diameter is 38 mm. The geometry described above is deliberately the same (except for the number of strain gauges) as the one designed, optimized and verified for the original CCBO method (Prof. Sugawara and Prof. Obara). This allowed the wealth of their experience to be drawn on. The geometry is described in full detail in Sugawara and Obara (1999).

The probe for the CCBM was designed as an alternative to the equipment developed for CCBO. The CCBM probe, which can be connected to an external control unit by cable (see Figure 3), thus enables observation of the stress changes in the rock mass (induced, for example, by underground mining activities). The probe consists of two parts:

- A measuring conical tip containing six strain gauges - two-element 90° tee-rosettes (longitudinal gauges and tangential gauges).
- The body of the probe containing an electronic multiplexed quarter strain gauge bridge MUX, analogue to digital converter A/D, microprocessor μP, stabilized power supply and TTL/RS-232 interface.

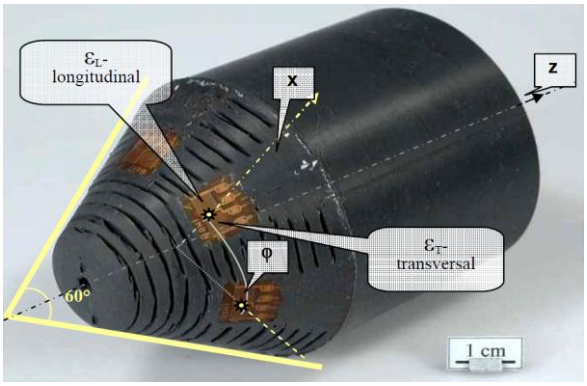

Figure 2 - CCBO gauges probe and representation of coordinate system used

Figure 3 - A gauges probe for long-term measurement of stress tensor changes (left side), registration unit PSION (right side)

Three principal modes of CCBM probe operation are available (detailed modes information can be found in Knejzlik and Rambousky (2008) and Knejzlik (2004)):

- Periodic manual reading of data using a portable computer or data-logger (notebook, Psion).
- Remote data transmission, which can be carried out using virtually any known method of computer communication.
- Implementation of the distributed control and measuring network.

The experiments described below were performed using the first mode – periodic manual data reading using a portable Psion data-logger.

The installation procedure of the CCBM probe is as follows:

- Drilling a borehole to the projected length - the quality of rock is examined from the core samples.
- Forming and polishing the bottom of the prepared borehole using a special conical drill bit (see Figure 4).
- Checking the homogeneity of the shaped borehole bottom by a TV inspection system - if the surface quality of the shaped borehole bottom is unsatisfactory (discontinuities or large grains,) it is necessary to continue drilling to a more suitable position to repeat the shaping and inspection procedure.
- Drying out the borehole bottom with compressed air if the surface quality is evaluated as satisfactory.
- Cementing the probe in place - a special kind of resin glue (epoxy type) is used to cement the probes, the handling equipment is fitted with a device which detects orientation, enabling

(together with knowledge of the direction and the inclination of the borehole) the determination of the location of strain gauges oriented in the space of the rock mass.

- The probe is ready to start measurement after proper glue setting and removal of the handling rods.

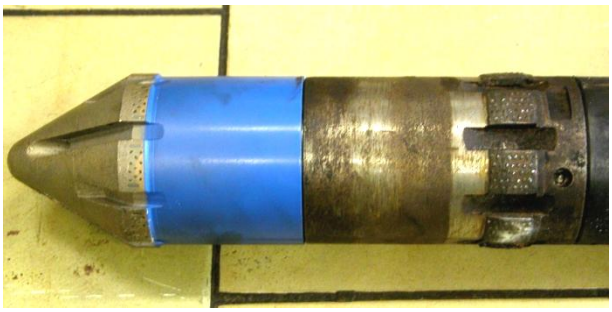

Figure 4 - Special conical drill bit used for shaping of bottom of installation borehole

COMPACT CONICAL ENDED BOREHOLE MONITORING METHOD (CCBM) - PRINCIPLES AND METHODOLOGY

The CCBM method is based on similar principles except that the 'destructive' overcoring phase is not performed. This method allows repeated measurement of strain on all sensors of the probe over a long period. In this case, however, only changes of the stress tensor in relation to the stress state at the time of probe installation (i.e. to the reference state) can be determined. This is the principal difference between the CCBO and CCBM methods. The evaluation of measurements is the same as in the case of the CCBO technique.

The dependence of the corresponding gauge sensor strain on the stress tensor for CCBO has been formulated in Sugawara and Obara (1999) and Obara and Sugawara (2003). For CCBM, it can be formulated as follows (Stas, *et al.*, 2011):

$$[\varepsilon_{\wedge}^{\Phi j}(t_i) + \varepsilon_{\wedge}^{\Phi j}(\Delta t)] \times E = |\boldsymbol{A}(\Lambda;\mu;\Phi_j)| \times [\,|\boldsymbol{\sigma}_i| + |\boldsymbol{S}(\Delta t)|]$$

Hence the following equation can be expressed:

$$\varepsilon_{\wedge}^{\Phi j}(\Delta t) \times E = |\boldsymbol{A}(\Lambda;\mu;\Phi_j)| \times |\boldsymbol{S}(\Delta t)|$$

where $\varepsilon_{\wedge}^{\Phi j}(t_i)$ and $\varepsilon_{\wedge}^{\Phi j}(\Delta t)$ are strain $\varepsilon_{\wedge}^{\Phi j}$ at the time of probe installation and differential strain related to time of installation respectively; $|\boldsymbol{\sigma}_i|$, $|\boldsymbol{S}(\Delta t)|$ are stress tensor at the time of installation t_i and induced stress tensor (stress changes at time Δt after installation) related to stress state $|\boldsymbol{\sigma}_i|$, respectively; E is Young's modulus and μ is Poisson's ratio. The optimal stress changes tensor of the whole system can be determined by calculating the differences of all ("j-") pairs of corresponding measurements ($\varepsilon_{\wedge}^{\Phi j}(\Delta t)$) and ideally implied strains ($\varepsilon_{\wedge\Phi j}(\Delta t) \equiv |\boldsymbol{A}(\Lambda;\mu;\Phi_j)| \times |\boldsymbol{S}(\Delta t)|/E$) using the method of least squares. A scheme of the CCBM is represented in Figure 2.

IN-SITU MONITORING OF THE INDUCED ROCK MASS STRESSES IN FRONT OF LONGWALL FACES

The development of the mining-induced stress ahead of the longwall face can be described through *in situ* observations of the installed CCBM probes. Applicability tests of the CCBM method were performed in several localities of the Czech part of the Upper Silesian Coal Basin. Changes in the vertical component of the induced stress at different positions of the longwall faces are of interest and were evaluated through readings from the installed CCBM probes. Results of the stress measurement at the three localities are described below. The rock stress monitoring was carried out at the Lazy collieries in the Karvina Coal Sub-basin at the two longwall panels No. 140 914 and 140 912 in coal seam N^{o} 504. Next, monitoring was performed in the longwall panel N^{o} 361 000 at the CSM Mine in the Karvina Coal Sub-basin in coal seam N^{o} 36. In most cases the CCBM probes were installed only in the overburden compact sandstone beds at vertical distances of 10 m to 20 m from the working coal seams. One CCBM

probe P1 was installed in the underlying bed of the working coal seam on the Lazy colliery (see Table 1). The installation boreholes were drilled from both the main and tail longwall gates at distances of 110 m to 540 m from the starting longwall face positions. Table 1 shows a basic description of the installed CCBM probes and the longwall panels.

Table 1 - Description of CCBM probe location

Name of probe	Colliery	No. longwall panel	Average coal seam thickness (m)	Average coal seam depth (m)	Length of longwall panel face (m)	Vertical probe position above (*under) coal seam (m)	CCBM probe distance from starting longwall face position (m)
L1	Lazy	140 914	4.1	690	110	16	180
L2						12	180
N1	Lazy	140 912	3.6	720	160 -180	16	540
N3						16	540
P1						*3	540
C1	CSM	361 000	1.8	980	180	16	110
C2						10	110

The first installed CCBM probes in front of longwall panel No. 140 914 showed satisfactory sensitivity to the mining activity. This finding was a strong impulse to use this probe for evaluation of the rock stresses in front of the longwall faces. The direct dependence of the stress changes on the progress of the longwall face is evident from subsequent events. The progress of the longwall face had to be temporarily discontinued due to technological problems (see the part inside the oval in Figure 5) from 20-23 February. This pause was immediately reflected in the evolution of the stress state behaviour of the rock mass during this period. Strain evolution registered by the gauges was retarded or even halted. The closer the position of the L1 probe was to the worked coal seam, the more distinctive the influence. The values of the stress changes on the CCBM probes L1 and L2 during this period are shown in Figure 5. S1, S2 and S3 in Figure 5 represent the components of the principal stresses.

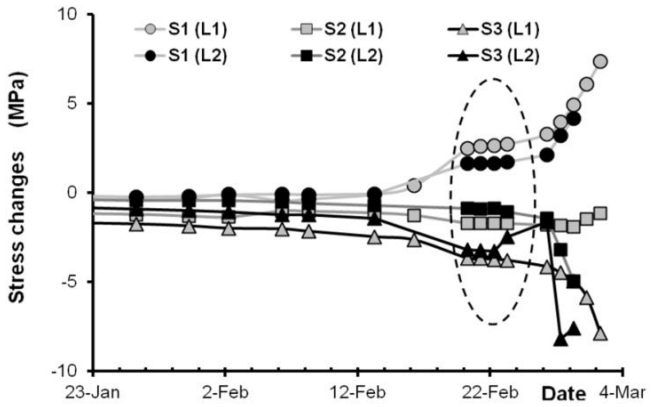

Figure 5 - Development of the stress changes on the L1 and L2 probes during longwall face stoppage

Mining-induced stress development

The observation by CCBM monitoring of the influence of the progress of the longwall face on the range of mining-induced stresses was evaluated on the basis of the development of the real volume component I_1 (first invariant, $I_1=S_1+S_2+S_3$, where S_1, S_2 and S_3 are components of the principal stresses). The one third of the first invariant value is plotted in the graphs in the next Figures 6, 7, 8 and 9 distinguish than batter. The first signs of change (insignificant) in the mining-induced stress, at almost all of the CCBM measuring probes, were recorded at distances from the longwall face ranging from 50 m to 70 m (see Table 2 and Figures 6 and 7). The range of these distances is at a lower level than the range of the mining-induced stresses determined according to the conventionally used monogram on the condition of the Upper Silesian Coal Basin. In one case, however, this range was recorded as higher than the range of

mining-induced stresses determined with the monogram, i.e., at more than 100 m (see Table 2, and Figures 8).

Table 2 - Range of the mining-induced stresses
(*) negative values represent compression loading, positive values represent relieving)

Name of probe	No. of longwall panel	Average coal seam depth / Theoretical vertical stress (m) / (MPa)	Maximal change of vertical component of induced stress *) percentage (MPa)	Distance from longwall face at maximal change of vertical component of induced stress (m)	Distance from longwall face at 10% change of the theoretical vertical stress component (m)	Influence range of induced stresses according to CCBM monitoring (m)	Influence range of induced stresses according to monogram (see Pict.1) (m)
L1	140 914	690 / -17	- 3.9	9	33	>100	93
L2			- 6,6	5	7	100 - 120	
N1	140 912	720 / -18	+7,7	20	27	50	87
N3			- 5.3	4	28	60	
P1			+2	0	1	58	
C1	361 000	980 / -23	- 3.5	22	28	51	70
C2			+13.3	3	34	70 - 80	

The more significant changes of the mine-induced stress in the overlying rock, at a 10% level of change from the theoretical vertical stress component, arise at a distance from the longwall face of c. from 1 m to 35 m (see Table 2 and Figures 6 - 8). From the development of changes in the vertical component of the mining-induced stresses and real volume component I_1 depending on the progress of the longwall faces in different mining and geological conditions, both additional compression loading and relieving of the rock mass are obvious (see Table 2 and Figures 6 - 9, where negative values of the stress changes represent compression loading, and positive values represent relieving). Figure 6 shows that cyclical compression loading and relieving of the overburden sandstone bed is probably due to its sequential caving. A different case (probe P1 placed in an underlying bed) of mining-induced stress development is represented in Figure 7. It is evident that real volume component I_1 demonstrates compression loading development of the stress, while the development of changes in the stress vertical component shows relieving up to 2 MPa. This was caused by the effect of the development of significant compression loading in a horizontal plane at the site of CCBM probe P1 (see Figure 7).

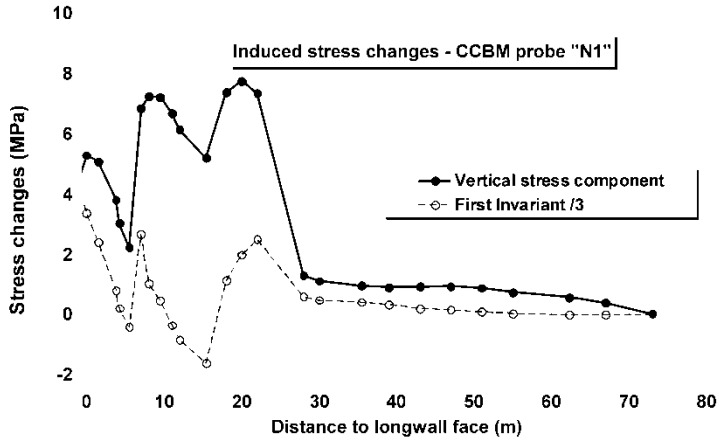

Figure 6 - Change of mining-induced stresses - CCBM probe N1

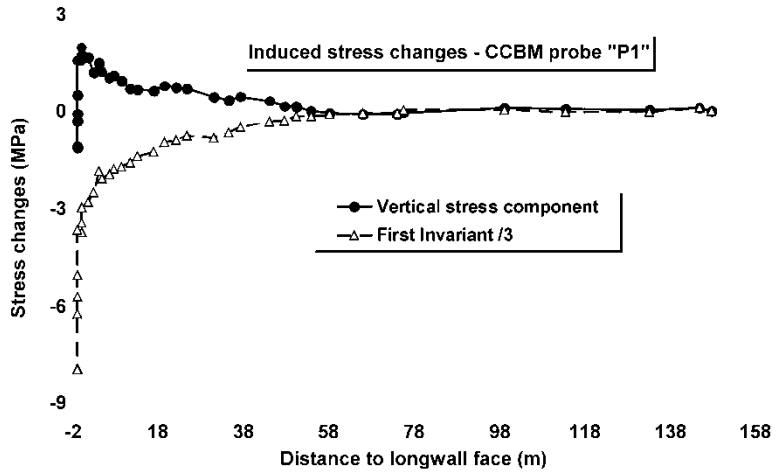

Figure 7 - Change of mining-induced stresses - CCBM probe P1

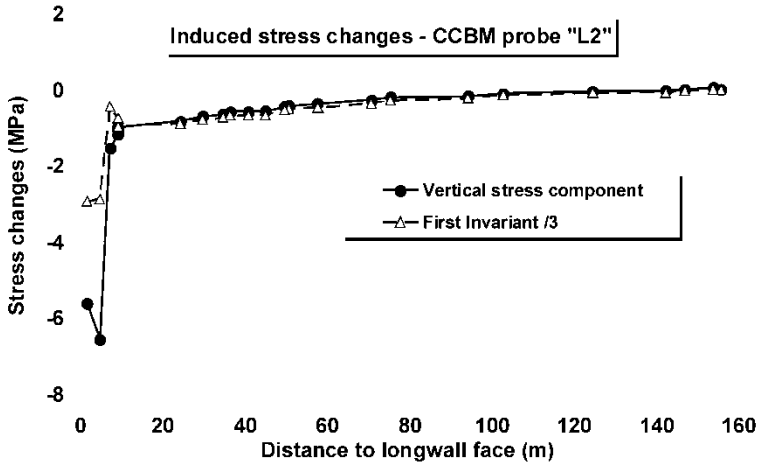

Figure 8 - Change of mining-induced stresses - CCBM probe L2

The next observed example of the development of mining-induced stress is represented in Figure 9 by measurement at the CSM colliery (Tables 1 and 2). Two CCBM probes C1 and C2 were installed in the overburden of the sandstone bed. In this area there were very simple mining conditions without any other mining work, and only the geological conditions were different at the placement of the CCBM probes C1 and C2. Probe C1 was placed in a relatively stable area without significant discontinuities and faults, while CCBM probe C2 was installed near to the regional fault "X", which probably affected the rock stress state at its location (see Figure 9). From the development of the mining-induced stresses on CCBM probes C1 and C2, we can see that the area of the rock mass lying under the inclined fault is relieved to a greater extent (about 56%) in comparison to value of the theoretical vertical stress component. The tensile character of all the principal components of the induced stress during the longwall face advance shows that the area close below the inclined fault is partially shaded, and thus the immediate influence of overburden loading might be deformed (Stas, *et al*., 2011).

CONCLUSIONS

On the basis of the results of the trial carried out using CCBM monitoring it can be stated that using the CCBM method provides the possibility of performing more detailed analysis of the development of the rock mass stress state during geomechanical processes induced by geotechnical works or the effects of mining. The CCBM monitoring of the mining-induced stresses provided the opportunity to perform a more detailed analysis of the development of the stress state through a strata equilibrium dynamics induced by the underground mining of the coal seams by the longwall method. This method can specify the range of induced stresses in different mining and geological conditions, but for generalization or more precise conclusions it will be necessary to conduct more CCBM monitoring of the rock mass stress state in the Upper Silesian Coal Basin.

The first systematic pilot project of the rock stress monitoring by the CCBO and CCBM methods will be performed at the Lazy Colliery in coal seam No. 504 during mining of longwall panel No. 140 704 next year, 2013. The depth of cover of the coal seam is about 750 m, the length of the longwall face is 205 m and the thickness of the mined coal seam is 6 m. There will be 12 monitoring stations with both CCBM and CCBO probes in different mining and geological conditions in the area surrounding the longwall panel of interest (see Figure 10). From Figure 10, it is evident that monitoring stations are to be placed in different areas with different rock mass stress states. The original rock stress state is influenced by previous mining workings in the surroundings, with both overlying coal seams and coal seam No. 504. The main and tail gates of longwall panel No. 140 704 mostly pass through areas with additional rock mass stress as a consequence of mining seams in the overburden (coal seams No. 512 and 530) and in the level coal seam No. 504 (adjacent to longwall panel No. 140 702).

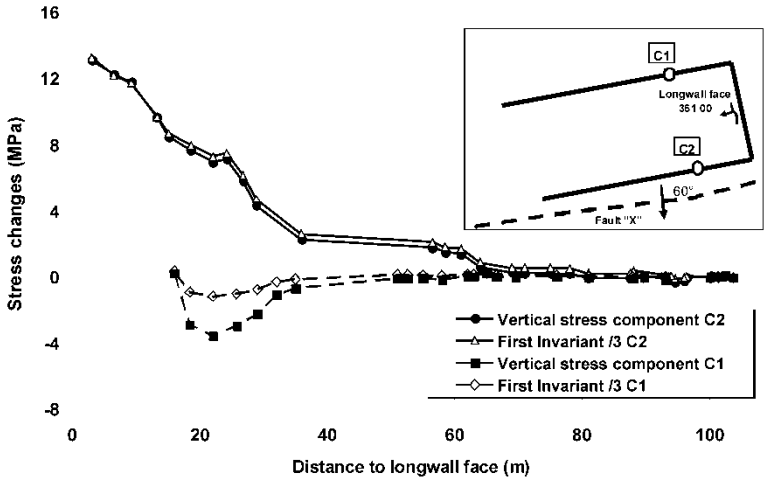

Figure 9 - Change of mining-induced stresses - CCBM probes C1 and C2

Figure 10 - Project for rock stress monitoring by CCBO and CCBM methods

Continuous knowledge of the stress state development can help to determine appropriate measures for managing the situation of high stress concentrations during mining below the competent roof strata for the next planned longwall panels in similar mining and geological conditions. This approach can also be helpful in ensuring the stability of underground structures, the selection of reinforcement systems and the *in situ* characteristics of the coal/rock mass.

ACKNOWLEDGEMENTS

This article was prepared in connection with a project of the Institute of Clean Technologies for Mining and Utilization of Raw Materials for Energy Use, reg. no. ED2.1.00/03.0082 (CZ.1.05/2.1.00/03.0082) supported by the Research and Development for Innovations Operational Programme, financed by the EU Structural Funds and from the state budget of the Czech Republic and is financially supported within the framework of the Safety Research Programme of the Czech Republic 2010 – 2015 (BV II/2-VS), the

project Safety aspects of executing mine work at depths of 800 m and greater (VG20102014034). This work was supported by the Czech Academy of Sciences projects ČR OZ 30860518.

REFERENCES

Knejzlik, J and Rambousky, Z, 2008. Recent solution of the distributed control and measurement system in the Jeronym Mine - modular system, *Acta geodynamica et geomaterialia*, 5(2):205-212.

Knejzlik, J, 2004. Data transmission from seismic stations via network AGNES using GSM-GPRS technology, *Acta Montana. Ser. A, B*, 1(1):73-76.

OKD, DPB, a s, 2005. Working rules of rockburst prevention in OKR (in Czech), Paskov.

Obara, Y and Sugawara, K, 2003. Updating the use of the CCBO cell in Japan: overcoring case studies, *International Journal of Rock Mechanics and Mining Sciences*, 40:1189-1203.

Sugawara, K and Obara, Y, 1999. Draft ISRM suggested method for *in-situ* stress measurement using the compact conical-ended borehole overcoring (CCBO) technique, *International Journal of Rock Mechanics and Mining Sciences*, 36:307-322.

Stas, L, Soucek, K, Knejzlik, L, Waclawik, P and Palla, L, 2011. Measurement of stress changes using a compact conical-ended borehole monitoring, *Geotechnical Testing Journal*, 34(6):685-693.

Stas, L, Knejzlik, J and Rambousky, Z, 2005. Conical strain gauge probes for stress measurement, in *Proceedings of Eurock 2005 - Impact of Human Activity on the Geological Environment*, Leiden: A.A.Balkema Publishers, pp 587-592.

IMPROVEMENTS IN LONG TENDON SUPPORT WITH PUMPABLE RESIN

Tom Meikle[1], Stephen C Tadolini[2], Robert Hawker[3] and Daniel Pollack[4]

ABSTRACT: Long tendon support systems provide several challenges when used as part of the secondary or primary support cycle. A two-component pumpable resin, Carbothix, has been in development for use with self-drilling rock bolts. Many of the attributes of this new resin system make it ideal for grouting long tendon support systems. While neat Portland cement grouts or polyester resin capsules have been used with long tendon support systems for many years, two-component pumpable resin systems overcome many of the shortcomings in these systems. The two-component systems dramatically improve the set-time to enable mining face advance with fewer delays, enable longer pumping distances, improve quality control, and enhance load transfer mechanisms. This paper describes the key benefits associated with a new pumpable resin and details the Coal Services Health/Workcover atmospheric testing results and cable load testing completed to date. It also details the results of the Australian mine site trials and the introduction of these systems into production use.

INTRODUCTION

Resin-grouted cable systems have been in use for many years. Tadolini (1994) detailed the development of these systems with the use of resin capsules for enhanced coal mine roof support, but the length of the tendons described were short (6 m) in comparison to long tendon systems used in Australia (13 m). Long tendon cable support systems are used in both coal and metal mines. Resin capsules are only used with long tendons (6 m to 8 m in length) for point anchoring to enable pre-tensioning of the cable prior to full encapsulation of the cable with a cement grout. Also, resin capsules can only be used with single strand cable systems, due to mixing and anchorage issues with twin-strand systems. These issues make them unsuitable for the majority of hard rock cable systems, which are twin-strand in configuration. In addition to the mixing and quality of anchorage issues, resin capsule anchoring is often difficult where variation in borehole size is experienced. Initially, Portland cement cable bolts were "bottom up" grouted, using a Portland cement/water mixture. In more recent years, with advanced grout technology, grouts with low shrinkage and high strength properties have been introduced. Low slump grouts have also been developed to allow "top down" grouting of cables, particularly those cables that are point anchored and pre-tensioned using resin capsules. However, current cement grouting systems (grout and equipment) have some disadvantages:

1. Quality of grout has always been an issue; very rarely do operators mix grout to manufacturer's specification, often relying on the operators visual observations to determine whether the grout was of the correct mixture.
2. Low slump grouts require pumps that can pump a thick grout; choice of suitable pump is limited.
3. Pumping distance is limited with current grout pumps; operators often add more water to allow pumping long distance, which adversely impacts the quality and strength of the material.
4. Grout is mainly supplied in 20 kg bags; therefore, grout waste is excessive when a small number of cables are to be grouted (for example, a row of cables in a continuous miner heading).
5. Grout strength development is relatively slow in comparison to resin systems, thus making tensioning of cable system only possible after hours of cure rather than minutes.

Carbothix two component resin

Carbothix can best be described in the following statements:

[1] *General Manger - Operations Minova Australia. Wyong, NSW Australia, tom.meikle@:minovaint.com, M: +61(0) 407 289 209*
[2] *Chief Technical Officer Minova USA. Georgetown, KY USA*
[3] *Civil Business Manager Australia/Asia, robert.hawker@minovaint.com, M: +61 418 680 001*
[4] *Mining Engineer, Minova Australia. Nowra, NSW Australia*

- Two component Urea Silicate bonding resin used for long tendon cables and strata reinforcement bolts, e.g. Wiborex and Fibre Reinforced Polymer (FRP) bolts
- Used in Self- Drilling Rock Bolts (SDRB)
- Delivered via two component pump and hoses
- Mixed in volume ratio from 1(Part A):1(Part B) or 1(Part A):2(Part B) depending on the application needs and strength requirements
- Mixed at grouting site
- Reacts to form thick paste for "top down" grouting within seconds of mixing and sets within minutes to provide early load transfer between steel tendon and strata
- Early set time allows cables to be fully tensioned in less than 60 min
- No reaction with borehole water
- Low application pressures
- Cured resin is highly resistant to acidic and alkaline environments

Using the Minova long distance pumping system, Carbothix resin has been supplied a distance up to 2.5 km in Germany.

History of Carbothix use for long tendon grouting

Xstrata Nickel first trialed the use of Carbothix in 2006 at the Craig mine as part of its Sudbury Basin operations support plan (Pritchard and McClellan, 2011). The resin was initially used for grouting hollow core fibreglass rebar but was soon investigated for use with long tendon support systems. Cable bolts up to 10 m in length have routinely been fully grouted at the operation with great success, achieving full encapsulation by using Carbothix materials.

Other cable applications at the mine have enabled cycle times to be reduced by up to 24 hours compared to Portland cement cable systems. This is because the resin sets within one minute of cable grouting, and tensioning can occur less than ten minutes later. The initial resin used was a fast setting 1:1 formulation to accommodate the cool rock conditions. Some difficulty was experienced with this resin when using longer cables, which required the development and use of a slower setting version.

Carbothix has now been "fully" implemented at the Xstrata Nickel - Fraser and Nickel Rim mines, Goldcorp Musselwhite mine, Ontario, Canada, Resolution Copper, Arizona, Vale Birchtree and T1 mines in Thompson Manitoba, USA.

INTRODUCTION OF CARBOTHIX TO AUSTRALIAN HARD ROCK MINES

Initial trials at Cosmos Mine, WA, owned by Xstrata, where underground air and product temperatures were around 40 °C, were less than promising. Carbothix 1:2, at 24°C, has a set time of around 90 s; at 40°C this time is greatly reduced to around 25 s. Furthermore, the cables were installed in 62 mm holes. This would require approximately 16 L of product, but the pump output was set at 10 L/min.

Due to the temperature of the product, excessive pump pressures were seen - up to 20 MPa. Typically, this indicated that the carbothix was setting faster than anticipated and that the pump was attempting to push solidified Carbothix down the annulus of the borehole. Due to these conditions and some safety concerns, the trial was prematurely terminated.

Developing a slow set Carbothix

Following the less than successful first trial at Cosmos mine, Minova and Xstrata Nickel drew up a set of actions before commencing the next trial. Minova would formulate a slow set resin; Xstrata Nickel would review their current cable bolt drilling process and make the necessary operational changes in order to drill a 52 - 55 mm hole. With this in mind, Minova had to develop a resin that would work within a wider range of temperatures and had the same or similar mechanical characteristics as the current formulation.

Minova Australia's technical department commenced developing a slow set resin in March 2011, and finalised the formulation in May 2011. Laboratory testing showed that Carbothix slow set would provide slower gel time in a higher temperature environment but still enable sufficient strength development for tensioning the cable whether the resin temperature was 20°C or 40°C. Note the gel time is the time for resin to become free flowing whilst the set time is the time when final resin setting has occurred. Figure 1 shows the gel and set time comparisons at selected temperatures. The slower setting material took 10 s longer to set at 40°C and 25 s longer to set at 20°C. The slower setting materials were also able to sustain adequate shear strength properties, as shown in Figure 2.

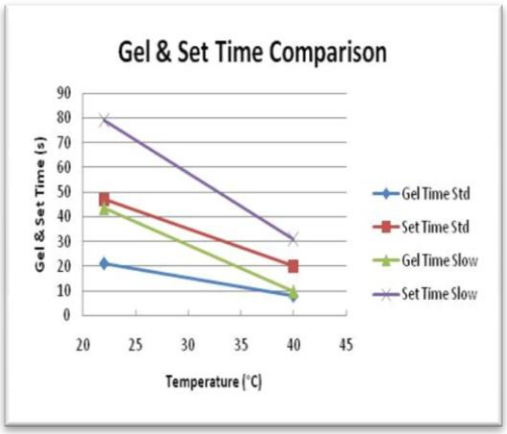

Figure 1 - Slow set resin gel and set time comparisons at selected temperatures

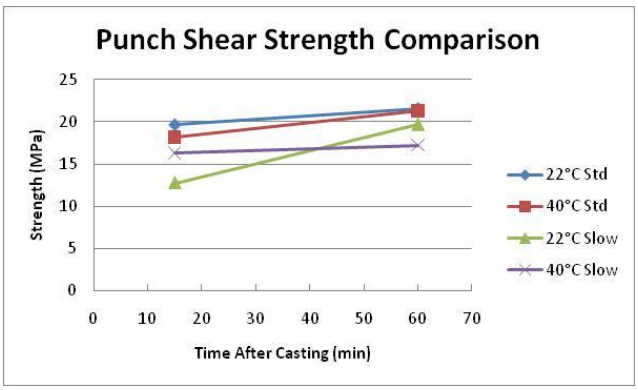

Figure 2 - Slow Set resin with shear strength properties at various temperatures

Surface trials of long tendon Carbothix grouting

Prior to carrying out underground trials, several surface trials were undertaken to:

- Ensure that the pumping system chosen could handle the product and deliver it at a consistent 1:2 ratio
- Ensure that the feed pipe system chosen could cope with system pressure
- Prove that 6 m and 8 m cables of various types could be fully encapsulated

Initial results in a laboratory environment, with Carbothix at 24 °C, were very encouraging; the pump delivered material at a consistent 1:2 ratio. Once the grout had set, cables were cut into sections to prove that full encapsulation had occurred. Figure 3 shows fully encapsulated twin-strand cables. Figure 4 shows a cross section of the Carbothix material fully encapsulating a megadowel strand bolt. The megadowel bolt is a 9 strand cable with a grout tube located in the center of the outside or sheath wires. The pump, shown in Figure 5a, is configured to deliver material at 1:2 ratios but that can be easily modified to pump 1:1 ratio depending on specific requirements. Smaller more mobile pumps are also available as shown Figure 5b.

Figure 3 - Cross-section of 6 m twin strand cables

Figure 4 - Cross-section of 8 m Megadowel

Figure 5a - Modified PHP pump

Figure 5b - Modified SK90 pump

IN HOUSE PRODUCT TESTING

Prior to use of Carbothix resin with long tendon supports, various tests were completed to compare the Carbothix's strength against both polyester capsule resin and also Portland cement cable grouts.

Initial punched shear testing, indicated the Carbothix resin was able to achieve one hour punched shear strengths of 26 MPa and 30 MPa after 24 hrs. This was compared to fast Lokset polyester resin, which achieved 24 MPa. Figure 6 shows punch shear results for various types of Lokset resins, Figure 7 shows Carbothix punch shear results.

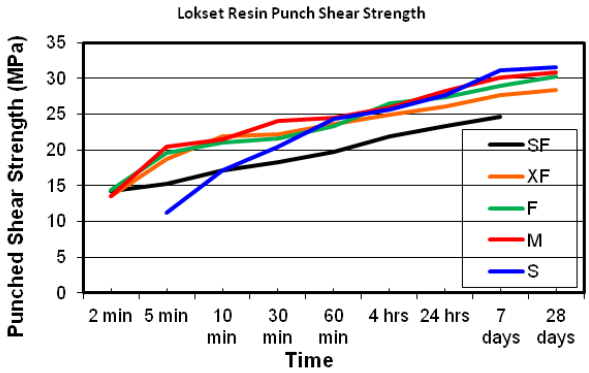

Figure 6 - punch shear results for various types of Lokset resins

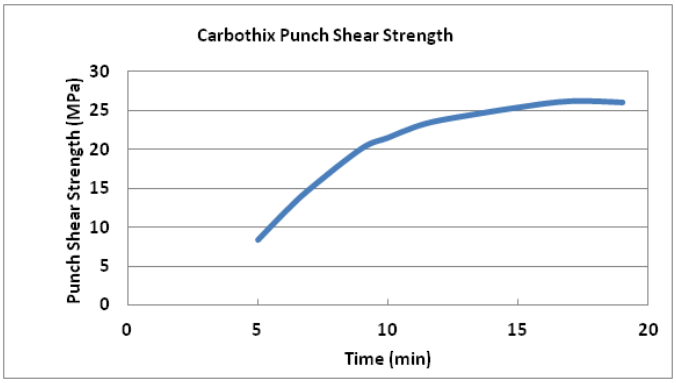

Figure 7 - Carbothix punch shear results

The Uniaxial compressive strength data for Carbothix was 70 MPa after 24 hours as shown in Figure 8, which is comparable to Portland cement cable grouts.

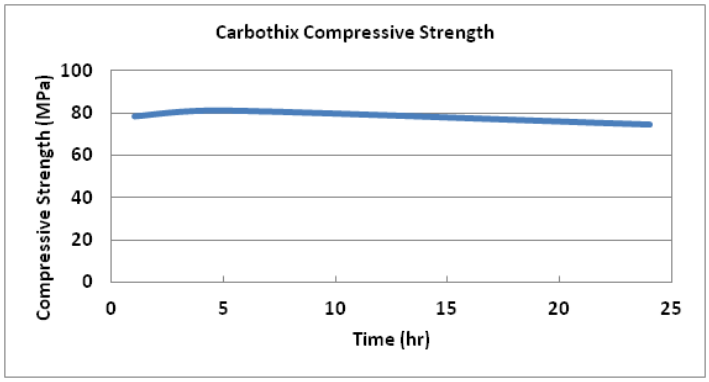

Figure 8 - Variation of the uniaxial compresive strength of Carbothex

To provide further confidence of the anchoring capability of Carbothix, further testing was done using various cable types and related borehole diameters. The laboratory testing method is shown in Figure 9. The cables were installed centrally then grouted in a steel pipe with 170 mm of anchorage medium and then "pulled" with a hydraulic jacking system. For a twin-strand bulbed cable, the Carbothix material reached anchorage strength of 7 kN in one hour. This compares with the identical style cable installed with General Portland (GP) cement that did not reach the 7 kN strength after 24 hours. This faster cure time makes it possible to post-tension the cables earlier, which can dramatically improve mining cycle times.

Figure 10 shows summary of results.

Figure 9 - The laboratory test set-up for pul testing of cables

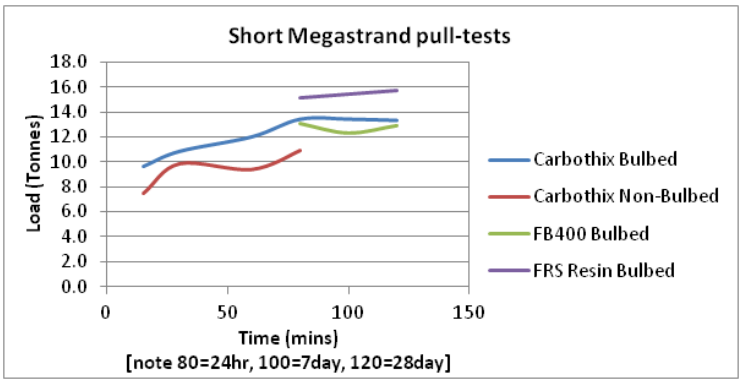

Figure 10 - Pull test results with pull duration

Further trials at Cosmos mine

Two further trials were carried out at Cosmos Mine using the new slow set formulation. In these trials, four different cable types were grouted in different ground conditions. The four types included single strand smooth cables, single strand bulbed cables, single strand de-bond cables, and twin-strand cables. The mine temperature varied between 31.8 °C and 36.1 °C due to various locations and ventilation conditions

in the mine. All of the cables were tensioned in excess of 20 t in less than 60 min. Subsequently, Xstrata Nickel Cosmos Mine has entered into a commercial arrangement with Minova Australia to supply Carbothix and accessories for long tendon grouting.

Four additional hard rock mines have commenced using Carbothix for cable grouting, and all of the mines are seeing substantial reductions in cycle times and outstanding support performance. Figure 11 shows a double strand cable installed and waiting for tensioning and plating.

Figure 11 - Double strand cable

INTRODUCTION OF CARBOTHIX TO AUSTRALIAN COAL MINES

The use of polymer materials that react *in situ* in underground coal mines is regulated under the Coal Mines Health and Safety Regulations 2006. These products are controlled using a license system, and the only systems exempt from these controls are traditional resin capsules.

Prior to the processing of the license application, the product must pass certain characterization tests, which include flash point, fire resistance, flame propagation, reaction temperature, oxygen indexing, and electrical resistance. Carbothix is the only pumpable resin approved for use with cable and bolting systems.

Minova Australia commenced the application process to the New South Wales (NSW) Department of Industry and Investment (DII) for Carbothix to be used in self-drilling rock bolts in 2010, and a limited "trial" license was granted that same year. The trial was limited to Tahmoor Mine, part of Xstrata Coal NSW Group. During these trials, air sampling was carried out by Coal Services Health to determine if Isocyanate was produced by the pumping process. Results showed that Isocyanate was not detected at any stage during the trial.

Following these trials, Minova Australia applied for an extended license to include the grouting of long tendon supports at any mine in NSW. This trial license was granted in November 2010.

Underground trials

The first underground trial was carried out at the Centennial Coal Mandalong mine. Ten 8-m-long cable trusses were installed to provide additional support in the LW12 tailgate, No 3 cut through area. All 20 cables were grouted with Carbothix standard set formulation due to the low underground temperature (18 degrees Celsius, and cables were trussed and tensioned after 30 min. Air analysis monitoring was carried out by Coal Services Health, and no MDI was detected.

Further underground trials were carried out at Centennial Coal Angus Place Mine, where several 8 m megadowels were grouted successfully using standard set resin. Again, air analysis was carried out by Coal Services Health, and zero Isocyanate MDI was detected.

Minova Australia has now applied to the NSW Department of Trade and Investmentfor a full license to allow full implementation of the system in coal mines in NSW.

CONCLUSIONS

There are several significant advantages of using Carbothix 1:2 resin for grouting long tendon cables with pumpable resin:

- Fast set allows early tensioning of cable bolts;
- Cables can be grouted immediately after tensioning;
- Ability to grout single cables, particularly in boggy or high shear ground;
- High early load transfer;
- Rapid resin set time; allows "in cycle" bolting;
- System can be adapted to be used with most grouted cables.

New developments of Carbothix grouting systems offer the advantage of safety, speed and reliability in a range of temperature conditions. The strengths are comparable to traditional cement-based anchorage systems while reducing mining cycle times. The recent acceptance of the material for coal mine applications is bringing forward several unique solutions for difficult ground conditions.

Use of Carbothix in the grouting of long high-capacity cables and truss systems has become routine at a number of operations leading to increase in development rates. Additionally, Carbothix is being used in self-drilling rock bolts) currently being tested in a full-scale program. The ultimate goal is to make the ground conditions safer for workers while improving operational efficiencies.

ACKNOWLEDGEMENTS

The authors would like to acknowledge the effort of the Minova Australia support teams in the development of this innovative solution. Special thanks are extended to Michael Rockhoff, Minova, for assisting with initial underground trials in Western Australia and Rob Hawker's team for developing the new slow set, low viscosity Carbothix 1:2 resin for these applications. We would also like to recognize the mine site personnel at Xstrata Nickel Cosmos Mine, Centennial Coal Mandalong and Angus Place Mines for providing underground trial sites and operational support.

REFERENCES

Tadolini, S, 1994. Resin grouted cables for enhanced coal mine roof support. *Technology News*. U.S. Bureau of Mines, United States Department of the Interior. No. 433.

Pritchard, C J and McClellan, R S, 2011. Injectable resin - a highly adaptable ground support anchoring system. *Canadian Institute ofMining Metallurgy and Petroleum Conference and Exhibition*.

IN-SITU PULL TESTING OF CABLE BOLTS ENCAPSULATED WITH INJECTION POLYURETHANE

Peter Craig[1] and Brett Murnane[2]

ABSTRACT: Polyurethane (PUR) injection into underground coal mine strata has been practiced in Australia as early as 1985. The ACARP report C100019 discussed several case studies of which one included PUR injection into resin anchored, pre-tensioned hollow central tube cable bolts.

In cases of rapid response to accelerating strata movement it is the preference of site geotechnical personnel to install immediate pre-tensioned cable support, followed by re-consolidation of the strata through injection of grout or PUR. Cementitious grouting of cable bolts has two operational time restrictions; 1) 24-48 hour restrictions can be placed on roadway widening or longwall chock removal while waiting for the grout to achieve adequate strength and 2) a 24 hour restriction being placed on PUR injection after grouting has taken place to avoid unwanted chemical reactions and heat generation. In the last few years, more mines, faced with time critical ground support, have been utilising hollow cable bolts as the support and the means of injecting PUR into the strata. The main reason is time, 24 hours lost to cementitious grout curing could be used in stabilising the strata by PUR injection into distant fractures, and operationally 24 hours gained on a longwall move represents a large financial advantage. It has been considered that foregoing cementitious grouting of cables and replacing it with PUR will reduce the load transfer of the cable bolt, but no readily available data exists on how much reduction in bond strength occurs. Underground short encapsulation cable pull tests were conducted at Springvale Colliery comparing cementitious grout against PUR at both 24 hours and nine days cure time.

INTRODUCTION

The application of polyurethane (PUR) injection is usually considered as a last resort for Australian coal mines due to the high cost and chemical hazards involved. PUR injection is typically used where control of the roof has been lost or it is considered it soon will be. The injection of PUR in situations, where the roof of a roadway has undergone considerable displacement/deformation and is highly fractured, has frequently resulted in successful outcomes (Buddery, 2003*).*

Injection of PUR into seven 7 wire cable bolts is increasingly practiced in US coal mines to provide corrosion protection, control of strata groundwater ingress and additional roof stabilisation (Faulkner 2012). It is possible to inject PUR up through the 1- 4 mm gaps of a cable bolt housing and wedge, whereas cementitious grout requires cables with a more significant opening over 10-12 mm diameter for pumping. Whereas the US coal mines typically use point anchored seven wire cables up to 36 t Ultimate Tensile Strength (UTS), Australia predominantly uses pre-tensioned, post grouted (cementitious) hollow strand cables typically 60 t UTS. The larger 10-12 mm diameter central injection tube of Australian hollow cable bolts allows pumping of either PUR or cementitious grout with little modification to standard equipment.

Research into the geotechnical aspects of Longwall recovery in Australian coal mines recommends that mines with weak roof should employ systematic cabling. Cable bolts should be at least 6 m in length, anchored outside the likely roof failure zone and be grouted at least 24 hours prior to commencement of chock removal (Hill, 2010). Cementitious grouting of cable bolts poses two operational time restrictions; 1) 24-48 hour restrictions can be placed on roadway widening or longwall chock removal while waiting for the grout to achieve adequate strength and 2) a 24 hour restriction is placed on PUR injection after grouting has taken. In more recent years at least three Australian mines used PUR for repeated Longwall recovery ground support due to problems experienced with previous recoveries and known geological issues. Operational reasons have led to the adoption of PUR injection through the 6-8 m long cable bolts to replace separate cementitious grouting of cable bolts and PUR strata injection.

Throughout December 2011, Springvale Colliery's Longwall 414 recovery experienced a small roof fall and significant chock convergence, extending the time from reaching zero chainage to last chock

[1] *Jennmar Australia Pty Ltd, Sydney, PCraig@jennmar.com.au, M: +61 (0) 419 018 998*
[2] *Springvale Coal Pty Ltd, Lidsdale*

recovered out to eight weeks. During that period PUR was injected on several occasions into the strata and successfully into cable bolts, which had failed to grout. In February 2012, after back analysis of events a test plan was developed with Jennmar to determine the bond strength of cable bolts injected with PUR.

UNDERGROUND TEST PLAN

Departmental approval

An application was made to the NSW Department of Primary Industries under Clause 49 of the Coal Mines Health and Safety Regulation 2006, to conduct a "High Risk Activity" in the application of polymeric material for strata control. The application, outlining the reasoning for the testing of bond strength of PUR with cable bolts, was approved for the location 416 panel, 1 C/T, a slant drivage indicated in the shaded area of Figure 1.

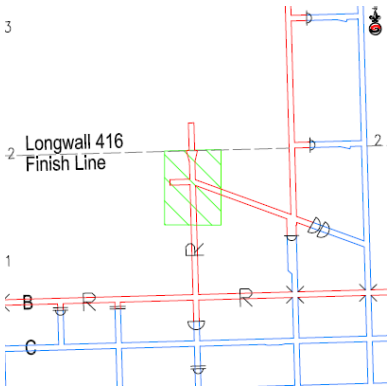

Figure 1 - Test area 416 panel

Pull test plan

Recent laboratory testing of fourteen different types of Australian cable bolts in sandstone (UCS of 19-25 MPa) identified that bulbed or nutcaged cables can have up to 400% higher load transfer capacity compared to plain-strand cables (Thomas, 2012). Considering the different modes of anchorage for plain and bulbed cables, it was necessary to test both types with PUR alongside grout for a comparison. The cables selected were; 1) Plain 28 mm hollow strand and 2) Bulbed 28 mm hollow strand. The plain strand is a nine wire 28 mm diameter cable with 63 t capacity, it has a 12 mm diameter central hollow tube for post-grouting. The bulbed strand is made from the same 28 mm diameter hollow strand but with 1 x 35 mm diameter non-collapsible bulb (nutcage) located in the middle of the 400 mm long pull test section. Both types of cable were installed into a hole drilled with 45 mm diameter twin-wing bits to suit Springvale mine drilling conditions through clay roof, the two types of cable are designed for use with 42 mm drill bits for the majority of mining conditions. The 28 mm hollow strand has had over one thousand cable bolt installations on Longwall recovery roadways as 6-8m cables and PUR injected. The contractors pumping the 1.8 m long pull test specimens were familiar with the PUR injection of the full scale 6-8 m product and they injected the test cables using the same method.

The test cables were separated into two locations, the PUR cables in the slant roadway and the cementitious grouted cables 50 m away in a stub. The separation of the cables into two locations enabled PUR injection and cementitious grouting on the same shift and inspection of the strata indicated the two sites were similar. This enabled the pull testing at 24 hours to be completed on both sets of cables on time.

The typical roof lithology at Springvale Colliery is a 3-4 m thick predominantly coal roof with two 100-200 mm thick claystone bands located within the bottom 1.2 m horizon. The pull test cable bond length was selected at the 1.3-1.7 m horizon to: a) avoid the dominant claystone bands; b) extend beyond immediate roof features and fractures; and 3) minimise the length of free cable to reduce strand rotation during pull testing. A roof core was taken during test cable installation in the area of the cementitious grouted cables; the stratigraphy referenced to the de-bonded test cables is shown in Figure 2. On the day of installation of the test specimens, the final bond length location was predominantly in coal but two thin claystone bands of 25-50 mm thick were present. Grout cube samples from the batch pumped into the test

specimens were collected for laboratory testing. The quality control for the PUR pumping was measurement of volume and pressure into each cable.

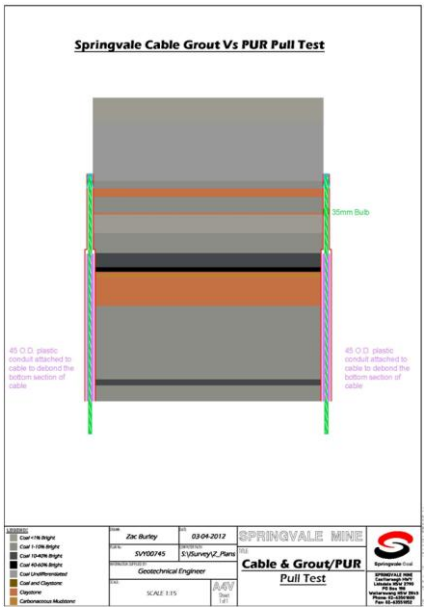

Figure 2 - Stratigraphy from core log referenced to test cables

RESULTS AND DISCUSSIONS

Grout and PUR properties

The top-down pumped high strength thixotropic grout was mixed at an approximate Water: Cement ratio (W/C) = 0.35 (5.25 litres per 15 kg bag). Typical Uniaxial Compressive Strengths (UCS) for the product at this water: cement ratio were 30 MPa at 1 d, 55 MPa at 7 d and 70 MPa at 28 d. The 50 mm cube samples taken underground from the mixture during test specimen grouting were tested at seven days to give a UCS values of between 45-49 MPa.

Nine test cables were pumped with Marithan N PUR in the same top-down manner as the grout, with pumping at a very steady pace to allow foaming to start and seal the bottom section before filling and pressurising the top bonded pull test section. Three cables failed due to excessive leakage of the packing material at the collar of the hole and subsequently failed the pull testing. The successful test cables took approximately 10 L of PUR each, which equates to a void fill of approximately 20 L considering the Marithan N used has an expansion factor of two. The theoretical volume of void around the 28 mm diameter test cables equated to 17 L. The pump pressures recorded to reach the 10 L of PUR was typically 40 bar, with four cables taking 100 bar which was most likely due to the foaming starting within the cable hollow tube before completion of the hole. The specification data sheet for Marithan N PUR is a laboratory compressive strength of 10 MPa and bonding strength to rock/concrete of 1 MPa.

Load displacement results (400 mm bond length)

The equipment used for 24 hours pull testing was a 30 t cable bolt tensioner of known ram area for conversion to metric tonnes. The displacement of the cable relative to the mine floor was measured from the cable tail protruding below the tensioner against a convergence pole fitted with mechanical dial gauge accurate to 0.1 mm. After the Bulbed 28 mm Hollow Strand unexpectedly reached the 30 t capacity of the tensioner used at 24 hours testing without peak load being achieved, the nine day tests included a 60 t hydraulic cylinder over a stem connected to a threaded barrel and wedge. The displacement measurements taken using the 60 t pull test cylinder were taken from the bottom of the protruding threaded stem. The displacement readings measured off the threaded stem were corrected for normal barrel draw over the wedges under load.
The foaming reaction of Marithan N PUR commences within 1-2 min and is completed within 3 min. The fast reaction of PUR has it achieving 90% of its strength within the first two hours (Buddery, 2003). The original plan was to include three bulbed cables with PUR at 24 hours and three at nine day to confirm the

strength over a reasonable time frame applicable to longwall recovery. Due to the three leaking failures during installation, only three bulbed test cables remained viable so one was completed at 24 hours with the remaining two at nine day.

The load versus bond displacements graphs were produced for each test cable as shown in Figures 3, 4 and 5. The peak load behaviour of both plain and bulbed strands in grout was a sudden release of load with a loud pop before reloading. The nature of the mechanical dial gauge setup jolted by the sudden movement prevented accurate reading of displacement after peak load was reached. This failure mode is likely related to the coal roof and is seen with rock bolts in coal roof and not in stronger rocks. It suggests the failure interface could be the coal or coal/grout interface. The PUR injected cables exhibited similar initial stiffness to the grouted cables but reached much lower peak loads and rapidly lost load but not in the sudden manner of the grouted cables.

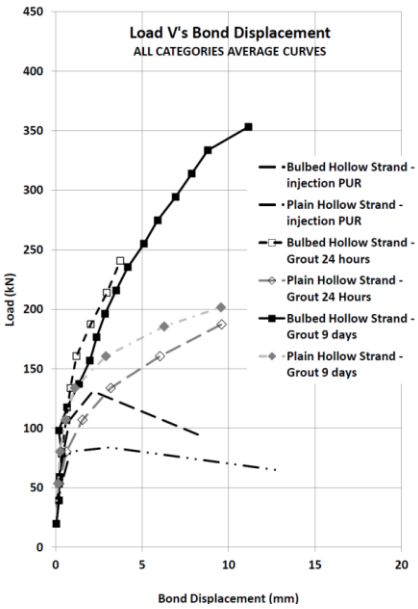

Figure 3 - Load displacement graphs, Average

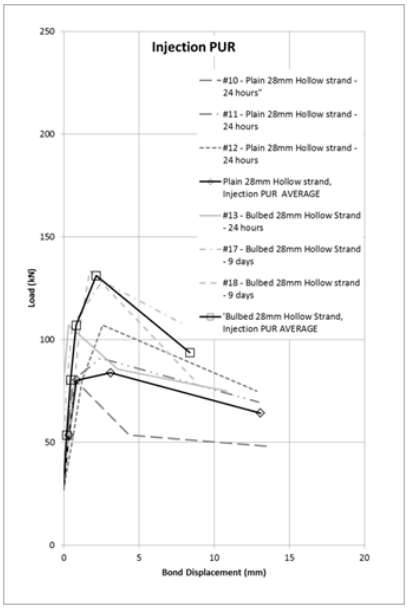

Figure 4 - Load displacement graphs, PUR

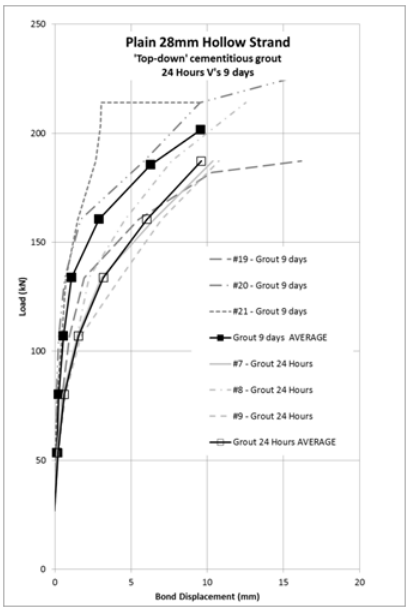

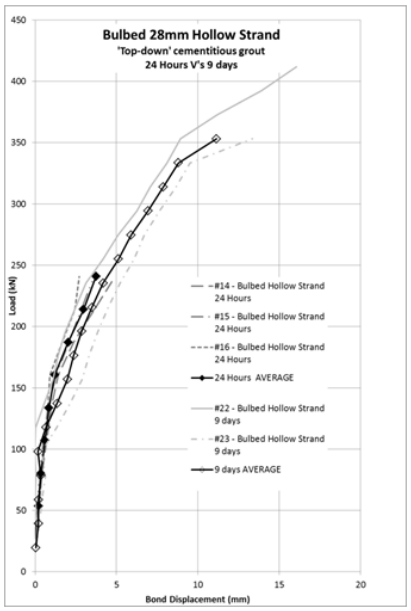

Figure 5 - Load displacement graph, cementitious grout

As shown in Figure 6, the average peak bond strength of PUR with the plain 28 mm hollow strand was 9 t per 400 mm bonded length, and for the bulbed 28 mm hollow strand was 14 t per 400 mm bonded length. The grouted test cable results for 24 h cure gave peak bond strength with the plain 28 mm hollow

strand as 20 t per 400 mm bonded length, and for the bulbed 28 mm hollow strand was in excess of 25 t per 400 mm bonded length (test were stopped due to equipment limit). The grouted test cable results for 9 d cure gave peak bond strength with the plain 28 mm hollow strand as 21 t per 400 mm bonded length, and for the bulbed 28 mm hollow strand was 39 t per 400 mm bonded length.

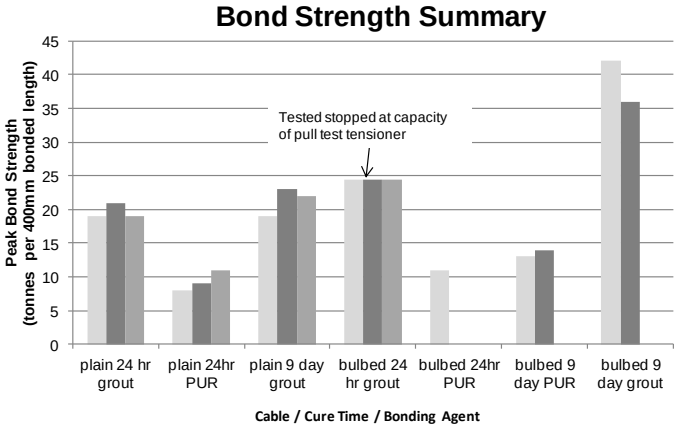

Figure 6 - Summary of bond strength results

Little published data exists on bond strength of rock or cable bolts bonded within a drill hole using injection PUR. The most relevant reference from laboratory tests conducted by Rock Mechanics Technology (Bigby, 2005) was that *Laboratory Short Encapsulation Pull* (LSEP) tests on expandable resins showed that PUR gave very poor load transfer characteristics, but that expandable resins base on polyester could provide a much higher level of load transfer though they still did meet the acceptance criteria recommended in the draft revision of BS7861-1:1996.

The expansion PUR used in Australia for the primary goal of migration into fractured ground, especially around a longwall recovery face, typically has an expansion ratio of around two. As illustrated in Figure 7, laboratory work on strata injection PUR completed in the Czech Republic (Snuparek, 2000) highlighted the rapid decrease in compressive strength as the foaming factor increased.

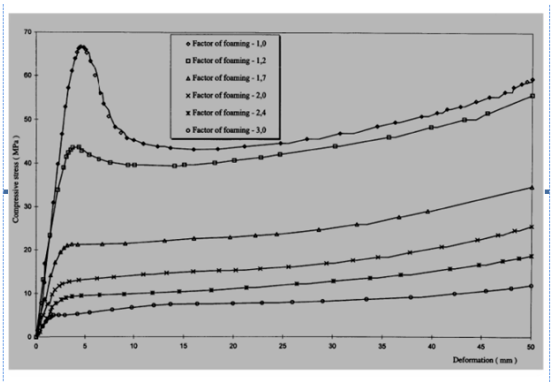

Figure 7 - Injection PUR compressive strength reduction with increased expansion ratio (Snuparek, 2000)

PUR injection into cable bolts in the US use a product with expansion ratio of 1:1 which gives a laboratory compressive strength of 20 MPa (Faulkner, 2012). The underground bond strength testing completed at Springvale Colliery was based on current Australian practices using a PUR with expansion ratio of 2:1. Optimisation of a PUR for strata injection function and combined cable bolt bond strength could utilise only slightly modifications on the current versions of Australian approved PUR to obtain higher strength.

CONCLUSIONS

Some Australian coal mining operations have recently used PUR injection through post-groutable cable bolts during longwall recovery support. The primary function of PUR injection in these scenarios is

reconsolidation of fractured strata, but the operational benefits of eliminating both cementitious grouting of cables, and drilling holes for PUR injection only; and instead injecting PUR into strata utilising the cable bolt is compelling.

Springvale Colliery's use of PUR injection into cable bolts during rapid response to deteriorating conditions in LW414 recovery raised the question of bond strength of injection PUR with cable bolts. The *in-situ* pull testing in Springvale Colliery coal roof with clay bands provided a comparison to cementitious grout and actual bond strengths for their strata with PUR injection into plain and bulbed cables.

Marithan N injection PUR in comparison to standard thixotropic cable bolt cementitious grout in Springvale Colliery coal roof gave a significant reduction in bond strength. The PUR compared to 24 h cured grout gave a 55% reduction in peak bond strength for the plain cable. Testing for the bulbed cable at 24 h was stopped at the 25 t equipment capacity, but even assuming this as peak strength it still has PUR being a 48% reduction in bond strength compared to grout at 24 h cure on a bulbed cable. The PUR compared to a nine day cured grout was a similar 57% reduction in bond strength for the plain cable, but a 67% reduction in bond strength for the bulbed cable.

The data presented may be useful in future testing for optimisation of possible PUR injection systems that have a dual purpose of rapid reconsolidation and a greater contribution to the load transfer of cable bolt ground support members.

ACKNOWLEDGEMENTS

Wilsons Mining Services for application of the Marithan PUR and associated product laboratory test results. RGN Mining Services for the quality installation of cable test specimens, roof core and cementitious grouting.

REFERENCES

Bigby, D and Reynolds, C, 2005. Development of the laboratory short encapsulation pull test for a revised British standard on rock reinforcement components used in coal mining. In *Proceedings of the 24th International Conference on Ground Control in Mining*, Morgantown, WV, August 2 - 4, pp 313-322, http://icgcm.conferenceacademy.com/papers/detail.aspx?subdomain=icgcm&iid=535.

The British Standard BS 7861-2007. Strata reinforcement support system components used in coal mines - Part 1. Specification for rock bolting and Part 2: Specification for Flexible systems for roof reinforcement.

Buddery, P, 2003. Cost effective use of PUR and optimising large-scale injected strata reinforcement. Report No: 00-180-ACR, ACARP Project C10019, Strata Engineering, Newcastle, Australia.

Faulkner, D, 2012. The development and application of polyurethane injectable cable bolts, In *Proceedings of the 31st International Conference on Ground Control in Mining*, Morgantown, WV, July 31- August 2, 5p. http://icgcm.conferenceacademy.com/papers/detail.aspx?subdomain=ICGCM&iid=1002.

Hill, D, 2010. Managing the geotechnical aspects of longwall face recovery. In *Proceedings of 10th Coal Operator's Conference*, University of Wollongong, 11–12th February, pp 84-87. http://ro.uow.edu.au/coal/321.

Snuparek, R, and Soucek, K, 2000. Laboratory testing of chemical grouts. Journal of *Tunnelling and Underground Space Technology*, 15(2):175-185.

Thomas, R, 2012. The load transfer properties of post - groutable cable bolts used in the Australian coal industry, In *Proceedings of the 31st International Conference on Ground Control in Mining*, Morgantown, WV, July 31- August 2, 10p. http://icgcm.conferenceacademy.com/papers/detail.aspx?subdomain=ICGCM&iid=1011.

VARIATION IN LOAD TRANSFER ALONG THE LENGTH OF FULLY ENCAPSULATED ROCK BOLTS, BASED ON THE INSTALLATION MIXING PARAMETERS

James Hillyer[1], Peter Craig[2], Shuqi Ma[1], Naj Aziz[1], Jan Nemcik[1] and Ting Ren[1]

ABSTRACT: The reinforcement quality of the fully resin encapsulated bolt depends on several factors, which are a combination of the bolt design configuration, bolt/hole diameter ratio and installation procedure. Gloving in bolt installation constitutes a challenging problem for effective strata reinforcement and the stability of gate roads and tunnels. A total of ten bolts were installed into ten 1.7 m long threaded steel pipes with different resin spin times, the pipes were retrieved from the installed holes in an underground mine road way roof and then cut into 100 mm long sections. The encapsulated bolts in the tube sections were then push tested. Significant variations were found in bond strength along the installed bolt length in the whole tube, with typically the top 200 mm of bolt being significantly lower (50%) in most cases due to gloving and unmixed resin components.

INTRODUCTION

An adequate rock bolting support system depends on five main physical components which are the resin, bolt, hole, machinery and rock type. Another important factor is the quality of the installation. (Wilkinson and Canbulat, 2005)

Campbell *et al.* (2004) investigation into the extent and mechanisms of gloving and un-mixed resin in fully encapsulated bolts highlighted the problems associated with quality of bolting operations. The development of a pressure front as the bolt encountering the resin cartridge as it is spun up the hole and radial expansion of the resin cartridge was suggested. Campbell *et al*. found gloving occurring over a wide range of bolt lengths, with the results showing anywhere between 30 mm to 790 mm affected. Typically the gloving affected around 500 mm of the up -hole end of the bolt.

The generalised bolt installation practice in Australian coal mines is to mix the rebar bolt through the length of the resin capsule for around 75% of the "spin time" followed by the remaining 25% of the spin time when the bolt is at the back of the hole. Operators stop mixing for the designated 'hold time' while the faster set resin hardens after which tensioning of the bolt and plate against the rock can occur. The need to improve productivity has led Australian coal mining operations to consider Spin-To-Stall (STS) bolt installation which eliminates hold time and can gain 20 s per bolt installed.

Anglo Coal pioneered the spin-to-stall system in South Africa at Goedehoop Colliery over a decade ago (Bugden, *et al.,* 2001). The spin-to-stall technique involves spinning continuously from initial mixing of the bolt through the resin capsule until the rig stalls the nut tight against the plate and rock face. The method of continually spinning a bolt until the shear pin breaks or until it tightens has been classified as an incorrect installation practice in Australia. Training of bolting operators by Australian bolting consumable manufacturers has taught that over mixing will damage the resin.

A project commenced to determine the bond strength variation along the length of a fully encapsulated bolt with varying installation techniques, including the spin-to-stall method. The resin, bolt, hole and machinery were fixed parameters with the rock replaced by steel tube. The installation variables investigated were those typically controlled by bolting operators or electronic automation programs which are mixing speed, mixing time and feed rate.

Bolts were installed into threaded steel tube underground at Springvale Colliery with a hydraulic bolting rig. The bolted tubes were subsequently transported to the University of Wollongong Rock Mechanics laboratory for further evaluation and analysis as part of an undergraduate thesis project. This

[1] *School of Civil, Mining and Environmental Engineering, UOW, Jameshillyer@gmail.com, M: 04 3344 4531. Contact: Naj Aziz <naj@uow.edu.au> Tel:02 42 213 449*
[2] *Jennmar Australia, pcraig@jennmar.com.au, M: 04 1901 8998*

collaborative opportunity was crucial as a learning base for similar studies to be undertaken on an ACARP funded project C21011.

STEEL PIPE METHOD OF INVESTIGATING BOND STRENGTH

Previous South African research

The study used similar methods to previous research conducted in South Africa on 20 mm diameter bolts installed through resin capsules into 800 mm long, 27 mm inside diameter threaded steel tubes. The South African study had sectioned the tubes as illustrated in Figure 1, with each section then tested by pushing the bolt through resin. The threaded steel tube ensures that the bond failure occurs between the bolt and resin interface.

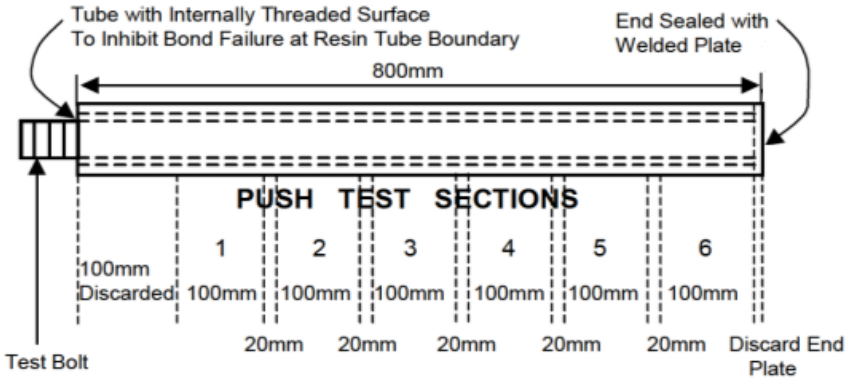

Figure 1 - Test bolt and steel pipe section (Altounyan, 2003)

The South African research used the maximum push test load for each section as the bond strength and this was plotted against the position along the bolt to come up with the "bolt bond strength profile". The trends obtained in the South African study are illustrated in Figure 2 and shows significant variation of bond strength along the bolt and also with different spin time.

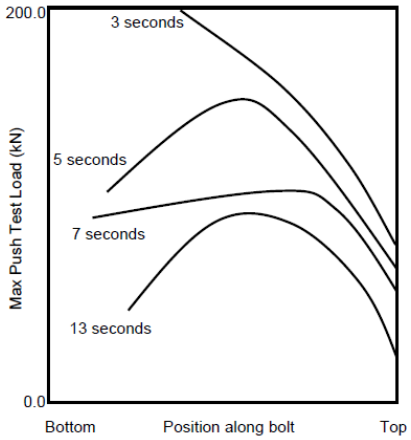

Figure 2 - South African bolt and resin 'bolt bond strength profile' (Altounyan, 2003)

The University of Wollongong has since further investigated the laboratory steel pipe push versus pull test methods. They have determined that the push test gives higher results than a pull test, and that the number of deformations (ribs) encapsulated within the length of pipe also affects the strength results (Aziz, *et al.*, 2006).

The study detailed herein maintained the use of push tests as it was most practically suited to the threaded steel tube after sectioning. The 1.7 m length of bolt and threaded steel tube was selected to simulate a 1.8 m long bolt and used dual speed 50% fast, 50% slow setting resin. The bolt selected was a 21.7 mm core diameter, 23.5 mm rib-rib diameter, JX rib profile with M24 thread as common to Australian mines.

Threaded steel pipe to simulate Australian drill holes

A review of the US Standard F432 and South African Standard SANS1532 steel pipe pull test methods led to the investigation of pipe diameters and threads to suit Australian sized bolts and drill hole. The US standard uses 25.4 mm (1") inside diameter, 32 mm (1 ¼") outside diameter pipe with a M27 x 3 mm cut thread. Both the US and South Africa commonly use 25.4 mm (1") vacuum drill bits for bolting and it is understandable that their laboratory test standards are developed to suit local products. The Australian industry standard is a 27-28 mm wet drill bit with an M24 (21.7 mm core diameter) rock bolt.

Seamless pipe of 28.5 mm internal diameter with 9.5 mm wall thickness was used for the study. A 1¼" - 7 UNC internal thread tap was selected as the minor diameter of 28.5 mm and major diameter of 32 mm suited the commercially available seamless pipe. The coarse series of thread was selected over a finer metric thread to provide good pipe/resin interface strength so that the bolt/resin interface would be the failure interface. Ten pipes were threaded and each blanked off at one end with a 300 mm x 300 mm plate welded on the other end. Holes were placed in the corners of the plate to allow bolting the pipe/plates into a borehole underground.

Underground installation of bolts into pipes

The bolting rig used underground was an electric powered mobile bolter with hydraulically powered drill motors. A 64 mm drill bit was used to form a drill hole in the roof large enough to fit the 48 mm outside diameter threaded steel tube. A drill steel was ran up and down each installed pipe with the water on to flush the pipe clean and align the rig prior to each resin and bolt installation. The rotation speed measured was 450 rpm without thrust and 420 rpm with thrust. The stall torque output was 220-250 N·m and the temperature of components was 24^{o}C.

The pipes were sectioned at the University of Wollongong Rock Mechanics laboratory into 100 mm long pieces as illustrated in Figure 3. Each section was push tested to determine the bond strength profile along the entire 1.8 m bolt/resin interface.

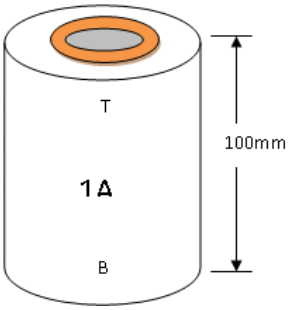

Figure 3 - Sectioned pipe with bolt and resin

The installation technique currently used in Australia could be described as the spin-and-hold method. The mixing parameters are listed below in Table 1 for the spin-and hold installations. Bolts three and four were installed with full speed rotation throughout the entire mixing. Bolt five was installed with low speed rotation during the entire mixing and bolt six had low speed during feeding of the bolt but full speed once the bolt reached the back of the hole.

Table 1 - Standard type of spin-and-hold installations

Test No	Bolt	Resin	Spin to Back		Spin at back		Hold	Length NOT encap from collar * (mm)
			Time (s)	Approx rpm	Time (s)	Approx rpm		
3	JX	J-Lok 1000 mm STS F/S oil based catalyst	9	420	3	450	All spin-and-hold installations were not tightened at all.	50
4	JX	J-Lok 1000 mm STS F/S oil based catalyst	9	420	3	450		170
5	JX	J-Lok 1000 mm STS F/S oil based catalyst	6	100	6	100		50
6	JX	J-Lok 1000 mm STS F/S oil based catalyst	6	100	6	450		200

The mixing parameters for the spin-to-stall installations are shown below in Table 2. Bolts seven and eight were installed with full speed rotation throughout the entire process. Bolts nine and ten were installed with low speed rotation during feeding of the bolt into the tube, but full speed once the bolt reached the back of the hole. Bolts 11 and 12 were installed by pushing the bolts through the resin without rotation, but full rotation was applied right through to stall once the bolt had reached the back of the hole.

Table 2 - Spin-to-stall installations

Test No	Bolt	Resin	Spin to back		Spin at Back			Thread tail below nut (mm)	Length NOT encap from collar * (mm)
			Time (s)	Approx rpm	Time at pin break (s)	Time at Stall (s)	Approx rpm		
7	JX	J-Lok 1000mm STS F/S oil based catalyst	8	420	28	35	450	120	100
8	JX	J-Lok 1000mm STS F/S oil based catalyst	8	420	29	33	450	76	170
9	JX	J-Lok 1000mm STS F/S oil based catalyst	6	100	18	22	450	80	150
10	JX	J-Lok 1000mm STS F/S oil based catalyst	6	100	13	17	450	48	180
11	JX	J-Lok 1000mm STS F/S oil based catalyst	6	0	10	12	450	52	110
12	JX	J-Lok 1000mm STS F/S oil based catalyst	6	0	11	14	450	48	0

RESULTS AND DISCUSSIONS

There were 150 x 100 mm long sections push tested, each with its own load displacement curve. The load displacement curves varied for each section but would generally be one of the types of loading illustrated below in Figure 4. Type A sections loaded rapidly to a peak load and residual loads held steady but lower. Type B sections loaded rapidly to an initial yield and subsequently loaded to a higher peak residual load before dropping load. Type C was much softer loading but maintained a residual load. The variations in load displacement curves are clearly evident in Figure 5 for typical sections of the entire bolt length tested. Also shown in Figure 5 the cross-sectional view of various bolt sections, clearly there were some spots of weak resin encapsulations and the severity of the poor bonding varied for different installations conditions.

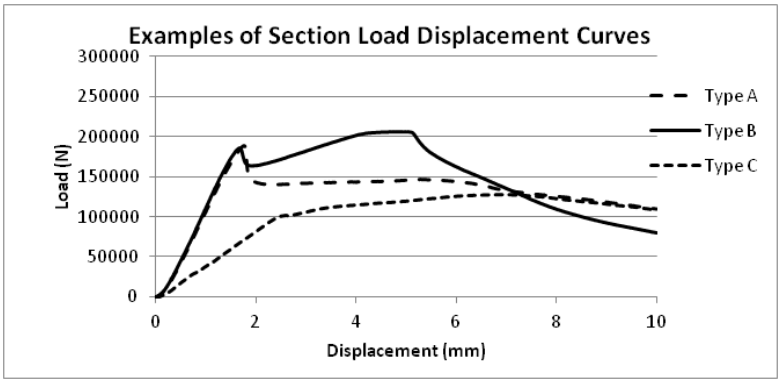

Figure 4 - Examples of load displacement curve types for the 100 mm push test sections bond strength profiles

The maximum load for each section within 10 mm displacement was taken as the peak load. The bond strength profile was determined for each bolt, with "best fit" curve applied as shown in Figure 6.

Bolts three and four were the current Australia typical spin-and-hold installation technique. The quality of bolts three and four was very high, with the gloving confined primarily to section A, and minimal air bubbles within the resin annulus. The average peak strength of these two bolts was used to compare the

effect of differing installation methods in the other groups of bolts, being 137 kN per section, and called the average baseline strength.

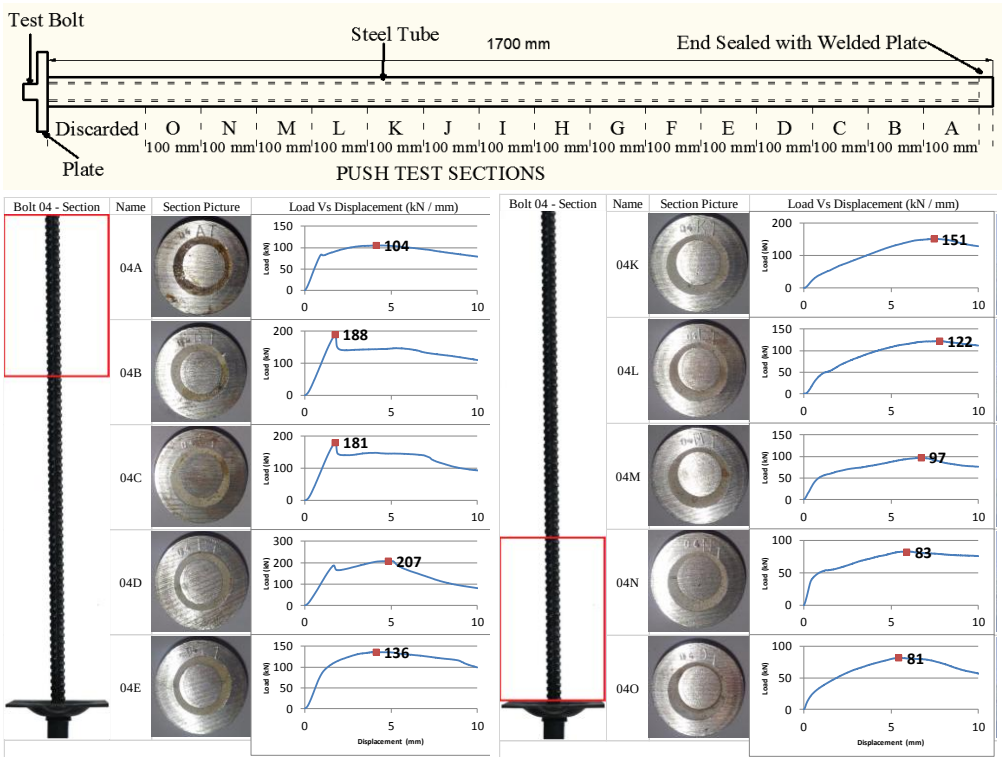

Figure 5 - Load transfer capacity of different 100 mm long sections on one bolted tube

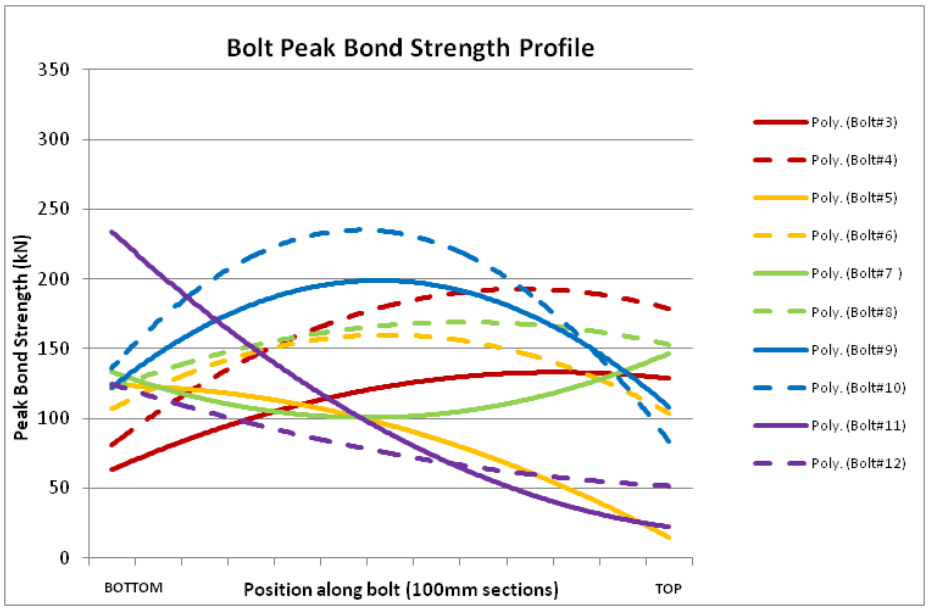

Figure 6 - Peak push load per section per bolt

Bolt five was slow rotation under-mixing and was the worst performing bolt, testing at 62% of the average baseline strength mentioned above. Visual inspection after testing revealed many flaws in the resin annulus along the entire length of the bolt. In the upper four sections there was excessive gloving that had completely enclosed the bolt, providing a much lower bond strength performance and significantly lowering the peak loads. Below the top 500 mm, the gloving had reduced to moderate or minimal, but there were air bubbles present in the resin annulus.

Bolt six was a spin-and hold installation with only a slow rotation during feed aimed at reducing over mixing of the bottom of the resin capsule. For bolt six, the overall quality was much greater than that of bolt five. But similar to bolt five, the top 200 mm had moderate to excessive gloving, and the gloving had completely enclosed the bolt section. Most of this bolt below the top 300 mm achieved the peak load between 5 mm and 10 mm displacement within the 100 mm sections.

Bolts seven and eight were a spin-to-stall with full rotation speed from the start to stall. In comparison to the baseline average strength all were directly on par. It did appear that the resin was over-mixed and lowered the average strengths. There was minimal gloving evident in both bolts.

Bolts nine and ten were spin-to-stall with slow rotation during feed aimed at minimising over mixing in the bottom part of the resin capsule, but full rotation was applied once the bolt reached the back of the hole and up until stall. When comparing bolts nine and ten to the baseline bolts, the average peak bond strengths were 28% higher, the average bond strengths were 44% higher. This installation method produced notably superior strengths, and when compared with bolts seven and eight, it is presumed that the slower mixing speed during installation prevented over-mixing of the resin but still enough to properly shred the resin capsule film.

Bolts eleven and twelve were pushed through the resin capsule without spinning then spun at full speed up to stall. Comparing bolts eleven and twelve to the baseline bolts; all three average strengths were notably lower than the average baseline strength. There was a shift in average strength in favour of the lower half of the bolts, and it is evident from inspection after testing that this method did not shred the resin capsule properly during the initial stages of mixing, therefore allowing for significant gloving in the upper half of the bolts.

Due to the variation in the 100 mm long section load displacement curves illustrated in Figure 4 further analysis was conducted by taking the load at 2 mm displacement for each section. Also, a method of bond strength being determined at the point of the gradient reaching 20 kN/mm was used.

Figure 7 below shows the average strength for each bolt using the various criteria; 1) Bond strength for each 100 mm section as the point the curve reaches 20 kN/mm gradient. 2) Peak bond strength for each 100 mm section, which can occur at any displacement depending on the shape of the curve. 3) Bond strength at 2 mm displacement for each 100 mm section.

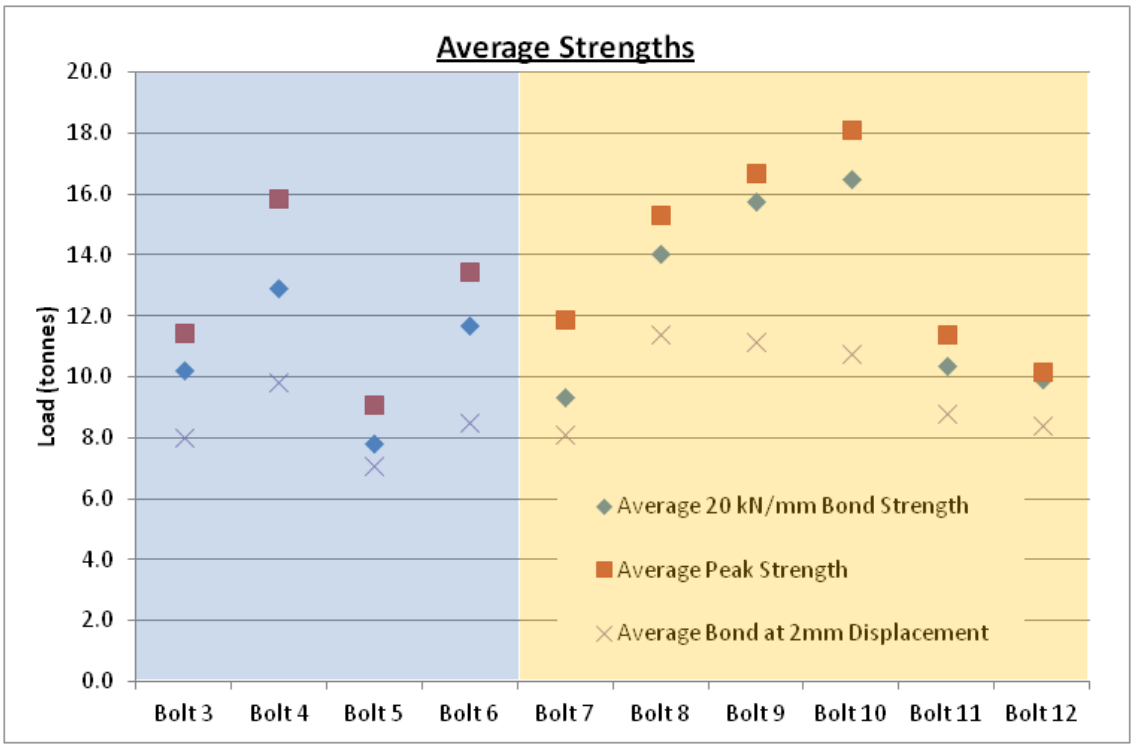

Figure 7 - Average push load per bolt tested at the stiffness of 20 kN / mm, at peak bond strength and peak bond strength within 2 mm displacement

CONCLUSIONS

There is significant variation of bond strength along individual rock bolts, with typically the top 200 mm of bolt being significantly lower (50%) in most cases due to gloving and unmixed resin components.

The typical Australian installation technique of spin-and-hold (Bolts 3 and 4) gave an average peak bond strength of 137 kN per 100 mm long push test section, which was used as a baseline for comparison of the other techniques.
Gloving and under mixing greatly reduced bond strength with slow rotation spin-and-hold (bolt five) and pushing through the capsule without spinning (Bolts 11 and 12) highlighting these effects.

Spin-to-stall installations (Bolts seven to ten) produced average bolt bond strengths, using the various presented criteria, equivalent to or better than spin and hold installations.

ACKNOWLEDGEMENTS

The authors would like to thank the following personnel;

- Ismet Canbulat and Jason Emery from Anglo American Metallurgical Coal for discussion and review of the project;
- Brett Murnane for assistance in arranging the underground installation of bolts into the threaded pipes at Springvale Colliery;
- Tim Gaudry from Jennmar for involvement in the underground testing;
- University of Wollongong laboratory staff.

REFERENCES

Altounyan, P, Bugden, A, O'Conner, D and Berry, R, 2003. Developments in improving the standard of installation and bond strength of full column resin roofbolts, In *proceedings 22nd International Conference on Ground Control in Mining*, Morgantwon, WV, August 6, pp 263-269. http://icgcm.conferenceacademy.com/papers/detail.aspx?subdomain=icgcm&iid=632.

Aziz, N and Web, B, 2003. Load transfer appraisal of bolts using short encapsulation push test. In *Proceedings of 4th Underground Coal Operators' Conference*. Wollongong. pp 72-80. (eds: N Aziz and R Kininmonth).http://ro.uow.edu.au/coal/162/.

Aziz, N, Jalalifar H and Concalves, J, 2006. Bolt Surface Configurations and Load Transfer Mechanism in proceedings 7th underground coal operators conference, Coal2006, Wollongong, 5-7 July , (eds, Aziz and Keilich), pp. 236-244. http: //ro.uow.edu.au/coal/51/.

Bugden, A, Minney and Altounyan, P, 2001. Improving roof control at a South African coal mine, In *proceedings of 20th International Conference on Ground Control in Mining*, Morgantown, WV, pp 95-104. http://icgcm.conferenceacademy.com/papers/detail.aspx?subdomain=icgcm&iid=716.

Campbell, R, Mould, R and MacGregor S, 2004. Investigation into the extent and mechanisms of gloving and un-mixed resin fully encapsulated roof bolts. In *Proceedings of Coal Operator's Conference*, University of Wollongong, 4-6 Feb, pp 203–214. http://ro.uow.edu.au/coal/145/.

Wilkinson, A, and Canbulat, I, 2005. An investigation into the support systems in South African collieries, In *proceedings of 24th International Conference on Ground Control in Mining*, Morgantown, WV, August, pp 294-301. http://icgcm.conferenceacademy.com/papers/detail.aspx?subdomain=icgcm&iid=533.

ROCK BOLT CORROSION - AN EXPERIMENTAL STUDY

Naj Aziz[1], Peter Craig[2], Jan Nemcik[1] and Faisal Hai[1]

ABSTRACT: The effect of long term exposure of full size bolts to corrosive environments is presented. A special test rig was used to test four bolts under different loading conditions. Four, X-grade identical profile bolts, each of 21.7 mm core diameter (23.7 mm full diameter) were subjected to prolong corrosion testing using acid sulphate water. The pH value of the circulated water varied between 3.4 and 4.3. The corrosion exposure test period lasted three and half years. Two bolts were axially loaded to 10 and 20 t force respectively, the third bolt was subjected to a 360 Nm torsion load and the fourth bolt was left unstressed to act as a reference bolt. After the test period ended, the bolts were stripped of their corroded coatings and weighted for weight loss. The diameter of each bolt was subsequently measured, and the loaded bolt samples were first tested non-destructively for tensile cracks and then tested for tensile failure. No cracks were found on post corrosion bolts tested non-destructively. The failure strength reduction on all four post-corroded bolts was significant, varying between 21% and 39%. The onset of corrosion was not confined to the targeted mid-section length of the bolt, however, the severest corrosion occurred at the anchored ends of the bolts.

INTRODUCTION

Corrosion is a physical alteration of a material from electrochemical reaction with its environment that often results in reduction of the mechanical properties of that material. Roof bolts are particularly susceptible to corrosion as they can be exposed in their working environment to ground water. Corrosion increases markedly in sulphide ore bodies due to acid runoff. Table 1 shows different types of corrosion that a rock bolt is likely to undergo when used for ground reinforcement. Of all the types of corrosion, pitting is particularly dangerous as it removes capacity for the bolt to deform with strata movements. Sudden failure of a bolt is likely to occur when pitting corrosion is experienced. The type and nature of corrosion depend on the nature of the ground condition and bolt encapsulation. Generally, the type of corrosion and severity of the corrosion varies along the bolt.

Historically the subject of steel corrosion has been of interest to civil and construction engineering. In mining, the interest in the topic is relatively new and following the introduction of bolting for ground support in mines and tunnelling. According to Baxter (1996) the early corrosion studies on rock bolting were carried out by Swedish and Finish researchers. Various publications include: Tuutti, 1982; Sundholm, 1990; Helfrich, 1990; Moving, 1994; Sundholm and Forsen, 1995; Satola and Aromaa, 2005. In the Australian context, the interest in bolt corrosion began in earnest in late 1990s, and the paper by Gray (1998) in which an emphasis was given to the Stress Corrosion Cracking (SCC). An ACARP project was initiated in 1999 to address the observed phenomenon of premature failure of rock bolts in a number of Australian coal mines, and with a particular focus on the problem of SCC in rock bolts (Hebblewhite, *et al.,* 2002, 2003a, and 2003b). Other Australian publications on corrosion include Gamboa and Atrens (2003), Hassell, *et al.*, (2005), and Vandermaat, *et al.,* (2012). The latter developed an apparatus to study stress corrosion cracking in full sized bolt specimens.

The rate of steel bolt corrosion is influenced by ground water composition, flow rates, water pH, temperature, CO_2 content, surface condition, presence of corrosion inhibitors, applied stresses, residual stresses (from workings, forming or welding operations) and any hydrogen sulphide concentrations (Henthorne, 1972; Spearing, 2010). Accordingly, a specialised test rig was constructed to study the effect of long term exposure on full size bolts, which are of current use in Australian mines. The study was undertaken in an environmentally controlled laboratory under different bolt loading conditions.

[1] *The University of Wollongong, School of Civil, Mining and Environmental Engineering, Wollongong, NSW 2522. naj@uow.edu.au, Tel: +61 (0 2) 42 213 449*
[2] *Jennmar Australia, PCraig@jennmar.com.au, M: 04 1901 8998*

Table 1 - Types of corrosion in steel

Forms	Categories	Description	
Uniform	Atmospheric	Corrosion of material exposed to air and its pollutants.	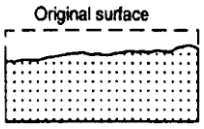
	Galvanic	Corrosion due to electrolysis	
Localised	Crevice	Localised corrosion occurring on confined, closely spaced metal to metal or non metal to metal component surfaces. It is localised corrosion occurring in small areas of stagnant solution in crevices on joints. Crevice corrosion can also occur as a result of differential aeration mechanisms.	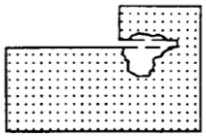
	Pitting	Highly localized corrosion occurring on a metal surface. Pitting is marked by the development of sharply defined holes "pits". Occurs as a process where the metal loss is accelerated by the presence of a small anode and a large cathode. A dangerous form of corrosion as it can cause failure where only small weight loss of metal is observed	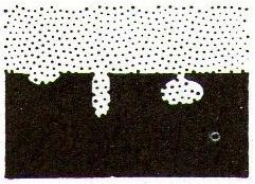
Mechanically Assisted Degradation	Erosion	The removal of a metal surface material by the action of numerous individual impacts of solid or liquid particles.	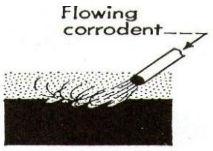
	Fretting	Occurs as the combined wear and corrosion between contacting surfaces, when the motion between the surfaces is restricted to very small amplitude oscillations. Oxidation is the most common element in the fretting process.	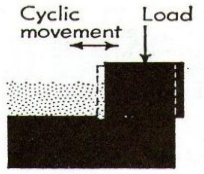
Environmentally Assisted Degradation	Corrosion Fatigue	The process in which a metal fractures prematurely under conditions of simultaneous and repeated cyclic stress loading. This is likely to occur at lower stress levels with fewer cycles than would be required in the absence of the corrosive environment.	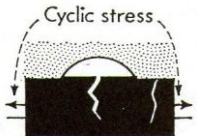
	Stress Corrosion Cracking	This is a progressive development and growth of brittle cracks in a metal due to the combined effects from localised corrosion and tensile stress.	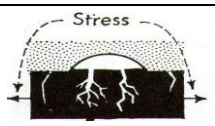
	Hydrogen Embrittlement	This results from the combined action of hydrogen and residual or tensile stress. This type of failure occurs in quenched and tempered high-strength steels. The presence of hydrogen in steel reduces the tensile ductility of the material	
	Bacterial Corrosion	Sulphate reducing bacteria (SRB) metabolising sulphate in anaerobic conditions produce the most common form of attack. The sulphate ions, as the waste product of such metabolism, react with the metal to give metal sulphides. A deposit of black iron sulphides results when iron is corroded in sulphate bearing water-saturated ground.	

EXPERIMENTAL PROCEDURE

The laboratory experiment involved four X-grade roof bolts subjected to similar environmental conditions to provide data on the effects of corrosion. The testing period lasted three and half years.

During the testing period the bolts were subjected to a corrosive environment using acid sulphate soil water with corrosive characteristics significantly greater than that can be found in most mine environments. This was necessary in order to speed up the corrosion process. The method adopted to study corrosion under various bolt loading conditions was as follows:

- Corrosion testing of a bolt axially loaded to 10 t force,
- Corrosion testing of a bolt axially loaded to 20 t force,
- Corrosion testing of a bolt subjected to torsion of 350 Nm, and
- Corrosion testing of a bolt section without loading as a reference bolt.

Factors such as pH, temperature, conductivity and salinity of the corrosive medium were constantly monitored and recorded. Water was sourced from acidic ground water drainage channels that flow into the Shoalhaven River in the South Coast of NSW, Australia. The acidity of the water was thus attributed to the regional acid sulphate soils

Test equipment

The corrosion testing apparatus consisted of a header tank which fed water to all test bolts as shown schematically in Figure 1. Figure 2 shows the laboratory experimental test rig. The dispersion of water on each tested bolt used 13 drippers spaced at 40 mm along a 720 mm long 100 mm diameter PVC manifold tubing, giving each bolt a wetting exposure length of between 520-540 mm. Water in the PVC manifild tubes was supplied from the main reserviour tank, placed about 500 mm above the PVC water manifold tubings. The length of each bolt loading frame was 770 mm. The dripped water was collected in plastic drip trays placed beneath each tested bolt and returned to the header tank for recirculation.

Bolt tensioning

Bolt tensioning was carried out using three strong Parallel Flanged Channel (PFC) steel frames, which allowed axial loading of two bolts to the predetermined loads of 10 and 20 t, and torsion of the third bolt. The 9.5 mm thick steel tensioning PFC frames consisted of two 150 mm x 75 mm sections. Two 150 mm square, 10 mm steel plates welded the two PFC steel channels together and were painted to protect and prevent them from influencing the bolt corrosion. The end-plates were drilled with 25 mm diameter holes to allow the bolt to pass through and sit between the beams spaced at 50 mm. The strength of the end-plates allowed the applied tension to be held by an interlocking nut against the sides of the frames as shown in the Figure 2 inset. The PFC section frames were designed to allow the water, that drip on to the bolts, to be collected in plastic trays placed underneath bolt mounted rigs. The reference bolt (non-tensioned) rested on top of the plastic drip tray, and the dripper tube was supported on a small plastic stand, just above the bolt. Figure 3 shows the procedure adopted for tensioning the bolt axially.

Test water

Water was sourced from Shoalhaven River (NSW, Australia) inlets. The Shoalhaven groundwater was acidic, with variable low pH value ranging between 3.4 to 4.3. The variation in the quality of the water was seasonal and at times the water was collected from two separate locations within a two square kilometre area. Due to the weathering of pyrites forming acid sulphate soil in this area, the water quality was of sulphuric acid concentration. The flow rate of dripping water to each bolt surface was kept between 3 - 5 L/h. Water in the circulation was regularly topped-up with fresh supplies, because of the losses occurring from spillage and evaporation.

Recycling of the water through the rig system was achieved using a small submersible pump with a float switch. Constant monitoring of the condition of the water was recorded as well as a titration analysis on four water samples at different times, spanning about three years of the experimental study. Table 2 shows the major chemicals present in the water and properties such as pH levels and conductivity. Figure

4 show the graph of PH level variations with time. Table 2 shows four water samples chemical analysis. Samples one to three were collected form Shoalhaven River inlet while sample four was from water from a local mine.

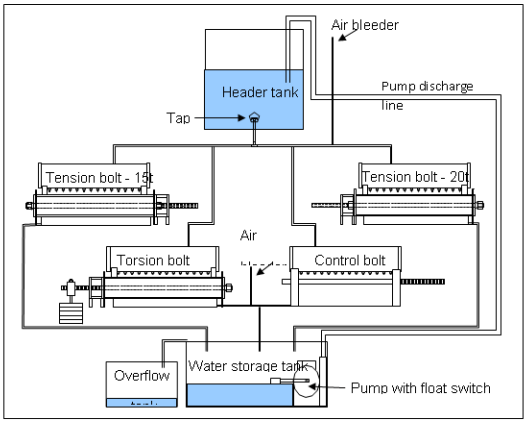

Figure 1 - The general layout of the bolt corrosion rig

Figure 2 - Corrosion testing rig

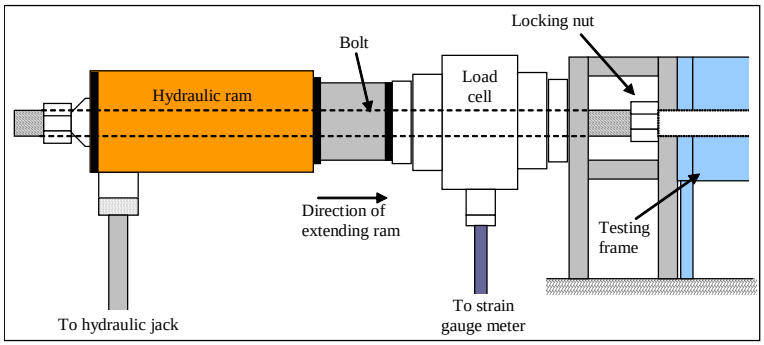

Figure 3 - Axial tensioning of bolts installed in the tension rig

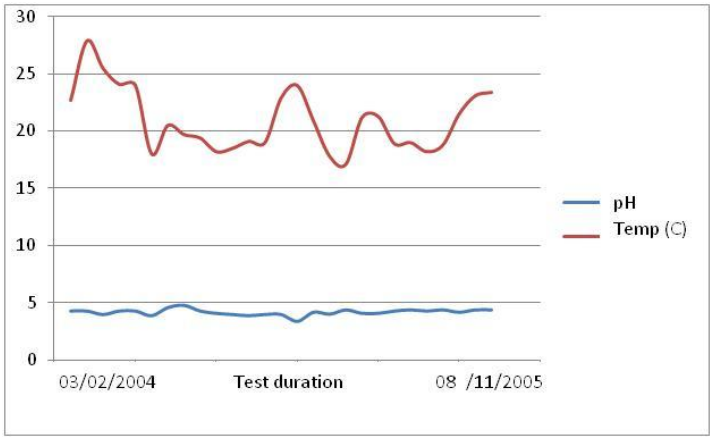

Figure 4 - Laboratory room temperature fluctuation and water Ph value

Table 2 shows the analysis of the water quality from Shoalhaven River and water quality of mine water collected from one mine in the southern coal field if Sydney Basin. It is clear from Table 2 and graphs in Figure 4, that the test water from Shoalhaven River was an aggressive solution that was suited to corrosion reactions in comparison from a typical mine water sample shown in Table 2. High concentrations of chloride ions as well as low pH level suggest that the solution was acidic. The large proportions of sulphates reinforced the weathering of the pyrite from the water origin, which assisted in decreasing any resistance to corrosion such as the formation of oxide layers. The sample solutions also show that the water had low dissolved oxygen content, which is not favoured in corrosive reactions;

however this was not thought to hinder corrosion in this test as oxygen was available to the metal surface from the atmosphere and the solution had a low pH and was not dependent on oxygen.

Table 2- Chemical analysis of test solutions, 1- 3 collected from Shoalhaven River with the fourth sample from a mine

	Sample 1 June 2002	Sample 2 May 2005	Sample 3 April 2006	Sample 4 (Mine water)
K (mg/L)	7.41	8.65		134.4
Ca (mg/L)	2.61	2.16	115	431.0
Al (mg/L)	60.4	47.6		10.21
Fe (mg/L)	69	74.8		1.00
Mg (mg/L)	60	58.2	130.7	533.7
Na (mg/L)	107.85	208.09	910	2850
Cl (mg/L)	217.55	62		5230.10
SO_4 (mg/L)	1059.44	1500		2380.80
Na/Cl	0.5	3.36		0.55
Cl/SO_4	0.21	0.41		2.2
pH	2.85	2.98	3.97	3.8
Electrical Conductivity (μS)	2008	2359	5080	18000
Dissolved Oxygen (mg/L)	8.3	9.7		
Total Dissolved Solids (ppm)	2.75	2.89		

Test bolts

Four M24 (22.0 mm core diameter) X-grade (AX) bolts were selected for this investigation. The chemical analysis conducted on the bolts is shown below in Table 3 and indicates a high carbon manganese steel. The post test samples were stripped of the corroded deposit layer to bare metal surface and had their diameters measured. The average diameter of the four tested samples pre and post-test is shown in Table 4.

Table 3 - Chemical analysis of the test bolts (source: Bureau Veritas Australia, 2012)

Bolt	C	Mn	P	S	Si	Ni	Cr	Mo	V	Al	Cu	B
Ref	0.43	0.73	0.010	0.027	0.22	0.10	0.16	0.03	0.002	0.002	0.30	0.0008
Tor	0.45	0.74	0.010	0.029	0.22	0.1	0.16	0.03	0.002	0.002	0.3	0.0008
T10	0.29	0.82	0.011	0.023	0.24	0.09	0.08	0.02	0.044	0.001	0.31	0.0007
T20	0.53	1.65	0.008	0.022	0.24	0.07	0.11	0.01	0.002	0.001	0.25	0.0011

NB: Ref; Reference bolt, Tor: torsion bolt; T10: 10 t tensioned bolt; T20; 20 t tensioned blt

Table 4 - Yield and ultimate strength failure load of the tested bolts

Bolt Status	Reduction in bolt diameter after corrosion test (%)	Reduction in bolt cross -section area (%)	Yield load (kN)	Change in yield load with respect to new bolt (%)	Failure load (kN)	Reduction in failure load bolt (%)
New bolt (P new) *	0	0	219.663		347.187	
20 t axially loaded (T_{20})	12.1	11.04	219.507	0	274.957	21
10 t axially loaded (T_{10})	12.5	11.40	150.518	31.5	211.354	39
300 Nm torsion Bolt (T_t)	9.65	8.81	126.930	42.2	211.518	39
Reference bolt (T_r)	12.6	11.50	128.119	41.6	222.164	36

* Initial bolt core diameter: 21. 7 mm; full diameter with ribs: 23.7 mm

Figure 5 shows pictures of various sections of pre and post-tested bolts. It is clear that there were some variations in the post-testing diameters along the length of each bolt. A noticeable and excessive corrosion occurred on the threaded bolt-ends section and at the sections of the bolts passing through the steel PFC end plate holes. These two sections were outside the direct water dripping zones. The threaded side of the bolt with maximum corrosion were for the purpose of bolt tensioning on the loading

frame sides. Figure 5 d, e and f show corroded bolt surfaces located in the vicinity of the PFC bolt tightening hole. This type of crevice corrosion is most likely to be the result of differential aeration mechanism.

Figure 6 shows the load-displacement graphs of various corrosion tested bolts as well as a new bolt, which was not subjected to the corrosion test. Table 4 shows the various bolts load-displacement values at yield as well as the ultimate strength values as seen in column six in Table 4.

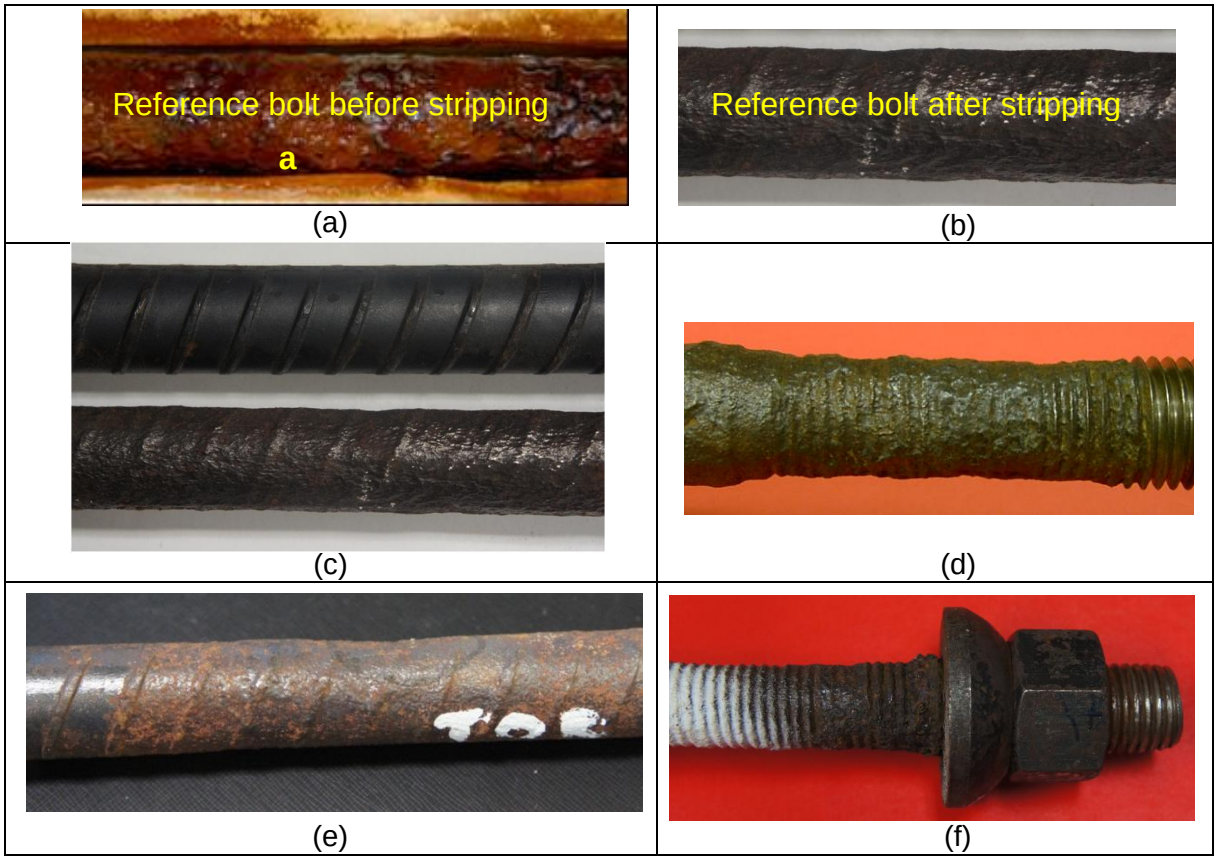

Figure 5 - Photos of parts of various corroded bolt sections compared with un- corroded section. Section (e) shows the evidence of crevice corrosion due to aeration at bolt end

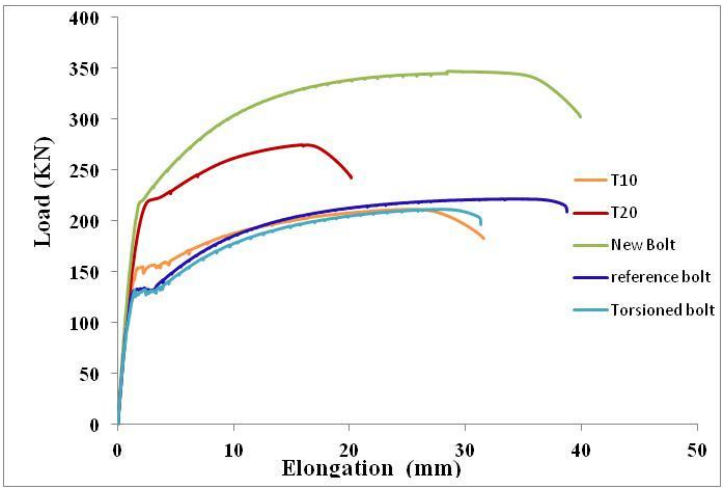

Figure 6 - Load displacement profiles of various bolts

One of the noticeable profiles of the load displacement graph was that the strength value of the 20 t tensioned bolt (T_{20}), was relatively greater than the other three bolts in the test. The peak load of P_{20} bolt was in the order of 274 kN (27.94 t). This level represented a reduction of around 21% in strength with

respect to the failure strength of a similar new bolt with its tensile strength failure load of 347 kN (35.38 t). The 10 t (T_{10}) tensioned bolt achieved 39% reduction in strength, and the reduction in strength of the torsion bolt (P_t) was 39% and the reference bolt (T_r) was 36%. The unusually lower percentage reduction in the failure load of the 20 t bolt as compared to other corroded bolts is likely to be attributed to the steel composition of the bolt as shown in Table 4. It is clear that the carbon and manganese content of the T_{20} bolt was greater than with other three bolts.

The average reduction in borehole diameter of all four bolts due to three and half years of corrosion testing was in the order of 11.7%. This is equivalent to a cross-sectional area reduction of around 10.7%. This level of cross-sectional area reduction was significantly less than the percentage reduction of the bolt tensile strength.

The accuracy and reliability of the corroded bolt diameter measurement were affected by the level of bolt surface irregularity due to the bolt surface pitting as well as near total erosion or corrosion of bolt profiles around the bolt. This made it difficult to differentiate measurements between core and full diameter bolt cross-section.

The weight loss measurement, before and after the test, could not be related solely to the designated wetted section of the bolt. There was some further corrosion at the bolt ends that anchored the bolt ends to the PFC steel loading frame. Thus, two forms of corrosion were identified in this experimental study, pitting and crevice corrosion. Pitting corrosion was evident in the mid-sections of the bolt directly along the dripping zone as seen in Figure 5 a, b and c. Crevice corrosion on the other hand occurred at the bolt ends as demonstrated in Figure 5 d, e and f. The mounting of the torsion bolt on the PFC tension frame also generated crevice corrosion as one side of the bolt required no direct axial loading, just torsion, thus leaving a free flow of air through the bolt surface as shown in Figure 5e. Normally crevice corrosion occurs in the confined space as a result of differential aeration mechanism. Also the excessively crevice corroded zone shown in Figure 5e was not in direct contact with the dripper waters as the last drip nozzle was some 60-70 mm away from either side of the rig side holes housing the bolt ends. This sort of corrosion is most likely to be observed underground at the collar of the installed bolt in a hole with less encapsulation, thus leading to the onset of stress corrosion cracking, particularly when the protruding bolt end is subjected to external shear loading or impact. According to Gray (2006) this kind of corrosion was often found in their field observations particularly at Angus Place Mine, NSW, with severe corrosion taking place along the free length of the bolt, even though there was no apparent free water. A damp corrosive atmosphere is sufficient to cause corrosion and perhaps this is because of the greater presence of free oxygen in air rather than under water. Also the excessive surface area of the threaded section of the bolt also has an influence.

A non-destructive test was carried out on T20 bolt to determine whether there was an onset of stress corrosion cracking of the sample after it was subjected to 20 t tension force. Using magnetic particle inspection, repeated tests on the sample produced negative results which indicated no cracks were found.

CONCLUSIONS

Prolonged experimental study using high carbon manganese X-grade rock bolt showed that significant corrosion has occurred in an aggressive low pH groundwater. Both pitting and crevice corrosion was identified as the type of corrosion that is most likely to occur along the tested bolt length. Using low pH water to speed up the corrosion process was considered as acceptable and viable methods of conducting bolt corrosion testing in the laboratory environment.

The ultimate tensile strength of bolts subjected to prolonged corrosion tests was reduced by between 21%, for 20 t bolt, and 39% of the reference bolt, compared with the ultimate tensile strength of a new similar type bolt. Both T_{10} and torsion bolts had near equal ultimate tensile strength reduction of 31%. The abnormally high load displacement profile of the T_{20} bolt was attributed to different composition steel with high carbon and manganese content in comparison to other three tested bolts

The average reduction in borehole diameter of all four bolts over the period of three and half years of corrosion testing was in the order of 11.7 %. This level of diameter reduction was significantly less the percentage reduction of the bolt tensile strength of between 21 and 39%.

ACKNOWLEDGEMENTS

The authors would like to thank Alan Grant, Ian laird and Robert Rowlan from the school of Civil, Mining and Environmental Engineering, faculty of Engineering, University of Wollongong for their assistance in the fabrication, maintenance, monitoring and supply of the field water during the four years of the experimental study programme. Special thanks to DSI and Jennmar Australia for supplying bolts for this particular study. Constructive comments and suggestions from Meitek Rataj of Sandvik and Glenn Sullivan of Moly-Cop are very much appreciated.

REFERENCES

Bureau Veritas Australia, 2012, Roof Bolt Material Identification report, Newcastle NSW 2304 Australia. 8p.

Tuutti, K, 1982. Corrosion of steel in concrete, CBI-research 4:82, 456p.

Sundholm, S, 1987. The quality control of rock bolts, *6th International Congress on Rock Mechanics, Montreal*, pp1225-1264.

Helfrich, H K, 1990. The durability of rock bolts, World Mining Equipment, April.

Moving, H, 1994, Corrosion test of rock bolts according to ASTM-B117. Document No. 10-13160.03, Marine, Materials Technology Centre for Applied Materials Research, August, Sandford, Norway (unpublished).

Sundholm, S and Forsen, O, 1995. Corrosion of rock bolts, cement mortar as corrosion protection of rock bolts, Laboratory of rock Engineering, Helsinki University of technology, Finland.

Baxter, D A, 1996. Do all rockbolts rust? Can Q.A help? But does it matter? In *Proceedings IX Australian Tunnelling Conference*, Australian Institution of Engineers, August, Sydney, pp175-190.

Spearing, A, Mondal, K and Bylapudi, G, 2010. The corrosion of rock anchors in US coasl mines, SME annual meeting, Phoenix, AZ, USA, February 28-March 3rd, 6p.

Gray, P, 1998. Stress corrosion cracking of rock bolts, *First Australasian Coal Operators Conference*, February, 18-20, University of Wollongong, pp 206-213.

Hebblewhite B, Fabjanczyk, M, and Gray, P, 2002. *Premature Rock Bolt Failure,* ACARP Project No. C8008, Final report, April.

Hebblewhite, B, Fabjanczyk, M and Gray, P, 2003, Investigations into rock bolt failures in the Australian coal mining industry, In *Proceedings of 4th Underground Coal operators Conference*, Wollongong, February 12-14, ISBN 0 8 6418 7785 (Eds. N Aziz, B Kinninmonth), pp 125-131. http://ro.uow.edu.au/coal/167/.

Gamboa, E and Atrens, A, 2003. Laboratory testing of rock bolt stress corrosion cracking, In *Proceedings of 4th Underground Coal Operators Conference*, Wollongong, February 12-14, ISBN 0 8 6418 7785 (Eds. N Aziz, B Kinninmonth, pp 132-153. http://ro.uow.edu.au/coal/169/.

Hebblewhite, B, Fabjanczyk, M, Gray, P and Crosky, A, 2003. Premature rock bolt failure through stress corrosion cracking, In *Proceedings 22nd International conference on Ground Control in Mining, ICGCM,* Morgantown, WV, pp 218-225.

Henthorne, M, 1971-1972. A CE refresher series on corrosion causes and control, Chemical Engineeering Magazine. A series of 12 articles written between May 17, 1971 through April 3, 1972. Reprinted by Carpenter Technology, Reading, Pennsylvania, USA.

Satola, I and Aromaa, J, 2005. The corrosion of rock bolts and cable bolts, in *Proceedings 5th International Symposium on Ground Support in Mining and Underground Construction*, Perth, September 28-30, pp 521-528,

Hassell, R, Villaescussa, E, Thompson, A G and Kinsella, B, 2005. Corrosion Assessment of ground support systems, In *Proceedings of 5th International Symposium on Ground Support in Mining and Underground Construction*, Perth, September 28-30, pp 529-544.

NEW APPROACH TO RESIN SAMPLE PREPARATION FOR STRENGTH TESTING

Naj Aziz[1], James Hillyer[1], David Joyce[2], Shuqi Ma[1], Jan Nemcik[1] and Arash Moslemi[1]

ABSTRACT: A new method of preparing multiple samples, from one resin mix portion, for strength testing is presented. The method is based on rapid mixing of the resin mechanically and forcing a select number of seven specially prepared moulds into the mixed resin. The system is applicable for both cylindrical and cube/prisms particularly suited for fast setting resin. The study demonstrated that the samples are easily prepared, uniform in composition, with little or no entrapped air. It was found that the samples yielded consistent uniaxial compressive strength values with a standard deviation of 0.47 and a coefficient of variation of 0.88%. The methods can be used for different sample sizes.

INTRODUCTION

There is no Australian standard for the evaluation of the mechanical properties of resins or cementitious grouts used for bolt or cable encapsulations; therefore there is no uniform method for testing resins for strength. Depending on the country of origin, resin manufacturers invariably use different specimen shapes and sizes to determine the strength properties of the resin or grout. Currently three standards available, which are likely to be used in Australia for strata reinforcement system components used in mines. They are:

1) The British Standard BS 7861: Strata Reinforcement support system components used in Coal Mines- Part 1. Specification for rock bolting (1996) and Part 2: Specification for Flexible systems for roof reinforcement;
2) American Standard for Testing Materials (ASTM) F 432- 10: Standard Specification for Roof and rock Bolts and Accessories; and
3) South African Standard SANS1534

There appears to exist a divided loyalty and preferred practices in testing for the strength of resin with regard to sample shape and size. Irrespective of the resin setting (fast, medium and slow set) the Uni-axial Compressive Strength (UCS) property is determined either by using 40 mm cubes, or cylindrically shaped samples, with varying sizes of 20, 30, 42 and 54 mm diameters. The 20 mm diameter size appears to be the most desirable size for testing fast set resin samples. In general, and in comparison with cube /prism, the cylindrical samples represent a better shape of sample preparation as well as being easily manipulated for different test needs. Normally the length to diameter ratio will be 2.5-3.0, in compliance with the suggested method for determining the UCS and deformability of rock material of International Society of Rock Mechanics (1979). Plastic drain pipe sections are used for making moulds.

The shape of the sample is not a major issue for samples preparation using slow setting resins. Both cube/prism and cylindrical shapes can be prepared and tested individually by mixing resin and mastic at a leisurely pace. The situation becomes more difficult in contrast when preparing the samples from fast setting resins, which typically have a setting time of 15-20 s. Accordingly, the proposed new approach allows several samples to be cast simultaneously from one resin mix batch, reducing sample variability. The method of resin mixing and sample preparation is the focus of discussion in this paper.

CURRENT PRACTICE

The present practice of determining the UCS value of a resin is to cast the resin in the desired shape, depending on one of the standard used and the resin type. For slow and medium setting resin, the current

[1] *University of Wollongong, NSW. naj@uow.edu.au, Tel: +61 (0 2) 42 213 449*
[2] *Minova Australia, Nowra, NSW, David.Joyce@minovaint.com, M: 04 1868 0005*

practice is to prepare the resin mastic and catalyst mix in a suitable container and then pouring the resin into the mould(s). The mould is made of steel or plastic tubes. Once filled the resin samples are left to harden/cure and then extracted from the moulds. Prior to resin pour, the mould is smeared with inert grease or lubricant sprays to ease sample extraction after casting. Figure 1 shows a typical sample being cast in a plastic mould. The past practice of axially splitting the moulds, especially the cylindrical plastic moulds, is not necessary as the cured or hardened samples are easily extracted from the mould because of the surface lubrication. A simple tapping of the hardened resin sample releases the sample free from the mould. A similar method can be used for cube/prism samples, however the open end side of the cube mould may not be as smooth and flat unless it is covered with a suitable plate so that the cube face is smooth and square. Testing cube samples, which are rough on one side, may not yield uniform test results.

With regard to fast setting resin sample casting, the situation is rather tedious. For 40 mm cubes and 42 mm and greater diameter cylindrical samples casting, a simple manual mixing of resin and mastic in each mould is the preferred practice, however for smaller sized cylindrical moulds of 20 or 30 mm the method of syringe style of suction practice is adopted. The drawback of casting sample by manual mixing and pouring includes:

- The difficulty of removing the air bubbles from the sample, unless the sample is subject to vibration,
- Non uniform composition of the sample mixtures as each sample has to be mixed and poured separately.
- One side of the cube sample will always remain rough, which could eventually influence the test results, and
- Mixing of the resin in the mould may not be uniform, unless the mixer is skilled.

In reality the test results of manually mixed resin samples will have variable values, which may lead to incorrect determination of the value of the sample UCS strength.

NEW APPROACH

A new approach currently being trialled is to produce several samples from a single resin/mastic mix. This is based on mixing a relatively large quantity of resin /mastic resin in one container mechanically and then has a number of readily prepared moulds forced into the resin mix as a single bunch. Once all the moulds are submerged in the resin mix, it will be allowed to harden which allows the samples to be knocked out of each mould by gently tapping the resin sample out of each mould in the block. Alternatively, the whole resin block is split or broken which allows separating the plastic moulds apart, which is followed by the extraction of the samples out of the plastic moulds. A gentle dowel tapping on each resin sample would facilitate sample extraction from the mould. A paint mixer mounted on to a hand held drill is suitable for resin mixing in the container. Figure 2 (a-f) shows the sequence of resin mixing and sample casting by moulds insertion of he moulds in the container. Ideally up to seven 30 mm diameter moulds can be cast in a 150 mm plastic pipe section.

Figure 1 - Various plastic pipe section moulds and typical moulds arrangement in mixing container. Note two samples in mould

For slow setting resin the insertion of the moulds into the mixed resin is not a major issue. Figure 3 shows a typical block of slow setting resin with 20 mm diameter samples being extracted from it. As shown there were six samples prepared from a single cast block, which was of a sufficient numbers to be tested. Note

that the entire resin sample prepared by moulds forced into the soft resin mix contained a minimum surface roughness as well as being devoid of large air bubbles. Once the samples were extracted from the moulds, their ends were cut perpendicular to the sample axis and then subsequently lapped if necessary and in compliance with the established standard requirements for sample end smoothness.

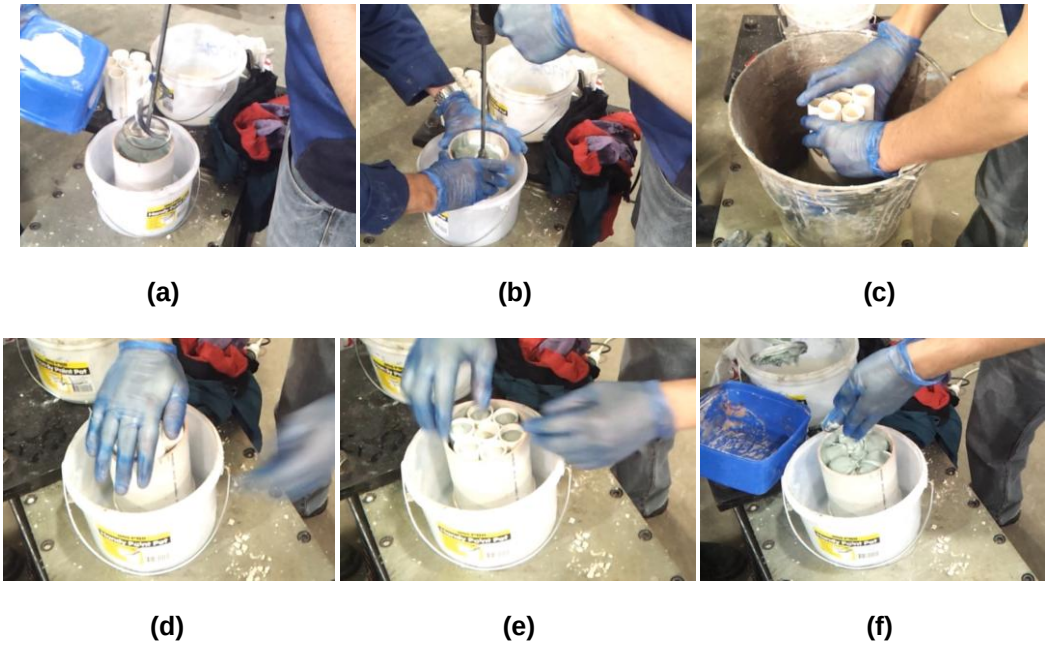

(a) **(b)** **(c)**

(d) **(e)** **(f)**

Figure 2 - Stages of resin mixing mechanically and sample casting in seven moulds simultaneously

It is worth noting that by forcing moulds into the resin will require some pushing force applied to enable the mould to be forced down the resin mix and this should be done as quickly as possible, because of the limited time available before the resin hardens. Experience will be gained by a few initial trials. Table 1 shows the results of one batch of seven samples being tested for the UCS values and Figure 4 shows post tested failed samples post test. It is clear that the quality of the samples and the results of the test have demonstrated the credibility of the new method of preparing resin samples. This kind of sample casting should also be suitable for cube/prism shapes. The average UCS value of the seven samples tested was 53.16 MPa, with a standard deviation of 0.47 and a coefficient of variation of 0.88%.

Table 1 - Failure load and UCS values of seven samples obtained from one resin/catalyst mix

Sample	Sample age (d)	Sample length (mm)	failure load (kN)	UCS (MPa)
1	4	78.52	36.8	53.88
2	4	78.56	36.1	53.08
3	4	78.29	35.6	52.41
4	4	78.48	36.7	53.38
5	4	78.55	36.3	52.99
6	4	78.12	36.2	53.45
7	4	78.29	36.0	52.91

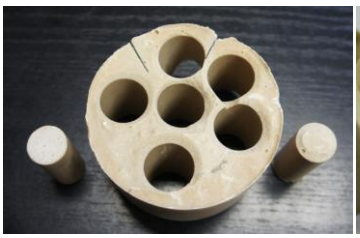

Figure 3 - Mould of slow setting resin and two 20 mm diameter samples

Figure 4 - Two 30 mm diameter tested samples

CONCLUSIONS

The new method of casting multiple samples in bunch represents a convenient method of preparing samples for strength testing. The prepared samples have been found to be of uniform composition and yielded consistent results. The proposed method of casting samples is:

- fast as no additional time is required for repeated casting;
- sample sides are uniform as the moulds are not split axially;
- the method can be applied to cylinder as well as cube sample preparation;
- the methods reduces the formation of voids and the composition of the cast sample is consistent.

ACKNOWLEDGEMENTS

Special thanks to Minova Australia of Nowra for providing resin and allowing the team frequent visits to Minova for carrying out the necessary preparatory work on the project. The laboratory support provided by Colin Devenish, the technical officer at the School of Civil, Mining and Environmental Engineering, Faculty of Engineering, University of Wollongong is greatly appreciated.

REFERENCES

The British Standard BS 7861: Strata Reinforcement support system components used in Coal Mines-Part 1. Specification for rock bolting (1996) and Part 2: Specification for Flexible systems for roof reinforcement,

American Standard for Testing Materials (ASTM) F 432-10: Standard Specification for Roof and rock Bolts and Accessories.

South African Standard SANS1534-2004, Resin capsules for use with tendon based support systems, published by Standards South Africa.

International Society of Rock Mechanics, 1979. Suggested methods for determining the uniaxial compressive strength and deformability of rock materials, *Int. J. Rock Mech.Min. Sci. and Geomechanics Abstract*, 16:135-40.

DILATIONAL SLIP ANGLE OF REBAR BOLTS UNDER AXIAL LOADING

Chen Cao, Jan Nemcik, Naj Aziz and Ting Ren

ABSTRACT: Mechanical interlock is an important component in load transfer capacity in the rockbolting system. It is in turn dominated by the rebar bolt profile configuration. To gain a deeper understanding of their interactions, rebar bolt units under axial loading were studied. Two kinds of failure mode have been identified, namely parallel shear and dilational slip failures. Based on some assumptions made, a universal upper limit of slipping angle of dilation slip failure can be found as the complementary angle of the grout material internal friction angle, which is also the minimum value of the bolt rib face angle. This theory can explain similar performances of rock bolts in pull-out tests while their face angles are large. In addition, once the geometric parameters of a rebar bolt profile are provided, more narrow slip angles range can be figured out via simple plots. As a result, the grout between the bolt profiles can be recognised as three sections, one works as part of the bolt profile, one carries out shear failure and the bottom part keeps intact.

INTRODUCTION

Steel bolts have been widely used for rock reinforcement in civil and mining engineering for several decades Bolts reinforce rock mass through restraining the deformation within the rock. To improve bolt loading capacity through the steel rebar, it is necessary to have a good understanding of the rock bolt behaviour in deformed medium. This can be acquired through analytical studies, laboratory tests and numerical modelling.

Monitoring of load transfer between the bolt, resin and rock strata indicates that the bolt profile plays an important role in generation of shear strength between the bolt and the surrounding rock. The short encapsulation pull out test of roof bolts indicates a significant increase of load transfer at a particular bolt rib profile spacing. Other variables such as profile rib angle, shape and size are also important parameters contributing to the load capacity of rock bolt systems.

The load transfer capacity of the bolt is governed by the shear strengths developed between the rock/grout and the grout/bolt interface interaction. Grout/rock interface failure can rarely occur in lab pull-out tests and in practice. As a result the bonding strength at the grout/bolt interface dominates the effect of rockbolting (Aziz, *et al.*, 2006; 2008).

It is commonly accepted that the bonding strength has three components: cohesion, friction and interlock. Singer (1990) demonstrated that there is no adhesion between the grout to bolt interface but in most cases reported, there is very little adhesion between grout-bolt, Aziz and Webb (2003).

The frictional component can be catalogued into the dilational slip, shear failure of surrounding medium and bolt unscrewing, Hyett *et al*. (1995). Each of them depends on the pressure generated at the bolt-grout interface, which in turn depends on the internal reaction forces of the three phase materials.

The mechanical interlock component plays an important role in bonding capacity and load transfer in the rockbolting system. It, in turn, is influenced by the bolt profile configuration. The profile configuration is defined by the rib profile shape, profile height, angle of wrap and spacing between the ribs, as shown in Figure 1.

In traditional rockbolting mechanism analysis, the effect of mechanical interlocking is often integrated into the analytical model in various manners, but do not concern with the rib geometry. In the so-called 'Interfacial Shear Stress' (ISS) model, the deformation of surrounding materials is lumped into a zero thickness interface, which is assigned with specific stress-strain behaviour to simulate the mechanical interlocking observed in pull-out tests. For example, Farmer (1975) has shown that exponential decay of the axial stress of the bolt occurs in the case of perfect bonding and elastic deformation. Li and Stillborg

School of Civil, Mining and Environmental Enginering,University of Wollongong, NSW, 2522, jnemcik@uow.edu.au, M: +61 0408 711 280

(1999) developed an ISS model for predicting the behaviour of rock bolts in pullout tests, in uniformly deformed rock mass and when subjected to opened joints. Ivnovic and Neilson (2009) developed a lumped parameter model with varying shear load failure properties along the fixed anchor length to analyse the bolt behaviour under static or dynamic loads. More recently, a tri-linear bond-slip model with residual strength at the grout-bolt interface is adopted and closed-form solutions are obtained for the prediction of full range behaviour of fully grouted rockbolts under axial load, Ren, *et al.* (2009) and Martin, *et al.* (2011).

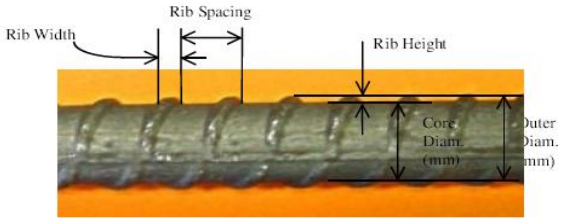

Figure 1 - Terminology of the rib profile of steel bolt.

How the bolt profile interacts with the grout material under axial loading is the focus of this study. It is a structurally based approach to reasoning the performances of the rock bolt when pull tested. A rib profile, shown in Figure 2, is only one unit of the bolt profile system which is the subject of discussion in this paper.

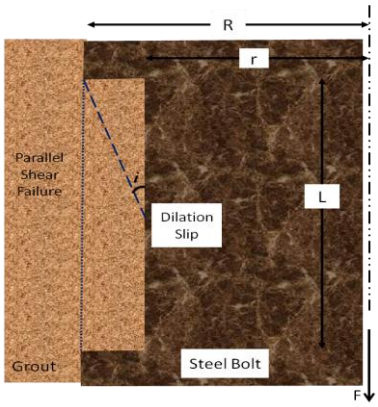

Figure 2 - Schematic diagram of one bolt unit. The load F is resultant force in axial direction; r is the core radius of the steel bolt; R equals to r plus rib height; L is rib spacing except rib itself; the dotted line indicates parallel shear failure surface; dashed line indicates the dilational slipping surface and the angle i is the slipping angle of the bolt unit.

The derived mathematical expressions of slipping angle, *i*, describe the initial orientation of dilational slip failure of the bolt unit; it is also the "real" face angle for the steel bolt. The aim of the theoretical predictions is to provide and understanding of the initial grout failure and to offer a new tool for research into the best profile geometries to reach optimum shear strength between the bolt and the surrounding medium.

FAILURE MODES OF ROCK BOLTS UNDER AXIAL LOADING

Failure modes of rock bolting subjected to axial loading are the major concern of the load transfer mechanism. Two kinds of failure modes can be identified via pull-out tests, namely direct parallel shear failure (indicated by dotted line in Figure 2) and dilational slip (indicated by the dashed line in Figure 2).

Direct parallel shear failure is charactered by a cylinder shaped failure surface. It is a characteristic failure pattern, which occurs for smooth surface bar (without profiles) along the bolt-grout contact, and for very closely spaced rebar (like a screw) along the rib tips of the bar. For one unit of a smooth bolt, the resultant axial load can be expressed as

$$F = 2\pi rL\tau \quad (1)$$

Where τ is the shear stress and once failure occurs, the shear stress can be calculated via Coulomb's failure criterion as:

$$\tau = c_{\text{grout-steel}} + p \cdot \tan\phi_{\text{grout-steel}} \quad (2)$$

Here c and ϕ are grout/steel interface properties and p represents the confining pressure when failure occurs.

In another situation, if a bolt has closely spaced ribs, parallel shear failure between the rib peaks will always occur. It can be found that during such failure, the grout between the profiles will remain as if it was part of the steel bar. In fact, a threaded bar can be thought of as a smooth bar with little larger diameter. The mechanical behaviour of threaded bar can be expressed using similar equations but replacing grout-steel properties with grout property only, thus:

$$F = 2\pi RL\tau \quad (3)$$

$$\tau = c_{\text{grout}} + p \cdot \tan\phi_{\text{grout}} \quad (4)$$

The load capacity of direct parallel shear failure is apparently lower if compared with ribbed steel bar of the same core diameter (Aydan, 1989; Ito, *et al.*, 2001; Aziz, *et al.*, 2008; Kilic, *et al.*, 2002). The force F is normally large and the resin is much softer than steel. Therefore, the direct parallel shear failure, without any dilatation can rarely occur for a common rebar bolt. That is, under normal circumstances dilatation will always occur, more or less, around the rebar bolt surface. If the confinement material is stiff, or say in hard rock, the initial dilatation can be depressed by increasing confinement pressure. In some cases where rock is very soft, the rib will push the surrounding material radially outwors and slip out from the initial flute.

THEORETICAL RANGE OF DILATIONAL SLIP DIRECTIONS

Problem of description and assumptions

From the failure modes analysis, the mechanism of dilational slip failure is the major concern of rebared rock bolting system. For one bolt unit, the initial failure is characterised by propagation of micro-cracks along a specific surface. Once the mobilised shear stress along this surface reaches a critical value, relative movement will take place. Then the post-failure behaviour will be governed by more complicated interaction as the initial confining pressure will be re-distributed.

In this paper, the post-failure behaviour will not be discussed, and the focus will be on the slipping angle analysis. Firstly, the following assumptions are made;

(1) Coulomb failure criterion is used to locate the failure surface within the grout material

(2) The initial confining pressure, p, is compressive and universal.

(3) The cohesion and friction at the resin-bolt contact are neglected.

Dilational slip failure of one unit bolt

Before slipping occurs, the axial force, F, cannot affect the initial horizontal stress field because they are perpendicular to each other. That is, p will keep its magnitude while F increases until relative movement takes place. In this procedure (shown in Figure 3):

$$\sigma_n = p\cos i - \frac{F}{A}\sin i \quad (5)$$

$$\tau = \frac{F}{A}\cos i - p\sin i \quad (6)$$

Where $A = \pi(R^2 - r^2)/\sin i$ is the conical area of the failure surface.

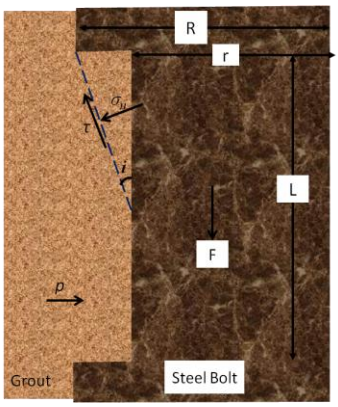

Figure 3 - Dilational slip just occurs along the dashed line

Once the relative movement along the supposed surface takes place, according to assumption (1), then the dilational slip failure follows

$$\tau = c + \sigma_n \cdot \tan\phi \quad (7)$$

Initial slipping angle analysis

Eq. (3) and (4) can be re-arranged as

$$F/A = \sigma_n \sin i + \tau \cos i \quad (8)$$

$$p = \sigma_n \cos i - \tau \sin i \quad (9)$$

Substitute shear stress, τ, in Eq. (7) and using Eq. (5),

$$p = \sigma_n \cos i - (c + \sigma_n \cdot \tan\phi)\sin i$$

This is the expression of confining pressure before it begins to change. The confining pressure is always positive (compression), so

$$\sigma_n \cos i - (c + \sigma_n \cdot \tan\phi)\sin i \geq 0$$

As $c \geq 0$, and $i \leq \frac{\pi}{2} - \phi$ (10)

This is the expression of the upper limit of the dilational slip angle. It demonstrates that the upper limit of slipping angle is solely dependent on the grout internal friction angle. For example, if the resin internal frictional angle = 35°, the dilation slip angle must be less than 55°, no matter what the real bolt face angle is.

The dilational slip angle reaches its maximum value $(\pi/2 - \phi)$ when c=0 and p=0. This is a kind of spontaneous dilational slip which is obviously not real for a rockbolting system. Thus the slipping angle will always be under this upper limit.

When the rib face angle is greater than the upper limit of slipping angle, the material between them will remain because there is no relative movement. In other words, grout material in this area will become part of the bolt profile, and in most cases, forever.

There are several research works of study on the bolt face angle. According to Tepfers (1973), slip on rebar can occur in two ways: (1) the rib can split the concrete by wedging action, and (2) the rib can crush the concrete. Tepfers also pointed out that a rib with a face angle between 40° and 105° produced about the same movement. Angle of the rib is defined in Figure 4. In addition, when concrete was crushed to a compacted powder, it became lodged in front of the ribs. However, Tepfers did not give any explanation of this phenomenon. The theory of upper limit of slipping angle derived in this paper is able to reason this experiment observation. If the internal friction angle of concrete is about 30°, then the bolt with face angle greater than 60° will produce the same performance.

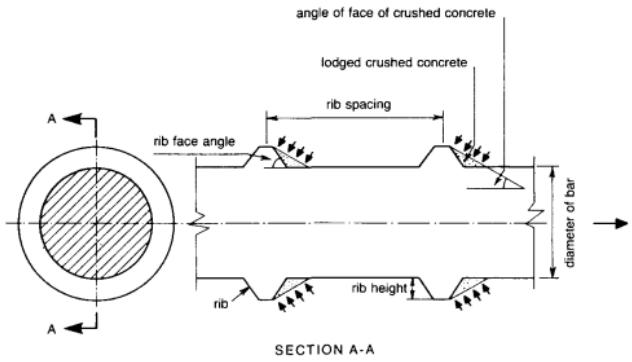

Figure 4 - The geometry of a deformed reinforcing bar and the mechanical interaction between the bar and the concrete, after Tepfers (1973)

Kilic, *et al.*, (2002) studied the effect of different shaped lugs on the steel bolt, by pullout tests. These were smooth bars, thread bars, single conical lugged bars and double conical lugged bars. The schematic illustration of two groups of their tests is shown in Figure 5; and the result of these tests is shown in Table 1.

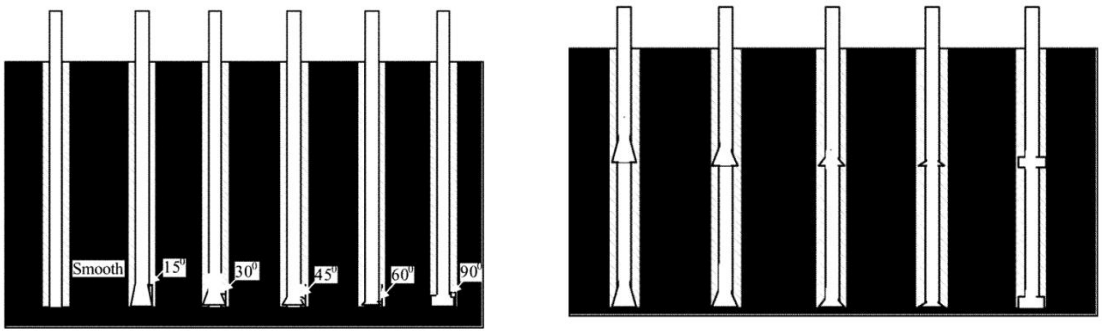

Figure 5 - Schematic illustration of two groups tests conducted by Kilic, *et al.*, (2002)

Table 1 - Pull out test results for different rock bolt types, after Kilic, *et al.*, (2002)

Bolt type	Yield load (kN)	Elastic displacement (mm)	Failure load (kN)
10° Single conical[a]	56	0.67	67.2
15° Single conical[a]	56	0.60	65.5
20° Single conical[a]	48	0.62	62.4
25° Single conical[a]	48	0.51	61.7
30° Single conical[a]	48	0.43	60.8
60° Single conical[a]	48	0.36	59.1
90° Single conical[a]	48	0.29	57.6
Smooth surfaces[b]	16	1.10	17.6
15° Single conical[b]	64	0.99	68.4
30° Single conical[b]	64	0.95	65.8
45° Single conical[b]	56	0.82	63.5
60° Single conical[b]	56	0.78	60.5
90° Single conical[b]	56	0.74	59.3
15° Double conical[b]	88	1.48	92.8
30° Double conical[b]	88	1.42	89.7
45° Double conical[b]	80	0.88	87.7
60° Double conical[b]	80	0.82	86.1
90° Double conical[b]	80	0.80	84.6

Their experimental results show a strong influence of the bolt profile on the load bearing capacity and deformational behaviour of the reinforecement system. It can also be found that the 60° bolts has very close performance with the 90° bolts (highlighted in Table 1). These results can be understood by, and also used to support to, the upper limit slipping angle theory conducted in this paper.

Slipping angle range for known rebar bolt

It should be noted that, according to previous analysis, the upper limit of the slipping angle is independent of bolt profile. In another word, it is universal whenever dilational slipping failure occurs for a bolt unit. For a known bolt however, the angle range of possible slipping can further be narrowed. Combine Eq. (5), (6) and (7), eliminate σ_n and τ, the axial load which causes dilational slip to occuris is

$$F_{dila} = \frac{\pi(R^2 - r^2)}{\sin i}\left[\frac{\cos\phi}{\cos(i+\phi)}c + p\tan(i+\phi)\right]$$

And Eq. (1) is the expression of the axial load capacity of the unit bolt for shear failure. So, if the dilational slip does occur, it will always have

$$F_{\text{shear failure}} \geq F_{\text{dilational slip}}$$

Combining with Eq. (5) leads to

$$2\pi RL(c + p\tan\phi) \geq \frac{\pi(R^2-r^2)}{\sin i}\left[\frac{\cos\phi}{\cos(i+\phi)}c + p\tan(i+\phi)\right] \quad (11)$$

To avoid cumbersome math, simply let p=0, then the equation can be easily solved as

$$\sin(\phi + 2i) \geq \frac{R^2-r^2}{RL}\cos\phi + \sin\phi \quad (12)$$

The domain satisfying this equation will be the theoretical slipping angle range for this bolt.

Here is an example. The bolt shown in Figure 1 is a commercial bolt of average rib spacing 12.5 mm, core diameter is measured to be 21.5 mm. After taking the average to the rib cross section, the average ribs height is found to be 1.35 mm and the average rib width is 2.8 mm. This leads to R=12.2 mm, r=10.8 mm, L=9.7 mm. Let the internal friction angle of the resin to be 35°, and put these parameters into Eq. (8) and solve, getting:

$$9° \leq i \leq 46°$$

The initial possible dilational slip direction for this bolt can be limited to a range of [9°, 46°], as shown in Figure 6. Consequently, resin between the bolt profile can be divided into three divisions in case of dilational slipping. The resin above face angle 46° (indicated as I in Figure 6) will move with the bolt and can be thought of as part of the bolt profile. Section II will experience shear failure, hence micro-cracks in this area are inevitable. The resin below 9° will keep intact with resin in the annulus and its strength not expected to change very much.

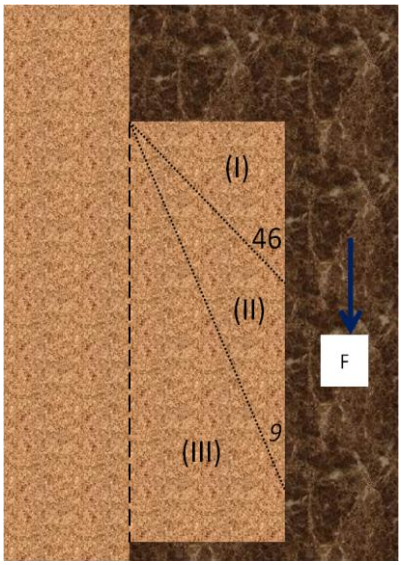

Figure 6 - The slipping angle range for rebar bolt in Figure 1

CONCLUSIONS

Mechanical interlock is an important component in load transfer capacity in rockbolting systems. It is dominated by the rebar bolt profile configuration which includes rib height, rib spacing, rib face angle and shape of rib cross section.. When an axial load is applied to cause failure of the rock bolt, two major failure modes can be identified as parallel shear failure and dilational slip. After introducing Coulomb's shear failure criterion, a universal upper limit of slipping angle can be calculated as the complementary angle of the grout internal friction angle. In addition, once the geometric parameters of a rebar bolt profile have been given, more accurate result can be achieved via simple plots. Consequently, the grout between the bolt profiles can be divided into three parts, one will be part of the bolt profile, one will undergo shear failure and the bottom part will remain unaffected.

REFERENCES

Aziz, N I and Webb, B, 2003. Study of load transfer capacity of bolts using short encapsulation push test, In *Proc. 4th Underground Coal Operators Conference*, Coal 2003, February 12-14, Wollongong, pp 72-80. (ed N Aziz and R Kininmonth). http://ro.uow.edu.au/coal/162/.

Aziz, N I, Jalalifar H and Concalves, J, 2006. Bolt surface configurations and load transfer mechanism, In *Proc.7th Underground Coal Operators Conference*, Coal 2006, Wollongong, 5-7 July, pp 236-244. http://ro.uow.edu.au/coal/51/.

Aziz, N, Jalalifar, H, Remennikov, A, Sinclair, S and Green, A, 2008. Optimisation of the bolt profile configuration for load transfer enhancement, In *Proc.8th Underground Coal Operators Conference*, Coal 2003, February 14-15, Wollongong, pp 125-131. (eds: N Aziz and J Nemcik), http://ro.uow.edu.au/coal/11/.

Singer, S P, 1990. Field verification of load transfer mechanics of fully grouted roof bolts, US Bureau of Mines, 9301.

Hyett, A J, Bawden, W F, Macsporran, G R and Moosavi, M, 1995. A constitutive law for bond failure of fully-grouted cable bolts using a modified Hoek cell, *Int. J. of Rock Mechanics and Min. Sci. & Geomech. Abstrs.*, 32(1):11-36.

Farmer, I W, 1975. Stress distribution along a resin grouted rock anchor. *Int J Rock Mech Min Sci Geomech Abstr*, 12:347-51.

Ren, F F, Yang, Z J, Chen, J F and Chen W W, 2010. An analytical analysis of the full-range behaviour of grouted rockbolts based on a tri-linear bond-slip model. *Construction and Building Materials*, 24:361-370.

Martin, L B, Tijani, M, Hadj-Hassen, F, 2011. A new analytical solution to the mechanical behaviour of fully grouted rockbolts subject to pull-out tests. *Construction and Building Materials*, 25:749-755.

Kilic, A, Yasar, E and Atis, C D, 2002. Effect of bar shape on the pull out capacity of fully grouted rockbolts. *Tunnelling and Underground Space Technology*, 18:1-6.

Ivanovic A and Neilson R D. 2009. Modelling of debonding along the fixed anchor length. *Int J Rock Mech Min Sci,* 46(4):699-707.

Aydan, O, 1989. The stabilisation of rock engineering structures by rock bolts, Geotechnical Engineering, Ph.D Thesis, Nagoya, Nagoya University, 202p.

Li, C and Stillborg, B, 1999. Analytical models for rock bolts. *Int J Rock Mechanics and Min. Sci. & Geomech. Abstrs*, 36(8):1013-29.

Ito, F, Nakahara, F, Kawano, R, Kang, S S and Obara, Y, 2001. Visualization of failure in a pull-out test of cable bolts using X-ray CT, *J Construction and Building Materials*,15:263-270.

Ren, F F, Yang, Z J, Chen, J F and Chen W W, 2010. An analytical analysis of the full-range behaviour of grouted rockbolts based on a tri-linear bond-slip model. *Construction and Building Materials*, 24:361-370.

Tepfers, R, 1973. A theory of bond applied to overlapped tensile reinforcement splices for deformed bar. Dissertation, Publication 73:2, Chalmers University of Technology, Division of Concrete Structures, Göteborg, Sweden, 328 pp.

STUDY ON THE BOLT-MESH-ANCHOR SUPPORT TECHNOLOGY FOR MINING ROADWAY IN COMPLEX COAL SEAM

Ying Chen, Hongwei Zhang and Bingjie Huo

ABSTRACT: The stability of mining roadway is affected significantly by the condition of the surrounding rock and stress regime, which is the key factor for determining the roadway support program. Located in syncline axis, the No.15 seam is a steep seam at - 230 m level in Changgouyu coal mine, the original flexible shield cannot meet the safety and production requirement. The No.15 seam is classified as unstable and relatively complex according to the analytic hierarchy process (AHP). The distribution characteristics of stress in the seam around the synclinal axis before and after mining are analysed by use of FLAC^{2D}. According to the complexity of the coal seam and the stress distribution characteristics, the supporting parameters using bolt-mesh-anchor were selected and implemented successfully in an underground roadway, which can be referred to as in the design of roadway support in similar complicated coal seams.

INTRODUCTION

Mining roadway layout and associated support play a key role in coal mining operations, which are the key technologies directly related to the benefits of coal production and safety. Over the years, researchers in China and abroad have conducted extensive and in-depth studies on the layout, location and support technology of mining roadway (Lu, *et al.*, 1998; Hou and Guo, 1996). Outcomes from these studies made positive contribution to the improvement of roadway support, working conditions of mine workers and the enhancement of coal mining efficiency (He and Yuan, 2004). When the mining roadway is driven in the coal seam, its stability is directly affected the occurrence of mining induced stress of coal seam. In addition, due to the low strength of the surrounding rock and poor bearing capacity of the coal rib, it has been difficult to maintain the integrity of the longwall roadway (Hou, *et al.*, 1999). It is therefore important to give due consideration of the influence factors in the design of roadway support system.

With the increase of mining depth and the complexity of mining conditions, the maintenance of mining roadways in complex coal seam have become increasingly problematic and influenced by geological structure, soft-broken surrounding rock as well as many mining factors (Chen, *et al.*, 2005). At present, the methods of the roadway support can be divided into three categories:

1. Passive support in the form of a variety of metal steel supports, arching and so on;
2. Active support based on bolt and anchor support which can establish function relation with the internal surrounding rock; and
3. Active reinforcement form by grouting which can improve the surrounding rock characters and the mechanical properties of surrounding rock fundamentally.

For complex coal seams, there is a need to understand the weight of all kinds of complex evaluation index for the control of surrounding rock stability. The support program needs to be designed for the major influence factors. A single support form should be adopted as far as possible to reduce the project volume and associated the support costs; if this cannot meet the safety requirement, then a the combination of different support method should be adopted so that their respective advantages can be utilised to promote the stability of surrounding rock.

This paper discusses an evaluation method in relation to the characteristics and support features of steep and complex coal seam, calculates a comprehensive evaluation value. The paper also describes the simulations and analysis of the influence of the syncline for dynamic stress. By considering the coal seam complexity and structure influence, the roadway support is designed and implemented in field application with good results.

Liaoning Technical University, College of Mining Engineering, Fuxin 123000, cyzx0824@yahoo@.com.cn

PROJECT OVERVIEW

The No.16 coal seam at - 230 m level is located in the vicinity of axis part and neighboring areas of the two branches of the Changgouyu synclinal in Changgouyu Coal Mine. Because of the effect of strata uplift and subsidence formation caused by ancient and contemporary tectonic movement, the syncline coal seams are formed in the pitching axis direction of due north, dipping at 29°. The coal thickness is 1.0~8.8 m, average 4.5 m. Both coal seam and the surrounding rock have poor stability, significant changes in coal thickness with rock partings, all of these have great impact on the mining and support (Figure 1).

Influenced by geological structure, the stress re-distribution has been strong in the mining roadway, leading to severe deformation of the surrounding rock, support impairment in roadway, especially with the sixteenth and seventeenth anti-eye located at the synclinal axis (as shown in Figure 1). The mining roadway was initially supported with "8" shape flexible support, each support was linked with four or eight steel ropes. Damage in the form of deformation, distortion and fracturing of the support has occurred frequently, therefore significantly compromise the support of roadway. The support is frequently deformed, twisted and cracked in the welding joints (Figure 2, 3) therefore seriously affect the support function. The deformation and guttering of the surrounding strata are increasing seriously, and although the roadway has been repaired for several times, its condition has seriously limits production efficiency and causes threat to production safety.

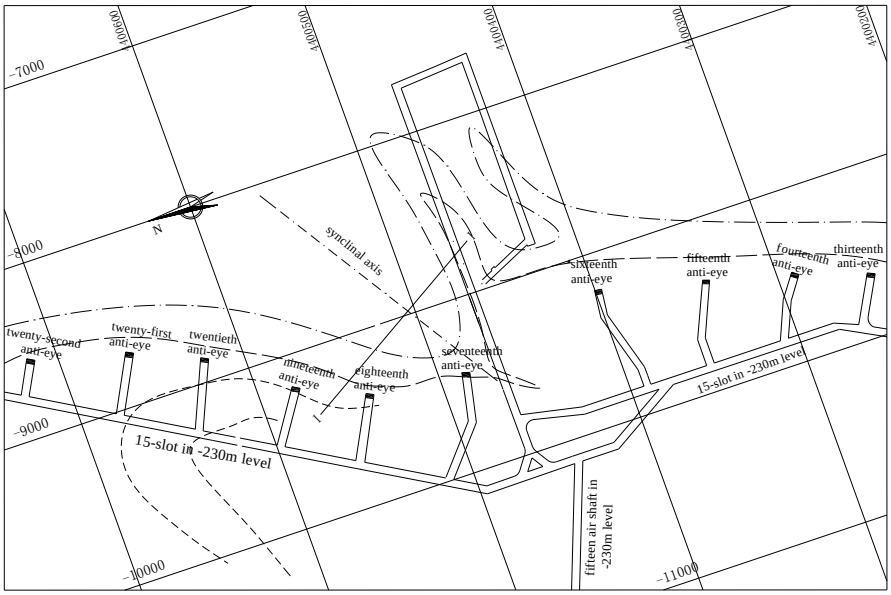

Figure 1 - A plan diagram showing the No.15 coal seam at - 230 m level

Figure 2 - Support crater cracking

Figure 3 - Support twist and deform

EVALUATION OF COAL SEAM COMPLEXITY

Many factors affect the coal seam complexity, these include geological structure, coal seam dip, thickness change the roof and floor condition of coal seam, the layers and thickness of dirt bands, the collapsing of karsts, the intrusion of magma and overburden depth, hydrological and geological condition.

Studies have shown that the coal seam complexity imposes significant influence on the support of the mining roadway (Huo, *et al.*, 2009). Therefore, it is necessary to evaluate the coal mine complexity before designing the roadway support. For this purpose, an evaluation system on the coal seam complexity is established by use of analytic hierarchy process (AHP). There are three steps in this evaluation criterion.

Firstly, identifying the influence index for coal seam complexity by describing the seam characters, the result can be one or zero; Secondly, according to the above index results and the weight of all indexes, calculate the evaluation marks of the indexes by an evaluation model. The total mark of all index influencing the coal seam complexity in which 100 means that the maximum influence on the complexity, and 0 means the minimum influence on the complexity; lastly, classifying the coal seam complexity based on the comprehensive evaluation marks. Based on the study references in China and overseas on the coal seam complexity, and considering the analysis of the influence index coal seam complexity as well as underground engineering applications, the complexity degree of the coal seam is classify as four grades. The classification types and criteria are shown in Table 1.

Table 1 - Classification and criteria of complexity of coal seam

Complexity classification of coal seam	Grade 1 Stable and simple	Grade 2 Relatively stable and fairly complex	Grade 3 Unstable and relatively complex	Grade 4 Extremely unstable and higly complex
Classification criteria (comprehensive evaluation marks)	<25	25～50	50～75	>75

According to the actual geological condition of No 15 coal seam at - 230 m level, the "evaluation system on the complexity of the coal seam V1.0" has been developed in VB6.0 language (Figure 4) (Wang, *et al.*, 2006; 2005). By inputting the identification index value of the complexity, the system produced a evaluation mark of 67 for the coal seam complexity. Comparing this mark with that of Table 1, the No.15 coal seam is classified as grade 3 - instable and relatively complex. Therefore, the following factors should be considered primarily when designing the support for the roadway:

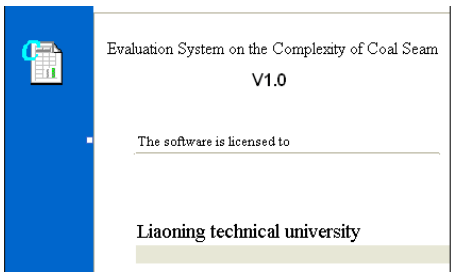

Figure 4 - The evaluation system on the complexity of the coal seam

(1) The support methods, material and engineering must be able to adapt to the changes of coal seam, such as the variation of coal seam dip, thickness, strength of the roof and floor, stress distribution caused by structure, etc.

(2) Giving priority to the flexible and active supports. The flexible supports can produce plasticity deformation, and unleash the energy of partial high stress zone. While the active supports can load weight punctually, strengthen the surrounding strata actively. It makes full use of the support ability of the surrounding rocks.

SIMULATION AND ANALYSIS OF THE STRESS STATE OF COAL AND ROCK MASS AT THE SYNCLINAL AXIS

To better understand stress environment of No.15 coal seam and provide the basis data for support, the ground stress of - 230 m level has been measured by use of stress relieving method. The results show that the ground stress field at - 230 m level is horizontal and mainly horizontal compressive stress. It has the presence of regional tectonic stress field with maximum principal stress of 13.82 MPa in the direction of NE90°. According to the measurement of the ground stress and the synclinal relative position, the

Changgouyu synclinal axis is vertical with the inclination of the stress field. Therefore, the synclinal axis is largely affected by horizontal compressive stress of present structural stress field. The coal and rock mass at the axial places are in large stress state.

Figures 5 and 6 respectively show the sectional profile along I-I in the Figure 1 and sectional profile model. By using FLAC^{2D}, the stress state of No. 15 coal seam at – 230 m level synclinal axis is simulated and analyzed before and after mining. The following can be concluded from the analysis of the stress state of coal seam at synclinal axis (Figure7, 8):

(1) The vertical stress distribution of coal seam at synclinal axis increases with the increase of burial depth. The vertical stress does not increase as isogradient, but increases as the shape of coal seam of synclinal axis with the hide depth.

(2) When the both flanks of synclinal axis are mined out, coal seam at the axis is influenced by mining stress, the vertical stress increases by 1.1~1.6 MPa compared with that of prior to mining, and the result is 10.4~11.2 MPa. The roof and floor stress of synclinal axis is larger, the stress near goaf increases to 12.8~13.6 MPa dramatically. The stress concentration factor is 1.20~1.26. The influence range is 10~15 m.

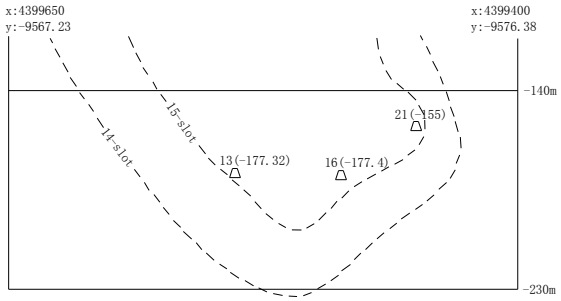

Figure 5 - I-I sectional profile

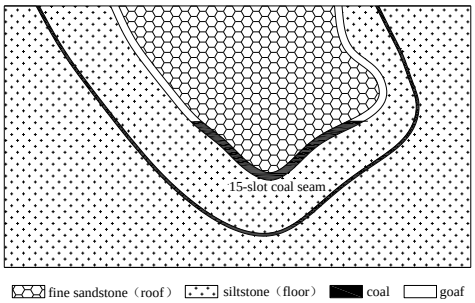

Figure 6 - I-I sectional profile model

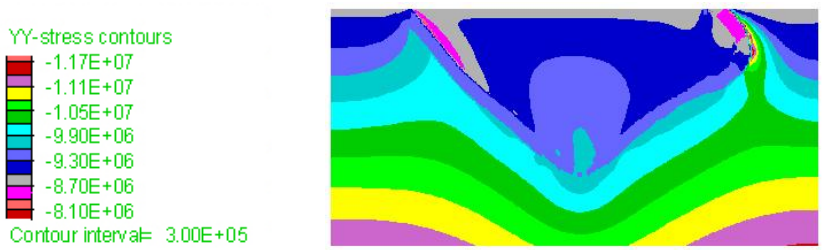

Figure 7 - Vertical stress distribution before coal mining

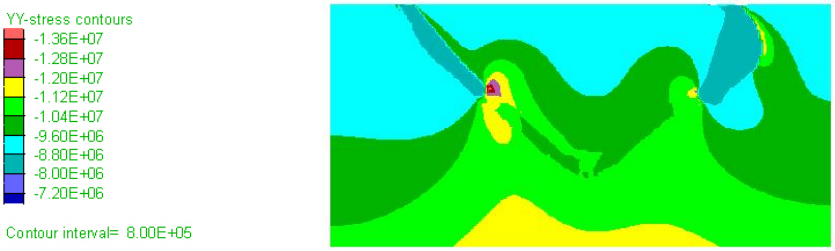

Figure 8 - Vertical stress distribution after coal mining

The followings can be concluded through the measurement of ground stress and the numerical simulation of stress state at synclinal axis:

(1) The measured principal stress direction is almost perpendicular to the layout of roadway. According to the maximum horizontal stress theory of roadway, one side of the roadway will have concentrated horizontal stress, and the area should be the key control part of the roadway.

(2) The numerical simulation shows that the stress concentration is formed in the synclinal axis coal seam before and after mining. The strength and intensity of the support equipment must be carefully considered.

STUDY ON THE SUPPORT METHOD OF THE MINING ROADWAY OF THE NO.15 COAL SEAM

Design of bolt support

The bolting has many advantages such as loading punctually, excellent support effect, low labour requirement, high efficiency, low capital cost (Wang, *et al.*, 2009; Zha, *et al.*, 2006). Because of that bolting is now widely promoted. Presently the bolting rate of coal roadway in China's state-owned key coal mines reaches 60%, this can be as higher as beyond 90% or even 100% in some coal areas (Kang and Wang, 2007). According to above analysis, the support method using bolting is selected in No.15 coal seam at - 230 m level. According to the distribution of structural stress field and the occurrence condition of coal seam, and considering similar engineering practice, and combining with the principle of asymmetrical support and controlling key part of the steep seam, the support program of 15-slot haulage roadway at - 230 m level is designed as bolt, anchor and metal mesh combined support. The support parameters are: three bolts thread steel for the roof and slope of the roadway respectively, and these bolts are of φ18 mm × 1800 mm. The row spacing is 650 mm, and the pitch spacing is 800 mm; the anchor length is 4000-5000 mm, one for the roof and sidewall respectively. The row spacing is 650 mm. The bolt is screwed on the end, hanging metal mesh on the roof. The original anchor stress of bolt is set as 20 kN, and the anchor is 30~50 kN. The distribution of roadway bolt and anchor is shown in Figure 9.

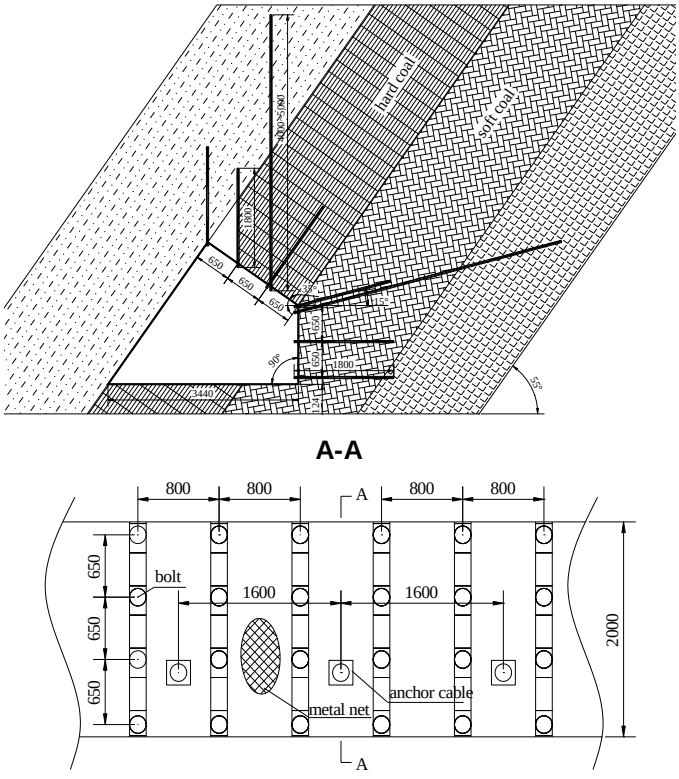

Figure 9 - Roadway geometry and the sectional view of the support (mm)

Pressure observation of the experimental roadway

The designed bolting program is implemented in the experimental roadway which is 100 m long. Pressure monitoring is carried out to determine if the roadway support design is reasonable or not, and provide the basis for further modifying and improving the support parameters.

(1) The monitoring shows that the maximum bolt force reaches 24 kN, anchor 30 kN, which are less than their respective failure load. Because of the anchors are cross-measure placed in deep seam, the coal and rock will experience sliding along the layer interface, it can lead to the anchor to bear shear failure

along the layer. If the sliding is violent, the diameter of anchor should to be increased to improve its shear strength.

(2) The different depth displacement values of roadway surrounding rock are rather limited. The maximum value reaches only 70 mm. The data shows that the designed length of bolt can control the displacement of the roadway deep surrounding rocks effectively. The displacement being limited is due to that the large coal seam dip, the stress along direction of the coal seam bedding caused by gravity will cause sliding of coal seam, so the bed separation along vertical direction of rock plane is less.

After monitoring for almost three months, the support effect in the test roadway is quite satisfactory. The support has greatly improved the maintenance status of the roadway. No maintenance is carried out during face mining. It reduces the labour intensity and the roadway maintenance cost with significant economic benefits.

CONCLUSIONS

(1) The complexity evaluation of the No.15 coal seam at the - 230 m level is carried out by means of "seam complexity analysis system V1.0". The coal seam is graded as III unstable and relatively complex type. It provides the basic data for the selection of support methods.

(2) The numerical simulation is carried out to study the stress conditions in the area of the No.15 coal seam's synclinal axis. The stress is concentrated before and after mining at the axis part of the seam. Hence the strength of the support equipment and support density should be improved appropriately.

(3) In view of the complexity of the No.15 coal seam, the stress condition of synclinal axis and the support characteristics for steep coal seam, the bolt support parameters for mining roadway are determined. Pressure monitoring shows that the support program is reasonable and the field economic benefits are significant.

(4) The coal seam complexity evaluation system has been applied to the research of roadway support deign for the first time, which makes the support method selection and the parameters determination being more scientific.

ACKNOWLEDGEMENTS

The authors would like to thank Geological Dynamic Division Institute for their continued support. Thanks for the basis data provided by the site staff in Changgouyu coal mine. The authors are very grateful to Dr. Ting Ren, University of Wollongong, for his help in modifying and improving this paper.

REFERENCES

Lu, S, Tang, L and Yang, X, 1998. Anchoring force and anchoring technology of cable, China Coal Industry Publishing House: Beijing, pp 44-45.

Hou, C, Guo, H, 1996. Orientation of technical development of rock bolting in in-seam gate-ways in China. *Journal of China Coal Society*, 21(2):113-118.

He, M and Yuan, H, 2004. Bolt theory and practice of coal mines in China, Science Press: Beijing, pp21-25.

Hou, C, Guo, L and Gou, P, 1999. Coal roadway bolting, China University of Mining and Technology Press: Xuzhou, pp7-17.

Chen, Y, Yu, X and Bai, J, 2005. Discussion on bolt and cable supporting technique of the complex roof, *Energy Technology and Management*, 6:6-7.

Wang, L, Miao, X and Dong, J, 2006. Numerical simulation of bolt-grouting support in soft roadway affected by mining, *Journal of Mining and Safety Engineering*, 23(1):39-42.

Wang, L, Li, M and Wang, X, 2005. Study on mechanisms and technology for bolting and grouting in special soft rock roadways under high stress, *Chinese Journal of Rock Mechanics and Engineering*, 24(16):2889-2893.

Wang, L, Zhang, Z and Zhang, J, 2009. Numerical simulation of bolt-grouting for gob-side entry in complex seam under a high stress, *Journal of Mining and Safety Engineering*, 26(2):145-149.

Huo, B, Zhang, H and Zhang, Z, 2009. Study on evaluation theory about complexity of coal seam, *World Sci-Tech R&D*, 31(3):433-438.

Zha, W, Xie, G and Luo, Y, 2006. Contrast testing study on steeply inclined seam roadway support under different support form, *Coal Mine Safety*, 6:4-6.

Kang, H and Wang, J, 2007. Rock bolting theory and complete technology for coal roadways, China Coal Industry Publishing House: Beijing, pp13-28.

TEAR TESTS OF GLASS FIBRE REINFORCED POLYMER SKIN SPRAY-ON LINER

Jan Nemcik, Ian Porter and Ernest Baafi

ABSTRACT: Current research into strata support automation in coal mine roadways requires development of a strong, tough and effective skin support that can be applied remotely. To investigate suitability of a glass fibre reinforced polymeric thin Spray-On Liner (TSL) numerous small and large scale samples were tested. These tests include; the tear load due to the lateral movement of TSL to fail in tear through the bolts installed in underground roadway roof, and the 'truser tear' due to the differential movement of the supported strata. The laboratory experiments suggested that a polymer based TSL can withstand substantial tear loads and despite the tear failure, the remaining TSL sheet can maintain strata support effectively. The tear strength tests were conducted using a standard 22 mm diameter steel bolt tearing the 5 mm thick polymer sheets reinforced with two or three glass fibre layers. The trouser tear tests were conducted with two and three layers of glass fibre reinforcement. The bolt tear tests indicated load bearing capacities in the range of 7.4 to 13.8 kN depending on the amount of reinforcement, while the trousers tear strength ranged from approximately 0.4 to 1.1 kN.

INTRODUCTION

During the ongoing TSL product development stage many small and large scale tests were carried out to evaluate the strength and failure modes of the TSL product itself and the rock-polymer composite material. These tests included tensile strength, three and four point bending strength, resistance to puncture, toughness and fatique tests of the polymeric product while the polymer-rock composite was tested for its reinforcement capabilities provided by the strong polymer to strata bond and the mechanical support of the strata by the polymeric sheet. These tests were reported in numerous publications (Lukey, *et al.,* 2008; Nemcik, *et al.*, 2009; Nemcik, *et al.*, 2011; Nemcik, *et al.,* 2012,). Two experiments were set up to investigate the tear loads when the rock bolt that pins the TSL to the strata tears through the TSL material and the 'trouser' tear of the TSL due to the differential movement of the supported strata.

BOCK BOLT-TSL TEAR TEST

The aim of this experiment is to determine the lateral loads on the rock bolt that tears through the glass fibre reinforced TSL. The basic principle of the tear test is shown in Figure 1. Several 5 mm thick polymer sheets 300x150 mm in size reinforced with two and three layers of glass fibre were prepared and cured overnight in the oven at a temperature of 60˚C. Preparation of the polymer sheets is shown in Figure 2. The edge of each sheet was clamped with steel brackets to enable anchorage of the sheet during testing. A 27 mm hole was drilled across the polymer sheet and a piece of standard Australian 22 mm diameter steel rock bolt was placed within.

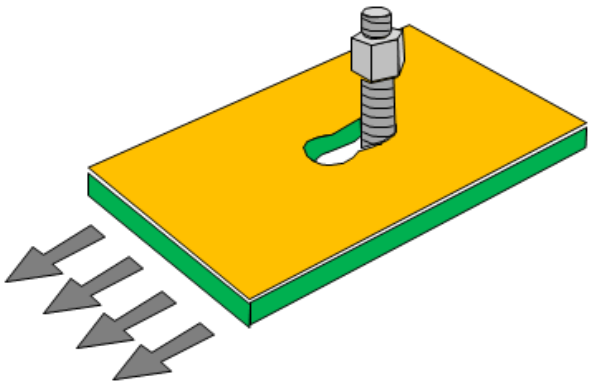

Figure 1 - Schematic diagram of the TSL tearing test

Faculty of Engineering, University of Wollongong, NSW, Australia, jnemcik@uow.edu.au, M: 04 0871 1280

Figure 2 - Preparation of the polymer based glass reinforced TSL

The TSL samples with the bolt in the hole were clamped into the 500 kN Instron servo-hydraulic universal testing machine and pulled appart at the rate of 5 mm/m while monitoring the applied load and displacements of each sample (Figure 3). In total, six samples were tested. Three samples were reinforced with two layers of glass fibre while the others contained three layers of glass fibre.

Figure 3 - The polymer sheet with steel rock bolt clamped into the 500 kN Instron servo-hydraulic universal testing machine and teared appart

The bolt tear resistance of samples that were reinforced with two glass fibre layers ranged approximately between 4 kN and 8 kN while the samples reinforced with three glass fibre layers tore at the applied load ranging from 6 kN to 12 kN (Figure 5). The measured tearing capacity of each polymer sheet versus displacement are graphed in Figures 4 and 5 while the results are detailed in Table 1.

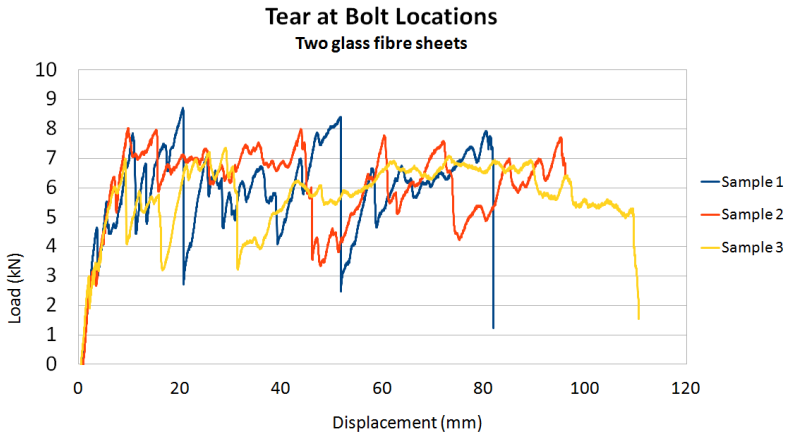

Figure 4 - The measured bolt tearing capacity of polymer samples reinforced with two glass fibre sheets

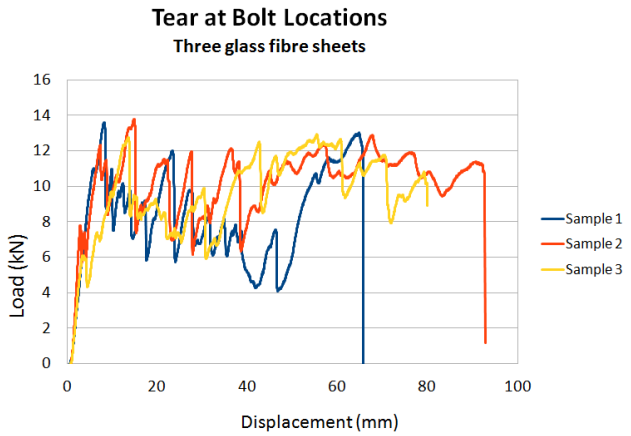

Figure 5 - The measured bolt tearing capacity of polymer samples reinforced with three glass fibre sheet

Table 1 - Results of the rock bolt - TSL tear

Number of glass sheets	Sample No.	Average sample thickness (mm)	Maximum applied load (kN)	Average allied load (kN)	Comments
2	1	5	8.7	6.0	Load fluctuation
2	2	5	8.0	6.3	Load fluctuation
2	3	5	7.4	5.9	Load fluctuation
3	1	5	13.6	8.4	Load fluctuation
3	2	5	13.8	10.4	Load fluctuation
3	3	5	12.9	10.0	Load fluctuation

The results indicate that the tested TSL-bolt tearing capacity may not be able to stop tearing action at high loads, however this is also the case for the currently used steel mesh that is readily deformable even at relatively low loads. If the bolt-TSL tear occurs in practice, its length would be shorter. Due to the toughness of the glass fibre reinforced TSL the tear would not compromise the TSL skin support substantially.

TROUSERS TEAR TEST

In accordance with AS 1683.12-2001, the trouser tear strength is the force required to propagate tear in the cut within the material divided by the material thickness. The basic principle of the trouser tear test is shown in Figure 6. Several polymer sheets 200x100 mm in size reinforced with two and three layers of glass fibre were prepared and cured in the oven at a temperature of 60˚C overnight. A 50 mm deep cut was prepared in each sheet to enable tear to propagate. The edges of each sheet were clamped with the steel brackets to grip each edge and pull in the opposite directions perpendicular to the polymer sheet to enable tearing of the material. The TSL samples were clamped into the 500 kN Instron servo-hydraulic universal testing machine and teared appart while monitoring the applied loads (Figure 7).

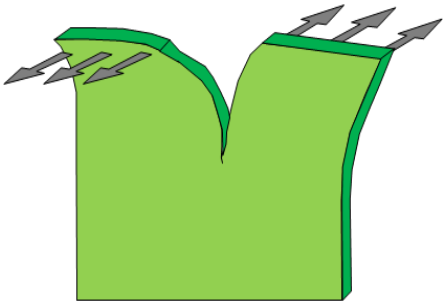

Figure 6 - Schematic diagram of the TSL tearing test

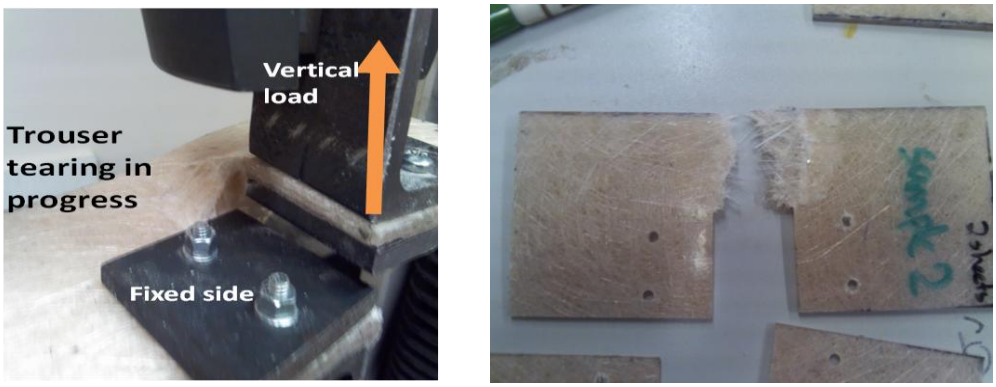

Figure 7 - TSL sample clamped in the 500 kN Instron servo-hydraulic universal testing machine and teared appart

In total, six samples were tested. At some stage the geometry of the polymer sample was modified to minimise tear in the wrong place. Three tested samples were reinforced with two layers of glass fibre while the others contained had three. The test results are shown in Table 2.

Table 2 - Results of the trouser tear tests

Number of glass sheets	Sample No.	Average sample thickness (mm)	Maximum applied load (kN)	Trouser tearing strength (kN/mm)	Comments
2	1	3.8	0.43	0.11	Teared
2	2	3.8	0.39	0.10	Teared
2	3	3.8	0.46	0.12	Teared
3	1	5.0	1.12	0.22	delaminated
3	2	5.0	0.96	0.19	delaminated
3	3	5.0	0.97	0.19	delaminated

The trouser tear resistance of samples that were reinforced with two glass fibre layers ranged from 0.10 to 0.12 kN/mm of sheet thickness while, as expected, the samples with three glass fibre layers tore at a higher load, which ranged from approximately 0.19 to 0.22 kN/mm. The measured tearing capacity of each polymer sheet versus displacement are graphed in Figures 8 and 9.

A delamination problem occurred in some tests where the TSL separated along the glass fibre layers as shown in Figure 10. This occurred due to the nature of laying the fibre during sample preparation. In ability of preparing samples with random fibre orientation may have contributed to the delamination problem. Delamination is unlikely to occur during TSL spray application. Futher tests need to be repeated with sprayed product.

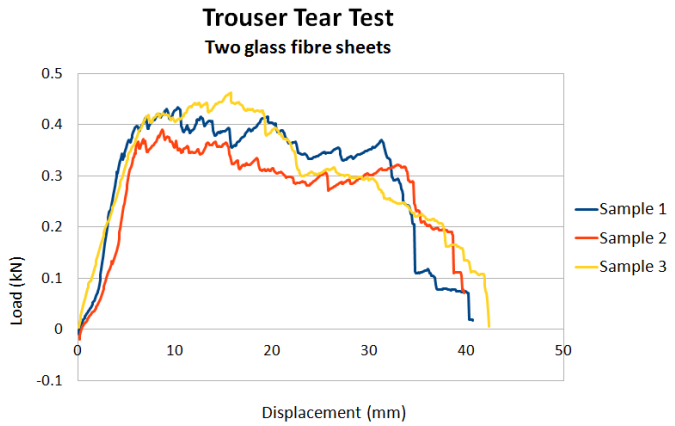

Figure 8 - The measured trouser tearing capacity of polymer samples reinforced with two glass fibre sheets

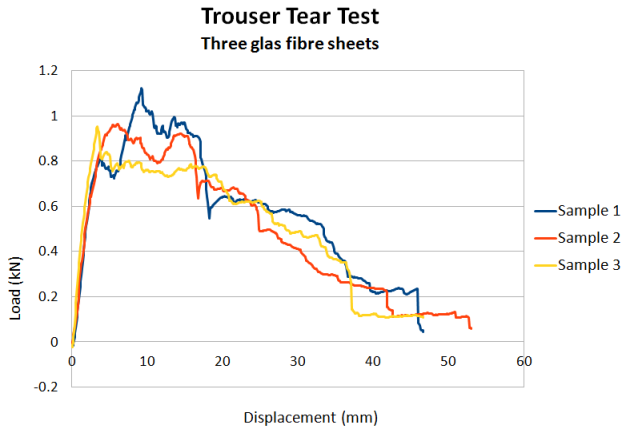

Figure 9 - Measured trouser tearing capacity of polymer samples reinforced with three glass fibre sheets

Figure 10 - Delamination along the glass fibre layers

DISCUSSIONS

The above tests indicate that the tested TSL material is tough and reasonably strong in tear. It should be noted that the samples were prepared in the laboratory under ideal conditions. The TSL was made by pouring the polymer into the mould furnished by several layers of glass fibre oriented parallel to the sheet surface. In practice, such sheet would be sprayed onto an uneven substrate with glass fibre that may be oriented in random directions. If the TSL is bonded well to the rock surface it will be subjected to the same differential deformations as would occur in the rock, resulting in tear. If the TSL bond fails, the TSL may not tear immediately but would provide normal confinement to the rock fracture surface generating skin reinforcement. Despite these differences the tearing tests indicate that the glass reinforced polymeric material is suitable to reinforce a relatively small roadway surface area located between the rock bolts making the tested TSL suitable for the mine roadway skin reinforcement.

No significant dynamic loads are experienced in most Australian coal mines. This has been confirmed using countless extensometry measurements that show the gradual strata movement with relatively small displacements until a predictable convergence and audible strata sound indicating imminent roof collapse. During the normal working life of a coal mine small differential displacements of the roadway skin may occur and can cause a bolt-TSL tear or a small trouser-type tear similar to the above tests. Under normal conditions this type of failure should not cause a significant problem as the remaining TSL adjacent to the tear would continue to support the roadway skin. During the collapse of mine roadway significant TSL tear could occur however, this problem would not be relevant as the TSL is not designed to control the overall stability of strata.

CONCLUSIONS

This study investigated the resistance of 5 mm thick glass fibre reinforced TSL to tear due to the differential movement of the steel bolt that restrains the TSL from lateral movement, and trouser tear that can occur during differential movement of the jointed strata. The tests indicate that the 5 mm thick TSL reinforced with three glass fibre sheets is capable of resisting bolt tear loads of up to approximately 14 kN and trouser tear of up to 1.1 kN. A delamination problem occurred at some of the trousers tear tests, where the TSL separated along the glass fibre layers. This occurred due to the nature of laying the fibre during sample preparation. The tearing capacity of the *in-situ* TSL may increase when the polymer and the mine roadway skin form a composite layer. Further tear tests of the sprayed TSL are recommended to provide more accurate data for future assessment of the TSL as a composite material as an alternative method to the current methods of the mine roadway skin support in Australian coal mines.

REFERENCES

Lukey, C, Spinks, G, Baafi, E, Porter, I and Nemcik, J, 2008. Polymer based alternative to steel mesh for coal mine strata reinforcement, In *Proceedings of 8th Underground Coal Operators Conference*. Wollongong. (eds: N Aziz and J Nemcik*),* pp. 110-116. http://ro.uow.edu.au/coal/9/.

Nemcik, J, Porter, I, Baafi, EY and Lukey, C, 2009. Geotechnical assessment of skin reinforcement in underground mines, In *Proceedings of 28th International Conference on Ground Control in Mining*, Morgantown, West Virginia, pp 256-260. http://icgcm.conferenceacademy.com/papers/detail.aspx?subdomain=ICGCM&iid=230.

Nemcik, J, Baafi, E, Porter, I and Lukey, C, 2009. Computer modelling of computer modelling of polymer liner reinforcement in underground mines, In *Proceedings of the Application of Computers and Operations Research in the Mineral Industry (APCOM) 2009 Conference*, Canadian Institute of Mining, Metallurgy and Petroleum, pp 532-547.

Nemcik, J, Porter, I, Baafi, E and Lukey, C, 2009 Geotechnical assessment of polymeric materials as skin reinforcement in underground Mines, *In Proceedings 8th Underground Coal Operators Conference*. Wollongong. (eds: N Aziz and J Nemcik), pp. 70-77. http://ro.uow.edu.au/coal/81/.

Nemcik, J, Porter, I, Baafi, E and Towns, J, 2011. Bearing capacity of a glass fibre reinforced polymer liner. In *Proceedings of 11th Underground Coal operators Conference*, Wollongong, February 10/11 (eds: N Aziz, B Kininmonth, J Nemcik and T Ren), pp 148 -153. http://ro.uow.edu.au/coal/351/.

Nemcik, J, Porter, I, Baafi, E and Navin, J, 2011. Determination of ultimate strength of tough skin, a glass reinforced polymer liner. In *Proceedings 11th Underground Coal operators Conference*, Wollongong, February 10/11 (eds: N Aziz, B Kininmonth, J Nemcik and T Ren), pp 154 -158. http://ro.uow.edu.au/coal/352/.

Nemcik, J, Porter, I and Baafi, E, 2011. Performance of polymer skin spray-on liner in coal mines. In *12th ISRM International Congress ob Rock Mechanics* (eds: Qian and Zhou), Beijing, China, 18-21, October. Published in Harmonising Rock Engineering and the Environment, 2012 Taylor and Francis Group, London, ISBN, 978-0-415-80444-8, pp 1565-1568.

Nemcik, J, Porter, I and Baafi, E, 2012. Performance of polymer skin spray-on liner in coal mines. In *12th ISRM International Congress ob Rock Mechanics* (eds: Qian and Zhou). London: Taylor & Francis Group, pp. 1565-1568.

Nemcik, J, Porter, I and Baafi, E, 2012. Stabilising rock surfaces with a glass reinforced polymer skin. In *Proceedings of 4th International Colloquium of Geomechanics and geophysics*, Ostravice, Czech Republic, 7-8 June 2012. Journal Acta Geodynamica et. Geomaterialia (Volume 2/2013).

AUSTRALIAN LONGWALL PANEL VENTILATION PRACTICES

Stewart Gillies[1] and Hsin Wei Wu[2]

ABSTRACT: A study has been undertaken into mine ventilation systems currently in use within Australian modern coal Longwall (LW) extraction mines. It reviews systems and discusses evolving changes being adopted to address the more complex challenges. There is a strong move to longer panels, wider faces, greater extraction heights, increased production rates, more efficient ventilation and decreased personnel. In addition mine workings are moving deeper which results in increased ventilation control issues such as higher total and respirable dust levels, greater seam gas contents in parallel with lower *in situ* permeabilities, spontaneous combustion and heat management issues. Currently there are a variety of LW panel ventilation circuits used in Australian underground coal mines due to various combinations of seam characteristics, gas emission rates, spontaneous combustion, geological features and surface constraints. The main issues usually addressed in the designing and planning of ventilation circuits for LW panels are airway velocity, gas concentrations, LW cutting methods (e.g. Bi-di, Uni-di or half web), ventilation of control devices, pressure differentials and leakage paths and understanding gas concentrations across the length and width of the goaf. If the ventilation circuit can manage the applied contaminant load (gases, heat and dust) at an acceptable cost and circuit duty, then supplementary controls, such as gas drainage, refrigeration and dust sprays and scrubbers, may not be required. The study has been undertaken based on reviews of LW mining operational practices in Australia.

INTRODUCTION

The purpose of this paper is to establish the state-of-the-art of Australian underground LW coal mining ventilation practices. Within Australia the two states where almost all underground coal mining activities take place are Queensland and New South Wales (NSW). The mining history, geology and regulations vary between these two states. This current study demonstrates significant changes from similar reviews undertaken by Schaller and Savidis (1983) and Mayes and Gillies (2001). In the first study it was found that mines almost exclusively used an "R" or "Z" ventilation approach similar to European practice whereas more recent studies show that many mines tend to use some form of U ventilation as used in the United States to ventilate their LWs. In the last ten years there has been a move for many mines to increase ventilation with the assistance of back boreholes and back airways or occasionally bleeders.

Currently there are a variety of LW panel ventilation circuits used in Australian underground coal mines due to various combinations of seam characteristics, gas emission rates, spontaneous combustion, geological features and surface constraints. The main issues usually addressed in the designing and planning of ventilation circuits for LW panels are face velocity, maingate intake velocity, tailgate and face return gas concentrations, flow direction in maingate conveyor roads (for heat, gas and dust management), LW cutting methods (e.g. Bi-di, Uni-di or half web), ventilation of maingates inbye of the faceline for (seal installations and holing of development roadways), contamination due to intake air passing goaf seals (if present), dilution of returns gas concentrations (mixing stations) if required, location of regulators with respect to pressure control, pressure differentials, leakage paths and of understanding gas concentrations across the length and width of the goaf. If the ventilation circuit can manage the applied contaminant load (gases, heat and dust) at an acceptable cost and circuit duty, then supplementary controls, such as gas drainage, refrigeration and dust sprays and scrubbers, may not be required. Various additional controls need be considered and incorporated into the ventilation circuit design where the ventilation circuit alone cannot handle the contaminant load.

The data for this review has been obtained from surveys of 13 LW mining operations in Queensland in the last ten years. Australia had in total about 30 operating LW mines in 2012 producing approximately 89 Mtpa. About 40 percent of these mines operate in Queensland. The average tonnage of individual mines in Queensland exceeds those in NSW. All Queensland LW mines operate in the Bowen Basin. The NSW LW mines operate within the Western, Southern, Hunter and Newcastle regions of the NSW Sydney Basin. Most Australian coal mines operate a single retreat LW installation but at any point in time a small

[1] *Union Pacific/Rocky Mountains Energy Mining Professor, Missouri University of Science and Technology, Rolla, Missouri. Tel: 1-573-3414365, gilliesst@mst.edu*
[2] *Director, Gillies Wu Mining Technology Pty Ltd. The Minserve Group, 1 Swann Road, Taringa, Queensland 4068. Tel: 61-7-33776734, h.wu@minserve.com.au*

number will have two retreat LWs in operation. By comparison the Australian underground coal production has increased significantly since the survey of Mayes and Gillies (2001). It was reported that in 1999 there were a total of 34 operating LWs in Australia producing approximately 67 Mtpa, 11 of which operated within the Queensland Bowen Basin and the remaining 23 within the Western, Southern, Hunter and Newcastle regions of the NSW Sydney Basin. All of these mines operated a single retreat LW except for one with two retreat LWs which was in the Illawarra Coalfield of NSW.

INDUSTRY CONDITIONS AND SURVEY

Over a number of years several formal or ad hoc surveys of coal mine ventilation were undertaken as part of mine design exercises. These have focused on a number of major issues including mine statistics, physical mine environment, main ventilation environment, development ventilation, LW ventilation, ventilation network analysis, ventilation monitoring and future considerations. The physical mine environment section deals with the physical parameters of the mine including seam cross section, roadway dimensions and physical layout of the pit. The main ventilation environment deals with main fan installations, issues affecting ventilation and related incidents and location of the critical or open splits. The development ventilation deals with ventilation layout in development and most importantly considerations for breaking through in development. The LW ventilation deals with extraction method and equipment, panel ventilation and sealing practices behind the active LW face. Ventilation network analysis and monitoring deals with the level of monitoring of ventilation parameters within the mine and how computerised network analysis is being utilised.

Currently there are a variety of LW panel ventilation circuits used in Australian underground coal mines due to various combinations of seam characteristics, gas emission rate, spontaneous combustion, geological features and surface constraints. The main issues to be addressed in designing and planning of the ventilation circuits for LW panels are as follows:

1. Face velocity,
2. Maingate intake velocity,
3. Tailgate and face return gas concentrations,
4. Flow direction in maingate conveyor road for heat and dust management,
5. LW cutting method for example, Bi-Di, Uni-Di or Half Web,
6. Ventilation of maingate inbye of the faceline for seal installation and holing of replacement development,
7. Contamination due to intake air passing goaf seals (if present),
8. Dilution of return gas concentrations (mixing stations or sewers) if required,
9. Location of regulators with respect to pressure control,
10. Pressure differentials and leakage paths,
11. Understanding gas concentrations across the length and width of the goaf,
12. Use of back airways or bleeders US style at back of LW panel.

If the ventilation can manage the applied contaminant load (gases, dust and heat) at an acceptable cost and circuit duty, then supplementary controls may not be required. However, where alternative control measures are required due to unacceptable conditions then the following as listed in Table 1 can be considered:

Within Australia the major factors that determine LW ventilation requirements and panel circuit design are heat, dust and seam gas concentrations. The control of heat is generally a function of intake air conditions and the amount of heat added to the air from the maingate LW equipment. This often is addressed during the summer months by introducing refrigerated air via a back panel shaft and homotropal LW belt ventilation arrangement. Pre drainage of seam gases prior to LW production can lead to the planned working section being largely dewatered and so dust inbye of the shearer generally cannot be controlled by ventilation alone. It is expected that the shearer cutting operations will generate considerable dust. Velocities of no more than 5.0 m/s of air across the LW face are necessary to avoid

raising additional dust. Dust controls such as additional systems of sprays, scrubbers and shearer clearers are considered in this situation.

Table 1 - Control measures and its effect for efficient longwall panel ventilation

	Control Measures	Effects of the Controls
1	Pre-drainage of working section	Reduce rib and LW gas emission
2	Post (goaf) drainage	Reduce LW gas emission
3	High capacity back return shafts	Goaf drainage with returns
4	Increase production to 7 d/week	Reduce gas emission peaks
5	Seal design and balancing	Use of adjacent development for intake
6	Dust suppression and water infusion	Allows intake velocities greater than 5 m/s
7	Increased local velocity or refrigeration	Heat management

Due to the statutory limits for methane concentrations in return airways and at the tailgate drive, the use of ventilation air as the sole control on the LW for gas control will require large and impractical quantities of air. Therefore gas concentrations on the LW face and in the tailgate will be controlled primarily by goaf drainage. Reduced gas content using pre-drainage reduces Specific Gas Emission (SGE) and insufficient pre-drainage results in increased SGE and hence increased LW gas make and increased goaf gas extraction rates. This means the maximum air quantity adopted for the LW face is generally between 40 and 80 m^3/s depending on the extracted seam height. Many modern Australian LWs extract a seam mining height ranging from 2.6 to 3.4 m and some times more.

Many modern mines have suitable reserves and design for a 300 m LW face width and variable annual LW production of up to about 8.0 Mtpa. A few faces are up to 400 m in length. There are various options used to reduce the CH_4 levels in LW return airways such as:

- Increased LW ventilation air quantity,
- Configuration of LW ventilation design,
- Increased goaf gas extraction efficiency,
- Increased seam pre-drainage to reduce face emission,
- Increased pre-drainage of adjacent seams to reduce SGE and/or
- Reduced LW production rate to hence reduce face emission.

Production from Australian LWs varies from about 0.7 to 8.0 Mtpa. The latter figure is from some of the newer "thick seam" mines. All underground mines have a combination of shaft and/or drift access for personnel, materials and ventilation. The production method on the face is predominantly Uni-di cutting due to gas and/or respirable concentrations of dust. Some mines in recent years have tried alternative methods for ventilating gateroad development including three heading development. However the additional cost of three headings has meant that these mines have reverted to two headings after mining of a few panels. Sealing practice has varied between the two states because of prescriptive new Queensland regulations introduced in the late 1990's requiring explosion pressure rated ventilation structures. However, NSW practice has largely been falling into line with Queensland's evolving practices.

Monitoring of gases within collieries is provided by both tube bundle and telemetry systems. Typically CO_2, CO, CH_4 and O_2 are reported. Those collieries with ventilation issues involving gas typically have a gas chromatograph to assist with the analysis of bag samples for other indicator gases. Ventilation network analysis is in most cases facilitated through the use of a mine ventilation computer network simulation program. The operation of these computer models is often supported by consultants who have assisted in the creation of up to date ventilation simulation models and then their maintenance.

LW VENTILATION DESIGN CONSIDERATIONS

The skeleton layout of an Australian LW mine is shown in Figure 1. In terms of ventilation nomenclature intake roadways are shown as blue, single arrow roadways while returns are shown as red, double arrow roadways. In this figure a borehole exists behind the current goaf and is shown as a circle with an intake

roadway connecting to the LW face roadway. Mines onerous ventilation conditions very often incur the expense of excavating a borehole.

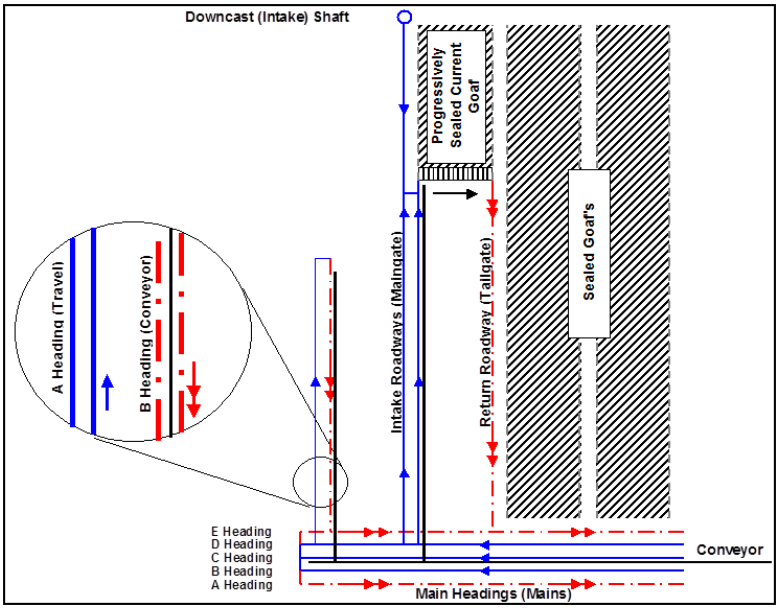

Figure 1 - Typical layout aspects of Australian LW mining

Australian LWs principally use a panel or section "U" ventilation layout with two roadway maingate development and have typically between five and seven mains roadways. In development, A Heading (as shown in Figure 1) is an intake roadway with B Heading the return roadway through which the panel conveyor runs. In the Mains, B, C, and D Headings are typically intake with flanking return roadways, A and E Headings. When all LWs are being extracted on one side of the mains only, D and E Headings may be used as return roadways with A, B and C Headings as intake roadways. The conveyor runs in the intake headings typically in C Heading. In Queensland C heading is segregated from either one or both of the other intake roadways. In NSW belt segregation is generally not undertaken to the same extent. The previous goafs are often sealed from the tailgate of the current LW with 140 kPa rated seals. The current goaf is progressively sealed on the maingate side as the LW retreats.

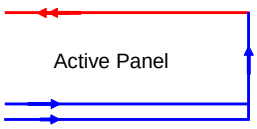

Figure 2 - Antitropal belt air **Figure 3 - Homotropal belt air** **Figure 4 - Downcasting borehole air**

Figure 2 shows an example of a traditional U ventilation approach. This is the most commonly used LW ventilation base model. This method minimises the induced ventilation pressure difference over both the current goaf and previous sealed goaf. This aspect is important when considering ventilation engineering design for operations in coal seams that have been demonstrated to have propensity for spontaneous combustion. The maingate belt headings have intake air flowing in the direction to the face, as shown, and termed antitropal. Air flowing in the reverse direction is termed homotropal.

The homotropal mode shown in Figure 3 is used for management of toxic seam gases, heat and dust. This method allows for a split of intake air to return via the B Heading to remove forms of ventilation contaminant away from the LW face. By locating the start of the split inbye of the location of the maingate B Heading contaminant source the contaminated air is not directed onto the LW face. However ventilation efficiency is lost as the air that passes along the maingate B Heading is lost from active use ventilating the LW face. The quantity of air lost from passing across the face varies but may be 20 to 25 m^3/s. The management of this homotropal split location can represent an operational issue as the split location is affected by constantly moving LW face/support equipment and discrete cut through locations.

Mine practice following the Moura No 2 mine disaster enquiry has generally been to install a pressure rated seal in the cut throughs behind the LW as the face retreats. The approach achieved popularity in

Queensland and is now well accepted in NSW. With more substantial structures present seal sites must be accessible for installation and ongoing access for inspection and maintenance. To provide access along the length of the A Heading roadway in the maingate in this ventilation approach auxiliary ducting ventilation is utilised. The use of auxiliary ventilation over increasingly longer distances as the LW retreats is problematic and hence this form of U ventilation is not employed without some variation.

Mines with more onerous ventilation requirements use a variation on the traditional "U" ventilation approach where a small diameter borehole (typically raisebored at 1.0 m diameter or more) has been excavated behind the current LW. The hole may be operated in a downcasting or upcasting mode and may be free venting or may be connected to a fan on the surface that is either pushing or pulling air. A free ventilating raisebore of diameter less than 1.0 m is generally only capable of providing or exhausting small quantities of air of the order of 10 m^3/s.

Figure 4 shows a LW panel with downcasting air in borehole. The use of a borehole will give a small drop in the overall mine resistance and an increase in airflow in the LW and on the face. Downcasting borehole air may become contaminated by gas as the goaf breathes out diurnally before the airflow reaches the face. This contamination may be considerable over distances such as when borehole air is used during installation of the last of a panel goaf seals. Borehole air can be routed to allow for access to the next LW's tailgate roadway which is a requirement for seal installation, inspection and maintenance. Sometimes downcasting boreholes pass refrigerated air in summer temperatures.

Figure 5 - Upcasting borehole

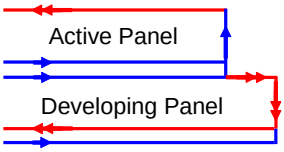

Figure 6a - Exhausting air via next panel

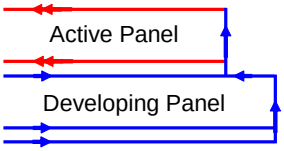

Figure 6b - Additional intake air from next panel

Figure 5 shows how boreholes may be operated in an upcasting mode. This method requires the installation of a surface fan on the borehole to provide the necessary pressure against the induced main fan ventilating pressures. This additional fan increases the number of operational issues when considering the running of multiple surface fan installations. Recirculation may be a possibility if multiple fans are not interlocked. The quantity provided by this additional fan is dependent on the sizing of the fan and hole dimensions. The distribution of pressures in the ventilation circuit has to be considered especially for spontaneous combustion reasons if exhausting large volumes of air with associated higher pressures. However, most of the pressure loss will be in the raisebore itself and not in the working horizon. The raisebore may be lined to prevent air leaking through cracks in the strata.

Exhausting boreholes assist removal of potential contamination from a seal installation site but can reduce the available quantity of air on the LW face. This method might also serve to offload some of the mains return requirements. Use of upcasting borehole air is far less popular that use of downcast air.

When an operation is well ahead in development it can make use of the newly completed next panel development to enhance ventilation in the current active panel. This approach is based on the "U" LW ventilation approach bringing intake air up the maingate of the current active LW panel and across the LW face before passing via the tailgate to the mains return. The workings in the adjacent newly developed panel can be used advantageously in either of two ways.

1. Some air from the active maingate A Heading can be brought past newly installed seals and then across the next LW's newly mined installation face road and returned to the mains return via the new B Heading belt road. This homotropal belt road return is also diluted with intake air from the next LW's maingate as shown in Figure 6a. The air provided inbye of the LW face in A Heading would be classed as return in some cases but would only carry contaminant sourced from the current active goaf's breathing.
2. Alternatively intake air from the newly developed panel having passed across the new face line is delivered to the inbye end of the current maingate. As shown in Figure 6b his extra intake air can then be used to assist dilution around the periphery of the current goaf by passing along the back road behind the active goaf.

Use of adjacent newly developed airways eliminates some of the need for borehole/small diameter shafts and associated capital costs behind the LW panels to provide ventilation to A Heading in the maingate for seal installation, maintenance and inspections. The added cost of this method is the development in advance of the next LW panel. Again in allowing ventilating of A Heading this approaches requires that seal installation follow closely behind LW operations. If the last open cut through inbye of the LW face is not sealed immediately following the LW retreat intake air may course indirectly behind the LW face through the goaf to the maingate or tailgate return. The introduction of air into the new goaf may have spontaneous combustion and/or face dust implications.

Figure 7 shows a panel ventilation approach based on a "Z" LW ventilation pattern. Part of the intake air comes up the maingate of the current panel workings. Additional intake air is brought up the tailgate (beside old workings) and across the LW face. Air exhausts behind the LW through the goaf. This method allows air to be coursed through the two caved roadways (maingate and tailgate) and through the next LW's tailgate roadway. All air is exhausted via a set of submain bleeders behind the LW panel.

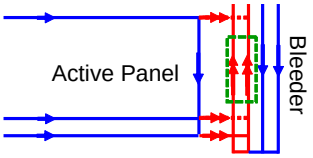

Figure 7 - "Z" LW ventilation with mixing chamber

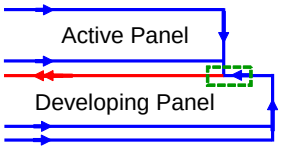

Figure 8 - Development air with mixing chamber

This ventilation method allows for significantly increased airflow in the pit. Much of this air is not necessarily directed onto the LW face due to ventilation induced face dust problems with excessive face velocities. The increased air available in the pit is used to dilute excessive quantities of gas present in the working section. Significantly increased ventilation pressures can also be achieved and directed across current workings and an incompletely sealed old group of goafs. This aids in draining seam gas from the goaf which is acting as gas reservoirs. This method would not be used in a seam that had demonstrated propensity for spontaneous combustion. A mixing chamber (restricted access/barricaded zone) may utilised to allow high concentration goaf gas to be diluted by uncontaminated air behind the current goaf.

Figure 8 shows a hybrid ventilation method utilising aspects of both U and Z ventilation approaches. Intake air is coursed towards the LW face along both the tailgate roadway and panel belt roadway. Intake air is also sourced from the next completely developed LW panel and passes along the sealed current goaf. Air returns from the LW face through the goaf to the last open cut through behind the face. At this point return air mixes with intake air from the next panel and is returned through a single roadway to the mains. This single roadway is barricaded, has restricted access and can be considered a "sewer" roadway. This ventilation method has being used to remove excessive quantities of gas present in the working section with consideration given to a seam with moderate propensity to spontaneous combustion. In this method the mixing chamber concept is utilised in the location where return air from the LW face is mixed with the intake airflow from the next LW panel. Due to the reorientation of the sewer roadway, development can be reversed from the traditional to minimise seal preparation and stopping destruction. Pressure distributions are very important due to face air intentionally passing through the immediate goaf to A Heading in the maingate. Seal installations have to be undertaken and monitored as soon as practicable coordinated with LW retreat.

RECENT DEVELOPMENT DATA IN LW MINES

Discussions with mine site ventilation officers have established the following parameters for typical current homotropal ventilation circuit design data:

1. LW belt road on homotropal ventilation running about 25 m^3/s at the maingate regulator,
2. 25 m^3/s passing around the back road or bleeder,
3. Up to 80 m^3/s air passing across the face into the tailgate,
4. 30 to 35 m^3/s air used for Mains with single continuous miner development,
5. Maintenance of LW panel circuit pressure of no more than 1.4 kPa.

6. Secondary supports are required in Tailgates outbye of the LW face and the minimum practice is 200 m of secondary supports.
7. LW panel pressures has been increasing when compared with mines in Central Queensland developed in the 1980s and 1990s.

A database of Ventsim models for 13 LW mines gathered over the last ten years by the authors is shown in Table 1. It can be noted that Mine D has two working LWs. From this information the reviewed LW panel ventilation pressures were varying from 250 to 1320 Pa (average 790 Pa) with LW face quantities ranging from 37 to 77 m^3/s (average 57 m^3/s) and roadway mining heights varying from 2.7 m to 3.8 m (average 3.2 m). Significant use of back boreholes (or shafts) within LW panels in Australia is a relatively new occurrence. Until the middle of the 1990s it was considered by many that the overlying strata was insufficiently competent for a borehole to be reliably drilled and to stand up for design life. Experience with sinking of shafts in many cases supported the view that overlying strata was weak and often incompetent; in this period a number of shafts and boreholes took much longer to complete that design expectation. Reference to Table 2 shows that in Queensland the situation is that back boreholes are now an integral part of most panel ventilation systems and is very much the norm to make use of. Of the 14 LW examples referred to in Table 2 nine are using back boreholes. These range from use of one or two small diameter boreholes each (less than 1.0m diameter) in four mines to cases where the borehole is greater than 2 m in diameter in three mines.

Table 2 - Summary of Queensland mines' LW panel ventilation and roadway dimension data

Mine	Panel Ventilation			Roadway		LW Panel			Comments	Beltway
	Pressure (Pa)	Total Q (m^3/s)	Face Q (m^3/s)	Width (m)	Height (m)	Face Height (m)	Length (m)	Face Position (m)		
A	1000	90	60	5.4	3.5	3.5	2170	2170	Highwall LW panel	Homotropal
B	250	93	70	6.2	3.5	3.8	860	860	1st LW; next panel intakes	Homotropal
C	1250	92	65	5.3	2.7	2.6	3650	3450	3 Hdgs; back shaft (2.5m) intake	Homotropal
D LW1	1200	110	77	5.4	3.4	3.4	3300	2550	Back shaft (2.2m) intake	Homotropal
D LW2	500	87	55	5.4	3.4	3.1	1650	550	Back Road intake	Homotropal
E	300	79	69	5.8	3.8	3.8	1200	520	Next panel intakes	Antitropal
F	480	54	37	5.3	2.9	2.9	3000	2780	Back Borehole (1.2m) intake	Homotropal
G	1300	70	48	5.2	3.2	3.2	2800	2475	Back Boreholes (0.6m & 0.8m) intake	Antitropal
H	1320	113	77	5.2	3.4	3.4	3050	1950	Back shaft (2.2m) return	Homotropal
I	300	70	43	4.8	3.3	3.2	1600	1300	Highwall LW panel; next panel intakes	Homotropal
J	1000	77	45	4.8	3.3	3.1	3000	2600	Back boreholes (0.6m & 0.5m) intake	Homotropal
K	930	79	45	5.0	3.0	3.0	3500	1200	Back boreholes (3 x 0.5m) intake	Homotropal
L	525	65	60	5.5	2.8	2.9	2800	2400	Back boreholes (2 x 0.7m) intake	Antitropal
M	650	73	50	5.2	2.6	2.2	2300	2100	Back boreholes (2 x 1.0m) intake	Homotropal
Average	**786**	**82**	**57**	**5.3**	**3.2**	**3.2**	**2491**			

Higher production in recent years with increased seam gas demands availability of more ventilation air for dilution in the LW panel. This has been achieved by a number of alternative strategies including

1. Use of back boreholes in most cases delivering down cast air for diluting the back road and tailgate ventilation,
2. The early cutting of development roadways in the next planned panel (adjacent to the current panel) and then use of these roadways to assist ventilation, as for three mines in Table 2.

A small number of mines find they have not needed to use back boreholes or air from the early development of next panel as they are working panels directly connected to a previously mined highwall and so do not need to ventilate a traditional mains. Australian mines before the mid 1990's generally passed intake air down the maingate to the face along both the transport and belt headings in an antitropal ventilation system. However depth, higher seam gases and higher temperatures mean that most mines now use homotropal maingate ventilation (with one heading carrying intake air and the other

carrying return air) meaning that relatively less fresh air reaches the face. The conclusion is that over a relatively short period additional pathways for high quantities of intake air to reach the panel face have been required. The industry has had to by necessity use back boreholes or, on occasions where development is ahead, use the newly excavated roads to supply required of air.

Within Australia there is currently limited use of true bleeder ventilation due to the propensity of Australian coal to spontaneous combustion. True bleeders refer to the US style of ventilating gas at the back of a panel with a number of parallel return roads. To provide ventilated access to the current goaf seals some mines are boring raises behind the LW panels and using in a downcasting mode for intake to the LW face or upcasting mode providing return capabilities. These back boreholes can be utilised for other purposes during LW installation (e.g. concrete drop holes) or during emergency scenarios as another means of access to the working seam and/or surface.

CONCLUSIONS

From the case studies discussed it can be seen that there are several underlying themes that are common within Australian LW mines. At the same time, however, there are also some extreme variations of ventilation approaches utilised to facilitate management of severe ventilation issues. Each of the 30 operating LW mines in Australia manages some or all of a combination of issues including spontaneous combustion, total and respirable dust, heat and explosible and toxic gases. The increasing depth of operations exacerbates most of these issues. The utilisation of two headings in maingate development is by far the most common approach across the industry. This limits the number of different LW ventilation methods possible and hence most operations use a variation of the traditional U ventilation approach. This method is also utilised to assist with the minimisation of pressure differential induced across the current and previous goaf's for spontaneous combustion reasons. A small number of operations use a variation of the Z ventilation approach but only to facilitate the ventilation management of extreme quantities of gas in a seam with little or no potential for spontaneous combustion. The use of panel back boreholes and small diameter shafts has become very popular. This shift has occurred in parallel with a move to use of homotropal LW maingates. 11 of the LWs in Table 1 have maingate homotropal airflow and only three have antitropal flow. Homotropal maingates have many advantages but in general need boreholes or extra development roadways to allow sufficient air to reach the face. Boreholes assist with reducing mine resistances in some instances and allow the ventilation of blind headings subject to gas inundation and development breakthroughs.

ACKNOWLEDGMENT

The authors wish to acknowledge thanks to Australian coal mines' personnel who have provided information that has assisted with the progression of this research.

REFERENCES

Mayes, T I and Gillies, A D S, 2001. An analysis of current Australian LW ventilation methods, In *Proceedings of Seventh International Mine Ventilation Congress*, Editor, S Wasilewski, Krakow, Polish Academy of Sciences, June, pp 793-800.

Schaller, S and Savidis, G, 1983. Some aspects of LW ventilation in Australian coal mining, In *Proceedings of the Symposium on Ventilation of Coal Mines*, Australasian Institute of Mining and Metallurgy, Illawarra Branch 21:1-10, 10-13 May, 1983.

REAL-TIME AIR VELOCITY MONITORING IN MINES - A QUINTESSENTIAL DESIGN PARAMETER FOR MANAGING MAJOR MINE HEALTH AND SAFETY HAZARDS

Bharath Belle

ABSTRACT: Mines should be safe places in which to work. These safe places are achieved by means of natural and mechanical means of ventilation. Air velocity is a quintessential ventilation design parameter in diagnosing and ascertaining the adequacy of ventilation for managing mine health and safety hazards. Although Australian coal mines are recognized as being the safest mines in the world using both real-time and tube bundle monitoring systems, monitoring of airflow at critical locations in real-time is glaringly deficient and poor ventilation monitoring practice. This paper discusses the needs for real-time velocity monitoring and the implementation benefits of it in mines. What is an acceptable velocity measurement error in the carbon era? Current carbon emission guidelines do not clarify the measurement challenges associated with air velocities, let alone air velocity accuracy. Historically, there are references to acceptable measurement errors ranging from ± 5 % to ± 20 %. Measured differences in monthly ventilation surveys against the real-time airflow monitoring were found to be 13.3 % resulting in annual carbon costs of A$580 000 for a CH_4 level of 0.2%. It is considered that, it is never too late to implement real-time velocity monitors in Australian mines, a safety enabler and a leading practice in the mature mining world.

INTRODUCTION

Mines should be safe places for all those who work in them. These safe places are achieved by means of natural and mechanical means of ventilation. Air velocity is a quintessential ventilation design parameter in diagnosing adequacy of ventilation for managing major mine health and safety hazards. Use of minimum air velocity as a design parameter is an integral part of various ventilation engineering planning spheres to provide assurance on regulatory requirements as well as quality of hazard controls in some form in most mining countries. Therefore, monitoring of air velocity and in turn air flow in real-time is an essential practice in assuring continuous provision of safe occupational environment.

Issues of velocity measurement in mines have been studied by various research agencies including, Thimmons and Kohler (1985), AAC (1990), Hardcastle *et al.* (1991, 1993), Casten (1995), Martikainen *et al.* (2011). A notable study is the work of Thimmons and Kohler (1985). This work noted after a review of measurement practices that flow determination is more of an art than a science. This demonstrates that during velocity compliance determination, it is possible to introduce the operator bias, i.e., novice or veteran, instrument bias, sampling location, and frequency of measurements as required by the respective safety regulations. In such instances, real-time velocity monitors provide ventilation engineers with non-emotional data for evaluating the underground conditions and effectiveness of the mine ventilation systems. This paper attempts to explore the needs, challenges and operational aspects of implementation of real-time velocity systems. Benefits derived from installing real-time air velocity monitoring installation on main fan systems at a Bowen basin coal mine are discussed.

According to McPherson (2006), prior to the invention of vane anemometers (Figure 1) in the nineteenth century, the only practicable means of measuring rates of airflow in mines was to observe the velocity of visible dust or smoke particles suspended in the air. It is still a practiced method by the 'shift boss' or 'deputies' to estimate the air movement or direction of flow in the absence of real-time velocity monitoring instruments at hand by simply throwing some float dust found in the roadways to gauge the airflow and direction at very low air velocities, i.e., non detectable instrument measurement ranges.

Recent global catastrophic events in some form can be attributed to the outcome of inadequate ventilation, lack of ventilation (air velocity) monitoring thus creation of a flammable gas mixture and absence of dedicated long term mine ventilation engineers (unlike contractors) who are responsible for airflow and gas management underground. These hazards when unmanaged would be dangerously unforgiving and are mostly managed by better mine ventilation conditions. Figures 2 and 3 show the

Anglo American Metallurgical Coal, Bharath.belle@angloamerican.com, Tel: +61 7 38341405

alarming fatal statistical consequence due to gas and dust explosions and frictional ignition potential in both gassy and non gassy mines.

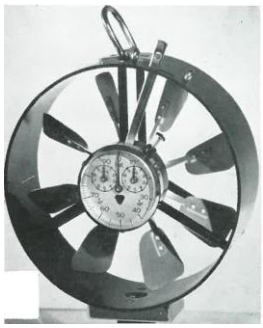

Figure 1 - Friedrichs Anemometer, Model 1400 (0.3038 m/s to 20.3 m/s), (Source: MVS Journal, 1957)

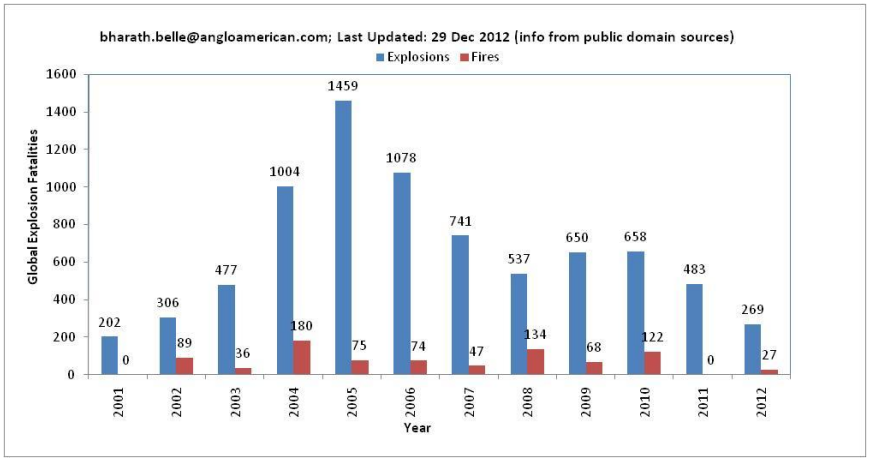

Figure 2 - Statistics on global mine explosions

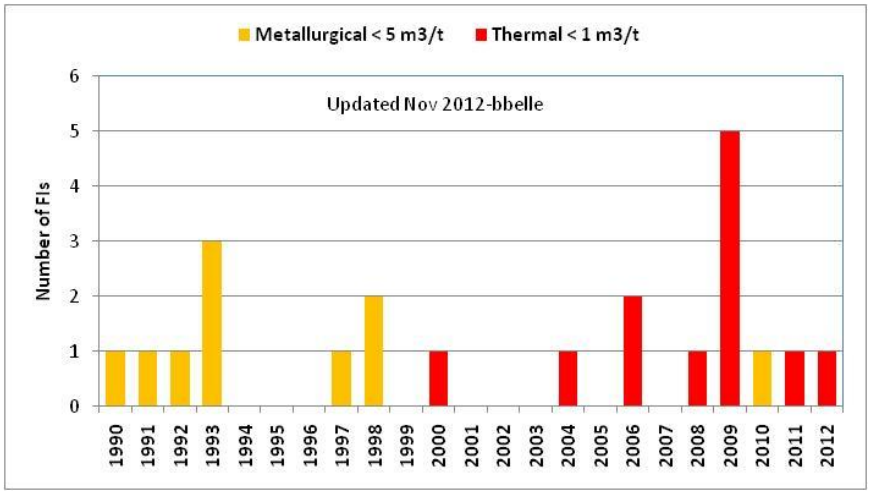

Figure 2 - FI incidents in gassy and non gassy mines (PS- reference to the use of FI limit of 5.75 m^3/t in PHMPs or COPs to be discouraged)

As seen above, explosion risks in coal mines are ever present because of inherent presence of methane gas. In order to minimize the risk profiles of these catastrophic events, it is timely that all interested parties in mines accept improvement opportunities in the following hierarchical control namely, air velocity (ventilation) monitoring:

- Accepting the need for continuous monitoring of hazards in the environment that is continuously changing (read gases and dust);

- Accepting the need for continuous monitoring of air velocity and ventilation that is continuously changing (read airflow) regardless of magnitude;
- Accepting that in a complex mine ventilation network, frequent manual ventilation monitoring in main returns or intakes is a cumbersome process and has practical limitations;
- Accepting the availability of Intrinsically Safe (IS) real-time monitoring tools for underground use in the current technologically advanced workplaces;
- Accepting that continuous air velocity monitoring devices can provide leading indicators of unanticipated conditions in the event of a failure or provide early warning of ventilation effectiveness or deficiencies;
- Accepting that traditional measurements aided by continuous monitoring would enhance the response time in the event of emergencies or re-entry;
- Accepting that approved IS real-time velocity monitors are available in Australia;
- Accepting that just as in other real-time gas monitoring tools, velocity monitors also need maintenance;
- Accepting that continuous velocity monitoring is a leading practice in other parts of the coal and metal mining world (UK, Canada, South Africa, and Poland);
- Accepting that improvements in velocity monitoring would assist the mines in controlling and providing improved quality of air;
- Accepting that real-time velocity monitor is a safety and production enabler.

ROLE OF AIR VELOCITY IN MINE DESIGNS AND REGULATIONS

Typical elements of occupational environment design are shown in Figure 4. These mining hazards resulting from natural and mining factors are managed by adequate mine ventilation using air velocity as a fundamental and quintessential design parameter. Air velocity expressed in metre per second (m/s) is the change of position and direction of moving air with time. Critical aspects that are considered in the design and planning of mine ventilation networks are air velocities and their direction in the working face, intake, return, tailgate, conveyor road, intake shafts, return shafts, main drifts, travel roads, haulage roads, longwall face, Last Through Road (LTR), over casts, bleeder road and regulators. These in turn with cross sectional area (m^2) would assist the mine ventilation engineer on the air flow rate (m^3/s) and in calculating the pressure differentials or calculating the efficiency of mine ventilation systems. Also, air velocity measurement along the maingate, mid-face and tailgate of a longwall enables the ventilation engineer to quantify the leakage of air into the goaf areas as well as estimate the heat loads and carry out in thermodynamic calculations.

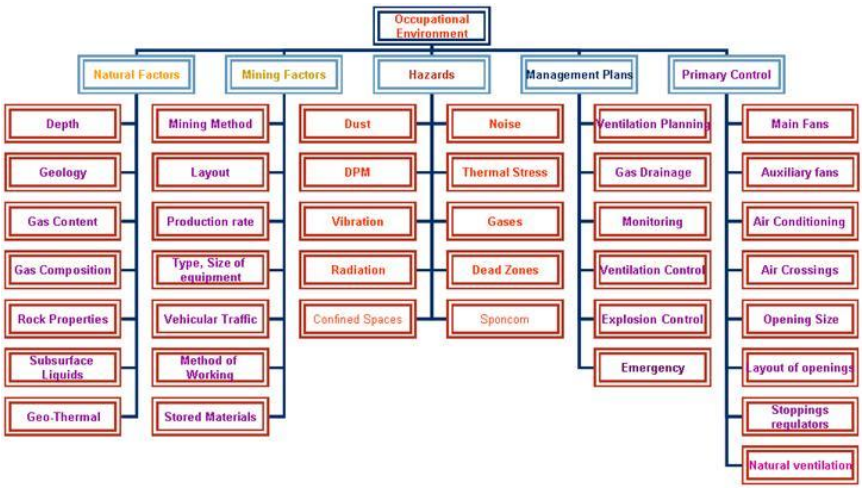

Figure 4 - Elements of occupational environment design

Typical ruling ventilation design parameters for various mineral types are shown in Figure 5. It must be noted that based on the place of operation (read continent), the ventilation ruling parameter may change due to the provision of minimum hazard limits at different commodities and mining countries.

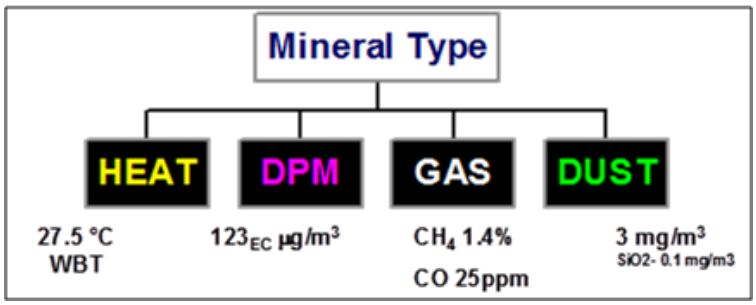

Figure 5 - Critical hazards in defining minimum air velocities

The methods considered for the minimum ventilation using air velocities for the working areas, viz.:

1) Ventilation for a minimum velocity (to dilute dust or gas or other identified hazards);
2) Ventilation for diesel engines to manage Diesel Particulate Matter (DPM) and gases;
3) Ventilation for heat management;
4) Ventilation for blasting re-entry time.

The normal design process is to calculate the air requirements using each of the above methods and to provide sufficient ventilation to meet the highest hazard management together with limit values prescribed in local regulations. This highest requirement is termed as the 'ruling parameter'. In some instances, this requirement is excessive or impractical and changes must be made to the mining or equipment parameters to reduce the ventilation requirements or cause another of the three parameters to become dominant.

Table 1 summarises an example of the air quantity requirements for the face ventilation system using various design criteria for identified hazards. The correct ventilation design factor used in the estimation can be debatable and the choice of factors is based on the individual operational experiences and the understanding of ventilation inflexibility needed during the life of the mine (LOM). In this example, measuring air velocity is the only means to ascertain the sufficient air quantities are supplied to manage the hazards, thus demonstrating the importance of measuring air velocities.

Table 1 - Example of determination of ventilation air quantity requirements

Condition	Design Criteria	Air Quantity	Leakage, 10%	Pressurisation, 15%	Required Air Quantity
		m^3/s	m^3/s	m^3/s	m^3/s
Legal-Min Std	0.25 $m^3/s/m^2$	2.72			
Re-entry multi-blast development	30 min wait; 8 air changes; 60 m tunnel	2.90			
Re-entry-Secondary blasting	10 min wait; 8 air changes; 30 m to face	4.36			
Dust clearance*	1.0 m/s	10.89			
Diesel Engine-DPM	0.0482 $m^3/s/kW$	6.884			
Diesel Engine-Avg. Heat**	0.065 $m^3/s/kW$	9.23			

*based on type of dust and make [this example is for kimberlite dust for a block cave, incline cave and sub level cave mining methods, Belle (2005)] ** It is assumed that the average intake air WBT will not exceed 18° C

The following paragraph summarizes the example expressions of air velocity in the ventilation code of practice (COP) and legislations of mining intensive countries. These requirements illustrate that manual

and or electronic means of real-time velocity monitoring devices would enable to provide assurance needed on meeting those compliance requirements.

- The QLD mine safety legislation requires that the Principal Hazard Management Pan (PHMP) must ensure that the ventilating air provided for the mine is of sufficient volume, velocity and quality to remove atmospheric contaminants from mining operations and maintain a healthy atmosphere at the mine during working hours. Also, it must ensure that the effective working temperature requirements are met. Effective temperatures are determined using wet bulb and dry bulb temperatures and air velocity. (Coal Mining Safety and Health Regulation 2001, Regulation 343-345)
- Controlled ventilation for a working place in each standing working place that is on the intake side of a working place and in each working place in an ERZ1 must provide for a ventilation current of an average velocity of at least 0.3 m/s measured across the cross-sectional area of the roadway in the working place. (Coal Mining Safety and Health Regulation 2001, Regulation 343-345)
- Mine safety legislation requires that in areas of the mine where persons work and travel, the ventilation system provides an average air velocity of at least 0·3 m/s measured across the work or travel area (Model Work Health and Safety (Mines) Regulations 2011 *Section 649)*
- The prescribed Chinese ventilation regulations, viz., minimum ventilation volume per person (4 m^3/min/person); decline travel airway velocity limit of 8.0 m/s; depending on location or activity a minimum ventilation velocity of 0.25-0.50 m/s and minimum diesel emission dilution factor of 0.06 m^3/s/kW.
- US regulation 30 CFR 75.350(b) limits belt air velocity to 5.08 m/s; 30 CFR 75.327(b) limits air velocity in trolley haulage entries to 1.27 m/s provided the methane content can be maintained below 1%.

Typically, ventilation systems are designed, implemented and monitored to manage the gaseous and particulate hazards. The following paragraphs reinforce the importance of 'air velocity' in mine ventilation designs and thus the need for accurate measurement requirements. Velocity values are widely published with accepted ventilation design standards on airways, viz., men and material shaft, dedicated intake shaft, exhaust shaft, travel road, conveyor road, working faces, main intake roadways, main return roadways (Jeppe, 1946; Lambrechts, 1974; Lambrechts and Howes, 1989; MVS Databook, 1999; McPherson, 2009). These proven or unproven 'design velocity' values (Table 2) have significant influence during mine planning in terms of main shaft and main airway sizes, number of roadways in mains or panels to carry certain design ventilation loads, e.g., six heading mains or eight heading mains, two heading roads or three heading roads in coal mines.

Table 2 - Typical ventilation design velocities (m/s)

Area	V1*	V2 (coal)**	V3** (metal)	Australian Guidelines***
Working faces	4	-	-	0.3
Conveyor drifts	5	5	5	
Main haulage routes	6	-	-	
Smooth lined mine airways	8	-	-	
Ventilation Shafts	20	18-22	18-22	
Decline Intakes	-	6-8	6-8	4-7
Dedicated Intake Shaft	-	18-22	18-22	
Downcast Shafts with hoisting	-	10-12	10-12	<10
Intake Airways	-	2-5	6-8	
Return Airways	-	3-5	6-8	
Overcasts	-	-	-	2-5
Auxiliary ventilated headings	-	-	-	0.5-0.75
Limit for safe pedestrian access+	-	-	-	<12

* McPherson (1984); Mousset-Jones (1986);** MVS Data Book (1999);***Draft
+If the second egress path is along the overcasts

Figure 6 show an example of a simulated ventilation model of an operating longwall coal mine with seven heading mains and an exhaust fan system and air velocities.

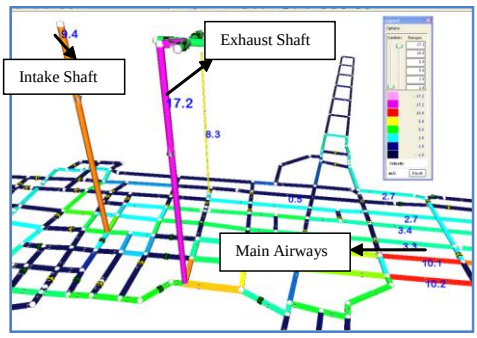

Figure 6 - Airway velocities of an operating gassy longwall coal mine

A summary of main airway velocities (excluding shafts) from few typical operating Australian coal mines is shown in Figure 7.

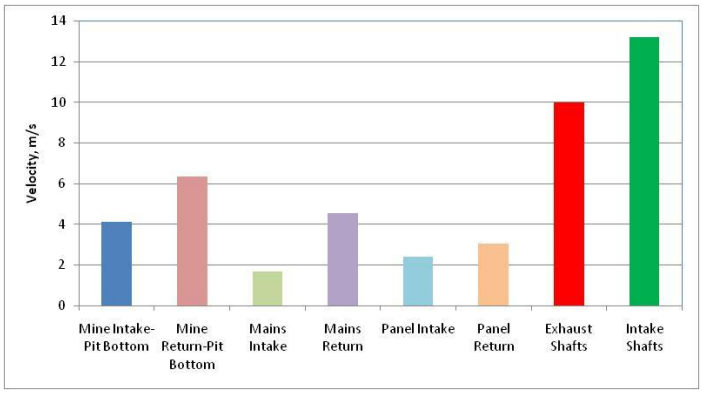

Figure 7 - Typical airway velocities in coal mines (Belle, 2012)

Amongst various air velocity design factors, another commonly quoted design air velocity is 4 m/s in conveyor road, face areas and intake airways. The basis for this value is to manage the physical discomfort of large dust particles (Figure 8) striking the skin (although not a health hazard) after McPherson (1984). The question is often less debated or questioned is if this conveyor road air velocity value still holds true based upon recent empirical data or studies based on increased daily production rates or speed of conveyor belts or if workers ever likely to be using that particular travel road (by walking) on a regular basis.

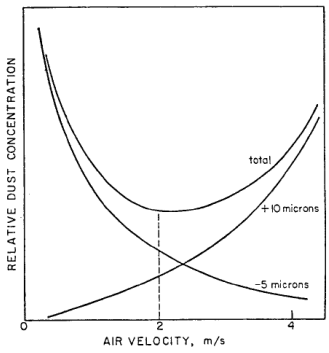

Figure 8 - Relationship between air velocity and relative dust concentrations (McPherson, 1984)

Real-time velocity monitoring leading practices

Air velocity is an indicator to monitor and control the hazards and is typically guided by design values. Traditionally, air velocity is monitored by a competent person (deputy or ventilation officer) by means of manual measurement tools such as vane anemometer by means of complete airway traverse or centerline measurements as required by the legislation or mine ventilation COP. However, in recent years, the need for electronic means of monitoring in real-time for management of hazards has become a

reality. Use of real-time velocity monitoring device and by measuring the airway size, airflow rates or gas make are readily determined.

Various studies have been done in the recent years on the use of real-time velocity monitoring in mines by research institutions or instrument suppliers. Real-time ventilation monitoring in coal and metal mines is a leading practice worldwide probably started in UK mines (vortex based velocity monitors). For example, almost all collieries in South Africa have been using the real-time air velocity monitoring devices underground over at least three decades. One of the limitations of these real-time velocity monitors for use in Australian underground coal mines is the complex process of approval certificates by the respective legislative or testing authorities for use in underground mines. However, some of these IS real-time velocity monitors are approved in other mining (coal and metal) countries such as UK, Poland, South Africa, Canada.

Summary of practical benefits from real-time air velocity monitoring are:

- Continuous monitoring of the efficiency of the mine environment system and mine safety in the prevention of mine fires, spontaneous combustion and explosion events.
- Estimation of real-time carbon monoxide, methane and other noxious gas flow rates as an indicator for Trigger Action Response Plans (TARPs) in PHMPs.
- Estimation of gas emissions during panel development and longwall retreat.
- Accurate determination of heat loads and air cooling capacity for thermal hazard management.
- Improved confidence in Ventilation Air Methane (VAM) emission data.
- Estimation and reconciliation of specific methane emissions (SME) for longwall panels and mine emissions.
- Utilisation of real-time air velocity parameter/tag in the widely used Longwall Visual Analyses (LVA) tool.

In the case of Australian mines, monitoring of airflow underground at critical locations in real-time is not an accepted practice and reasons for its non-use are not documented. Anecdotal evidence indicates that perceived maintenance systems prohibit the pursuit of air velocity monitoring systems. Another commonly expressed reason is that the ventilation systems do not change frequently. Other debate typically diverts into the choice between real-time velocity or real-time pressure differential measurement which ultimately results in neither of the systems being considered. What has become noticeable is that most explosions or fire events have occurred in a smallest 'window' of change that occurred to the ventilation systems.

Figure 9 show the typical locations of real-time velocity monitoring in bord and pillar sections (left), underground velocity check using Kestrel (a digital anemometer) in low seam ~ 2 m (middle) and high seam (4.5 m) seam (right) coal mines in South Africa.

Figure 9 - Location of real-time velocity monitoring and correlation of underground installation in various mining heights in South African collieries

Real-time air velocity monitors in conjunction with CO, CH_4 and smoke sensors are typically placed at intake and return airways. At the beginning of the shift the Kestrels are calibrated against the known air velocities on the surface and later used underground to check if there are any significant deviations from the real-time vortex real-time velocity monitors. Typically the shift boss would calls the control room operator on surface and check the real-time air velocity readings for any significant deviations. Figure 10

shows the hand held Kestrel calibration on the surface, real-time vortex type air velocity sensor and mobile real-time monitoring sensor cluster of velocity, CH_4, CO and smoke sensors.

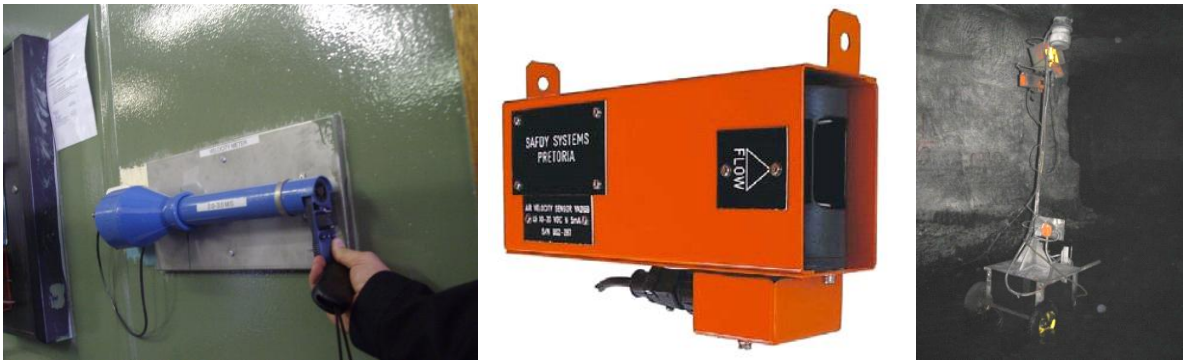

Figure 10 - Calibration of Kestrels on surface (left), vortex real-time velocity monitor (centre); CH_4, CO, smoke and velocity monitoring instrument cluster in section return (right) in South African collieries

ROLE OF VELOCITY MEASUREMENT - LW FACE AND MAIN FAN DUCT VELOCITY PROFILES - AN OBSERVATION

Velocity measurement is an quintessential activity in an underground mine to monitor the hazards on a daily basis by the deputies and ventilation officers. Application of air velocity is typically expanded to understanding the ventilation system effectiveness through velocity profiles like roadways, mine fan ducts and shafts. Velocity profiles are typically carried out to establish the velocity at different points along the longwall face or main fan ducts. Traditionally longwall face velocities of between 1.8 to 2.5 m/s have been considered optimum for longwall operations at conventional height. However, these values have evolved over time. Similarly, main fan duct velocity profiles would provide the main fan operational characteristics and air turbulence profiles in the main fan ducts.

Longwall face velocities

Figure 11 shows the LW face air velocities measured on two consecutive days by two different operators on three different longwall faces. Similarly Figure 12 shows the longwall main gate, panel intakes and return air velocities measured at three different longwalls. It is noted that they are also influenced by the location of shearer along the longwall face or if the shearer is operating. For example (Figure 11), for LW 3 (right), shearer was operational on day one (LW3-A); shearer was standing still at main gate chock ten and tail gate chock 160 on day two and three respectively.

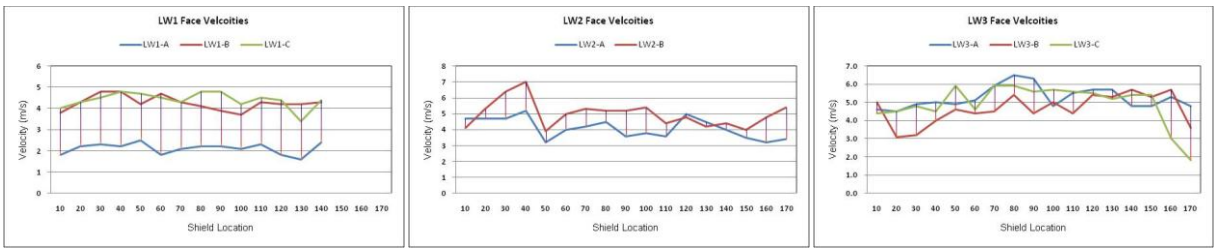

Figure 11 - Influence of manual velocity measurement by different operators in different longwall faces

Measured air velocities when the shearer was operational were higher than when it is standing still at TG or main gate position. However, it is not true for LW2, where the results were opposite to that of LW3. It is important to note that these measurements are typically measured using instruments such as Kestrels (not vane anemometers that are used by the ventilation engineer).

Figure 13 provides the longwall face velocity contours of measured longwall face air velocity data, viz., Chock 15 (top Left), Chock 75 (top middle), Chock 115 with shearer present (bottom Left) and Chock 135 (bottom right). As seen from these profiles based on air velocity measurements, these velocity contours can provide both a visual depiction of the air flow pattern and also a means of quantifying airflow. These

profiles are useful to understand the possible location or presence of gas as well as possible scenarios for ventilation to leak into the goaf. Furthermore, it demonstrates the need to locate the daily velocity measurements taken by deputies throughout the industry. These air velocity readings along with the wet bulb temperature (WBT) and dry bulb temperature (DBT), which would provide the longwall effective temperatures and their status in relation to the TARPs.

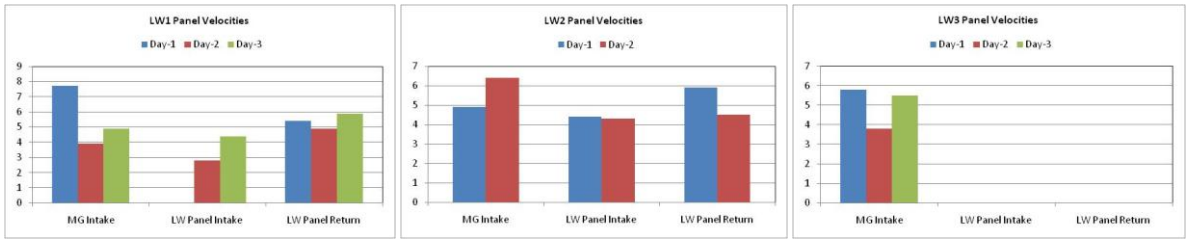

Figure 12 - Operator influences on measured air velocities along the longwall face

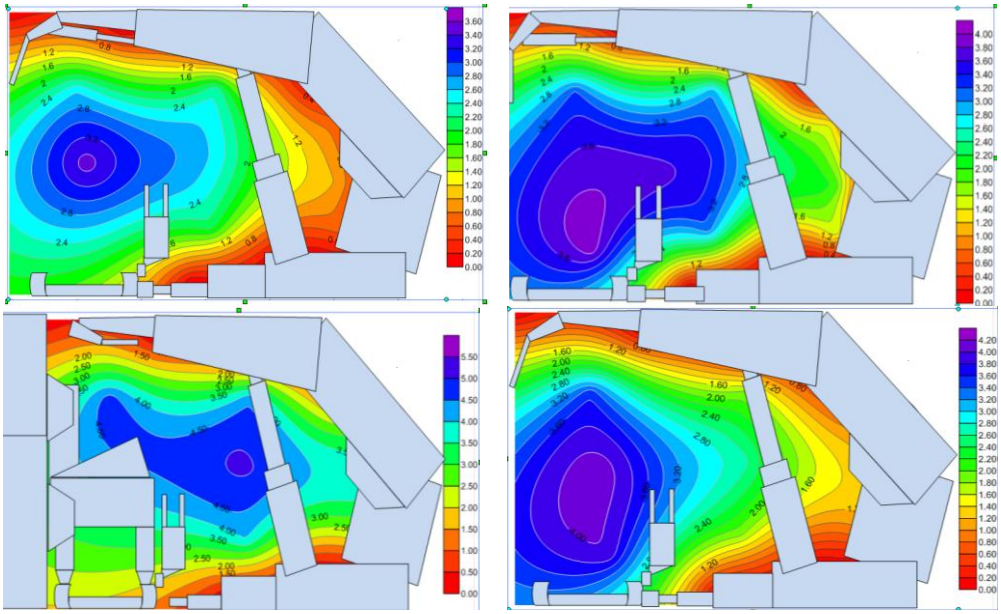

Figure 13 - Isovels along the longwall face maingate (top left), mid gate (top right), shearer (bottom left) and tailgate (bottom right) locations

These velocity profiles would enable the operator on the Frictional Ignition (FI) potential to ventilation leakage potential into the goaf area. In the prevention of FI, critical monitoring parameters of interest are methane, section or face air velocity, alarm settings of these monitors (Belle, *et al.*, 2012). In all or most of FI incident investigation reports it is noted that there was a failure to analyse the pre-ignition gas trends or velocity trends due to limited manual gas records or unconnected real-time gas recording and data collection system or velocity measurements. Improvement in collection of this crucial information is worth the effort for improved understanding and management of FI risks in the LW or development face areas. Therefore, real-time velocity monitoring installation along the longwall face would be a step in the right direction to the mining industry.

From measurement examples (longwall), it is noticed that without major changes to the ventilation flow, the differences in air velocity readings are significant despite each observer using the similar equipment and measurement techniques. These differences translate themselves onto some other parameters such as determining the effective temperatures for thermal stress or longwall panel gas make or longwall panel CO make. The resulting outputs further translate themselves onto the TARPs or longwall Specific Methane Emission (SME) models, monthly ventilation survey reports or review of simulations models such as Ventsim, or even during accident investigations on Frictional Ignitions (FI). Therefore the need to measure the air velocity beyond the statutory measurement location and their frequencies is increasingly becoming a practical reality.

Main fan duct velocity profiles

Figures 14 and 15 shows the isovels of main fan ducts measured from two different exhaust shafts (A and B) with a total seven different fans. These velocity profiles provide a graphical presentation of any issues that can be identified in main fan performance or turbulence associated with the shaft bend designs. What is valuable is that the velocity measurements derived from velocity pressure measurements provide the status of the fans or its future long term use. The isolvel plots suggest that they are definitely different to ideal velocity contours obtained in Computational Fluid Dynamic (CFD) simulations provide by main fan suppliers.

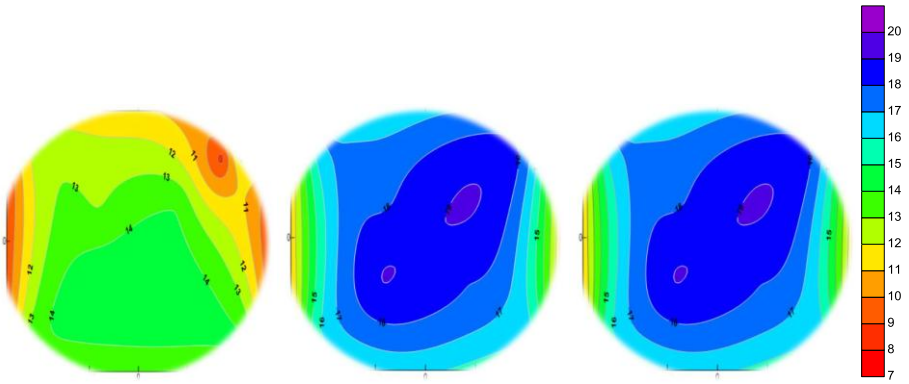

Figure 14 - Isovels measured at three different fan ducts from an exhaust shaft-A

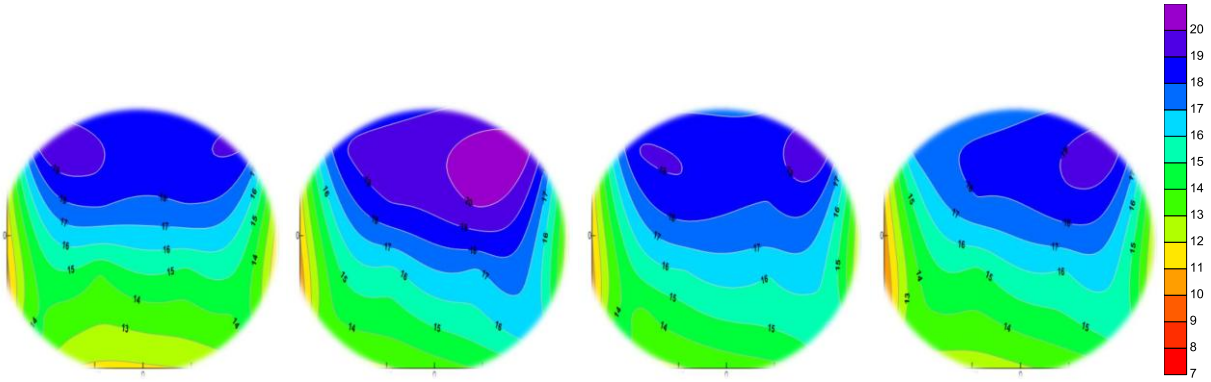

Figure 15 - Isovels measured at four different fan ducts from an exhaust shaft-B

There are several studies on the use of correction factors (including factory correction factors and their given range of velocities) in the literatures; its application in practice is remote. For example Thimmons and Kohler (1975) have suggested that the measurement should always be made at a minimum distance of three roadway diameters upstream of an obstruction and ten roadway diameters downstream of an obstruction. In reality, presence of these ideal locations is scarce or simply they do not exist. Measurement experiences suggest that each operation or a location underground or even the velocity contour profiles of a roadway which is dynamic is different and thus development or application of these correction factors are remote.

Critical measurement aspects that are commonly faced by the ventilation surveyors underground and during surface fan performance evaluations are:

1. Art of velocity measurement (years of experience u/g and correlating monthly ventilation reports to independent surveys);
2. Practical locations of velocity readings to be taken underground (high velocity turbulent regions or sharp bends);
3. Instruments used and their calibration on surface (kestrel or vane anemometers);
4. Underground environment conditions (humid and dusty vs. comfortable conditions);

5. Time constraints and understanding of significance of 'velocity values' to be used after the ventilation surveys.

Above pragmatic measurement challenges offer the users the benefits of fixed real-time velocity monitoring systems to minimise various operator (human) errors identified above.

Australian experiences of real-time velocity monitoring on main fans

With no means of measuring emissions from the mine in real-time and without compromising current mine monitoring systems dedicated for mine safety, specifically sponcom, explosion prevention and management of thermal stress, the need for dedicated real-time airflow monitoring at strategic underground locations is quintessential. Typically, during most shifts various measurements are taken and ideally these are analysed for suitable trends. These trends at times may identify the deficiencies in controls or measurement errors. For example, analyses of recorded underground data on temperature measurements and associated air velocities suggested that LW mid face temperatures were higher than the tailgate temperatures with constant ventilation flow. Later the measurement bias was rectified through toolbox talk, whereby temperatures and air velocity were taken at the same time on each shift and at the same location on a consistent basis. These accurate data are typically used to evaluate the performance and effectiveness of the mine cooling systems.

Figure 16 shows possible location for real-time velocity monitoring system in an underground drift which is a common practice in overseas mines.

Figure 16 - Suitable location for real-time air velocity measurements to carry out performance evaluation of Bulk Air Cooler (BAC)

In recent past, the introduction of a carbon price on Green House Gas (GHG) emission has further necessitated the need for accurate airflow data from mine exhaust systems. The biggest variable in the carbon emission is the airflow. Most mines have established the emission inventory using the existing manual ventilation measurement practices in accordance with the obligations of the National Greenhouse and Energy Reporting Scheme (NGERS) Act (2007). The NGERS Act underpins the Carbon Pricing Mechanism which was introduced on 1st July 2012. The mine Ventilation Air Methane (VAM) is a significant constituent (over 70%) of past, current and future underground carbon emissions.

A significant opportunity exists in Australian coal mines to build a robust, compliant, accurate and transparent VAM reporting system through improved real-time airflow monitoring systems instead of the current user of manual monthly ventilation surveys. Both internal and later external VAM compliance audits have identified the need for a paradigm shift in VAM monitoring systems in terms of resolution and frequency of measurement of key data components. The common findings from most carbon audits is that the current single monthly ventilation survey data for VAM estimation is deemed as a 'Potential Risk of Non-Compliance' due to the materiality of 'Run-of-Mine Coal Extracted from Gassy Underground Mine' emissions. Typically any changes in ventilation system (such as slowing down of fans or maintenance of a single fan or brief power failures) or errors associated with the ventilation measurement are not captured in the estimated carbon emissions. This is because the monthly ventilation surveys do not capture them. For example, 400 m^3/s of airflow with 0.3% methane, 10% changes in airflow alone would relate to additional carbon tax of AUD$1.4 million per annum. Similarly, a 5% error in manual measurement flow at 0.36% methane over a 5 year period would have an emission cost of AUD$10.9 million at carbon price of AUD$23. Acknowledging these significant costs, the VAM monitoring system considered by mines is typically independent of current systems which are dedicated to mine safety.

As a proactive approach, most mines are implementing the underground use of approved IS ultrasonic flow monitoring devices at the exhaust shaft fan ducts. It is also noted that a handful of coal mines are in the process of implementing these real-time monitors underground. Current installation of monitoring systems at exhaust shaft fan ducts or underground shaft bottoms incorporate independent measurement of real-time exhaust airflow, CH_4, CO_2, temperature (WBT and DBT), moisture and pressure to improve VAM measurement accuracy which is a largest variable in the VAM greenhouse gas estimates. The introduction of leading practice of real-time monitoring of airflow and low range gas measurements at fan ducts will enable mines to produce transparent emission reports and also enable immunisation from carbon tax estimation errors. Recently, these systems have been implemented at mines in NSW, Moranbah North Mine and are also proposed to the new Grosvenor mine.

Figure 17 shows the implementation of real-time ultrasonic air velocity monitoring system installed on main fan ducts. Figure 18 demonstrates the daily real-time air flows measured at individual fans (for a period of 34 d) and the average airflow measured over a period of 5 months. The average airflow measured from underground surveys over a period of five months was 253 m^3/s. Similarly, the average flow recorded using real-time air velocity for a period of 32 d was 219.78 m^3/s with a difference of 13.25 %. Other benefits of obtaining the air velocity trends from each fans is to evaluate individual fan performance against the planned airflow in mine ventilation designs and ventilation simulation models. In this example, it is easily noticeable that Fan A is significantly different than the other two main fans. In addition, the impact of airflow measurements is significant on the estimation of greenhouse gases as well as associated annual costs in the region of $580 000 for a methane concentration level of 0.2%. Table 3 provides the carbon costs associated with variations in measured velocities and methane concentrations.

Figure 17 - Installation of real-time air velocity monitoring on main fan ducts

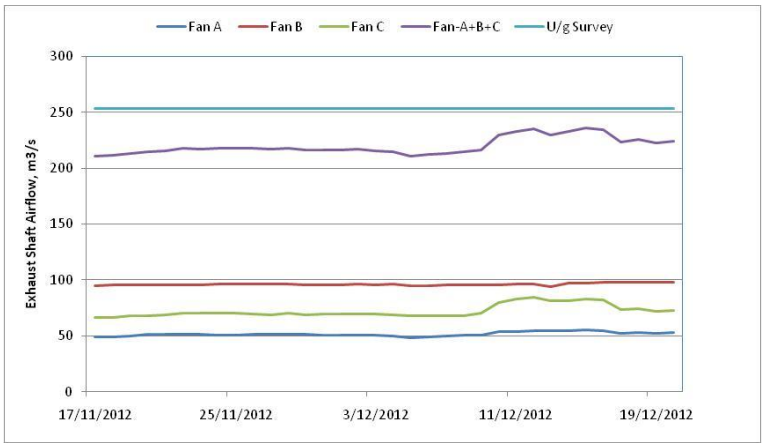

Figure 18 - Differences between real-time air velocity monitoring on exhaust shaft and u/g ventilation surveys

Another significant parameter that is used in determining the airflow is the area of a roadway. Typically, 5% is considered to be an acceptable error during underground airway measurement survey. Even with this low level of acceptable error the carbon cost is significant, i.e., at 0.2% methane level for a roadway area of 20.30 m^2, 5% accepted error in airway area (m^2) would be costing around ±$200 000 per annum (Table 3).

Table 3 - Cost of carbon with variation in methane levels and various accuracy levels on measured air velocity

Air Velocity, m/s	8	8.5	9	9.5	10	10.5	11	11.5	12
CH4, %	-20%	-15%	-10%	-5%	0%	5%	10%	15%	20%
0.025	$ 390,588	$ 415,000	$ 439,411	$ 463,823	$ 488,235	$ 512,647	$ 537,058	$ 561,470	$ 585,882
0.05	$ 781,176	$ 829,999	$ 878,823	$ 927,646	$ 976,470	$1,025,293	$1,074,117	$1,122,940	$1,171,763
0.075	$ 1,171,763	$1,244,999	$1,318,234	$1,391,469	$1,464,704	$1,537,940	$1,611,175	$1,684,410	$1,757,645
0.1	$ 1,562,351	$1,659,998	$1,757,645	$1,855,292	$1,952,939	$2,050,586	$2,148,233	$2,245,880	$2,343,527
0.125	$ 1,952,939	$2,074,998	$2,197,057	$2,319,115	$2,441,174	$2,563,233	$2,685,291	$2,807,350	$2,929,409
0.15	$ 2,343,527	$2,489,997	$2,636,468	$2,782,938	$2,929,409	$3,075,879	$3,222,350	$3,368,820	$3,515,290
0.175	$ 2,734,115	$2,904,997	$3,075,879	$3,246,761	$3,417,644	$3,588,526	$3,759,408	$3,930,290	$4,101,172
0.2	$ 3,124,703	$3,319,997	$3,515,290	$3,710,584	$3,905,878	$4,101,172	$4,296,466	$4,491,760	$4,687,054
0.225	$ 3,515,290	$3,734,996	$3,954,702	$4,174,407	$4,394,113	$4,613,819	$4,833,524	$5,053,230	$5,272,936
0.25	$ 3,905,878	$4,149,996	$4,394,113	$4,638,230	$4,882,348	$5,126,465	$5,370,583	$5,614,700	$5,858,817

What is an acceptable velocity measurement error in the carbon era? Current guidelines do not necessarily clarify the measurement challenges associated with air velocities, let alone measurement air velocity accuracy. Historically, there are few references to acceptable measurement errors. Thimmons and Kohler (1985) have expressed the definitions on accuracy requirements for mine ventilation applications. They had expressed the accuracy of ± 20 % is satisfactory based on the ventilation measurement practices of 1970s. Also, recently, there are suggestion of ± 5 % error value that is viewed as an acceptable air velocity measurement error in an underground mine (Martikainen, *et al.*, 2011). Considering the recent financial impacts, lack of a standard on an acceptable measureable error persists and in addition, which velocity measurement instrument to be seen as a 'reference true velocity measurement device' to estimate the accuracy of a velocity measurement device needs to be established by the mining industry.

ENVIRONMENTAL MONITORING SYSTEM, MAINTENANCE DILEMMA AND IMPLEMENTATION BENEFITS

Continuous on-line velocity monitoring systems will facilitate the establishment and maintenance of a safe environment underground if well installed, maintained and monitored. Such a system will give early warning of a fire, spontaneous combustion heating, abnormal methane or carbon monoxide gas concentrations and a failure or weakening of the air flow. Prompt response can then be taken to deal safely with the abnormal situation provided controls are in force and manageable. Interested parties in determining the real-time velocity monitoring strategy are the ventilation officer, mine manager assisted by the mechanical and electrical engineering manager. Most of the Australian coal mines incorporate CH_4, CO, CO_2, and O_2, barometric pressure monitoring systems stationed at strategic locations along the intake, return and longwall face and on the surface. The monitoring of air velocity at strategic positions will indicate the status of the air distribution in the mine on a continuous basis. For example, the ventilation and heat simulation software tools like Ventsim Visual have the facility to incorporate real-time velocity tags for live simulations. The real-time velocity monitors will give early warning of a weakening in airflow or a ventilation failure. It will also indicate a weakening trend in airflow and action can therefore be taken before a gas accumulation develops. Benefits of real-time velocity monitors will provide ventilation engineers additional information on whether an increase in gas levels is due to increase in gas release rate or reduced ventilation.

Just as in real-time and tube bundle environmental monitoring systems, the maintenance of real-time velocity monitoring system is of vital importance. Confidence in the system will be lost if the system is not maintained and kept in a fully operational condition as in other real-time measurement parameters such as CH_4, CO, O_2 sensors. All existing real-time and tube bundle systems require adequate maintenance as per the Australian Standard (AS) 2290.3. Failure to address this will lead to misinterpretation of conditions underground and should be addressed without delay by relevant person responsible for the installation and maintenance of the monitoring systems. As in the case of existing environmental monitoring systems, the inspection should include provision for frequency of cleaning of monitors, testing of response of monitors, replacing malfunctioning monitors, a documentation system to include installation, cleaning, testing and replacement dates. As in the case of existing environmental monitoring systems, air velocity monitors must be provided with battery back-up power which must switch on automatically in the event of a power failure.

CONCLUSIONS

The monitoring of air velocity at strategic positions will indicate the status of the air distribution in the mine on a continuous basis. The velocity monitors will give early warning of a weakening in airflow or a

ventilation failure. It will also indicate a weakening trend in airflow and action can therefore be taken before a gas accumulation develops. Benefits of real-time velocity monitors will provide the ventilation engineers additional information on whether the increase in gas levels is due to increase in gas release rate or reduced ventilation.

Use of real-time air velocity monitoring technology underground can aid the ventilation engineers, longwall operators, technical services managers, safety officers and emergency response personnel for any unanticipated surprises on gas or ventilation situation and develop speedy interventions and thereby reduce production downtime. Therefore, monitoring of air flow in real-time is essential and is a leading practice in evaluating the performance of underground environment conditions and must be pursued by the Australian mining industry into the next decade.

Air velocity and area of a roadway, and wet bulb temperatures (WBT) and dry bulb temperatures (DBT), CH_4, CO_2, barometric pressure are the key parameters that will assist in understanding the key hazards (gas, dust, sponcom, thermal), associated risks and the effectiveness of controls provided at the workplace. Therefore, it is important that these parameters are accurately measured by those who are responsible for them.

It is hoped that the implementation of real-time velocity monitors that are glaringly absent in the Australian coal mines that have one of the best gas monitoring systems would consider this improvement opportunity to clear out any distractive comments or criticisms on Australian Safety and Health Systems. In author's opinion, it is never too late to implement the real-time velocity monitors in mines, a life saving safety enabler and a leading practice that exists in the rest of the coal mining countries.

ACKNOWLEDGEMENTS

The author is indebted to various sources of knowledge that were developed in the past that have resulted in a better understanding of velocity monitoring in mines. Author also acknowledges the efforts of M Borg, R Nel, F Casey, K Martin, N Stanton of Moranbah North mine, and D Broad, S Coppard and D Dwyer of Grasstree Mine for collation of relevant longwall data and sharing of air velocity monitoring implementation challenges that assisted in the preparation of this paper. The author also acknowledges Prof. Naj Aziz of University of Wollongong for the technical review and positive contributions to this paper.

REFERENCES

AAC, 1990. Environmental monitoring systems, Anglo American Corporation, Johannesburg, South Africa.

Australian Standard (AS), 1990. Electrical equipment for coal mines –maintenance and overhaul, Part 3: Maintenance of gas detecting and monitoring equipment, Standards Australia, NSW, Australia, pp 33.

Belle, B, 2005. Pre-feasibility ventilation design of high production block, incline and sub level cave mining study report, Anglo American Internal Document, South Africa.

Belle, B, Carey, D and Robertson, B, 2012. Prevention of frictional ignition in coal mines using chilled water sprays - Towards a leading practice, in *Proceedings of 12th Coal operators' conference*, University of Wollongong, Australia. pp 176-185, http://ro.uow.edu.au/coal/405/.

Belle, B, 2012. An internal FI and global methane and coal dust explosion database, Australia.

Belle, B, 2012. A Case for revision of time-honoured mine ventilation design parameters-main airways, 14th United States/North American Mine Ventilation Symposium, 2012 - Calizaya & Nelson © 2012, University of Utah, Dept. of Mining Engineering, USA, pp 3-11.

Casten, T P, 1995. Air velocity measurements in underground excavations, M.Sc., Thesis, University of Reno, Nevada, USA, pp 169.

Coal Mining Safety and Health Regulation 2001. Regulation 343-345, Australia.

Draft Code of Practice, 2012. Ventilation of Underground Mines, Metalliferous and Coal Mines Combined, Australia.

McPherson, M, 2006. Ventilation surveys, Chapter 6, Subsurface ventilation engineering, USA.

Hardcastle, S, Granier, M and Butler, K, 1991. Electronic vane anemometry-Finding a suitable replacement of mechanical analog devices for mine airflow measurements, in *Proceedings of 5th US Mine ventilation symposium*, Morgantown, Chapter 60, pp 482-493.

Hardcastle, S, Granier, M and Butler, K, 1993, Electronic anemometry-recommended instruments and methods for routine mine airflow measurements, in *Proceedings of 6th US Mine ventilation symposium*, Utah, Chapter 86, pp 571-576.

Jeppe, C B, 1946. Gold mining on the Witwatersrand, Vol-II, Published by The Transvaal Chamber of Mines, South Africa.

Lambrechts, J De V and Howes, M J, 1989. Mine ventilation economics, Chapter 33, Environmental engineering in South African mines, The Mine Ventilation Society of South Africa.

Lambrechts, J De V, 1974. Mine ventilation economics, The ventilation of South African Gold Mines, 1974, pp 449-474.

Mine Ventilation Society of South Africa (MVS) Data Book, 1999. The mine ventilation practitioner's data book, Volume 2, The mine ventilation society of South Africa, Edited By A. Patterson.

McPherson, M J, 1984. Mine ventilation planning in the 80's, *International Journal of Mining Engineering*, 2(3):185-227.

McPherson, M J, 2009. Subsurface Ventilation Engineering, Published by Mine Ventilation Services, Inc., USA.

Martikainen, A L, Taylor CD and Mazzella A L, 2011. Effects of obstructions, sample size and sample rate on ultrasonic anemometer measurements underground, SME Annual Meeting, Pre-Print 11-010, USA.

Mousset-Jones, P, 1986. A survey of mine ventilation practices, Mackay School of Mines, USA, pp 19.

NGERS Act, 2007, National greenhouse and energy reporting act, Australia.

Thimmons, E D and Kohler, J L, 1985. Measurement of Air Velocity in Mines, BOM RI 8971, USA.

FULL SCALE EXPLOSION TESTING AND DESIGN OF GYPSUM PLASTER VENTILATION SEALS

Verne Mutton[1] and Michael Salu[2]

ABSTRACT: This paper describes recent research to evaluate Gypsum plaster seal designs in the full-scale pressure test facility at Londonderry, NSW. After the Moura Number 2 Mine explosion a review of the safety of coal mine operations resulted in changes to mining legislation where ventilation control devices (VCDs) were required to be tested in an internationally recognised mine testing explosion gallery to achieve over pressure ratings of 14, 35, 70, 140 or 345 kPa. Since this disaster, Minova has live tested all VCD designs to provide validation test data for design purposes. In recent years validation and certification of seal designs has been undertaken by Queensland Registered Professional Engineers (RPEQs) using laboratory measured seal material properties as input to 3-dimensional numerical models. As an engineering material, mining plaster has properties that approximate to those of a low-strength concrete. Unlike concrete, mining plaster gains strength extremely rapidly and this makes it ideal for constructing seals where downtime while waiting for material strength literally costs money. As a result of these properties, Sprayplast UW VCDs can be rapidly brought into service as explosion rated and/or water holding seals and stoppings. Previous full-scale explosion testing carried out in Australia at Testsafe's Londonderry Explosion Gallery (Pearson, 1999) has shown that mining plaster stoppings can resist significant blast pressures.

This paper describes a recent series of full-scale explosion tests carried out at the Londonderry Testing facility in NSW, which were intended to build on experience gained from earlier tests carried out at the Lake Lynn experimental mine in the USA and at Londonderry, NSW in 1999. The testing process and instrumentation layout will be described in which each seal design was subjected to a series of explosions progressively increasing in intensity until seal failure resulted. Two seal designs at 100 and 150 mm nominal thickness were constructed and instrumented to provide time-related overpressure and wall deflection response during the controlled series of explosions in separate test programs. Suppliers worked to develop reliable engineering designs, with results of the testing used to calibrate a numerical engineering model for Sprayplast UW mining plaster that can be used to design seals for overpressures up to the maximum currently legislated in Australia. The model can also be used to design bulkhead thicknesses for water retention. In addition to theoretical analysis, this paper also considers some of the practicalities of seal location, design, construction and maintenance.

INTRODUCTION

After the Moura No 2 Mine explosion in 1994 there were changes to mining legislation in Queensland that required all Ventilation Ccontrol Ddevices (VCDs) to have been tested in an internationally recognised laboratory. Although most VCDs are now designed by registered professional engineers in Queensland, there is a variation in design practises and outcomes with no design methodology common to the coal industry in Australia.

In contrast the coal industry in the United States now has a set of guidelines, the "final rule" for mine seals issued in 2008. This replaced historic requirements set in 1992 where seal design only required a seal to survive a 20-psi test explosion at the National Institute for Occupational Safety and Health (NIOSH) Lake Lynn Experimental Mine (LLEM) without any visible structural damage and within certain leakage bounds. Seal design strength was increased and there are specified new requirements for the engineering and construction of mine seals (MSHA seal reference). New seal designs (Zipf, *et al.*, 2010) must resist a design pressure-time curve, remain elastic to withstand repeat overpressures, have adequate anchorage to the surrounding strata, and consider roof-to-floor convergence.

In Australia there is a variation in both software being used by designers and in their ability to design structures that are subject to transient loads. Characterisation of seal construction materials provides important input for design using Finite Eelement Numerical Methods (FEM). Gyspum plaster products

[1] *Senior Mining Engineer, Minova Australia (part of the Orica Group),verne.mutton@minovaint.com, M: 04 1749 6550*
[2] *Principal Structural Engineer, Parsons Brinckerhoff (Australia) Pty Ltd*

used in VCD construction must be "fit for purpose" in the range of conditions they will be subject to over their life.

The Queensland Mines Inspectorate stipulates (Taylor, 2011) now that designs are to be examined using numerical computer models by registered engineers. Parsons Brinckerhoff believes that valid designs with a greater degree of confidence are possible when numerical (FEM) models are calibrated from the results of live seal testing in controlled experimental conditions.

In 1997 at Lake Lynn Experimental Mine, Tecrete Industries (Weiss, *et al.*, 1999) designed an explosion seal and stopping test program in which instrumentation was introduced for the first time to measure the structural response of VCDs when subject to transient loads. Using linear variable transducers, accelerometers and carefully situated overpressure monitoring, live test data was captured that would be useful to enable the design of VCDs in a wide range of roadway sizes and pressures ratings ranging from 14 kPa (2 psi) to 345 kPa (50 psi). With this data numerical models were constructed.

Parsons Brinckerhoff designed a series of explosion tests that would provide 138 kPa (20 psi) and 345 kPa (50 psi) Gypsum plaster seal designs around the testing facility available at Londonderry, NSW.

Thus thinner seals were modelled that could replicate a normal mine sized seal. Nominal thickness seals of 100 and 150 mm were chosen as they were found to provide sufficient data to be able to predict the performance of high pressure rated seals. As per the MSHA requirement it could be seen how the seal designs reacted under multi explosions. Natural gas was used to replicate an explosion in a coal mine as opposed to using high explosive charges or water pressure as in the LLEM hydraulic test facility. The pressures generated in the tunnel gas enclosure subject the VCD to rapid load. Even pressure is experienced across the structure at any given time, making structural response more easily simulated with a FEM model. There is a possibility that acceleration and additional loading of the VCD could occur under rapid loading, which cannot be simulated by applying hydraulic pressure to a seal. Materials when subjected to rapid loads exhibit higher strength capacity over and above their capacity under static loading. Seal displacement data during these tests showed that the pressure across the seals was uniform. Hysteresis (permanent displacement) was measured for each seal design during successive testing.

USE OF GYPSUM BASED PLASTERS IN MINE SEALING

Gypsum based plaster materials have been widely used for dry application spraying of stoppings and seals within Australian coal mines since the mid 1990s and these are intermediate in strength and stiffness between Portland cement based shotcrete and high yield grouts. Gypsum based products can either be manufactured from naturally occurring crystal Gypsum deposits, desert sand or synthetically from industrial processes such as a by product from the lime scrubbing of sulphur from power station flue gases (Germany).

Mitchell (Mitchell, 1971) reports studies in 1968 to develop bulkheads for mines in the United Kingdom and in the Ruhr and Saar districts of Germany. These studies resulted in the Gypsum bulkheads which withstood 1480 kPa (215 psi) and failed at 1790 kPa (260 psi) in explosion trials that developed impulses of up to 100 psi-seconds. At this time Gypsum was preferred by British, Czechoslovakian, and German coal miners who believed it to be the most effective, easiest to use, and least costly seal material. British miners used "Hardstem" and "Hardstop," which are proprietary products made by heating ground Gypsum under controlled conditions, mixed with water and wet pumped in between two form walls.

These materials have fast set times allowing high-speed building. Strength gain is rapid with 70% of the 28 d strength being gained in the first 24 hours. Unlike cement based materials, Gypsum based plasters expand on setting. Sprayplast UW used in the explosion tested seals is highly resistant to wet-dry cycles with only 3% water absorption measured in 28 d of submersion. Uniaxial compression tests on six 50 mm diameter x 100 mm length cores (Refer to Figure 1) show the average strength of Sprayplast UW is significantly stronger than Gypsum plaster product live tested by Tecrete Industries (Pearson, 1999).

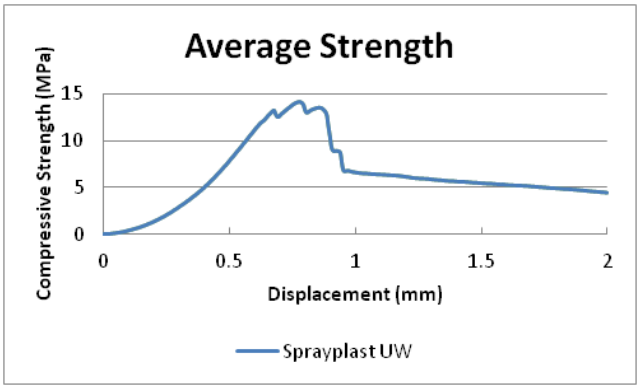

Figure 1 - Compressive strength versus displacement

EXPLOSION TESTING OF SPRAYPLAST UW SEAL DESIGNS

Two designs of ventilation seal were subjected to natural gas-air explosions inside the TestSafe Explosions Gallery to determine their ultimate explosion resistance and measure the structural response of each wall to transient explosion loads. To provide a wide enough range of data for designing 20 psi (138 kPa) and 50 psi (345 kPa) seals firstly a 150 mm nominal thickness wall was constructed and tested and then a 100 mm nominal thickness wall was built.

DESCRIPTION OF SEAL DESIGNS

The seals were erected within a circular 2.7 m diameter tunnel (Gallery) of high strength concrete pipe, about 10 m from the closed end of the Gallery. The Gallery has a flat concrete floor that reduces the maximum available height to 2.4 m. (See Figure 2 for Gallery layout).

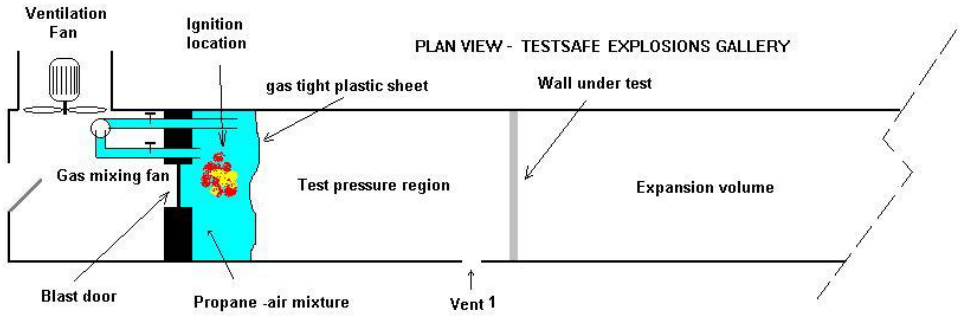

Figure 2 - Schematic plan view of test configuration (Pearson, 2012)

The inner surface of the seal site was prepared by jack hammering so as to provide a rough surface for the grout to adhere to, simulating trimming a normal roadway seal key back to solid material. Three vertical telescopic steel poles were spaced approximately 1000 mm apart (See Figure 4) and were held onto the shell of the Gallery with "Dynabolts". The 1170 mm width sheets of Tecmesh^{TM} were overlapped by 100 mm and attached to the steel telescoping poles using zip ties, forming an in-plane vertical formwork wall. The sheet edges of Tecmesh^{TM} were attached to each other by wire crimps using closing pliers.

Sprayplast UW used for both 100 mm and the 150 mm designs was sprayed onto the backing formwork with a Reed Sova pump using the dry application shotcrete process.

Nine thickness indicators were evenly distributed over the formwork for each seal using 16 mm I.D black pipe with a 40x40x3 mm steel backing plate as a guide to guarantee a minimum sprayed thickness. (See Figure 3).

Prior to testing, both seals were exposed to about 150 mm depth of water at their bases due to leakage into the gallery. Each seal was subjected to explosion pressures incrementally until structural failure occurred.

Figure 3 - Depth indicator attached to Tecmesh sheet formwork

Figure 4 - Formwork for 100 mm seal

MONITORING STRUCTURAL RESPONSE-EQUIPMENT AND METHOD

As in a previous test program at LLEM (Weiss, *et al*., 1999) both seal designs were instrumented to measure response to transient loads in order to provide data for FEM calibration.

Explosion overpressure (Pearson, 2012) was measured using RS type 461-373 pressure transducers. These had a working range of zero to ten bar and an output voltage range of zero to five VDC.

The deflection of the seal under the applied load was also measured using RS - "Miniature linear motion position sensors". These had a range of 38.1 mm and operate on the principle of variable resistance actuated by a spring loaded push rod. These were held rigidly in place on a steel frame which was itself Dyna-bolted to the interior of the gallery (See Figure 5). One sensor was located at the approximate centre of the seal and another approximately half way to the edge from the centre. Data sampling these devices for all except tests 1-3 was at a rate of 1000 scans per second. During each test, time related pressures and seal deflections were recorded at this sample rate.

A portion of the Gallery was partitioned off with a plastic sheet held in place with plastic conduit. The edges of the plastic sheet partition within the Gallery (See Figure 6) were sealed against the inner wall of the Gallery using rapid setting expanding polyurethane foam. Once the blast door was closed and sealed, natural gas was mixed into this volume with a target concentration. Once this concentration was achieved the gas supply and mixing fan were isolated and the explosive gas mixture ignited remotely.

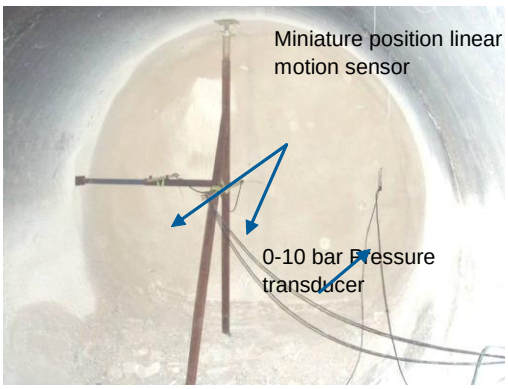

Figure 5 - Layout of instruments for measuring structural response

Figure 6 - Plastic curtain to seal gas volume

The volume of the gas/air mixture was increased incrementally over several tests on order to change the applied explosion overpressure and ultimately cause the seal to fail.

TEST RESULTS

There was no air leakage found through the seals during the test series. No discernible cracks were visible within the body of the seals before final failure. Results of the explosion testing are found in Table 2 (Pearson, 2012).

Table 2 - Explosion test data showing seal pressure and deflection

Test Number	Seal Thickness	Peak Pressure kPa (gauge)	Initial Side Position	Peak Side Deflection	Final Side Position	Initial Centre Position	Peak Centre Deflection	Final Centre Position
5	150	66	0.40	1.20	0.40	0.75	2.35	0.80
6	150	136	0.38	2.05	0.40	0.70	3.85	0.92
7	150	175	0.38	2.55	0.45	0.88	4.85	1.00
8	150	222	0.42	3.54	0.62	1.00	7.20	1.40
10	150	250	0.76	4.50	1.00	1.70	9.40	2.30
11	150	330	0.84	NA	NA	2.10	NA	NA
12	100	50	0.00	1.47	0.05	0.00	2.05	0.06
13	100	160	0.05	6.20	0.70	0.05	9.90	1.15
14	100	214	0.50	NA	NA	0.90	NA	NA

A typical plot is shown for Test 13 of the 100 mm seal design shown in Figure 7 where peak centre deflection is 9.9 mm and final centre position is 1.15 mm indicating a minor amount of permanent deformation.

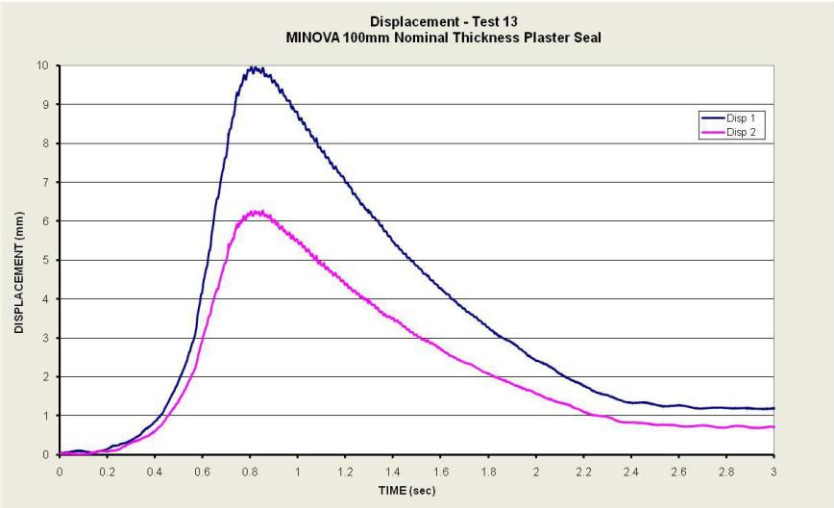

Figure 7 - Seal displacement versus time in Test 13

STRUCTURAL DESIGN ASPECTS OF SEALS

Minova Gypsum plaster stoppings have previously been full-scale blast tested at Londonderry Occupational Safety Centre (Pearson, 1999) at Londonderry, NSW using pressures up to 48 kPa (7 psi). The results from these tests together with a literature review which includes research papers from ACARP indicated that Gypsum plaster is a suitable material for construction of rated seals but unfortunately there is no recognised method for design of these seals from engineering first principles. There are no design standards such as AS3600 (Concrete structures) that give guidance on Gypsum based plasters as a construction material despite the fact that as a cost effective product it is used for low cost dwellings in developing countries of the world.

Extrapolation of low blast pressures and thin stopping thicknesses to provide designs to much higher pressures such as 140 kPa and 345 kPa (20 and 50 psi) is fraught with danger. Large factors of safety (more correctly termed "factors of ignorance") have been applied previously to Gypsum plaster seal

designs and the increasing requirement of engineering Certification of stoppings and seals has lead to this Gypsum plaster seal testing program.

To keep the testing as close to typical underground mine conditions as possible within the constraints of the Londonderry testing facility, seal thicknesses of 100 mm and 150 mm were selected. These gave parametric "strength" ratios (height to thickness) of 24 and 16 respectively. Assuming that a 140 kPa plaster seal will be 200 to 300 mm thick and that a 345 kPa plaster seal will be 400 to 500 mm thick and that mine roadway heights can vary from 2.4 m to 4.2 m high, then the expected height to thickness ratios for actual mine seals will be in the range of 10 to 20, which is a reasonably good match.

The Londonderry testing setup, as previously described, was for a circular shape seal so that the maximum blast pressure available could be used for testing. Previous tests at Londonderry have tested rectangular shape seals but the asymmetric test configuration due to structural limitations in the gallery limits the blast pressures to approximately 70 kPa, which would be insufficient for the proposed tests. To convert the test results from circular seals to a useable form for the rectangular seals typical in underground mines, the approach used was to create a 3D computer finite element model of the circular seal and calibrate the material properties to those actually achieve during blast testing. The material properties could then be applied to a model with typical roadway dimension e.g. 3 m high x 6 m wide and a safe thickness determined for any overpressure as required.

One advantage of the Londonderry test and instrumentation setup was that a continuous set of pressure and deflection values were available for each test and these proved to be very interesting when plotted for each test. (Refer to Figure 8)

Only two seals were constructed, but each was subjected to multiple explosions and the results show a number of interesting features:

1. Hysteresis. The seals did not appear to exhibit classical elastic behaviour but instead showed permanent deformation after each test. This incremental permanent deformation was typically 5% of the peak deflection experienced at the centre of the seal during each blast. This possibly indicates a degree of internal damage or fine cracking that was not evident from visual inspection and is a reaction to very rapid loading during each explosion. This can be seen in the pressure-displacement data where the same seal follows different pressure-time curves in successive tests as shown in Figure 8.

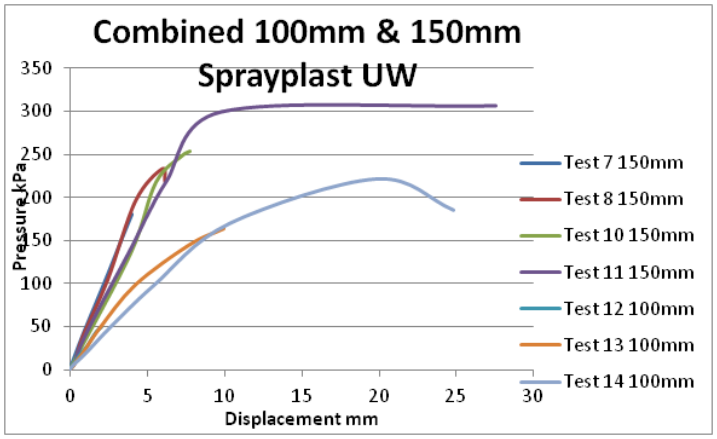

Figure 8 - Pressure versus displacement at seal centre

2. Each successive test at increasing pressure appeared to cause very little more permanent deformation when considering the increased pressure of each blast.
3. The bending mechanism is exhibited in stoppings with low aspect ratios as shown in Figure 9. The material stiffness of the 100/mm thick seal appeared to be less than the material stiffness of the 150/mm thickness seal taking into account the different bending stiffness's, which in this case differ by a factor of 3.4. The difference can be accounted for by the "arching action" of the thicker seal (Refer to Figure 9 for arching mechanism), where a proportion of the load is carried by direct compression through the seal rather than by bending (Parsons, *et al.,* 2000), as illustrated in Figures 8 and 9.

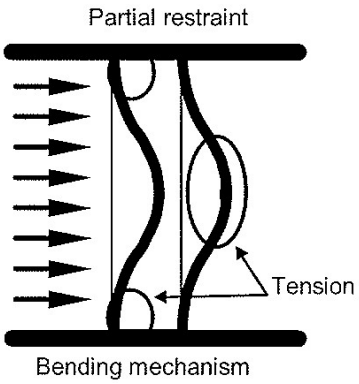

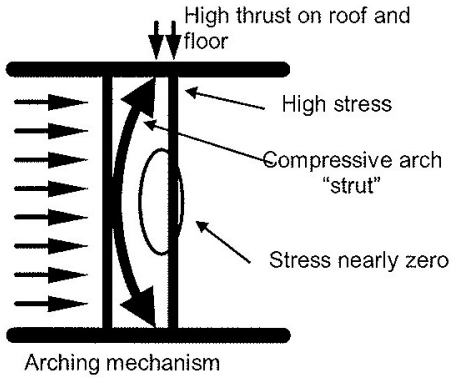

Figure 9 - Bending mechanism

Figure 10 - Seal arching mechanism

(For Figures 9 and 10 refer to Pearson, *et al.*, 2000)

The results of the full-scale testing have allowed the development of a simple design tool for estimating thicknesses for any roadway size and for any design pressure. In order to simulate the seal test results a numerical model of each seal within the 2.7 m diameter Londonderry tunnel was compiled. Figure 11 shows a deflection plot of a seal within the gallery tunnel.

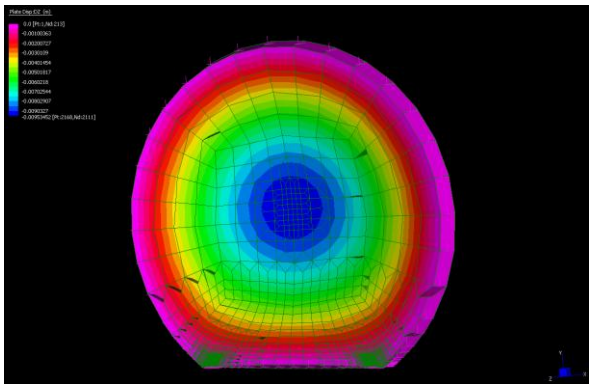

Figure 11 - Peak Londonderry seal deflection during a blast

From the calibration of this model, the designer is able to extrapolate to build a model of 20 and 50 psi explosion rated seals in a range of dimensions typically found within mine roadways. A seal displacement plot for a mine roadway with a rectangular shape is shown in Figure 12.

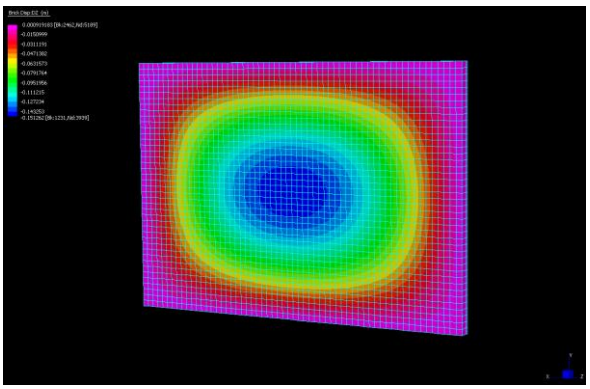

Figure 12- Peak mine seal deflection during a blast

If a mine requests a specific factor of safety to be applied to say a final seal, then this can be accommodated by designing the seal using a blast pressure equal to the design pressure of x factor of safety. For example, final seal design pressure 345 kPa and a factor of safety of three results in a total design pressure of 345 x 3 = 1035 kPa (150 psi).

ASSESSMENT OF DYNAMIC FACTOR APPLICABLE TO FULL-SCALE TESTS

The gas/air mixture used in the testing produced a relatively slow rise-time explosion, when compared with commercial high explosives. This type of explosion closely simulates actual underground coal mine gas explosions and subsequent coal dust explosions. The rise time for the explosions was in the order of 0.8 to 1 s. The natural frequency of the tested seals has been calculated as follows, for their first mode of vibration:

Seal Thickness (mm)	Blast Pressure (kPa)	Pressure Rise Time (ms)	Seal Natural Period (ms)
113	164	750	15
163*	250	1000	13

*Note that this thickness is an estimate, assuming that the 150 mm nominal seal was constructed 13 mm thicker as the 100 mm nominal seal

In both cases, it can be seen that the natural periods of vibration of the seal was substantially shorter than the rise time of the explosions. This means that the seals had time to fully absorb the pressure loading and in effect the pressure experienced was equivalent to a static load. So the pressures experienced during the tests were "actual" pressures and the "dynamic load factor" can be taken as 1.0. For the purposes of structural design, the loads are considered to be "ultimate" loads using terminology from Australian Standards and the design thicknesses derived from these test results are said to have a "safety factor" greater than 1. Using Australian Standard AS1170.0 notation the equation is:

$R^*/S^* > 1.0$

Where R^* is the ultimate strength of the seal and S^* is the design blast pressure.

Using a calibrated engineering model, the calculated seal thickness can sometimes be quite thin for low roadway heights. In such cases, it is recommended that minimum seal thicknesses should apply and that any design methodology should have such safety considerations included.

For example, for 140 kPa seals a recommended minimum thickness is 300/mm for all but the lowest heights and for 345 kPa, 450 mm is recommended. These minimum thicknesses provide a degree of robustness to the seals, which enables them to withstand accidental vehicle impacts and even unforeseen water pressure.

Seal thickness and type can be governed by the need to satisfy the requirement to provide an effective barrier after the effects of roadway convergence and an increased leakage path length.

Using the results from modelling of the seal explosion tests it has been possible to reduce a 20 psi explosion rated seal thickness from 450 mm to 300 mm in roadways heights up to 3.6 m within a 6 m maximum width mine roadway.

Another application for Gypsum plaster seals is as water-retaining bulkheads. The gypsum is typically blended with cement and other additives to make it water resistant but without losing its rapid-setting qualities. Tests have shown that this product will only absorb ≈ 3% moisture and it does not shrink during its period of strength gain. With the full-scale testing results now available, Gypsum plaster seals can confidently be designed to retain high heads of water of 30 m (equivalent to 300 kPa pressure) or more. With bulkheads and other water retaining structures such as dams, the type of load on the structure is quite different from a blast load. Water pressure is a continuous pressure that may last for the life of the mine and over time it may soften the strata surrounding the bulkhead and compromise its safety. To account for the long-term loading effects of water, it is recommended that a minimum factor of safety of two should be applied to water retaining bulkheads and some mines currently require factors of safety of up to four for combined explosion rated seals/bulkheads.

When considering the factors affecting the structural integrity of a ventilation control device such as a seal or stopping or a water control device such as a bulkhead, it is important to understand that engineering design of the device itself is only one link in a chain of requirements. Every one of those requirements is equally important because just as the weakest link determines the strength of a chain then a deficiency in any of the six factors outlined below will lead to a loss of structural strength of the seal. Particularly due to the erosion and strata softening potential of water, it is recommended that a program of pre and post injection be carried out at bulkhead sites that will be subject to ten or more metres of water head:

1. Geology. The device must be located in a region of sound material. More specifically, it should not be located in a weak or heavily faulted zone. Bulkheads should be located where the surrounding strata will be able to withstand the expected water head without piping (loss of material from the strata) or infiltration past the device.
2. Site and preparation. The device must be located away from intersections for a sufficient distance the strength is not compromise. All soft, loose, crumbly and otherwise unsuitable material must be removed to provide a sound base all around the device. For bulkheads, this generally includes cutting a "keyway" into the roof, ribs and floor to provide additional security and water sealing.
3. Design: The device must be designed by a competent engineer, experienced in design of VCDs and bulkheads and using proven methodologies. A signed design certificate should clearly state the design parameters adopted.
4. Materials: The materials used must be of the highest quality and suitable for the task. Records such as batch numbers must be provided with each consignment to provide full traceability in the event that defective material is discovered at a future time.
5. Construction: The device must be constructed strictly in accordance with the Engineering Certification and any drawings, specifications or construction notes should be provided by the designer and the material supplier. The most common construction defect of sprayed plaster devices is insufficient thickness. Depth gauges must be used to confirm the sprayed thickness and a sufficient quantity of product must be on hand before construction commences to complete the device, to provide another means of checking that the required thickness has been achieved.
6. Maintenance: Sometimes overlooked, a mine manager and ventilation officer has an on-going obligation to regularly inspect all ventilation control devices and bulkheads to ensure that they are continuing to perform as expected. Issues such as convergence, accidental damage and latent defects in the seal or strata can cause major problems if they are not picked up early.

CONCLUSIONS

The 100 mm seal that withstood a 160 kPa explosion, was destroyed during a 214 kPa explosion. The 150 mm seal withstanding a 250 kPa explosion, was destroyed during a 330 kPa explosion.

Tests have shown that Sprayplast UW seals will withstand scaled explosions within the pressure range required by Australian coal mine legislation. This explosion test program adds to a series of programs in which seals and stoppings since 1991 have been designed from the results of live explosion testing.

There is no accepted or universal guideline within Australia to assist registered professional engineers in the design of VCDs for the underground coal industry. However he "final rule" developed by MSHA provides thorough guidance.

Instrumentation showed that the seal response provided under explosion loading behaved in accordance with commonly accepted structural theories. Results from testing were consistent with the Tecrete results of 1999 testing of Gypsum based plaster stoppings. A computer model which can to be used to design seal thickness for a variety of roadway geometries and design overpressures based on results of live testing has been developed. Seal designs provided by numerical analysis have to be correctly sited, constructed and maintained in order to ensure their long-term effectiveness.

ACKNOWLEDGEMENTS

We would like to thank Minova Australia for giving permission to publish this paper. The assistance given by David Joyce, Chris Lukey and Minova Operations during the construction of the seals and explosion testing was fundamental to the success of this research. Special thanks also go to David Pearson of Testsafe, Workcover NSW for his contribution and leadership.

REFERENCES

Pearson, D, 1999. Explosion pressure tests on "ventmine" plaster stoppings. Londonderry Occupational Safety Centre, NSW. (Internal Report).

MSHA website ventilation seal reference: http://www.msha.gov/Seals/SealsSingleSource2007.asp.

Zipf Jr, R K, Mohamed, K M and McMahon, G W, 2010. Design and analysis of a new method to test mine seals. National Institute for Occupational Safety and Health (NIOSH), Pittsburgh, Pennsylvania USA.

Taylor, G, Safety Bulletin No. 107, Mine Seals, Mines Inspectorate, Queensland.

Weiss, E S, Cashdollar, K L, Mutton, I V S, Kohli, D R and Slivensky, W A, 1999. Evaluation of reinforced cementitious seals. *Report of Investigation 9647,* National Institute for Occupational Safety and Health, Lake Lynn Experimental Mine, PA.

Mitchell, D W, 1971. Explosion proof bulkheads-present practises. Pittsburgh Mining and Safety Research Centre, Pittsburgh, PA. *Report of Investigation 7581.*

Pearson, D, 2012. Explosion testing of sprayplast UW gypsum based plaster seal designs. *Testsafe Report No: TR 33828a* (For Minova Australia Pty Ltd).

Pearson, R D, Gillies, A D S, Green, A R, Day, R and Dux, P, 2000. Evaluation of a full scale pressure test for ventilation control devices. *ACARP Project No: C8006*, Testsafe Report No: TR 20815.

DESIGN AND FIELD TRIALS OF WATER-MIST BASED VENTURI SYSTEMS FOR DUST MITIGATION ON LONGWALL FACES

Ting Ren[1], Shivakumar Karekal[2], Graeme Cooper[3], Zhongwei Wang[1] and Brian Plush[1]

ABSTRACT: Dust generation from longwall chock movement and the Beam Stage Loader/crusher (BSL) is a major source of air contamination on modern longwall faces. If not controlled effectively, much of these respirable dust particles would disperse quickly into the longwall due to high face ventilation velocities, contributing significantly to higher dust levels. A new water mist based venturi system has been developed for the purpose of suppressing respirable dust from longwall chock movements close to the maingate (MG). The unit is powered by compressed air and water using an ultrasonic nozzle embedded in a venturi body. The ultrasonic nozzle is capable of producing ultra fine water mist with droplet sizes ranging from 1 to 100 µm. Laboratory tests indicate that the ultrasonic nozzle (MAL-1300-B), when combined with a 70 mm (diameter) x 143 mm (length) venturi body, was can produce an optimum spray covering a distance over 10 m. Further tests show that a combination of air supply at 6 bar and water at 4 bar produces the optimum water mist thrust with inducted air velocity over 8 m/s. The venturi system was built as a stand alone unit using fire resistant and antistatic materials and can be easily hooked under the chock canopy with a magnetic base. The system can be powered by compressed air and water supplied to the longwall face and adjusted with the spray angle to achieve the droplet size and velocity needed for dust suppression and diversion. Computational Fluid Dynamics (CFD) modelling was undertaken to gain a better understanding of face ventilation and dust flow patterns to optimise the spray orientation of the venturi system for field trial installation. CFD modelling results show that the operating conditions of sprays with the best mitigation performance vary according to the source of dust, a better dust mitigation effect can be achieved when the venturi units on longwall chock are installed at 20° down towards the floor and tilted 45° along the face. Field trials were conducted at two underground longwall mines in QLD and NSW. Three venturi units were installed on Chock No 6 on the longwall with an additional unit trialled at the BSL to mitigate dust from longwall outbye. Dust measurements with real time monitoring Personal Dust Monitor (PDM) and gravimetric samplers indicate dust mitigation efficiency up to 30% has been achieved in both trials.

INTRODUCTION

Respirable dust particles can be generated from several sources on the longwall, primarily shear cutting, chock movements, BSL and intake contaminations. As the supports are lowered and advanced, crushed coal and/or roof rock drops from the top of the canopy into the air flow on the longwall face. As a result, chock movements can be a significant source of respirable dust for shearer operators when chocks are advanced upwind of the shearer during a maingate to tailgate cut.

Gillies and Wu (2007; 2008) conducted extensive real-time respirable dust monitoring and baseline surveys on Australian longwalls. During the cutting sequence from Maingate (MG) to Tailgate (TG), 1-5 MG Chocks were advanced immediately after the shearer passed. This action leads to dust falling from the advancing chocks; dust levels registered by both PDM units were increased significantly, accounting for about 47.8% of total longwall dust make at the Shearer MG operator's position during the cutting cycle. Similar observations have also been reported at other mines in Australia. The dust baseline survey results demonstrated the importance of reducing respirable dust generated from the movement of MG chocks thereby significantly mitigating total dust make to the longwall face. Dust monitoring also showed that the BSL can be another major dust contributor, even for longwalls equipped with a BSL dust scrubber. Dust surveys indicated that the scrubber can cleanse only a portion of the air travelling to the face, allowing a high proportion of the dust particles to escape over the BSL and to end up on the longwall face, increasing the threshold dust levels in the ventilation air.

[1] *University of Wollongong, tren@uow.edu.au, Tel: +61 2 4221 4186*
[2] *CSIRO Earth Science and Resource Engineering*
[3] *Tecpro Australia*

Water sprinklers/hoses are widely used for dust control on longwalls to suppress the dust particles before they become airborne. However, conventional hydraulic water sprays are not effective on respirable dust. With typical diameters of 200-600 µm sprays, the droplets are much larger than the dust particles they are attempting to suppress. Water drops that are too large will not collide with the finest, most hazardous dust particles smaller than 10 µm. The attraction of water droplets and dust particles is most likely to occur when their dimension is of similar size.

With the support of ACARP, a new type of venturi system based on ultrafine water mist technology has been developed to reduce respirable dust contamination on medium and thick seam longwall faces, particularly those dust particles from the advancement of MG chocks and the intake ventilation passing the BSL. The venturi system was initially fabricated and tested in the laboratory and field trialled near the MG chocks in two longwalls extracting medium to thick seams. Detailed CFD modelling studies of the airflow dust particle dispersion patterns from MG chocks and the BSL was conducted to determine the optimum positioning of the water mist venturi unit(s) for effective dust control. System performance was evaluated in terms of Dust Mititigation Efficiency (DME) in two underground coal mines. This paper describes the design, laboratory testing, CFD modelling and the field trial results of the water mist based venturi units for longwall dust mitigation at two underground coal mines.

DESIGN OF A WATER MIST BASED VENTURI SYSTEM

Several industrial processes need the atomising of liquids into fine and very fine droplets. In the majority of industrial processes a fine liquid atomisation can be obtained by means of air assisted atomisers, where compressed air supplies the required energy to break the liquid and to throw the droplets at a given distance from the atomiser. Ultrasonic atomisers produce the finest sprays available with air assistance for industrial processes such as dust suppression. Water and air do not mix in a confined volume before leaving the nozzle and therefore their feed pressures can be adjusted independently without influencing each other. This allows for a very wide regulation range on the liquid capacity and makes it easier to reach the desired operating conditions. Figure 1 shows a typical ultrasonic nozzle and the fine mist produced by such a device.

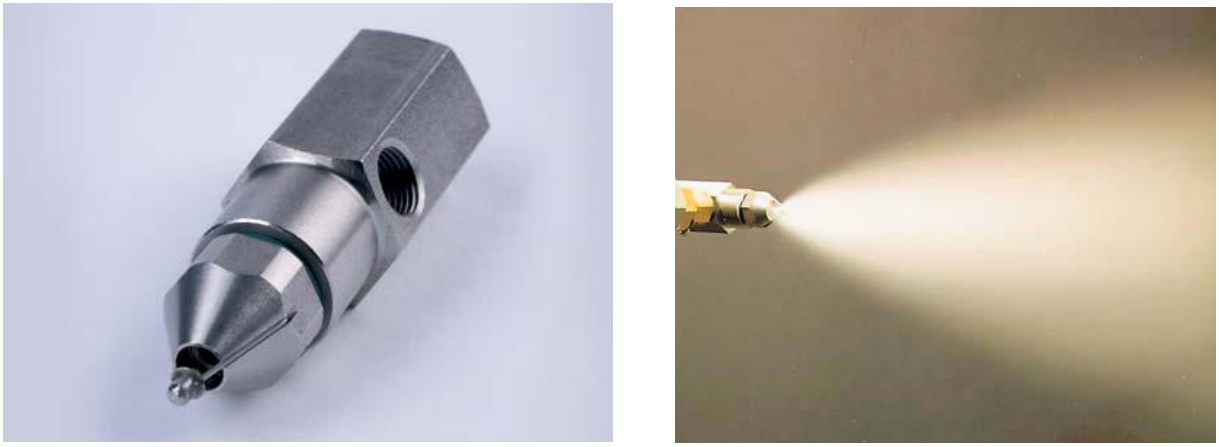

Figure 1 - A typical ultrasonic nozzle and the fine mist produced

Venturi apparatus has been used in many industry processes. As fluid flows through a length of pipe of varying diameter, the velocity of the fluid increases as the cross sectional area decreases, and the static pressure correspondingly decreases. According to the laws governing fluid dynamics, a fluid's velocity must increase as it passes through a constriction to satisfy the principle of continuity, while its pressure must decrease to satisfy the principle of conservation of mechanical energy. A venturi can therefore be used to mix a liquid such as water with gas or air. If a pump forces liquid through a tube connected to a system consisting of a venturi to increase the liquid speed, the diameter decreases, a short piece of tube with a small hole in it, and last a venturi that decreases speed (so the pipe gets wider again), the gas or air would be drawn in through the small hole because of changes in pressure. At the end of the system, a mixture of liquid and gas would appear. Therefore by embedding an ultrasonic nozzle with a venturi apparatus, a water mist venturi system can be built.

Considering the limited space when a chock is lowered, the unit had to be compact enough to leave enough clearance between the AFC and any spalling coal lumps so that the units could avoid being

knocked off or damaged after installation. At this stage, it was designed to be operated manually following the movements of the MG chocks but with the potential of being integrated into the longwall automation system should the system prove effective and robust after the field trials.

Figure 2 shows a schematic layout of a prototype venturi developed in this project. The venturi system essentially consists of a water mist generating chamber incorporating mounting holes via which water and compressed air can be introduced to the ultrasonic atomisers to produce very fine droplets. Water is ejected through a number of orifices into the nozzle air outlet channel, where the high velocity air stream produces the first liquid breakup through a shearing action. The air stream, carrying the droplets, collides with a resonator placed in front of the nozzle outlet channel that generates a field of high frequency sound waves. Water delivered to the resonator is shattered into fine droplets which are carried downstream by the air by-passing the resonator. The system was designed to perform the following two functions:

- To produce uniformly distributed ultra fine water droplets for encapsulating and trapping a high proportion of the respirable dust particles before they become airborne and reach the walkway area.
- To induce a controlled volume of water-mist airflow with sufficient momentum for diverting and suppressing respirable dust clouds off the walkway area along the face.

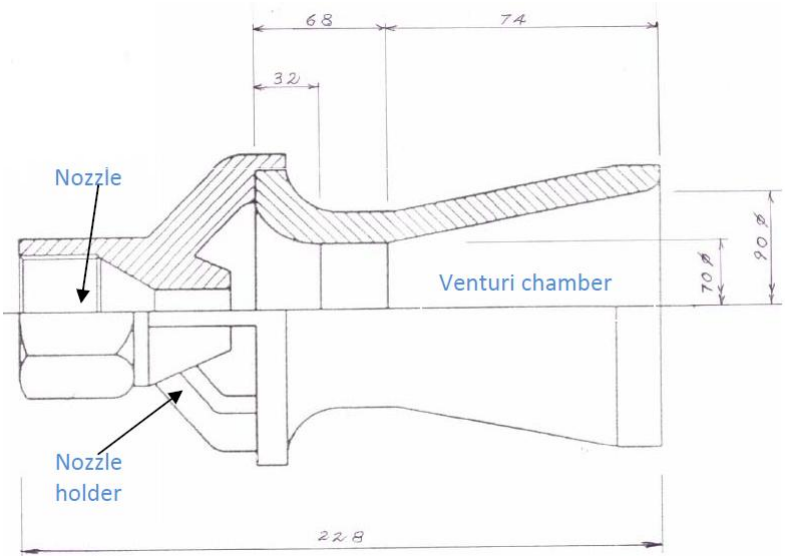

Figure 2 - A schematic layout of a prototype venturi (unit in mm, not to scale)

To achieve the above design requirements, comprehensive laboratory tests were carried out with different venturi chamber diameters (42 ~ 70 mm), venturi lengths, methods for mounting the ultrasonic nozzles, as well as air pressures (ranging from 2~8 bar) and water pressures (ranging from 1~6 bar). The ultrasonic nozzle holder assembly with different nozzles was used to test the best combination by varying the distances between the nozzle and the venturi to optimise the water mist production and air induction effect. Test results indicated that the 70 mm (diameter) x 143 mm (length) venturi was capable of producing an optimum spray coverage and spray distance of approximately 10~12 m in the underground environment. The ultrasonic nozzle used was MAL 1300 B1, as shown in Figure 3. Figure 4 shows the various parts of the venturi unit and laboratory testing process.

The novelty of this new system is its capability to draw air into the chamber to carry the atomised droplets downstream with sufficient momentum for maximum dust particle attraction and controlled diversion away from the walkway area. In order to utilise the existing water and compressed air supply on the longwall face, the system was built as a stand-alone module with a magnetic base which can be easily attached to the chocks' canopy and adjusted with the right spray angle to achieve the droplet size and velocity needed for dust suppression and diversion.

Laboratory tests showed that having a ratio of 2:1 air to water seems to produce the best atomisation for the ultra fine water mist nozzle, i.e. if liquid pressure is 3 bar, ideal air pressure would be 6 bar. Water consumption at 3 bar liquid pressure and 6 bar air pressure would then be 2.15 L/min or 0.0358 L/s. The mist produced was of such a fine size that it remained airborne as a 'dry fog'. As the mist evaporated, it

had an evaporative cooling effect which, over a period of time, could effectively reduce temperatures on the longwall face. Further tests showed that at an air pressure of 6 bar and water pressure of 4 bar, the water mist produced by the venturi unit was found to travel over 8 m with inducted air velocity over 8 m/s. Water consumption in this case was about 2 L/min for a single unit. Figure 5 shows the air and water coupling pipelines and manifold regulating the first prototype water mist venturi systems for field trials.

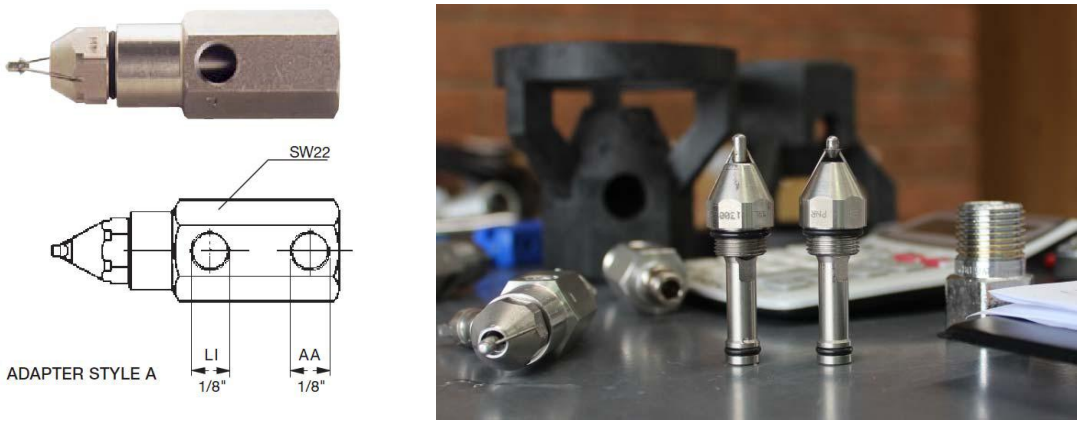

Figure 3 - Ultrasonic nozzles MAL 1300 B1 and MAD 1131 B1

Figure 4 - Design and testing of the water mist based venturi system

A complexity during the development of the venturi system was that all materials used for the unit have to comply with combustion propagation characteristics requirements of MDG 3006 MTR8.8.2.b and antistatic properties (electrical resistivity) requirements of MDG 3006 MTR8. 8.3, prior to any field trials in underground coal mines in NSW. Therefore a new material had to be sourced and tested by the Mine Safety Technology Centre, NSW Department of Trade and Investment. All the materials used for the final venturi units passed the required tests and satisfied the above requirements. Figure 6 shows the complete assembly of four venturi units using the Fire Resistance and Antistatic (FRAS) materials.

Figure 5 - Air and water coupling pipelines and associated manifold regulating the venturi units and the assembled first prototype unit for field trial

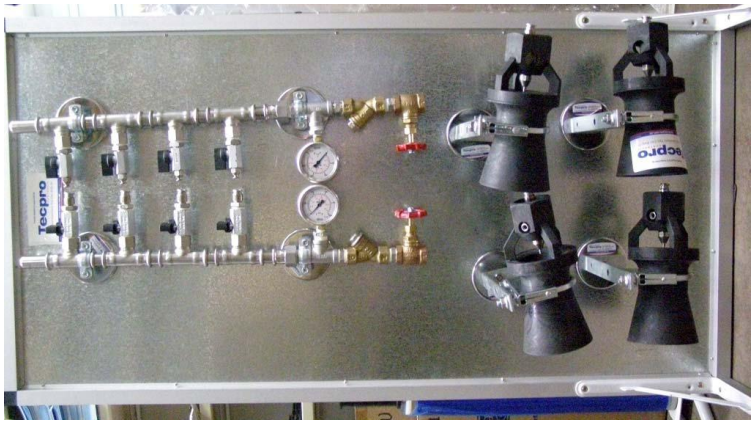

Figure 6 - An assembly of four venturi units made up of fire resistance and antistatic (FRAS) material

CFD MODELLING OF DUST DISPERSION FROM MG CHOCKS AND BSL

CFD models

A major challenge in this study has been the understanding of the dispersion of dust particles from chock movement in the turbulent flows on the longwall face, and the optimum position of venturi units under the canopy to suppress and divert the dust clouds. CFD has proved to be capable of investigating a series of factor affecting the behaviour of longwall dust, such as the impact of ventilation, cutting sequence and local geological conditions (Ren and Balusu, 2005; 2010).

In this study, a full scale longwall face, with 103 chocks, shearer, AFC, BSL and belt conveyor equipped along the face and MG was built up in the design modeller under the Ansys 13 Workbench (2010) on the basis of information collected from a mine site. The longwall face has a physical domain of 156.5 m (face length) X 50 m (MG length) X 3.5 m (face cutting height), and the last cut through 45 m outbye the face. The longwall shearer was located 10 m away from the MG. The model was meshed using the tetrahedron method with over 1.8 million elements. Figure 7 is a snapshot of the longwall CFD model and computational mesh.

Base model simulations were carried out with a face airflow rate of 45 m3/s without the intervention of any dust controls. The base-case CFD models were calibrated and validated against field ventilation survey data and subsequently used for further parametric studies of the water mist venturi systems.

Modelling of water mist venturi

To optimise the position of the water mist venturi units on the MG chocks, the base CFD models were used to conduct parametric studies on a number of combinations of venturi positions along the MG chocks (1-6) and on the AFC/BSL plate, including:

1. With venturi attached the chock canopy, with

- Venturi at canopy level - towards the coal face;
- Venturi at canopy level but tilted along the face (10~45˚);
- Venturi tilted down and along the face.

2. With venturi stationed on the AFC/BSL plate, with

- Venturi spray towards the coal face;
- Venturi spray with angles along the face.

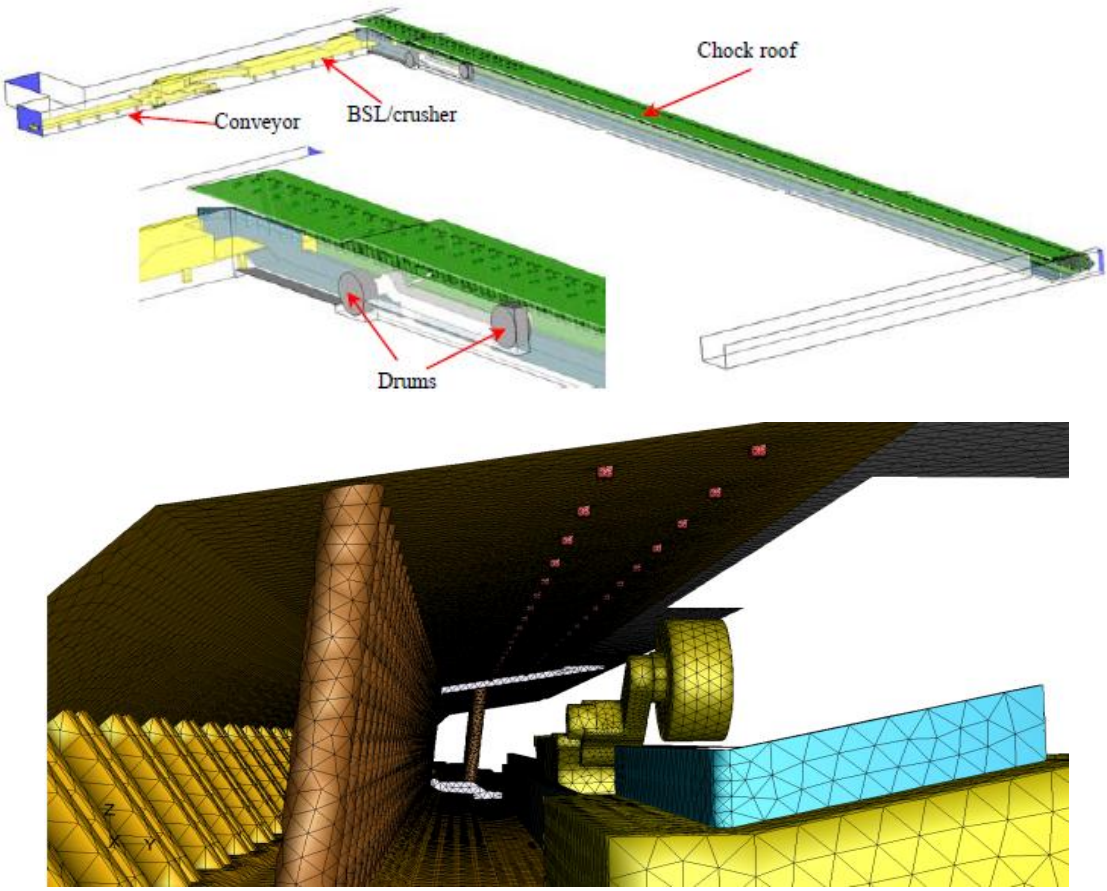

Figure 7 - Layout of the longwall CFD model and computational mesh

In all cases, the water mist injection was modelled as 'air spray' as much of the spray would be of compressed air with a small portion of fogged water droplets. This also avoids the complexity of modelling multiphase flow which would require much computing power and time. Figures 8 to 10 respectively show the impact of venturi units oriented at different locations on the diversion of dust particles from both MG chocks and the BSL transfer point.

CFD modelling results show that the operating conditions of sprays with the best mitigation performance may vary according to the source of dust. To achieve an overall good mitigation effect, it is suggested that sprays in the face should be operated at 20° down and tilted 45° along the face; sprays on the AFC/BSL spill plate should be operated at 30° towards the floor and 20° along face. Results from the CFD modelling were used to assist field trials of the newly developed water mist based venturi systems as described below.

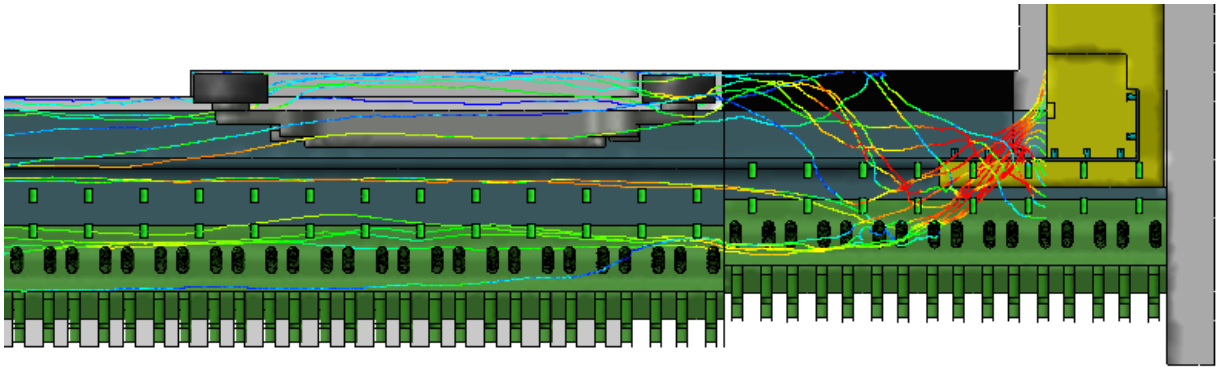

(a) Venturi units operating at level and titled 20° along face

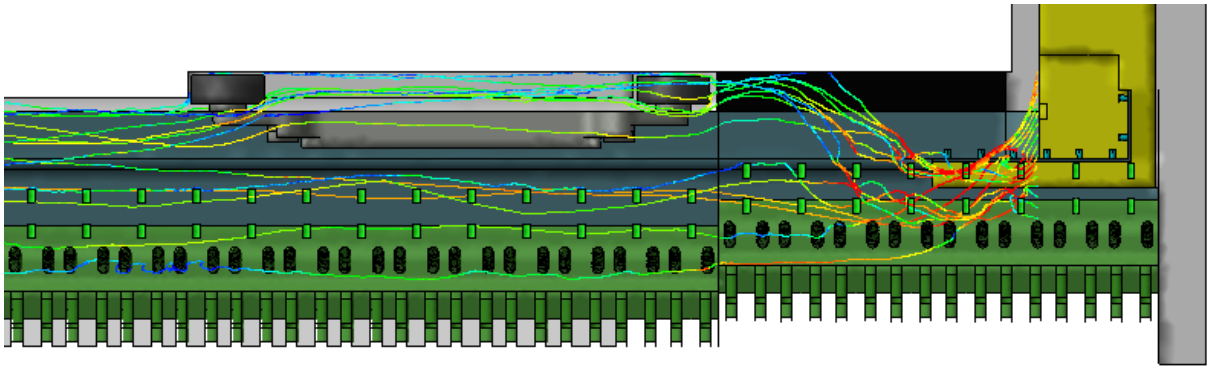

(b) Venturi units operating at 20° down and titled 30° along face

Figure 8 - Dust dispersion pattern with venturi units operating at different orientations - dust from MG chocks and BSL

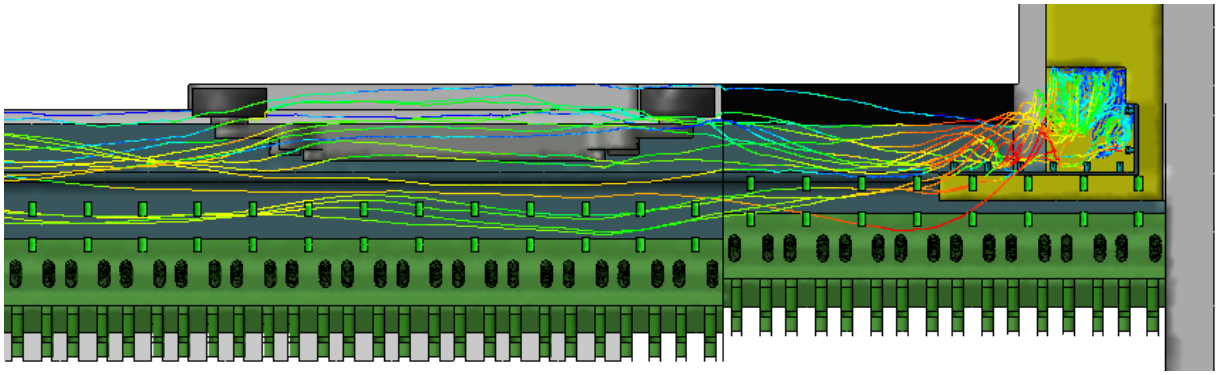

(a) Venturi units operating at level and titled 20° along face

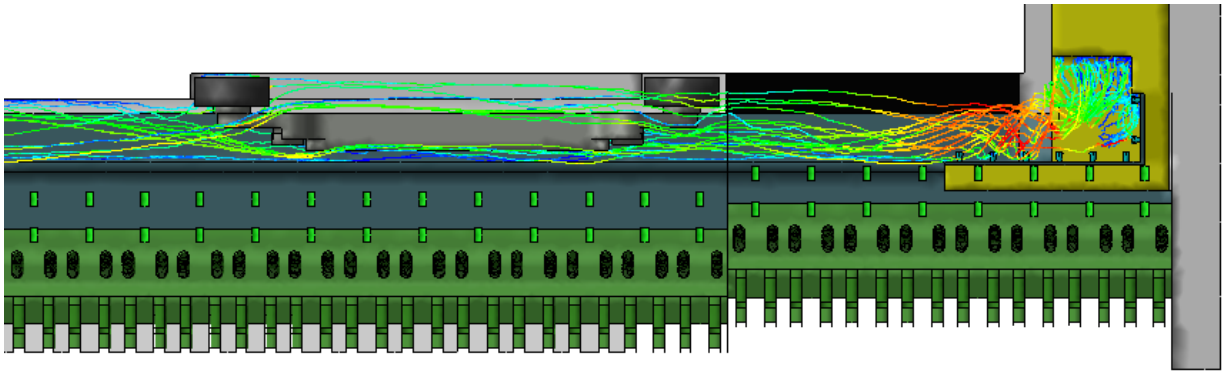

(b) Venturi units operating at 20° down and titled 30° along face

Figure 9 - Dust dispersion pattern with venturi units operating at different orientations at the spill plate - dust from BSL

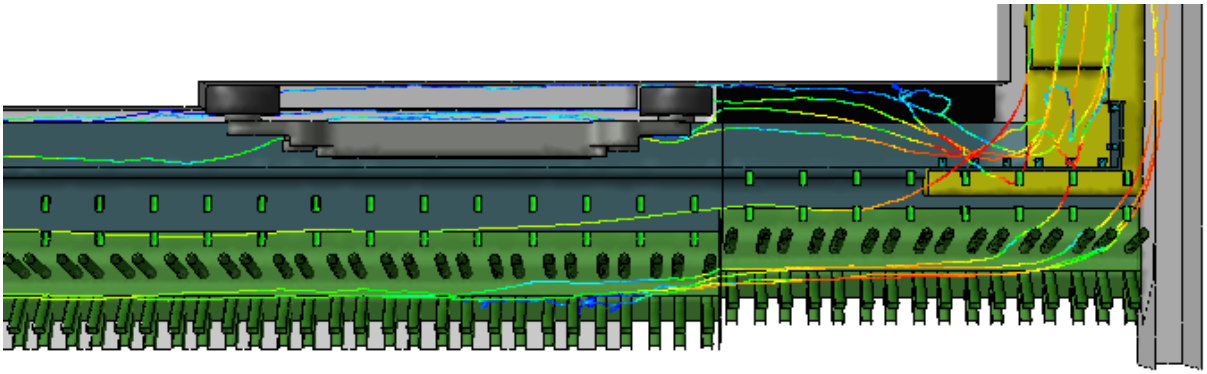

(a) Venturi units operating at level and titled 20° along face

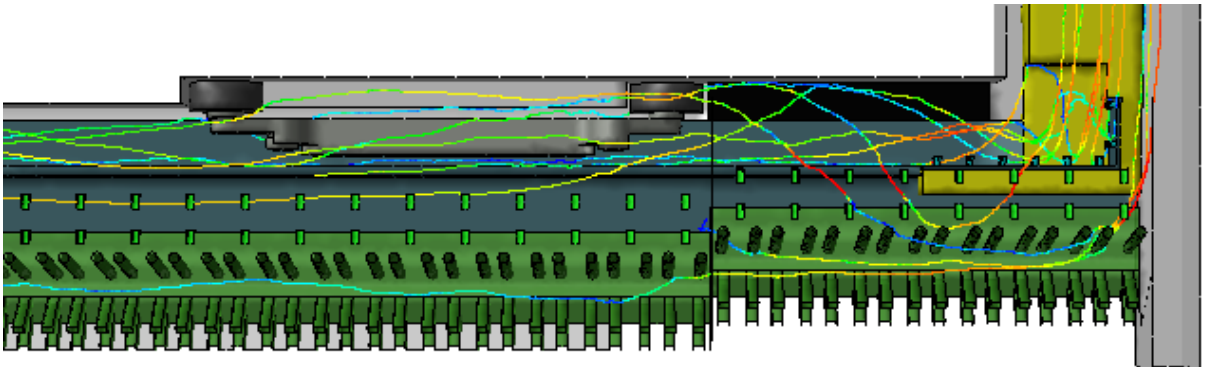

(b) Venturi units operating at 20° down and titled 30° along face

Figure 10 - Dust dispersion pattern with venturi units operating at different orientations - dust from BSL and outbye dust

FIELD TRIALS AND PERFORMANCE EVALUATIONS

Field trials at MINE A

The first field trials were conducted at a longwall face in the Bowen Basin, QLD. Wu Mining Technology Pty Ltd was commissioned by MINE A to undertake a real time dust survey on their production face to establish the improved longwall respirable dust situation during cutting operational cycles after the installation of a water mist venturi system. Figure 11 shows the face layout indicating the location of the water mist venturi system. The dust sampling was undertaken at MG Drive, Chock No 8 and shadowing shearer operators. Ventilation conditions and the position of shearer and manned position during cutting operational cycles were also recorded.

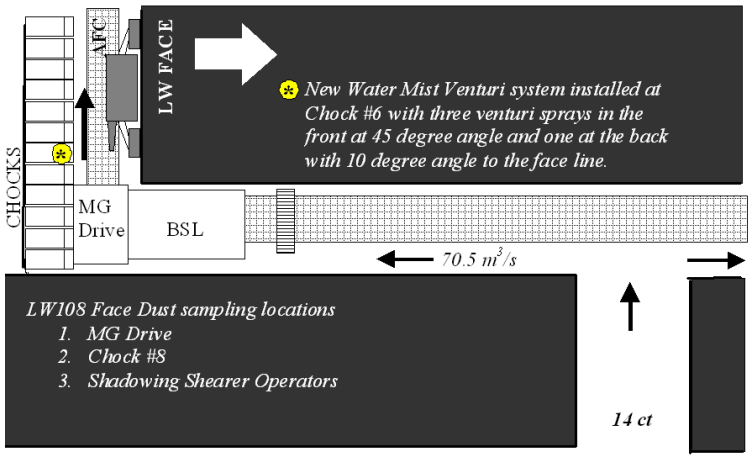

Figure 11 - Venturi units attached to the canopy of the longwall chock for field trials

Table 1 shows a summary of the test results on the effectiveness of the installed venturi system on dust mitigation. A comparison of the dust levels and dust made at the Chock No 8 (PDM stationary) and shearer operator (PDM shadowing) shows that the water mist venturi system has reduced the dust levels by 20~30% at Chock No 8 and 8~31% for the dust exposure levels of shearer operator.

Table 1 - A summary of test results from field trials at MINE A

Test cycle conditions (22 December 2010)	Average dust concentration at monitoring positions (mg/m^3)	
	Chock #8 position	MG shearer operator
Shearer cycle #1 sprays Off	0.24	0.93
Shearer cycle #2 sprays On	0.19	0.64
Dust reduction (%)	20.6%	31.3%

Test cycle conditions (23 December 2010)	Average dust concentration at monitoring positions (mg/m^3)	
	Chock #8 position	MG shearer operator
Shearer cycle #1 sprays Off	0.73	0.94
Shearer cycle #2 sprays On	0.51	0.86
Dust reduction (%)	30.5%	8.4%

Observations of field trial at MINE A

The mine management was happy to see the trial results and the longwall crew welcomed the venturi system. This initial trial demonstrated that the water mist based venturi units can be used to reduce dust contamination from longwall chock movements. During the trial period, the venturi units adequately cleared of the floor and other equipment and posed no interference to the longwall production process. This enabled the units to survive the longwall environment allowing its continued use for dust mitigation. A concern raised during the trial was the wetting of water mist. When the venturi units were turned on, the water mists can travel quite some distance (greater than 20 m) along the face and can wet the longwall operator(s). This problem could be avoid or minimised by positioning the units further under the canopy or by turning off the units once the advance of the first five MG chocks was completed. During the trials, the venturi units were turned on during the entire production cycle (even after the advance of first five MG chocks). These units were designed to be used only during the advance period of these MG chocks and they should be turned off once the chock movement is completed. This would avoid the wetting and visibility problems.

Field trials at MINE B

Field trials were conducted at MINE B in NSW along with dust surveys to evaluate the dust mitigation efficiency on the venturi units installed on the MG chock and BSL. A benchmark test was undertaken specifically designed to measure the amount of dust produced during shield movement in the maingate area as the longwall progresses with further sampling taken for venturi sprays installed at the maingate (BSL) and at Chock No 6. The longwall was vented with an air flow rate of around 45 m^3/s during the field trial.

Based on the trial experience at MINE A, four venturi units were delivered to MINE B and installed for field trials of which three units were installed on Chock No 6, and one unit on the maingate BSL. Figure 12 shows the installation of the venturi units on the BSL/maingate (Figure 12.a) and the longwall Chock No 6. As shown in Figure 12.b, these units were installed just under the canopy forehead and tilted along the face at angles between 15-20° down and 45° along the face, as indicated by CFD modelling. Air and water supplied to these units were around 6 bar and 3.5 bar respectively, with a water consumption of 2 L/min per unit (total of 6 L/min for three units). The induced airflow velocity at the outlet mouth of the venturi unit would be around 8 m/s according the lab test results, thus having some momentum for diverting and streamlining respirable dust clouds off the walkway area along the face.

(a) Venturi unit installed on the BSL in the maingate **(b) Venturi units installed on MG Chock**

Figure 12 - The installation of the venturi units on the longwall face

Dust Mitigation Efficiency evaluation

Dust Mitigation Efficiency (DME) was conducted according to AS2985 (Workplace Atmospheres - Method for sampling and gravimetric determination of respirable dust) using an approved universal pump and sample heads (Plush, *et al.*, 2012). The gravimetric sampling for exposure levels relies on a time weighted average to determine personal exposure levels of employees working on a producing face. The gravimetric heads would need to be changed during the testing process in order to measure dust loads generated firstly as a benchmark dust production of the operating longwall and then when the venturi sprays are operating. The weighed difference would indicate DME.

Figure 13 shows the dust production at different longwall chocks when the BSL venturi was off and on. The results show that this single venturi unit has reduced dust production along the longwall face between 5~13%.

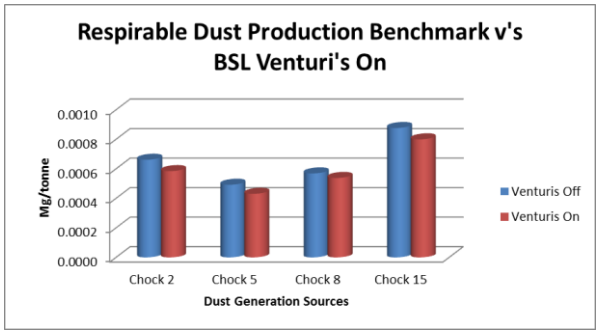

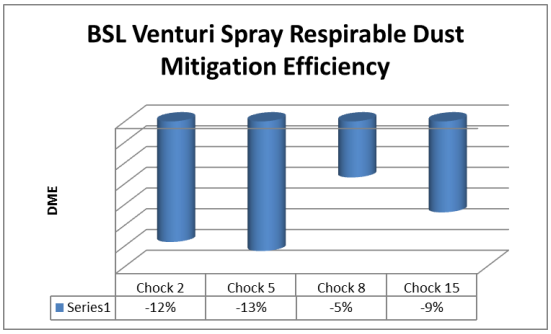

Figure 13 - Respirable dust production with BSL venturi system off and on

Figure 14 shows the dust production at different longwall chocks when the venturi units on Chock No 6 were off and on. The results show that dust reduction up to 27% on Chock No 8 has been achieved.

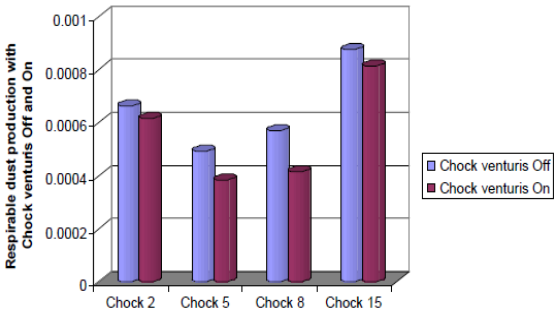

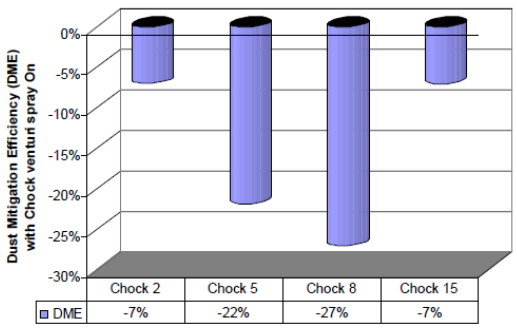

Figure 14 - Respirable dust production with venturi system off and on

Figure 15 shows the combined respirable dust mitigation efficiency. Overall dust mitigation efficiency up to 35% has been achieved at Chock No 5 and 16% down to Chock No 15. The results of the testing show that the venturi sprays have a significant effect on respirable dust in the maingate area, more specifically from Chock No 2 to Chock No 15. The BSL venturi saw a reduction of respirable dust by 12% at Chock No 2, 13% at Chock No 5, 5% at Chock No 8 and 9% at Chock No 15.

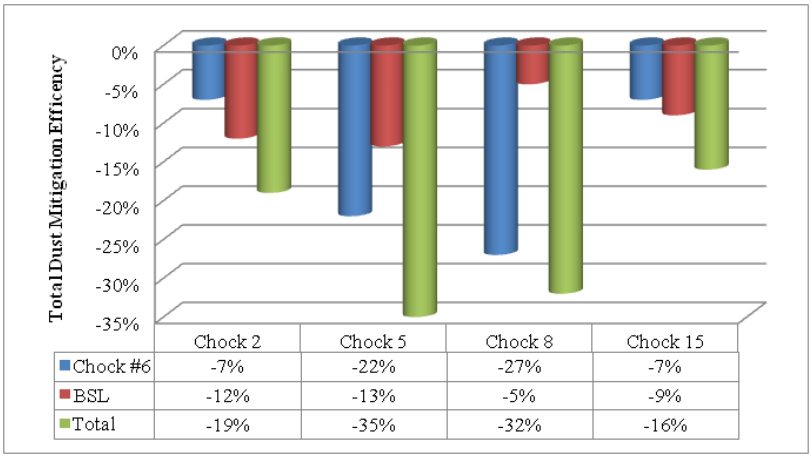

	Chock 2	Chock 5	Chock 8	Chock 15
Chock #6	-7%	-22%	-27%	-7%
BSL	-12%	-13%	-5%	-9%
Total	-19%	-35%	-32%	-16%

Figure 15 - Total respirable dust mitigation efficiency with both BSL and Chock No 6 venturi units operating

Field trial observations at MINE B

The management team at MINE B strongly supported the field trials during the entire project and was pleased to see the encouraging results. The longwall crew also welcomed the venturi system as a new tool for combating dust contamination on the longwalls. Field trials demonstrated that the design of the water mist based venturi units has been a success to reduce dust contamination from longwall chock movements and the maingate/BSL.

The positions of these venturi units, either on the BSL or MG chocks, are important in diverting and suppressing the dust clouds with minimum wetting issue on the longwall. The installation and adjustment of these units has been simple and straight forward without any disturbance to existing equipment or operation. Again these venturi units demonstrated their robustness and remained clear of the floor and other equipment without being damaged during the trials. However the issue of wetting by the water mist travelling along the face has been noticed during the tests. When the venturi units are turned on, the water mist can travels some distance along the face, and at some point, the water mist cloud would be more widely dispersed across the face. Although offering additional benefits of dust suppression and cooling, it does however have the side-effect of wetting and in some case, causing poor visibility.

This problem can be minimised by positioning the units further towards the front under the canopy or by turning off the units once the advance of the 1~5 MG chocks were completed. Again during the trials, the venturi units were turned on during the entire production cycle (even after the advance of 1~5 MG chocks). It should be noted that these units should be used only during the advance period of 1~5 MG chocks and be turned off once the chock movement is completed. This would avoid the problem of over wetting and potential visibility problems.

CONCLUSIONS

Longwall chock movements have been identified as a significant source of dust exposure to longwall operators when chocks are advanced upwind of the shearer during MG to TG cutting. Using the latest development of ultrasonic nozzle technology and CFD modelling results, a new water mist venturi system has been designed and field trialled successfully to mitigate dust particles from MG chock movements. Field trials at two underground longwall mines indicated a respirable dust reduction up to 30% when these units are installed on longwall Chock No 6 and BSL discharge point. Field observations proved that the design of the water mist based venturi unit is robust and safe to use in underground coal mines for dust mitigation. Further trials are needed to improve its operation and eliminate face wetting by incorporating the venturi operation into the longwall automation system. The potential for the application

of this technology in other areas of mining are enormous, particularly in underground coal mines and hard rock mines. Such units can be deployed for dust mitigation in roadway drivage heading, tunnelling, surface stockpiling and mineral processing plants.

ACKNOWLEDGEMENTS

The authors are grateful to ACARP for funding the research work presented in this paper, and the strong support from many mines for the development and field trials of the venturi systems, particularly Broadmeadow, Moranbah North and Metropolitan mines.

REFERENCES

Gillies, S and Wu, H W, 2007. Mine real time personal respirable dust and diesel particulate matter monitoring, Proceedings, *Queensland Mining Industry Health and Safety Conference*, Townsville, pp 407-416.

Gillies, S and Wu, H W, 2008. Underground atmosphere real time personal respirable dust and diesel particulate matter direct monitoring, in *Proceedings of 8th Underground Coal Operators' Conference* (Eds: N Aziz and J Nemcik), 14 - 15 February 2008, Wollongong, Australia. pp 143-154. http://ro.uow.edu.au/coal/14/.

Ren, T and Balusu, R, 2005. Dust control technology development for longwall faces - simulation studies, ACARP Project C13019, Exploration and Ming Report, P2005/394, September 2005, pp90.

Ren, T and Balusu, R, 2010. The use of CFD modelling as a tool for solving mining health and safety problems, in *Proceedings of 10th Underground Coal Operators' Conference* (Eds: N Aziz and J Nemcik), 11-12 Feb 2010, Wollongong, Australia. Pp 339-349. http://ro.uow.edu.au/coal/319/.

Plush, B, Ren, T and Aziz, N, 2012. A critical evaluation of dust sampling methodologies in longwall mining in Australia and the USA, in *Proceedings of 12th Coal Operators' Conference*, University of Wollongong & the Australasian Institute of Mining and Metallurgy, 2012, pp 193-201. http://ro.uow.edu.au/coal/407/.

DELAYING SPONTANEOUS COMBUSTION OF REACTIVE COALS THROUGH INHIBITION

Basil Beamish[1], Patrick McLellan[2], Homero Endara[2], Umit Turunc[2], Michael Raab[2] and Rowan Beamish[1,3]

ABSTRACT: A moist coal adiabatic oven test has been used to quantify the effect of applying an anti-oxidant agent to reactive coals from Australia and the US. For the dosage rate applied, the anti-oxidant significantly reduces the coal self-heating rate and extends the time taken to reach thermal runaway by a factor of three for sub-bituminous coal and by a factor of two for the same application to high volatile C bituminous coal. The laboratory result obtained for sub-bituminous coal from Powder River Basin is in direct agreement with the practical site experience of applying the anti-oxidant product as a spontaneous combustion management control. Consequently, it is now possible to benchmark the application of the anti-oxidant to any reactive coal prior to mining as part of developing a leading practice spontaneous combustion management plan.

INTRODUCTION

Low rank coals are known to have a high propensity to spontaneously combust and the mining, storage and transport of such coals poses a significant hazard for management planning. One solution to mitigating this hazard is to apply inhibiting agents to delay the onset of thermal runaway that can ultimately lead to a spontaneous ignition event. Smith *et al.* (1988) studied the effects of a range of inhibitors on coal spontaneous combustion, with varying degrees of success. The index parameter used to quantify the effectiveness of each inhibitor was the minimum Self-heating Temperature (SHT) of the coal as defined by earlier work of Smith and Lazzara (1987). This index parameter does not provide any time perspective of the inhibition delay in reaching thermal runaway and there has been no subsequent publication of any practical application of their findings.

Recent advances in coal spontaneous combustion testing (Beamish and Beamish, 2012a, 2012b) provide the opportunity to quantify the effectiveness of applying inhibiting agents (in the form of anti-oxidants) to reactive coals to delay self-heating reaching thermal runaway. This paper presents the results of a series of laboratory trials supported by site experience of an anti-oxidant product developed the industry, which has been applied to three reactive coals of differing coal rank and geographical setting.

ADIABATIC OVEN TESTING

Coal samples

Details of the samples used in this study are contained in Table 1. The two major benchmark coals are Kideco (Indonesia) and Spring Creek (New Zealand), which covers a rank range from sub-bituminous C to high volatile B bituminous. Site experience with each of these coals indicates that heating events will develop in loosely piled coal in approximately 10-15 d for the Kideco coal and 40-60 d for Spring Creek coal.

The reactive coals used in this study fall within the rank range of the two benchmark coals. Sample PRB is from the Powder River Basin and the other two coals are from Australian coal basins. There is also a fundamental difference in coal type between the two Australian coal samples, which is readily identifiable from a Suggate Rank (Suggate, 2000, 1998) plot (Figure 1). Sample AUS1 is inertinite-rich as it plots below the New Zealand coal band, whereas sample AUS2 is vitrinite-rich as it plots within the New Zealand coal band as defined by Suggate (1998). The Kideco, Spring Creek and PRB coals are all vitrinite-rich.

[1] *B3 Mining Services Pty Ltd, PO Box 1565, Toowong BC QLD 4066, basil@b3miningservices.com, M: +61 488 708 949*
[2] *GE Power & Water, Water & Process Technologies*
[3] *The University of Queensland, School of Mechanical and Mining Engineering, Brisbane QLD 4072*

Table 1 - Coal quality data for benchmark and reactive coal samples

Sample	R_{70} (°C/h)	Volatile matter (%, dmmf)	Calorific value (Btu/lb, mmmf)	ASTM rank	Ash content (%, db)	Sulphur content (%, db)	Moisture content (%, ar)
Benchmark coals							
Kideco	28.57	51.6	9755	subC	1.8	0.10	24.0
Spring Creek	5.87	41.3	13749	hvBb	1.2	0.30	11.7
Reactive coals							
PRB	23.09	47.4	9801	subB	6.8	0.62	24.3
AUS1	14.61	30.2	10540	subA	11.5	0.12	17.0
AUS2	9.38	44.5	12198	hvCb	3.9	0.72	14.1

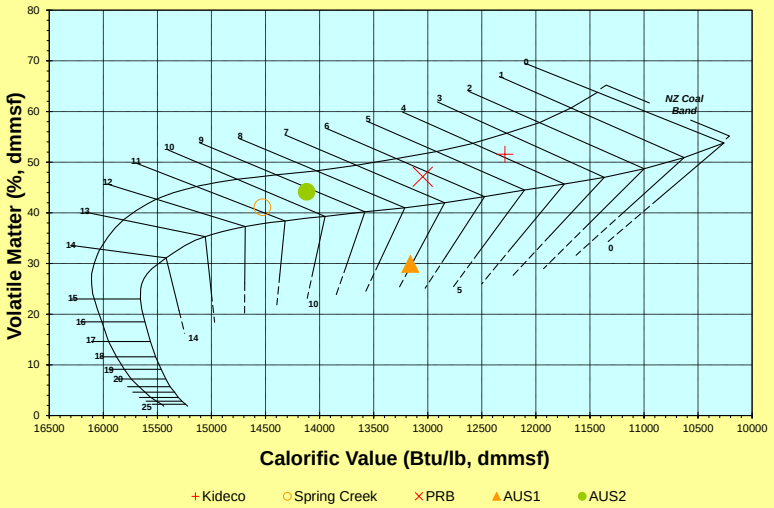

Figure 1 - Suggate rank plot of coal samples used in the study

Self-heating test procedures

The R_{70} testing procedure essentially involves drying a 150 g sample of <212 μm crushed coal at 110 °C under nitrogen for approximately 16 hours (Beamish, 2005). Whilst still under nitrogen, the coal is cooled to 40 °C before being transferred to an adiabatic oven. Once the coal temperature has equilibrated at 40 °C under a nitrogen flow in the adiabatic oven, oxygen is passed through the sample at 50 mL/min. A data logger records the temperature rise due to the self-heating of the coal. The time taken for the coal temperature to reach 70 °C is used to calculate the average self-heating rate for the rise in temperature due to adiabatic oxidation. This is known as the R_{70} index, which is in units of °C/h and is a good indicator of the intrinsic coal reactivity towards oxygen.

A more indicative test that quantifies coal self-heating behaviour from low ambient temperature to thermal runaway, known as Moist Adiabatic Benchmark (MAB) testing has been developed (Beamish and Beamish, 2011). The major changes from the normal R_{70} method for MAB testing are, testing the coal with its as-received moisture content from the ambient mine start temperature, an increased sample size of approximately 200 g and a decreased oxygen flow rate of 10 mL/min. Increasing the sample size to 200 g provides a greater mass of coal to react that is still manageable without modifying the reaction vessel. Decreasing the oxygen flow rate to 10 mL/min reduces any cooling effect experienced by the coal from moisture evaporation as it self-heats. Effectively, these changes optimise the worst case scenario of developing a heating from as-mined coal.

Anti-oxidant

The anti-oxidant applied to the coals in this study is currently being used to treat large quantities of Powder River Basin coal at an opencut mine producing 15 Mt/a. Normal treatment rates range from 45-225 g/t of coal depending on the characteristics of the coal, climatic factors and the duration of

inhibition effectiveness required. Dosage requirements for solids treatment are known to be particle size dependent, hence increased (surface area equivalent) dose rates were applied for laboratory testing to compensate for the <212 µm crushed coal samples.

Adequate mixing is critical for effective treatment, as with all chemical applications, to ensure a uniform distribution of the anti-oxidant throughout the coal. In site applications, moisture addition can be minimised and mixing enhanced, by using specialty foam to distribute the anti-oxidant during the material handling process. Additional moisture is required under laboratory conditions, to effectively wet the <212 µm coal and uniformly distribute the active chemical.

ADIABATIC TESTING RESULTS AND DISCUSSIONS

R_{70} self-heating rate values and coal reactivity

The R_{70} self-heating curves for each sample are shown in Figure 2. Their respective R_{70} values are contained in Table 1. It can be seen that the Australian samples have an ultra-high intrinsic spontaneous combustion reactivity rating and the Powder River Basin and Kideco samples have and extremely high intrinsic spontaneous combustion reactivity rating based on Queensland conditions. It should be noted that this test is performed on a dry basis and it does not provide any indication of the moderating influence of the coal moisture content on self-heating. It also does not provide a reliable indication of the time taken for a coal to reach thermal runaway. In this particular example the coal reactivity is dominated by the rank order of the coals.

Effectiveness of anti-oxidant in delaying thermal runaway

The MAB test results for raw and treated Powder River Basin coal are shown in Figure 3. The relative benchmark scale indicates that the time taken for spontaneous combustion issues in a loose stockpile of raw PRB coal would be in the order of 13 to 20 d. Actual site experience with this coal indicates that heating events at the mine can take place in 15 d. Hence, the MAB test provides an acceptable match with site experience for this coal and the PRB coal now provides a benchmark in its own right for comparing the effectiveness of spontaneous combustion inhibiting agents.

The self-heating curve of the treated coal shows the effectiveness of the inhibitor at reducing the initial self-heating rate as it reaches a maximum of 43.9 °C after 13 hours and actually loses heat over the next ten hours before the self-heating begins to accelerate again at a much more reduced rate compared to the raw coal. The time taken to reach thermal runaway is substantially prolonged (almost three times the raw coal) and according to the benchmark performance scale in Figure 3 the time taken for spontaneous combustion issues in a loose stockpile of treated PRB coal would be in the order of 34 to 51 d. This result is consistent with actual site experience using the anti-oxidant.

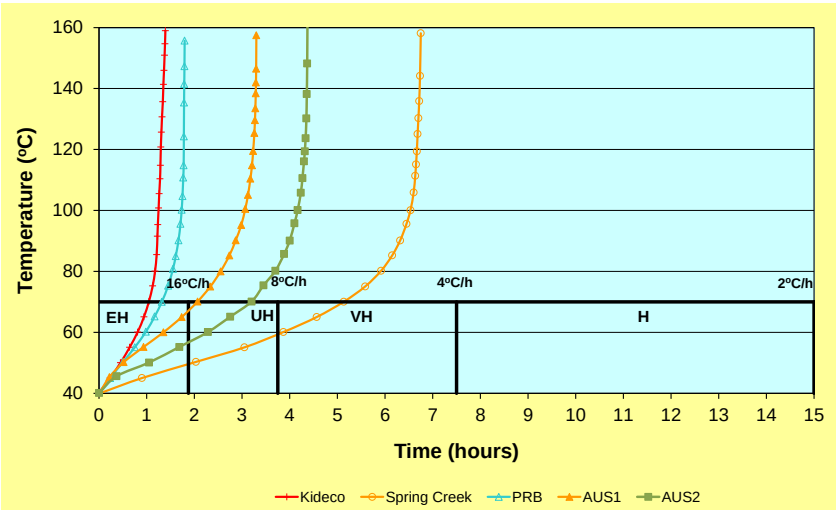

Figure 2 - Adiabatic self-heating curves for samples tested using the normal R_{70} test procedure, showing intrinsic spontaneous combustion reactivity ratings based on Queensland conditions (H = High, VH = Very High, UH = Ultra High, EH = Extremely High)

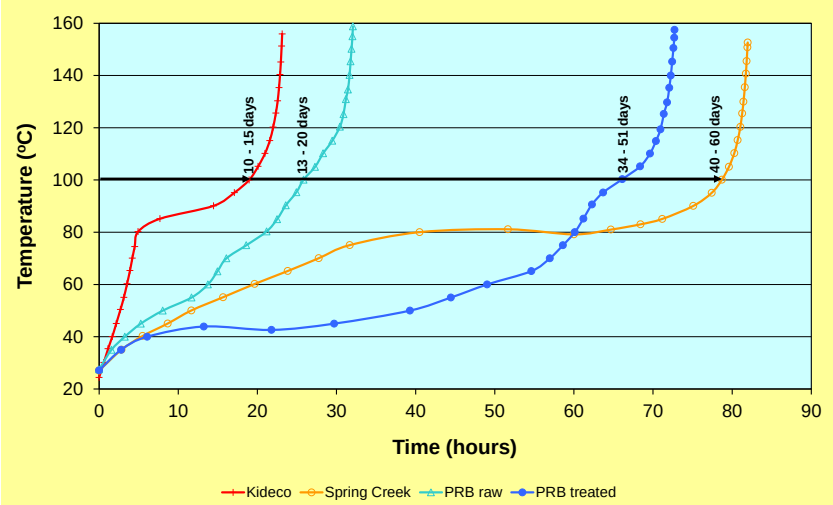

Figure 3 - Moist adiabatic benchmark test results for Powder River Basin raw coal and treated coal using an inhibitor application of 100 g/t (surface area equivalent dose rate)

The two Australian coals are located in areas that often experience wet season conditions and many spontaneous combustion incidents in stockpiles have been observed during this climatic period. The MAB test results for raw and treated AUS1 coal are shown in Figure 4. The relative benchmark scale indicates that the time taken for spontaneous combustion issues in a loose stockpile of raw AUS1 coal would be in the order of 16 to 24 d. This is consistent with the known behaviour of the coal in operations.

The self-heating curve of the treated AUS1 coal shows a different response to the PRB coal, as the initial delay in self-heating is not as dramatic, but as the test progresses there is a significant prolonged delay in self-heating once the coal reaches approximately 70 °C. This difference in the shape of the self-heating curve of the two treated coals could possibly be a function of the different pore structure associated with the maceral composition of the two coals. The AUS1 coal is inertinite-rich, which is usually associated with a high macroporosity, whereas the PRB coal is vitrinite-rich, which is usually associated with a high microporosity. It may also be that there is a fundamental difference in the way that each coal interacts with the anti-oxidant. Again, the time taken to reach thermal runaway is substantially prolonged (three times the raw coal) and according to the benchmark performance scale in Figure 4 the time taken for spontaneous combustion issues in a loose stockpile of treated AUS1 coal would be in the order of 51 to 76 d.

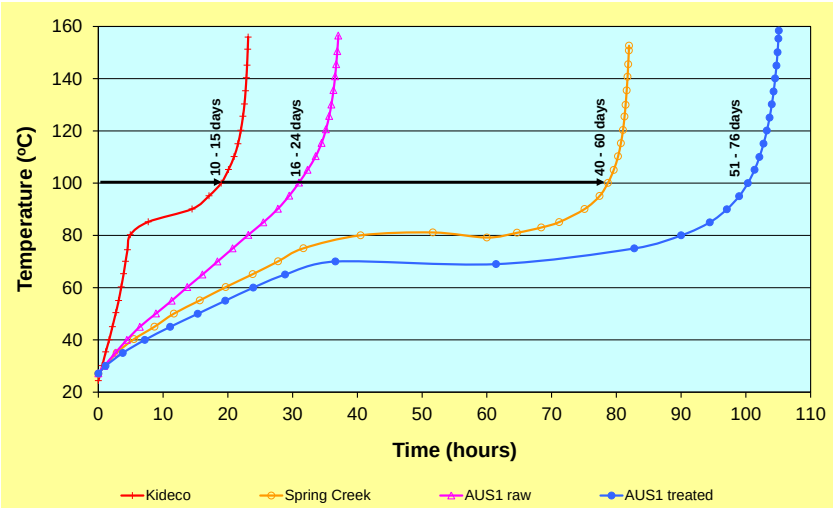

Figure 4- Moist adiabatic benchmark test results for AUS1 raw coal and treated coal using an inhibitor application of 100 g/t (surface area equivalent dose rate)

The MAB test results for raw and treated AUS2 coal are shown in Figure 5. The relative benchmark scale indicates that the time taken for spontaneous combustion issues in a loose stockpile of raw AUS2 coal would be in the order of 16 to 25 d. It is interesting to note that this value is almost identical to the AUS1

coal test, yet the AUS1 coal is over 50% more reactive than the AUS2 coal as shown by the R_{70} self-heating rate value. The reason for this result is that the AUS2 coal has approximately 3% less moisture and hence the heat loss from evaporation during the initial coal self-heating is less. In fact the AUS2 coal reaches 90°C sooner than the AUS1 coal as a result, but it then goes through a decrease in self-heating rate until oxidation sites become available after moisture has been evolved. Again the difference in shape between the two self-heating rate curves appears to be a function of the AUS2 coal being vitrinite-rich compared to the AUS1 coal being inertinite-rich. The increased rank of the AUS2 coal would also alter the coal microstructure.

The self-heating curve of the treated AUS2 coal shows a similar response to the PRB coal, in terms of its shape. The time taken to reach thermal runaway is approximately double that of the raw coal and according to the benchmark performance scale in Figure 5 the time taken for spontaneous combustion issues in a loose stockpile of treated AUS2 coal would be in the order of 30 to 44 d.

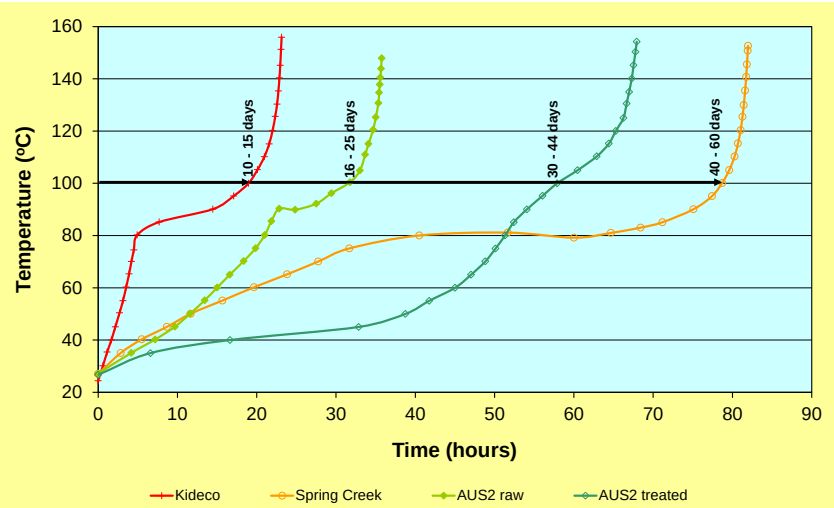

Figure 5 - Moist adiabatic benchmark test results for AUS2 raw coal and treated coal using an inhibitor application of 100 g/t (surface area equivalent dose rate)

For each of the three coals tested in this study the delay in reaching thermal runaway created by the anti-oxidant application shows that it is possible to manage each of these coals in an effective manner to mitigate the risk of spontaneous combustion related events. At this time the anti-oxidant treatment has been successfully implemented in opencut operations of the Powder River Basin. The chemical agent has an added benefit as it also acts as a dust suppressant. It would also reduce calorific value loss of the coal given the nature of its effectiveness to reduce the rate of coal oxidation.

Underground coal mines that are operating with reactive coals could also benefit from the application of this anti-oxidant to mitigate against goaf heatings. The dust suppressant aspect of the product could also benefit mines using seamgas drainage. Again this would be an added benefit since gas drainage of reactive coals increases the propensity of the coal to self-heat, as the drainage process removes both moisture and gas from the coal pore structure thus freeing up reactive sites for oxidation to take place.

CONCLUSIONS

Mitigation of coal spontaneous combustion has been successfully practiced in the Powder River Basin for a considerable time now using the systematic application of an anti-oxidant. The effectiveness of this chemical to inhibit coal self-heating and delay thermal runaway has been quantified using adiabatic oven testing procedures, which produce results in agreement with site experience. The same laboratory testing procedures have also shown that the anti-oxidant is just as effective on an Australian sub-bituminous coal and an Australian high volatile C bituminous coal. There appears to be a relationship between rank and the delay time to thermal runaway as the higher rank coal shows a delay by a factor of two, whereas the lower rank coal shows a delay by a factor of three.

These results have significant practical implications for the successful management of mining, storage and transport of these coals. The success of applying anti-oxidants in the Powder River Basin can be

transferred to Australian operations in a sound scientific manner by simulated laboratory testing in conjunction with closely monitored field trials.

ACKNOWLEDGEMENTS

The authors would like to thank the Coal Industry for their continued support of spontaneous combustion benchmarking, along with The General Electric Company and UniQuest Pty Limited for granting permission to publish this paper.

REFERENCES

Beamish, B B, 2005. Comparison of the R70 self-heating rate of New Zealand and Australian coals to Suggate rank parameter, *International Journal of Coal Geology*, 64(1-2):139-144.

Beamish, B and Beamish, R, 2011. Experience with using a moist coal adiabatic oven testing method for spontaneous combustion assessment, in *Proceedings 10th Underground Coal Operator's Conference* (ed: N Aziz and J Nemcik), pp 264-268, (University of Wollongong and The Australasian Institute of Mining and Metallurgy), http://ro.uow.edu.au/coal/382/.

Beamish, B and Beamish, R, 2012a. Testing and sampling requirements for input to spontaneous combustion risk assessment, in *Proceedings of the Australian Mine Ventilation Conference* (eds: B Beamish and D Chalmers), pp 15-21 (The Australasian Institute of Mining and Metallurgy: Melbourne).

Beamish, B and Beamish, R, 2012b. Benchmarking coal self-heating using a moist adiabatic oven test, in *Proceedings of the 14th US/North American Mine Ventilation Symposium* (eds:F Calizaya and M G Nelson), pp 423-427 (University of Utah, Department of Mining Engineering, Utah, USA).

Smith, A C and Lazzara, C P, 1987. Spontaneous combustion studies of US coals, US Bureau of Mines Report of Investigations RI 9079.

Smith, A C, Miron, Y and Lazzara, C P, 1988. Inhibition of spontaneous combustion of coal, US Bureau of Mines Report of Investigations RI 9196.

Suggate, R P, 1998. Analytical variation in Australian coals related to coal type and rank, *International Journal of Coal Geology*, 37:179-206.

Suggate, R P, 2000. The Rank (Sr) scale: its basis and its application as a maturity index for all coals, *New Zealand Journal of Geology and Geophysics*, 43:521-553.

REMOTE MONITORING OF SUBSURFACE HEATINGS IN OPENCUT COAL MINES

John Malos[1], Basil Beamish[2], Lance Munday[1], Peter Reid[1] and Craig James[1]

ABSTRACT: The detection and monitoring of spontaneous combustion (sponcom) events in opencut coal mines are significant hazard management issues. Currently, the only way of locating sponcom incidents is by manual inspection, whether by visual examination or by use of hand-held thermal cameras, often putting personnel at risk. These inspections are also limited in terms of access and coverage. Therefore, there is a need to implement a convenient remote means to detect and monitor the state of subsurface heatings in opencut coal mines over extended areas for significant periods of time. A versatile self-contained imaging system has been developed that is deployed using an unmanned aerial vehicle. The system eliminates the safety hazard of personnel accidentally entering hot ground and being exposed to toxic gases often associated with heatings. Results obtained from the imaging system is presented, which generates thermal and visible geo-referenced images that can be overlaid onto a digital map of the surveyed area. The data allow rapid detection and accurate localisation of anomalous heat levels within target areas that can be updated on the mine plan for management purposes, and thus enables mitigation strategies to be monitored for effectiveness.

INTRODUCTION

Management of self-heating of coal is an important issue for safety and productivity of open cut coal mining. There are a limited number of methods for effective monitoring of associated ground heating and outbreaks of spontaneous combustion, due to the often large areas that require regular inspection. Traditionally, monitoring is performed via spot inspections by qualified staff or via infrequent manned aerial thermal imaging surveys, either of which involves OH and S risks to staff and/or expense prohibiting regular deployment.

Unmanned aircraft systems (UAS) and lightweight, low-cost thermal imaging cameras have become commercially available in recent years and provide an alternative monitoring solution. In combination they provide a cost-effective solution to the challenge of undertaking sufficiently regular thermal imaging surveys for management of coal-related ground heating and spontaneous combustion outbreaks (Vasterling, *et al.,* 2010a, 2010b; Sheng, 2010).

CSIRO has developed a proof-of-concept lightweight imaging payload deployed on a UAS that is capable of automated mission-based mapping of target areas. The system has been trialled at non-active coal mine workings in which residual heatings persist and thereby present realistic field-trialling scenarios. This paper details the basic configuration of the system used together with imaging results from these preliminary trials, thereby demonstrating the potential of the system for general use within the industry to improve detection, safety and cost effectiveness of this novel mode of spontaneous combustion management in open cut coal mines.

PROTOTYPE SYSTEM

UAS-based mapping is a relatively new technology that is being rapidly adopted in numerous commercial contexts, and is receiving growing interest from the mining industry for the safety and productivity gains that can be provided. At present, relatively few UASs offer the facility for autonomous operation, instead being operated remotely by qualified pilots. Furthermore, application of these systems to specific industries often warrants an OEM-based approach to permit a tailoring of the UAS to the payload being carried, which in turn warrants tailoring to the specific application area. CSIRO has developed a proof-of-concept system which combines an autonomous UAS with OEM-modifications to support a thermal imaging payload designed for aerial surveying of mining operations. The system (Figure 1) consists of a self contained imaging payload carried by a commercially available UAS.

[1] *CSIRO Division of Earth Science and Resource Engineering, john.malos@csiro.au, M: 04 1815 4863*
[2] *B3 Mining Services Pty Ltd, PO Box 1565, Toowong BC QLD 4066, basil@b3miningservices.com, M: +61 488 708 949*

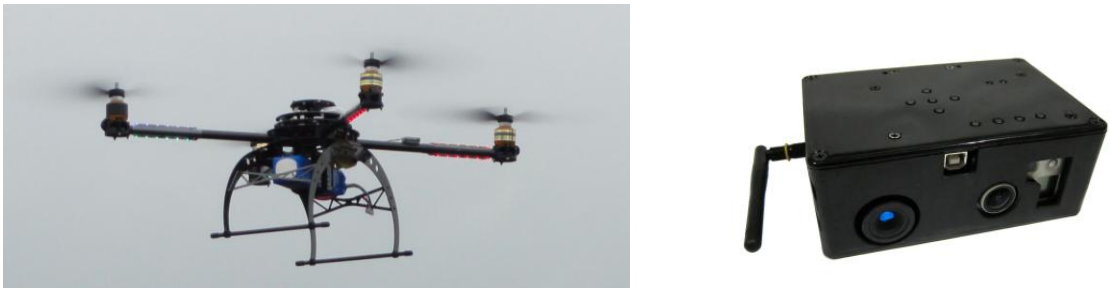

Figure 1- UAS and imaging payload

The UAS has the following specifications:

- autonomous GPS-waypoint-controlled flight (see Figure 2);
- wholly battery powered;
- durations of approximately 10-15 min per mission, but unlimited in the number of missions;
- a portable wireless base-station for mission control; and
- a camera mounting system.

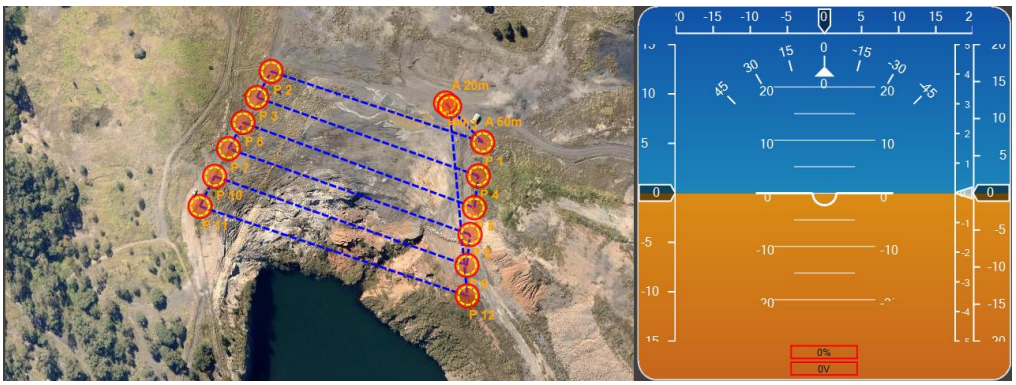

Figure 2 - Screenshot from base-station software application illustrating waypoint-planning facility for imaging-path planning

The imaging platform is a self-contained imaging payload consisting of:

- a thermal infrared (TIR) analogue video camera employing an uncooled micro-bolometer sensor array;
- a digital video recorder to record the TIR camera video signal;
- a visible-band spectrum digital video camera; and
- a self-contained battery power source.

FIELD TRIALS

An example false-colour overlay image of thermal activity of old mine spoil is shown in Figure 3, in which ground heating is readily discernable. The yellow and orange regions represent temperatures in the range of roughly 60^{o}C through to 200^{o}C, whereas the blue regions are of order 20^{o}C to 30^{o}C. These temperatures correspond to spot surface and sub-surface measurements taken using hand-probes since the TIR images in the present system are not calibrated for temperature.

The utility of aerial TIR image overlay is immediately evident from this particular field example. The boundaries and extent of heating are readily discernible which would otherwise only be partially detected from accompanying ground-level visible expressions such as ground sweating and fume emissions. Furthermore, smaller scale features that may be easily missed by visual inspection are prominent in the

TIR overlay; the regions marked by red arrows demonstrated clear expression of heating during ground-based inspections, however the small region indicated by the blue arrow did not show any visible expression of heating and would otherwise have not been detected in establishing the extent of the sub-surface heating progress.

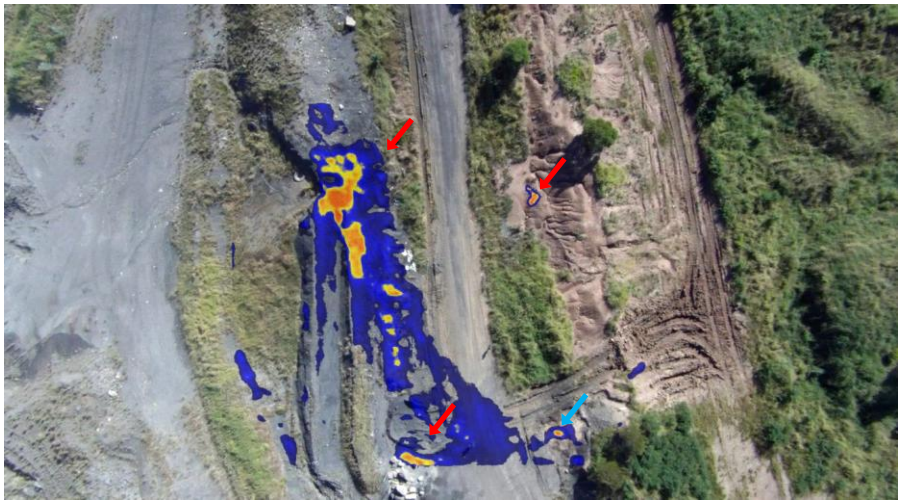

Figure 3 - Thermal and visible-band overlay image of old mine spoil

Results of a test of the capability to create mosaics of overlapping images are shown in Figure 4. This was taken at surface workings of a decommissioned coal mine using an artificial heat source (an electric element operating at 150^{o}C), readily identifiable as the small orange spot in the false-colour overlay. Sufficient feature contrast was found to exist between video frames from the TIR camera so as to permit stitching together of the infrared mosaic image and thereby maintain exposure consistency between constituent frames. The process is scalable and can be extended in order to construct a large mosaic of an extended area, particularly applicable in the opencut context in which leases are sizeable.

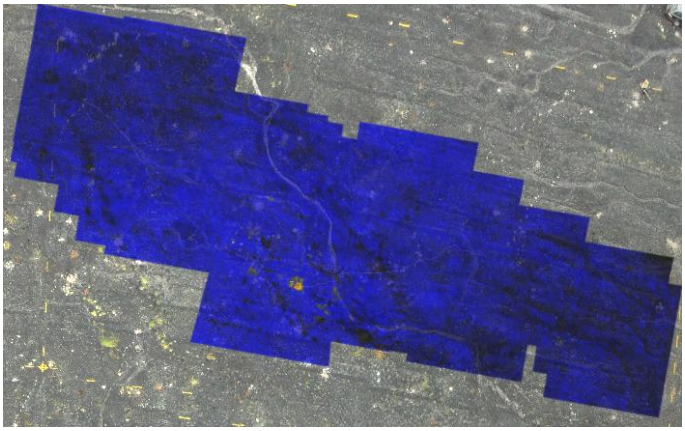

Figure 4 - TIR and visible-band mosaic created solely from image features of the composite images

The system was trialled at a third decommissioned site where surface heatings were ongoing and extended over a larger area. The flight plan shown in Figure 2 was executed and individual images from the TIR and visible-band video frames were retrieved. Since the UAS has the facility for recording flight data during a mission, it is therefore possible to determine the camera attitude orientation in space (azimuth, pitch and roll) as well as the geodetic position and height (latitude, longitude, altitude), which in turn allows the individual frames to be registered within geographical information systems. Figure 5 shows the image and flight path data imported into GoogleEarth, with which it is possible to present the collection of perspective-corrected imaging results in their approximate position and orientation, and with reference to the executed flight plan, shortly after the flight. This facility is easily adaptable to enable this mode of presentation to be generated in real time as the flight progresses.

Subsequent to data acquisition, the TIR and visible-band video sequences were processed, selecting individual frames from each to respectively include in single TIR and visible-band mosaic images. The resulting large image (5653 x 5740) is down-scaled for presentation and shown in Figure 6. As in Figure 3, the yellow and orange regions represent temperatures in the range of roughly 60^{o}C through to 200^{o}C, whereas the blue regions are of order 20^{o}C to 30^{o}C. Using these images, a comprehensive assessment of the full extent of the heatings can be readily discerned. Subsequent trials are planned in order to assess any time-evolution of the heating. Once again, due to the facilities available with the UAS, the same flight path can be re-flown and the resulting mosaics directly compared in order to easily and effectively track the progress of heating.

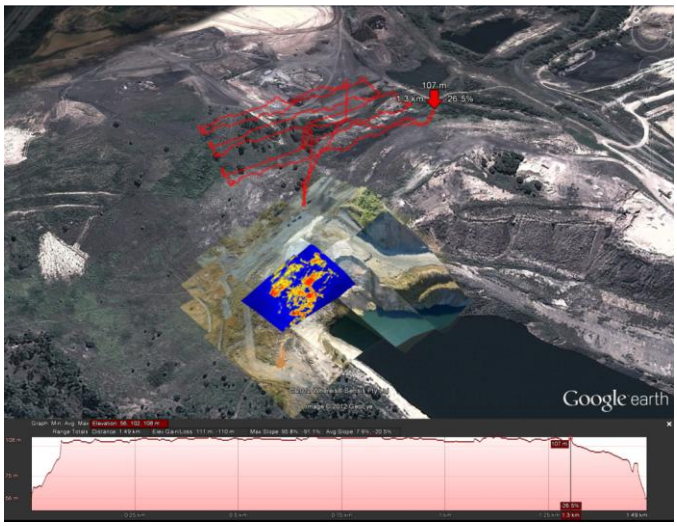

Figure 5 - Mission flight path data imported into the GoogleEarth geographical information program. The red curve is the 3D position recorded by the onboard navigation and control systems of the Unmanned Arial Vehicle (UAV). Also shown (bottom inset) is the altitude series as a function of flight path distance (in kilometres). Individual image frames from the TIR and visible-band video sequences are keystone-corrected and overlaid on the GE terrain using information derived from the UAV attitude and position at the time each image was recorded.

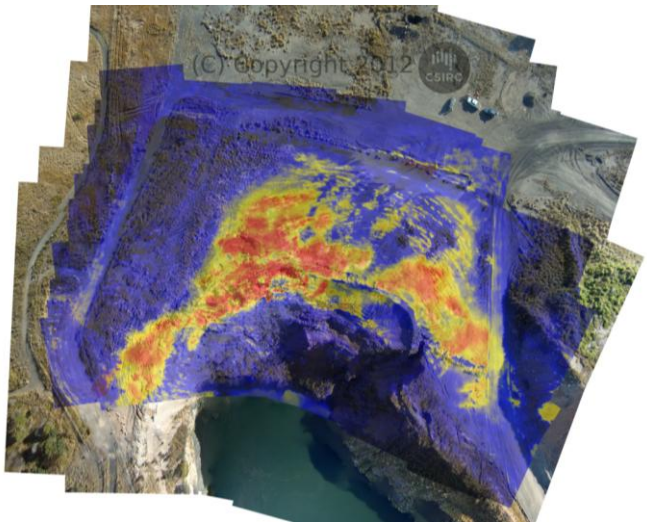

Figure 6 - TIR and visible-band mosaic of survey region exhibiting extended surface and sub-surface heatings

In addition to production of image mosaics, the quality of data obtained from the prototype system permits the retrieval of 3D information of the surface via photogrammetric principles and those employed in structure-from-motion techniques. Figure 7 shows a further trial of a heatings-prone excavation in which TIR and visible-band mosaics were similarly constructed as in Figure 6. Software applications were then employed to retrieve the 3D information from the image sets and generate a 3D mesh of points representing the inferred geometry of the imaged surface. The combination of the 3D mesh and the

high-resolution mosaic imagery permits the construction of the 3D models shown, and in which the position of heatings in the context of the surface relief can be made. Such capability creates numerous additional possibilities, such as being able to plan mitigation strategies in response to the accessibility of active heating, as well as for volumetric analyses that may help project the extent and depth of areas of surface expression.

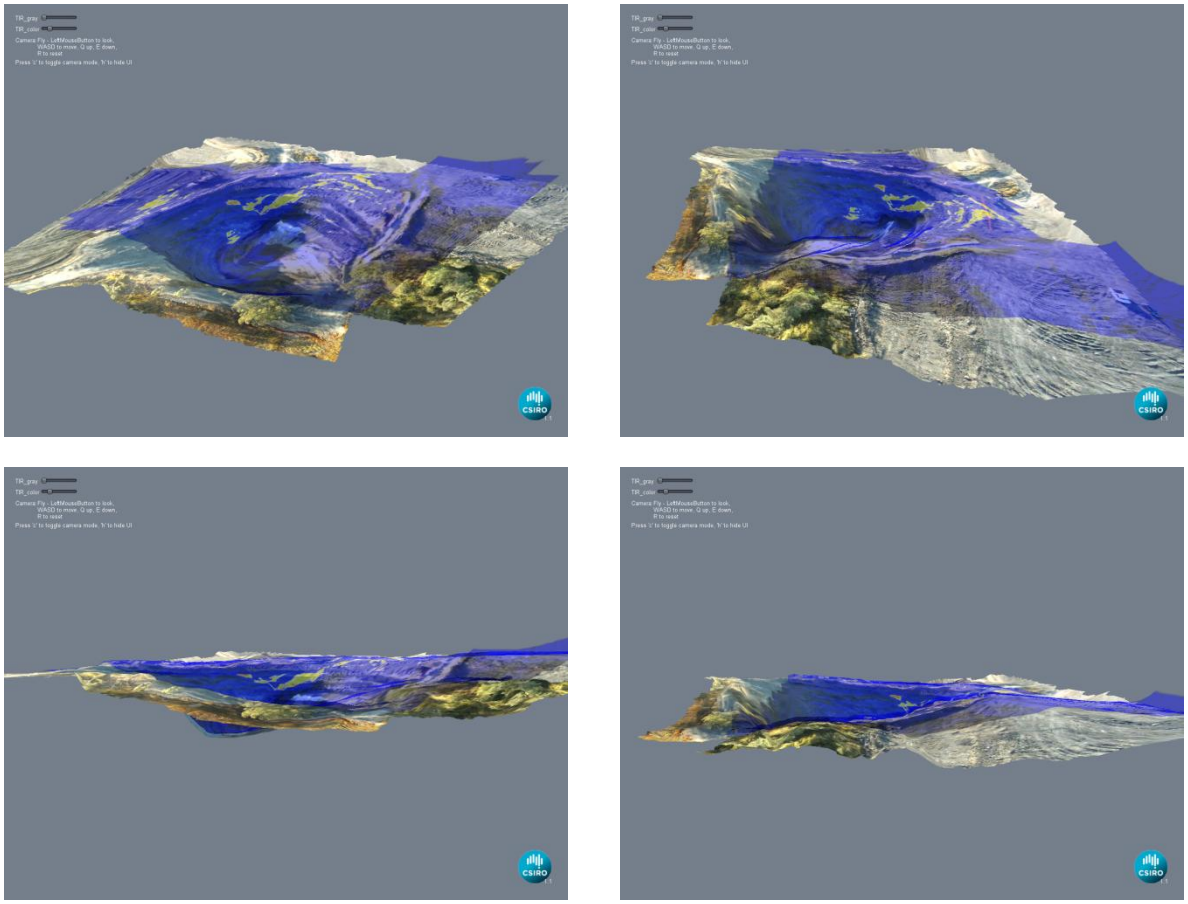

Figure 7 - Four different view of a model constructed from the 3D information present within the TIR and visible-band video frames

CONCLUSIONS

The advent of commercially accessible unmanned aerial systems in combination with lightweight thermal infrared and visible-band imaging systems has permitted the development of a new capability in management of coal-related surface heatings in the opencut context. In particular, the aspects of low-cost, high-flexibility and convenience, and the wealth of spatial and temporal information that can be obtained from this straightforward imaging measurement, makes this approach immediately suitable for employing in sponcom-related management and for defining new standards of practice in the industry.

REFERENCES

Vasterling, M, Schlömer, S, Ehrler, C and Fischer, C, 2010a. Thermal imaging of subsurface coal fires by means of an Unmanned Aerial Vehicle (UAV) in the Autonomous Province Xinjiang, PRC, oral presentation at *European Geosciences Union General Assembly 2010*, Vienna 2-7 May. EGU2010-8664.

Vasterling, M, Schlömer, S, Ehrler, C and Fischer, C, 2010b. Correlation of surface temperature and remote thermal infrared measurements using an unmanned aerial vehicle, paper presented to *Second International Conference on Coal Fire Research 2010*, Berlin.

Sheng, H, Chao, H, Coopmans, C, Han, J, McKee, M, and Chen, Y, 2010. Low-cost UAV-Based thermal infrared remote sensing: platform, calibration and applications, in IEEE/ASME *International Conference on Mechatronic and Embedded Systems and Applications* 2010, Qingdao. pp 38-43.

PREDICTION AND CONTROL OF SPONTANEOUS COMBUSTION IN THICK COAL SEAMS

Ramakrishna Morla, Rao Balusu, Krishna Tanguturi and Manoj Khanal

ABSTRACT: Spontaneous combustion is one of the causes of fire in underground coal mines especially in thick coal seams, which may cause loss of working personnel, production, valuable reserves, and damage or loss of expensive mining equipment. The blasting gallery method in an 11 m thick seam in Indian geological conditions was considered to model prediction and control of spontaneous combustion (sponcom) in thick coal seams. To find sponcom properties of the coal, gas evolution test, sponcom propensity test, differential scanning calorimetry and crossing point temperature tests were conducted for the specified thick seam. The knowledge of goaf gas behaviour in the blasting gallery extraction method during sponcom can be useful in controlling and minimizing the effects of fire. The paper discusses the application of computational fluid dynamic simulations to investigate the goaf gas behaviour at the time of sponcom in the blasting gallery panels. Computational fluid dynamic simulations studies were also conducted with ascentional and descentional ventilation systems with inert gas injection at a single injection point, multiple injection points and at various inert gas flow rates. The results indicate that the descentional ventilation system is useful for goaf inertisation and multiple inert gas injection points are more effective than the single point injection. The paper also presents the effect of sealing of bottom rooms by inertisation.

INTRODUCTION

Charbonnages de France, a French mining company developed a method called Blasting Gallery (BG) to extract a thick coal seam at its Carmaux Colliery. The method is more suitable for thick seams up to 15 m height where the seam is already developed by the bord and pillar system (Yarlagadda, *et al*., 2011). The main advantage of this method is the high percentage of recovery (up to 85%) with less capital investment. However, if the coal seam is highly susceptible to sponcom then this method has fire and explosion issues. In this case, there will be a loss of production, machinery and coal reserves. The present paper discusses a case study taken from an Indian coal mine which has various sponcom tests details and a record of sponcom control measures adopted for its thick seam BG panel.

GDK 10 Incline Mine

GDK10 Incline mine of Singareni Collieries Company Limited (SCCL) is located in the southern part of India. The mine has two workable seams (III seam and IV seam). The thickness and gradient of the III seam are 11 m and one in seven respectively. Since 1987 the BG method has been employed to extract the coal reserves in III seam. The panel areas of III seam BG panels vary from 9000 m^2 to 33 000 m^2, which depend on the incubation period of the coal, strata condition and availability of machinery. Figure 1 shows the layout of III seam BG panel. It has 12 workable pillars of 40 m X 48 m size surrounded by barrier pillars. The width and height of the galleries (road ways) are 4.8 m and 3 m respectively. The roadways at barrier pillars are closed with explosion proof or temporary stoppings. Middle level (58L) is a haulage road to transport men and material and both 57L and 59L are used for belt conveyor. Air flow quantity of 40 m^3/s is used to ventilate the panel. The ventilation control devices like brattice and ventilation doors are used to send sufficient intake air to all the working places in the panel. During depillaring the pillars are divided into two stooks/slices, which are extracted by drilling long holes with jumbo drills and blasted with special type of explosives. Remote control operated load haul dumpers (LHD) are used to load and transfer the blasted coal.

COAL SEAM SPONCOM CHARACTERIZATION

The spontaneous combustion of coal seam is dependent on various factors such as moisture content, rank of coal, availability of oxygen, temperature, geological disturbances, ventilation, etc. The sponcom

CSIRO Earth Science and Resource Engineering, Pullenvale-4069, QLD, Australia, ramakrishna.morla@csiro.au, Tel: 07 3327 4504

laboratory tests provide background understanding of how coal reacts with oxygen. The III seam sponcom propensity tests were conducted in India and Australia, and the results are discussed below.

Gas evolution test

The Gas evolution test (GET) was carried out to know the gas evolution parameters of a coal seam under oxidation conditions, and to develop fire indicators which can indicate the different stage of heating that happens in a coal seam (Clarkson, 2009). Approximately 70 grams of coal was placed in the sponcom vessel in the hot storage oven. A thermocouple placed in the centre of the spontaneous combustion vessel was used to monitor the coal temperature while a second thermocouple monitored the vessel temperature. Wet air was flowed through the vessel at approximately 10^{-6} m^3/s. The coal was heated in 20°C steps to approximately 160°C and then a 40°C step to approximately 200°C at 0.4°C per minute. The temperature was maintained at each step while gas samples were taken for chromatographic analysis. The GET of III seam was conducted at the SIMTARS coal testing laboratory. Figure 2 indicates that CH_4, CO_2, CO percentages are increasing with the increase in temperature. The percentage of H_2 increases from 50°C to 180°C and after 180°C it decreases. On the other hand, O_2 percentage decreases with increase in temperature to zero above 210°C.

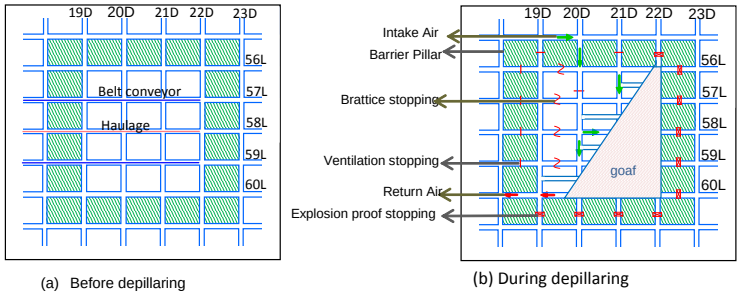

Figure 1 - Layout of the BG panel

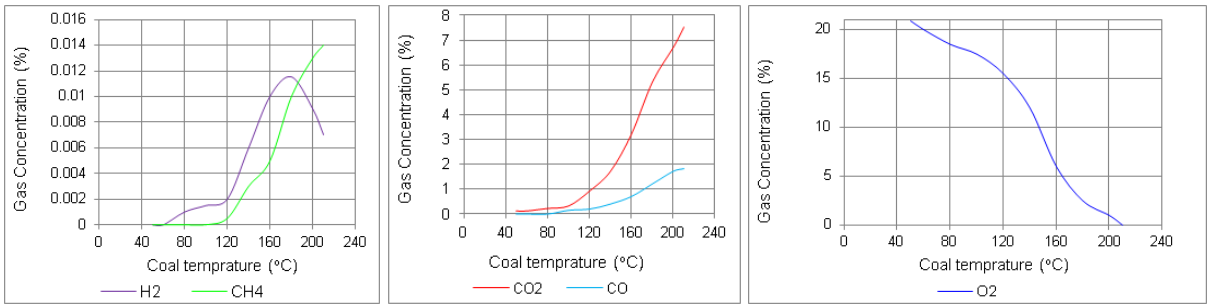

(a) Methane and Hydrogen **(b) CO_2 and CO** **(c) Oxygen**

Figure 2- Gas evolution behaviour for GDK 10 Incline coal seam

Based on the gas evolution test, several sponcom indicators like CO/O_2 ratio, Graham's ratio, Morris ratio and young's ratios were derived for the III seam and are furnished in Table 1.

Table 1 - Indicator ratios derived from gas evolution test

Temperature (°C)	47.8	65.4	85.2	105.8	129.6	154.7	173.5	211.0
O_2 deficiency	0.18	0.34	0.96	3.160	6.790	13.79	19.42	20.47
Graham's ratio	1.10	1.50	1.78	2.200	3.130	4.230	6.270	9.110
Morris ratio	5.34	11.6	18.0	24.04	23.23	19.66	14.08	9.460
CO/O_2 ratio	0.03	0.06	0.08	0.130	0.190	0.220	0.240	0.250
Young's ratio	0.27	0.23	0.20	0.160	0.160	0.180	0.250	0.360

Sponcom propensity test

Coal samples of III seam were tested at the University of Queensland sponcom test laboratory to determine R70 values. The coal samples were brought to the ambient start temperature of 40°C by

flushing with inert N_2; after achieving the study state temperature, O_2 was allowed to pass through the sample. The oxidation of coal continuous and the temperature of the sample rose linearly up to a temperature of 70°C. The time taken for the coal temperature to reach 70°C was used to calculate the average self-heating rate for the rise in temperature. This is known as the R70 index, which is in units of °C/h and is a good indicator of the intrinsic coal reactivity towards oxygen (Beamish, 2009; Beamish, *et al*., 2012).

The R70 values of coal samples with percentage of ash content are shown in Figure 3 and Table 2. The R70 values of the mining seam are in between 0.91°C/h to 3.63°C/h; the results show that the samples are reactive towards O_2, and their intrinsic spontaneous combustion propensity rating varies throughout the seam profile (Beamish, 2009). There is a distinct increase in coal self-heating temperature at the top (sample-1) and the bottom (sample-5) which shows that the samples are relatively more reactive than the middle section sample (sample-3); which may be due to the presence of high ash content in excess of 50%.

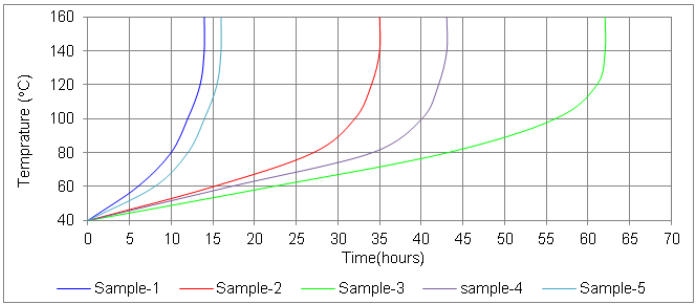

Figure 3 - Adiabatic self-heating curves for III seam samples of GDK10 incline mine

Table 2 - Results of sponcom propensity test

Sample	Location of the sample (III Seam top to bottom)	Ash content (% Dry Basis)	R70 (°C/h)
Sample-1	1.1 m	19.4	3.63
Sample-2	3.3 m	17.3	1.32
Sample-3	5.5 m	51.8	0.91
Sample-4	7.7 m	15.8	1.11
Sample-5	11 m	18.9	2.88

Differential Scanning Calorimetry (DSC) and Crossing Point Temperature (CPT) tests

In this test, coal samples are subjected to a controlled temperature where the energy inputs are measured and compared as a function of temperature (Mohalik, *et al*., 2009). The DSC thermo gram onset temperature of III seam coal is 61.52°C. The low onset temperature indicates that the coal seam is prone to spontaneous heating.

The rate of rise in coal temperature during coal oxidation becomes greater under favourable conditions. The temperature at that point where the coal temperature begins to exceed the surrounding temperature is called CPT. Since 1974 this test is most commonly used to find out sponcom propensity of coal seams in Indian coal mines. A coal seam with CPT 160°C and moisture content of 2% is poorly susceptible to sponcom whereas coal seam with CPT 140°C - 160°C and with moisture content of 2%-5% is moderately susceptible. A coal seam with CPT 120°C - 140°C and moisture content of more than 5% is highly susceptible to sponcom. The CPT and moisture content of III seam coal were found to be 138°C and 7.5% respectively. The results of the CPT along with proximate analysis of DSC thermo gram are shown in Table 3. The DSC and CPT tests were conducted at the Central institute of Mining and Fuel Research (CIMFER), India.

EARLY STAGE SPONCOM PATTERNS IN THE BG GOAF

The main reason for sponcom development in extraction panels is the presence of coal and high percentage of O_2 in the goaf region. Geological disturbances, shale bands, improper drilling and blasting, inefficient loading, and leaving coal in the form of curtains can leave a significant amount of coal in the goaf regions. Similarly, pressure variations between ventilation stoppings, unproductive ventilation

system and inefficient inertisation are the reasons for the presence of high O_2 percentages in the goaf regions.

Computational Fluid Dynamic (CFD) simulation studies were conducted to simulate the airflow patterns in BG goaf with 40 m^3/s airflow quantity as boundary condition. The predicted gas distribution pattern of CO during early stage of development of sponcom is shown in Figure 4.

Results indicate that the amount of CO produced from heating at the goaf corner (22D/60L) would disperse over a wide area in the BG goaf. Even when the concentration of CO reaches 3% in the goaf, the return air CO levels were only around 1 ppm. Therefore, it is critical to monitor CO levels in the goaf for early detection of sponcom in the goaf area. In order to control/regulate the sponcom, simulations were carried out with effective inertisation using CO_2 gas.

Table 3 - DSC thermo gram results of GDK 10 Incline coal seam

DSC results of III seam of GDK10 Incline mine	
Crossing point temperature	138^{o}C
Ignition point temperature	157^{o}C
Percentage of mixture content	7.50
Percentage of ash content	11.1
Percentage of volatile matter	31.6
Percentage of fixed carbon	49.8
Percentage of Pyritic Sulphur	0.10
Percentage of organic Sulphar	0.13

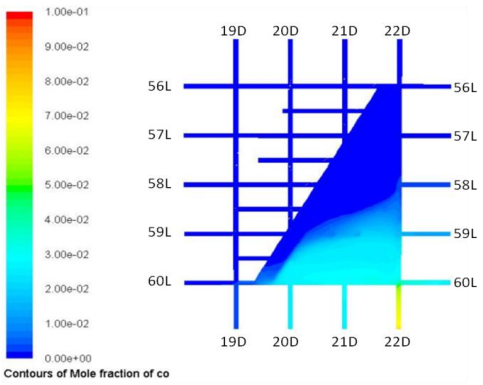

Figure 4 - Early stage of spontaneous combustion in the goaf

DEVELOPMENT OF PROACTIVE SPONCOM CONTROL STRATEGIES

Ventilation

Airflow quantity of 40 m^3/s was taken as a boundary condition for this model. Figure 5 shows the O_2 distribution pattern in the BG goaf region for both ascentional and descentional ventilation systems. From the figure, it can be seen that in both cases, the O_2 percentages are high. CH_4 is a lighter gas, and its specific gravity is 0.554 so it tends to escape from the topmost levels/dips of a goaf. In the descentional ventilation system, CH_4 moves opposite to the air flow direction hence, there is less goaf airflow flush and offers advantages for goaf inertisation. In an ascentional ventilation system both CH_4 and air move in the same direction hence, O_2 concentration in the goaf is very high.

Inertisation from a seal

In longwall mines, various inertisation techniques at different locations and with various flow rates and gases are available (Balusu, *et al*., 2005; Ren, *et al*., 2005; Claassen, 2011). Mine ventilation simulation softwares are also available to simulate the inertisation and mine fires (Gillies and Wu, 2007).

Figure 6 shows the inertisation results when 0.03 m^3/s of CO_2 was injected from upper level (left figure) and middle level (right figure) of the panel. The modelling results show that the inert gas injection via seal

56L/22D has little impact on goaf; CO_2 dissipated along the air flow and O_2 level remains above 19% in most of the goaf regions. However, improved inertisation can be achieved by injecting CO_2 through the middle part of the goaf, i.e., 58L/22D.

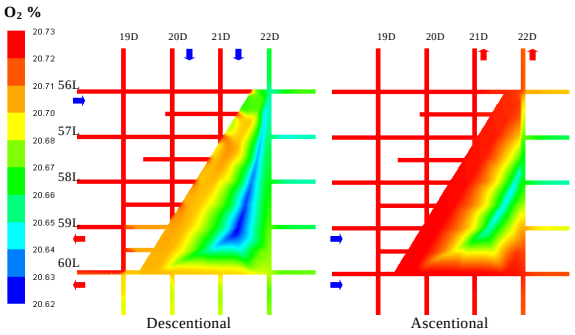

Figure 5 - Oxygen distribution patterns in the goaf area for panel with descentional and ascentional ventilation systems (Yarlagadda, *et al*., 2011)

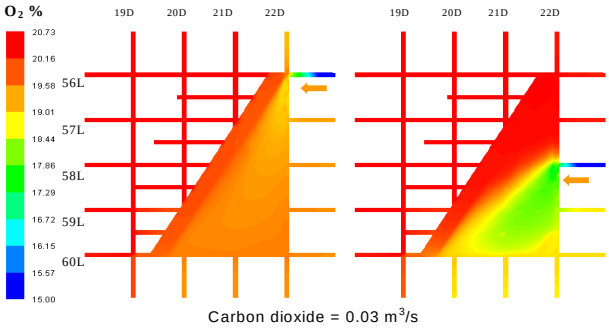

Figure 6 - Inertisation results by injecting CO_2 via seal 56L/22D and 58L/22D with 0.03 m^3/s injection rate

Inertisation with different CO_2 injection rates

Figure 7 shows the injection of CO_2 at the middle level from 58L/22D with flow rates of 0.03 m^3/s and 0.1 m^3/s respectively. It can be seen that there is no variation in O_2 percentages in the goaf and most of the inert gas was flushed out through the return air. It shows that the inert gas injection location is very important for efficient goaf inertisation.

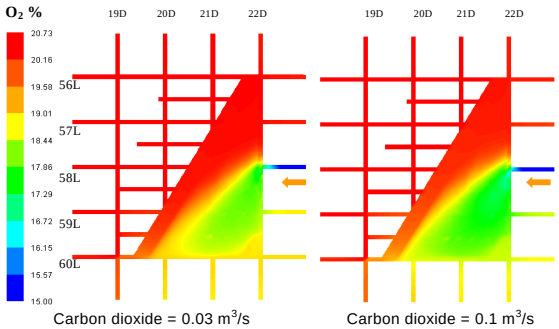

Figure 7 - Comparison of goaf inertisation results with different CO_2 injection rates (0.03 m^3/s VS 0.1 m^3/s)

Inertisation from multiple seals

Figure 8 shows the inertisation from a combination of injection points, such as 56L/22D, 58L/22D and 60L/22D. The results show that improved concentration of CO_2 in the goaf, and significant amount of CO_2 (5%) is in the working face of the goaf. At the goaf corner, the percentage of O_2 is reduced to 17%. The

inert gas injection from the multiple points (Figure 8) with 0.03 m^3/s was achieved better goaf inertisation than the single injection point with same flow rate (Figure 6). From the figure, it is clear that the multiple injection points are more effective than the single injection point.

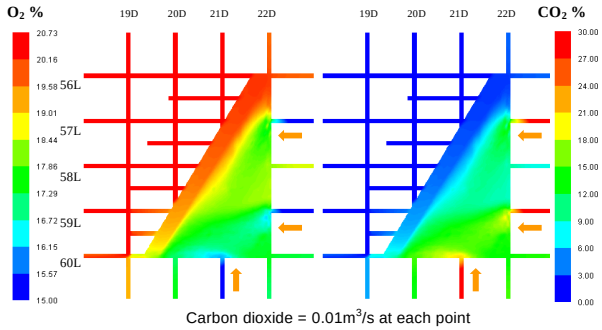

Figure 8 - Inertisation results by injecting CO_2 via multiple seals 56L22D, 58L22D and 60L22D with 0.01 m^3/s injection rate at each point

Rooms closed at lower part of the BG panel

Figure 9 shows the inertisation from 57L/22D, 59/L22D and 21D/60L with 0.02 m^3/s injection rate at each point while rooms at 59L and 60L are closed, the simulation results show that inertisation from the multiple points with closing of bottom rooms cause better inertisation in the goaf region. In the goaf region the CO_2 percentage increased to 20% and O_2 percentage decreases to 15%. The concentration of CO_2 along the working face region also improved.

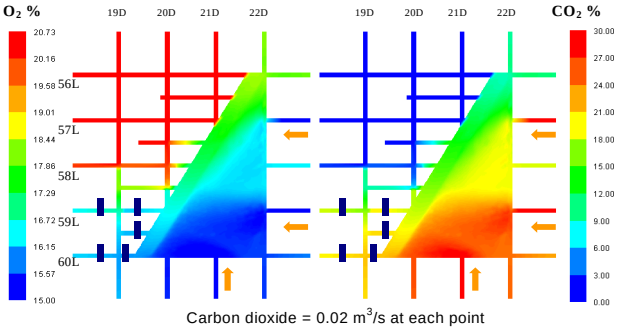

Figure 9 - Inertisation results by injecting CO_2 via multiple seals with 0.02 m^3/s injection rate at each point - rooms 59L and 60L sealed off

FIELD DEMONSTRATION STUDIES IN BG PANEL

Field studies were carried out with the descentional ventilation system at an air flow rate of 40 m^3/s. Inertisation with CO_2 was carried out from lower levels with an extensive gas monitoring system. Figure 10 shows the BG panel where the field trials were carried out along with the inertisation monitoring points (one to seven). The panel has nine workable pillars and about 9000 m^2 of area. The goaf inertisation was initiated about three months after starting of the panel. The inert gas injection rate was 2 t/d to 12 t/d. To improve the caving pattern, the induced blasting was enhanced by significantly reducing the blasting interval to 5 m and by increasing the depth of the blasting hole to 10 m.

The amount of inert gas injected into the panel with the increase in injection points throughout the working period of BG panel is shown in Figure 11. It shows that after 160 d, the amount of CO_2 injected was more than six tonnes per day, and the number of injection points increased to six.

During the initial stage, coal exaction was carried out from lower levels of the BG panel, however, the caving was not fully performed and the goaf was in the initial stage of formation for almost three months from the start of panel. The trends of O_2 and CO_2 at 60L/18D are shown in Figure 12. The results show that after 140 d (after bottom most rooms closed), the percentage of CO_2 increased sharply and there is a gradual reduction of O_2 percentage. During the panel extraction, traces of CO were not found.

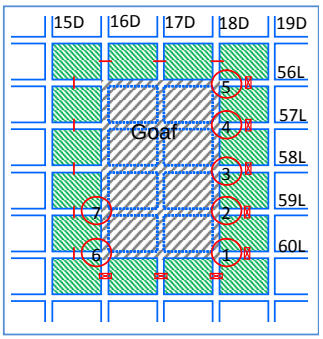

Figure 10 - Inertisation and monitoring plan of BG panel for field trails

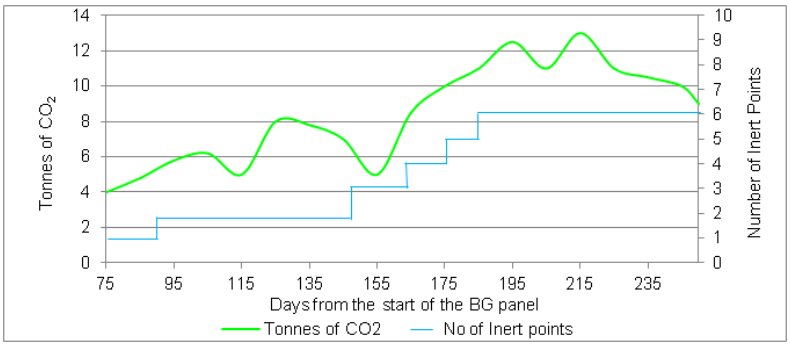

Figure 11 - Inert gas injection rate during panel extraction

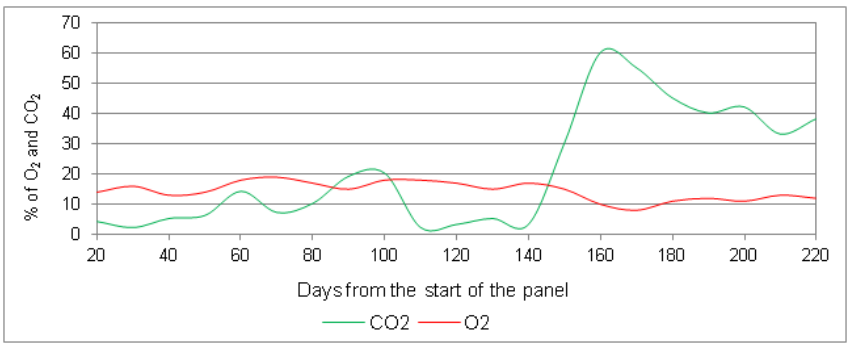

Figure 12 - O_2 and CO_2 percentages during the panel extraction

CONCLUSIONS

As per III seam coal sponcom laboratory investigations, the coal is highly prone to sponcom. The crossing point temperature of the coal is 138^{o}C. The R70 values of the coal seam vary from 0.91 to 3.63^{o}C/h. The DSC thermo gram onset temperature is 61.52^{o}C. GET values indicated increased percentages of CH_4, CO_2, CO and H_2 with increasing temperature and reduction in O_2 percentage with increasing temperature.

As per the CFD simulations, during early stages of sponcom, CO spreads in all direction from source. In descentional ventilation system CH_4 moves opposite to the air flow direction hence, less goaf airflow flush and offers advantages for goaf inertisation. The inertisation from the inbye locations of the goaf region is effective compared to the inertisation from the outbye locations. The multiple inert gas injection points cover more goaf area and provide efficient goaf inertisation compared to the single point inertisation. Inertisation by sealing the bottom most room provides effective inertisation.

Field studies demonstrated that descentional ventilation system with improved induced blasting pattern and effective inertisation from multiple points with bottom levels sealed off has enabled successful extraction of the panel without sponcom development in the goaf area.

REFERENCES

Balusu, R, Ren, T and Humprhries, P, 2005. Proactive inertisation strategies and technology development. *ACARP report* C12020, 2005.

Balusu, R, Yarlagadda, S, Ren, T, Karekal, S, Adhikary, D, Tom, L, Tanguturi, K and Morla, R, 2012. Mine fire prevention and control. *APP Project report* CLM-07-17.

Beamish, B, 2009. Spontaneous combustion assessment of samples from GDK 10 inclines UniQuest Project No 15842, 52p.

Beamish, B, McLellan, P, Turunc, U, Rab, M and Beamish, R, 2012. Quantifying spontaneous combustion inhibition of reactive coals. *14th United States/ North American Mine Ventilation Symposium, 2012*. pp 436-440.

Claassen, C, 2011. Goaf inertisation and sealing utilising methane from in-seam gas drainage system. In *Proceedings of 11th Underground Coal Operators Conference.* pp 369-374. http://ro.uow.edu.au/coal/380/.

Clarkson, F, 2009. Determination of the spontaneous combustion propensity of coals from GDK 10 Incline No 3 seam, SIMTARS Report OG420162F1, 45p.

Gillies, A D S and Wu, H W, 2007. Inertisation and mine fires simulation using Computer Software. *ACARP project Report* C14025.

Mohalik, N, Panigrahi, D, Singh, V and Singh, R, 2009. Assessment of spontaneous heating of coal by differential scanning calorimetric technique. In *Proceedings of Underground Coal Operators' Conference 2009*. pp 303- 310. http://ro.uow.edu.au/coal/113/.

Ren, T, Balusu, R and Humphries, P, 2005. Development of innovative goaf inertisation practices to improve coal mine safety. In *Proceedings of Underground Coal Operators Conference 2005*. pp 315-322. http://ro.uow.edu.au/coal/181/.

Yarlagadda, S, Balusu, R, Liu, T and Reddy, V, B, 2011. Proactive strategies for prevention and control of fires in bord and pillar mines working in thick coal seams. In *Proceedings of 11th Underground Coal Operators Conference*. pp 249- 256. http://ro.uow.edu.au/coal/365/.

PIKER RIVER ROYAL COMMISSION OUTCOMES

Stewart Bell

ABSTRACT: On the 19th November 2010 29 men died when a methane explosion ripped through the Pike River coal mine near Greymouth on the South Island of New Zealand. Two survivors staggered out of the mine one hour after the initial explosion but the mine remains a tomb for the Pike 29. Over the next few weeks three further explosions occurred until the mine was inerted using the GAG jet inertisation device and then sealed.

This paper summarises the finding of the Royal Commission of Inquiry that was convened in December 2010 by the New Zealand Government, to address the questions of: What went wrong at Pike. Why were the previous lessons from mine disasters in developed countries around the world not learned and what is the potential to learn from this event. The report from the Royal Commission was provided to the Governor General of New Zealand on the 30th October 2012.

Pike was a coal mine with difficult geological and topographical conditions. This mine needed the best of everything but this didn't happen and 29 people paid the ultimate price.

This presentation will set the context of Pike, look at the rescue recovery operation and cover the Royal Commission report and what the future holds for the New Zealand coal mining industry. The paper extensively references the information contained within the report of the Royal Commission.

The bodies have not been recovered and the definitive cause of the disaster has not been determined but the Royal Commission uncovered a litany of problems that lead to the explosion on the 19th November. These problems should have been addressed. This disaster was avoidable

INTRODUCTION

Pike River underground coal mine is located on the eastern side of the Paparoa Range about 45 km north east of Greymouth. The seam lies below the Paparoa National Park and dips in an easterly direction. The resource is estimated to contain approximately 40 Mt of a coal that is a low ash, high fluidity, coking coal (Whittall, 2006). The Brunner seam dips from the outcrop in the western escarpment to the east at an angle of between 11 and 20 degrees and varies in thickness between 2 and 13 m mainly lying in the range 4 to 9 m (Whittall 2006). There is a predominantly methane seam gas, generally the gas content ranging between 3 and 6 m^3/t, though some bore samples have been higher than this (Whittall, 2006). The seam was accessed via a single 2.3 km long tunnel driven in stone to access the eastern side of the coal seam where it intersected the Hawera Fault. Development of pit bottom began in early 2009. By November 2010 the development had reached the stage outlined in Figure 1 below. Of particular significance to the development of the mine was the collapse of the bottom of the main ventilation shaft during construction requiring a bypass to be constructed to connect to the upper shaft. The seam depth below the surface varies considerably because of the surface terrain ranging between about 60 m to over 100 m.

In November 2010 Pike River was still in start up mode and was behind in its development schedule.

At the time of the first explosion ventilation was provided by a single fan placed underground adjacent to the base of the upcast shaft extracting about 120 m^3/s of air.

Methane concentrations within the mine were managed through a combination of ventilation and some pre-drainage through in seam holes originally drilled to map the limits of the coal seam. Development was undertaken by continuous miners and a road header was used to excavate roadways in stone. Secondary extraction was to be undertaken using the hydro mining technique. This technique uses high pressure water jets to cut the coal, which then was washed into a flume to be transported out of the mine.

Deputy Director General and Commissioner for Mine Safety and Health, Department of Minerals and Energy Brisbane QLD 4000, Stewart.Bell@dnrm.qld.gov.au, 32371474

Hydromining is not a commonly used mining techniqhue and with the thick coal seams prevalent at Pike River ventilation needs to be carefully managed.

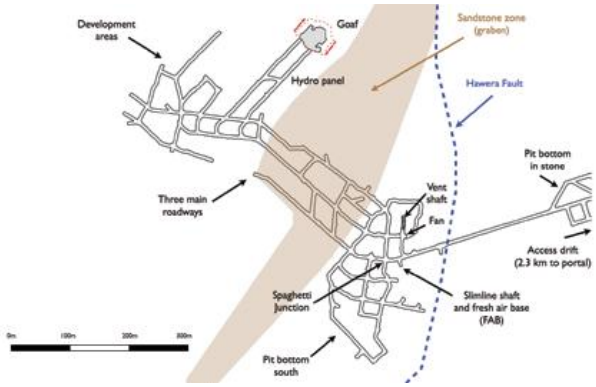

Figure 1 - The mine plan as at November 2010 (PRRC, 2012)

THE TRAGEDY

At approximately 3:45 pm on Friday November 19 2010, there was a violent explosion within the mine. All communications and power were lost to the underground mine. The main fan stopped and the auxiliary fan failed to initiate. At the time of the explosion 31 men were underground, 29 perished and two who were within the stone drift were able to escape after about an hour and a half. Analysis of the gases exiting the fan shaft was consistent with a methane explosion having occurred. Detailed analysis suggests that the volume methane involved would have been somewhere in the range of 1000 to 2000 m^3. This volume of methane suggests that it must have originated in the goaf of the hydropanel. The volume of gas that exploded is thought to have been somewhere in the range 10 000 to 30 000 m^3. It is not clear what ignited the atmosphere, though there were a number of potential ignition sources identified. It is believed that all men died instantaneously either from the pressure wave of the explosion or from asphyxiation or carbon monoxide poisoning.

There were three subsequent explosions on 24, 26 and 28 November. Again it is thought that the primary fuel was methane though there is evidence of coal dust contributing to the fourth explosion. These appear to have been ignited close to the fan shaft, probably by an ongoing fire within the mine.

Suppression of the residual active fire(s) and prevention of subsequent explosions was achieved by deploying the GAG jet inertisation system (Figure 2 and 3). The process of establishing control was complicated by the rugged surface terrain and access to the area above the mine only being feasible by helicopter. It took many weeks to drill boreholes to establish that the mine atmosphere had been rendered inert and for the mine portal to be sealed and the fan shaft capped safely (Figure 4).

Since that time it has not been possible to safely re-enter the mine and retrieve the bodies. Some progress has been made in recovering a limited section of the stone drift.

RECOMMENDATIONS OF THE ROYAL COMMISSION

The Royal Commission investigated the tragedy and made 16 recommendations in an effort to prevent a repeat of this tragedy. The recommendations are listed below verbatim from the report (PRRC, 2012).

Recommendation 1: To improve New Zealand's poor record in health and safety, a new Crown agent focusing solely on health and safety should be established.

- The Crown agent should have an executive board accountable to a minister.
- The chief executive of the Crown agent should be employed by and be accountable to the board.
- The Crown agent should be responsible for administering health and safety in line with strategies agreed with the responsible minister, and should provide policy advice to the minister in consultation with the Ministry of Business, Innovation and Employment.

- The ministry should monitor the Crown agency on behalf of the minister.
- The Crown agency should be funded by the current levies but the basis of the levies should be reviewed for high-hazard industries.

Figure 2 - Fire burning at top of fan shaft after fourth explosion (NZ Police, 2012)

Figure 3 - The GAG jet inertisaion system in operation at Pike River (NZ Police, 2012)

Recommendation 2: An effective regulatory framework for underground coal mining should be established urgently.

- The government should establish an expert task force to carry out the work. Its members should include health and safety experts and industry, regulator and worker health and safety representatives, supported by specialist technical experts.
- The expert task force should be separate from the ministerial task force that is reviewing whether New Zealand's entire health and safety system is fit for purpose.
- The expert task force should consult the Queensland and New South Wales frameworks as best practice.
- In the interests of time, the expert task force should consider the immediate development of approved codes of practice, to be replaced by regulation where appropriate.

- The expert task force should consider addressing urgently the specific issues identified by the commission including:
    - the removal of the 'all practicable steps' qualification from the mandatory provisions of the regulations, including those relating to ingress and egress;
    - the provision of better health and safety information by the employer to the regulator, including notification of all high-potential incidents;
    - requiring employers to have a comprehensive and auditable health and safety management system;
    - mandating the statutory positions necessary to ensure healthy and safe mining (including a statutory mine manager and ventilation officer), and identifying their key functions and the relevant qualifications, competencies and training;
    - defining standards for ventilation control devices, such as stoppings;
    - defining the requirements of underground gas monitoring systems;
    - prohibiting the placement of main fans underground and requiring them to be protected against
    - explosions and other hazards, in accordance with the most appropriate international standards;
    - clarifying the restricted zone within which electrical equipment requires protection; and
    - updating electrical safety requirements in the light of new technology.

Figure 4 - The capped fan shaft, showing the evasee where it was deposited after the fourth explosion (NZ Police, 2012)

Recommendation 3: Regulators need to collaborate to ensure that health and safety is considered as early as possible and before permits are issued.

Recommendation 4: The Crown minerals regime should be changed to ensure that health and safety is an integral part of permit allocation and monitoring.

- The proposals in Review of the Crown Minerals Act 1991 Regime are endorsed.
- Mining permits should have a general condition requiring the need for compliance with the Health and Safety in Employment Act 1992 and regulations.
- The Ministry of Business, Innovation and Employment should provide information to prospective permit holders on health and safety laws and regulations.
- The ministry should review the information required from applicants for mining permits and the way it assesses applications against the criteria in the minerals programme.

Recommendation 5: The statutory responsibilities of directors for health and safety in the workplace should be reviewed to better reflect their governance responsibilities.

Recommendation 6: The health and safety regulator should issue an approved code of practice to guide directors on how good governance practices can be used to manage health and safety risks.

Recommendation 7: Directors should rigorously review and monitor their organisation's compliance with health and safety law and best practice.

Recommendation 8: Managers in underground coal mines should be appropriately trained in health and safety.

Recommendation 9: The health and safety regulator should issue an approved code of practice to guide managers on health and safety risks, drawing on both their legal responsibilities and best practice. In the meantime, managers should consult the best practice guidance available.

Recommendation 10: Current regulations imposing general health and safety duties on the statutory mine manager should be extended to include detailed responsibilities for overseeing critical features of the company's health and safety management systems.

- The new regulations should have regard to the Queensland legislation applying to the mine's senior site executive.
- The statutory mine manager should be protected by new procedures requiring disclosure to the regulator when the employer does not accept the manager's proposals for improving health and safety.

Recommendation 11: Worker participation in health and safety in underground coal mines should be improved through legislative and administrative changes.

- Legislative changes should:
  - require operators of underground coal mines to have documented worker participation systems;
  - ensure all workers, including contractors, are competent to work safely, are supervised and are included in the mine's worker participation system;
  - empower trained worker health and safety representatives to perform inspections and stop activities where there is an immediate danger of serious harm;
  - require the results of monitoring and investigation of health and safety in the workplace to be automatically made available to workers; and
  - allow unions to appoint check inspectors with the same powers as the worker health and safety representatives.
- The regulator should:
  - issue an approved code of practice on employee participation;
  - promote workers' rights and obligations through education and publicity; and
  - ensure that inspectors routinely consult workers and health and safety representatives as part of audits and inspections.

Recommendation 12: The regulator should supervise the granting of mining qualifications to mining managers and workers.

- The regulator should lead the work to strengthen standards so that they are comparable with those of Australia.
- The regulator should work with Australian counterparts towards developing a joint accreditation process with Australia and an Australia/New Zealand board of examiners.
- Additional statutory roles and qualifications are required in new regulations, including a statutory ventilation officer and an agreed level of industry training and supervision for all new or inexperienced workers.

- The regulator should work with the Accident Compensation Corporation and others on raising the standards of health and safety consultants.

Recommendation 13: Emergency management in underground coal mines needs urgent attention.

- Operators of underground coal mines should be required by legislation to have a current and comprehensive emergency management plan that is audited and tested regularly.
- The emergency management plan should be developed in consultation with the workers and the Mines Rescue Service.
- The emergency management plan should specify the facilities available within the mine, such as emergency equipment, refuges and changeover stations, and emergency exits.
- The emergency management plan should contain a strategy for notifying next of kin and ensuring that genuine enquirers receive appropriate information.
- The mining operator must keep and regularly update a comprehensive list of emergency contact details for all workers.
- The emergency management plan needs to be compatible with CIMS, the co-ordinated incident management system used by New Zealand's emergency services and the police.
- The regulator should include the emergency management plan in its audit programme.

Recommendation 14: The implementation of the co-ordinated incident management system (CIMS) in underground coal mine emergencies should be reviewed urgently.

- The implementation of CIMS should be reviewed to ensure that emergencies in underground coal mines are well managed.
- The review team should include the mining industry, police, emergency services, the Mines Rescue Service and the regulator.
- The CIMS framework should be rigorously tested by regular practical exercises at underground coal mines.
- The incident controller at an underground coal mine emergency must have mining expertise and, together with the incident management team, must be responsible for co-ordinating the emergency effort and approving key decisions. This does not prevent a government agency such as the police from being the lead agency or from maintaining its command structure.

Recommendation 15: The activities of the New Zealand Mines Rescue Service need to be supported by legislation.

- The Mines Rescue Trust Act 1992 should reflect the functions performed by the Mines Rescue Service.
- The adequacy and fairness of the current levies imposed on mines to fund the service need to be reviewed.

Recommendation 16: To support effective emergency management, operators of underground coal mines should be required to have modern equipment and facilities.

- Operators should be required to have equipment and facilities suitable for self-rescue by workers during an emergency.
- Operators should be required to include, in their emergency management plans, provisions for continued monitoring of underground atmospheric conditions during an emergency.
- Operators should be required to install facilities that will support emergency mine sealing and
- Inertisation

DISCUSSIONS

The Royal Commission concluded that there was need for major reform of the way coal is mined in underground coal mines in New Zealand. These changes must be enacted urgently. There are lessons for government, regulators, employers and workers (PRRC, 2012).

There is a need to reform the way that the government administers health and safety in mining. Health and Safety should be an integral part of the design for a new mine long before it starts development or operation. Health and Safety compliance should be a condition of mining permits.

The mines inspectorate requires major reform in order to be effective. There are inherent difficulties in attempting to adequately inspect a very small, specialized high risk industry. There are a number of changes that the Department of Labour (DOL) must undertake in order to have an effective mines inspectorate. These relate to such things as:

- Adequate resourcing and support of inspectors
- Recognising the particular needs of high hazard industries
- Improving transparency of DOL reporting
- Improving the focus on health and safety
- Defining a clearer role for DOL in administering the legislation
- Implementing a modern compliance strategy

The legislation needs to be improved. The Commission recommended an expert task force be convened to investigate the way forward. The legislation relating to worker participation should be strengthened, including the right to have trained workplace representatives to carry out inspection and stop work if workers are in immediate danger. The Commission identified the lack of union check inspectors as a serious deficiency. Employers and workers in general need to be better educated in the advantages of active worker participation in health and safety management. In addition the governance by boards of directors of companies needs to be improved to overtly include health and safety responsibilities.

The mining regulations require major improvement to keep pace with industry changes and best practice. The major change should be the requirement of employers to have comprehensive and auditable health and safety management systems including principal hazard management plans (PHMPs). The regulator needs to issue an approved code of practice describing the minimum specifications of PHMPs. In addition the regulations should be changed to comprehensively identify key statutory roles, duties and qualifications, including the positions of statutory mine manager and ventilation officer. They should align the new regulations with the Australian approach to determining the training requirements for all workers.

Workplace safety and health legislation has been weakened in New Zealand over the last 20 years with a greater reliance on self regulation and cooperation between the regulator and those being regulated. This "soft touch" legislation has resulted in New Zealand having one of the worst health and safety records in the developed world.

The management of emergencies needs major enhancement. There should be regulatory guidance for the development of procedures for emergency management, including the requirement for regular testing of the emergency management plans, this testing should include the demonstration of the capacity for every worker to be able to safely escape the mine, as well as demonstrating that the mine emergency management process is effective. The application of the emergency services Coordinated Incident Management System (CIMS) needs to be overhauled so that it can be applied more effectively where high hazard industries are involved. The review should include a range of stakeholders including employers, the Mines Rescue Service, the regulator, worker representative and the emergency agencies. It is vital that the key decision on whether to enter a mine or not lies with the incident controller and the incident management team on the spot.

The funding mechanism for the Mines Rescue Service should be reviewed to ensure it has the capacity to provide the services required to help mines manage emergencies. The Commission was not critical of the New Zealand Mines Rescue Service but recognised that funding for the service was an issue

It is essential that mines have the equipment and facilities to enable miners to rescue themselves, including the capacity to monitor the early warnings of gas levels, modern breathing apparatus, changeover stations, navigation aids, alternate means of egress, adequate transport, robust and redundant communications systems and personnel tracking equipment. The mining company should be able to monitor the mine environment independent of underground power, through a tube bundle sampling system. These things should be legislative requirements.

The Commission was of the view that Pike River had a sub standard gas monitoring system and this made immediate re-entry into the mine impossible. In fact the mine had no fully functional gas monitors in the mine ventilation return.

As has been found elsewhere, it is essential that mines have the capacity to rapidly seal all or part of a mine in an emergency, so that the atmosphere can be controlled. The capacity to externally inert a mine should be investigated.

There is no doubt Pike River was a difficult mine to operate. The topography, highly faulted geology, high methane levels, poor gas monitoring and ongoing financial constraints lead to the fact that the mine never operated on a sustainable basis and lurched from one problem to the next. A workforce with a large percentage of greenskins and a fluid management structure meant that a reservoir of corporate memory was never achieved. The Commission looked to find areas where Pike River had met normal standards but were unable to do so. In the words of several witnesses this mine was a disaster waiting to happen and with 21 high methane events, reported but not acted upon, in the month before the disaster an explosion was inevitable and 29 men paid the ultimate price.

It is recommended that interested persons access the full Royal Commission report available on their website http://pikeriver.royalcommission.govt.nz/.

These reforms need to be made as soon as possible. It is the view of the Royal Commission that:

> *"The Pike River tragedy was preventable but administrative and regulatory reforms are urgently needed to reduce the likelihood of further tragedies.*
>
> *The Pike River tragedy contains lessons for government, regulators, employers and workers, especially in high-hazard industries such as coal mining, where the frequency of major accidents is low, but accidents can have catastrophic results." (Page 29, PRRC, 2012 Volume 1)*

ACKNOWLEDGEMENTS

The author would like to dedicate this paper to the families of the 29 miners who died at Pike River in the hope that we will learn from this disaster and prevent such a tragedy from ever happening again.

REFERENCES

NZ Police, 2012. Operaion Pike Website https://www.police.govt.nz/operation_pike/videos_photos accessed 30 November 2012.

PRRC, 2012. Royal Commission on the Pike River Coal Mine tragedy, 2012. Wellington, New Zealand. ISBN 978-0-477-10377-0, October 2012.

Whittall, P, 2006. Pike River Coal - hydraulic mine design on New Zealand's west coast, in Aziz, N (ed), *Coal 2006: Coal Operators' Conference*, University of Wollongong & the Australasian Institute of Mining and Metallurgy, pp 155-163. http://ro.uow.edu.au/coal/43/.

ENSURING THE SURVIVAL OF CRITICAL INFORMATION SOURCES AFTER AN UNDERGROUND INCIDENT - CAN IT BE ACHIEVED?

Darren Brady[1], David Cliff[2], Geoffrey Nugent[3], Seamus Devlin[4], Steve Tonegato[4] and Peter Mason[5]

ABSTRACT: Through a risk management process ACARP Project C19010 (Emergency Response: Mine Entry Data Management) identified critical information decision makers required to make informed, risk based decisions on whether mines rescue teams could enter or remain in a mine in response to an incident. The project also developed a proof of concept software tool to assist making informed and considered, risked based decisions founded on predetermined relevant and reliable information. One of the questions that presented most commonly throughout this project was how can operations effectively sustain the systems which could provide this required information once an incident occurs. This leads to other questions such as; what level and type of incident could render our existing systems obsolete in an emergency? And what contingencies do operations have in place or available to them to counter this risk? To assist address these issues an extension to ACARP Project C19010 was sought and successful, allowing a scoping study to research and identify existing and future strategies, systems and hardware which have the potential to support and provide the information requirements of decision makers during or after an incident at an underground coal mine. This paper outlines findings to date, of the ACARP Project C19010 extension.

INTRODUCTION

In an effort to ensure that *emergency* mine re-entry processes were developed using risk management methodologies, Queensland Mines Rescue Service (QMRS) facilitated a comprehensive risk assessment involving all key stake holders including New South Wales Mines Rescue (NSWMR). The risk assessment took four days to complete and resulted in identifying what information was required to make a risk based decision on the deployment of rescue teams underground. A task group was formed that converted the risk assessment into mine re-entry guidelines from which the Australian Coal Association Research Program (ACARP) funded project C19010 "Emergency Response: Mine Entry Data Management" developed a decision support system. The system known as Mine Re-entry Assessment System (MRAS) incorporates check lists of the information determined to be required as well as the capability of accessing information known prior to the event. Making use of the this tool with underpinning risk management logic, assists decision makers to make informed, quality decisions in a timely manner (Brady, *et al.,* 2012).

Workshops in Queensland, New South Wales and New Zealand were held as part of the information dissemination process of the project as well as presentations at local and international conferences. A common question and one that was raised many times by the project team themselves was "will the systems providing the information identified as being critical survive the event?" This question led to others such as; what can mines do to protect these systems? What type and magnitude of event will compromise systems? What contingencies are in place or available to cover such events?

One of the main findings of this project was that mining operations give little consideration to the locality and survivability of information and communication systems critical to obtaining the required information after an incident of any type or size. The recommendations made in the project report (Nugent, *et al.,* 2011) included the following;

[1] *Mine Safety Institute of Australia Pty Ltd*
[2] *Minerals Industry Safety and Health Centre, Sustainable Minerals Institute, University of Queensland, d.cliff@mishc.uq.edu.au, 07 3346 4086*
[3] *BHP Billiton Mitsubishi Alliance, Broadmeadow Mine*
[4] *NSW Mines Rescue Service*
[5] *Coal Mine Technical Services*

There is an urgent need to assess and determine the general capability and capacity of existing critical mine monitoring and communication systems to provide reliable and relevant information during emergencies of varied types and size. The research should include:

- The general status of Australian underground coal mines environmental monitoring and communications systems capabilities and capacities to provide adequate information after an incident.
- What structural design specifications and strategic positioning considerations (including contingences) for environmental monitoring and communications systems would be considered best practice for emergency response?
- The current status of existing systems available and suitable for Australian underground coal mines relevant to the scope.
- The current status of any research and development being carried out or pending applicable to the scope.
- What further specific research is needed to assist industry in implementing the functional specification developed in the original C19010 project and recommendations of how such research could best be achieved?

This is by no means the first time that recommendations of this type have been made. The report on the Warden's Inquiry into the Moura No.2 Mine disaster (Windridge, 1995) stated "The loss of telephone communication with the five South crew at the time of the first explosion left no means of ascertaining the status of those persons without some form of entry to the mine. There appears a need to examine explosion resistant means of communication".

The task group that was formed following the Warden's inquiry to look at Mines Rescue Strategy Development (Task Group No. 4, 1996) determined that with regards to existing practice, knowledge of conditions underground after an incident would be insufficient for accurate assessment of the mine environment. The task group identified "The highest priority need is for a communications system which would survive an incident and provide ongoing two way communications between escaping or trapped miners and rescue personnel on the surface".

With regard to gas monitoring, Task Group four recommended that fixed tube bundles and gas chromatographs should be made available at all mines as the primary method of measuring post incident mine atmospheric conditions, something that many Australian mines have achieved. The recommendation went further stating that tube bundle systems should include:

- protection of tubes from damage,
- locations of sampling points designed for both normal and post incident atmospheric conditions,
- modularisation using boreholes to minimise delay in transmission and analysis as well as to make the system as robust as possible,
- techniques for verifying tube integrity which could be routinely applied post incident.

For real time systems the Task Group 4 recommended "*Research into the development of robust telemetric sensors for gas analysis and other environmental parameters, over ranges existing after incidents, should be prioritised."* (Task Group No. 4, 1996)

Task Group 4 also highlighted that both pre-installed and post-incident boreholes should be considered when developing Aided Rescue Management Plans.

The New South Wales Department of Primary Industries Mine Design Guidelines MDG 1003 (Windblast Guideline), (Mine Safety Operations Division, 2007) states "The mine must establish and maintain a robust system of gas monitoring capable of providing real time gas analysis of explosive gases in the Hazardous zone - Windblast before, during and after a windblast."

The New South Wales Department of Primary Industries Mine Design Guidelines MDG1020 Guidelines for underground emergency escape systems and the provision of self rescuers (Mines Rescue Working

Group and Mine Safety Operations Division, 2010) identifies that a main risk in a mine's emergency escape system is that the monitoring system does not survive the event. The guideline indicates that integrity and protection of the system during an event, and contingencies in the event of a failure need to be considered. Also the design, construction and installation of hardware associated with the emergency communication apparatus, need to assure the integrity of the system during any event that causes an emergency, and that the risk assessment and risk management systems must aim to preserve the functionality of the system through a catastrophic event.

Even with all of these recommendations and requirements, the underground coal mining industry is not in the position it should be to ensure ongoing reliable information/data during and post incident. With this knowledge and knowing that the information identified in ACARP project C19010 as critical for decision makers was possibly not going to be available during an incident, the project team made a successful application to ACARP for an extension to the project to address the research recommended. The aim of the extension being to research and identify existing and future strategies, systems and hardware which have the potential to support and provide the information requirements of decision makers during or after an incident at an underground coal mine.

C19010 PROJECT EXTENSION

Industry risk assessment

One of the initial tasks the project team completed was an industry risk assessment to assess and analyse the potential incidents that could impact effective communications and mine monitoring systems supplying data and information. This risk assessment defined critical data/information sources (Figure 1), the types of sensors/hardware collecting data (Figure 2) and the transmission medium of that data/information (Figure 3). A detailed hazard analysis was then conducted to identify the incidents that could compromise the capture, supply and transmission of the critical data/information to the post-incident management team (Figure 4). These threats were analysed for their consequences and potential magnitude. The current preventative and mitigation controls employed to maintain access to this data and information were also identified. It became very apparent during this process that most of the systems set up to collect and transmit critical data/information were done so in a manner that addressed the day to day requirements for this information with little consideration given to expected measurements or increasing the chance of survivability during or following an event. Despite this it appears systems are scoped, designed and installed for "peace time mining". Where possible the industry risk assessment team identified areas requiring improvement.

An issue that was identified as requiring urgent investigation was the need for independent intrinsically safe power supplies for systems providing critical data, such as gas monitoring and communications, when underground power is lost. The use of battery backup to address this problem although useful to overcome short duration power supply issues, is not adequate for an ongoing response that may last more than several days. Recent events in Australia and at Pike River in New Zealand have involved responses and withdrawal to the surface best measured in weeks rather than days, and would far exceed battery backup capacity to keep systems operational. The project team have organised for manufacturers, certification experts and electrical inspectors to meet to try and come up with a solution to provide power for ongoing provision of critical data from such systems during extended periods of underground power loss.

Another area that became obvious during the risk assessment was the need for "hardening" of sensors and other hardware, including transmission media to protect against both over pressure and flying debris. It is recognised that hardening of the sensors by the manufacturers although important is not going to be achieved in the short term. For this reason the project team has recommended further investigation into designing retro fitted physical protection to critical hardware. There is also a need to investigate the most appropriate means of installation of hardware and transmission media (including tube bundle sample tubes). The positioning of the hardware also needs to be considered as part of the installation. Communication hardware such as telephones may be better placed in cut throughs rather than main headings to provide protection.

It is normal practice following an incident such as an explosion underground to ring all underground phones and regularly communicate over the intercom systems (DAC) to try and get a response from workers underground. One of the problems frequently faced at these times is knowing whether the communications are still operational. There is a need for a means of testing to be built into hardware. A

desirable feature on intercom type systems is an override button, allowing the surface operator to activate the talk function at the unit underground allowing them to hear what was happening in that area.

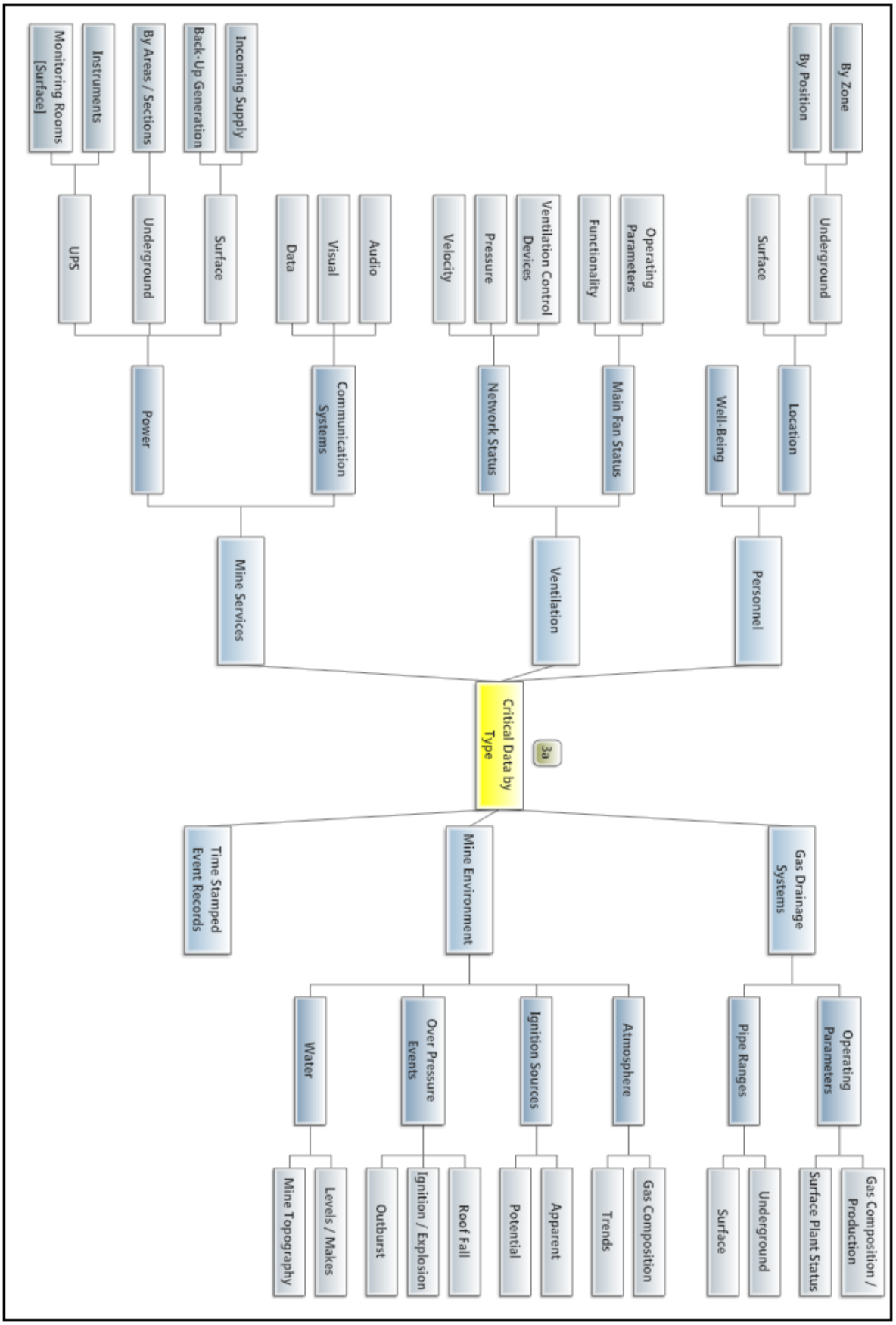

Figure 1 - Critical data by type

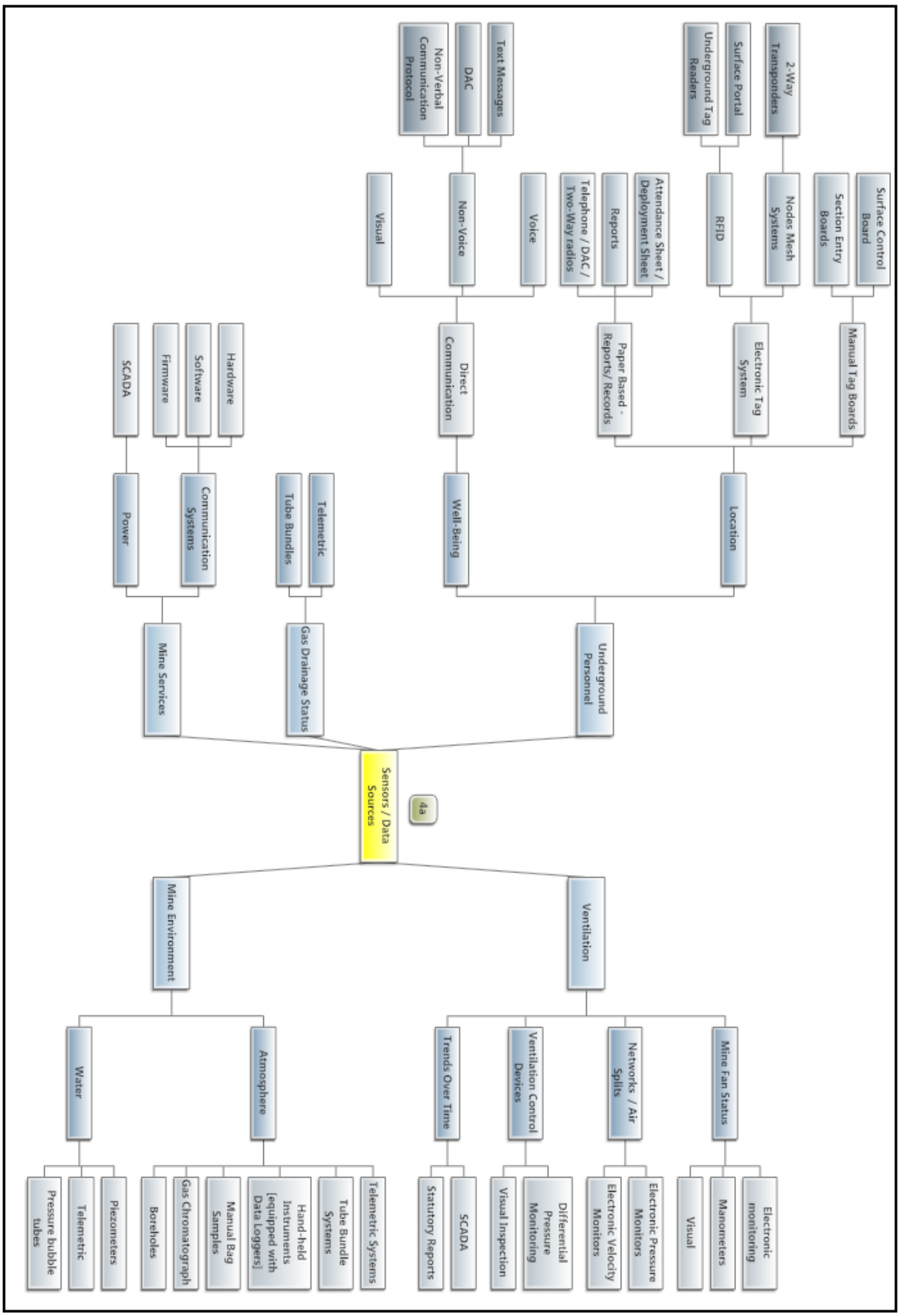

Figure 2 - Critical sensors/data sources

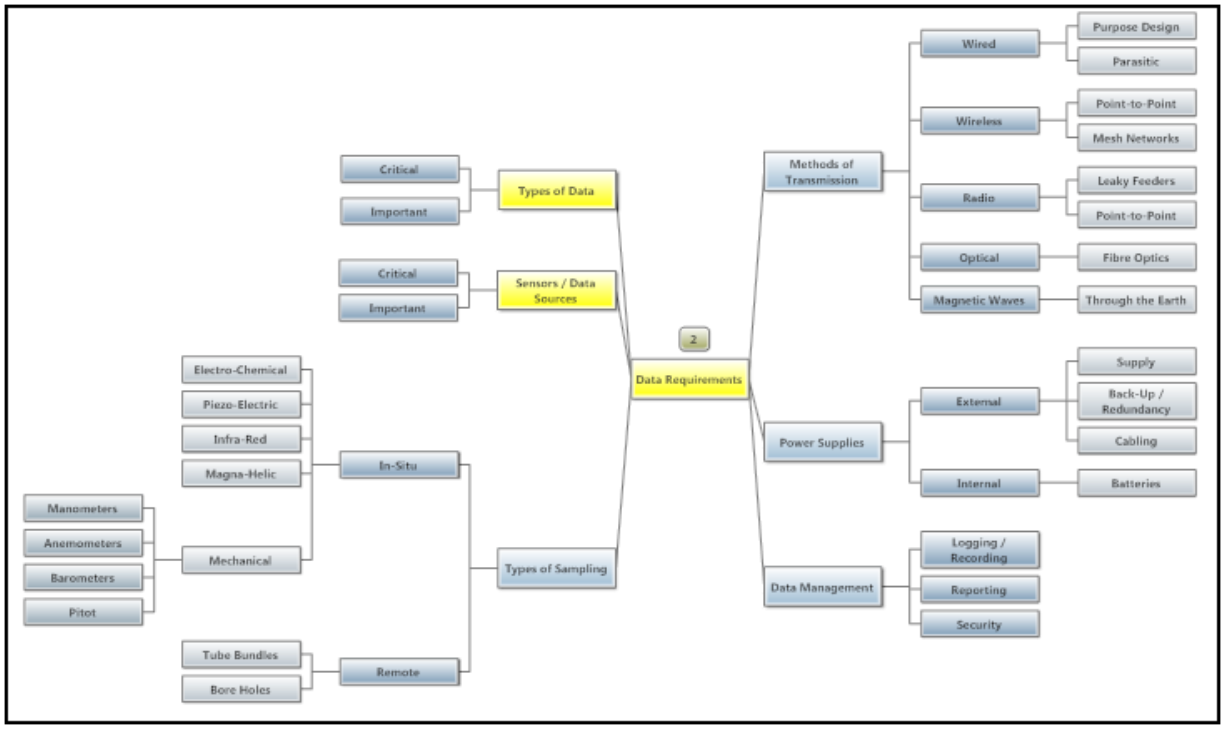

Figure 3 - Data requirements

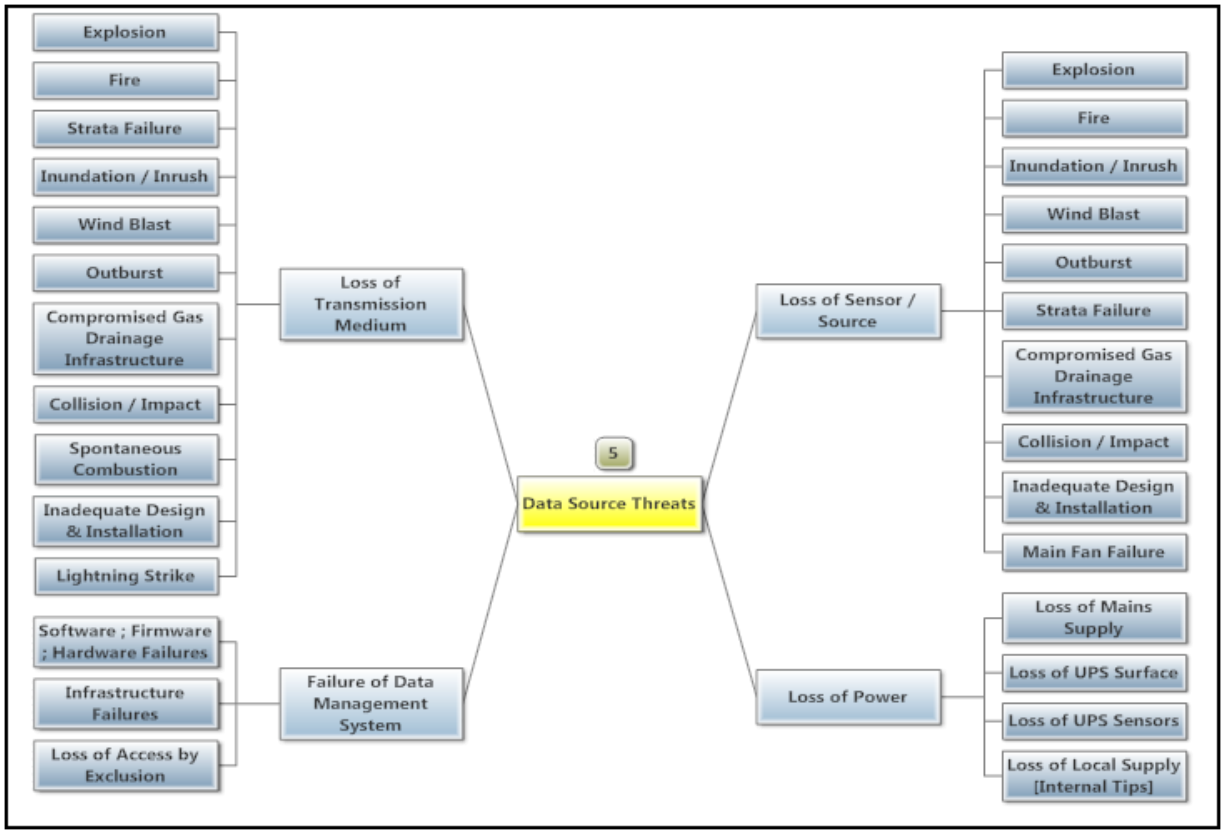

Figure 4- Data source threats

The need for systems with inbuilt component redundancy, to increase the probability that the system could survive an explosion, was also identified. It was determined probable that borehole based systems would be required and if information was to be available in a timely manner these bore holes would need to be pre drilled with a risk based approach utilised to determine required locations.

International mining industry

Communications with international research, statutory and mines rescue organisations revealed similar issues and concerns with the survivability of critical data and communication infrastructure during or following an event. There has been no evidence that any country has found a solution. The approach of most is to make use of bore holes for monitoring where possible. International attention seems to have focused more on communications rather than data with the United States leading the way.

Following the Sago, Aracoma, and Darby disasters in the United States in 2006 the Mine Improvement and New Emergency Response Act of 2006 (MINER Act) was introduced requiring mine operators to adopt underground communications and electronic tracking (CT) systems to meet specific performance goals (NIOSH, 2011). Two requirements were;

- Submission of an Emergency Response Plan (ERP) that provides for a means of communication with the surface for underground workers with inbuilt component redundancy such as a secondary telephone or equivalent two-way communication. The ERP also must provide for above-ground personnel to be able to determine the current, or immediately pre-accident, location of all underground personnel. Any system so utilised must be functional, reliable, and calculated to remain serviceable in a post-accident setting.
- Submission of plan for approval that provides for post-accident communication between underground and surface personnel via a wireless two-way medium, and an electronic tracking system that permits surface personnel to determine the location of any persons trapped underground or set forth within the plan the reasons such provisions cannot be adopted. Where such plan sets forth the reasons such provisions cannot be adopted, the plan must set forth the operator's alternative means of compliance. Such an alternative must approximate, as closely as possible, the degree of functional utility and safety protection provided by the wireless two-way medium and electronic tracking system.

These wireless systems often make use of nodes that if configured with redundancy and survivability in mind can continue to operate if a node is destroyed as they are able to "re-route" the communication via an alternative pathway not using that node. There are however still some uncertainties as to the survivability of these systems as they exist but work is continuing to improve them.

Other industries

The project team looked at other industries that also rely on data and information transmitted to a central point from which decisions are made. What was obvious was that underground coal mining was unique in the conditions under which these systems have to operate and what they would be exposed to by way of undesirable events. The petrochemical industry uses similar types of gas sensors but these are installed in open areas unlike those in the confinement of an underground coal mine. In general the installation standards are higher in the petrochemical industry with use made of cable trays and protective ducting for transmission cables. Because they are located on the surface, exclusion zones don't pose the same problems as they do for underground installations and provision of more than one power supply for gas monitoring systems as a contingency to power monitoring systems is much easier to accommodate.

CASE STUDIES

There are enough example cases of data and communications remaining operational after incidents to know that it is possible for systems to survive and worth the effort to protect them in case of such events. There are also cases where systems are destroyed so survivability will depend on amongst other things the nature, location and magnitude of the event. The following are a few examples that highlight where systems have continued to provide information.

Moura No 2 Qld Australia

Workers in the 1NW section at Moura No 2 reported ears popping and some were thrown at the time of the explosion. Contact with the surface was however possible via telephone (this was how the surface learnt of the event). The estimated over pressure at the site of the explosion (512 Panel) was 8psi (Stephan, *et al.*, 1994). A tube bundle system was installed at Moura No. 2 and although not all tubes were sampling from intended locations results from the system and subsequent gas chromatograph

analysis of samples collected via the tube bundle system provided valuable information on the status of the underground environment. These tubes were unprotected but installation was performed to a high standard with tubes attached to a catenary wire being tied off every 300 mm. Subsequent analyses of data coming from the tube bundle system (Golledge, *et al.,* 1995) determined the most likely sampling locations for tubes following the initial explosion to be as detailed in Table 1.

Table 1 - Likely sampling locations following initial explosion

Sampling Point	Original Location	Status
1	4 South	Relocated to same air split as Point 9 17 CIT Dips
3	Fan North Return	Unaffected
4	Fan South Return	Unaffected
5	512 Seals	Severed in 4 South Level
6	5 South Bottom Returns	Severed in 4 South Level and severely pinched
7	5 South Top Return	Severed in 4 South Level
8	1NW Return	Unaffected (integrity doubtful)
9	17 C/T Dips	Unaffected
16	512 Top Returns	Severed in 4 South Level
19	Dips North Return	Unaffected

Pike River New Zealand

It is rare that video evidence of an underground coal mine explosion exists, however the video camera at the portal at the Pike River Mine in New Zealand captured footage of all four explosions in November 2010. The images from the camera provided useful information during response to this disaster including the direction of ventilation flow. The camera was in a position that meant it survived all four explosions. The video along with observations and the condition of the two survivors allow an estimation of the forces and velocity of the initial explosion. The velocity of gas exiting the portal was calculated as being between 30 and 70 m/s (108-252 km/h). Almost 2000 m inbye the portal, was a telephone positioned only one metre from the corner of the main drift and the outbye rib of B1 cut through (Figure 5). In this position the phone would have been exposed to most of the force travelling up the drift. This phone was fixed to a rib bolt whereby the bracket of the phone slipped over the bolt and a nut used to hold the bracket in place. The cable was also firmly anchored so that it could not stress the connector, directly below the phone. The cable then ran up the main drift predominantly in the centre of the roadway clipped to a catenary wire. This phone withstood the velocity and over pressure of the explosion and was operational and used by one of the survivors to phone the surface. The standard of installation is the most likely reason the phone remained operational. Observations of installation standards of phones in Australian underground coal mines would suggest that many would not have withstood such an event. Although this phone remained operational after the initial explosion, it may have been better placed on the inbye rib of the cut through where it would have been less likely to be exposed to flying debris and the force of the explosion. The mine's Voicecom (intercom system) at the portal was also operational after the initial explosion but it is not known for certain whether this system or telephones inbye of the phone used at B1 were operational. The mine's real-time gas monitoring system was not operational following the initial explosion.

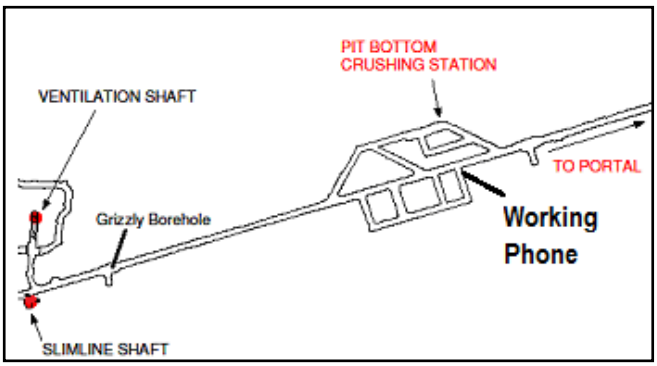

Figure 5 - Location of phone used after initial explosion

Roof fall in drift

A recent significant roof fall in a drift at a mine disrupted communications and power, however six of the eight tube bundle lines in service that were run in the drift survived. The tube bundle installed was in two bundles of five core tube. The five core tube has five tubes encapsulated in an outer protective sheath. Review of vacuum pressures (Figure 6) and sample flow rates (Figure 7) post incident shows that the tubes were not broken but instead squashed. The two tubes that were not operational after the event were squashed to the extent that sample could not be drawn through them, so no measurements were possible.

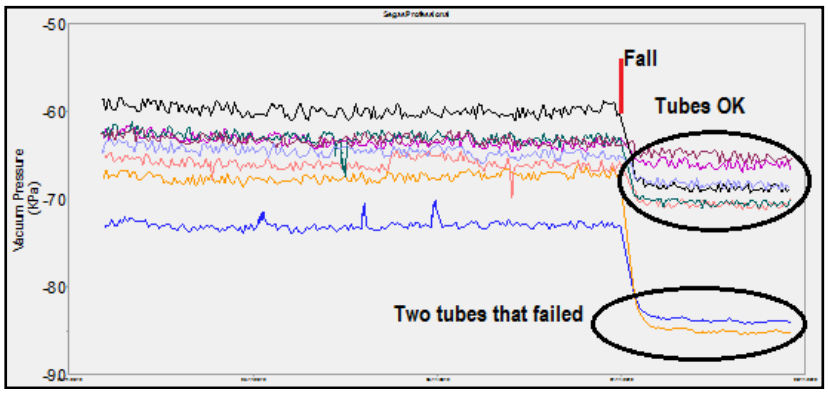

Figure 6 - Tube vacuum pressures

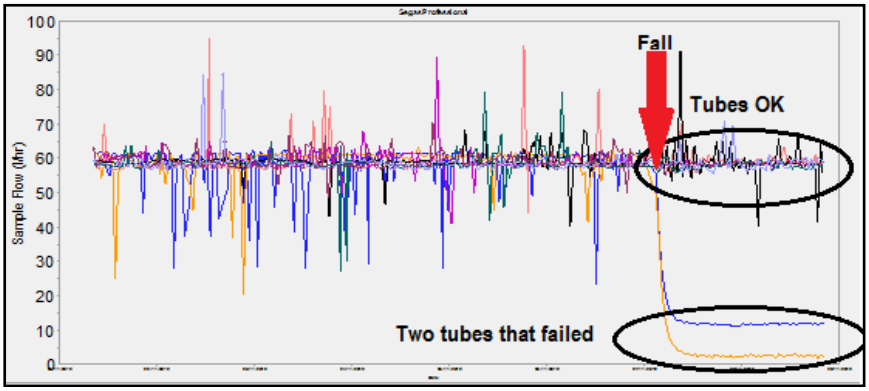

Figure 7 - Sample flows

When tubes are squashed it is important to remember that with the extra resistance leakage paths not previously favoured may eventuate. Any such leakage would influence the accuracy of the results. The onset of leakage in a sample line monitoring an area normally returning low oxygen concentrations (such as a sealed goaf) is easily picked up by an increase in oxygen. It is however more difficult to determine whether a general body type sample is still monitoring from the intended location as increases in oxygen when original samples contain those close to fresh air are difficult to detect. Figure 8 shows there was no change to the oxygen concentration for the location with approximately 10% oxygen and a slight increase in one of the tubes returning over 20% oxygen, indicating that at least some leakage was occurring in this tube. To be assured that general body type samples were still monitoring from the intended locations, review of other gas components would need to be undertaken in conjunction with changes to vacuum pressure.

This example highlights that additional protection of the tubing, in this case the outer sheathing of the five core bundle, can afford the protection required to allow ongoing tube bundle analysis even after a significant fall. Mine sites should evaluate areas of elevated risk for tubes where additional protection is required.

Willow Creek Utah USA

Four explosions occurred at the Willow Creek Mine over 31 min beginning 11:48pm 31st July 2000. A Personal Emergency Device (PED) system was in use at the mine, and was instrumental in alerting miners underground of the need to evacuate with miners working in active and remote areas of the mine

at the time of the explosion notified using the PED. These miners all safely exited the mine (Mckinney, *et al.*, 2001).

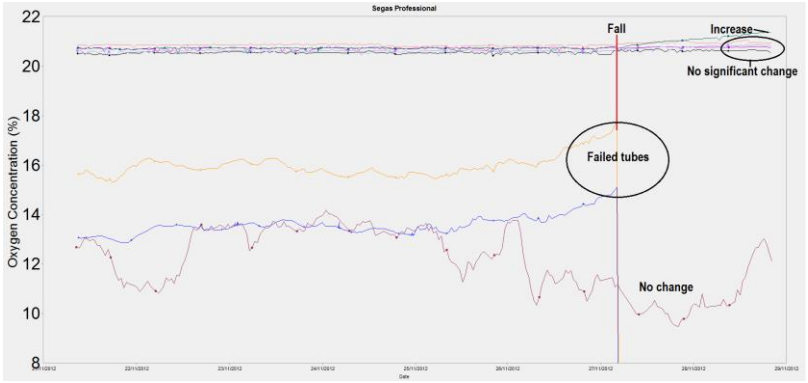

Figure 8 - Oxygen concentrations

Following the initial explosion on the headgate (maingate) side of the D-3 goaf elevated CO readings occurred in the bleeder entries and in the D-3 No. 1 headgate entry. The monitors near the headgate bleeder connector regulators experienced a communication failure. Data from the CO monitors near the tailgate regulators at the bleeder entries indicated concentrations in excess of 50 ppm (maximum sensor could measure) shortly after the explosion. Data from the CO monitor at MPL B2 showed that the concentrations began to increase approximately 21 min after the explosion and, within an additional two minutes, the readings were in excess of 50 ppm. Data from the CO monitors in the No. 1 headgate entry outbye the face revealed that elevated concentrations of CO occurred at the monitor locations near the longwall face. Data from each outbye sensor also showed elevated concentrations. This explosion occurred in the No. 1 headgate entry of the D-3 section near the longwall set-up rooms and is estimated to have generated pressures of approximately 5 psi near the origin. The force exiting the headgate into the bleeder entries was approximately three psi. The force reaching the tailgate bleeder regulators was probably two psi.

This example shows how monitoring sensors are not all necessarily destroyed. It also highlights the problem of measuring ranges for these types of sensors, often limited to 50 ppm, which is fine during normal operations but off scale during an event.

THE NEXT STAGE

Although the extension project is still not completed, the project team has collected enough evidence to show that the likelihood of survivability of data and information sources can be increased by fitting mechanical protection and improved installation standards including the siting of hardware. To assist mine sites improve the chance of ongoing data and information supply ACARP have approved further funding for the project team to conduct testing that will expose modified/protected hardware and transmission media to over pressure events and flame fronts to establish best practice based on scientific and engineering testing.

CONCLUSIONS

- General practice at most Australian underground coal mines is for mine communication and monitoring systems to be designed, located and installed to address the proactive risk management of principle and major hazards but give little consideration to a system's purpose, requirements or functionality post any incident - systems are currently designed and installed for "peace time mining".
- It is possible for monitoring systems and communications to remain operational after events, including explosions.
- Installation standards and siting of hardware can have a significant influence on the survivability of systems delivering critical information.

- Post incident use should be considered in specifications, installation standards and location of data and communication infrastructure.
- More can be done to ensure that data required and communications are available post incident.
- Unless improvements are introduced to increase survivability of critical sources of data and information, significant delays to aided rescue can be expected.

REFERENCES

Brady, D, Nugent, G, Cliff, D, Devlin, S and Grieves, J, 2012. A New approach to decision making for mines rescue deployment. *2012 SME Annual Meeting and Exhibition, Meeting Preprints* Seattle, USA 2012 PP 353-356.

Golledge, P, Humphreys, D, Cliff, D, Reinhardt, D and Hester, C, 1995. Report of investigation of various matters associated with explosions at Moura No. 2 underground mine on 7 and 9 August 1994. Report R005-94/95, SIMTARS, DME, January 1995.

McKinney, R, Crocco W, Tortorea, J S, Wirth, G J, Weaver, CA, Urosek, J E, Beiter, D A, and Stephan, C R, 2001. United States Department Of Labour Mine Safety And Health Administration Coal Mine Safety And Health, Report Of Investigation Underground Coal Mine Explosions July 31 - August 1, 2000 Willow Creek Mine - Msha Id. No. 42-02113 Plateau Mining Corporation Helper, Carbon County, Utah.

Mines Rescue Working Group and Mine Safety Operations Division of Industry and Investment NSW, 2010. Mine design guidelines MDG 1020 guidelines for underground emergency escape systems and the provision of self rescuers. New South Wales Department of Primary Industries.

Mine Safety Operations Division, 2007. Mine design guidelines MDG1003 windblast guideline New South Wales Department of Primary Industries.

NIOSH, 2011. Tutorial on Wireless Communication and Electronic Tracking Part 1: Technology Overview. National Institute for Occupational Safety and Health (NIOSH) Mining Division. http://www.msha.gov/techsupp/PEDLocating/WirelessCommandTrack2009.pdf. [Accessed: 28 December 2012].

Nugent G, Devlin, S, Grieves, J, Cliff, D and Brady, D, 2011. Emergency response: mine entry data management, Australian Coal Association Research Program Project No. C19010.

Stephan, C R, Urosek, J E and Giardino, D A, 1994. A technical evaluation of information provided by the Department of Minerals and Energy, Brisbane, Queensland Australia concerning the Underground Coal Mine Explosions Moura No. 2 Mines, Moura, Queensland, Australia, August 7 and 9.

Task Group No. 4, 1996. Moura No. 2 inquiry warden's report implementation: Task Group No. 4 Report - Mines Rescue Strategy Development

Windridge, F, 1995. Warden's inquiry. Report on an Accident at Moura No. 2 Underground Mine on Sunday, 7 August 1994.

EARLY FIRE DETECTION IN UNDERGROUND COALMINES

Frank Mendham[1], David Cliff[2], Tim Horberry[3] and Andre De Kock[4]

ABSTRACT: Analysis of mine fire growth and spread is important for improving safe emergency egress for mine workers in fires. In fire engineering, a 'design fire' is the term that describes the characterisation of a fire in relation to its growth and decay. Defining the design fire is the starting point for managing the fire risk of a mine and is the basis for further analysis of emergency response. A current Minerals Industry Safety and Health Centre (MISHC) PhD project is researching methods of improving fire life safety and asset loss control in mining using Video Based Fire Detection (VBFD) in the context of fixed plant fires. Experiments were carried out at Safety in Mines Testing and Research Station (SIMTARS) facilities. This research was part of the MISHC project to better understand the detection capabilities of VBFD in relation to weak plumes from the early combustion of coal associated with fixed plant. This part of the research specifically deals with assessing the physical dimensions and shape of the low energy, non-flaming weak plumes formed from smouldering coal fires. It demonstrates how experimental methods were used to successfully validate the corresponding numerical simulation of the design fire so it can be used for further research.

INTRODUCTION

This paper reports on a part of an ongoing research program that assesses the small smouldering combustion type fires that are the subject of Video Based Fire Detection (VBFD).

The purpose of the primary research is to assess if (VBFD) is an effective means of improving fire life safety and asset loss control in mining.

These fires are likely to occur on fixed plant in such locations where VBFD could be located to detect such early stage smouldering. One of the most commonly reported sources of potential ignition associated with fixed plant in underground coal mines is the frictional overheating of conveyor belt bearings and rollers that are in the process of failure through seizing.

The types of fires prevalent at this early stage of combustion are quite small in terms of the energy released in the coal combustion process and are usually without flames. They typically produce a plume of visible products of pyrolysis termed pyrolates. In the subject research these pyrolates include condensed fragments of volatile hydrocarbons, water vapour and gases such as Carbon Monoxide (CO) resulting from the pyrolysis of coal and grease. Under appropriate conditions there is potential for rapid fire growth and spread, so these small fixed plant fires are considered quite dangerous to mine workers.

This plume analysis and its relationship to the design fire's mass loss rate is the main focus of this paper. Design fires are typically described in a graphical format, which compares Heat Release Rate (HRR) measured in Kilowatts (kW) or products of combustion, such as smoke and pyrolates, against time. Low energy plumes with small or no flames are termed 'weak plumes'. The experimental and numerical assessments of the design fire plume dimensions were compared.

Clearly defining the design fire was a critical step in this VBFD study, as the ongoing accuracy of the research depends on repeatability of the design fire throughout the experiments. The objective of this research therefore was to prove that the numerically estimated plume dimensions could be validated experimentally.

[1] *PhD Candidate, Minerals Industry Safety and Health Centre, Sustainable Minerals Institute, University of Queensland, f.mendham@uq.edu.au, M: +61 4 2140 7633*
[2] *Professor of Occupational Health and Safety in Mining, and Director, Minerals Industry Safety and Health Centre, Sustainable Minerals Institute, University of Queensland*
[3] *Associate Professor of Human Factors, Minerals Industry Safety and Health Centre, Sustainable Minerals Institute, University of Queensland*
[4] *A/Director - Mining Research and Development Centre, SIMTARS*

METHOD

Experimental method

Testing of pyrolates produced from a thin layer of coal and grease on simulated overheated bearings was experimentally carried out at the Safety in Mines Testing and Research Station (SIMTARS) in Queensland, Australia. The experimental purpose was to simulate a frictional heating fire on a typical underground mine conveyor belt bearing or roller, in pre-failure mode.

Study Design. Experimental data relating to the visibility of small sample coal combustion plumes was collected across a range of tests. The sensitivity analysis that was introduced involved varying the levels of ventilation and luminous intensity. Three levels of the two parameters were applied over six repetitions of each experiment. In total, this resulted in 54 individual tests being included in the experimental plan (i.e. 3 air velocity levels x 3 luminosity levels x 6 repetitions). The intention was to alter the shape or visibility, or both, of the plumes to test the capability of VBFD under a range of light conditions and plume shapes. The tests were carried out over several days. The data was analysed to compare the time taken for VBFD to recognise the pyrolate plumes associated with the simulated conveyor belt bearing fires.

Equipment: A circular steel plate of 250 mm diameter was used as the simulated bearing surface with a propane gas burner rig, as shown in Figure 1, used to heat the underside of the steel plate. In an operating underground coalmine the surface of the simulated bearing housing is likely be covered with a thin layer of coal dust. The estimated mass of coal dust was 40 g, having a thickness of 5 mm based on previous mine observations. Due to the likely failure of the bearing's mechanical seal, a small amount of grease was included. The grease quantity was approximately 40 g at a thickness of 3 mm. Figure 2 shows the simulated bearing housing surface with a layer of grease on the left hand side plate and grease covered with a coal dust layer on the right hand side plate.

Figure 1 - Heater unit

Figure 2 - Simulated bearing housings with surface coal and grease

Procedure: A thermocouple was placed 5 mm above the surface of the coal layer. The temperature at this point was continuously logged at 10 s intervals throughout each test. The air stream was directed towards the fire and adjusted to achieve three levels of air velocity and subsequent plume shapes.

An initial heating of the simulated bearing housing was carried out to record the surface temperature prior to the introduction of the coal and grease samples. Figure 3 depicts the metal surface being heated and shows the location of the thermocouple. Figure 4 shows an example of a pyrolate plume resulting from heating a coal and grease sample on the simulated bearing housing plate.

In relation to the repeatability of the experiments, six repetitions of each experiment were planned using coal and grease samples of approximately the same amount (40 g each). The samples were applied to the metal plate using the same application tool for each experiment to achieve consistent coal and grease dimensions and quantities.

Figure 3 - Heated simulated bearing housing without fuel

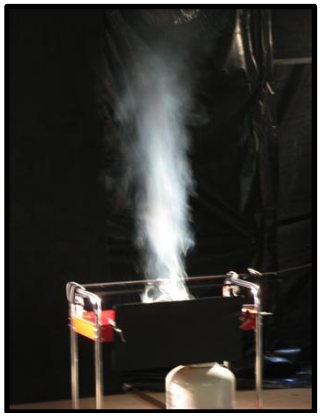

Figure 4 - Typical smoke plume resulting from heating the coal and grease fuel mixture

Data Recorded: For each repetition of each set of experimental conditions involving variations of airflow and light intensity levels, the following parameters were measured and recorded: -

1. Air velocity;
2. Light intensity;
3. Coal surface temperature at commencement of test;
4. CO levels of three CO monitors at commencement of test;
5. VBFD activation time;
6. Coal surface temperature at VBFD activation;
7. CO levels of three CO monitors at VBFD activation.

The height and width of the plumes were estimated from VBFD recordings, video camera recordings and still photographs, for each fire repetition at 'growth', 'fully developed' and 'decay' phases. The visual data was synchronised with recorded time data and readings associated with the coal surface temperature.

The simulated bearing surface was heated to a temperature up to a maximum of 384 ºC using a propane gas burner producing 909 W applied directly to the under surface of the metal plate.

Figure 5 shows the temperature curve of the simulated bearing housing upper surface. This setup was applied to all repetitions of each set of experiments. The metal surface was heated in each experiment until the VBFD detected smoke, or if smoke was not detected by the VBFD, until the plume production was reduced to an insignificant rate due to consumption of the fuel source. The temperature curve associated with the simulated bearing housing surface shown in Figure 5 was also incorporated in the CFD models.

Air velocity was a significant contributing factor to the plume shape and dimensions. Three axial fan settings were used to establish the low, medium and high levels of air velocity used in the testing. The air velocities were recorded using a calibrated hotwire anemometer, as follows:

1. Low air velocity - 0.11 m/s;
2. Medium velocity - 0.5 m/s;
3. High velocity - 1.6 m/s.

For the purpose of brevity in this paper, only the three low air velocities by the six repetitions (that is, eighteen studies in total) are considered in the results presented.

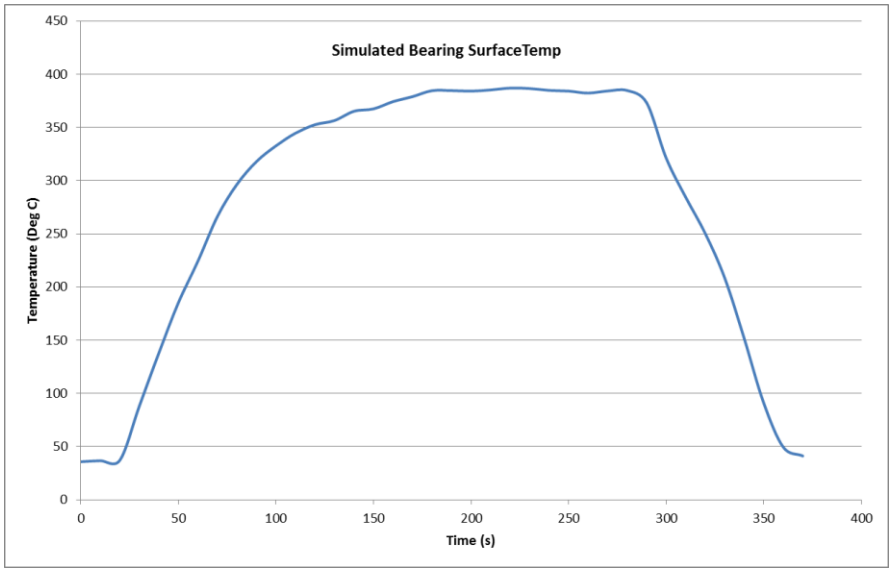

Figure 5 - Surface temperature of simulated bearing housing

Numerical assessment method

Several Computational Fluid Dynamics (CFD) models were developed after the SIMTARS VBFD experiments in order to make use of the actual physical setup parameters and the experimental space dimensions. This was done in preference to using estimated parameters before the experiments so as to reduce uncertainty in the CFD models.

The purpose of the CFD models was firstly to compare the numerical results with the experimental results in terms of similarity of plume dimensions and related characteristics.

Secondly, if the numerical CFD simulations were validated by the experimental results, CFD would be considered a useful tool for simulating the design fire in a range of computer generated mine environments for further analysis. These potential environments would vary in air velocity, ambient temperature, spacial dimensions, obscuration and light intensity levels.

The CFD program utilised for the modelling was Fire Dynamics Simulator (FDS) Version 5 (McGrattan, *et al*., 2007). This software is widely used in the field of fire engineering for estimating fire conditions within built structures and transport tunnels to assist in the development of safe design. The CFD modelsoftware solves numerically a large eddy simulation form of the Navier-Stokes equations appropriate for low-speed, thermally-driven flow, with an emphasis on smoke and heat transport from fires. Further investigation into the use of an alternative CFD model that models chemical combustion was not concluded at the time of writing this paper

The CFD models were useful in estimating the pyrolate plume dimensions and temperature in the model space by resolving mass continuity and energy conservation equations for the smouldering combustion of the coal samples. It was assumed for the simulated conveyor belt bearing housing that the coal layer itself would offer negligible resistance to the release and subsequent flow of pyrolates from the porous dust samples. It was further assumed, and subsequently shown experimentally, that the resistance by the coal layer to the released pyrolates from the grease layer located below the coal sample was also negligible.

The Cox and Kumar explanation provided in the SFPE Handbook 3rd Edition (Cox and Kumar, 2002) discusses how the behaviour of solid combustibles during pyrolysis can be described using the mass and energy conservation principles in the following terms: -

> "This application of the conservation of mass and energy is subject to the boundary conditions set by the gas phase. Because of this low resistance to the release of pyrolates, the CFD engine can incorporate the mass continuity and energy conservation equations.

The mass continuity equation is: -

$$\frac{\partial \rho_s}{\partial t} + \frac{\partial}{\partial x_j}(\rho u_j) = 0$$

with ρ_s being the instantaneous local density of the solid.

The energy conservation equation is: -

$$\frac{\partial}{\partial t}(\rho_s c_s T_s) + \frac{\partial}{\partial x_j}(\rho u_j c_p T_s) = \frac{\partial}{\partial x_j}\left(k_s \frac{\partial T_s}{\partial x_j} - \dot{q}_R\right) - H_p \frac{\partial \rho_s}{\partial t}$$

with Hp being the heat of pyrolysis.

The terms on the left side represent the unsteady accumulation of energy in the solid together with the energy carried by the gas pyrolysates through the elementary control volume.

The right side comprises terms describing thermal conduction, the influence of in-depth absorption of thermal radiation, and the energy lost in the phase change.

An Arrhenius pyrolysis rate equation closes the system of equations:

$$\frac{\partial \rho_s}{\partial t} = -B\rho_s \exp\left(-\frac{E_s}{RT_s}\right)$$

These equations are solved by the CFD model subject to the boundary conditions at the solid surface that:

$$\dot{q}''_{\text{net}} = -k_s \frac{\partial T}{\partial x_j}$$

where $\dot{q}''$ net represents the net heat transfer to the solid. "(Cox and Kumar, 2002)

RESULTS

The shape and dimensions of the pyrolate plumes from small smouldering coal fires plumes is the subject of this paper. A close correlation was found to exist between the shape and dimensions of the CFD simulated pyrolate plumes and the experimental plumes that were observed and measured. These plumes were used as the target source of 'smoke' for the VBFD assessment carried out at SIMTARS. Being able to validate a numerical model of the design fire is very important, as CFD models may now be used as a means of incorporating the virtual design fire in any CFD modelled mine environment for ongoing VBFD or other research.

In relation to the plume formation, the time synchronised simulated bearing housing surface temperature that heated the coal and the relationship to the coal surface temperature are graphically shown in Figure 6.

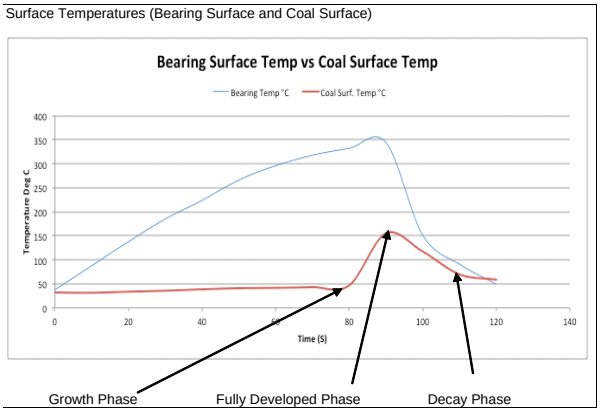

Figure 6 - Assessment of numerical, experimental and analytical plume dimensions

In Table 1, images from the CFD model and photographs of the experiment are compared at the three fire development stages, growth, fully developed and decay stage.

Table 1 - Comparison of pyrolate plumes

Growth Phase	Fully Developed Phase	Decay Phase
CFD Simulation Result		
		
Experimental Result		
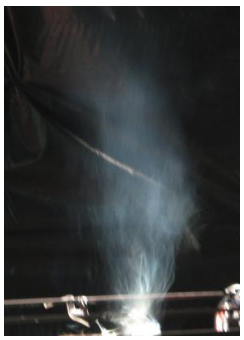		

Observations

Growth Phase:

The CFD simulation indicates that the pyrolate plume width is approximately 200 mm and extends to the ceiling 3.65 m above the fire surface. This is validated by the experiment, as shown in the Table 1 growth phase image.

Fully Developed Phase:

The plume appears considerably denser in the fully developed phase CFD simulation and in the experiment photograph at the same stage of growth. In both the simulation and the experiment, the width of the plume is the same diameter as the heated metal surface, which is 250 mm. Stratification of the pyrolate plume is occurring at approximately 3 m above the fire surface in both the simulated and experimental images.

Decay Phase:

In the decay phase, the plume is at its weakest and most turbulent. Stratification remains below the ceiling even though the plume is diminishing in width to 200 mm in both the CFD simulation and in the image of the experiment.

Furthermore, it was observed that the rate of accumulation of smoke or pyrolate particulates in the plume in the subject experiments was not as a result of flaming combustion, but of radiant heat transfer through the heated metal surface of the simulated bearing housing. Also it was noted that when the coal was heated, a pyrolate plume formed. The entrainment of nearby air diluted and cooled the pyrolate plume as it rose above the hot surface.

DISCUSSIONS / CONCLUSIONS

The experimentation carried out at SIMTARS as part of the VBFD early fire detection in coalmines project has been successful in validating the numerically modelled CFD simulation of the subject design fire.

Importantly, further CFD models of specific mine layouts incorporating their environmental conditions may be developed in the future to include this validated design fire. This provides the ability to safely estimate the movement of early developing fires in underground mines and also assists in the ongoing development of VBFD.

The research has produced some very positive findings to support the further development of CFD simulated design fires and VBFD for mine site use. A number of correlations between the results of the weak plume analysis of the subject design fires used for this VBFD research and the methods developed by Drysdale (Drysdale, 1998) for much stronger plumes have been demonstrated. This is particularly evident in the dimensions of the plume size at the various stages of design fire development.

From a practical viewpoint, in relation to non-flaming weak pyrolate plumes, when the plume entrains air, a possible flammable pyrolates mixture with air above the Lower Explosive Limit (LEL) can form. Delayed flaming can occur within the pyrolate plume or beyond, if a pilot ignition source exhibiting an adequately strong energy level above Minimum Ignition Energy (MIE) level is introduced.

Where adequately strong ignition sources, such as a frictional sparks or a hot metal shard from a failing bearing housing may become present in conjunction with a space that has accumulated a significant volume of volatile hydrocarbons from a pyrolate plume, the potential for an explosion exists.

It is clear that weak low energy non-flaming plumes in underground coalmines are a complex topic with many variables that might affect the outcome. Little previous research has been carried out in this area; as such, the studies reported in this paper could not build on an established body of knowledge here, however this fact underpins the importance of the research itself.

REFERENCES

Cox, G and Kumar, S, 2002. Modelling enclosure fires using CFD. In *The SFPE Handbook of Fire Protection Engineering, 3rd edition*, National Fire Protection Association and Society of Fire Protection Engineers. USA.

Drysdale, D, 1998. *An Introduction to Fire Dynamics, Second Edition*. John Wiley and Sons. NY.

Heskestad, G, 1995. *Fire Plumes, Section 2, Chapter 2, The SFPE Handbook of Fire Protection Engineering, 2nd edition*, National Fire Protection Association and Society of Fire Protection Engineers. USA.

McGrattan, K, Klein, B, Hostikka, S and Floyd, J, 2007. *NIST Special Publication 1018-5 - Fire Dynamics Simulator (Version 5) - Technical Reference Guide*, Baltimore, Maryland, USA.

Yokoi, S, 1960. Study of the prevention of fire spread caused by hot upward currents. *Building Research Institute, Report No. 34*, Tokyo.

AN ENGINEERED APPROACH TO BUSHFIRE MANAGEMENT

Frank Mendham[1,2]

ABSTRACT: In the summer of 2010 to 2011, enhanced levels of vegetation occurred across Queensland due to a number of major rainfall events. New mining operations, as well as significant coal seam gas gathering developments, were considered to be under threat from bushfire hazards during the impending dry season due to abnormal natural fuel loads. This paper outlines a risk based fire management strategy using high level multi-discipline systematic risk analysis tools, including fault tree analysis, to develop controls that were viable in terms of implementation and cost. A quantitative approach to the designation of fire risk zones was applied through the calculation of thermal radiation caused by potential fire in vegetation surrounding exposed areas. The methods used to perform these calculations were derived from the Australian Standard AS 3959:2009 - construction of buildings in bushfire prone areas. Bushfires are a significant risk in Australian conditions. Putting in place measures to protect local worker communities, process assets, cultural heritage values and the environment, was seen as essential under current and impending climatic and ecological conditions. The use of a risk based approach offered an effective, quantifiable and reproducible system to meet this challenge.

INTRODUCTION

The initial development of the engineered approach to bushfire management was developed out of a requirement to reduce the life safety risks and risks associated with asset loss in relation to a major Coal Seam Gas (CSG) operator's upstream surface facilities in Queensland. The predominant hazard was seen as an uncontrolled fire event due to high residual fuel loads resulting from recent above average rainfall and dry hot summer weather forecasts. To address the identified credible threat, a high level Fire Management Strategy (FMS) was developed with a particular focus on the CSG operator's gas gathering network surface equipment, but with the flexibility to address existing infrastructure, as well as future development. A risk based approach was taken to develop the FMS and through this process, a thorough and detailed analysis of the issues surrounding the potential associated threats to personnel, property, cultural heritage and environmental assets caused by fire, whether planned or wild, was conducted. This methodology has since been effectively applied to further scenarios involving a Bowen Basin coal mine and a Victorian alpine zinc mine. The approach is therefore seen as being particularly relevant to existing and future mining.

In order to identify the conditions resulting from the occurrence of an unwanted event, extensive Fault Tree Analysis (FTA) workshops were facilitated. In these workshops professionals from a range of engineering and science disciplines worked together to understand the problem and to identify areas that needed to be managed to reduce the level of risk. The FTA workshop project team was split into three areas consistent with the three contributing key events leading to the top level event; fuel sources, ignition sources, and exposures. Each of the key events were then further analysed in risk workshops, where the team evaluated the available risk treatments, and risk acceptance criteria. The range of risk treatments consisted of operational, procedural and engineering risk management controls. Several hundred fault tree inputs were identified and assessed.

As part of the development of the FMS, a review of the 'Final Report Recommendations' of the 2009 Victorian Bushfires Royal Commission was carried out. Fifteen (15) key recommendations were identified as relevant, and appropriate actions were included as part of the overall FMS. The purpose of the overarching FMS was to provide a guideline for the development of subordinate site specific Fire Management Plans (FMPs) that can be developed, reviewed, modified and deployed, as needs change, by the mining operators' staff and contractors.

It is important to note that a level of 'on the job' training and experience is required to develop the competence to complete the assessments, as fire management specific terms, measurements and calculations are required to determine essential outcomes based on the application of Australian Standard AS3959: 2009 'Construction of Buildings in Bushfire Prone Areas' (Standards Australia, 2009).

[1] *PhD Candidate, Minerals Industry Safety and Health Centre, Sustainable Minerals Institute, University of Queensland, f.mendham@uq.edu.au, M: +61 4 2140 7633*
[2] *Technical Director - Industrial Fire and Risk Engineering, WSP Asia Pacific*

In some situations, such as where life safety exposures exist, or where asset exposures exist under certain conditions relating to sloping ground or where limited available separating distance from fire sources exists, a higher level assessment is required. This assessment involves fire modelling, engineering calculations and experienced judgement.

Fire fighting training and equipment options were addressed in this project. The options ranged from a do nothing reliance on fixed fire suppression and passive systems in infrastructure facilities to a fully operational industrial fire brigade. The FMS was intended to be a living document, which reflects current research in bushfire management and the changing needs of the mining operator and the fire risks facing its operations.

FIRE MANAGEMENT STRATEGY

In relation to uncontrolled fire events, the FMS delivers a framework that provides a uniform, structured and planned tool for managing the asset by minimising fire life safety risk, fire exposure risk to environmental and cultural heritage artefacts, losses associated with property and subsequent reputational risk.

The solution to address the original CSG operators' challenge involved the development of a FMS or guideline that could be applied by users as guidance in developing site specific FMPs. The preservation and improvement of the associated agricultural portfolio and the natural environment was also a key factor addressed by this risk management framework. The FMS achieved its purpose by allowing the development of site-specific FMPs across the variety of sites that make up the gas field or mine site. These site-specific FMPs are developed to assist in making decisions in land and asset management on an ongoing basis providing for the protection of life, the environment, items of cultural heritage and assets, from the threat of bushfires.

The FMS development project addressed the following:

1. Conduct a thorough and detailed risk analysis of the issues surrounding the potential associated risks to personnel, property, cultural heritage and environmental assets caused by fire, whether planned or wild;
2. Develop suitable preparedness and response strategies for gas plants, wells, rig sites, agricultural land, environmentally and culturally sensitive areas and general plant and equipment;
3. Set out the requirements for managing fire on non operator owned properties with a particular focus on preventing fire spread from the gas gathering network surface equipment;
4. Establish a Bushfire Management Plan template for sites, which cover building requirements, asset protection zones, fuel management, access and emergency response measures consistent with legislative and business requirements;
5. Review and include any relevant findings from the Victorian Fire Board 'Black Saturday Report';
6. Establish equipment needs and requirements; and
7. Establish training and competency requirements.

Fire risk analysis

A focussed FTA workshop was facilitated and documented, determining a wide range of 'trigger events' leading to the 'top level event' - which was recorded as an 'Unwanted Planned or Unplanned Fire Event'. The fault trees were developed at this workshop by project teams, comprising of both the CSG operator and the fire and risk engineering team. Likewise, subsequent mine projects in Queensland and Victoria were carried out in a similar way, but with the benefit of experience of the original CSG project.

In risk analysis, the graphical construct FTA is considered useful for modelling the system conditions using binary variables (0's and 1's) that may result in the occurrence of an unwanted event. The significance of the output event (otherwise known as the 'top level event') is nominally recognised as the 'consequence factor' associated with risk, therefore values of probability (random variables) are not normally applied.

Boolean logic 'AND' gates and 'OR' gates are used in FTA. For example, both logic inputs of a two (2) input 'AND' gate need to be concurrently a logic level '1' or 'TRUE' for the output of the 'AND' gate to be '1' or 'TRUE'. Any other combination would result in a logic '0' or 'FALSE' output. For an 'OR' gate, either logic input or both logic inputs can be a '1' or a 'TRUE' level for the output to be 'ONE' or 'TRUE'.

The combination of events in an 'AND' gate configuration or even a single event, as in the case of an 'OR' configuration, is required to trigger the output of the fault tree (to achieve a value '1'), so input event probability (or risk likelihood factor) is not associated with fault trees.

The consequence levels associated with the fault tree top level event can be graded either qualitatively, or quantitatively. For the purpose of a qualitative assessment, it was considered that any event that was acceptable would signify a consequence value of '0', while any event that was unacceptable would have a consequence value of '1'. Acceptability was based on the operators risk appetite.

An overall reduction of risk may be achieved by preventing fault tree outputs from 'triggering'. This is realised through implementing risk mitigation controls that reduce the likelihood or probability of achieving a '1' input condition into a logic gate.

Three (3) risk workshops were facilitated as part of the fire risk analysis component of the FMS project, where risk registers were developed based on the information coming from the initial FTA.

A diverse disciplinary range of team members attended the sessions, which were focussed on determining and documenting the level of risk and risk management treatments acceptable to the CSG operator in relation to the contributors of the identified 'Unwanted - Planned or Unplanned Fire'.

As stated earlier, the contributors to this risk consist of: 'Fuel Sources', 'Ignition Sources' and 'Exposures', with each requiring specific risk management.

- Workshop one addressed 'Fuel Sources', which included a significant representation by ecological and environmental professionals.
- Workshop two addressed 'Ignition Sources' and 'Exposures', and was attended primarily by health and safety professionals and fire and risk engineers.
- Workshop three addressed, 'Ignition Sources' and 'Exposures' and was attended by a wide range of engineers and scientists.

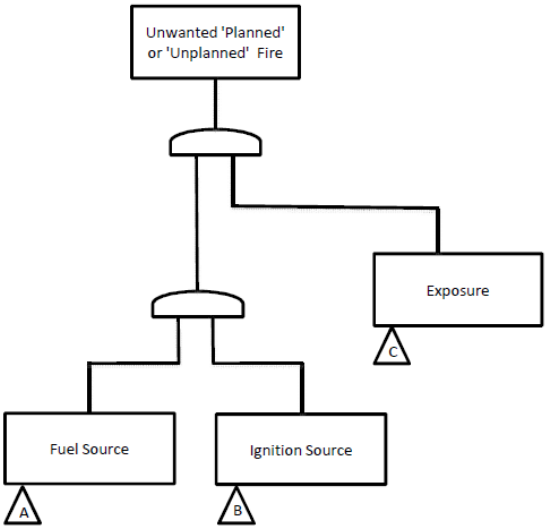

Figure 1 - Fault tree analysis

Fire risk was assessed in two ways:

1. The risk of fire spread from the operators property or assets
2. The risk of fire spread to the operators property or assets

The developed risk treatments were considered achievable and relevant to the operations with the range of risk treatments consisting of operational, procedural and engineering risk management controls. A key benefit of the combined FTA and traditional risk matrix approach is that it takes both a 'bottom up' and 'top down' approach. The 'bottom up' approach addresses measures required to reduce the likelihood of fuel sources becoming 'readily combustible' and ignition sources becoming 'adequately strong'. The 'top down' approach addresses the protection of exposures, such as life safety, the environment, cultural heritage values and assets, given the occurrence of an 'Unwanted Planned or Unplanned Fire'.

In this way, the risks are managed such that at least two 'layers of protection' exist: one layer to reduce the fire risk and another layer to reduce the fire exposure. Both methods reduce the risk of 'losses'. This risk-based approach has since been successfully deployed at a Victorian and a Queensland mine.

Bushfire preparedness and response strategies for mines

The stay or go policy in relation to mine sites and remote drill pads and the like, will require the decision to be a core responsibility of the management team that by the nature of their role will have all the relevant site information: Fire Danger Index (FDI) and weather information for the site, as well as FMPs. Any site that has been identified as being 'at risk' to the extent that the stay or go policy has to be considered should be assessed in accordance with Method 2 of AS3959 (Standards Australia, 2009) to establish if further controls can be made to mitigate the risk prior to any manned operations to the site.

While both management and individuals will make choices about what to do and how best to prepare in advance of a fire occurring, the emphasis should be on taking protective action rather than choice or options. Drilling or other activities on sites at risk from bushfire need to be scheduled outside of the bushfire season, however if essential work is deemed to be vital to business continuity then on days where the FDI raises the bushfire risk above moderate (High; Extreme; or Catastrophic) all access to these activities should be prohibited.

The stay or go policy must be considered in the light of available information. For example in a worst-case scenario, a bushfire might travel at 1.5 km/h in a forest or woodland and faster in grassland. To ensure safe escape routes are available evacuation must take place before the fire is within approximately 3 km of the site. Access and choices of travel determine whether or not escape routes to defendable locations are practical and are not vulnerable (tops of ridges). When the fire is within approximately 2 km, ember attack may cause spot fires that may impact on escape routes, therefore alternative routes need to be identified and documented in the site FMP. These considerations are site specific and as such, need to be documented for each FMP.

In the event of a bushfire approaching a manned site, a decision to leave site should be made early. Any decision to stay on site and defend assets should only be made if appropriately trained staff with suitable fire fighting equipment is in place and the site has been proven to be able through a bushfire engineering study to provide a safe place of refuge.

In the instance of the Victorian (underground) gold mine, the mineshaft with refuge chamber was considered the safest refuge location. To ensure safe egress is possible, the design and maintenance of access roads is imperative in ensuring staff are able to securely leave the site.

To ensure this, site planners and machinery operators should be suitably trained in the design and construction of access roads, so regular inspection and reporting of damage to these roads are important in maintaining safe egress integrity.

Engineered approach

The Australian Standard AS3959: 2009 'Construction of Buildings in Bushfire Prone Areas' (Standards Australia, 2009) is the basis of determining the impact of fire on various targets, including those typically located at mines and similar industrial facilities in close proximity to vegetation. Its' application requires the assessor to carry out either a basic assessment of the minimum separation distance, known as an Asset Protection Zone (APZ), between a potential vegetation fire and infrastructure under the 'Method 1' approach, or a more rigorous assessment involving engineering analysis and judgement, under AS3959's 'Method 2' approach.

It is recommended that only persons competent in each assessment area be engaged to carry out this work. Both approaches estimate radiant heat flux at the target based on the distance from the subject vegetation fire by vegetation type or category.

The AS3959 (Standards Australia, 2009) Method 1 approach is quite appropriate in most circumstances to estimate an APZ, however the 'granularity' of the Method 1 table in AS3959 (Standards Australia, 2009) is quite coarse. As a result, tabulated separation distances between the target and the source take wide steps and often overstate the required vegetation clearance distance.

The slope of the ground also restricts Method 1's applicability and maximum Fire Danger Index (FDI) levels listed in the table. The Method 1 assessment procedure represents a useful, streamlined approach to risk mitigation for buildings or infrastructure located on the vegetation interface, however, often it will result in an inaccurate risk model for structures exposed to unique vegetation topography or shape.

In cases where life safety is the dominant risk, or where high value assets, such as overland conveyors are at threat, the analytical AS3959 (Standards Australia, 2009) Method 2, in conjunction with performance based fire engineered construction solutions, is recommended.

The Method 2 assessment procedure provides the calculation methodology and accepted inputs that the Method 1 assessment matrix was derived from. The Method 1 assessment procedure focuses purely on radiant heat and is non-granular in assessment. Primary limitations with the Method 1 assessment procedure include:

1. There is no consideration of flame contact.
2. Upslope vegetation is considered as being level
3. Vegetation slopes are divided into 5-degree increments with the highest slope in the range determining the vegetation slope.
4. The site slope, being the slope between the vegetation and the building is not differentiated from the slope within the vegetation.
5. The structure receiver is measured opposite the midpoint of the flame, which is often inaccurate.
6. Vegetation width may be less than the predefined 100 m.
7. Radiant heat shielding from the surrounding landscape is not considered.

The Method 2 detailed procedure for determining the radiant heat flux measure, referred to as Bushfire Attack Level (BAL) was originally published as a model proposed by Tan (Tan, *et al.*, 2005). This model builds upon the Drysdale (Drysdale, 1985) radiant heat model to create a three-dimensional landscape to model the bushfire within.

The model contains two sets of equations: one, that models bushfire behaviour, while the other models radiation. Key to the fire behaviour model is the determination of the configuration or view factor as shown in Figure 2.

This factor is assessed via an algorithm that tilts the flame as a flat panel emitting radiant heat to determine the worst possible case scenario. The main variables that determine the view factor include:

1. Fire Danger Index (FDI);
2. Vegetation type;
3. Site slope (slope between the vegetation and the structure);
4. Vegetation slope (slope within the vegetation);
5. Vegetation width; and
6. Elevation of receiver (the most vulnerable height of the structure).

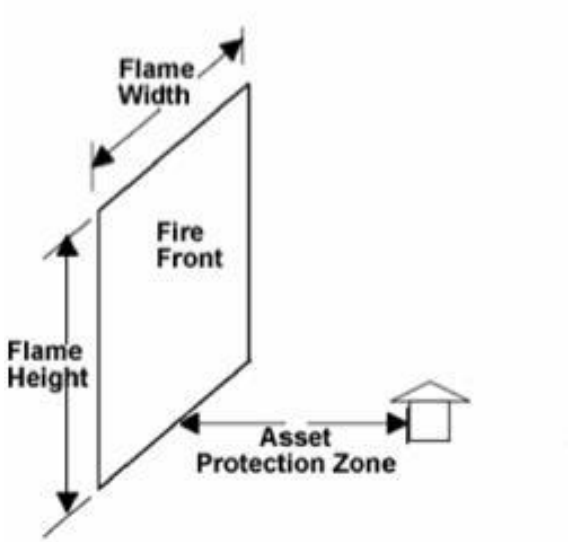

Figure 2 - Theoretical radiating surface of bushfire

By specifying an accurate peak elevation of receiver, the flame trigonometry provides a more accurate view factor for determining radiant heat. This is due to the path between the midpoint of the tilted flame and the receiver being increased or decreased.

The vegetation interface often leads to topography where the site slope does not match the vegetation slope. By specifying a more accurate elevation of receiver, a design fire that more closely represents the real world scenario can be used to assess bushfire risk.

An assumption of the view factor calculation is that the radiant heat panel is a blackbody of evenly distributed heat. Therefore the panel can be divided into multiple pieces to effectively add or subtract from the model to equate to the view factor of the receiver. Using this methodology the width of the flame and subsequent radiant heat flux that will impact on the site can be predicted. Furthermore, using this methodology, any shielding effect can be quantified by the subtractive methodology of the view factor model. The rate of spread determines the flame length, fire intensity and the radiant heat flux.

A fire in vegetation will eventually reach equilibrium rate of spread. Grass and woodland take 5-10 min to reach equilibrium and forest in 12-45 min in winds above 4 m/s. AS3959 (Standards Australia, 2009) design fires are based on a bushfire in equilibrium or a quasi-steady state.

The main acceptance criteria are based on life safety and the requirement to provide a safe refuge for any persons located at the facility whilst the fire front passes. Where a safe refuge is not available, the radiant heat flux will need to be below 2.1 kW/m² to provide an acceptable level of protection, as shown in Table 1 (Assael and Kakosimos, 2010). In this situation the APZs will need to provide sufficient setbacks to ensure that a radiant heat flux of 2.1 kW/m² is not exceeded where there is no shielding or safe refuge.

Table 1 - Effects on humans of radiant heat (Assael and Kakosimos, 2010)

Radiant Heat (kW/m^2)	Impact
37.5	100% lethality in 1 min 1% lethality in 10 s
25.0	100% lethality in 1 min Significant injury in 10 s
12.5	1% lethality in 1 min 1st degree burns in 10 s
4.0	No lethality 2nd degree burns probable Pain after exposure of 20 s
1.6	Acceptable limit for prolonged exposure

A second consideration is the structures and assets within the facility, which may consist of combustibles, which will begin to distort and char at a radiant heat flux of between 10 kW/m² and 12 kW/m².

Therefore any radiant heat flux from a bushfire impacting on the facility assets will need to be below 10 kW/m^2.

AREA SPECIFIC FIRE MANAGEMENT PLANNING

Preparedness and response strategies were embedded into risk controls and risk registers. Risk registers were developed for 'ignition sources,' 'fuel sources,' and 'exposures.' These risk registers were aimed at identifying a level risk that is acceptable to the CSG operator and subsequently for miners.

As a part of the risk assessment carried out, the risk registers developed considered requirements for managing fire on non-operator owned properties, in particular where gas gathering network surface equipment was located.

The findings of the Black Saturday Report (Victorian Govt, 2009) indicated that a requirement to manage ignition sources (overhead power lines in the case of the Black Saturday fires) should be incorporated in the operators FMS. The gas gathering network in this situation and subsequent mine scenarios, was considered in a similar way to overhead power lines. A FMP template was developed in conjunction with the FMS strategy, including FMP development procedures and a sample FMP.

The Victorian Fire Board's Black Saturday report (Victorian Govt., 2009) was considered as part of the development of the FMS. Where appropriate, findings from the report were incorporated into the FMS. Options for fire fighting and fire protection needs of the operator were developed to assist in informed decision making in relation to fire fighting training and fire equipment needs.

A range of competency and subsequent training requirements exist for the development of FMPs and for potential fire fighting activities. Some of these training requirements are legislated, depending on the level of activities undertaken with respect to each.

FMP development using AS3959 Method 1 (Standards Australia, 2009) by mine operational staff was enabled as part of this project through the development of field manuals, which included 'step by step' instructions via flow charts and a comprehensive set of reference data in appendices.

Figure 3 shows an example of a flow chart developed to enable creation of specific area FMPs.

CONCLUSIONS

This paper demonstrates an example of how a risk based approach to the development of a FMS to address bushfires was conducted. It further demonstrates how a thorough and detailed analysis of the issues surrounding the risks to personnel, property, cultural heritage and environmental assets caused by fire, whether planned or wild, can be addressed using a multi-discipline approach to minimise the impact on the environment using engineered methods.

The purpose of the overarching FMS was to provide a guideline for the development of site specific FMPs that can be implemented by the operators' staff and contractors.

It is important to note that a level of 'on the job' training and experience is required to develop the competence to complete the assessments, as fire management specific terms, measurements and calculations are required to determine essential outcomes, based on the application of Australian Standard AS3959:2009 'Construction of Buildings in Bushfire Prone Areas' (Standards Australia, 2009).

A 'Fire Management Strategy - Field Management Plan Procedure' document was developed as part of this project, to facilitate the collection of field data required for the Method 1 assessment approach as detailed in AS3959, to allow the development of FMPs.

As part of the development of the FMS, a review of the 'Final Report Recommendations' of the 2009 Victorian Bushfires Royal Commission (Victorian Govt., 2009) was carried out. Fifteen (15) key recommendations were identified as relevant, and appropriate actions incorporated as part of the overall FMS.

The Fire management Strategy was intended to be a 'living document', which reflects current research in bushfire management and the changing needs of mining and the fire risks facing its operations.

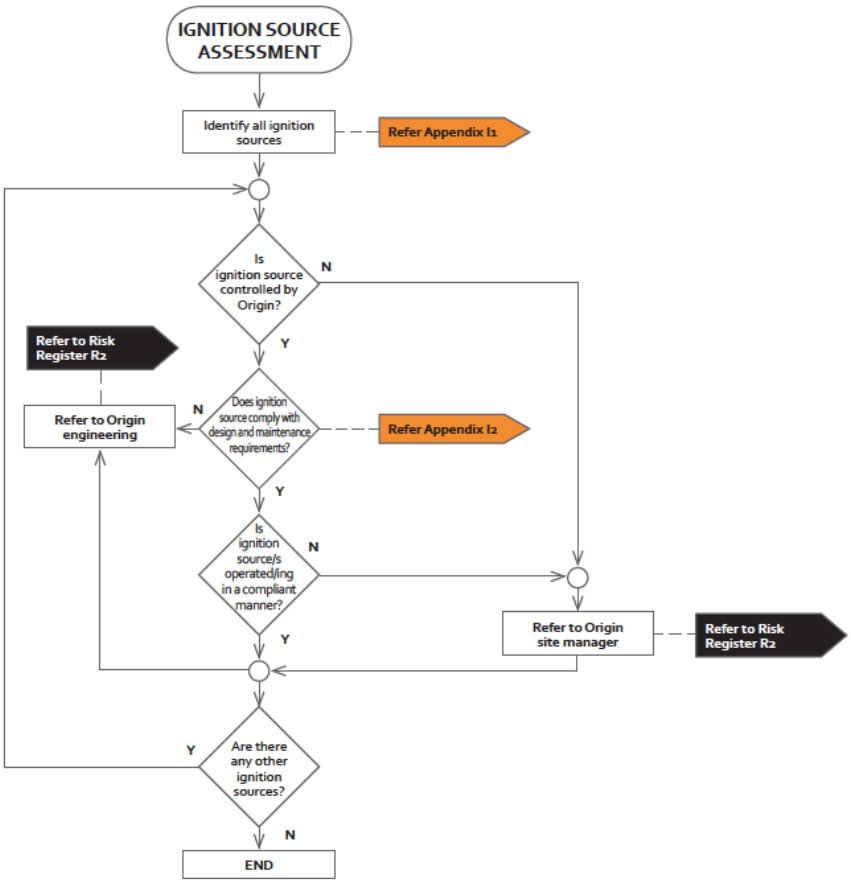

Figure 3 - Typical example of guidance provided in FMP development template

REFERENCES

Assael and Kakosimos, 2010, Fires, explosions, and toxic gas dispersions: effects calculation and risk, *CRC Press*, Florida, USA.

Drysdale, D, 1985. An introduction to Fire Dynamics. John Wiley and Sons. New York.

Standards Australia, 2009, AS 3959:2009 Construction of buildings in bushfire-prone areas, Standards Australia, Sydney.

Tan, Z, Midgley, S and Douglas, G, 2005. A computerised model for bushfire attack assessment and its applications in bushfire protection planning, at *16 the Congress of the Modelling and Simulation*. Society of Australia and New Zealand (MODSIM 05), Melbourne, 12-15 December 2005.

Victorian Bushfires Royal Commission, 2009. Final Report - Summary, Parliament of Victoria, Melbourne.

CROSS-MEASURE DIRECTIONAL DRILLING

Frank Hungerford[1,2] and Ting Ren[1]

ABSTRACT: The development of directional drilling in the coal industry has been driven by the need to provide reliable in-seam gas drainage ahead of development. The same technology has been utilised for cross-measure drilling in adjacent seams other than the working seam and also in surrounding strata. The equipment and technology utilised for the applications of directional drilling in cross-measure applications is identified. The process of designing both lateral and vertical aspects of the drilling is explained with specific reference to the limitations and practices of directional control during the inter-burden section of each borehole. Cross-measure drilling applications of in-seam pre and post gas drainage, goaf gas drainage, water management and in-rush protection as well as exploration are described to explain the ways the technology has been utilised.

INTRODUCTION

Although underground drilling has evolved from rotary drilling to directional drilling for gas drainage, the ability to steer and locate boreholes with directional drilling has created opportunities to access horizons (or targets) other than that of the drill site location.

As with in-seam drilling, it is essential to have prior knowledge of the environment to be drilled. This allows logical limitations to be applied to project planning to ensure equipment security and enhance the prospects of achieving favourable goals. The in-seam component is similar to directional in-seam drilling. The added challenge involves dealing with the variations presented with the cross-measure component. Borehole design has to provide a design path in the vertical plane usually complicated by being incorporated with a lateral design path. The drillers then attempt to follow these paths while dealing with the variability of environment with changing strata and stability.

The various applications of cross-measure and cross-measure in-seam drilling have been developed and employed in Australia, the USA, China and other countries. These have their challenges in both the planning and the drilling stages.

DIRECTIONAL DRILLING

While in-seam rotary drilling was being used for gas drainage, rotary drilling was and still is employed to drill relatively straight boreholes angled through the strata and coal measures under and over longwall blocks. These boreholes provide post-drainage by removing gas released from the underlying seams after stress relief as the longwall face passes. In some instances, similar boreholes have been drilled into the strata above the longwall block to provide gas drainage of the goaf.

Directional drilling has provided the ability to drill boreholes through, into and along strata surrounding the working seam. Early application of cross-measure, in-seam direction drilling was trialled as part of an in-seam directional development project (Hungerford, *et al*., 1988) and has since evolved as an established practice. This provides the opportunity to locate boreholes in positions which can provide pre and post gas drainage, exploration, water drainage and inrush protection.

The equipment used is the same as for in-seam directional drilling with some allowances for the various vertical angles at the collar and options to manage unstable environments and stronger strata in the cross-measure sections. Although the required capacity of a drilling system for cross-measure is dependent of the length of boreholes to be drilled, the established standard equipment set for longhole drilling in the 1980's and 90's (Hungerford, 1995) includes:

- 75 kW, 1000 v electro-hydraulic power unit,

[1] *School of Civil, Mining & Environmental Engineering, University of Wollongong, Wollongong, NSW 2522, Australia, FHungerford@vli.com.au, Tel: +61 2 4964 2300*
[2] *Global Technical Services Manager, Drilling Division, Valley Longwall International Pty Ltd*

- Integrated methane monitor,
- 250 l/min @ 8 MPa high pressure water pump,
- 135 kN thrust and pull,
- 1500 to 2000 Nm torque, NQ rod capacity rotation unit,
- track mounted,
- compact enough to operate in a mine roadway and allow vehicles to pass.

The specifications for directional drilling equipment have been upgraded with an HQ rod chuck capacity for over-core recovery. Since there will always be some uncertainty in the stability of the environment to be drilled and no fall-back recovery option of mining recovery of bogged equipment, the option of over-coring needs to be available with the HQ rod capacity. To supplement that precaution, if boggy conditions are expected, the design depths need to be limited to the over-coring depth capacity. If cross-measure drilling is the main aim of a drilling project, it is preferred that the feed frame of the drill rig be supplied with an angled setup option so standpipes can be installed at appropriate vertical angles to suit the design of the project. Track mounted drill rigs are limited in the vertical angle at which they can be mounted.

CHD rods are utilised with an electronic survey tool and 2-7/8" downhole motor. Electronic survey tools are an integral component in the process of steering the drilling.

The standard 4/5 lobe Accu-drill downhole motor has been used extensively in cross-measure drilling with good results. Penetration rates are dependent of the strength of the strata being drilled with 0.2 m/min a common penetration rate in the sandstone with a compressive strength in the order of 60 MPa. Recently, more powerful 5/6 and 7/8 lobe downhole motors have been introduced with good drilling performance.

The PCD bit design impacts on penetration rate and performance. Drill bits from Asahi and Drilling Products Inc. (DPI) have been used with various options available in the shape of the face (convex versus flat) and arrangement of cutters. Some bits of a particular design have been very effective then following supplies have suffered from quality control problems which tend to negate previous reputations gained. In each case, the drillers have to assess how the current bit is performing, alter drilling parameters to establish reasonable penetration rates or ultimately replace the bit. Reliability and robustness then become as important to the performance of the drill bit. Inter-burden strata strength has a direct influence on the penetration rates achievable and when it exceeds 60 MPa, penetration rates can be expected to reduce dramatically. In these cases, the option of using tungsten tipped tri-cone roller bits for the stone section of drilling is available but only over short intervals due to the limited life of these bits in this environment.

DRILLING ENVIRONMENT

As for any directional drilling, an assessment of the expected drilling conditions is required. Not only does it serve to provide the drillers with an indication of what to expect and what precautions they may need to employ, but it also has an influence on the design of the drilling. Ideally, the drilling environment needs to be stable enough to support an open borehole over the length of the drilling along the target horizon, and for long enough through the cross-measure section to allow for installation of casing if required. The state of the strata at the drill site determines whether the standpipe is installed directly into the face or has to be directed into the roof or floor strata.

Since access is not usually available to inspect the inter-burden strata and seams, initially the drilling relies on studying geological logs from any existing vertical exploration boreholes in the area. Some idea of the nature and stability of the inter-burden strata can be defined but ultimately, the most comprehensive knowledge is established from prior and current experience in drilling the environment. The presence of fractured horizons and clay bands with the expectation of swelling when in contact with water is the main point of caution. Prior knowledge of thick soft clay bands has shaped drilling projects by limiting drilling to targeting coal seams above the clay band to avoid intersection/interaction. If substantial clay bands are to be penetrated, a reliable plan needs to be established involving drilling a pilot borehole, reaming and installing casing through the area to allow unimpeded drilling beyond.

With any drilling, the drilling horizon has to be reasonably stable to allow drilling to progress. The drilling horizon has to support the initial drilling and then the borehole has to remain open to be effective for its design purpose. Assessment of this also relies on both exploration data and prior experience. The gaining of additional knowledge and experience is an ongoing learning process as drilling progresses. Particular zones of interest are the inter-faces between the stone strata and the target coal seam which have been found to be unstable in many instances and require stabilising by extended flushing and rotation before drilling can continue. It is not uncommon to have to over-core through this section to release a bogged set of rods.

STRATIGRAPHY OF VERTICAL SECTION

The key information required from the vertical stratigraphy through the coal measures is the thickness and location of the target seam or strata, adjacent coal seams and distinguishing strata in the inter-burden to be crossed. The inter-burden seams and main strata members are used to monitor the progress through the inter-burden and compare relative positions with the vertical design.

The thickness of the target seam and the vertical displacement required to reach it determines the vertical entry angle, angle through the inter-burden and angle at which to intersect the target seam and be able to curve vertically to "land" within the seam to continue the in-seam drilling.

Contours of the working seam (or Reduced Levels (RL's) of the surrounding workings) are required to determine the profile of the target seam both in the area of intersection and along the length of the in-seam section of drilling. For drilling along a horizon in the strata outside the seam, the seam profile provides a reference horizon to which the vertical profile can be designed.

The logical design sequence is to complete the lateral design first then plot it on the mine plan to allow the seam profile along the path of drilling to be determined. The profile of the target seam can be incorporated on that profile and then design the vertical borehole profile to suit.

LATERAL DESIGN

The lateral design is the relative position left or right of a horizontal reference line along a target azimuth. This allows boreholes to be positioned in specific locations parallel to roadways, at specific spacing or to intersect a known location or feature.

Designing lateral borehole layouts for cross-measure, in-seam or parallel strata drilling is the similar to designing for in-seam drilling (Figure 1). The only variation is specific allowance for the reduced ability to curve laterally when it coincides with a section or borehole which requires a curve in the vertical design. The usual options are to design both vertical and lateral curves at reduced rates so their combined curve is within the capabilities of the downhole motor, design the borehole so the vertical and lateral curves do not coincide (Table 1) or reduce the vertical angle and lateral off-set angle so the extent of curving is reduced.

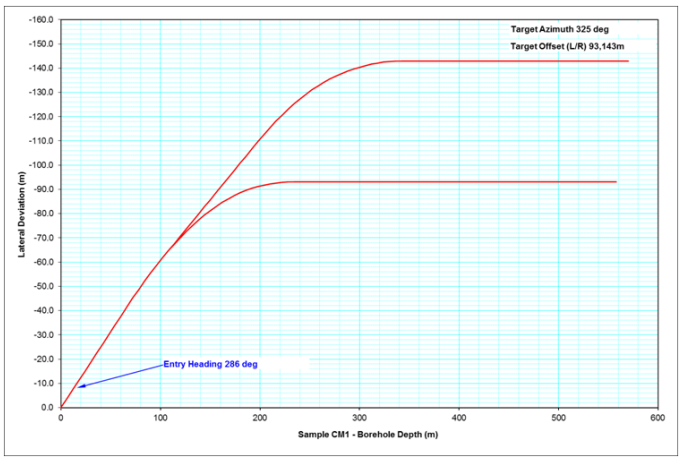

Figure 1 - Lateral deviation design

Table 1 - Design survey data

DEPTH m	AZIMUTH deg	PITCH deg	DRIFT deg	DOWN TRACK	LEFT/ RIGHT	UP/ DOWN
	Entry Hdg					
0	286.00	-7.00	-39.00	0.00	0.00	0.00
6	286.00	-7.00	-39.00	4.63	-3.75	-0.73
12	286.00	-7.00	-39.00	9.26	-7.50	-1.46
18	286.00	-7.00	-39.00	13.88	-11.24	-2.19
24	286.00	-6.00	-39.00	18.52	-14.99	-2.87
30	286.00	-5.00	-39.00	23.16	-18.75	-3.45
36	286.00	-4.00	-39.00	27.81	-22.52	-3.92
42	286.00	-3.00	-39.00	32.46	-26.29	-4.28
48	286.00	-2.00	-39.00	37.12	-30.06	-4.55
54	286.00	-2.00	-39.00	41.78	-33.83	-4.76
60	286.00	-1.00	-39.00	46.44	-37.61	-4.91
66	286.00	0.00	-39.00	51.10	-41.38	-4.97
72	287.50	1.00	-37.50	55.81	-45.10	-4.91
78	289.00	1.50	-36.00	60.62	-48.68	-4.78
84	290.50	1.50	-34.50	65.52	-52.15	-4.63
90	292.00	1.50	-33.00	70.50	-55.48	-4.47
96	293.50	1.50	-31.50	75.58	-58.68	-4.31
102	295.00	1.50	-30.00	80.73	-61.74	-4.15

If multiple legs are required from a single standpipe, the preferred option is to plan any branching after the cross-measure section to improve chances of successful branching and utilise better lateral control in coal compared to stone. In each case, the inner leg of any set is designed first within the limits of lateral deviation rates then additional legs designed as an extension out to a wider lateral deviation.

VERTICAL PROFILE

When the lateral design is completed, the planned borehole(s) can be plotted on the relevant mine plan to confirm the correct positioning. Using the seam contours along the line of the borehole, the profile of the target seam (and any inter-burden seams) can be incorporated on the profile using the established vertical separation and then design the vertical borehole profile (Figure 2). Adjustments in either vertical or lateral design can be made progressively to bring the design parameters within the capabilities of the drilling.

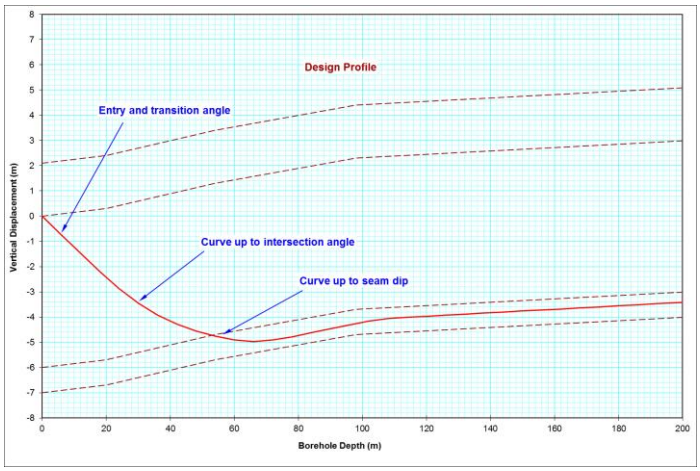

Figure 2 - Design profile of cross-measure in-seam borehole

The vertical entry angle can be determined and limited by several factors including:

- vertical displacement to reach the target seam or horizon,
- any design or distance restrictions within which the target horizon must be reached,
- height of the drill site limiting angled rod handling from the collar, through the drill rig and out the back to the water swivel,
- range of vertical angles at which the drill rig can be mounted,
- height of the feed frame of the drill rig.

Additional allowances are required for rod handling if catering for the ability to over-core in the case of potential bogging in adverse drilling environment. The vertical angle is limited with a single unit, track mounted rig where the hydraulic power unit is incorporated in the rig.

Where the entry angle does not match that required to transect the inter-burden section, the borehole can be curved down or up to achieve the angle required. As drilling progresses through the inter-burden, the strata being penetrating needs to be compared with that of the lithology to monitor progress through the inter-burden. Adjustments can be made to the design vertical profile when the strata is intersected higher or lower than expected. As each inter-burden drilling section is completed, the lithology can be modified to match that defined by the drilling.

The angle transecting the inter-burden may be too big to recover from to remain within the target seam after it has been intersected. The thickness of the target seam or distance into the target seam of the planned drilling dictates the differential angle at which the seam can be intersected while still maintaining the ability to curve vertically to "land" the borehole within the seam. The differential angle is then combined with the dip of the seam in the direction of drilling to determine the vertical angle of drilling desired to intersect the seam. The design has to indicate a point from which to curve the borehole to achieve the desired intersection angle and continue to the seam (Figure 2). From the intersection with the seam, the borehole can then be curved vertically to run parallel with the target horizon in seam or strata. For a very close intersection, a preferred differential angle of three degrees is needed, which only requires three survey intervals to get the borehole parallel to the target horizon.

The stability of the inter-burden and interfaces between strata and seam also has an influence on the vertical angles. The steeper angle of transition through the inter-burden reduces the contact distance through any particular strata and thus reduces the potentially adverse exposure to the strata.

When in-seam drilling, the plan is then to curve the borehole up to intersect the seam roof to confirm the profile before branching to continue the drilling. This practice also provides numerous opportunities for branch points should ongoing drilling encounter unstable conditions. As mentioned earlier, the rate of curve may have to be reduced if coinciding with a section of borehole requiring a lateral curve.

APPLICATIONS

Cross-measure in-seam drilling for pre and post drainage

The first example of directional drilling being employed was during the research and development project at Appin Colliery (Hungerford, *et al.*, 1988). Short-hole rotary drilling had been employed to provide post-drainage of gas released from the underlying seams during longwall extraction. An initial vertical cored borehole was drilled from the Bulli seam down through the underlying coal measures. This borehole defined the location and thickness of each coal seam, major stone strata and the presence of clay bands. The presence of a significant (1.2 m thick) soft clay (tuff) band in the upper section of the Wongawilli seam prompted the decision to limit cross-measure drilling to the Balgownie seam (14.09 m below the floor of the Bulli seam) to avoid the potential problems of drilling low angled boreholes through the clay.

The initial trial at cross-measure, in-seam drilling of the Balgownie seam (Hungerford, *et al.*, 1988) from the end of LW15 produced a 923 m long borehole (Figure 3) which was branched for second leg, 857 m long and 40 m to the left. These boreholes produced moderate pre-drainage gas flows before the advancing longwall face crossed the end of the boreholes. From that point, very high gas flows were produced with beneficial gas control at the longwall face. This practice has been tried for other longwall blocks and at other mines (Figure 4) with mixed results in drilling control, gas flows and management.

Directional drilling has allowed drilling to access and provide more contact with the coal seams below each longwall block. With post-drainage applications, the target seam is usually below the current extraction seam with the drilling providing an attempt to pre-drain gas before longwall extraction. With longwall extraction, boreholes are then in position to provide post-drainage by drawing off as much of the released gas as possible. In China, there is a propensity to drive roadways in stone under the seam being mined to provide access for gas drainage rotary drilling. The opportunity exists to drill directional in-seam boreholes from these stone roadways to target the seam above for more efficient pre-drainage of gas.

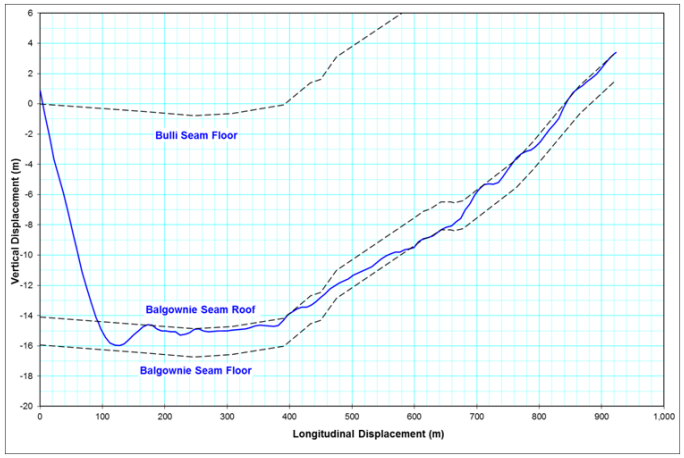

Figure 3 - Initial cross-measure in-seam trial in the Balgownie seam (Hungerford, *et al.*, 1988)

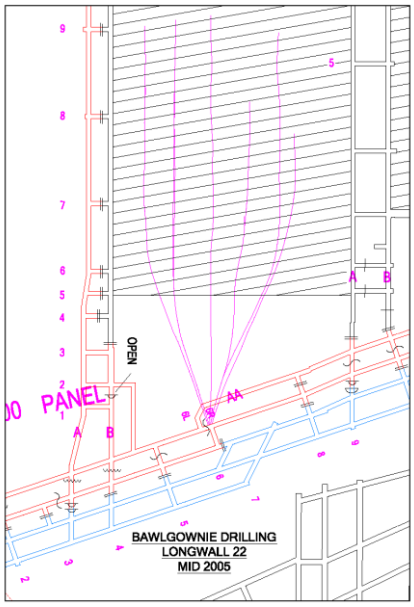

Figure 4 - Successful Balgownie seam cross-measure drilling pattern

Where early exploration in the Appin project identified the soft clay member within the Wongawilli seam as a problem to penetrate and maintain open, drilling in mines to the south found the clay member to be more stable. Drilling through the clay still presents stability problems after exposure to water so the installation of casing is required to allow ongoing drilling. One established practice is to drill the directional borehole through the clay, ream the borehole to a bigger diameter then install casing before continuing with the directional drilling. All drilling, reaming and installation of casing has to be completed within a day before swelling of the clay presents further problems.

A recent development has been to directional drill to the top of the clay, ream out to that depth, drill through the clay with casing fitted with a retractable bit, remove the bit then continue directional drilling. These practices have allowed access to the lower sections of the Wongawilli seam from the Bulli seam for pre-drainage.

Goaf drainage

Cross-measure drilling into the strata above and parallel to the working seam has allowed gas to be drained from the goaf to control gas at the longwall face (Figure 5) (Kravits, *et al*., 1993). This practice has been in place in the USA for some time and has recently been introduced to some Australian mines. In China, there is a practice of driving sewer roadways along the length of the longwall blocks in the stone strata above. To replace these successfully with directional boreholes will provide large cost savings.

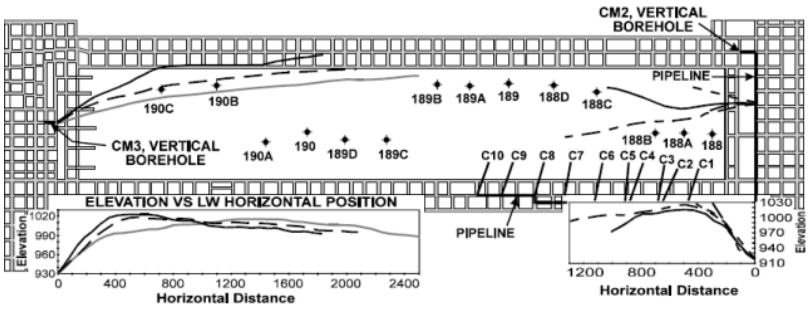

Figure 5 - Underground directional goaf drainage holes (Kravits, *et al.*, 1993)

The applications in Australia have been limited but the potential benefits are starting to be realised. Drilling has been directed into the strata above the seam adjacent to the tailgate roadway (Figure 6). These boreholes have been reamed from a diameter of 96 mm to 145 mm to improve gas flow potential. This reaming has limited the borehole lengths to 500 m to be manageable with an alternate set of more robust rods (NWJ) being employed for the reaming.

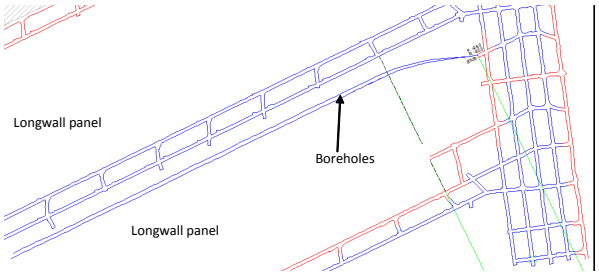

Figure 6 - Goaf drainage boreholes

This practice has many options in terms of distance from the roadway, height above the seam, trajectory, number and diameter of boreholes. The preferred option is to target a known coal seam for easier drilling (Figure 7) while alternative options are to drill along a design path at a prescribed vertical separation, either parallel to the working seam or at a prescribed vertical angle slightly up or down.

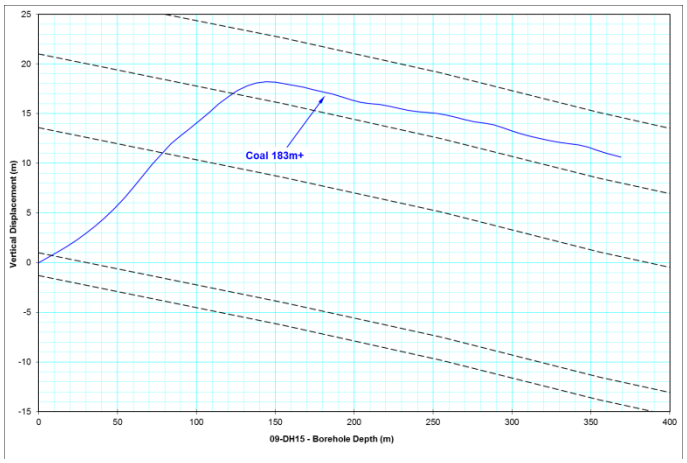

Figure 7 - Goaf drainage borehole profile

Access allows these boreholes to be installed along the length of tailgate side of the longwall block but drill site configuration is limited with boreholes having to be curved to suit (Figure 8).

Water drainage and in-rush protection

Accessing coal seams above and below the current mining horizon has also been employed to provide water drainage of overlying or underlying flooded old workings (Hungerford, 2012). Being capable of drilling within these seams also allows drilling to provide in-rush protection from flooded old workings.

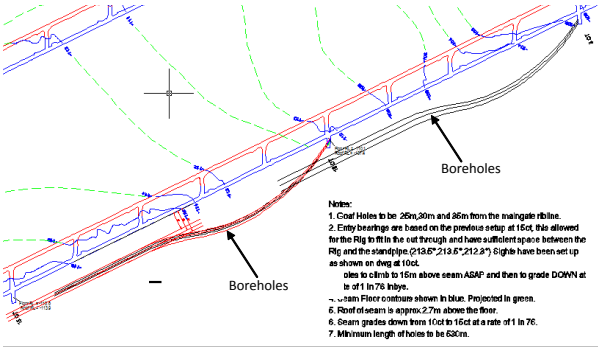

Figure 8 - Flanking goaf drainage boreholes

Exploration

In-seam exploration drilling is usually confined to directional drilling within the working seam with progressive definition of the seam profile as the borehole advances. Intersection with a full displacement fault (Figure 9) requires cross-measure drilling to find the seam and define the displacement (Hungerford, 2011) to design further cross-measure drilling needed to continue drilling in the seam beyond the fault.

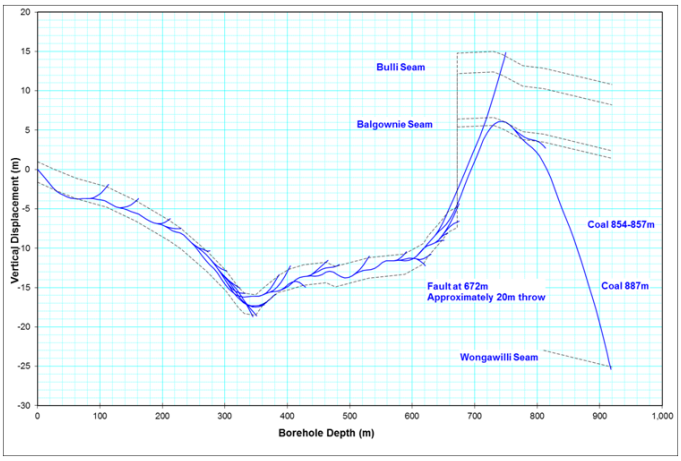

Figure 9 - Cross-measure in-seam drill for exploration (Hungerford, 2011)

Cross-measure in-seam drilling for pre-drainage

A common practice in China is to drive roadways in stone below the working seam to provide access to rotary drill into the seam for pre-drainage (Figure 10) (Hungerford, 2008).

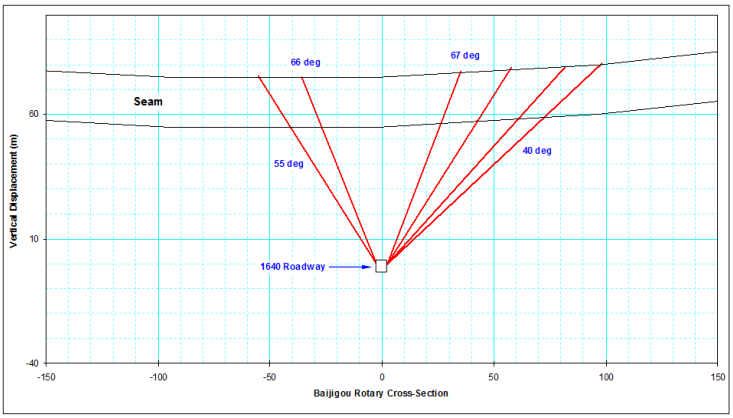

Figure 10 - Rotary cross-measure drilling for gas drainage (Hungerford, 2008)

A gas drainage project at Baijogou mine in China utilised cross-measure drilling to drain gas from a longwall block previously inaccessible from a below seam stone roadway (Hungerford, 2008). The drilling utilised tungsten tipped tri-cone bits to penetrate the 130 MPa stone up to the seam before reverting to PCD bits to drill the coal seam (Figure 11). The 20 m thickness of the seam allowed a more abrupt angle of intersection with the seam which assisted in managing instable conditions at the stone/coal interface. In most cases, two coal legs were drilled from each stone cross-measure section of drilling (Figure 12).

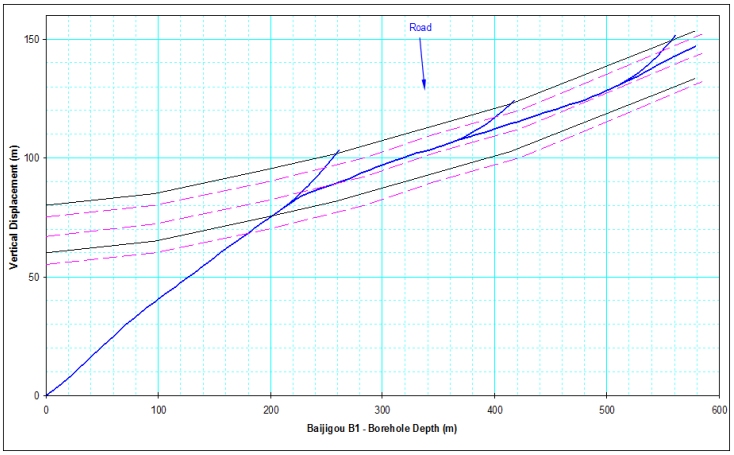

Figure 11 - Baijigou cross-measure in-seam profile (Hungerford, 2008)

The project involved two stages. The original cross-block drilling was followed by along block drilling to replace a failed attempt of SIS drilling (Figure 12). The stone drilling sections of each borehole are shown in blue.

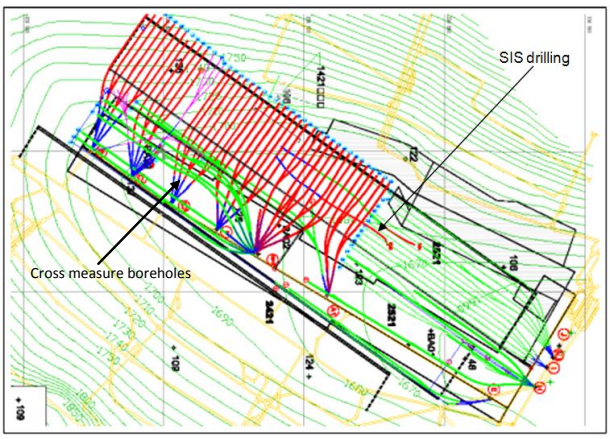

Figure 12 - Baijigou gas drainage layout (Hungerford, 2008)

CONCLUSIONS

The development of directional drilling for in-seam drilling has provided the coal mining industry the technology to accurately position boreholes within the working seam for gas drainage, exploration, water management and in-rush protection. The ability to position boreholes through planned locations and horizons has opened the opportunity to use directional drilling for more applications.

Directional drilling is now regularly used in projects involving cross-measure drilling for:

- Pre-drainage of gas from seams other than the current working seam,
- Positioning boreholes in strata above the seam to enable post-drainage of gas from goaf zones above longwall blocks,
- Positioning boreholes in strata or seams under seams to allow post-drainage from zones of stress relief under longwall goaf,

- Exploration ahead of development,
- Water drainage, management and in-rush protection from flooded workings in seams other than the current working seam.

There are challenges in managing complicated drilling environments other than that found in coal seams when drilling outside the seam boundaries but as new conditions are encountered, drilling procedures and practices have evolved to manage them. As more experience is gained, the cross-measure drilling practices are becoming more manageable and creating opportunities for other applications.

REFERENCES

Hungerford, F, Saghafi, A and Williams, R J, 1988. In-seam and cross measure methane predrainage by long-hole drilling. *End of grant report NERDDP project No. 874*.

Hungerford, F and Thomson, S, 1996. The application of drilling and surveying technology to Australian coal mining. Symposium on geology in longwall mining, University of New South Wales, Sydney.

Kravits, S, Schwoebel, J and Chiari, D, 1993. Utilisation of horizontal in-mine gob ventilation boreholes at Cambria Slop No. 33 Mine, Paper 9338 in *Proceedings of the 1993 International Coalbed Methane Symposium*, Birmingham, Alabama.

Hungerford, F, 2012. Inrush protection drilling. *4th Asian Mining Congress*, Kolkata, India, 28 January 2012.

Hungerford, F and Ren, T, 2011. Evolution of in-seam drilling for gas drainage. *Australian Mining Ventilation Conference.* University of NSW, Sydney, Sept 2011.

Hungerford, F, 2008. In-seam directional drilling for gas drainage - PR China. Coal Tech Asia 2008, Global Leaders Institute Summit. Beijing 18-19th November 2008.

A NEW *IN-SITU* METHOD FOR MEASURING SIMULTANEOUSLY COAL SEAM GAS CONTENT AND PERMEABILITY

John Pope[1] and Quentin Morgan[2]

ABSTRACT: This paper will describe a new method for measuring simultaneously coal seam gas content and permeability that can be performed on existing coal quality holes. The goal of the work was to provide an operational expedient and cost effective method for achieving these simultaneous measurements reliably and accurately. This reported method involves combining an established gas testing technique, based on downhole Raman spectroscopy, with an established permeability testing technique, based on open hole inflate straddle packer technology. This paper describes these two key enabling technology platforms and the means developed to facilitate simultaneous operations of both. A standard test program is also described, encompassing a review of test planning, test methods, and operational considerations required to successfully combine these measurement methods. In addition, the steps required to validate data integrity and ensure accuracy while optimising operational efficiencies are discussed. The conclusions of the work indicated that proper selection of equipment options and careful coordination of the test plans typically used for the two methods results in successful integration of the testing methods and simultaneous measurement of gas content and permeability in coal seams.

INTRODUCTION

Coal plays an important role as the primary source of energy for the generation of electricity worldwide. However, the coalification process that converts plant matter to fuel also produces methane and carbon dioxide gases. The release of coal gases during mining, can pose serious safety challenges through two mechanisms - outburst and explosive gas.

Generally, less permeable coals containing higher methane gas contents contain higher gas pressures and so pose a higher outburst risk. In addition, more permeable coals containing higher methane gas contents flow more gas, more quickly, into underground mine spaces and so pose a higher explosive gas risk.

Existing *ex situ* techniques (i.e. those conducted on fluid, gas or rock samples removed from coal seams) for measuring gas content and permeability require collection and laboratory analysis of core samples. In some cases, those samples do not reflect the complex, distributed characteristics of the coal seam being evaluated. In some cases, the analyses of those samples are complicated by changes to the samples that may occur during collection.

This paper describes a new technique for measuring concurrently gas content and permeability *in situ* and subsurface (i.e. conducted on the coal seams as they reside, without removing samples to surface). This technique integrates Reservoir Raman spectroscopy (RRS) with Drill Stem Testing (DST) technology and focuses on *in situ* measurement of fluids drawn from the coal cleats into a wellbore or tubing.

This integration provides some advantages in that it can be performed more quickly and at a greater density than typical *ex situ* methods. This *in situ* methodology is well suited to challenging downhole environments such as those containing friable coals, mixed carbon dioxide and methane gases, and trace amounts of gases. And it can be performed in existing coal quality holes (i.e. holes cored in order to obtain samples of coal for laboratory testing of quality and other metrics), obviating need for special cores or core holes for gas analysis.

Challenges of the new technique include the need to manage fluids wisely in order to insure representative data and to minimise operational time.

[1] *WellDog Pty Ltd, Brisbane QLD 4000, Email: jpope@weldog.com, O: 07 3218 2175*
[2] *WellDog Pty Ltd, Brisbane QLD 4000, Email: qmorgan@welldog.com, M: 0417 760 685*

ENABLING TECHNOLOGIES

Reservoir Raman Spectroscopy (RRS)

Raman spectroscopy is a well-established laboratory chemical analysis technique. It was invented after the discovery of the Raman Effect in 1928, for which Sir Chandasekhra Venkata won the Nobel Prize for Physics in 1930. Obtaining reliably measurements with Raman spectrometers in a borehole is not trivial. Most Raman spectrometers are bulky, difficult to operate, and require substantial electrical power - in many cases occupying entire benches in the laboratory. Over the past ten years, the RRS technology has undergone continuous improvement to reduce size, improve ruggedness, increase sensitivity and expand operating temperature range.

Several articles (Koval and Pope, 2006; Pope, 2006; Pope, 2009; Renouf and Pope, 2011) and technical papers (Pope, *et al.*, 2004; Lamarre and Pope, 2007; Pope, 2009a; Pope, 2009b) have been published on the measurement principle and disclosing case histories testifying to the system reliability, operational efficacy and accuracy of this technique compared to core-derived estimates of gas content.

In situ flow capacity testing from surface holes

Flow capacity (and thus bulk permeability), along with other reservoir parameters, can be determined from monitoring and analysis of pressure transients induced in a coal seam using DST technology, suitable for multi-zone open hole environments. This technique has been employed extensively by both coal mining and coal seam gas operators in order to avoid the challenges associated with *ex situ* analysis of permeability on coal core samples.

A variety of tubing and wireline deployed technology platforms have been developed to isolate target seams and induce pressure transients. Tubing deployed systems are commonly referred to as DST systems, while wireline deployed alternatives are referred to as pump-out systems. Both categories are further classified according to the type of packers employed, setting methods and the control system used to actuate the tester valve. Table 1 summarises capabilities of each type, with only one, the Tubing Pressure Actuated (TPA) system type, deemed suitable for facilitating simultaneous production and logging of formation fluids.

Table 1 - Comparison of alternative *in situ* flow capacity testing technology platforms

System Actuation Type	Conveyance Method		Application Types			RRS Wireline Access	Multi-Cycle Circulation
	Wireline	Tubing	Off Bottom	Single Trip MZ	Open Hole		
Annulus Pressure	✗	✓	✓	✗	✗	✓	✓
Compression Set	✗	✓	✗	✗	✓	✓	✗
Internal Control Line	✗	✓	✓	✓	✓	✗	✗
External Control Line	✗	✓	✓	✓	✓	✗	✓
Positive Pressure Pump-Out	✓	✗	✓	✓	✓	✗	N/A
Hydraulic Amplifier Pump-Out	✓	✓	✓	✓	✓	✗	N/A
Tubing Rotation Actuated	✗	✓	✓	✓	✓	✓	✗
Tubing Pressure Actuated	✗	✓	✓	✓	✓	✓	✓

Tubing pressure actuated DST technology

The TPA system, as depicted in Figure 1, features a fully integrated design, with all functions mechanically and hydraulically interlinked. These functions are accessed via a zero-displacement setting tool, which incorporates a balanced valve that is manipulated by altering height of the work string stickup. The zero-displacement feature minimises pressure perturbations during tool manipulation, thereby optimising pressure data quality. In the packer setting position, pressure is applied onto a full water column in the work string to actuate the inflate packers straddling the Zone Of Interest (ZOI), with setting pressure communicated from upper to lower packers via the interval pipe used to set test height.

While technical due-diligence is crucial in shaping test selection and test design, uncertainties in reservoir characteristics may require changes to the test design during execution in order to optimize validity of pressure transient analyses. Access to real-time formation pressures during the flow and shut-in periods is therefore crucial. A wireless surface readout formation pressure monitoring system is therefore included between the straddle packers.

The wireless system relays pressure data to surface using a low frequency electromagnetic (E-M) signal propagated through the surrounding overburden to one or more receivers staked in the ground at surface. This eliminates the need for complex inductive coupling systems or wet-mate connections and associated wireline equipment, thus saving costs and mitigating interruptions to rig operations.

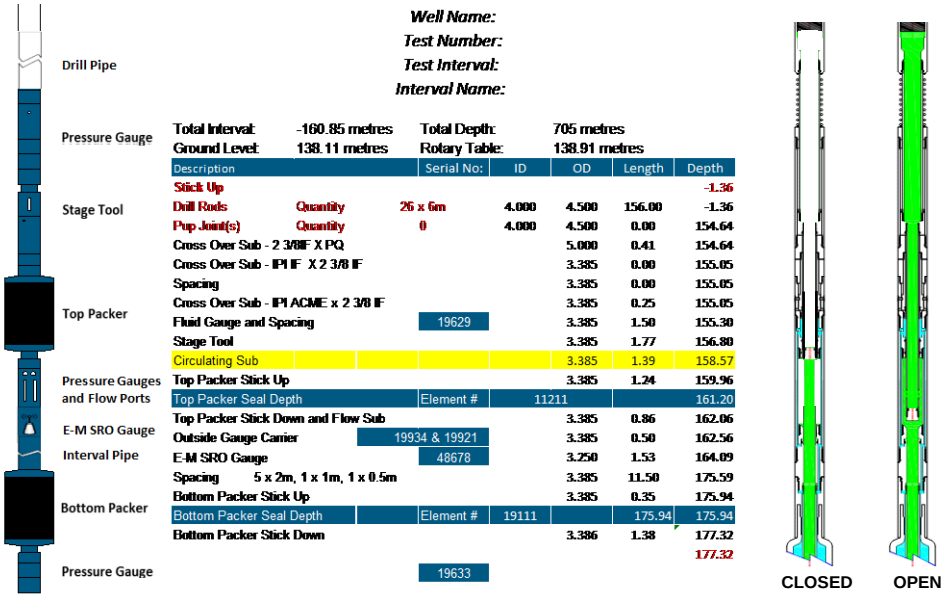

Figure 1 - Tubing pressure actuated DST system

Wireline entry guide system

To facilitate concurrent wireline operations and manipulation of the setting tool in the TPA DST system a unique load-bearing Wireline Entry Guide (WEG) system has been developed. A stack-up diagram of the integral Flow and Pressure Control Equipment (FPCE) system, which is connected to the work string, is shown in Figure 2. The design of the WEG (items 1-3), is shown in Figure 3.

Figure 3 reveals how the weight of the entire work string is supported by a cage, comprising a system of rods that connects the FPCE system to the top drive via flanged crossovers either end of the rods. This ensures that the wireline pack-off unit mounted in the top of the lower flange is not subjected to any loads, enabling a standard design to be used. The number, height and spacing of the rods, bolt design with the flanges and the geometry of the flanges ensures that loads will always be evenly distributed, and that the pack-off unit can be fully disassembled, and if need be replaced, without having to dissemble the cage.

To enable the RRS logging tool to be quickly and easily deployed the FPCE system also features specially designed load bearing quick union connections (items 7 and 8 in Figure 2). Together, the WEG and FPCE system design enables RSS logging operations to be conducted independently of changes to the TPA DST setting tool position.

As a result, it is possible to monitor real-time the solubilised methane concentration of produced fluid entering the work string during the main flow period, and/or log solubilised methane concentration profiles during the final shut-in period. In so doing, provided the produced fluid is not contaminated by filtrate or other extraneous sources, determination of coal seam gas content does not involve having to extend overall test duration beyond that required to determine flow capacity.

Another benefit of the WEG system is that any gas liberated from the fluid or coal prior to or during testing is contained within the sealed work string and can be readily flushed prior to further rig floor operations.

As a result, testing involves no additional risk - in fact, this type of surface pressure and gas control is improved over that available on a typical mineral rig.

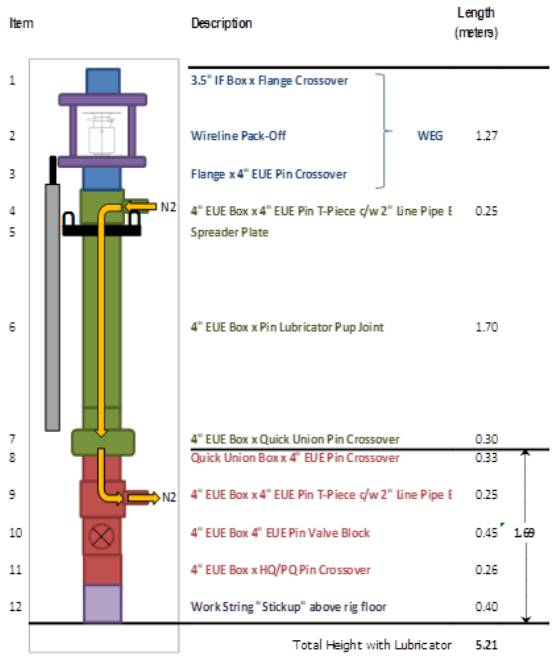

Figure 2 - WEG and FPCE stack-up configuration

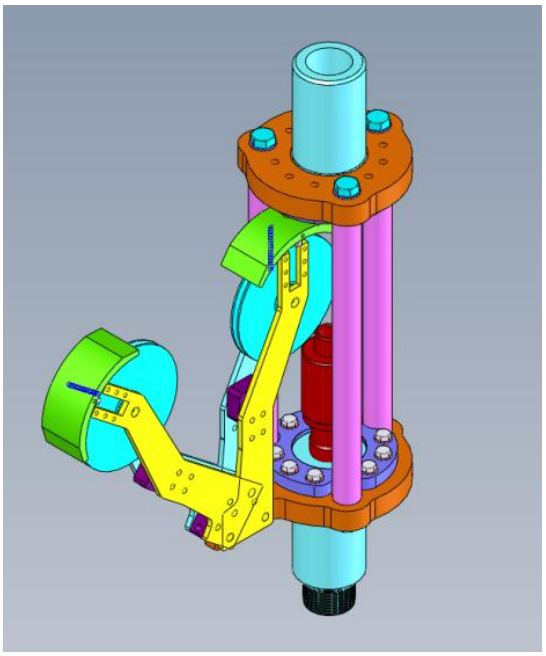

Figure 3 - Top drive wireline entry system

GENERIC TEST PROGRAM

In order to quantify permeability, skin and other coal seam reservoir parameters a variety of test types can be conducted, including Injection Fall Off Testing (IFOT), Diagnostic Fracture Injection Test (DFIT), tank tests and slug tests. All these test types however involve injection of fluids into the coal seam. In order to measure gas content using the RRS logging tool, native fluids need to be withdrawn from the coal seam. As a consequence, a conventional flowing/build-up DST is performed, comprising an initial pre-flow and build-up, followed by a main flow period and final build-up period, which must be of sufficient duration to establish pseudo radial flow conditions. Reservoir pressure is estimated from analysis of the initial build-up data, with analysis of final build-up used to derive flow capacity and other reservoir parameters.

This test type is widely used, with execution governed using well-established procedures and best practices. In the interest of brevity therefore, only innovations introduced to accommodate simultaneous measurement of coal seam gas content will be discussed.

Test design

A flow chart with appropriate evaluation criteria has been developed to guide decisions on whether to test for coal seam flow capacity and/or gas content, and if not gas content, whether to instead employ an IFOT test type. Furthermore, the evaluation criteria are chosen to enable decisions to be made prior to, or during, testing.

Fluid cushion

In order to limit potential for fines production a dynamic nitrogen cushion is employed in place of water that can be gradually bled off during the pre-flow to minimise reservoir shock and limit amount of gas liberated from solution in order to optimise the quality of pressure transient analysis. To limit nitrogen requirements, a hybrid nitrogen-over-water cushion is employed for deeper seams, using a bespoke formula to quantify volume ratios.

Fluid management

A number of innovations have also been developed to manage production and purging of produced fluid. Some of these are aimed at maximising fluid cleanliness, with others focusing on ways to displace produced fluid under pressure. This precaution is necessary in order to prevent solubilised methane from being liberated as free gas, which would compromise computation of gas content.

One such innovation involves partially displacing the produced fluid up the work string. This is achieved by applying nitrogen pressure down the work string until the total pressure at the bottom of the work string is equal to hydrostatic. The TPA DST setting tool is then moved to the circulating position, after which the nitrogen pressure in the work string is slowly bled off. The drop in work string pressure causes water to enter from the annulus, which is continuously topped up from surface - no pressure need be applied.

This procedure essentially reduces ambient temperature of the produced fluid column, and need only be adopted for applications where coal seam temperature exceeds the operating temperature range of the RRS logging tool.

Another innovation involves displacing the produced fluid under pressure all the way to surface, past a manifold shown in Figure 4, which incorporates an optically transparent sapphire window. This allows fluid properties to be interrogated by a surface RRS instrument, obviating need to log produce fluid *in-situ* on wireline. The choke manifold also features four sensor wells in the flow line to measure water rate, pressure, temperature and conductivity.

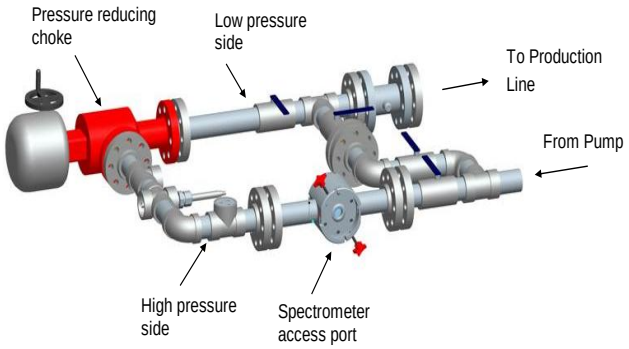

Figure 4 - RRS surface choke manifold

This procedure does extend overall test durations somewhat, however, as displacement of the produced fluid past a surface RRS instrument would need to be delayed until after the main shut-in period has been completed. However, this technique does enable applications of this integrated service to be extended into small hole sizes (HQ or less).

If RRS logs of fluid produced during the main flow period is not deemed sufficiently representative of reservoir conditions, it will be necessary to withdraw additional fluid from the coal seam. Two options are available for fluid removal, with choice dependent on two key factors; additional volume that needs to be withdrawn and available time:

- Move the TPA DST setting tool to the open position, allowing additional reservoir fluid to be introduced below the pre-existing column of produced fluid.
- Move the TPA DST setting tool to the circulate position to purge the work string contents and reset the cushion.

Purging produced fluid involves first filling the work string with clean water, and then circulating the entire contents up the annulus with additional clean water until conductivity of the annulus returns is the same as the clean water. Nitrogen pressure is then applied down the work string to reset the dynamic cushion, prior to moving the TPA DST setting tool to the open position.

A typical timeline for conducting tests using this new integrated gas content and flow capacity testing capability on a 24 h rig is shown in Figure 5, using an example of main shut-in period. In an actual test, the

duration of the main shut-in period would be optimised to end once pseudo radial flow conditions have been established.

A typical test, therefore, would extend from 13 hr to 20 hr, depending on reservoir flow rate and residual mud and/or fines present in the wellbore. Tests have been regularly completed in the field over this range of operational times.

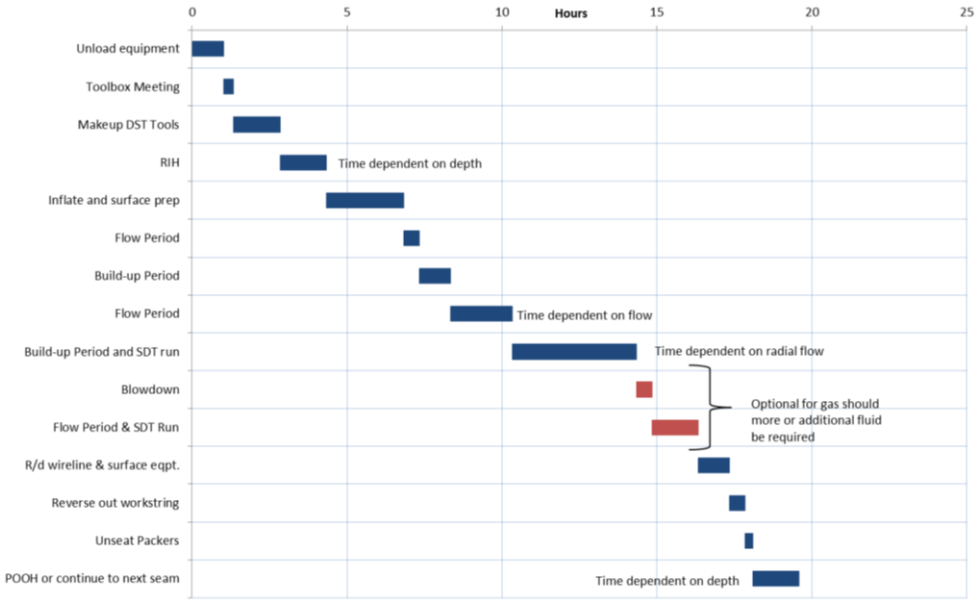

Figure 5 - Idealised RRS and TPA DST test program on a 24 hour Rig

DATA VALIDATION

In addition to measuring solubilised gas concentrations, the RRS instrument also acquires measurements of solubilised pressure, temperature and conductivity on a continuous basis, as shown in example log in Figure 6. These parameters are needed to derive an appropriate constant for use with the solubility law, which in turn allows the measured methane and other gas concentrations to be equated to an effective partial pressure for each gas. These values are in turn used to determine the gas content for each species in the coal seam, using appropriate isotherms.

Determining partial pressure of solubilised (dissolved) gas in formation water can be achieved using a number of bubble point analysis techniques, such as head-space analysis of bottom hole samples or water-gas ratio measurements. However, these techniques can be affected by production perturbations from the surrounding coal, presence of residual solids, and fluid contributions from other completed zones. Thus, a single point measurement in a wellbore cannot be certain to represent the local reservoir. Definitive results can only be obtained by performing continuous measurements, in depth and/or time.

A distinctive feature of the RRS technology is its ability to obtain self-consistent data that simplifies the task of validating measurements prior to analysis. Firstly, the conductivity readings are used to distinguish between reservoir fluid, invasion fluid and completion fluid. Secondly, the pressure reading is used to confirm fluid column height, and is validated against measurements acquired by the various pressure gauges installed in the TPA DST test string.

Thirdly, the log of solubilised gas concentration shows the theoretical saturation curve (blue line, Figure 6, log at right) which closes matches measured values in the upper section of the fluid column. Lastly, the region of uniform measured concentration values (below about 550 m) represents under-saturated conditions. The concentrations measured in that region therefore represent the native concentration of gas in the coal seam and can be used to calculate the gas partial pressure in the coal seam.

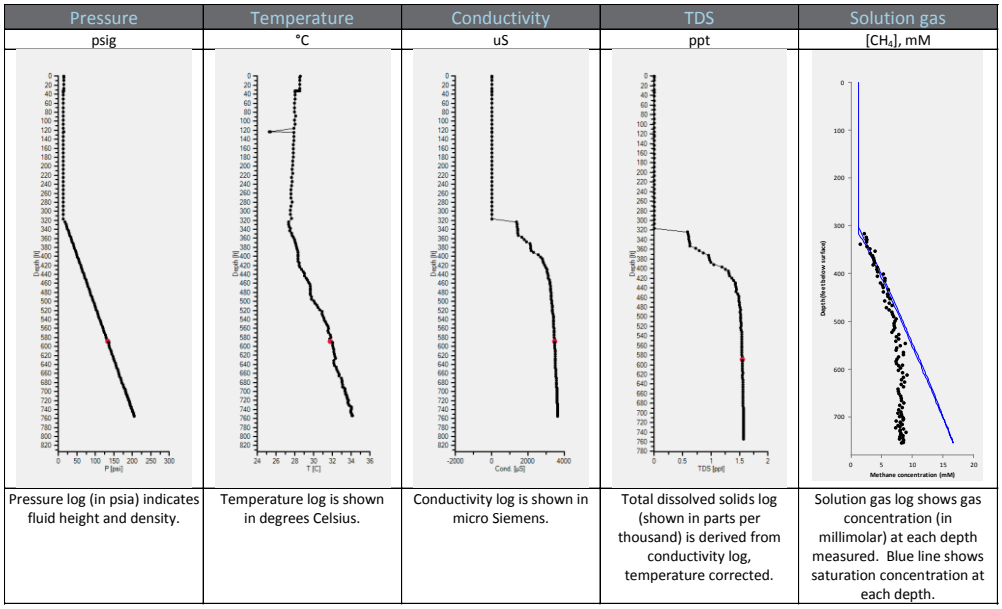

Figure 6 - Example RRS logs

SUMMARY

The integration of unique RRS technology with TPA DST technology has been successfully trialled for a number of large coal mine operators, with perceived advantages of the combined service encompassing the following:

- Provides a means for quantifying coal seam flow capacity and gas content at in-situ conditions using proven testing methods.
- The core-less measurement principle can be performed in existing coal quality holes, greatly reducing number of dedicated gas testing core holes required.
- The reduction in overall well count reduces mapping costs and time.
- The core-less measurements yields immediate results, further reducing time required to develop and implement pre-drainage strategies.
- Avoids data uncertainty associated with ex situ and rock-based measurement techniques.
- Widely accepted by coal seam gas auditors, enabling mine operators to book gas assets if desired.

REFERENCES

Koval, E and Pope, J, 2006. Seeing a reservoir's character from solution gas, *World Oil,* November, pp 144-146.

Lamarre, R A and Pope, J, 2007. Critical gas content technology provides coalbed-methane-reservoir data, SPE 103539, *Journal of Petroleum Technology*, 59(11):108-113.

Pope, J, Buttry, D, Lamarre, R, Noecker, B, MacDonald, S, LaReau, B, Malone, P, Van Lieu, N, Perosli, D, Accurso, M, Harak, D, Kutz, R, Luker,S and Martin, R, 2005. Downhole geochemical analysis of gas content and critical desorption pressure for carbonaceous reservoirs. In *Proceedings West Texas Geological Society Fall Symposiium.* 26-28 October 2005.

Pope, J M, 2006. Get accurate, CBM reservoir data, *E and P*, September.

Pope, J M, 2009. CBM challenges, *World Coal*, December, pp 51-54.

Pope, J M, 2009. Best Practices for multi-zone coalbed methane completions, 0933, International Coalbed and Shale Gas Symposium 2009, 18-22 May 2009.

Pope, J M, 2009. Retaining coalbed methane water discharge permits, 0934, International Coalbed and Shale Gas Symposium 2009, 18-22 May 2009.

Renouf, P and Pope, J, 2011. Measuring gas content without cores, *CBM Review,* September.

CYCLIC INERT GAS INJECTION - AN ALTERNATIVE APPROACH TO STIMULATE GAS DRAINAGE FROM TIGHT COAL ZONES

Dennis J Black

ABSTRACT: Traditional methods of coal seam gas drainage depend on reducing the reservoir pressure to enable gas desorption from the coal matrix. Studies in coal mine gas drainage, particularly in coal seams that are deeply undersaturated and have low permeability, found the rate of reservoir pressure reduction was prohibitively slow. In such conditions, lengthy production delays were experienced while additional gas drainage drilling was undertaken in an attempt to reduce seam gas content below specified threshold limits. Such additional drilling represents a high additional operating cost and typically yields low total gas production whilst adversely impacting the mine's gas drainage drilling schedule and potentially leading to coal production delays. kA novel method to enhance gas drainage from tight coal zones, known as cyclic inert gas injection, which does not rely on reservoir pressure reduction to stimulate gas flow is proposed.

INTRODUCTION

Gas drainage is an integral part of many underground coal mines, with efficient and effective gas management required to support safe and productive mine operations. In gassy mines, such as those operating in the Bulli seam, located in the Southern Sydney Basin, Australia, there has been a reliance on Underground to Inseam (UIS) drilling to pre-drain the working seam to reduce the gas content below prescribed threshold limits ahead of mine development. In rural areas, such as Central Queensland, Surface to Inseam (SIS) methods, in particular Medium Radius Drilling (MRD) has become an effective drilling method to access and extract coal seam gas. Figure 1 illustrates a variety of UIS and SIS drilling methods that are available for use in coal seam gas drainage.

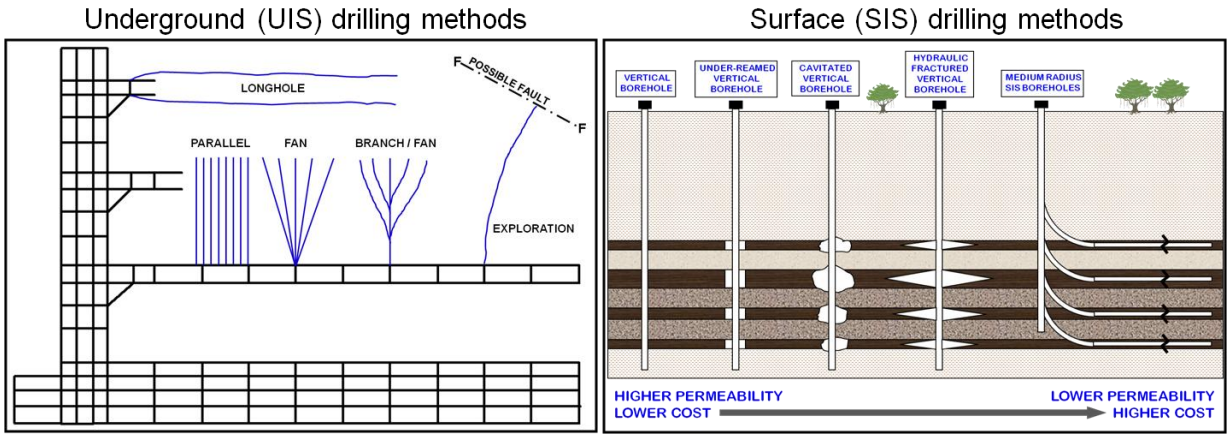

Figure 1 - Underground and Surface based drilling methods / patterns available for use in coal seam gas drainage

Due to the many restrictions associated with access and operations within an underground coal mine UIS drill rigs are much smaller than surface drill rigs and therefore are limited to drilling shorter, smaller diameter boreholes. In order to achieve the required gas content reduction prior to mining, UIS drainage relies on drilling a larger number of closely spaced boreholes to drain the coal seam in a relatively short period. The drainage time available for UIS is typically less than 12 months. In comparison, SIS drainage typically involves drilling a small number of long MRD boreholes, in excess of 1500 m, that flank the planned future gateroad driveage. Given the high cost of SIS gas drainage the MRD boreholes should be installed such that they are afforded a lengthy drainage window, which should be at least three years ahead of planned mining in the area.

Pacific Mining and Gas Management Consultants, Australia. www.pacificmgm.com.au, black.dennis@bigpond.com, M: +61 (0) 401 999 542

Conventional UIS and SIS gas drainage methods are dependent upon reducing the reservoir pressure within the particular coal seam from the *in situ* condition to the Critical Desorption Pressure (CDP) corresponding to the sorption isotherm for the given coal / gas mix (Durucan and Shi, 2009). Such methods, although relatively simple are not particularly efficient as the reduction in reservoir pressure also corresponds to a reduction in the rate of gas production from the borehole (Puri and Stein, 1989). In deeply undersaturated conditions a significant pressure reduction may be required to reach the CDP, as illustrated in the case of CO_2 rich coal seam gas conditions in Figure 2, which requires a pressure reduction of approximately 3000 kPa to reach the CDP.

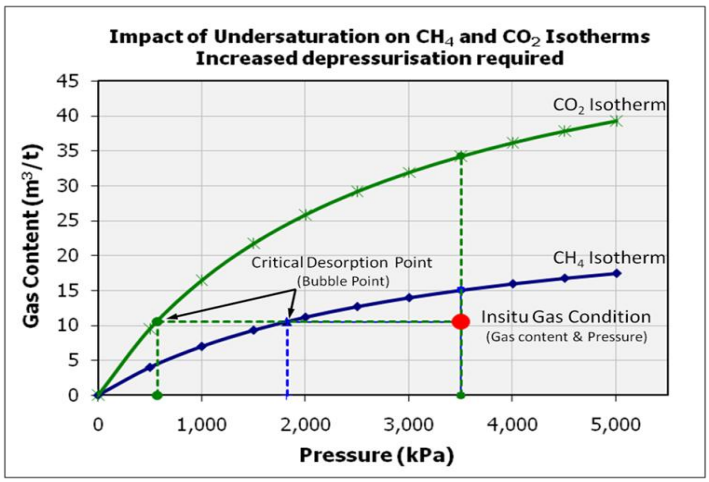

Figure 2 - Typical Bulli seam gas content and reservoir pressure condition relative to CH_4 and CO_2 isotherms

Figure 3 presents data that highlights the relationship between gas production from conventional UIS boreholes and Degree of Saturation (DoS) of the coal seam. In such conditions where the permeability of the coal seam is also low, the time period required to achieve even a small pressure reduction may be prohibitively long resulting in negligible gas content reduction within the available drainage window. Where such conditions exist it is recommended that the coal seam in the tight coal zone be treated with an additional gas drainage enhancement technique to enhance the permeability of the coal and increase the rate of gas flow from the coal.

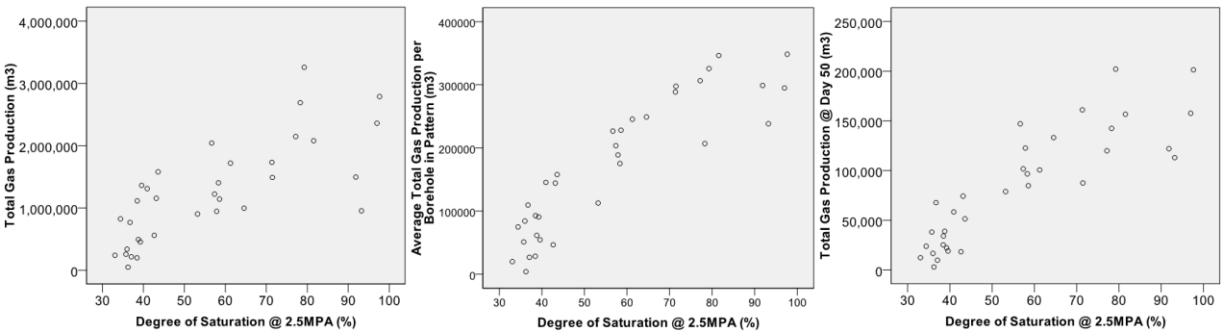

Figure 3 - Data indicating relationship between UIS gas production and Degree of Saturation

DEGREE OF SATURATION

Coal that contains the maximum amount of gas at reservoir pressure and temperature conditions is said to be 'saturated', whereas coal that contains less than the theoretical maximum is referred to as 'undersaturated'. Gas is most easily drained from coal seams that are fully saturated (Lamarre, 2007). Slightly undersaturated coals behave similarly to saturated coals with only a short delay prior to first gas production followed by a steady, strong, rising gas production rate. In deeply undersaturated coal the critical desorption pressure, which is the pressure at which consistent gas production can be expected, is significantly less than the initial reservoir pressure and requires extensive dewatering prior to initiation of gas production.

In a study of the economic impact of gas saturation on coals in the United States (Seidle and O'Connor, 2007) determined that as coal became less saturated, the gas production profile weakened exhibiting a longer dewatering time and lower peak production rate. Compared to a fully saturated coal, a coal that was 60% undersaturated required five times as long to reach the peak gas production rate and the magnitude was one sixth that of the saturated coal. Gas saturation is therefore an important coal property and its impact on gas production must be considered.

The DoS used in this analysis represents the ratio of measured to saturated gas content (Equation 1). The measured gas content (V_{meas}) is determined using the method described in Australian Standard AS3980 (Standards Australia, 1999). The saturated gas content (V_{sat}) is calculated using the modified Langmuir equation (Equation 2), which requires prior knowledge of the Langmuir constants of volume (V_L) and pressure (P_L), determined during gas adsorption testing, and the initial reservoir pressure (P_i), determined through the use of pressure measuring devices, such as piezometers.

$$DoS = \frac{V_{meas}}{V_{sat}} \cdot 100 \quad (1)$$

where:
DoS = degree of saturation (%);
V_{meas} = measured gas content (m^3/t);
V_{sat} = saturated gas content (m^3/t).

$$V_{sat} = V_L \cdot \frac{P_i}{P_i + P_L} \quad (2)$$

where:
V_{sat} = saturated gas content (m^3/t);
V_L = Langmuir volume constant (m^3/t);
P_i = initial reservoir pressure (kPa);
P_L = Langmuir pressure constant (kPa).

The Langmuir equation can also be used to determine the critical desorption pressure (P_d) corresponding to a given measured gas content (Equation 3) and therefore the reservoir pressure reduction ($P_i - P_d$) required to reach the critical desorption point.

$$P_d = P_L \cdot \frac{V_{meas}}{V_L - V_{meas}} \quad (3)$$

where:
P_d = critical desorption pressure (kPa);
P_L = Langmuir pressure constant (kPa);
V_L = Langmuir volume constant (m^3/t);
V_{meas} = measured gas content (m^3/t).

Data collected from 18 piezometers installed into the Bulli seam were used to monitor changes in seam pressure in response to advancing mine working and gas drainage. Figure 4 shows the advance of UIS gas drainage drilling and mine development along with the change in recorded average monthly seam pressure over an eight month period.

Of particular significance in this example is the fact that in the inbye part of the gateroad development that had historically been very slow and difficult to drain, the hydrostatic pressure within the coal seam just prior to roadway development is quite high, approximately 1000 kPa, and the rate of pressure reduction appears slower than the more easily drained outbye areas. Referring to the sorption isotherm curve for this CO_2 rich area, shown in Figure 2, where the *in situ* gas content is 10.5 m^3/t, it can been seen that the corresponding critical desorption point is 570 kPa. In this case, where the reservoir pressure remains above the critical desorption pressure, the slow rate of gas production from the inbye part of the mining area is largely attributable to the deep undersaturation in the area and highlights the need for significantly increased drainage time, or the use of a drainage enhancement technique to stimulate gas flow from such deeply undersaturated areas.

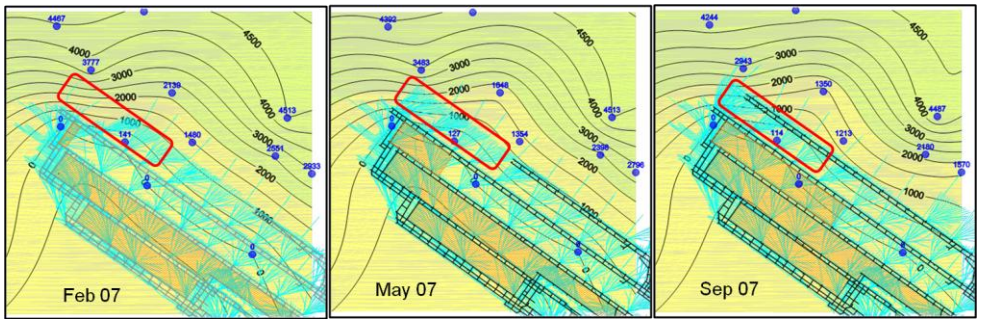

Figure 4 - Impact of gas drainage and mine development on measured hydrostatic pressure in the Bulli seam

ENHANCED COALBED METHANE DRAINAGE

Enhanced Coalbed Methane (ECBM) is a technique used to increase the rate of coal seam methane gas production that involves the injection of an inert gas, typically CO_2 and/or N_2, into a coal seam to stimulate gas desorption and increase total coal seam gas production (Stevenson, *et al*., 1993; Durucan and Shi, 2009). A cross-section view of a surface based ECBM process is illustrated in Figure 5. A similar method was proposed by Battino and Hargraves (1982) for to stimulate gas production from UIS boreholes which involved injecting compressed air into CO_2 rich coal and N_2 into CH_4 rich coal through a central borehole to accelerate gas production from adjacent producer boreholes.

The injection of CO_2 or N_2 into the coal seam, referred to as inert gas stripping, reduces the partial pressure of CH_4 in the free gas phase stimulating the desorption of CH_4 from the coal matrix (Brown, *et al*., 1996, Durucan and Shi, 2009; Mazumder and Wolf, 2008). The movement of the inert gas through the coal seam 'sweeps' the desorbed seam gas toward the production borehole(s).

The use of ECBM to enhance coal seam gas production was first trialled in 1993 in a small scale N_2-ECBM pilot project in the Fruitland formation, San Juan Basin and CO_2-ECBM pilot project in the Manville formation, Alberta (Ham and Kantzas, 2008; Saghafi, 2009). A typical ECBM drilling pattern consists of a central gas injection borehole surrounded by a number of dedicated gas production boreholes, used to extract the seam gas / injected gas mixture from the coal seam.

The process of CO_2 adsorption does however induce swelling of the coal matrix which can reduce permeability and have a detrimental impact on the ability to inject additional gas into the coal seam. During CO_2-ECBM at the Allison Unit pilot project in the San Juan Basin a reduction in permeability of more than two orders of magnitude was experienced as a result of sorption induced swelling (Durucan and Shi, 2009).

N_2 is considered a superior gas for use in ECBM injection for methane production as it achieves a greater sweep efficiency and is less likely to induce sorption related permeability reduction (Oudinot, *et al*., 2007; Durucan and Shi, 2009). Injection of N_2 following CO_2 at the Tiffany ECBM pilot in the San Juan basin not only reversed the permeability reduction caused by the previous CO_2 injection but enhanced the rate of N_2 injection into the coal seam (Oudinot, *et al*., 2007; Durucan and Shi, 2009).

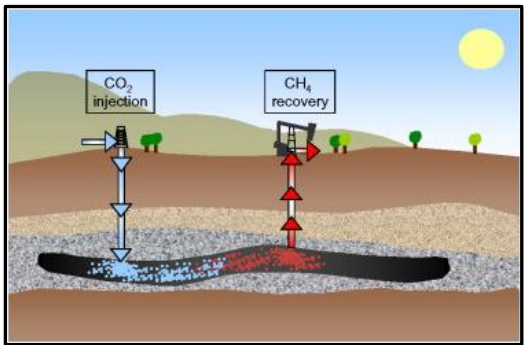

Figure 5 - Illustration of the CO_2-ECBM technique to stimulate coal seam methane gas production

The effectiveness of ECBM is highly dependent on prevailing geological conditions, the properties of the coal seam gas reservoir, the layout of the injection and production boreholes and the design of the injection program. To be effective the injected inert gas must be in contact with the coal matrix for sufficient time to stimulate desorption and sweep seam gas from a large area of the coal seam. In cases where the face cleat and geological structures align sub-parallel to the path between the injection and production boreholes the injected gas is more likely to take a direct path toward the production borehole resulting in low sweep efficiency and reduced effectiveness of the ECBM method. The adverse effect of a geological structure on ECBM in a UIS application that allows the injected gas to flow directly to the adjacent producers boreholes is illustrated in Figure 6 where pattern A illustrates the desired migration of injected inert gas and pattern B illustrates the effect of the injected inert gas flowing directly to the producer boreholes along the structures present in the coal seam.

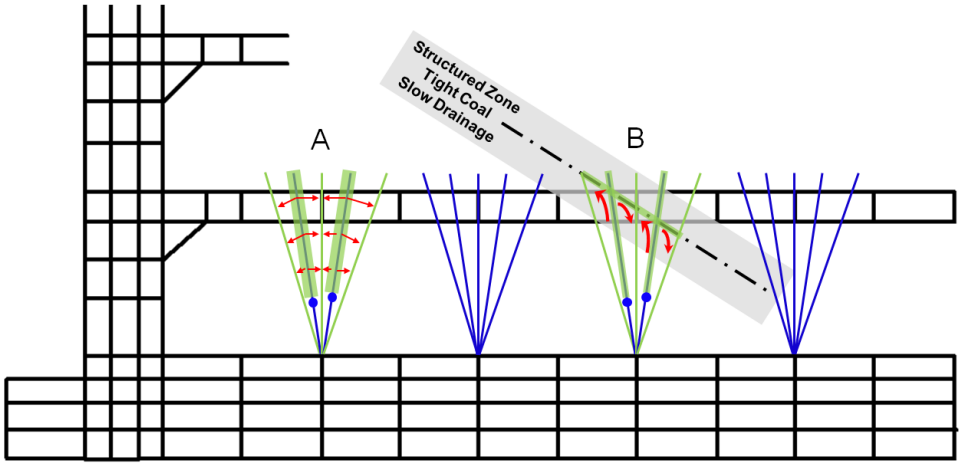

Figure 6 - Illustration of the adverse effects of geological structures on the effectiveness of ECBM

Given the fact that many coal seams are highly structured and likely to feature multiple potential paths that may render a conventional ECBM treatment through SIS or UIS boreholes ineffective, it is necessary to develop a new enhancement technique that is better suited for use, and able to stimulate gas production from such disturbed zones. Such a technique is referred to as Cyclic Inert Gas Injection (CIGI) (Black, 2011; Black, *et al*., 2011).

CYCLIC INERT GAS INJECTION

Unlike conventional ECBM, CIGI does not rely on the broad sweeping effect of inert gas flow through the coal seam between the injection and production boreholes and is well suited to areas where geological structures may be present.

CIGI involves injecting a heated inert gas, such as N_2, into a coal seam through a dual purpose injection-production borehole at a pressure greater than reservoir pressure and less than fracture initiation pressure to penetrate the cleat and flood the coal structure surrounding the injection borehole. Upon completion of the injection phase the borehole is shut-in for a period to encourage desorption of CH_4 from the coal matrix. After sufficient hold time the borehole is opened to produce a mixture of desorbed CH_4 and inert gas. The cycle of inject-hold-produce is repeated multiple times and the intent is to grow the size of the treated coal zone with each stimulation treatment cycle. Figure 7 illustrates the major components of a CIGI project and the progressive increase in the size of the treated coal zone during a five cycle coal seam stimulation treatment through a single vertical borehole.

The technical advantages of the CIGI treatment over conventional gas drainage and ECBM to enhance coal seam gas production are able to be realised through combining the following key characteristics of coal seam gas reservoirs:

- When inert gas is injected into a coal seam at a pressure greater than reservoir pressure and less than fracture initiation pressure the pores expand as the inert gas permeates through the coal seam, opening the cleat and penetrating deep into the formation;

- The presence of fractures and geological discontinuities are not detrimental to the process as they provide additional pathways that facilitate inert gas penetration into the coal seam thereby increasing the size of the treated zone;
- Due to the non-elastic nature of coal many of the flow paths that open during the gas injection stage will, to varying degrees, remain open when the gas pressure is released, thus increasing the number and size of potential gas flow paths within the coal seam (Harpalani and Zhao, 1989).
- At the conclusion of each inert gas injection cycle the injection borehole should be sealed shut for a specified time period to encourage the diffusion of seam gas from the coal matrix. The reduced partial pressure of the inert gas within the cleat and fracture network of the coal promotes CH_4 desorption from the coal matrix;
- The temperature of the inert gas should be increased prior to injection into the coal seam. The process of heat transfer from the injected gas increases the temperature of the coal seam thus energising the CH_4 gas molecules and increasing the rate of movement out of the coal matrix;
- Increasing the temperature of the coal also has a positive effect of reducing the gas sorption capacity of coal which in turn increases the relative degree of saturation of the CH_4 / inert gas mix.
- Given the mixed gas sorption isotherm of a CH_4/N_2 gas mix is lower than for pure CH_4, the process of injecting N_2 into a coal seam to form a mixed seam gas will serve to reduce the effective gas sorption capacity of the coal within the treatment zone thereby creating a localised increase in the relative degree of saturation, as illustrated in Figure 8; and
- During the gas production phase a reduction in pressure within the cleat and fracture network, and the change in effective stress, will cause the coal matrix to swell which may lead to a reduction in permeability. However this effect will be counteracted by the process of matrix shrinkage which occurs as CH_4 is desorbed. After having been subjected to multiple inject-hold-produce cycles the CH_4 content of the coal is expected to be substantially less than the pre-treatment state resulting in a net increase in effective permeability of the coal seam within the treatment zone.

Laboratory studies undertaken at the University of Wollongong (UoW) examined the effect of displacing adsorbed gases in coal using N_2 injection (Florentin, *et al*., 2010). The work involved injection of N_2 into coal samples saturated with binary CO_2/CH_4 gas in a high pressure triaxial gas chamber to a pressure of 3.0 MPa. Results indicate the injection of N_2 caused both gases to be displaced from coal delivering a 20% increase in CH_4 production from the coal samples. The study also recorded strain changes both perpendicular and parallel to coal layering/bedding, indicating an increase in coal permeability.

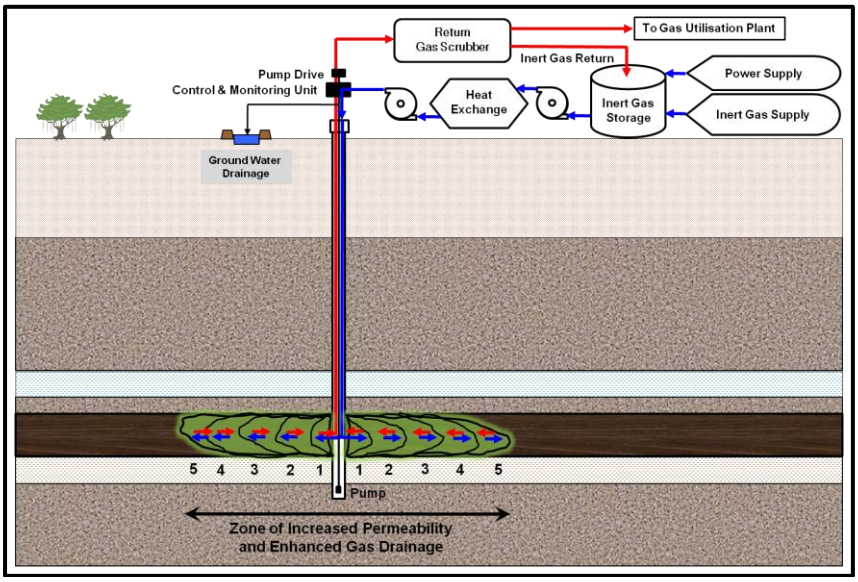

Figure 7 - Illustration of a five (5) cycle CIGI treatment to increase coal seam permeability coal production

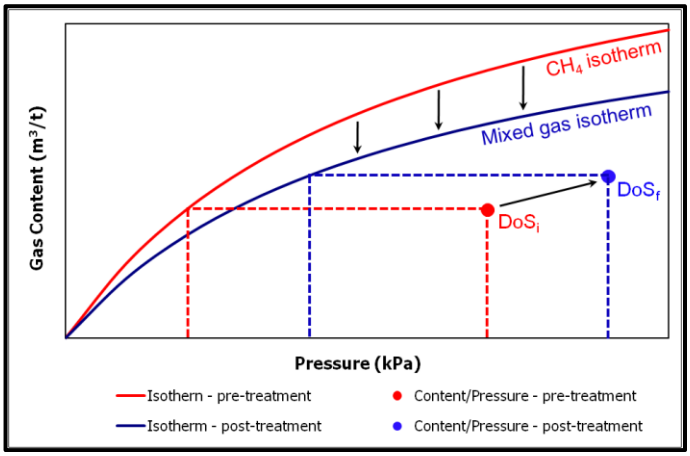

Figure 8 - Localised increase in degree of saturation (DoS) resulting from the proposed CIGI treatment

Figure 9 provides an example of a UIS drilling pattern to illustrate the effect of the CIGI treatment to enhance gas production from a tight coal zone that would otherwise be extremely difficult to drain using conventional drainage methods. If not effectively treated to stimulate gas production and reduce the gas content of the seam prior to scheduled development of the gateroads through the effected zone, production delays are likely. In this example a packer assembly would be securely installed within the borehole, nominally at least 25 m from the borehole collar, prior to the commencement of the various branches that have been drilled into and through the tight coal zone. Multiple cycles of inert gas injection would then be applied to the borehole through the packer assembly to allow inert gas to penetrate into the tight coal zone as illustrated.

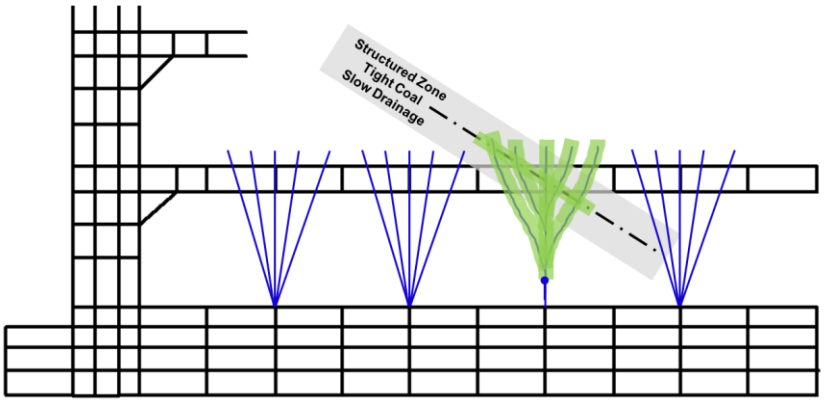

Figure 9 - Illustration of a CIGI treatment in a UIS drilling pattern to treat a tight coal zone ahead of gateroad development

Upon completion of the hold stage of each inert gas injection cycle, when the borehole is opened to release the gas, it is expected that the composition of the produced gas will be a combination of both seam gas and the injected inert gas. In the majority of coal mine gas drainage operations the production of a mixed gas, particularly if only utilising CIGI to enhance gas production from isolated tight gas zones, will not have an adverse effect on typical site based gas utilisation processes such as flaring and reciprocating gas engine electricity generators. Should the gas be produced for sale into the commercial natural gas market it can be expected that the gas will require additional processing to remove the inert gas from the drained gas mixture prior to sale and utilisation.

CONCLUSIONS AND RECOMMENDATIONS

A new technique to enhance coal seam gas production is proposed which involves the cyclic injection of an inert gas into the coal seam through a common injection/production borehole. The use of a single dual-purpose (injection/production) well eliminates the risk of bypass and low sweep efficiency that exists with conventional ECBM methods. The proposed cyclic inert gas injection technique utilises a combination of four independently proven processes (i) matrix swelling and shrinkage in response to

adsorption/desorption, (ii) gas diffusion from the coal matrix in response to gas concentration gradient, (iii) reduced sorption capacity of coal at elevated temperature, and (iv) gas flow from the treated coal seam to the injection/production well due to pressure gradient upon completion of each inject-hold-release cycle. By cyclic inert gas injection it is proposed to increase the *in situ* gas condition, raising the mixed gas content and gas pressure, thereby raising the energy state of the seam gas surrounding the injection borehole. Through injection of inert gas, such as N_2, the isotherm of the mixed gas would be reduced relative to a localised increase in the mixed gas content of the coal seam, thereby increasing the degree of saturation and reducing the reservoir pressure reduction required to reach the critical desorption point on the isotherm.

The development of the cyclic inert gas injection method offers potentially significant benefits to coal mine operators in being able to enhance coal seam gas drainage, particularly from tight coal zones that may be extremely difficult to drain using conventional methods.

REFERENCES

Battino, S and Hargraves, A J, 1982. Seam gas drainage experiments in some collieries of B.H.P., *Seam gas drainage with particular reference to the working seam*, (ed: A J Hargraves), University of Wollongong, Wollongong, pp 157-171.

Black, D J, 2011. Factors affecting the drainage of gas from coal and methods to improve drainage effectiveness, PhD thesis, University of Wollongong, Australia. http://www.uow.edu.au/eng/outburst/html/Completed%20Thesis/Completed_Thesis.html.

Black, D J, Aziz, N I, and Ren, T X, 2011. Enhanced gas drainage from undersaturated coalbed methane reservoirs, in *Proceedings of the 3rd Asia Pacific Coalbed Methane Symposium*, University of Queensland, Brisbane, 3-6 May, Paper No.50, 8p.

Brown, K, Casey, D A, Enever, J R, Facer, R A and Wright, K, 1996. New South Wales coal seam methane potential, *Geological Survey of NSW Coal and Petroleum Geology*, Department of Mineral Resources, Petroleum Bulletin 2.

Durucan, S and Shi, J, 2009. Improving the CO_2 well injectivity and enhanced coalbed methane production performance in coal seams, *International Journal of Coal Geology*, 77:214-221.

Florentin, R, Aziz, N, Black, D, Nghiem, L and Baris, K, 2010. Recovery of stored gas in coal by nitrogen injection - a laboratory study, in *Proceedings of the 10th Underground Coal Operators Conference*, Wollongong, 11-12 February, pp 217-228. http://ro.uow.edu.au/coal/310/.

Ham, Y and Kantzas, A, 2008. Development of coalbed methane in Australia: unique approaches and tools, *CIPC/SPE Gas Technology Symposium*, Society of Petroleum Engineers, Calgary, Alberta, 16-19 June, 8p. (SPE-114992).

Harpalani, S and Zhao, X, 1989. An investigation of the effect of gas desorption on coal permeability, in *Proceedings of the 1989 International Coalbed Methane Symposium*, University of Alabama, Tuscaloosa, 17-20 April, pp 57-64.

Lamarre, R A, 2007, Downhole geomechanical analysis of critical desorption pressure and gas content for carbonaceous reservoirs. *SPE Annual Technical Workshop on Coalbed Methane*, Society of Petroleum Engineers, Durango, Colorado, 27-29 March.

Mazumder, S and Wolf, K H, 2008. Differential swelling and permeability change of coal in response to CO_2 injection for ECBM, *International Journal of Coal Geology*, 74:123-138.

Oudinot, A Y, Schepers, K C and Reeves, S R, 2007. Gas injection and breakthrough trends as observed in ECBM sequestration pilot projects and field demonstrations, in *Proceedings of the 2007 International Coalbed Methane Symposium*, University of Alabama, Tuscaloosa, 24-25 May, 13p. Paper No.0714.

Puri, R and Stein, M H, 1989. Method of coalbed methane production, *US Patent* 4883122.

Saghafi, A, 2009. Enhanced coal bed methane (ECBM) and CO_2 storage in Australian coals [online], *The Australian Institute of Energy*, 43p. Available from: http://aie.org.au/Content/NavigationMenu/SydneyBranch/PastTechnicalMeetings/saghaficsm.pdf [Accessed: November 2010].

Seidle, J P, and O'Connor, L S, 2007. The impact of undersaturation on coal gas economics, *SPE Rocky Mountain Oil & Gas Technology Symposium*, Society of Petroleum Engineers, Denver, Colorado 16-18 April. (SPE-107731).

Standards Association of Australia, 1999. Guide to the determination of gas content of coal - direct desorption method. Australian Standard AS3980:1999.

Stevenson, M D, Pinczewski, W V and Downey, R A, 1993. Economic evaluation of nitrogen injection for coal seam gas recovery, *SPE Gas Technology Symposium*, Society of Petroleum Engineers, Calgary, Canada, 28-30 June, 14p. (SPE-26199).

A CRITICAL ANALYSIS OF GAS DATA IN RELATION TO GAS DRAINABILITY IN BULLI SEAM

Lei Zhang[1], Ting Ren[1], Naj Aziz[1], Jan Nemcik[1] and Andrew Hyslop[2]

ABSTRACT: To prevent the outburst fatality, outburst threshold limits was established. It is the stipulation of limits on seam gas content prior to mining. The outburst threshold limits varied linearly based on gas composition, increasing from a minimum in CO_2 rich conditions to a maximum in CH_4 rich conditions. It is believed that the gas data of the drainage boreholes are closely related to the gas drainability in Bulli Seam. A total of 519 sample results from Metropolitan mine has been examined. It was found that Q_1, Q_2 and Q_3 components increased in response to increasing measured total gas content Q_M. Statistical analysis also shows an increasing trend in the Q_1:Q_M and Q_2:Q_M ratio corresponding to increased Q_M, but there was a decrease in trend in the Q_3:Q_M ratio corresponding to increased Q_M. A power relationship was considered to more accurately represent the average of each gas content component relative to Q_M, especially for "Fail" samples. The average value of CO_2 composition of "Pass" samples is 73.5 % and it was 82.6 % for "Fail" samples. The zone with CH_4/ (CH_4+CO_2) ratio of less than 0.2 includes 171 "Fail" samples, accounting for 88.1 % of total "Fail" samples.

INTRODUCTION

The generation of coal bed methane during coalification occurs in two ways (Singh and Singh, 1999): (a) metabolic activity of biological agencies (biological process) and (b) thermal cracking of hydrogen-rich substances (thermogenic process). In comparison, gas in Sydney Basin coals has been derived from multiple sources, including (Faiz, *et al.*, 2007): (a) thermogenic CH_4 and higher hydrocarbons formed at deep burial during the Jurassic and Early Cretaceous periods, (b) secondary biogenic CH_4 formed since Late Cretaceous uplift, and (c) CO_2 derived mostly from intermittent igneous activity between the Permian and Tertiary periods. Coal seam gas generally comprises CH_4 with subordinate amounts of CO_2, C_2H_6, higher hydrocarbons (C_{2+}) and N_2. However, in some parts of the Sydney Basin, coals contain over 90% CO_2 and up to 12% C_2H_6 (Faiz, *et al.*, 2007). Clayton (1998) reviewed the geochemistry of seam gas and listed four sources for CO_2 gas in coal seams: (a) decarboxylation reactions of kerogen and soluble organic matter during burial heating of the coal, (b) mineral reactions such as thermal decomposition or dissolution of carbonates or other metamorphic reactions, (c) bacterial oxidation of organic matter and (d) magmatic intrusion.

Faiz and Hutton (1995) reported variable amounts of CO_2 and CH_4 occurring within the Illawarra Coal Measures. It is believed that the CH_4 and other hydrocarbons present within the Southern Coalfield were formed as by-product of the coalification process and most of the CO_2 was introduced during periodic igneous activity. The variations of CO_2 and CH_4 are mainly related to the geological structure and depth. The variations in the gas composition have no clear relationship with the coal composition or rank but show well-defined relationships with stratigraphy and geological structure. High proportions of CH_4 occur in the synclinal structures whereas the CO_2 content increases towards structural highs. Extensive areas of pure CO_2 gas occur on anticlines and domes. In structural lows, local pockets of high CO_2 concentrations are found near some dykes and related faults. Increasing concentrations of CO_2 also occur in the stratigraphically higher levels. Migration of gases mainly occurred upwards in aqueous solution, down the pressure gradient. During the upward migration of gas-saturated solutions, gas was continually released from the solution due to decreasing pressure. Due to the lower solubility of CH_4 relative to CO_2, CH_4 was exsolved within the deeper strata whereas increasing amounts of CO_2 being exsolved within the shallower strata. Therefore, in most parts of the Southern Coalfield, increasing amounts of CO_2 gas occur at shallower depths.

High gas content and hence the concentration of methane and carbon dioxide gas typically in close proximity to geological structures, have been identified as a major contributing factor in the coal and gas outburst phenomenon (Lama, 1995). The Bulli seam in Australia, which is located in the southern Sydney Basin, is extremely prone to the occurrence of coal and gas outbursts. Totally 12 lives have been lost as a result of outbursts in the history of mining in the Bulli seam (Harvey and Singh, 1998). As pointed by

[1] *University of Wollongong, Wollongong, NSW, Australia, 2500. Email: lz811@uowmail.edu.au, M: 04 2542 1368*
[2] *Metropolitan Colliery Pty Ltd, Peabody Energy Australia, Helensburgh, NSW, Australia, 2508*

Black (2012), in addition to the explosion and outburst risk, accumulations of methane and carbon dioxide in underground mines may exceed the diluting capacity of the mine ventilation system and hence exceeding prescribed maximum concentration limits. To prevent excessive build up of gas, coal production is required to cease until the gas concentration in the mine ventilation air is reduced below the statutory limit. Operation of the ventilation system alone to manage high gas emission in the gassy mines with highly permeable coal seams may result in frequent and prolonged production delays. In such mines the use of gas drainage is required to assist the mine ventilation system in reducing the coal seam gas content, minimize the risk of a dangerous gas accumulation, reduce the risk of an outburst, improve ventilation air quality, reduce ventilation costs, and ultimately make mining safer and more efficient (Lama, 1980; Kahil and Masszi, 1982; Clark, *et al.*, 1983).

Several mines operating the Bulli seam have coal seam zones which are difficult to drain. Metropolitan Colliery is one of such mines. The mine has experienced difficulties in reducing gas content within the available drainage lead time in an area of MG22, as the coal seam would not drain even with additional drainage boreholes. The Bulli coal seam appears to be CO_2 rich in the concerned area. A research program has been undertaken at the University of Wollongong aimed at: (a) identifying the main reasons for "hard-to-drain" zones in areas between 8-11 c/t of MG 22; (b) establishing the fingerprints of coals that give early warning signs for future drainage process; (c) Coal seam flushing using N_2 gas to drain the coal in the hard-to-drain areas. In order to identify the main reasons for "hard-to-drain" and give early warning signs, the study is currently engaged in examining the field drainage data. This paper provides the latest on the research results of critical analysis of the whole gas data base in this research program.

BULLI SEAM OUTBURST THRESHOLD LIMITS (TLV) ANALYSIS

As a result of the investigation into the last fatal Bulli seam outburst at West Cliff Colliery on 25 January 1994, a directive was issued to all Bulli seam coal mine operators, under the authority of the Coal Mines Regulation Act 1982, prescribing Threshold Limit Values (TLV), among with other actions, to be implemented to prevent future coal and gas outbursts (Clarke, 1994; NSWDMR, 1995; Black, 2012). The TLV represent the maximum allowable gas content, relative to seam gas composition, considered safe for mine operations. Mine operators are required to ensure seam gas content has been reduced below the applicable TLV prior to mining. The outburst threshold limits varied linearly based on gas composition, increasing from a minimum in CO_2 rich conditions to a maximum in CH_4 rich conditions. According to the test results from BHP Gas Lab, the whole database of Metropolitan Colliery containing totally 519 sample results was studied. From the mining level values in the database, the threshold limits was generated. As shown in Figure 1, the gas content was 6.0 m^3/t for pure CO_2 and 9.5 m^3/t for pure CH_4. Thus the test gas content for coal sample is under this TLV limit, accordingly the tested samples will be marked as "Pass", if they are under the TLV limit, otherwise it will be marked as "Fail".

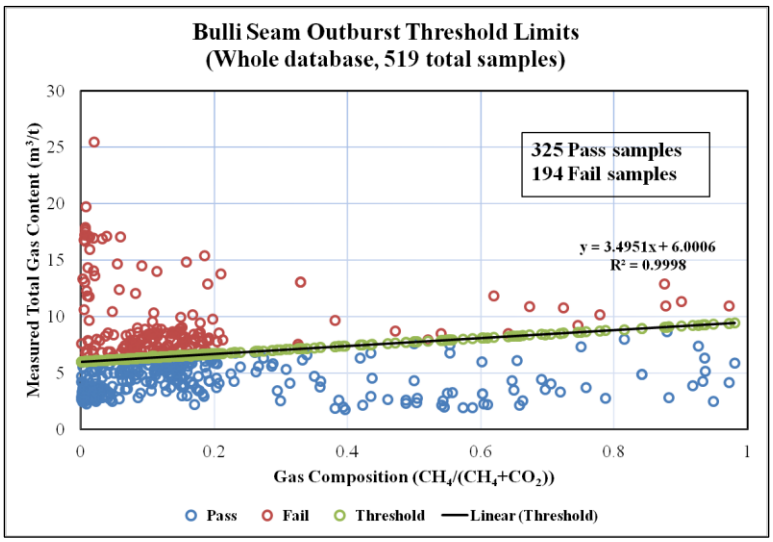

Figure 1 - Bulli Seam outburst threshold limits (whole data base)

Figure 1 shows the whole gas composition data scatter, ranging from CO_2 rich to CH_4 rich area. From 519 samples tested, 325 samples are "Pass" samples, accounting for 62.6 %, while 194 samples are "Fail" samples, accounting for 37.4 %. The value of total gas content of "Fail" samples ranges from 6.14 m^3/t to

25.44 m^3/t. The average value of measured total gas content Q_M of "Pass" samples is 4.4 m^3/t and 9.2 m^3/t for "Fail" samples. The average value of CH_4 concentration of "Pass" samples is 17.1 % and 14.0 % for "Fail" samples, while the average value of CO_2 concentration of "Pass" samples is 73.5 % and 82.6 % for "Fail" samples, which indicates the seam of this area is CO_2 rich condition. The zone of gas composition CH_4/ (CH_4+CO_2) less than 0.2 includes 171 "Fail" samples, accounting for 88.1 % of total "Fail" samples. Including the "Pass" samples, 41.0 % of samples in the zone of gas composition CH_4/ (CH_4+CO_2) less than 0.2 are failed, compared with 22.5 % in the gas composition zone CH_4/ (CH_4+CO_2) more than 0.2.

Q_1 GAS CONTENT COMPONENT ANALYSIS

The Q_1 component of measured total gas content (Q_M) represents the gas lost from a coal sample, during core recovery stage and prior to being sealed in a gas desorption canister. Figure 2a shows the distribution of Q_1 gas content data relative to Q_M. The average Q_1 gas content is 0.5 m^3/t for the whole database, 0.2 m^3/t for "Pass" samples and 1.0 m^3/t for "Fail" samples. Q_1 increased in response to increasing Q_M. Figure 2b shows the distribution of Q_1:Q_M ratio data relative to Q_M. Although a high degree of scatter was evident, the statistical analysis confirmed an increase in the Q_1:Q_M ratio corresponding to increased Q_M. The average Q_1:Q_M ratio is 6.0 % for the whole database, 4.0 % for "Pass" samples and 9.5 % for "Fail" samples.

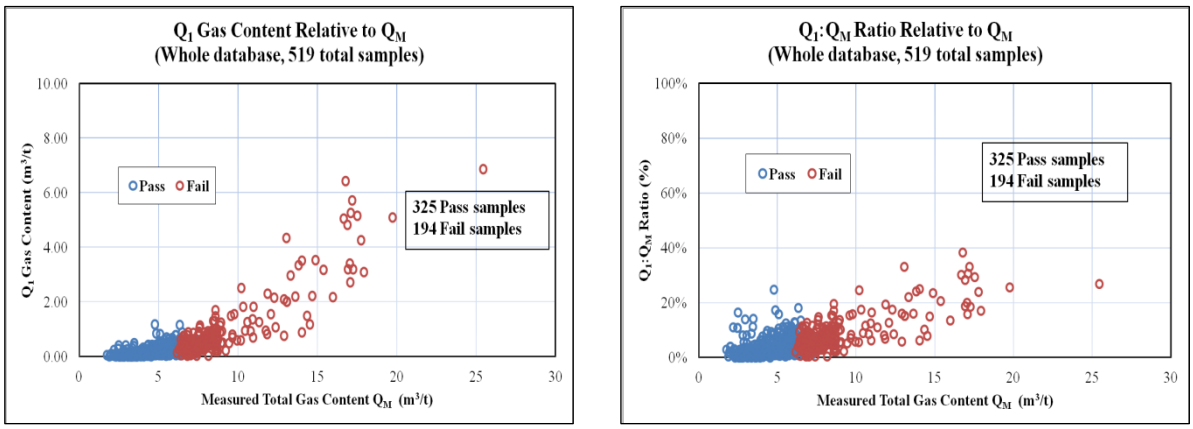

(a) **(b)**

Figure 2 - Distribution of Q_1 gas content and Q_1:Q_M ratio relative to Q_M (whole data base)

Figure 3a shows the distribution of Q_1 data relative to the gas composition (CH_4 %) of each sample. In the 0-20 % CH_4 gas composition zone, the average Q_1 gas content is 0.6 m^3/t for all the samples, 0.2 m^3/t for "Pass" samples and 1.1 m^3/t for "Fail" samples, while in the 20-80 % CH_4 gas composition zone the average Q_1 gas content is 0.3 m^3/t for all the samples, 0.2 m^3/t for "Pass" samples and 0.9 m^3/t for "Fail" samples. Figure 3b shows the distribution of the Q_1:Q_M ratio data relative to gas composition. In the 0-20 % CH_4 gas composition zone the average Q_1:Q_M ratio is 6.3 % for all the samples, 4.1 % for "Pass" samples and 9.5 % for "Fail" samples, while in the 20-80 % CH_4 gas composition zone the average ratio is 4.7 % for all the samples, 3.5 % for "Pass" samples and 8.7 % for "Fail" samples.

Q_2 GAS CONTENT COMPONENT ANALYSIS

The Q_2 component of measured total gas content (Q_M) represents the measurable gas desorbed from as-received coal sample during the laboratory gas emission testing at atmospheric pressure. Figure 4a shows the distribution of Q_2 gas content data relative to Q_M. The average Q_2 gas content is 1.2 m^3/t for the whole database, 0.6 m^3/t for "Pass" samples and 2.2 m^3/t for "Fail" samples. Q_2 increased in response to increasing Q_M. Figure 4b shows the distribution of Q_2:Q_M ratio data relative to Q_M. Although a high degree of scatter was evident, statistical analysis confirmed an increase in the Q_2:Q_M ratio corresponding to increased Q_M. The average Q_2:Q_M ratio is 17.1 % for the whole database, 14.1 % for "Pass" samples and 22.0 % for "Fail" samples.

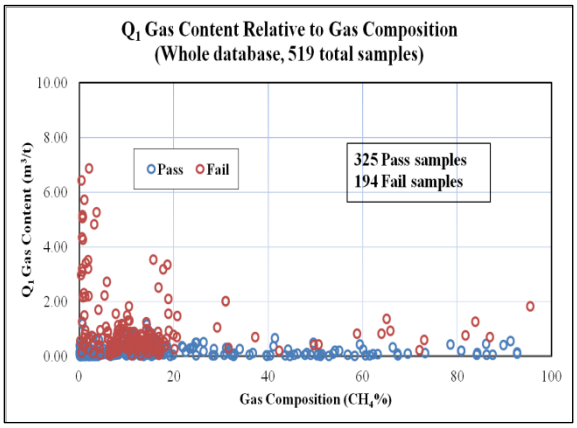

(a)

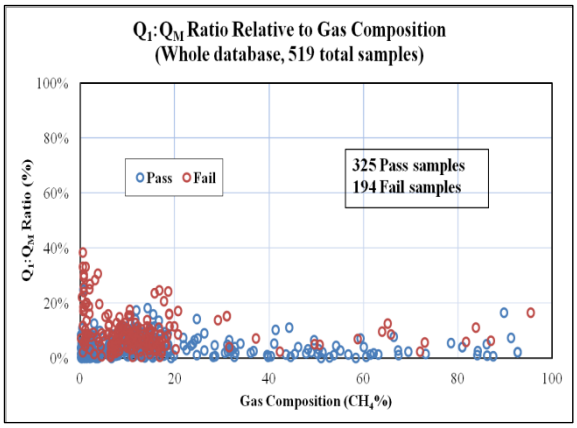

(b)

Figure 3 - Distribution of Q_1 gas content and Q_1:Q_M ratio relative to gas composition (whole data base)

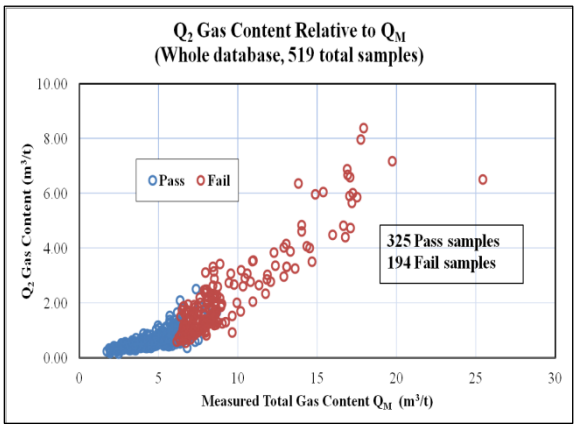

(a)

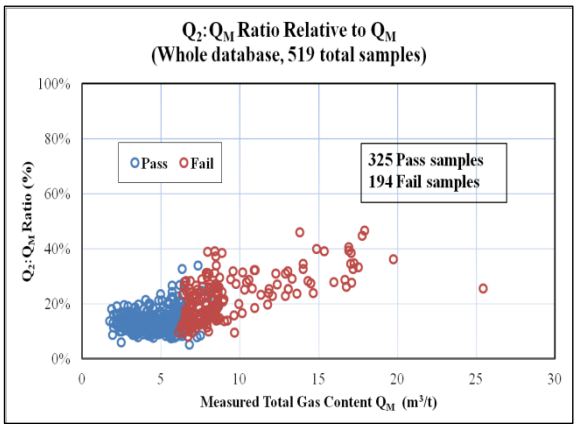

(b)

Figure 4 - Distribution of Q_2 gas content and Q_2:Q_M ratio relative to Q_M (whole data base)

Figure 5a shows the distribution of Q_2 data relative to the gas composition (CH_4 %) of each sample. In the 0-20 % CH_4 gas composition zone the average Q_2 gas content is 1.3 m^3/t for all the samples, 0.6 m^3/t for "Pass" samples and 2.2 m^3/t for "Fail" samples, while in the 20-80 % CH_4 gas composition zone the average Q_2 gas content is 0.9 m^3/t for all the samples, 0.6 m^3/t for "Pass" samples and 2.1 m^3/t for "Fail" samples. Figure 5b shows the distribution of the Q_2:Q_M ratio data relative to gas composition. In the 0-20 % CH_4 gas composition zone the average Q_2:Q_M ratio is 17.5 % for all the samples, 14.3 % for "Pass" samples and 22.2 % for "Fail" samples, while in the 20-80 % CH_4 gas composition zone the average Q_2:Q_M ratio is 15.1 % for all the samples, 13.5 % for "Pass" samples and 20.7 % for "Fail" samples.

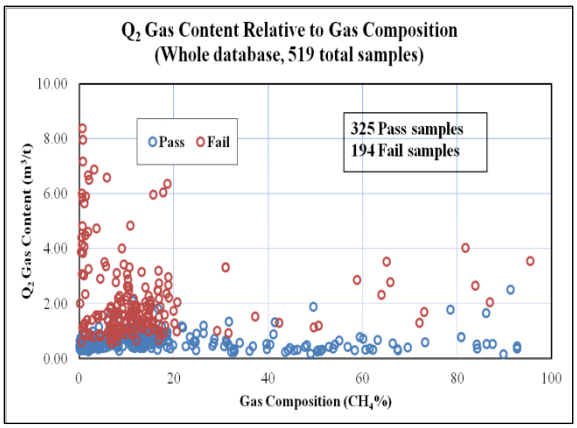

(a)

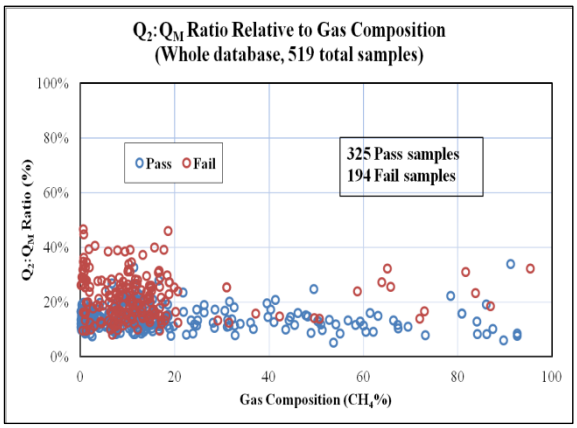

(b)

Figure 5 - Distribution of Q_2 gas content and Q_2:Q_M ratio relative to gas composition (whole data base)

Q_3 GAS CONTENT COMPONENT ANALYSIS

The Q_3 component of measured total gas content (Q_M) represents the gas released from a coal sample following crushing to less than 212 µm. Figure 6a shows the distribution of Q_3 gas content data relative to Q_M. The average of Q_3 gas content is 4.5 m^3/t for the whole database, 3.6 m^3/t for "Pass" samples and 6.0 m^3/t for "Fail" samples. Q_3 increased in response to increasing Q_M. Figure 4b shows the distribution of Q_3:Q_M ratio data relative to Q_M. Although a high degree of scatter was evident, statistical analysis confirmed a decrease in the Q_3:Q_M ratio, corresponding to increased Q_M. The average Q_3:Q_M ratio is 76.9 % for the whole database, 81.9 % for "Pass" samples and 68.5 % for "Fail" samples.

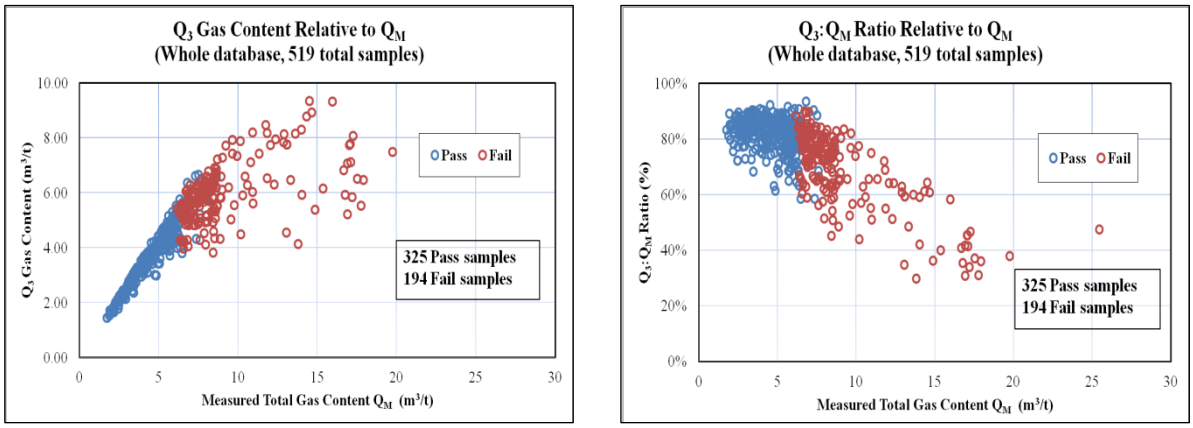

(a) **(b)**

Figure 6 - Distribution of Q_3 gas content and Q_3:Q_M ratio relative to Q_M (whole data base)

Figure 7a shows the distribution of Q_3 data relative to the gas composition (CH_4 %) of each sample. In the 0-20 % CH_4 gas composition zone the average Q_3 gas content is 4.5 m^3/t for all the samples, 3.6 m^3/t for "Pass" samples and 5.9 m^3/t for "Fail" samples, while in the 20-80 % CH_4 gas composition zone the average Q_3 gas content is 4.3 m^3/t for all the samples, 3.5 m^3/t for "Pass" samples and 6.9 m^3/t for "Fail" samples. Figure 7b shows the distribution of the Q_3:Q_M ratio data relative to gas composition. In the 0-20 % CH_4 gas composition zone the average Q_3:Q_M ratio is 76.2 % for all the samples, 81.6 % for "Pass" samples and 68.3 % for "Fail" samples, while in the 20-80 % CH_4 gas composition zone the average Q_3:Q_M ratio is 80.2 % for all the samples, 83.0 % for "Pass" samples and 70.6 % for "Fail" samples.

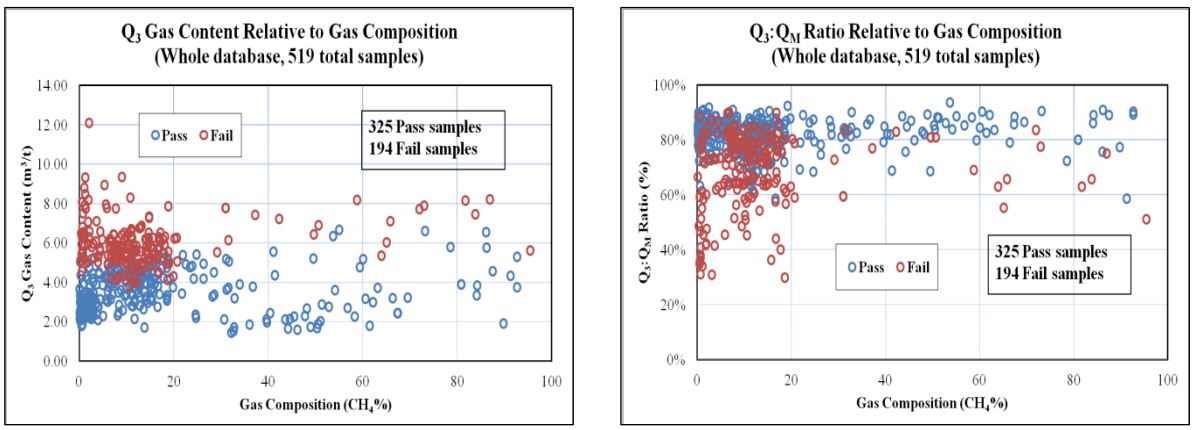

(a) **(b)**

Figure 7 - Distribution of Q_3 gas content and Q_3:Q_M ratio relative to gas composition (whole data base)

COMBINED GAS CONTENT COMPONENTS ANALYSIS

Figure 8 shows the results of the gas content component values Q_1, Q_2 and Q_3, plotted relative to Q_M for each sample of whole database. A linear trend line was plotted to represent the average relationship of each gas content component relative to Q_M. As shown in Figure 8a, for "Pass" samples, $Q_1 = 0.047Q_M$, $Q_2 = 0.1469Q_M$ and $Q_3 = 0.8062Q_M$. The statistical correlation is greater for Q_3 gas component, which indicates a better linear relationship between Q_3 and Q_M for "Pass" samples. As shown in Figure 8b, for

"Fail" samples, $Q_1 = 0.1384Q_M$, $Q_2 = 0.2599Q_M$ and $Q_3 = 0.6017Q_M$. The statistical correlation is small for Q_3 gas component, which indicates a non linear relationship between Q_3 and Q_M for "Fail" samples.

Figure 9 shows the results of the gas content component values, Q_1, Q_2 and Q_3, plotted relative to Q_M for each sample with the power trend line. As shown in Figure 9a, for "Pass" samples, $Q_1 = 0.0029Q_M^{2.4819}$, $Q_2 = 0.1172Q_M^{1.1046}$ and $Q_3 = 0.9102Q_M^{0.9241}$. For "Fail" samples, shown in Figure 9b, $Q_1 = 0.0017Q_M^{2.7218}$, $Q_2 = 0.0365Q_M^{1.7947}$ and $Q_3 = 2.642Q_M^{0.3686}$. The statistical correlation is greater for power trend line than linear trend line, which indicates a power relationship was considered to more accurately represent the average of each gas content component relative to Q_M. Figure 9b shows gas content of Q_1 and Q_2 gas component increase sharply with the increasing total gas content Q_M.

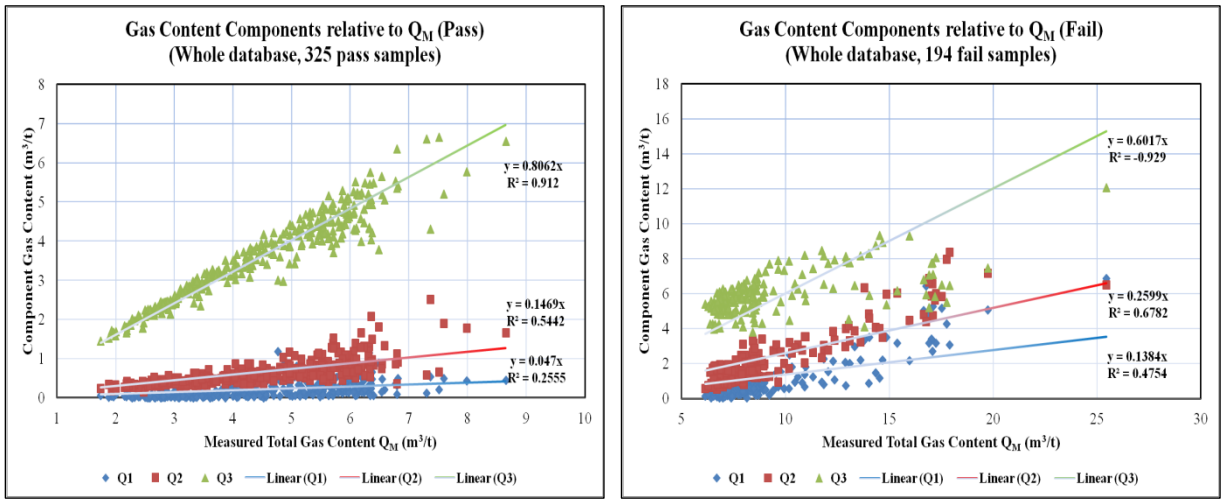

(a) **(b)**

Figure 8 - Gas content component relative to Q_M (whole data base, linear relationship)

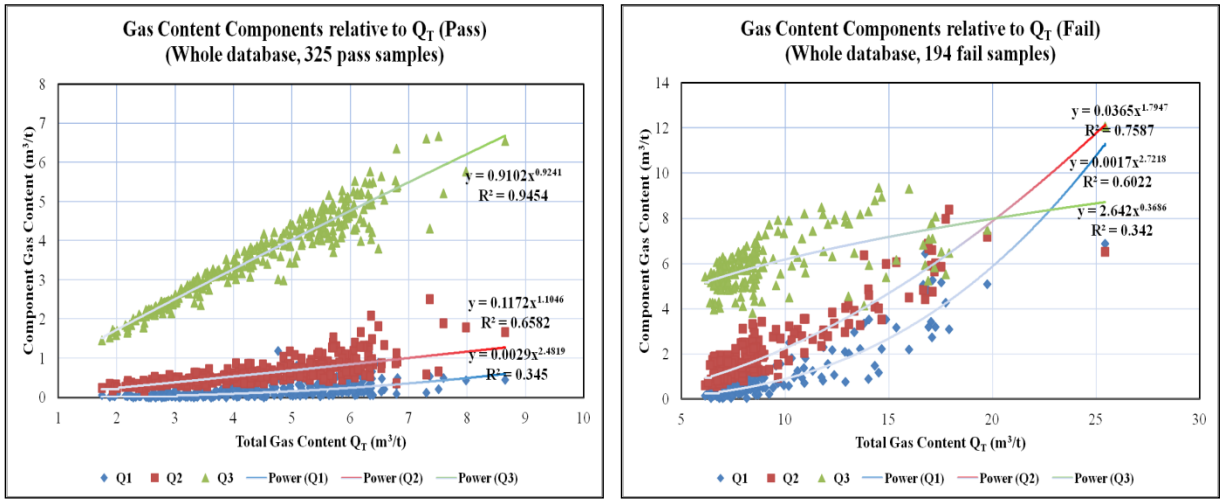

(a) **(b)**

Figure 9 - Gas content component relative to Q_M (whole data base, power relationship)

CONCLUSIONS

An analysis of the whole gas database found that the Q_1, Q_2 and Q_3 components increased in response to increasing measured total gas content Q_M. Statistical analysis also shows an increase trend in the Q_1:Q_M and Q_2:Q_M ratio corresponding to increased Q_M, but an decrease trend in the Q_3:Q_M ratio corresponding to increased Q_M. No clear correlation was found between the gas components and their ratio corresponding to the gas composition. Because of the seam is CO_2 rich, the samples are mainly located in areas with less than 20 % CH_4.

It can be concluded that, a linear trend line can be fitted to represent the average relationship of each gas content component relative to Q_M of the whole gas database as well as typical hard-to-drain area. The statistical correlation shows a better linear trend line fitting for "Pass" samples than "Fail" samples

especially Q_3 gas component. A power relationship was considered to more accurately represent the average of each gas content component relative to Q_M, especially for "Fail" samples. Analysis also shows that Q_1 and Q_2 gas component increased more sharply than Q_3 with the increase of Q_M, especially for "Fail" samples.

The whole database contains 519 samples, from CO_2 rich to CH_4 rich area. The average value of CO_2 composition of "Pass" samples is 73.5 % and 82.6 % for "Fail" samples. The zone with CH_4/ (CH_4+CO_2) ratio less than 0.2 includes 171 "Fail" samples, accounting for 88.1 % of total "Fail" samples. Including the "Pass" samples, 41.0 % of samples in the zone with CH_4/ (CH_4+CO_2) ratio less than 0.2 are failed, compared with 22.5 % when in the zone with CH_4/ (CH_4+CO_2) ratio greater than 0.2.

ACKNOWLEDGMENT

The research financial support from Metropolitan Colliery of Peabody Energy Australia is appreciated. The field trial support and gas data collections assistance from Metropolitan Colliery are gratefully acknowledged. University of Wollongong Scholarship and Scholarship from China Scholarship Council are also acknowledged.

REFERENCES

Black, D, 2012. Factors affecting the drainage of gas from coal and methods to improve drainage effectiveness, PhD thesis, University of Wollongong, Wollongong. http://www.uow.edu.au/eng/outburst/html/Completed%20Thesis/D%20Black%20PhD%20Thesis.pdf.

Clark, D A, Battino, S and Lunarzewski, L, 1983. Prevention and control of outbursts by pre-drainage of seam gas at Metropolitan colliery - a review, *Alleviation of Coal and Gas Outbursts in Coal Mines - Seminar 3*, Coordinating Committee on Outburst Research, September. http://www.uow.edu.au/eng/outburst/html/Research%20&%20Publication/Committee%20on%20Outburst%20Research/Chapter%2018.pdf.

Clarke, M, 1994. Notice pursuant to Section 63 Coal Mines Regulation Act 1982, New South Wales Department of Mineral Resources – Coal Mining Inspectorate and Engineering Branch, 11 May.

Clayton, J L, 1998. Geochemistry of coalbed gas - a review, *International Journal of Coal Geology* 35(1-4): 159-173.

Faiz, M and Hutton, A C, 1995. Geological controls on the distribution of CH_4 and CO_2 in coal seams of the southern coalfield, NSW, Australia. *International Symposium-CUM-Workshop on Management and Control of High Gas Emissions and Outbursts in Underground Coal Mines*, Wollongong, NSW, Australia, 375-383. http://www.uow.edu.au/eng/outburst/html/Research%20&%20Publication/Committee%20on%20Outburst%20Research/Chapter%2018.pdf.

Faiz, M, Saghafi, A, Sherwood, N and Wang, I, 2007. The influence of petrological properties and burial history on coal seam methane reservoir characterisation, Sydney Basin, Australia. *International Journal of Coal Geology,* 70(1-3):193-208.

Harvey, C R and Singh, R N, 1998. A review of fatal outburst incidents in the Bulli seam, in *Proceedings of the 1st Australasian Coal Operators' Conference COAL98*, University of Wollongong, 18-20 February, 649-658.

Kahil, A A and Masszi, D, 1982. Technical considerations for the design of a demethanation program, in *Proceedings of the Symposium on Seam Gas Drainage with Particular Reference to the Working Seam*, (ed: A J Hargraves), Australasian Institute of Mining and Metallurgy - Illawarra Branch, University of Wollongong, Wollongong, Australia, 11-14 May, 99-104.

Lama, R D, 1980. Drainage of methane from the solid at West Cliff Colliery - Optimisation of drainage hole design parameters, *Commonwealth Scientific and Industrial Research Organisation, Division of Applied Geomechanics*, Geomechanics of coal mining report No.18.

Lama, R D, 1995. Safe gas content threshold value for safety against outbursts in the mining of the Bulli seam, *International Symposium on Management and Control of High Gas Emissions and Outbursts in Underground Coal Mines*, (ed: R D Lama), Wollongong, 20-24 March, 175-189.

New South Wales Department of Mineral Resources (NSWDMR), 1995. Outburst Mining Guideline MDG No.1004, Coal Mining Inspectorate and Engineering Branch, Department of Mineral Resources New South Wales.

Singh, A and Singh, B D, 1999. Methane gas: An unconventional energy resource. *Indian Academy of Science.*

ESTIMATION OF FUGITIVE EMISSIONS FROM OPEN CUT COAL MINING AND MEASUREABLE GAS CONTENT

Abouna Saghafi

ABSTRACT: To evaluate fugitive emissions from open cut coal mines, emission factor values of 3.2 m^3/t and 1.2 m^3/t have been used for the two main Australian coal-producing states of New South Wales and Queensland, respectively. CSIRO developed these values in the early 1990s. They were meant for use as average regional values (Tier 2 method), but were subsequently used for all mines, irrespective of the level of 'gassiness' of specific coal seams and strata. Over the past decade, A new method has been developed for Australian open cut mining that is specific to each mine site (Tier 3 method). The proposed method has been adopted by National Greenhouse and Energy Reporting and is the basis of Method 2 or 3 for calculation of emissions. The new method is based on an emission model, which considers the coal seams and sedimentary gas-bearing horizons (layers) as individual gas reservoir units. These units release part or all of their gas during mining. The main data required are *in situ* gas content, gas composition and thickness of the gas-bearing horizons within the column of strata above and below the mine base. In this method, drilling can be reduced by partitioning the mine site into 'gas zones' in which similar patterns of gas distribution are expected. Two to three core drillings are required to characterise a gas zone and to provide the main input of the model. Routine geophysical log data can also provide the thickness of gas-bearing layers. Because of the limitations of the standard gas content measuring method, different commercial laboratories claim various limits of detection (i.e. measurability). However, in view of the very different global warming potential values of coal seam gas components, different limits of measurability can lead to significant differences in the estimation of fugitive emissions.

INTRODUCTION

In the early 1990s, a method of estimating fugitive gas emissions from open cut coal mines based on direct measurement of gas plumes emitted from 17 open cut coal mines in the Sydney and Bowen Basins was developed (Saghafi and Williams, 1992; Williams and Saghafi, 1993; Williams, *et al.*, 1996). Emissions from these mines were determined using an air pollution technique, involving the measurement of wind speed and gas concentration above the ground in the proximity of emissions sources (one or a group of coal mines). Subsequently, an average emission factor (*EF*) of 1.2 m^3/t methane (CH_4) was established (equivalent to 0.017 t of carbon dioxide (CO_2) per tonne of raw coal) for open cuts of the Bowen Basin and an *EF* value of 3.2 m^3/t (or 0.045 t of CO_2 per tonne of raw coal) for the open cut mines of the Hunter Coalfield (for details, see Saghafi, 2012a). These numbers were the basis for what is called Method 1 (see National Greenhouse and Energy Reporting (NGER) documents, 2009).

Over the past decade, several studies have been undertaken to improve the method of fugitive emissions estimation. The effort was culminated in, the development of a mine-specific method (Tier 3 method) to calculate *EF*s (Saghafi, *et al.*, 2003, 2005a, 2005b, 2008; Saghafi, 2010a, 2010b, 2012a). This paper explains this new method, which is described under Method 2 or 3 in the NGER documents (NGER, 2009). A main input parameter in the new emission model is the gas content of coal seams and gas-bearing horizons in overburden and underburden strata. Using the standard method (Standards Australia, 1999) for measuring the gas content of open cut coals may not produce correct results for low-gas-content coals. Hence, a detectable limit of gas content should be agreed upon, or a suitable method of gas content testing for low-gas-content coals should be developed (Saghafi, 2010c, 2012b). In this paper, the effect of using various gas content detectability limits on the evaluation of fugitive emissions is discussed.

CSIRO Energy Technology, P.O. Box 52, North Ryde, NSW 1670, Abouna.Saghafi@csiro.au, Tel: 02 9490 8670

THE NEW TIER 3 METHOD FOR ESTIMATION OF FUGITIVE EMISSIONS FROM OPEN CUT COAL MINES

A new approach is used to develop a mine-specific method of estimating fugitive emissions from open cut mines. The approach considers a coal mine as a gas reservoir and assumes that the total volume of emissions from the mine, including exploration boreholes, spoil piles, and transport and haulage of coal products, is equal to the volume of gas initially trapped in the reservoir. If a coal mine advances at a certain regular pace over its life, this approach assumes that emissions would be equal to the volume of gas contained in a column of strata of constant width that includes the overburden and part of the interburden. This column of strata is called the 'gas release zone' (Saghafi, *et al.*, 2005a, 2008; Saghafi, 2012).

Using the new method, the gas release zone is partitioned into a number of gas-bearing horizons that we called 'emission layers' (Saghafi, *et al.*, 2008). The layers are first identified according to their lithology (type of material). The layering can be further refined if the gas content and gas composition vary significantly along the height of the layer (e.g. a coal seam with significant interburden bands).

Figure 1 shows a schematic of a gas release zone in an open cut mine in which the emission layers are identified based on the lithology of the layer (coal, shale and rock). Each layer (i) is characterised by its thickness (h_i), material density (ρ_i), and gas content (c_i) and gas composition. Two coefficients (α_i and β_i) are also attributed to each layer. The production coefficient (α_i) takes on values of 1 or 0 depending on whether the layer is mined (α_i=1) or not mined (α_i=0). This latter is the case of thin, uneconomical seams in the overburden, and any coal or rock horizon in the underburden. The emission coefficient (β_i), which varies between 0.0 and 1.0, presents the extent of gas release from the layer. A value of β_i=1.0 indicates that the totality of gas trapped in the layer is released during mining. A value of β_i <1 indicates that only part of the layer's gas is released during mining, and a β_i=0.0 indicates that no gas is released from layer i (the case of a coal seam far below the base of the mine).

Using the above notations, the emission from layer i as a result of mining is:

$$q_i = \beta_i c_i \rho_i h_i \tag{1}$$

q_i is the emission from layer i and is quantified in terms of m^3 of gas per m^2 of ground surface (assuming that gas content is in m^3/t, height in m and density in t/m^3 or g/cc). Hence the total emissions from all n layers would be:

$$Q = \beta_1 c_1 \rho_1 h_1 + \beta_2 c_2 \rho_2 h_2 + ... + \beta_i c_i \rho_i h_i + ... + \beta_n c_n \rho_n h_n \tag{2}$$

The quantity Q, expressed in m^3 gas per m^2 ground surface, is the total emissions from coal mine. It is also called emission density in this paper.

Since fugitive emissions are usually expressed in terms of volume of gas liberated per tonne of raw coal extracted, the potential mass of mined coal in the column of strata that forms the gas release zone (Figure 1) should be evaluated. For an individual layer i, the mass of coal that can be produced is:

$$p_i = \alpha_i \rho_i h_i \tag{3}$$

where p_i is the raw coal produced from layer i, and is expressed in tonnes per m^2 of the ground surface. It follows that the total coal production from all n layers is:

$$P = \alpha_1 \rho_1 h_1 + \alpha_2 \rho_2 h_2 + ... + \alpha_i \rho_i h_i + ... + \alpha_n \rho_n h_n \tag{4}$$

where P (total coal production from the gas release zone) is expressed in terms of tonnes of coal per m^2 of ground surface.

Hence, the EF for a specific site is:

$$EF = \frac{Q}{P} \tag{5}$$

which gives *EF* in terms of m^3 of gas per tonne of coal mined (similar to gas content unit).

Using the EF value, the model can take into account the temporary stoppage of mining, in which case the new annual production will be P_r and the emissions volume will be $EF \times P_r$. Note that *EF* calculated by this method should not be affected by temporary stoppages of coal production. However, if mining is completely stopped, the applicability of this model also stops. This is because emissions would continue, but at a much-reduced rate.

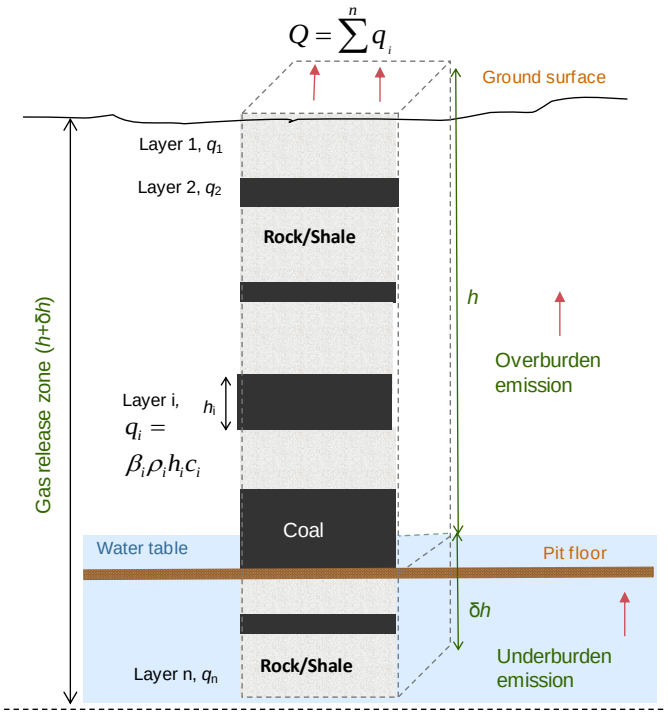

Figure 1 - The new mine-specific emission model showing the gas release zone and emissions layers, not to scale (modified from Saghafi, *et al.*, 2005, 2008; Saghafi, 2012a)

Gas content in terms of CO_2 equivalent

The climate impact of a given mass of a gas emitted to the atmosphere depends on its radiative properties and its atmospheric life span. Global Warming Potential (GWP) is a measure of this impact. GWP is calculated by using the radiative and lifetime of the gas in atmosphere. It varies for different gases according to the time span chosen, reflecting the lifetimes of CH_4 and CO_2 in the atmosphere (Climate Change, 1995). For a time span of 100 years, if CO_2 GWP is taken as 1.0, then the GWP for CH_4 relative to CO_2 is 21 in terms of mass and 8.4 in terms of volume. Note that in later IPCC documents a GWP of 25 for CH_4 is also reported (IPCC, 2007). For greenhouse gas inventory purposes, gas emissions must be reported in CO_2-equivalent (CO_2-e). Therefore, the CH_4 emissions are converted to CO_2 using the GWP factor for CH_4. Another component of coal seam gas in Australia is nitrogen (N_2), for which GWP=0.

If the composition of desorbed gas is known, the measured gas content (C_m) can be converted to CO_2-e gas content ($C_{co2\text{-}e}$) as follows:

$$C_{CO_2-e} = \frac{C_m (CO_2\% + 8.4 CH_4\%)}{100} \qquad (6)$$

Estimation of the emission coefficient β

The value of β indicates how much of the total gas initially in a layer is liberated during mining. It is plausible to assume that any overburden layer releases all its gas (β=1) in the course of mining. For the coal seams and gas-bearing strata in the underburden, β is less than 1.0, because these layers partially release their gas during mining. We can assume that at a depth of more than 20 to 30 m below the base

of the mine, coal seams retain their gas and β=0.0 for these seams (Saghafi, *et al.*, 2005, 2008; Saghafi, 2012a). A simple method to estimate β in the underburden is to use a linear function of depth (Saghafi, *et al.,* 2008; Saghafi, 2012a), with β=1.0 at the base of mining and β=0.0 at a depth of δh below the base of the pit. Figure 2 shows schematically the variation of β from the ground surface to a distance δh below the base of the pit. Saghafi, *et al*., (2005, 2008) suggested a value of δh=20 m for Australian mines. The value of β in the underburden is:

$$\beta = 1.0 - \frac{z-h}{\delta h} \tag{7}$$

Note that the water table and the extent of fracturing of the ground below the pit floor affect the values of β, and can be set to follow other functions (for a more detailed discussion, see Saghafi, 2012a).

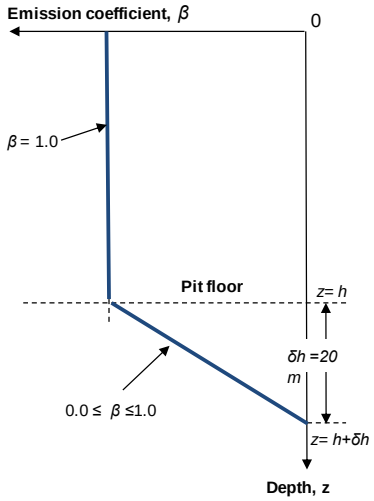

Figure 2 - Emission coefficient β as a function of depth, not to scale (modified from Saghafi, *et al.*, 2005a, 2008, Saghafi, 2012a)

Variability of gas content and gas composition in shallow strata

The large variation in gas content and composition at shallow depths makes the production of a gas distribution model a tedious task. Hence, a number of core holes are required to quantify the distribution of gas in shallow strata. The number of boreholes can be reduced by initially partitioning the mine lease into several 'gas domains' and 'gas zones' (Saghafi, *et al.*, 2008; Saghafi, 2010a, 2010b) in which the local geology, strata layout and hydrology follow similar patterns, so that similar gas patterns can be expected. In each gas zone, at least two boreholes should be drilled and cored for gas content and gas composition. Mine routine exploration boreholes can be used for these measurements. For example, exploration boreholes are subjected to routine geophysical logging, and data such as the thickness of various emission layers, and possibly the porosity of rock layers, can be provided by the log data (Saghafi, *et al.*, 2011). The number of cores from each hole should be at least equal to the number of gas-bearing horizons. Overall, delineating gas zones is a first step in reducing gas drilling. Combining routine exploration drilling with gas testing could substantially reduce the cost of drilling and coring.

Uncertainty of emissions estimate

As discussed, the volume of emissions from a mine site in terms of emissions density, Q, is calculated by summing the individual emissions (q_i) from layers in the gas release zone. If the uncertainty of emissions from the layer i is δq_i, then the uncertainty of the total emissions (emissions density δQ) is:

$$\delta Q = \sqrt{\sum \delta q_i^{\,2} + 2\sum\sum q_i q_j} \tag{8}$$

Assuming that emission uncertainties of different layers are independent of each other, the second term of square root nullifies and the uncertainty of the total emissions would be:

$$\delta Q = \sqrt{\sum \delta q_i^{\,2}} \tag{9}$$

Moreover, assuming that all other measurement errors, except error of gas content, are negligible, it can be shown (Saghafi, 2012a) that the absolute uncertainty of emissions density (δ*Q*) is:

$$\delta Q = \sqrt{\varepsilon_1^{\,2} q_1^{\,2} + \varepsilon_2^{\,2} q_2^{\,2} + \ldots + \varepsilon_i^{\,2} q_i^{\,2} + \ldots + \varepsilon_n^{\,2} q_n^{\,2}} \tag{10}$$

where $\varepsilon_i = \delta c_i / c_i$ is the relative error of measurement of gas content for samples collected from gas-bearing layer *i*. The relative uncertainty of emissions is calculated by dividing the value of absolute uncertainty by the value of emissions:

$$\frac{\delta Q}{Q} = \frac{\sqrt{\varepsilon_1^{\,2} q_1^{\,2} + \varepsilon_2^{\,2} q_i^{\,2} + \ldots + \varepsilon_i^{\,2} q_i^{\,2} + \ldots + \varepsilon_n^{\,2} q_n^{\,2}}}{q_1 + q_2 + \ldots + q_i + \ldots + q_n} \tag{11}$$

If the relative errors of gas content for all gas-bearing layers are of similar magnitude, it can be shown that the uncertainty of emissions density is:

$$\delta Q = \varepsilon \sqrt{q_1^{\,2} + q_2^{\,2} + \ldots + q_i^{\,2} + \ldots + q_n^{\,2}} \tag{12}$$

In this equation, ε is an average relative error associated with the measurement of gas content. Depending on the confidence level required, the emissions estimate is reported as $Q \pm k\,\delta Q$. The coefficient *k* is the coverage factor; for a confidence level of 95%, *k*=1.96.

EXAMPLE APPLICATION OF THE MODEL TO AN OPEN CUT COAL MINE

The emission model presented here is readily amenable to a spreadsheet calculation. The input data for the model are gas content, gas composition, thickness, density and *α* and *β* coefficients for the layer. The output data are emission density (*Q* in Eq. 2) and emission factor (*EF* in Eq. 5).

Figure 3 shows a spreadsheet calculation for estimating emissions from a shallow, open cut coal mine, with a maximum depth of ~ 80 m. Coal seams identified as seams 1-3 are to be mined. Seam 4 is a thin seam at a depth of 90 m and is not mined. Using the new method, the strata are first divided into nine layers based on the nature of materials each layer contains. Each coal seam is identified as a single layer. The inputs to the model for each layer are its thickness, average density, average gas content, gas composition, and coefficient *α* and *β*. Coefficient *α* is zero for all layers except seams 1-3. Equation (7) is used to evaluate the value of *β* assuming that δ*h*=20 m. Hence for Seam 4, which is located about 10-11 m below the base of the mine, *β*=0.4.

Equations (2) to (5) are then used to calculate emission density and *EF*. Spreadsheet calculation delivers an emission density (*Q*) of 136.58 m^3 CO_2-e per m^2 of ground surface and an *EF* value of 8.0 m^3 CO_2-e per tonne of coal mined. Note that these calculations use data from a single borehole. Drilling more holes in the area will produce a pattern (contour) of *EF* in the area, allowing the hypothesis of single or multiple gas zones to be tested.

			Emission model inputs										Emission model outputs			
								Gas composition (%)			Layer attributes		Coal production & emissions		Uncertainty	
	Layer position	Lithology	Depth from (m)	Depth to (m)	Layer height (m)	Density (t/m^3)	Gas content (m^3/t)	CH_4	CO_2	Gas content, CO_2-e (m^3/t)	*α*	*β*	*p* (t/m^2)	*q* (m^3/m^2)	δ*q*	δ*q*^{2}
Overburden	1	Conglomerate & sandstone	0.0	65.2	65.2	2.5	0.05	29.33	70.67	0.16	0	1.0	0.00	25.75	6.44	41.4
	2	**Seam 1**	65.2	69.3	4.1	1.5	1.06	41.73	58.27	4.32	1	1.0	6.15	26.57	6.64	44.1
	3	Tuff & claystone	69.3	72.6	3.4	2.5	0.05	43.06	56.94	0.21	0	1.0	0.00	1.76	0.44	0.2
	4	**Seam 2**	72.6	78.5	5.9	1.6	1.27	44.72	55.28	5.46	1	1.0	9.42	51.49	12.87	165.7
	5	Carbonaceous mudstone	78.5	79.9	1.4	2.3	0.15	46.02	53.98	0.66	0	1.0	0.00	2.09	0.52	0.3
	6	**Seam 3**	79.9	80.9	1.0	1.5	1.39	46.46	53.54	6.17	1	1.0	1.51	9.30	2.33	5.4
Underburden	7	Siltstone, shale & stony coal	80.9	91.6	10.6	2.2	0.20	48.54	51.46	0.92	0	0.7	0.00	15.16	3.79	14.4
	8	**Seam 4**	91.6	92.1	0.5	1.4	1.68	50.54	49.46	7.95	0	0.4	0.00	2.54	0.63	0.4
	9	Claystone and tuff	92.1	100.9	8.9	2.3	0.10	52.22	47.78	0.48	0	0.2	0.00	1.93	0.48	0.2

Figure 3 - Spreadsheet calculation of the emission factor using the Tier 3 model; seams 1 to 3 are mined

The uncertainty of emissions can be calculated using the quadratic additions method. To simplify the calculation, it can be assumed that the main source of uncertainty is gas content. If all other uncertainties are omitted, Equation (10) can be used. To further simplify the calculation, we assume that for all layers the relative uncertainty of gas content testing is equal and is about 25%. Then Equation (11) can be used, which delivers an uncertainty of about ±16.50 m^3/m^2 for emission density and an uncertainty of ±0.97 m^3/t for *EF*. These uncertainty values are valid for a confidence level of 68%. At a 95% confidence level, the emissions should be reported as:

Q = 136.58 ±32.33 m^3/m^2 (CO_2-e vol)

EF= 8.00 ±1.89 m^3/t (CO_2-e vol).

To calculate emission factor in terms of CO_2 equivalent mass (CO_2-e mass), a density of 0.00178 t/m^3 for CO_2 is used (15°C and 101.325 kPa):

EF= 0.014 ±0.003 t CO_2 per t coal (CO_2-e mass).

LIMIT OF MEASURABILITY OF GAS CONTENT AND EMISSIONS EVALUATION

The limit of measurability is an issue for determining the gas content of low-gas-content coals from shallow seams in open cuts. The standard guideline (AS 3980-1999) was prepared for mine safety and for prediction of outburst potentials and high gas emissions. Therefore, low gas content determination was not an issue, and it has only recently become a focus of research.

Currently, a limit of measurability (or detection limit) of 0.1-0.5 m^3/t of gas content of coal is achievable in Australian gas laboratories. The newly published ACARP guidelines for the implementation of NGER Method 2 or 3 for open cut coal mine fugitive emissions reporting (ACARP, 2011), recommend using a detection limit of 0.5 m^3/t for gas content of open cut coals when using the gas content data to estimate emissions. This limit of detectability is set irrespective of gas type. If the gas is mainly CH_4 then this limit in terms of CO_2 equivalent is ~4.2 m^3/t and if the seam gas is a mixture of 50% CH_4 and 50% CO_2 the limit would be 2.3 m^3/t CO_2 e. For gas contents below 0.5 m^3/t the guidelines recommend to use a default value of 0.125 m^3/t CO_2-e vol (or 0.000 233 t CO_2 per tonne of coal, CO_2-e mass) irrespective of composition of seam gas.

Because of the large differences in the GWP of various gases, using a 0.5 m^3/t limit irrespective of gas type and then applying a default value of 0.125 m^3/t CO_2-e vol can produce significant differences in the estimated emissions for mines that otherwise have similar magnitudes for their real emissions (in terms of CO_2-e vol).

For instance, assume a coal mine (Mine 1) that extracts a single coal seam at a depth of 70 m. For simplicity of calculation it is also assumed that there is no other significant gas-bearing layers in the overburden or to a depth of 20 m in the underburden. The seam gas is made mainly of CH_4 (90%) with remaining CO_2 (10%). Measured gas content is 0.45 m^3/t. Using Eq. (6) the CO_2-e gas content for the mined seam is 3.447 m^3/t CO_2-e which is also the *EF* for this mine since the only gas emitting horizon is the mined coal seam. However, because the gas content falls below suggested measurability limit the *EF* for this mine would be the default value of 0.125 m^3/t CO_2-e.

Now assume a neighbouring mine (Mine 2), which also extracts a single coal seam at open cut depth of 70 m, but with gas mainly made of CO_2 (90%) with remaining CH_4 (10%). The measured gas content is 0.55 m^3/t. The CO_2-e gas content for the mined seam is 0.495 m^3/t CO_2-e (Eq. 6), which is also the *EF* for this mine. The gas content for this mine is above the recommended measurability limit and therefore the true *EF* applies. These data reported in Table 1, show that although Mine 2 produces some seven times less CO_2-e gas than Mine 1, it is attributed four times more CO_2-e gas than Mine 1.

Table 1 - Comparison of attributed emission factors for two mines of different gas mixtures using recommended gas content measurability limit of 0.5 m^3/t

Coal mine	Measured gas content (m^3/t)	CH_4 (%)	CO_2 (%)	Gas content (m^3/t, CO_2-e)	Emission factor (m^3/t, CO_2-e, vol)
Mine 1	0.45	90	10	3.447	0.125
Mine 2	0.55	10	90	0.495	0.495

A new standard for low gas content testing is urgently required in view of the variation in gas mix in different coal mines. A new standard method should enable measurement of gas content of open cut coals, as well as low-rank coals and coals from shallow underground mines. A joint CSIRO-ACARP study (C18050) to develop a new method for determining the gas content of low-gas-content coals has been completed (Saghafi, 2012b). Two commercial laboratories took part in this study and built two prototypes according to the CSIRO design. The prototype systems were trialled by measuring the gas content of two suites of coals from two open cuts. This study (C18050) showed that it is possible to lower the limit of measurability by one order of magnitude. The study was a first major step in adopting a new method for measurement of the gas content of coals from open cuts. The results from this study will be the subject of a future paper.

CONCLUSIONS

A mine-specific emission model for estimating fugitive emissions from open cut coal mines has been developed. The model meets the requirement of the industry and regulatory bodies for calculating emissions on a mine-specific basis (Tier 3 method). The method, which has been adopted by NGER, is used to establish the NGER guidelines for calculating emissions from open cut mines. The model assumes that gas is emitted from a gas release zone, which consists of gas-bearing horizons or emission layers in the overburden, and the mining-affected section of the underburden. The key inputs to the emission model are thickness, gas content and gas composition of the gas-bearing layers. The outputs of the model are gas emission density, expressed in terms of m^3 of gas released per m^2 of ground surface, and *EF*, expressed in terms of m^3 of gas released per tonne of raw coal produced.

Since gas content and gas composition are the main input parameters of the model, gas content must be measured in 2–3 locations over a particular site to enable accurate quantification of gas distribution.
The standard method of gas content measurement is not suitable for the low-gas-content coals of open cut mines. Therefore, some limits for measurability of gas content are required. A measurability limit of 0.5 m^3/t has been suggested. However, such a high limit for low-gas-content coals can lead to erroneous calculations. One issue is the large differences in GWP for various gases. For example, a coal mine with seam gas rich in CH_4 but with gas content below 0.5 m^3/t is attributed a CO_2-e emission level much smaller than its real emissions. In contrast, a mine with seam gas rich in CO_2 but with gas content above 0.5 m^3/t is attributed its true CO_2-e emissions. It is suggested that adaptation of a suitable standard for low-gas-content coal is now urgently required to allow proper calculation of fugitive emissions from open cut mines.

ACKNOWLEDGEMENTS

The author wishes to thank CSIRO and Australian Coal Association Research Program for providing the necessary funds to allow the development of the Tier 3 method of estimating emissions from open cut coal mines. Assistance from coal mines and their staff in New South Wales and Queensland has been invaluable and they are sincerely thanked. My thanks go also to many of my CSIRO colleagues, including J. Carras, C. David, S. Day, C. Dokumcu, M. Drummond, R. Fry, P. Hoarau, A. Lange, A. Quintanar, D. Roberts and D. Williams, who contributed at various stages to mine emissions projects over the past two decades. My thanks are extended to Jim Edwards of CSIRO Energy Technology for reviewing this paper.

REFERENCES

Australian Coal Association Research Program, 2011. Guidelines for implantation of NGER method 2 or 3 for open cut coal mine fugitive GHG emissions reporting (ACARP Project C20005). *ACARP publication*, December 2011, 27 p.

Climate Change, 1995. The Science of Climate Change: Summary for Policymakers and Technical Summary of the Working Group I Report, p. 22. http://unfccc.int/ghg_data/items/3825.php.

IPCC, 2007. IPCC fourth assessment report: Climate change 2007. Working group I: The physical science basis. Section 2.10.2, Direct Global Warming Potentials. http://www.ipcc.ch/publications_and_data/ar4/wg1/en/ch2s2-10-2.html.

National Greenhouse and Energy Reporting (NGER) Act 2007, 2009. National Greenhouse and Energy Reporting (Measurement) Determination 2008. Prepared by the Office of Legislative Drafting and Publishing, Attorney General's Department, Canberra, 238p.

Saghafi, A, 2010a. A tier 3 method for estimating fugitive emissions from open cut coal mining: application to Bowen Basin Coalfields, In *Proceedings of 6th Bowen Basin Symposium, Back in the Black*, GSA Coal Geology Group, MacKay, Qld, October 6-8, pp 101-109.

Saghafi, A, 2010b. A tier 3 method for estimating fugitive emissions from open cut coal mining: application to Hunter Coalfield, In *Proceedings of 37th Symposium on the Geology of Sydney Basin*, 6-7 May, Pokolbin, Hunter Valley, Australia, CD Publication, Paper 19, 9p.

Saghafi, A, 2010c. Novel methods of coal seam gas content determination for estimation of greenhouse gas emissions from mining, in *Proceedings of the 27th Annual International Pittsburgh Coal Conference*, 11-14 October, Istanbul, Turkey, CD Publication, 9p.

Saghafi, A, 2012a. A tier 3 method to estimate fugitive gas emissions from surface coal mining. *International Journal of Coal Geology*,100:14-25.

Saghafi, A, 2012b. Developing a new method for measurement of gas content of low gas content coals (ACARP project C18050). CSIRO Investigation Report EP115419, 70p.

Saghafi, A, Day, S J, Fry, R, Quintanar, A, Roberts, D, Williams, D J and Carras, J N, 2005a. Development of an improved methodology for estimation of fugitive seam gas emissions from open cut mining (ACARP project C12072). *CSIRO Investigation Report ET/IR 74*. ACARP Publication, 1 July 2005, 55p.

Saghafi, A, Day, S J, and Carras, J N, 2005b. Gas properties of shallow Bowen Basin coal seams and gas leaks to the atmosphere. In: *Bowen Basin Symposium 2005: The Future for Coal*. Geological Society of Australia Coal Geology Group and the Bowen Basin Geologists Group, 12-14 October, Qld, Australia, pp 267-271.

Saghafi, A, Day, S, Williams, D J, Roberts, D B, Quintanar, A and Carras, J N, 2003. Toward the development of an improved methodology for estimating fugitive seam gas emissions from open cut mining (ACARP Project C9063). *ACARP Publication*, 1 February 2003, 49p.

Saghafi, A, Hatherly, P and Pinetown, K, 2011. Towards an optimal gas sampling and estimation guideline for GHG emissions from open cut coal mines (ACARP Project C19005). *CSIRO Investigation Report EP113374. ACARP Publication*, 20 July 2011, 74p.

Saghafi, A, Roberts, D, Fry, R, Quintanar, A, Day, S, Lange, T, Hoarau, P, Dokumcu, C and Carras, J, 2008. Evaluating a tier 3 method for estimating fugitive emissions from open cut coal mining (ACARP Project C15076). CSIRO Investigation Report ET/IR 1011R, 120p.

Saghafi, A and Williams, D J, 1992. Estimation of methane emission from Australian coal mines. In: *Symposium on Coalbed Methane Research and Development in Australia*. Townsville, Australia. Vol. 5, pp. 7-13.

Standards Australia, 1999. Guide to the determination of gas content of coal - Direct desorption method. AS 3980-1999, Standards Association of Australia.

Williams, D J and Saghafi, A, 1993. Methane emissions from coal mining - A prospective. *The Coal Journal*, 41:37-40.

Williams, D J, Saghafi, A and Lama, R D, 1996. Methane emissions from coal mining*, IEA Greenhouse Gas R&D Programme*, Report Number PH2/5, June 1996, Paris, 180p.

A FRACTAL THEORY BASED FRACTIONAL DIFFUSION MODEL OF METHANE IN COAL AND EXPERIMENTAL VERIFICATION

Haina Jiang[1,2] and Yuanping Cheng[1,2]

ABSTRACT: Structure parameter θ that reflects the dynamic character of methane in coal and fractal dimension d_f that reflects the static structure of coal were introduced into Fick's model, and based on the assumption that the diffusion is memorable by introducing a parameter ν, a Fractional order of diffusion model was established (the FFD Model). Several adsorption and desorption experiments on anthracite coal with different grain sizes (0.2-0.25 mm, 1-3 mm) were performed under different equilibrium pressures (1 MPa, 4 MPa) to determine the parameters and to confirm the validity of the FFD Model. On that basis, further desorption experiment of pulverized coal was conducted to validate the applicability of the FFD Model on pulverised coal. The results showed that the desorption rate of the 0.045-0.075 mm grain size coal is seven times of the 0.106-0.25 mm grain size coal. The implications of the study are for the pulverising phenomenon during the coal and gas outburst. The desorption velocity will increase rapidly, resulting in the dramatic increase of expansion energy of methane, and this further accelerates the pulverising process - a positive feedback effect between desorption velocity and dusting process. This can be used to explain the phenomenon of the gas-solid two phases flow and the piston effect during the coal and gas outburst.

INTRODUCTION

Coal seam is a dual pore reservoir system that is composed of matrix pores and fractures (Warren and Root, 1963). The matrix pores in a coal seam can absorb 95 percent of the total amount of methane because of their large internal surface area (Gray, 1987). The size distribution of the matrix pores is within the nanometer to micrometer range (Cai, *et al.*, 2013). Fractures are the primary channels for gas migration, and their sizes are inconsistent, ranging from a few inches to several inches (Gan, *et al.*, 1972). Therefore, it can be stated that the pore structure of coal is heterogeneous, which suggests that the pore structure plays an important role in understanding the mechanism for the diffusion of methane in coal.

Because of the complexity of the coal pore structure, the migration of methane in coal is significantly different from its migration in traditional media. Researchers generally accept that the migration of methane in coal simultaneously exists in the following two states: laminar flow in the fracture, which can be described by Darcy's Law where pressure is the driving force, and movement through diffusion in the coal matrix, which can be described by Fick's diffusion law where the concentration gradient in the matrix is the driving force (Yi, *et al.*, 2009; Adler, *et al.*, 1990).

The diffusion model has received increasing attention following the development and utilization of coalbed methane (CBM) resources. Cui *et al.* (2004) reported that the diffusivity had an inverse relationship with the reservoir pressure based on the use of the dual diffusion resistance model to calculate the diffusivity of CH_4, CO_2, and N_2 under different pressures. Other researchers, including Busch *et al.* (2004), Pillalamarry *et al.* (2011), Saghafi *et al.* (2007) and Shi and Durucan (2003) , conducted similar research on this topic. The single pore diffusion model, derived from Fick's second law, is widely used because of its simplicity and ease of use despite the low degree of fitting. Smith and William (1984) conducted experiments on six coal samples from the San Juan Basin to verify the applicability of the single pore diffusion model. Their results indicated that the single pore diffusion model is only suitable for the first 50% of the desorption gas.

The diffusivity of methane in coal has also attracted the interest of many researchers (Cui, *et al*., (2004); Busch, *et al.*, (2004); Pillalamarry, *et al.*, (2011); Saghafi, *et al.*, (2007); Shi and Durucan (2003); Charrière, *et al.*, (2010); Clarkson and Bustin, (1999); Nandi and Walker, (1970); Siemons, *et al.*, (2007)). Some conclusions have been obtained regarding the diffusivity of methane in coal, such as the adsorption kinetics under high and low pressures are related to the character of the gas, the moisture and the temperature. Based on Fick's classical diffusion model, Smith and William (1984) calculated the

[1] *National Engineering Research Center of Coal Gas Control, M: +86 (0)13952231131*
[2] *Faculty of Safety Engineering, China University of Mining and Technology, Xuzhou, Jiangsu 221116, China.*

effective diffusion coefficient and concluded that the effective diffusion coefficient of the coal sample varied little with the depth of the coal sample. Nandi and Walker (1975) also examined coal samples from three regions of America to calculate the effective diffusion coefficient and concluded that diffusion coefficients of two of the samples will increase with the increase of the average diffusion concentration under high methane concentrations. Based on this result, Nandi and Walker (1975) believed that the concentration dependent diffusivity results follow a nonlinear adsorption process. However, Bielickiet and Perkins (1972) obtained the pressure dependent diffusivity, and based on this result, he believed that Fick's diffusion model was not suitable for coal because, from a theoretical perspective, the diffusivity in Fick's model is a constant that was not dependent on concentration and pressure. Smith and William (1984) reported that the causes of errors in Fick's diffusion model are due to the assumptions of sample homogeneity and isotropy. Smith and Keller (1985) studied the influence of nonlinear adsorption of a single medium on the diffusion and adsorption parameters and concluded that the magnitudes of the dynamic parameter in the linear and nonlinear adsorption models were different despite the similar adsorption rate curves. In addition, Smith and Keller (1985) also observed that the nonlinear adsorption behaviour is particularly obvious when the concentration significantly changes, especially during the gravimetric method experiment that was used to determine the adsorption rate.

The objectives of this paper are to solve the problems that exist in Fick's classical diffusion model, such as the inability of the model to describe heterogonous coal and the dynamic transport process of methane in coal. Therefore, in this paper, we introduce the fractal dimension (d_f), which can describe the heterogeneous nature of coal, and the structure parameter (θ), which can describe the dynamic transport of methane in coal into Fick's classical diffusion model. In addition, it is assumed that the transport process is memorable and can be described by a fractional partial differential equation of the time variable (t). Therefore, a fractal theory based Fractional diffusion model of methane in coal was established (FFD Model). To verify the validity of the FFD Model, three different types of coals from China were used in an adsorption and desorption experiment and other studies. The different relationships between the fractal dimensions, the structure parameter (θ), the grain size and pressure are also discussed.

EXPERIMENTAL METHODS

Physical property parameters of the coal

In this paper, three types of coal samples were collected, including long flame coal from Tie Fa, coking coal from Tun Lan, and anthracite from Da Nin. According to the Sample Preparation Method (GB 474-2008, 2008) standard, the coal sample was sieved in the laboratory to obtain samples with the grain sizes of 0.075-0.2 mm, 0.106-0.2, 0.2-0.25 mm, 1-3 mm, and 20-30 mm. The maceral and mineral contents and the vitrinite reflectance of the 0.2-0.25 mm grain size coal sample were determined using metallographic microscopes and micro-spectrophotometic methods (ZEISSaxio Imager M1 m) based on the Method of Determining Marcel Group Composition and Mineral Coal (GB/T8899-1998, 1998) and <Method of Determining Microscopically the Reflectance of Vitrinite in Coal (GB/T6948-2008, 2008) standards. Based on the Proximate Analysis of Coal (GB/T212-2008, 2008) standard, a fully automated industrial analyser (5E-6600) was used to perform the industrial analysis with the 0.074-0.2 mm grain size coal sample. The determination of the multipoint BET and average pore diameters with the 0.2-0.25 mm grain size coal samples is based on The Materials by mercury Porosimetry and Gas Ddsorption - Part 2:Analysis of Microopores and Macropores by Gas adsorption (GB/T21650.2-2008, 2008) using the liquid nitrogen adsorption technique (77.35 K, 101.3 kPa) and the AUTOSORB-1 gas adsorption analyser. The experimental results from these analyses are presented in Table 1.

Table 1 - Basic physical property parameters of the coal samples

Maceral and mineral (vol.%)					Proximate analysis/%				Average Pore Diameter/ Å	Multipoint BET /(m^2/g)
Vitrinite	Intertinite	Liptinite	Mineral	Vitrinite reflectance	M_{ad}	A_d	V_{daf}	FC_d		
77.8	14.1	0	8.1	3.6	3.46	25.63	8.61	68.05	36.01	43.77

CO_2 adsorption isotherm analysis

Experiments on the adsorption of CO_2 gas were conducted in a HCA gas adsorption instrument using the high pressure volumetric analysis method. The laboratory procedure followed the Method of Determining Methane Adsorption Capacity in Coal Standard MT/T 752-1997 (1997). All of the samples were prepared

by grinding and sieving to a size range of 0.2~0.25 mm and 1~3 mm. Up to 50 g of the samples were weighed for the adsorption experiment, and the samples were then sealed in the coal canister. After verifying the air tightness of the coal canister, helium gas (He) was applied to determine the dead space of the canister. The samples were outgassed overnight in a 60℃ thermostatic water bath under vacuum to a final pressure of 0.25 Pa. After these pretreatment steps, the coal samples were placed into a 30℃ thermostatic water bath for the adsorption isotherm experiment. The tests were conducted under equilibrium pressures of 1 MPa and 4 MPa for all of the samples. The procedure for performing the test is as follows: a certain pressure of CO_2 was injected into a reference canister with a known volume. Then, the reference canister was connected to the coal canister after the pressure in the reference canister reached equilibrium. The connecting valve was then closed after the pressure in the coal canister reached the predetermined pressure, and the equilibrium pressure of the reference canister and the equilibrium adsorption pressure in the coal canister were recorded. The amount of adsorbed gas was then calculated as the difference of the amount of gas in the dead space of the coal canister from the amount of gas that moved from the reference canister to the coal canister.

Desorption experiments

Experiments examining the desorption of CH_4 gas were conducted in a desorption instrument using the coal seam methane content from rapid determination equipment (FM4WP-1). All of the samples were prepared by grinding and sieving to a size range of 0.2~0.25 mm and 1~3 mm. A certain amount of coal (to fill the coal canister) for the adsorption experiment was weighed and then sealed in the coal canister. After verifying the air tightness of the coal canister, the samples were outgassed overnight in a 60℃ thermostatic water bath under vacuum to a final pressure of 0.25 Pa. After these pretreatment steps, CH_4 with a purity of 99.99% was injected into the coal canister to a certain pressure, and then the canister was placed into a 30℃ thermostatic water bath to reach adsorption equilibrium. After recording the equilibrium pressure, the coal canister valve was opened as quickly as possible, and once the pressure reached zero, the canister was rapidly connected to the desorption graduate. The amount of gas desorbed over two hours and the ambient and atmospheric pressures were also recorded. After two hours, the canister valve was tightened as quickly as possible to perform the residual gas content measurement. This measurement consisted of placing the canister that underwent desorption for two hours into vacuum degassing equipment in a 95℃ bath; Gas chromatographs were then used to determine the components of the gas. After vacuum degasification, the sample in the vacuum canister was transferred into a ball-milling canister for a second grinding until the grain sizes of 80% of the coal sample were less than 0.25 mm, then the samples were outgassed and then reground until there was no longer outgassing. Then, the total gas content was calculated as the sum of the two hours of desorbed gas and the residual gas.

ESTABLISHMENT OF THE FFD MODEL

Solution of FFD model

The adsorption processes are commonly interpreted by comparison with standard solutions of Fick's model. Fick's model (Zhao, 1991) used for Euclidean geometry is:

$$\frac{\partial c(r,t)}{\partial t} = \frac{D}{r^{d-1}} \frac{\partial}{\partial r}\left(r^{d-1} \frac{\partial c(r,t)}{\partial r} \right) \quad (1)$$

where c is the diffusion concentration of the components (kg/kg), d is the dimension for Euclidean geometry, D is the diffusivity (m^2/s), r is the radius of the coal particles (m), and t is the time (s).

The pore structure is the primary factor that affects the diffusive transportation of methane in coal; however, Fick's classical diffusion model cannot describe the influence of the pore structure on the diffusive transport process. By considering the structures of the pores in the coal to be diffusive structures, the Euclidean dimension (d) in Eq.(1) was substituted with the fractal dimension, d_f. Based on simulations, Zhang *et al.* (2004) concluded the following: The diffusivity (D) in fractal structures is not a constant but rather a function of the position, r, in the form of $D = D_0 r^{-\theta}$, where D_0 is the pre-exponential coefficient and θ is a structure parameter that can describe the fractal dimensionality of the path of the diffusive component on the porous material and is related to the fractal dimension (d_f). In addition, it is assumed that the diffusive transport in fractal structures is memorable; therefore, the first-order partial

differential equation about time is changed into a υ fractional-order partial differential equation (Yi, *et al.*, 2009).

Through the above series substitution, the fractal theory based FFD model of methane in coal was established:

$$\frac{\partial c^{\upsilon}(r,t)}{\partial t^{\upsilon}} = \frac{D_0}{r^{d_f-1}} \frac{\partial}{\partial r}\left(r^{d_f-1-\theta} \frac{\partial c(r,t)}{\partial r} \right), \ 0<\upsilon\le 1 \tag{2}$$

Where $c(r,t)$ is the concentration of the diffusion component; for coal particles, the concentration c_0 is at the adsorption equilibrium. Concentration gradients along the radii of the coal particles will appear after the coal particles have been exposed to atmospheric conditions because of the reduction of the concentration at the surface of the coal particles. The adsorbed gas becomes free gas, and the diffusion from the center of the coal particle to the surface occurred. The surface concentration is c_1, and the initial and boundary conditions are:

$$c(r,t)\big|_{t=0} = c_0, \ 0\le r<r_0 \tag{2a}$$

$$\frac{\partial c(r,t)}{\partial r}\Big|_{r=0} = 0, \ t\ge 0 \tag{2b}$$

$$c(r,t)\Big|_{r=r_0} = c_1, \ t\ge 0 \tag{2c}$$

where c_0 is the initial concentration in an adsorbent, kg/m^3 and r_0 is the granule radius, m.

By performing the transform of $u(r,t)=c(r,t)-c_1$, Eq. (2) becomes,

$$\frac{\partial u^{\upsilon}(r,t)}{\partial t^{\upsilon}} = \frac{D_0}{r^{d_f-1}} \frac{\partial}{\partial r}\left(r^{d_f-1-\theta} \frac{\partial u(r,t)}{\partial r} \right), \ 0<\upsilon\le 1 \tag{3}$$

$$u(r,t)\big|_{t=0} = c_0-c_1, \ 0\le r<r_0 \tag{3a}$$

$$\frac{\partial u(r,t)}{\partial r}\Big|_{r=0} = 0, \ t\ge 0 \tag{3b}$$

$$u(r,t)\Big|_{r=r_0} = 0, \ t\ge 0 \tag{3c}$$

The solution of the Eq. (3) is:

$$\frac{c_0-c(r,t)}{c_0-c_1} = 1-\sum_{n=1}^{\infty} \frac{2}{\mu_n J_{1-\alpha}(\mu_n)} \left(\frac{r}{r_0}\right)^{\frac{d_w-d_f}{2}} \cdot J_{-\alpha}\left[\mu_n\left(\frac{r}{r_0}\right)^{\frac{d_w}{2}}\right] \cdot e^{-D_0\left(\frac{\mu_n d_w}{2r_0^{d_w/2}}\right)^2 t^{\upsilon}} \tag{4}$$

The cumulative diffusion amount at time *t* was expressed in Q_t and the limiting diffusion amount when $t\to\infty$ was expressed as Q_∞:

$$\frac{Q_t}{Q_\infty} = \frac{c_0-\overline{c(r,t)}}{c_0-c_1} = 1-\sum_{n=1}^{\infty} \frac{4d_f}{d_w{\mu_n}^2} e^{-\left(\frac{\mu_n d_w}{2}\right)^2 \frac{D_0}{r_0^{d_w}} t^{\upsilon}} \tag{5}$$

where

$$\overline{c(r,t)} = \frac{d_f}{r_0^{d_f}} \int_0^{r_0} c(r,t) r^{d_f - 1} dr \quad (6)$$

when the parameters in Eq. (4)、 Eq. (5) change into the following values: $d_f = 3$, $\theta = 0$, correspondingly, $d_w = 2$, $D_0 = D$, $\alpha = -0.5$, $\mu_n = n\pi$, $J_{0.5}(\frac{n\pi r}{r_0}) = \sqrt{\frac{2r_0}{n\pi^2 r}} \sin(\frac{n\pi r}{r_0})$, $J_{1.5}(n\pi) = \sqrt{\frac{2}{n\pi^2}}(-1)^{n+1}$

Eq. (4) and Eq. (5) were changed into:

$$\frac{c_0 - c(r,t)}{c_0 - c_1} = 1 - \frac{2r_0}{\pi r} \sum_{n=1}^{\infty} \frac{(-1)^{n+1}}{n} \cdot \sin(\frac{n\pi r}{r_0}) \cdot e^{-D_0 \left(\frac{n\pi}{r_0}\right)^2 t} \quad (7)$$

$$\frac{Q_t}{Q_\infty} = 1 - \sum_{n=1}^{\infty} \frac{6}{(n\pi)^2} e^{-(n\pi)^2 \frac{D_0}{r_0^2} t} \quad (8)$$

This result is the solution of Fick's diffusion model. From this solution, it can be seen that Fick's model is a special condition of the FFD Model; therefore, the validity of the FFD Model is confirmed (Qilin, 2004; Society, 1986).

Determination of the parameters

In this paper, the fractal dimension is determined from an analysis of multiplayer adsorption to a fractal surface according to the FHH equation (Radliński, *et al.*, 2009; Triolo and Child, 1984; Allen, *et al.*, 1985; Yao, *et al.*, 2009; Machnikowski, *et al.*, 2004; Wang, *et al.*, 2011). The structure parameter (θ) was calculated using the exact-enumeration method (Gorenflo, *et al*., 2007; Turk, *et al*., 1987; Xin, 1997). The diffusivity (*D*) was obtained through its definition (Donghui, 2004), the calculated results are shown in Table 2:

Table 2 - The calculated results of the diffusivity

Pressure/MPa	Grain size/mm	D_{avt}/(m^2/s)	d_f	θ	D_0/(m^2/s)
1	0.2-0.25	4.05689E-11	2.5841	1.7036	2.59166E-18
	1-3	4.24814E-10	2.5185	1.6165	2.15161E-15
4	0.2-0.25	4.05742E-11	2.7149	1.8772	4.83959E-19
	1-3	4.2487E-10	2.6266	1.7600	7.35474E-16

It can be seen from Table 2 that the fractal dimension (d_f) of the long flame coal from TieFa is between 2.4~2.55; and within the experimental pressure range (1 MPa-4 MPa), the fractal dimension (d_f) will increase with pressure because the surface structure was damaged and becomes more complex with increasing pressure. The fractal dimension (d_f) will increase with the decreasing grain size of the coal because the large and medium pores disappeared and the micropore porosity relatively increased, which caused the coal structure to become complex. θ is a parameter that can reflect the dynamic walk process in the porous media; therefore, it is consistent with the fractal dimension (d_f). The structure parameter (θ) for the long flame coal from TieFa is between 1.5~1.9. The magnitudes of the pre-exponential coefficient (D_0) are between 10^{-19}~10^{-15} and the average diffusivity (D_{avt}) rate is between 10^{-12}~10^{-10}; this result is consistent with the results of previous researchers (Busch, *et al.*, 2004; Pillalamarry, *et al.*, 2011; Saghafi, *et al.*, 2007; Shi and Durucan, 2003). Furthermore, from Table 2 also it can observed that the diffusivity in the FFD Model has little variance with the pressure and can be

basically considered to remain constant with pressure. The diffusivity in the FFD Model will increase with the grain size and first increase then decrease with the coal types.

A COMPARATIVE ANALYSIS OF FICK'S MODEL AND THE FFD MODEL

By substituting d_f, θ, and D_0 into Eq. (8) and applying the positive zero of the Bessel function, the relative desorption amounts of the different coal samples (three coal types and two grain sizes) can be calculated for CH_4 at 273 K with time at different initial pressures (1 MPa and 4 MPa). The results from the FFD Model and Fick's model for comparison with experimental data are shown in Figure 1a and Figure 1b. In addition, the parameter ν was obtained by fitting the FFD Model with the experimental data, and it represents the trend of the desorption curve. The gradient of the curve will increase with the increase of υ, especially during the initial stage of the desorption curve.

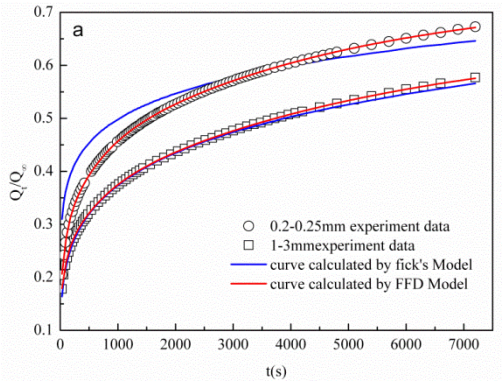

Figure 1a - The desorption curve of anthracite from DaNing at different pressures (a: 1 MPa)

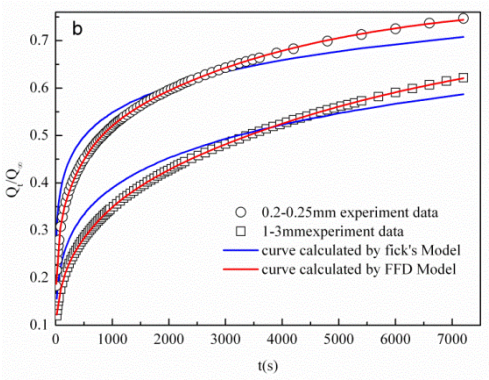

Figure 1b - The desorption curve of anthracite from DaNing at different pressures (b: 4 MPa)

It can be seen from Figure 1a and Figure 1b that the trend of the relative desorption curve has basically similar pattern, i.e., the desorption rate is fast initially. The influence of the microstructure pore will be apparent with the increase of diffusion time, and the difference between the FFD Model and Fick's model becomes more obvious. The diffusion channel will be regular when the d_f, θ are small, and the calculated relative adsorption volume will also be small.

From Figure 1a, Figure 1b, it can also be observed that at the initial stage, the relative adsorption curve for the FFD Model is lower than Fick's model because at the initial time, the influence of the structure parameter θ is not obvious but the fractal dimension d_f is smaller than in Fick's model. With the increase in time, the influence of the structure parameter θ becomes obvious, but there is no structure parameter θ in Fick's model; therefore, Fick's model cannot be used to describe the dynamic movement process of gas in the porous coal, and consequently, the growth rate of the relative adsorption curve of Fick's model is less than the FFD Model, the relative adsorption curve in the FFD Model will intercept the curve of Fick's model. A comparison of the two models is as shown in Table 3:

Table 3 - A comparison of the FFD Model and Fick's model results

Pressure/MPa	Grain size/mm	υ	D_F /(m^2/s)	Correlation coefficient in Fick's model	Correlation coefficient in FFD Model
1	0.2-0.25	0.32	1.11E-11	0.97253	0.99475
	1-3	0.52	5.01E-10	0.98531	0.99325
4	0.2-0.25	0.34	1.37E-11	0.96515	0.99482
	1-3	0.7	5.50E-10	0.97568	0.99475

It can be seen from Table 3 that the degree of curve-fitting for the FFD Model is higher than that of Fick's model. Furthermore, Fick's model is not suitable for the desorption of small grain sized coal, as well as for describing the desorption process under high pressure.

SUITABILITY OF THE FFD MODEL FOR PULVERISED COAL

During coal and gas outburst, the coal that were ejected can be transported by the gas, and the high pressure gas in ejected coal has the explosive characteristics, and this can break the outburst coal further, resulting in the accumulation of large volumes of pulverised coal in the outburst solids.

The quick desorption of the pulverized coal will then further speed up the dusting process - a positive feedback effect between desorption velocity of pulverized coal and dusting process. Based on this observation, additional desorption experiments were conducted using the pulverized coal to study its effect on coal and gas outburst and the suitability of the FFD Model on pulverised coal.

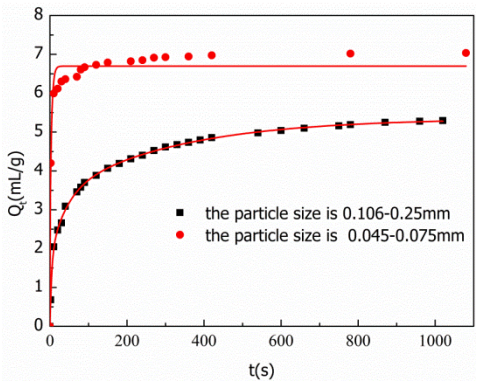

Figure 2 - Desorption isotherm of methane in pulverised coal

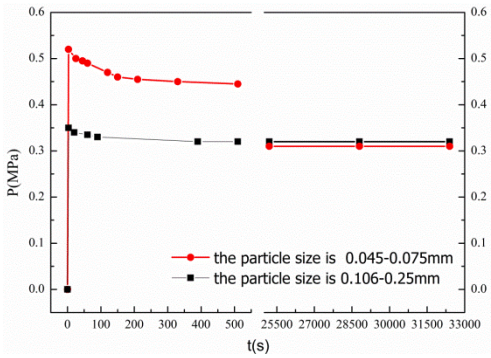

Figure 3 - The adsorption rate curves on 0.045-0.075 mm and 0.106-0.25 mm grain size coal

When the coal was crushed into a certain size, the pore in it will be damaged, and in this case, the coal can be considered to be isotropy, thus it can be assumed that $d_f = 3$, correspondingly, $\theta = 0$, take the value of d_f and θ into the Eq. (8), the average diffusivity D_{avt} and memorable parameter ν were obtained, the results are shown in Table 4.

Table 4 - The fitting result of FFD Model on 0.045-0.075 mm and 0.106-0.25 mm grain size coal

Grain size/mm	Equilibrium pressure/MPa	υ	d_f	θ	Correlation coefficient
0.045-0.075	0.32	0.19	3	0	0.9551
0.106-0.25	0.31	0.21	3	0	0.9998

From the Figure 2 and Table 4, it can be observed that the fitting degree of 0.106-0.25 mm grain size coal is higher than the 0.045-0.075 mm grain size coal. This indicates that the FFD Model is not suitable for the pulverized coal, and another model should be used.

CONCLUSIONS

The fractal dimension, d_f , of the long flame coal from TieFa, is between 2.4~2.55; within the experimental pressure range (1-4 MPa), the fractal dimension, d_f , will increase with pressure due to the damage of the surface structure. The fractal dimension, d_f , will increase with the decreasing grain size of the coal because of the reduction of the large and medium pores and the increase in micropore porosity, causing the coal structure to become more complex. The structure parameter θ is a parameter that can reflect the dynamic adsorption process in the porous media and is consistent with the fractal dimension, d_f . The structure parameter θ for the long flame coal from TieFa is between 1.5~1.9. The magnitudes of the average diffusivity D_{avt} in the FFDModel are between 10^{-12}~10^{-10}, and this parameter can be basically considered to remain constant with pressure. The magnitudes of the pre-exponential coefficient D_0 are between10^{-19}~10^{-15}. This result is consistent with the results of other researchers. The diffusivity in the FFD Model increases with the grain size.

The relative adsorption curve of the FFD Model is initially lower than that of Fick's model because at the initial stage, the influence of the structure parameter θ is not obvious but the fractal dimension d_f is smaller than that in Fick's model. As time increases, the influence of the structure parameter θ becomes evident. As there is no structure parameter θ in Fick's model, it therefore cannot be used to describe the dynamic movement process of gas in the porous coal. The growth rate of the relative adsorption curve of Fick's model is lower than the FFD Model, and that the relative adsorption curve in the FFD Model will eventually intersect that of Fick's model.

The fitting degree of the FFD Model is higher than Fick's model. Furthermore, Fick's model is neither suitable for describing the desorption of gas in small grain sized coal, and nor for describing the desorption process under high pressure. Equally, the FFD Model is not suitable for the pulverized coal.

REFERENCES

Adler, P M, Jacquin, C G and Quiblier, J A, 1990. Flow in simulated porous media. *International Journal of Multiphase Flow*, 16(4):691-712.

Allen, M, Brown, G J and Miles, N J, 1995. Measurement of boundary fractal dimensions: review of current techniques. *Powder Technology*, 84(1):1-14.

Busch, A, Gensterblum, Y, Krooss, B M and Littke, R, 2004. Methane and carbon dioxide adsorption-diffusion experiments on coal: upscaling and modelling. *International Journal of Coal Geology*, 60(2-4):151-168.

Bielicki, R J and Perkins, J H, 1972. Methane diffusion parameters for sized coal particles: a measuring apparatus and some preliminary results. United States. Bureau of Mines. p12.

Charrière, D, Pokryszka, Z and Behra, P, 2010. Effect of pressure and temperature on diffusion of CO2 and CH4 into coal from the Lorraine basin (France). *International Journal of Coal Geology*, 81(4):373-380.

Clarkson, C R and Bustin, R M, 1999. The effect of pore structure and gas pressure upon the transport properties of coal: a laboratory and modelling study. 2. Adsorption rate modelling. *Fuel*, 78(11):1345-1362.

Coal science research institute of coal analysis laboratory, 2008. Yunnan coalfield geological exploration company 143 team, proximate analysis of coal. In *GB/T 212-2008*, General Administration of Quality Supervision: 2008.

Cui, X, Bustin, R M and Dipple, G, 2004. Selective transport of CO2, CH4, and N2 in coals: insights from modelling of experimental gas adsorption data. *Fuel*, 83(3):293-303.

Cai, Y, Liu, D, Pan, Z, Yao, Y, Li, J and Qiu, Y, 2013. Pore structure and its impact on CH4 adsorption capacity and flow capability of bituminous and subbituminous coals from Northeast China. *Fuel*, 103:258-268.

Donghui, Z, Mingheng, S and Jin Feng, Y H, 2004. Diffusion characteristic in fractal porous media(I). *Journal of engineering thermophysics*, 25(5):822-824. (in Chinese).

Fushun Branch, China Coal Science Research Institute, 1997. Determine method of methane adsorption capacity in coal. In *MT/T 752-1997*, Industry standard - coal: 1997.

Gan, H, Nandi, S P and Walker Jr, P L, 1972. Nature of the porosity in American coals. *Fuel*, 51(4):272-277.

Gorenflo, R, Mainardi, F and Vivoli, A, 2007. Continuous-time random walk and parametric subordination in fractional diffusion. *Chaos, Solitons & Fractals*, 34(1):87-103.

Gray, I, 1987. Reservoir engineering in coal seams: Part 1 - The physical process of gas storage and movement in coal seams. SPE Reservoir Engineering, 2(1):28-34.

Laboratory of Coal Science Research Institute, 2008. National Coal Quality Supervision center, sample preparation method. In *GB 474-2008*, General Administration of Quality Supervision: 2008.

Machnikowski, J, Grzyb, B, Weber, J V, Frackowiak, E, Rouzaud, J N and Béguin, F, 2004. Structural and electrochemical characterisation of nitrogen enriched carbons produced by the co-pyrolysis of coal-tar pitch with polyacrylonitrile. *Electrochimica Acta*, 49(3):423-432.

Nandi, S P and Walker Jr, P L, 1970. Activated diffusion of methane in coal. *Fuel*, 49(3):309-323.

Nandi, S P and Walker Jr, P L, 1975. Activated diffusion of methane from coals at elevated pressures. *Fuel*, 54(2):81-86.

Pillalamarry, M, Harpalani, S and Liu, S, 2011. Gas diffusion behavior of coal and its impact on production from coalbed methane reservoirs. *International Journal of Coal Geology*, 86(4):342-348.

Qilin, Y, 2004. *Mathematical physics equation and the special function*. Tsinghua University Press, p6.

Society, J O C C, 1986. Theory of methane diffusion from coal cuttings and its application. *Journal of China coal society*, (3):87-94.

Radliński, A P, Busbridge, T L, Gray, E M A, Blach, T P and Cookson, D J, 2009. Small angle X-ray scattering mapping and kinetics study of sub-critical CO2 sorption by two Australian coals. *International Journal of Coal Geology*, 77(1-2):80-89.

Saghafi, A, Faiz, M and Roberts, D, 2007. CO2 storage and gas diffusivity properties of coals from Sydney Basin, Australia. *International Journal of Coal Geology*, 70(1-3):240-254.

Shi, J Q and Durucan, S, 2003. A bidisperse pore diffusion model for methane displacement desorption in coal by CO2 injection. *Fuel*, 82(10):1219-1229.

Siemons, N, Wolf, K A A and Bruining, J, 2007. Interpretation of carbon dioxide diffusion behavior in coals. *International Journal of Coal Geology*, 72(3-4):315-324.

Smith, D M and Williams, F L, 1984. Diffusion models for gas production from coals: Application to methane content determination. *Fuel*, 63(2):251-255.

Smith, D M and Keller, J F, 1985. Nonlinear sorption effects on the determination of diffusion/sorption parameters. *Industrial & Engineering Chemistry Fundamentals*, 24(4):497-499.

The Chinese academy of sciences institute of process engineering, 2008. The physical and chemical analysis and test center, the materials by mercury porosimetry and gas adsorption - Part 2: Analysis of mesopores and macropores by gas adsorption. In *GB/T 21650.2-2008*, General Administration of Quality Supervision.

Triolo, R and Child, H R, 1984. Small-angle neutron scattering study of coal extract solutions in pyridine. *Fuel,* 63(2):274-279.

Turk, G A, Cobb, T B, Jankowski, D J, Wolsky, A M and Sparrow, F T, 1987. CO2 Transport: A new application of the assignment problem. *Energy*, 12(2):123-130.

Wang, S, Yu, B, Zheng, Q, Duan, Y and Fang, Q, 2011. A fractal model for the starting pressure gradient for Bingham fluids in porous media embedded with randomly distributed fractal-like tree networks. *Advances in Water Resources*, 34(12):1574-1580.

Warren, J and Root, P, 1963. The behaviour of naturally fractured reservoirs. society of petroleum englineers jounal, 426:245-255.

Xian branch, 1998. Coal scientific research institute, method of determining marcel group composition and mineral coal. In *GB/T 8899-1998*, General Administration of Quality Supervision.

Xian branch ,2008. Coal scientific research institute, Method of determining microscopically the reflectance of vitrinite in coal. In *GB/T 6948-2008*, General Administration of Quality Supervision.

Xin, Hw, 1997. Reaction kinetics in fractal media. Shanghai Scientific and Technological Education Press: Shanghai.

Yi, J, Akkutlu, I Y, Karacan, C Ö and Clarkson, C R, 2009. Gas sorption and transport in coals: A poroelastic medium approach. *International Journal of Coal Geology*, 77(1-2):137-144.

Yao, Y, Liu, D, Tang, D, Tang, S, Huang, W, Liu, Z and Che, Y, 2009. Fractal characterisation of seepage-pores of coals from China: An investigation on permeability of coals. *Computers and amp; Geosciences*, 35(6):1159-1166.

Zhao, X, 1991. An experimental study of methane diffusion in coal using transient approach. Ph.D Dissertation. University of Arizona.

Zhang, D, Mingheng, S and Jin Feng, Y H, 2004. Diffusion characteristic in fractal porous media (α). *Journal of engineering thermophysics*, 25(5):825-827. (in Chinese).

A STUDY OF COAL SWELLING-CONTROLLED CO_2 DIFFUSION PROCESSES

Wei Li[1,2,3], Yuanping Cheng[1,2] , Liguo Wang[1,2] and Junhui Mo[1,2]

ABSTRACT: CO_2 sequestration in deep and unmineable coalbeds is regarded as a viable option for carbon storage. CO_2 diffusion is a key assessment parameter to effectively seal CO_2 in the coal seam. By conducting laboratory tests of coal CO_2 desorption and unsteady gas diffusion theory model calculation, the desorption dynamic characteristics of Yaojie coal was studied under the condition of constant temperature and different balance pressure, and the CO_2 diffusion coefficient was obtained through the non-steady diffusion model at different time. The results show that the higher the balance pressure, the greater the diffusion coefficient under the same condition. As the pressure drops, the CO_2 diffusion coefficient gradually decreases as time increases, and the CO_2 desorption mass fraction has a linear relationship with the diffusion coefficient. It is observed that under high pressures, the diffusion coefficient initially increases, then gently decreases. The non-steady CO_2 diffusion in Yaojie coal relates to the CO_2 swelling effect of the coal, especially in high pressure condition, the glass transition of coal with CO_2 maybe the governing factor leading to the nonlinear diffusion of CO_2 in coal.

INTRODUCTION

Carbon dioxide (CO_2) storage (CCS) in unmineable coal seams is regarded as one of the possible approaches to mitigate the ever increasing CO_2 concentration in the atmosphere resulting from human activities since the ndustrial Revolution. Injection of CO_2 into unmineable coal seams not only provides a solution for long term storage of CO_2 but also provides the added advantage of Enhancing Coalbed Methane Recovery (ECBM). Experimental studies of CO_2 sequestration were conducted in many countries. When CO_2 is injected, gas flow in the coal seam consists of the diffusion in coal matrix and the transport in coal cleat, of which the Fick diffusion model and Dracy's law can be used to describe these processes respectively. The diffusion coefficient controlled by concentration is normally far less than that controlled by pressure gradient, hence the time of transfusion is negligible when compared with the time of diffusion, the diffusion flow is the dominant coefficient of the gas transport process in the coal sample. The rate of CO_2 diffusion in the coal seam determines the effectiveness of sealing up CO_2 for safe storage. For this purpose, many scholars have conducted studies in the area of CO_2 adsorption and diffusion in coal.

Findings by many scholars indicated that the diffusion of gas in coal could be adopted by the description of Bidisperse diffusion model(Cui, *et al.*, 2004; Shi, *et al.*, 2003), by considering the diffusion in the form of surface diffusion in micropore as well as the pore diffusion in middle or larger pores; Based on the diffusion mechanism of Bidispere, Wei, *et al.,*(2007) adopted the diffusion theory of Maxwell-Stephen with numerical calculation, and draw conclusion of the diffusion feature of mixed gas CO_2 and CH_4; Pan, *et al.*, (2010) discovered the notable influence of water and gas diffusion in coal, with more water in coal the diffusion coefficient drops off remarkably; Based on the second law of Fick, Zhang, *et al*.,(2010) concluded that the effective diffusion coefficient of CH_4 and CO_2 would increase when the adsorption temperature goes up, and the effective diffusion coefficient has a relationship of "U" with the coal rank; the expansion of coal caused by the absorption of CO_2 was confirmed by many experiments, and it was concluded the interaction of CO_2 and coal in microcosmic, the physical and molecule structure could be changed by this interaction. Studies of the diffusion influence of CO_2 in coal are still limited, and the gas diffusion in coal is always regarded as the diffusion in steady state, without considering the influence of the diffusion of gas and coal interaction.

In view of the coal and CO_2 outburst hazard in Yaojie Mine, this paper investigates the desorption diffusion characteristics of CO_2 in coal samples from Yaojie. Using the unstable diffusion model and adsorption method, the diffusion coefficient was studied as well as the diffusion characteristics and mechanism of CO_2 in coal sample under different pressures.

[1] *National Engineering Research Center for Coal Gas control, M: +86 (0)13952231131*
[2] *Faculty of Safety Engineering*
[3] *The Key Laboratory of Coal-based CO2 Capture and Geological Storage, China University of Mining and Technology, Xuzhou, Jiangsu 221116, China*

SAMPLING AND ANALYTICAL PROCEDURES

Coal samples

In this study, Haishiwan coal was used as an adsorbent. The proximate and ultimate analyses for the Argonne premium coal samples are presented in Table 1.

Table 1 - Compositional analyses of Haishiwan coal samples

Proximate analysis				Maceral analysis				
moisture (wt %)	volatile (wt %)	ash (wt %)	fixed carbon (wt %)	vitrinite (wt %)	inertinite (wt %)	Exinite (wt %)	mineral (wt %)	vitrinite reflectance (%)R_{omax}
1.01	30.10	3.39	66.85	48.68	47.35	2.85	1.14	0.93

CO_2 desorption experiments

Experiments on the desorption of CO_2 gas were conducted in a desorption instrument using the coal seam methane content from rapid determination equipment (FM4WP-1). All of the samples were prepared by grinding and sieving to a size range of 2 mm. A certain amount of coal (50 g) for the adsorption experiment was weighed and then sealed in the coal canister. After verifying the air tightness of the canister, the samples were outgassed overnight in a 60°C thermostatic water bath under vacuum to a final pressure of 0.25 Pa. After these pretreatment steps, CO2 with a purity of 99.99% was charged into the canister to a certain pressure, and then the canister was placed into a 30°C thermostatic water bath to reach adsorption equilibrium. After recording the equilibrium pressure, the coal canister valve was opened as quickly as possible, and once the pressure reached zero, the canister was rapidly connected to the desorption apparatus. The amount of gas desorbed over two hours and the ambient and atmospheric pressures were also recorded. After two hours, the canister valve was tightened as quickly as possible to perform the residual gas content measurement. This measurement consists of placing the canister that undergone desorption for two hours into vacuum degassing pump in a 30°C bath; Gas chromatographs were then used to determine the components of the gas. After vacuum degasification, the sample in the vacuum canister was transferred into a ball-milling canister for a second grinding until the grain sizes of 80% of the coal sample were less than 0.25 mm, then the samples were outgassed and reground until there was no longer outgassing. Then, the total gas content was calculated as the sum of the two hours of desorbed gas and the residual gas.

DIFFUSION COEFFICIENTS MODEL

The process of gas diffusion in micropore, macropore and fracture is controlled by various diffusion mechanisms. The pore size and pore structure of coal are related directly to the diffusion mechanisms and thus diffusivity. If the slack coal is assumed as spheroidal coal particle, and the gas concentration only depends on the spherical coal particle radius then the three dimensional diffusion model can be expressed as follows:

$$\frac{\partial(rC)}{\partial t} = D\frac{\partial^2(rC)}{\partial r^2} \tag{1}$$

with the initial condition: $C\big|_{t=0} = f(r) = C_1$,

with the boundary condition: $C\big|_{r=a} = C_0$,

where *C* is the gas concentration in the spheroidal coal particle(%); *D* is the diffusion coefficient (mm^2/s); *r,* the spherical coal particle radius(mm).

The diffusion model and diffusivity derivation of the three-dimensional sphere sample with radius of a can be seen in Jian*, et al.,* (2012).

$$F = \frac{M_t}{M_\infty} = 6\frac{\sqrt{Dt}}{a\sqrt{\pi}} - 3\frac{Dt}{a^2} \quad (2)$$

where M_t is the mass of the spheroidal coal particles desorption of CO_2 at a given time (ml), M_∞ is the mass of spheroidal coal particles after complete desorption of CO_2 for a very long time(ml), *a* is the average radius of spheroidal coal particle(mm).

If *D* depends on time, then

$$F = \frac{6}{\sqrt{\pi}}\frac{\sqrt{\int_0^t D\mathrm{d}t'}}{a} - 3\frac{\int_0^t D\mathrm{d}t'}{a^2} \quad (3)$$

Assume that; $x = \frac{\sqrt{\int_0^t D\mathrm{d}t'}}{a}$, Eq. (3) is solved, then:

$$x = \frac{1}{\sqrt{\pi}} - \sqrt{\frac{1}{\pi} - \frac{F}{3}} \quad (4)$$

If $y = a^2x^2$, then, the diffusion coefficients D at a given time can be obtained as

$$D = \frac{\mathrm{d}y}{\mathrm{d}t} = \frac{\mathrm{d}y}{\mathrm{d}x}\frac{\mathrm{d}x}{\mathrm{d}F}\frac{\mathrm{d}F}{\mathrm{d}t} \quad (5)$$

The relationship between t and F can be obtained by using polynomial fitting. The curve fitting formula and Eq. (4) are input into Eq. (5), we can obtain the D that changes with time t.

RESULTS AND DISCUSSIONS

CO_2 desorption

The balance pressures of desorption range from low (0.85 MPa, 1.74 MPa, 2.20 MPa) to high pressure (7.92 MPa) at 30°C, the dynamic curve of Yaojie coal desorption is shown in Figure 2.

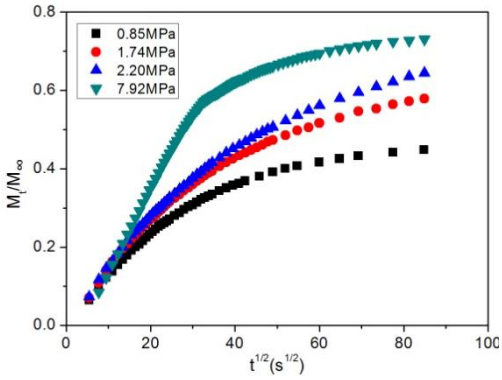

Figure 1 - Desorption kinetic curves of CO_2 at different pressures

As the balance pressure of adsorption increases, the CO_2 desorption becomes larger in 120 min, the curve of desorption could be divided into two phases, one is high desorption and the other in low desorption phase. The desorption curve at low pressure is relatively smooth, whilst two distinctive parts can be observed at the high pressure.

As explained in Section two, the migration process of gas molecule in coal can be expressed as:

$$F = \frac{M_t}{M_\infty} = k_1\sqrt{t} + k_2 t \approx kt^n \quad (6)$$

where: *K* is constant; *n* is diffusion indexed number.

Ritger *et al*. (1987) provided a relationship of diffusion type and n in different coal geometrical characteristics, for sphere coal particle, when n=0.43, it follows Fick's diffusion model (Figure 2), when it was at low pressure, the Yaojie coal diffusion index number $n \approx 0.43$, which follows Fick's diffusion law; when it was in high pressure, the diffusion index number *n*>0.43, it follows anomalous diffusion, indicating that the diffusion of CO_2 is not only determined by the concentration gradient, but also other influential coefficients at high CO_2 pressure.

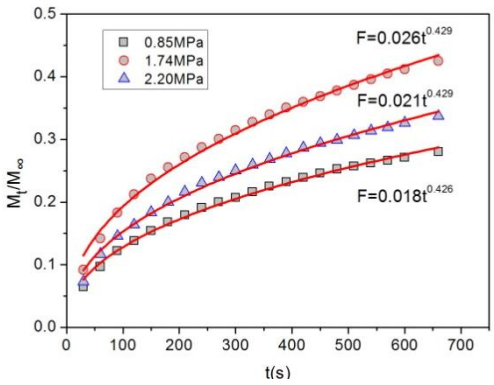

Figure 2 - Power relation equations of time versus CO_2 mass fraction (*F*)

Based on the calculation model of diffusion coefficient in section 1.3, the relationship of CO_2 diffusion time and diffusion coefficient in different pressures can be drawn as in Figure 3. Diffusion coefficient of CO_2 is 1.83×10^{-6}-9.08×10^{-5} mm^2/s in the low pressure, which is approximately the same result as reported by Zhang et al(2010). As time increases, the value of diffusion coefficient D declines rapidly in the initial phase and then gradually flats out. The high pressure diffusion coefficient of CO_2 is 4.76×10^{-6}-1.91×10^{-4} mm^2/s, the value of D in high pressure is one order of magnitude greater than that in low pressure.

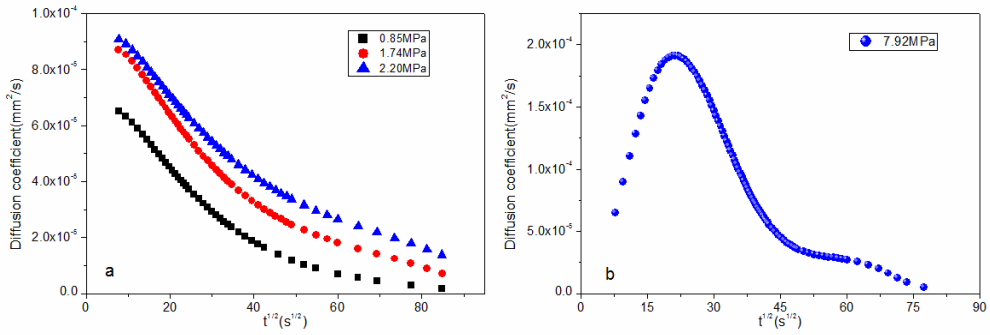

Figure 3 - Relation between CO_2 diffusivity and square root of time for different pressure

Figure 4 and Table 2 show a linear relationship between the mass fraction of CO_2 and diffusion coefficient D in low pressure. As CO_2 desorption takes place from coal, D drops gradually, and its variation rate also drops as the desorption equilibrium pressure increases. The adsorption of CO_2 would cause swelling of coal, and in high pressure, the numerical value of D with the mass coefficient of CO_2 desorption shows a near parabolic shape, which increases at first and then decreases with the increase of CO_2 desorption. Due to the high reaction rate of CO_2 with coal, such as the shape memory effect, the adsorption swelling effect etc, the interaction of coal with CO_2 appears to influence or even control CO_2 desorption from coal.

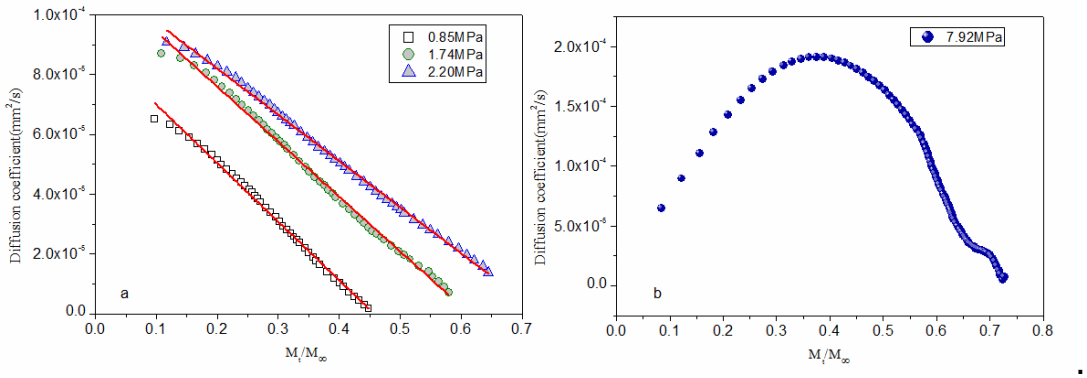

Figure 4 - Relation between diffusivity and mass fraction of CO_2 cumulative desorption in coal

Table 2 - Linear relation equations of *D* versus CO_2 mass fraction (*F*), and the correlation coefficient (R^2)

Experimental balance pressure (MPa)	Linear relation	R^2
0.85	D=-1.95×10^{-4}F+8.95×10^{-5}	0.995
1.74	D=-1.83×10^{-4}F+1.13×10^{-4}	0.996
2.20	D=-1.54×10^{-4}F+1.13×10^{-4}	0.997

Discussion of CO_2 diffusion mechanism

The transport of gas in coal may be influenced by temperature, pressure, moisture content, ash, coal rank, and maceral components (Mathews, *et al*., 2011). The pore structure of coal directly influences gas diffusion. Considering the pore size and mean free path of gas molecule, the multi-disperse gas diffusion mechanisms in coal can be classified as self-diffusion, transition diffusion, Knudsen diffusion and surface diffusion (He, *et al*., 2001; Zhang, *et al*., 2011).

Coal has greater affinity for CO_2 than for CH_4, thus leading to greater adsorption of CO_2 than CH_4 at the same pressure. The majority of CO_2 is thought to be adsorbed onto the surface of micropores in the coal matrix. However, the interactions between CO_2 and coal are considered to be complex. Pan and Connell (2007) suggested that coal swells as a direct result of gas adsorption and gas pressure. Chemically, coal structure, excluding anthracites and the high rank coals that are graphitic in their nature, is generally viewed as a macromolecular network of cross-linked (chemically bonded and physically entangled) chains or clusters of aromatic rings(Romanov, 2007; Li and Zhou, 2001). A CO_2 molecule placed between the polymer chains of coal disrupts partly the original structure if the sorption takes place in locations where the available volume between the chains is smaller than the actual volume of the CO_2 molecule (Mazumder, *et al*., 2011).

The swelling of coal by a penetrant can be referred to as, an increase in the volume occupied by the coal as a result of the visco-elastic relaxation of its highly cross-linked macromolecular structure (Suuberg, 1997). Although the macro molecular network structure does not dissolve, the penetrant is almost universally termed as solvent. Thus a coal-coal hydrogen bond or any other weaker bond will be replaced by a coal-solvent bond only if the new coal solvent bond is thermodynamically favoured. If intra-molecular bonding in the coal contributes significantly to its structural integrity, then strong coal-solvent bonding should disrupt such a structure, which results in coal swelling (Larsen, 2004). Mastalerz *et al*. (2012) found that these absorption bands increased in intensity as CO2 pressure increased (Figure 5), The diffusion process is closely interlinked to the dynamic volumetric swelling of coal. The increase in volume of a coal sample is a function of time. Only the adsorbent that has diffused into the "bulk" structure induces coal swelling.

Unswollen coal is in a glassy state (not in the lowest energy state) under typical reservoir conditions. The temperature required to cause a transition from glass to rubber is the glass transition temperature (Mackinnon and Hall, 1996). High-pressure CO_2 on the macromolecular structure of coal shows that the glass transition temperature of coal decreases with CO_2 pressure significantly (Larsen, 2004; Day, *et al*., 2008), indicating that high-pressure CO_2 diffuses through the coal matrix, causing significant plasticization effects, and changes in the macromolecular structure of coal. The glass transition temperature of Wyodak coal are 395.1 K and 349.2 K at various CO_2 pressures of 0 MPa and 3 MPa

(Mirzaeian and Hall, 2006), respectively. Structural changes induced during this process include swelling, microcavity formation and primary phase transition requiring rearrangements of each chain segments. As compared to the glassy state of coal, in the rubbery state the crosslink polymeric chains can move separately and rapidly by a process involving rotation of main chain bonds so that the equilibrium is obtained almost instantaneously. Thus, the initial penetrant volume will be less than the equilibrium volume fraction, CO_2 diffusion coefficient in rubber state is faster than that in the glass state of coal (Govindjee and Simo, 1993; Mazumder, *et al*., 2011).

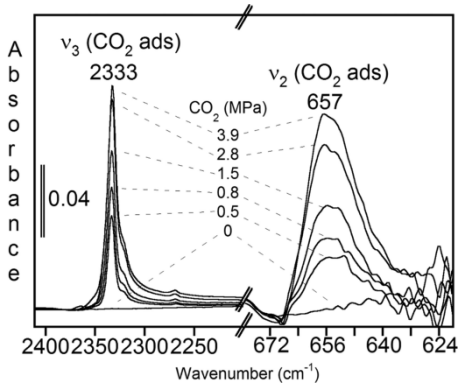

Figure 5 - Graph of *in situ* ATR-FTIR spectra of sorbed CO_2 on vitrain lithotype from Lower Block (LB) as a function of increasing CO2 pressure (0.5, 0.8, 1.5, 2.8, and 3.9 MPa). (Mastalerz, *et al.*, 2012)

If the diffusion is controlled by the volume fraction gradient between the centre and the outside of the glass state coal matrix, the diffusion mechanism is Fickian. CO_2 diffusion coefficient linearly decreases as coal matrix shrinking after CO_2 desorping at low pressure. High pressure CO_2 saturated coal can develop into rubber state on a lower glass transition temperature easily. If the transport is controlled by a stress gradient induced by the penetration of molecules, the diffusion mechanism is anomalous. At this early stage, CO_2 diffusion speed increases quickly with time, The part free volume is frozen with the CO_2 desorption and reduction at high pressure, coal transform into glass state once again, CO_2 diffusion coefficient linearly decreases with time, and which is higher than diffusion coefficient at lower pressure. Simultaneously, the interactions of coal with CO_2 concerning the mechanisms of diffusion, the strength of interactions, and the irreversibility of uptake for the permanent disposal of CO_2 into coal fields are complicated. Further research is needed for a mechanism of CO_2 diffusion in the coal.

CONCLUSIONS

The CO_2 diffusion coefficient (D) is of un-steady state for coal samples from Yaojie. Under identical conditions, the higher the desorption equilibrium pressure, the larger the diffusion coefficient. The value of D is 1.83×10^{-6}-9.08×10^{-5} mm^2/s at low pressure, and 4.76×10^{-6}-1.91×10^{-4} mm^2/s at high pressure, which is one order of magnitude larger than that in low pressure. As desorption time increases, the value of D reduces rapidly in the initial phase, and then it levels off gradually. The CO_2 mass fraction desorption and the diffusion coefficient has a linear relationship under low pressure and parabolic relationship at high pressure respectively. The un-steady gas diffusion in Yaojie coal is a result of CO_2 adsorption swelling, particularly at high pressures, the coal containing CO2 undergoes glass transition to high-elastic state, which is probably the governing factor lead to the abnormal and non-linear gas diffusion.

REFERENCES

Charrière, D, Pokryszka, Z and Behra, P, 2010. Effect of pressure and temperature on diffusion of CO_2 and CH_4 into coal from the Lorraine basin (France). *International Journal of Coal Geology,* 81:373-380.

Cui, X J, Bustin, R M and Dipple, G, 2004. Selective transport of CO_2, CH_4, and N_2 in coals: insights from modelling of experimental gas adsorption data. *Fuel*, 83:293-303.

Day, S, Fry, R and Sakurovs, R, 2008. Swelling of Australian coals in supercritical CO_2. *International Journal of Coal Geology*, 74:41-52.

Goodman, A L, Favors, R N and John, W L, 2006. Argonne coal structure rearrangement caused by sorption of CO_2. *Energy and Fuels*, 20:2537-2543.

Govindjee, S and Simo, J C, 1993. Coupled stress-diffusion: Case II. *J. Mech. Phys. Solids*,41:863-887.

He, X Q and Nie, B S, 2001. Diffusion mechanism of porous gases in coal seams. *Journal of China University of Mining and Technology*, 30:29-32.

Jian, X, Guan, P and Zhang, W, 2012. Carbon dioxide sorption and diffusion in coals: Experimental investigation and modelling. *Sci China Earth Sci*, 55:633-643.

Larsen, J W, 2004. The effects of dissolved CO_2 on coal structure and properties. *International Journal of Coal Geology*, 57:63-70.

Li, K S and Zhou, A N, 2001. Progress of coal-base material researches. *Polymer materials science and engineering*, 17:19-22.

Li, W, Cheng, Y P and Yang, Y F, 2011. Research on the genesis and accumulation of carbon dioxide in the Yaojie coalfield. *Journal of China University of Mining and Technology*, 40:190-195.

Mackinnon, A J, Hall, P J, 1996. Observation of first- and second-order transitions during the heating of argonne premium coals. *Energy & Fuels*, 9:25-32.

Marecka, A and Mianowski, A, 1998. Kinetics of CO_2 and CH_4 sorption on high rank coal at ambient temperatures. *Fuel*, 77:1691-1696.

Mastalerz, M, Goodman, A and Chirdon, D, 2012. Coal litho types before, during, and after Exposure to CO2: Insights from Direct Fourier Transform Infrared Investigation. *Energy and Fuels*, 26(6):3586-3591.

Mathews, J P, Van duin, A C T and Chaffee, A L, 2011. The utility of coal molecular models. *Fuel Processing Technology*, 92:718-728.

Mazumder, S, Vermolen, F and Bruining, J, 2011. Analysis of a model for anomalous - diffusion behaviour of CO_2 in the macromolecular-network structure of coal. *SPE Journal*, 16:856-863.

Mirzaeian, M and Hall, P J, 2006. The Interactions of coal with CO_2 and Its effects on coal structure. *Energy & Fuels*, 20:2022-2027.

Pan, Z J, Connell, L D and Camilleri, M, 2010. Effects of matrix moisture on gas diffusion and flow in coal. *Fuel*, 89:3207-3217.

Pan, Z and Connell, L D, 2007. A theoretical model for gas adsorption-induced coal swelling. *International Journal of Coal Geology*, 69:243-252.

Ritger, P L and Peppas, N A, 1987. Transport of penetrants in the macromolecular structure of coals. *Fuel*, 66:815-826.

Romanov, V, 2007. Coal chemistry for mechanical engineers: from macromolecular thermodynamics to reservoir simulation. *Energy Fuels*, 21:1646-1654.

Shi, S Q and Durucan, S, 2003. A bidisperse pore diffusion model for methane displacement desorption in coal by CO_2 injection. *Fuel*, 82:1219-1229.

Suuberg, E M, 1997. Comments regarding the use of coal swelling to count hydrogen-bond cross-links in coals. *Energy Fuels*, 11:1103-1104.

Wei, X R and Wang, G X, 2007. Massarotto P. Numerical simulation of multicomponent gas diffusion and flowin coals for CO_2 enhanced coalbed methane recovery. *Chemical Engineering Science*, 62:4193-4203.

Zhang, D F, Cui, Y J and Li, S G, 2011. Adsorption and diffusion behaviours of methane and carbon dioxide on various rank coals. *Journal of China coal Society*, 10:1693-1698.

Zhang, X D, Liu, Y H, Sang and S X, 2011. Study of the gas diffusion mechanism in high rank coal reservoirs. *Journal of China University of Mining and Technology*, 40:43-48.

INTERNATIONAL EXPERIENCE OF GAS EMISSION AND GAS OUTBURST PREVENTION IN UNDERGROUND COAL MINES

Thomas Imgrund[1] and Rob Thomas[2]

ABSTRACT: With increasing depth of cover, control of gas emissions and prevention of gas outbursts has become a more and more important issue in mine design and mine operation. Long term experience in these fields exists, especially in Australia, Germany, China, Kazakhstan and Ukraine. Based on local conditions including geology, market conditions and mining regulations, different approaches have been developed in these countries. Changes in these parameters have however exposed the limitations of traditional solutions. While the Australian approach is based on the premise that gas content will be reduced below specific threshold values ahead of mining, opportunities of pre-drainage are limited in low permeability coal such as that encountered e.g. in Germany and China. In the case of multi seam mining, a highly effective increase in permeability can however be achieved through pressure relief by unconventional mining sequences. Although practiced at several mines in Europe and Asia, realising this in open market conditions requires a high quality of planning in regard to mine layout, mine development and gas drainage as well as the appropriate geotechnical assessments. A key factor is access and extraction of the first seam at or near to virgin gas contents. Mining at high gas contents by applying local exploration and pressure relief drilling has been practiced in a successful and safe way in several European mines. This has to be connected with a proper management system and safety system, allowing efficient reactions to identified hazards. Apart from international experience and development, the paper will also discuss current and future approaches of technology transfer. Merging the future development in gas drainage with unconventional approaches is therefore an opportunity for accessing deep and difficult deposits.

INTRODUCTION

Methane and in some deposits carbon dioxide, are the predominant gases contained in coal. These gases are adsorbed to the coal matrix and also occur within voids in both, coal and surrounding rock. Gas is released as a result of mining coal and the subsequent pressure release in the surrounding strata. At certain concentrations and volumes, these gases cause major risks of explosions and asphyxiation. Methane is known as a source of underground explosions resulting in large numbers of fatalities. More recent accidents as at Pike River Mine in New Zealand and Upper Big Branch Mine in the USA are in our mind. Apart from being a safety risk in the mine operation, methane from coal mines is an energy source which could be utilised by various technologies for heat or power generation. Regarding the climate, methane is also identified as a greenhouse gas, which is 21 times more harmful to global warming compared to carbon dioxide (United Nations Economic Comission for Europe, 2010). Hence, systematic capture and utilisation is a major target in terms of sustainability and reduction of carbon taxes.

The release of gas during mining is a complex process depending on various factors. Among others, the gas content, permeability, stresses, coal structure, tectonic faults and the stratigraphic sequence of coal and rock layers have an influence (Lama and Bodziony, 1996). In certain conditions, gas is released suddenly, known as a gas outburst. This phenomena has occurred in most coal producing countries during the history of coal mining. With the recent development of the worldwide market, technical and political conditions, mining of coal prone to gas outbursts nowadays only takes place in a few countries. A lot of experience gained in the past has disappeared. Today apart from Australia, gas outbursts are a significant problem in China, Kazakhstan, Ukraine, Germany, Turkey and Mexico.

In most cases, gas desorption is a slow process. In longwall operations, gas is released from the coal face as well as from adjacent seams and rock layers. In a first stage, gas emissions are controlled by diluting and discharging the gas by the mine ventilation system. It is the nature of this process, that the gas concentration passes the explosive range. The zone where this happens, requires particular consideration. If gas emissions cannot be controlled by ventilation only, gas drainage is necessary.

[1] *DMT GmbH & Co.KG, Essen, Germany, thomas.imgrund@dmt.de, M: +49 170 921 77 03*
[2] *Golda Assocites Pty Lt*

Although being common problems in the international coal mining industry, different measures are carried out for both, gas emission control and gas outburst prevention. Some of these differences are fundamental. These differences are a result of individual geological conditions, mining practices, technological standards, market environments and experiences. Furthermore, there are unequal structures of state authorities and safety regulations. On the one hand there are flexible, risk assessment based regulations as e.g. in Australia or Germany and on the other hand there are rather inflexible, strict regulations as in the CIS countries or China. However, all of them have their own reasonable background in historic mine accidents and local mining practices.

Apart from the regulations there are fundamental differences in the geology of mined coal deposits. While conditions at Australian coal mines are currently characterised by depths of below 500 m, medium to high permeability and single seam mining, the coal mines in China, CIS countries and Europe are often characterised by depths of more than 500 m, permeability far below 0.1 Milidarcy and multi seam mining. In coal mining a maximum mining depth of more than 1500 m has been reached in Germany (Hucke, *et al.*, 2006) and in doing so, gas management controls have experienced some limitations at these depths. The information about the actually practised methods of gas emission control and outburst prevention as reviewed in this paper has mainly been gathered from various engineering assignments in different countries.

GAS OUTBURST PREVENTION

Particularly in the case of gas outburst prevention the internationally applied strategies possess significant differences. In Australia the gas outburst risk is assessed based on gas content tests during exploration (Black and Aziz, 2010). Based on gas composition and coal structure outburst threshold values are defined. If these threshold values are exceeded, the gas content has to be reduced by pre-drainage. The results are checked by compliance tests. Surface to In-seam (SIS) or Underground In-seam (UIS) drilling is used with high efficiency in most cases. Where pre-drainage has been unsuccessful, remote controlled heading has been used e.g. at BHP's Appin Colliery (Henderson, *et al.*, 2008). From its introduction, the system of threshold values has been successful with no fatalities caused by gas outbursts. Although factors additional to the gas content lead to an actual gas outburst risk, by this procedure a key factor is eliminated. Hence, no further parameters have to be investigated and assessed. In the recent past however, areas of low permeability have resulted in insufficient pre-drainage results and the consequent sterilisation of coal reserves. Considering the development of mines towards greater and greater depths and new projects targeting deeper deposits, this may therefore become a more crucial issue in the future.

About 70% of the worlds' underground coal production is from China which operates a high number of gassy mines (United States Environmental Protection Agency, 2010). In China, the gas outburst risk of coal seams is classified based on four factors: the gas pressure, tectonic faults, the desorption rate and the coal strength (Xue, *et al.*, 2010). This classification is valid for an entire seam at a mine. Hence, the differences in the distribution of gas contents, desorption rates and coal strength, especially at tectonic faults, are not assessed in a selective way. For the prevention of gas outbursts the reduction of gas contents has priority. Pre-drainage is applied using underground in-seam boreholes or penetrating the target seam by cross measure boreholes at high density. In cases of low permeability, drainage periods of around five years are common. Alternately heading and pre-drainage at the coal face is a further method resulting in considerable regular downtimes of roadway development. Wherever possible, over- or undermining is also used to increase permeability (Figure 1). This is known as sacrificial or protection seam mining. If gas contents however cannot be reduced in a reasonable way, local measures such as water injection are applied. In China, gas outburst prevention follows fixed and detailed procedures with a low grade of flexibility. Cost control is not of importance with the priority being maximum safety. Notwithstanding the strict regulations and intense drilling programs, gas outbursts with fatalities still occur.

Some of the largest gas outbursts in the world have occurred in Kazakhstan with a maximum of 1.3 million m³ of gas being released during one coal and gas outburst (Baimukhametov, *et al.*, 2009). The level of risk and the number of gas outbursts have resulted in a strict and area wide classification of whole seams or parts of seams. This classification is based on the depth and the occurrence of outbursts in the past. As in China, protection seam mining is applied wherever possible. Otherwise, pre-drainage using UIS or SIS boreholes is carried out, but efficiency is limited due to low permeability at depths of up to 800 m. Local drilling of pressure relief boreholes is the main method used in in-seam developments. As most historic gas outbursts have occurred in contact with tectonic faults, exploration drilling in advance of the

heading plays a major role. The effectiveness of pre-drainage or pressure relief is checked during heading by special short in-seam boreholes allowing an assessment of coal fine volumes and gas release. Similar assessments are common within other Commonwealth of Independent States (CIS) countries and Europe. These measures are in accordance with strict regulations and detailed procedures which are fixed for each single heading. Although work is done according to regulations and very intense exploration and pressure relief drilling is carried out, gas outbursts with fatalities have still occurred during the last few years. As heading advance is significantly limited with this method, essential work is done on improving the assessment of the gas outburst hazard and the identification of tectonic faults in advance of the heading.

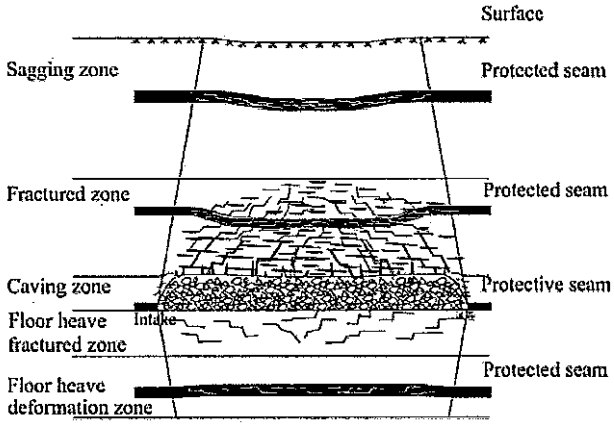

Figure 1 - Pressure relief by over- and undermining (Cheng, *et al.*, 2011)

In Ukraine the gas outburst risk of a seam is defined based on depth, coal rank and gas content. During development and extraction, seismo-acoustic monitoring methods have been developed by local institutes and are used for the identification of actual hazards. Pre-drainage is usually not efficient due to low permeability, but multi seam mining sometimes allows a reduction of gas contents by over- or undermining. Local measures of outburst prevention are common, such as inductor shock firing. This measure is based on a considerable different philosophy as gas outbursts are provoked by blasting with the workforce being removed from the area beforehand.

Currently two mines in Germany, Ibbenbueren and Prosper-Haniel mine coal prone to gas outbursts. Since 1903 alone in the state of North Rhine Westphalia more than 400 gas outbursts have been reported (Imgrund, 2012). Due to continuous improvement of identification of hazardous zones and prevention measures no fatalities have occurred since 1990. Gas outburst prevention in the German mining industry is based on a selective risk assessment in two stages. In a first step, the suspicion of a gas outburst hazard is checked. For this, gas content tests are carried out during exploration and later during the in-seam development. Usually the threshold value is 9 m³/t desorbable gas content, but in the case of tectonic faulting, abutment pressure or gas emission anomalies, the value is reduced to 5.5 m³/t (Mine Inspectorate of the State of North Rhine-Westfalia, 1996). As in other countries, the reduction of gas content is a prior target. Due to very low permeability at depth of greater than 1000 m, pre-drainage is however a limited option. Stress relief by over- or undermining is systematically used where possible. If threshold values are exceeded and gas contents cannot be reduced prior to heading advance, exploration drilling is done in progressive stages depending on the level of the gas content (Figure 2).

Fan shaped sets of boreholes are drilled in advance of the heading, usually covering a section of one week heading advance. A safety zone around the roadway is maintained by overlapping all sides. Furthermore, desorption is assessed by using the online monitoring and referring the gas emissions to the coal production and gas content. As a further step, an actual gas outburst hazard is checked based on the results of these measures. Pressure relief drilling is executed in case of an actual hazard being identified (Figure 3). The equipment is the same as that used for exploration boreholes, however critically, the procedure in this case targets a controlled elimination of the gas outburst hazard under safe conditions. Special Trigger Action Response Plans (TARPs) are also used to lower the risk levels even further.

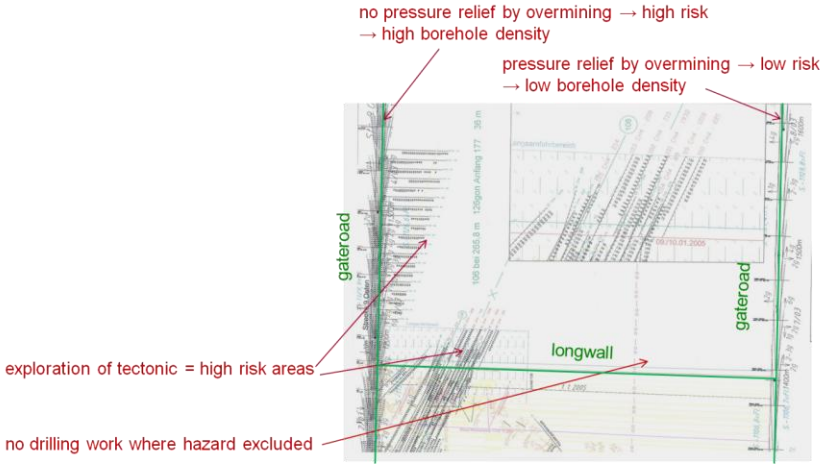

Figure 2 - Selective exploration and pressure relief drilling

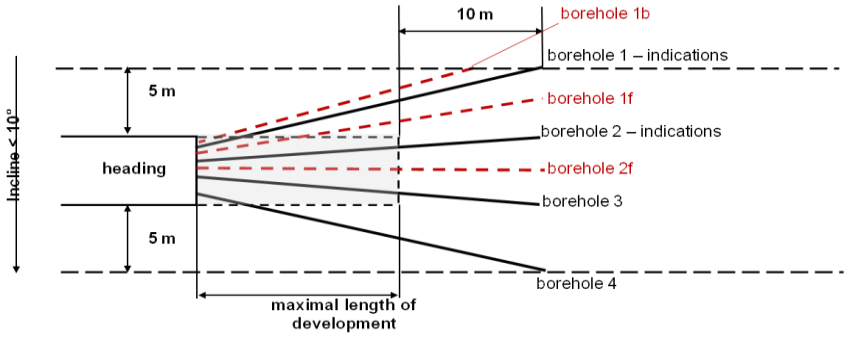

Figure 3 - Pressure relief drilling (Kunz and Imgrund, 2010)

As gas outbursts cannot be avoided by 100 %, the residual risk has to be managed systematically. Avoiding injuries and fatalities therefore is the main target. This is achieved by a management structure adjusted to the outburst risk and certain measures covering e.g. increased monitoring and communication systems, supply of breathable air, removal of the workforce from endangered areas and remote mining (e.g. with ploughs). Downtimes and costs associated with the safety measures are reduced as far as possible by a selective assessment of the gas outburst risk.

GAS EMISSION CONTROL

Although some methods of ventilation and gas drainage are basically similar throughout the world, there are also considerable country specific differences. Ventilation of longwalls in Australia typically utilises U or Y systems depending on gas emissions and the risk of spontaneous combustion. Access is by two or three heading roadways. This allows ventilation layouts and air flows to be adjusted to the expected gas emissions. Some mines use bleeder systems with part of the return air being discharged via the back end of the longwall panel. The high longwall output in many cases requires pre-drainage even below gas outburst threshold values and further post drainage from the gob area. Due to the comparative low depth and predominant single seam mining, post drainage is successfully executed by surface gob wells drilled in advance of the longwall face. Underground cross measure boreholes are less common, but floor holes are drilled in some mines.

In Chinese longwalls the U system of ventilation is common with some companies also using Y system ventilation based on double used roadways. However, single entry gate roads are state of the art. At high seam thickness, some mines use additional superjacent gate roads. As an additional return airway they are positioned in the upper section of the seam with 2.5 % CH_4 general body being permitted. Based on mine safety regulations, gas drainage is required at defined levels of gas emissions. Especially in single seam operations e.g. in Shanxi Province, pre-drainage by UIS boreholes is executed. While parallel boreholes being drilled from the gate roads are the traditional method, directional longhole drilling recently has been applied e.g. at Shenhua Group. Underground cross measure boreholes are the most usual practise where seams in the roof are a major source of gas emissions. Usually these boreholes are

drilled in advance of the longwall from niches in the tail gate or from small raises driven from the tail gate into the roof of the worked seam (Figure 4).

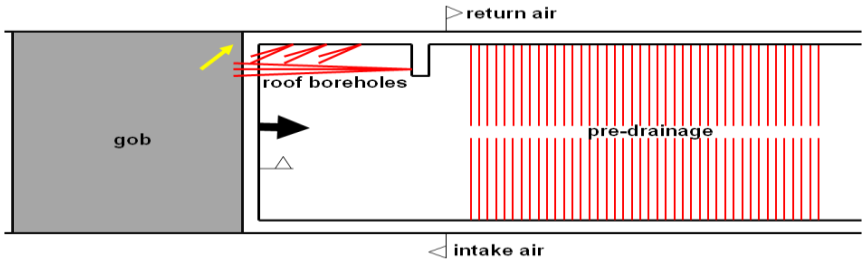

Figure 4 - Typical gas drainage layout at Chinese mine

Some mines apply gas drainage roadways driven in the roof of the worked seam and parallel to the tailgate (Figure 5). Being sealed by a dam and not being accessible after drivage, gas is drained directly from this roadway.

At low to medium depth, some mines (e.g. at Inner Mongolia and Anhui Provinces) apply surface goaf wells. A further very common system is draining gas from the sealed goaf area. For this, the tail gate is closed in the rear of the longwall by bags filled with waste rock or sand. Goaf gas is drained via pipes inserted into these dams and operated on suction. It is the nature of this layout, that the drained gas is close to or even within the explosive range. Often a mixture of different gas drainage methods is used.

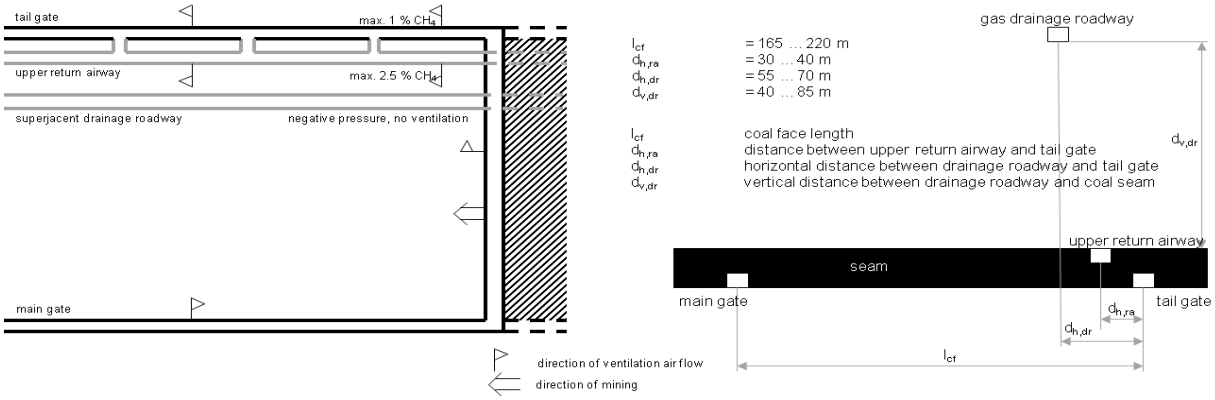

Figure 5 - Thick seam mining with superjacent tail gate and gas drainage roadway

The layout of Russian longwall panels is quite close to Australian methods with two entry heading gate roads being common. U system, but at higher gas emissions also Y system ventilation is applied. Some mines in Siberia use bleeder systems. Pre-drainage is mandatory at gas contents of 9 m³/t. Parallel UIS boreholes are drilled from the gate roads. The efficiency is often very low due to low permeability of the coal. Post drainage utilises cross measure roof holes drilled from the return airway or by surface gob wells (Figure 6).

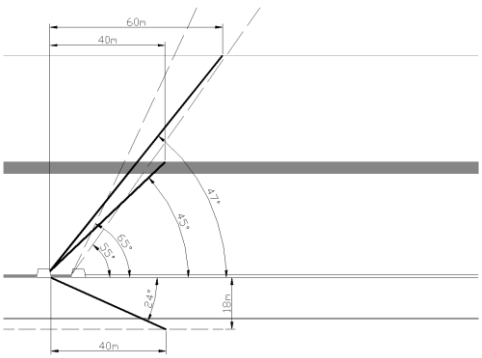

Figure 6 - Underground cross measure roof and floor boreholes drilled from gate road

Within the European Union, coal mines in Germany, the UK, Poland, Czech Republic and Romania apply gas drainage. According to the respective national regulations, either U system or Y system ventilation is preferred. While Y system ventilation and double used roadways are not permitted in the UK due to the risk of spontaneous combustion, this method has been successfully used in Germany and Poland even in seams prone to spontaneous combustion. The gob area is sealed by a concrete roadside pack. The system of double use roadways is also used due to the need to avoid irregular subsidence and zones of abutment pressure in multi seam mining. Gas drainage is applied where ventilation alone is not capable of controlling gas emissions. Pre-drainage has been successful in some cases, but compared to Australia or the US, the efficiency is low due to permeabilities down to 10^{-4} Milidarcy (Meiners, 1987). In Germany good pre-drainage results have been achieved in cases of previous over- or undermining. However, in multi seam environments, post drainage by roof and floor boreholes is often required.. Surface gob wells are not common due to high depth, existence of gob areas in the roof and difficult access from the surface due to scattered ownership or buildings. Highly efficient cross measure boreholes are drilled at the return end of the longwall. In case of double used roadways boreholes are drilled after the main subsidence is completed and there is full access to the boreholes during the entire lifetime of a panel (Figure 7).

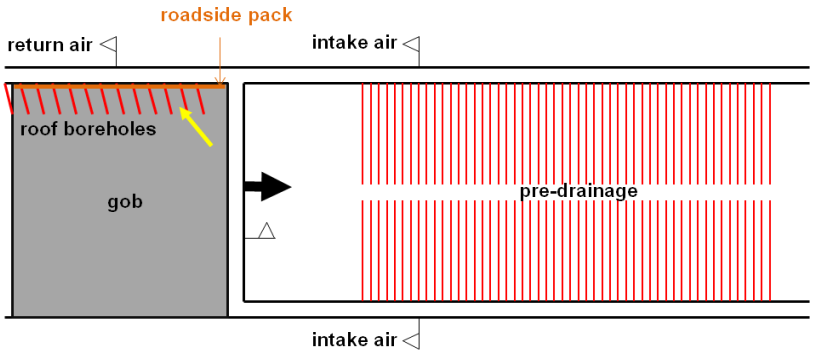

Figure 7 - Roof borehole layout at Y ventilation system

In the UK at some mines a back return system has been applied while access to the boreholes is limited to the area close to the longwall (Pitts, 2008). Further boreholes being served by a sacrificial pipeline (Figure 8).

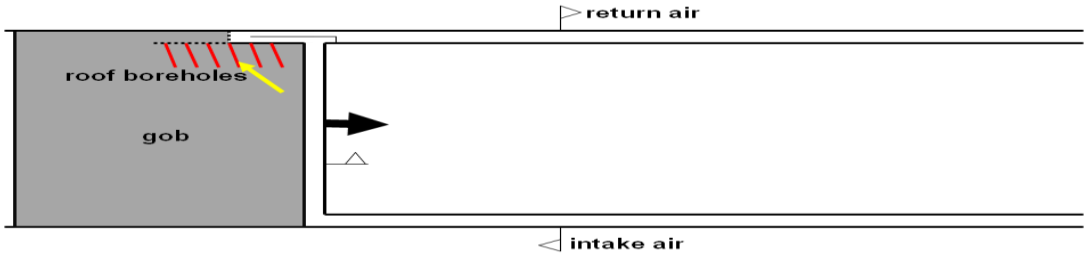

Figure 8 - Roof borehole layout at a UK coal mine

In the US both, room and pillar and longwall mining, are common methods with several mines combining the systems. Longwall panels usually are vented by a U system via multi entry gate roads. Bleeder systems are applied with 2 % CH_4 general body being permitted (U.S. Government, 2012). Pre-drainage is similar to Australia using UIS or SIS drilling. Low depth and high permeability allow efficient pre-drainage. Post drainage is basing on surface gob wells.

TECHNOLOGY TRANSFER OPTIONS

Any transfer of technology has to consider the fact that any measures of ventilation and gas drainage - and especially gas outburst prevention - have been adjusted to local conditions. These conditions are not only related to geology and mining methods, but also the structure of legislation and authorities as well as the history of mine accidents. Mine safety regulations e.g. in the CIS countries or China are very strict and detailed instructions are defined for both mine design and operation. Duly authorised institutes have to be involved in key stages of mine planning and approval processes. In contrast to this, in Australia and

Western Europe a risk assessment based approach is common. However, there is some potential in transferring overseas approaches and adjusting them to other environments. Merging international experience may bear opportunities for the Australian coal mining industry as well as for Australian technology to be transferred overseas.

In Australia the risk assessment regarding gas outburst hazards is primarily based on gas contents and coal structure. The system of threshold values has been very successful since its introduction based on the investigations of Lama (Black, 2011). Today, zones of lower permeability at increasing depths lead to difficulties in pre-drainage (Gray, 2012). Apart from the ongoing research and development of pre-drainage technologies, recent development targets defining threshold values are more selective. Nevertheless, the potential of this approach is limited if the coal cannot be pre-drained to the required threshold values. With respect to German and Chinese approaches, safe mining is also feasible at gas contents exceeding gas outburst threshold values. There are a wide range of factors which lead to a gas outburst, including but not being limited to desorption rates, permeability, gas pressure, coal strength and structure, tectonics and stress regimes. For operational practice, it is reasonable to assess those parameters which are crucial and also allow an easy measurement with low risk of errors or wrong interpretation. In most cases gas outbursts are limited to tectonic faults. German mines have made good experience with focus on local measures of exploration and pressure relief drilling according to tectonic faulting. As also small scale faults with displacement far below the seam thickness can cause a gas outburst hazard, the assessment of surface exploration borehole data and seismic measurement is not sufficient. Underground exploration drilling and proper projection of the course of faults by surveyors and geologists is a base of gas outburst risk assessment. The assessment can be executed step wise based on different parameters. As a further parameter, desorption can be assessed by using the stationary ventilation and gas monitoring and referring gas emissions to the gas volumes originally stored in the removed coal. Being more complex than an assessment based on gas contents only, there must be a clear management structure, an efficient flow of information and clear TARPs in place.

In Australia as well as in Europe and Asia there is much experience in pre-drainage, but with fundamental differences. The productivity of gassy Australian mines and intense research and development has resulted in a high level of pre-drainage technology, especially directional drilling and hydro fracturing, as well as an in deep understanding of processes occurring along gas drainage such as shrinkage and swelling of the coal matrix. At worst, local or area wide mining conditions, which are characterised by e.g. high depth, intense tectonic faulting and low permeability, state of the art drainage technologies may come to a temporary or even ultimate dead end. Experience from China, Kazakhstan and Europe shows that stress relief by over - or undermining is an efficient way to increase permeability. Leaving pure empirical approaches behind, numeric modelling is a fundamental support in understanding geotechnical and gas related aspects along with over- or undermining (Figure 9). While undermining of target seams clearly reduces gas contents, the negative and positive effects on strata control have to be considered as well. Last but not least, multi seam mining with unconventional mining sequences requires a well organised production schedule.

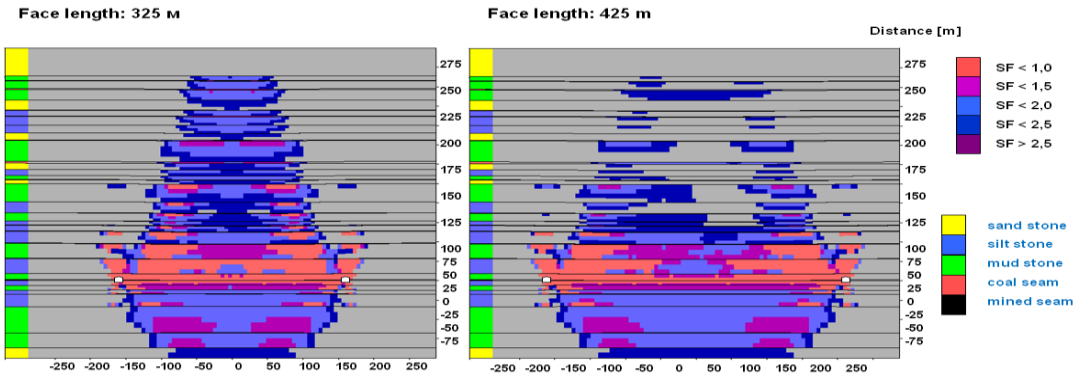

Figure 9 - Example of numeric modelling of gob zone with Flac 2D

At sections where directional drilling or hydro fracturing is not feasible due to either local tectonic faults or low permeability, limited use of exploration and pressure relief drilling from the coal face may be an alternative to abandoning coal reserves. As this requires coal seams to be mined at gas contents above generally accepted threshold values, this obviously requires higher safety standards and proper management of the residual risk.

In multi seam mining in Europe and China, double use roadways, underground cross measure boreholes and special gas drainage roadways are recognised as effective control measures. Accepting that these are fundamentally different from Australian and US mining layouts and gas drainage layouts, certain aspects of these approaches bear big advantages for multi-seam mining and mining at increased depth. Moreover, acknowledging the fact that the economic environments and ground conditions in the CIS countries, China, Europe and Australia are quite different, the cost of these supposedly expensive measures can be reduced through appropriate modifications to the mining and/or gas drainage process.

REFERENCES

Baimukhametov, D, Polchin, A, Dauov, T and Ogay, S, 2009. Gate road development in high gas content coal seams at Karaganda Basin coal mines, Kazakhstan, *Underground Coal Operators' Conference*, (Eds. Aziz, N.), University of Wollongong & the Australasian Institute of Mining and Metallurgy, 2009, pp 90-95. http://ro.uow.edu.au/coal/85/.

Black, D J and Aziz, N, 2010. Outburst threshold limits - current research outcomes, *Underground Coal Operators' Conference*, University of Wollongong & the Australasian Institute of Mining and Metallurgy, 2009, paper 295. http://ro.uow.edu.au/coal/295/.

Black, D J, 2011. Factors affecting the drainage of gas from coal and methods to improve drainage effectiveness, PhD thesis, University of Wollongong, Wollongong.

Cheng, Y, Weng, H and Wang, L, 2011. Regional gas drainage techniques and applications in Chinese coal mines, *11th Underground Coal Operator's Conference*, University of Wollongong & the Australasian Institute of Mining and Metallurgy, 2011, pp 335-342. http://ro.uow.edu.au/coal/375/.

Gray, I, 2012. Mining gassy coals, *12th Coal Operators' Conference*, University of Wollongong & the Australasian Institute of Mining and Metallurgy, 2012, 99 249 - 259. http://ro.uow.edu.au/coal/414/.

Henderson, J, Jones, B and Esler, R, 2008. Introduction of remote mining, paper presented to Gas and Outburst Seminar, Wollongong.

Hucke, A, Studeny, A, Ruppel, U and Witthaus, H, 2006. The advantage of combining numerical simulation, physical modelling and *in-situ* monitoring for roadway planning, *Glueckauf Mining Report*er, 2:13-20.

Imgrund, T, 2012. Gas outburst prevention - International experience, paper presented to 2nd International Research and Practise Conference, Problems regarding methane in coal mines and ways of their solution, 26-27 June, Karaganda.

Kunz, E and Imgrund, T, 2010. Pre-drainage of deep coal seams, paper presented to Workshop on Coal Mine Methane Recovery and Utilisation in Ukraine, Donetsk, 21-22 September.

Lama, R D and Bodziony, J, 1996. Sudden outbursts of gas and coal in underground coal mines, Final report ACARP project C4034. http://www.uow.edu.au/eng/outburst/pdfs/C4034%20Final%20Report.pdf.

Meiners, H, 1987. Gas flow processes in coal seams under influence of mining, PhD thesis, University of Aachen.

Mine Inspectorate of the State of North Rhine-Westfalia, 1996. *Gas Outburst Guideline*, Mine Verlag Glueckauf GmbH: Essen.

Pitts, M, 2008. Effective gas drainage in low-permeability coals - a case study, paper presented to Guizhou CMM Workshop, 15-17 July, Guiyang.

Xue, S, Reece, D and Yarlagadda, S, 2010. APP coal mine health and safety project 1 report - Identify and collate leading safety technologies, CSIRO Earth Science and Resource Engineering Report EP106702, CSIRO: Kenmore.

U.S. Government, 2012. *Code of Federal Regulations, Title 30, Mineral Resources*, National Archieves and Records Administration: Washington.

United Nations Economic Comission for Europe, 2010. *Best practise guidance for effective methane drainage and use in coal mines*, ECE Energy Series No. 31, United Nations Economic Commission for Europe: Geneva.

United States Environmental Protection Agency (U.S. EPA), 2010. *Coal Mine Methane Country Profiles*, Global Methane Initiative: Washington.

CARBON SEQUESTRATION IN COAL MEASURES ROCKS

Ian Porter[1], Jae Dawes[1], Long Nghiem[1] and Jim Somerville[2]

ABSTRACT: It is a widely held belief that anthropogenic addition of greenhouse gases to the atmosphere will lead to rapid climate change. It is also a widely held belief that the burning of fossil fuels for power generation is a major contributor to these anthropogenic additions, predominantly the emission of carbon dioxide and the consequential increase in carbon dioxide levels in the atmosphere. Irrespective of the cause and effect of the increased carbon dioxide levels it is in the interest of the coal mining industry to work with various partners to develop methods of reducing the rate of emission of carbon dioxide to the atmosphere. Carbon capture and sequestration has the potential to meet that objective. This paper looks at the various methods of carbon sequestration and presents the published results from various laboratory and theoretical studies to determine the potential for carbon sequestration in coal measures rocks.

INTRODUCTION

A common consensus is that human development has greatly contributed to increased atmospheric levels of greenhouse gases - particularly methane and carbon dioxide (the 2nd and 3rd most prolific greenhouse contributors, behind water vapour). It has been determined that greenhouse gas emissions have increased since the Industrial Revolution with concentrations of carbon dioxide having risen from 280 ppm to approximately 350-380 ppm (Bachu, 2003; Normile, 2009). With these rises in greenhouse gases it is believed that rapid climate change will occur, leading to unacceptable social and economic problems. The emission of carbon dioxide and the consequential increase in carbon dioxide levels in the atmosphere is of particular concern, and irrespective of the cause and effect of the increased carbon dioxide levels it is in the interest of the coal mining industry to work with various partners to develop methods of reducing the rate of emission of carbon dioxide to the atmosphere.

The most theoretically promising option to reduce carbon dioxide is Carbon Capture and Sequestration (CCS) (Metz, *et al.*, 2005). CCS involves capturing CO_2 from large point emitters (such as power stations) and storing it for a geological time frame. CCS involves:

- separation of carbon dioxide from industrial point sources;
- transport to site;
- long term storage in atmospheric isolation.

According to Metz *et al.* (2005), CCS could reduce CO_2 emissions from pulverised coal power stations by 80-90%. Figure 1 shows the amount of carbon dioxide emitted from a regular power plant in comparison to CO_2 emitted from a power plant with a carbon capture regime implemented. Although more carbon dioxide is produced, due to the increased fuel required per unit of electricity released to the grid, the amount of carbon dioxide emitted is significantly less. The widespread application of CCS depends on future advances in technology. At present the technology exists to allow for each individual stage of CCS, e.g. CO_2 has been pumped underground for use in Enhanced Oil Recovery (EOR), the technology to drill wells deep into the earth has been proven by the successful exploitation of natural oil and gas reserves, the use of pipelines to distribute oil and gas is a routine occurrence, however, the various technologies have not been put together into a system that can economically and safely sequester carbon dioxide on a geological timeframe.

Studies have shown that CO_2 can be theoretically stored in the ocean (Marchetti, 1977; Holloway and Savage, 1993), soil (McCarl, *et al.*, 2007), saline aquifers (Allen, *et al.*, 2005; Bachu, *et al.*, 1994), coal (Bachu, 2000; Larsen, 2004; Fitzgerald, *et al.*, 2005; Shackley and Gough, 2006; Orr, 2009) and sandstone (Korbol and Kaddour, 1995; Nowak, 2007).

[1] *School of Civil, Mining and Environmental Engineering, University of Wollongong, Australia, iporter@uow.edu.au, Tel: +61 2 42213450*
[2] *Institute of Petroleum Engineering, Heriot-Watt University, Scotland.*

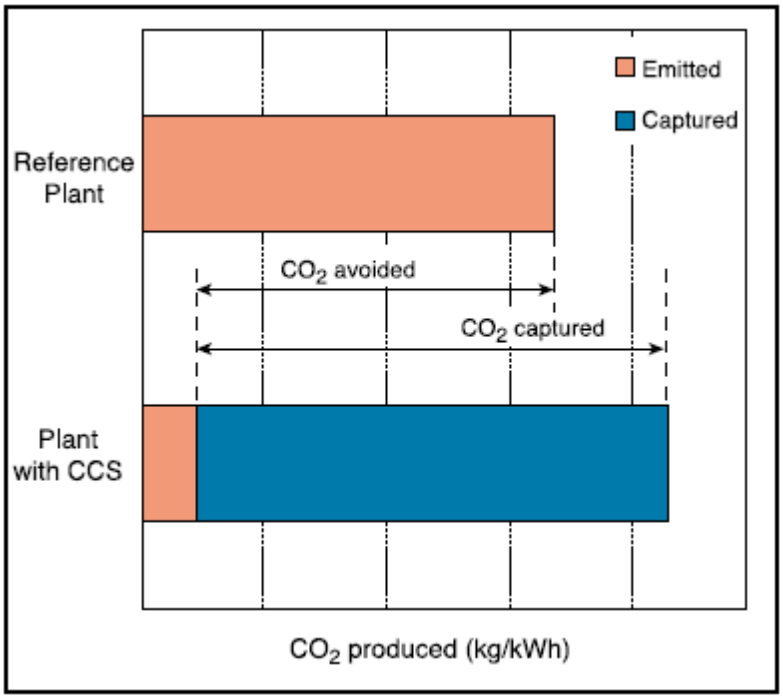

Figure 1 - CO_2 emissions for power stations with and without capture. (Metz, *et al.,* 2005)

OCEAN SEQUESTRATION

According to Metz *et al.* (2005) there are several viable methods for ocean sequestration:

- dissolution - CO_2 is injected by ship or pipe at depths greater than 1000 m where the carbon dioxide dissolves into the water and becomes part of the equilibrium;
- lakes - carbon dioxide is deposited onto the sea floor deeper than 3000 m. At these depths CO_2 is denser than sea water and is capable of forming lakes which settle on the floor and prevent the spread of CO_2 into the environment;
- conversion - converting CO_2 into solid bicarbonates (with the use of limestone) and storing them in the ocean. Bicarbonates are extremely stable and would be capable of withstanding the erosion and pressures that they would be subjected to at great depths that are required for sequestration;
- store CO_2 in solid clathrate hydrates already on the ocean floor, or create new hydrates.

Each of these systems has merit, but an obvious demerit is the potential effect on the ocean equilibrium and subsequent effect on ocean ecosystems.

SOIL SEQUESTRATION

It has been suggested (McCarl, *et al.*, 2007; Parliamentary Library, 2011) that sequestering carbon into soil could improve the health and productivity of the soil. There are two ways to sequester carbon in soils; increase carbon levels in soils or convert organic matter into a more stable form of carbon. The former involves returning plant material to the soil. McCarl *et al.* (2007) concluded that when plant material was returned to the soil or the amount of lost carbon reduced, or both, then the overall health of the soil would improve. For the latter biochar can be considered as a viable option (Krull, 2010; McCarl, *et al.*, 2007; Parliamentary Library, 2011; Victoria Parliament, 2010). Biochar is a charcoal that is produced when organic materials (manure, wood chips, crops, coal) are burned in an oxygen-depleted environment; the process is conducted at high temperatures and is known as pyrolysis (Krull, 2010). It utilises production processes similar to coke making.

The sequestration of carbon dioxide into soils is dependent on a number of factors. The climate (temperature and precipitation), geology of the surrounds (texture, mineralogy), vegetation types and the land management practises employed all affect the ability of soil to sorb and store carbon dioxide (McCarl, *et al.*, 2007; Victoria Parliament, 2010). These factors all affect the soil residence time (Jastrow, *et al.,* 2007), i.e. the time for the stored carbon to be released back into the atmosphere. There is evidence that the residence time associated with biochars can range from hundreds of years to several thousand of years (Lehman, *et al.*, 2008). Figure 2 (Lehman, 2007) shows the natural carbon cycle in comparison to the biochar carbon cycle.

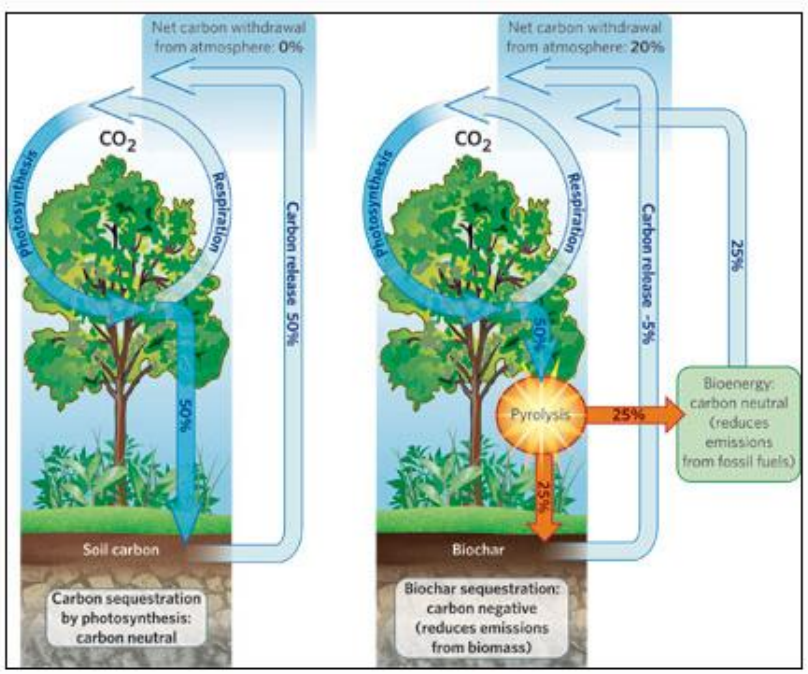

Figure 2 - Natural carbon cycle verse biochar carbon cycle (Lehmann, 2007)

Whatever the merits or demerits of soil sequestration there must be an ability to store CO_2 for geologically significant periods.

GEOLOGICAL SEQUESTRATION

There is general agreement (Metz, *et al.*, 2005; IEA, 2004; Bachu, 2003; Holloway, 1997; Orr, 2009) that the most suitable geological formations, as illustrated in Figure 3, for carbon sequestration are:

- deep saline aquifers;
- depleted oil and gas reservoirs (including coal bed methane);
- rock formations, such as sandstone, limestone and shale, and uneconomical coal seams.

Sequestration in deep saline aquifers and depleted oil and gas reservoirs

There are currently two significant commercial projects; Sleipner, Norway and In Salah, Algeria, that utilise deep saline aquifers for CO_2 storage. These two projects are similar, in that they harvest the CO_2 from extracted CH_4, and store it in deep saline aquifers. The Sleipner project is the world's longest running sequestration project, with the first CO_2 sequestration occurring in 1996 (Korbol and Kaddour, 1995). Sleipner utilises a deep saline aquifer for sequestration that sits around 1700 m above the gas deposit, Figure 4, while In Salah exploits a saline aquifer down dip of gas production. Both of these projects sequester approximately 1Gt CO_2 annually (Metz, *et al.*, 2005).

Storage of CO_2 is a 'by-product' of EOR at the Weyburn oil field in Canada. The CO_2 is pumped into the formation to drive out the last drops of oil that would otherwise be irrecoverable and in the process is captured in the sandstone formation.

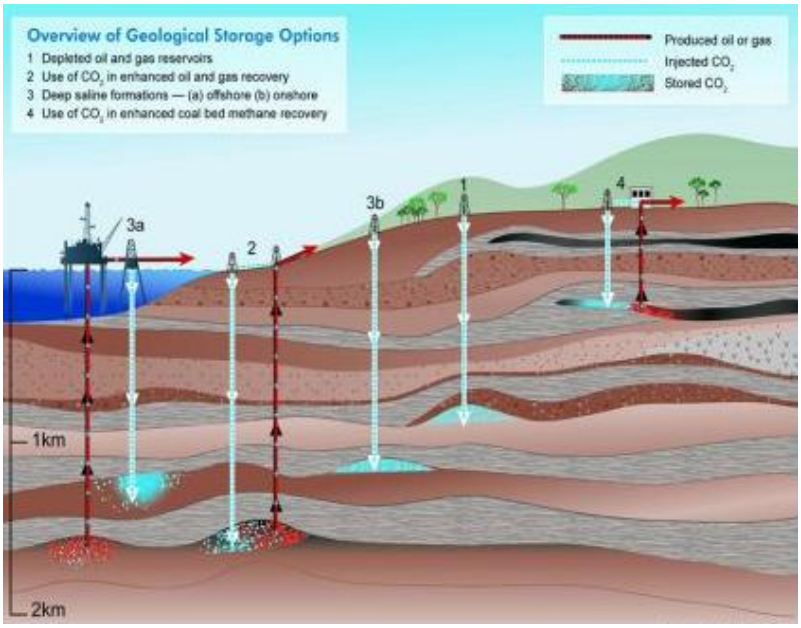

Figure 3 - Methods for storing CO_2 in underground geological formations (Metz, *et al.*, 2005)

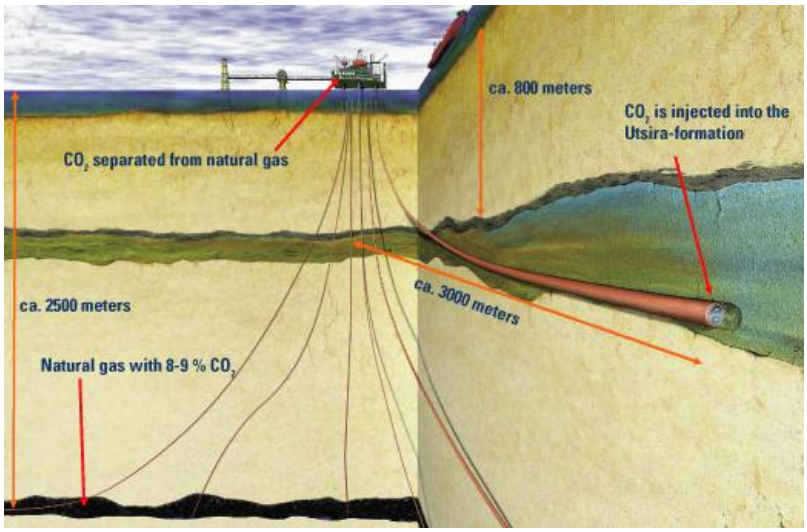

Figure 4 - Carbon dioxide injection at the Sleipner gas field (image courtesy of Statoil)

Sequestration in coal measures rocks

For CO_2 to be held in geological formations some form of trapping mechanism must be present, this may be in the form of an impermeable caprock, dissolution in formation water or geochemical trapping where the CO_2 is mineralised. Geochemical trapping results in the most stable form of carbon storage, but this may take thousands of years and as such some form of lower order trapping must initially take place.

Carbon dioxide is stored in coal measures rock by the process of adsorption (often simply termed sorption), where the gas is held on the rocks' surface. With this process, coal for example, may theoretically hold 40 to 60 m^3 of CO_2 per tonne of coal at 5 - 6 MPa (Gaucher, *et al.*, 2011). In addition to storing CO_2 in uneconomical seams, the CO_2 can be used in an Enhanced Coal Bed Methane (ECBM) operation, Figure 5, as CH_4 is preferentially displaced by CO_2 in coal.

Charrière *et al.* (2010) conducted tests on the effects of temperature and pressure on the diffusion of CH_4 and CO_2 into coal. They found that at a pressure of 5.15 MPa a coal from the Lorraine Basin, France, could adsorb 1.55 mmol/g of CO_2, approximately 34 m^3/t. Similar experiments have been conducted elsewhere (Busch, *et al.,* 2003) where over 54 m^3/t was adsorbed on a coal from Illinois. A common element in these works is the use of a small sample mass, 5 g or less, of finely powdered coal, and

temperature and pressures that are sub-critical for CO_2. The results are then used to infer what would happen *in situ*.

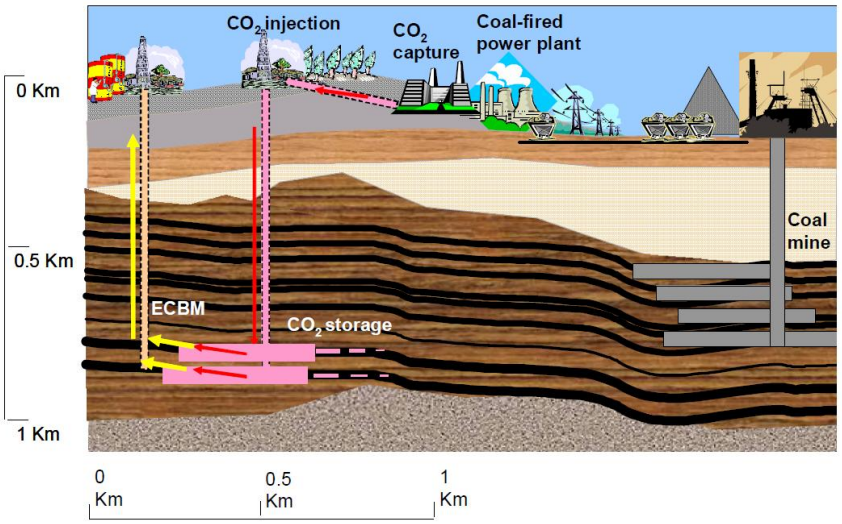

Figure 5 - Enhanced coal bed methane operation (Gaucher, *et al.*, 2011)

Florentin *et al.* (2009) reported on work conducted on coal samples of varying particle size, up to 54 mm diameter core. The findings showed similar total sorption capacities between the varying particle sizes, however the time to reach equilibrium was longer in the solid core samples. It takes at least three days to reach the equilibrium pressure in coal fragments and four days in 54 mm core. In coal fragments, around 70% of the equilibrium pressure was reached during the first 360 min, while in the 54 mm core only 30% of the equilibrium pressure was reached in the same period. As before these results were obtained from samples at sub-critical temperatures and pressure.

Supercritical fluids are substances that are at a temperature and pressure greater than the critical point, Figure 6, such that they cannot be identified as a liquid or a gas. They are capable of effusing through solids (like a gas) and dissolving materials (like a liquid). The most important sequestration property of supercritical fluids is the greatly increased density. When the density increases, the volume of a gas reduces, as such, high density CO_2 takes up much less volume than low density gas, allowing more carbon dioxide to be stored in the same volume. Due to the pressure and temperature requirements to keep CO_2 in the supercritical phase, carbon sequestration occurs at depths greater than 800 m. This is the approximate depth at which the earth's temperature and pressure matches that of supercritical CO_2 - 31.1°C and 7.39 MPa. There are, of course, variations in this due to geothermal gradients and density of surrounding rocks (Bachu, *et al.*, 1994).

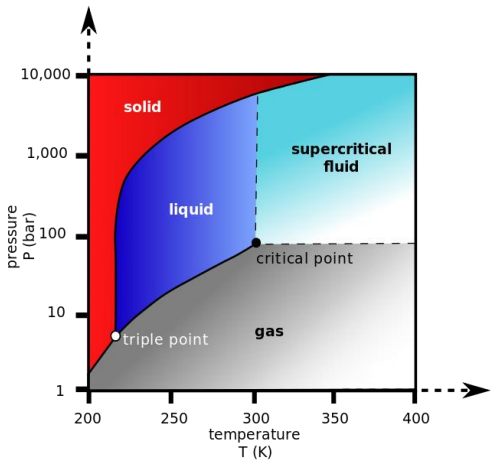

Figure 6 - Phase diagram for carbon dioxide (open source)

Zhang *et al.* (2011), shows that the sorption capacity for CO_2 increases with pressure, but at some pressure beyond the critical pressure it then decreases. This may be a result of the swelling behaviour of the coal under different gas pressures (Day, *et al.,* 2010). These studies and the work reported previously have all been in coal, but the rocks of the coal measures all have the ability to sequester CO_2, obviously to varying degrees.

Sequestration in sandstone and limestone is usually in the context of storage in deep saline formations as discussed previously, however, other coal measures rocks such as carbonaceous shales, particularly those rich in carbonaceous matter (MRSCP, 2005) have the ability to adsorb CO_2 in a manner similar to that of coal. It was reported (MRSCP, 2005) that these shales are often multifunctional; acting as seals for underlying reservoirs, as source rocks for oil-and-gas reservoirs, and are unconventional gas reservoirs themselves. As with ECBM extraction, CO_2 injection into unconventional carbonaceous shale reservoirs could be used to enhance existing gas production. It is believed the carbonaceous shales would adsorb the CO_2 into the shale matrix, similar to coal, permitting long-term CO_2 storage, even at relatively shallow depths (Nuttall, *et al.,* 2005).

Testing core samples under supercritical conditions

As stated previously, most laboratory testing is conducted on small samples of powdered coal, this is particularly true of tests conducted at supercritical conditions. In order to test core samples at supercritical conditions a new high pressure bomb had to be designed. The bomb was based on those used by Florentin *et al.* (2009). Australian Standard, AS1210-2010 Pressure Vessels (Standards Australia Limited, 2010), was used to guide the design process and the final design is shown in Figure 7. For the design and construction of the bomb, marine grade aluminium was chosen as it is resistant to gas erosion. To conform to Australian Standards:

- the bomb must be categorized according to its hazard level;
- the design pressure and operating pressure must allow for a reasonable factor of safety;
- extra precautions must be in place for materials that undergo a phase change whilst contained in the vessel;
- design drawings must be to Australian Standards;
- machining and construction must be done by a competent person;
- the final design needs to be audited by a qualified certifier.

In order to avoid weak spots caused by welds or stress concentrations where the base meets the side wall, the vessel was machined from solid bar and incorporates a hemispherical finish to the base. The bomb is capable of taking 100 mm long 54 mm diameter cores at pressures up to 10 MPa.

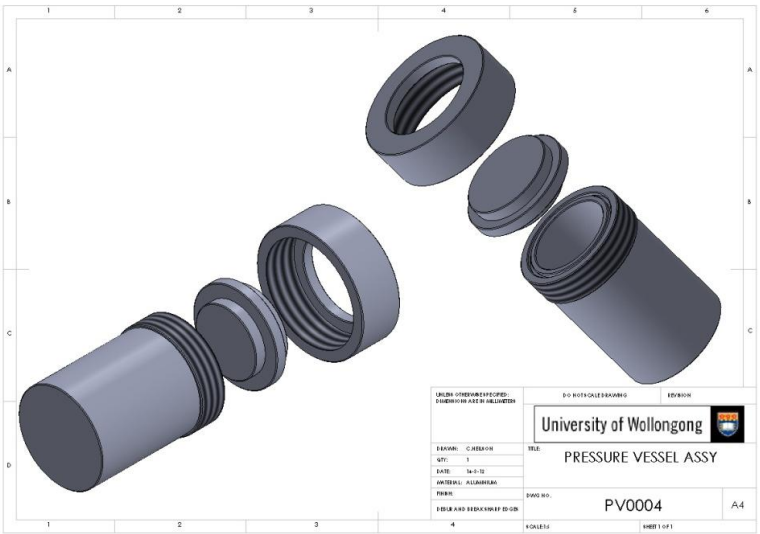

Figure 7 - Pressure vessel for use at supercritical pressures

CONCLUSIONS

At present the only practical application of carbon sequestration is in deep saline aquifers and depleted oil reservoirs. Initial findings have shown that carbon sequestration in these sinks is both feasible and practical. The problem with sequestering carbon dioxide from coal fired power stations in large saline aquifers and depleted oil fields is that these sites are often at some distance from the power station, requiring expensive and expansive transport solutions to get the carbon dioxide to the site.

A potential solution is to utilise coal measures rocks to sequester CO_2. As coal has the greatest sorption capacity by some measure over other coal measures rocks, it would appear that storing CO_2 in uneconomical coal seams, possibly as a by product of enhanced coal bed methane extraction, is the most cost effective and efficient option. The major problem with this approach is that a coal seam that is uneconomical at present may not be in the future. Some countries, the UK for example, have for that reason specifically legislated that CO_2 cannot be sequestered in coal seams.

Although both sandstone and limestone can sequester about 30% the volume of CO_2 that coal can, there is much more of it and, at depth, it is not constrained by being a potential resource. It is necessary to test samples of these rocks under supercritical conditions as they may behave differently to that of coal at elevated pressures. Another potential coal measures rock is carbonaceous shale, where evidence suggests that some shales with high organic content adsorb carbon in a manner similar to coal. Thus, even if legislation or future potential prevents the use of uneconomical coal seams for sequestering CO_2, other coal measures rocks may provide a local solution for coal fired power stations.

ACKNOWLEDGEMENTS

The authors would like to acknowledge Mr Alan Grant and Mr Cameron Neilson, Senior Technical Officers in the Faculty of Engineering, University of Wollongong, for their input to the design and construction of the modified pressure vessel.

REFERENCES

Allen, D E, Strazisar, B R, Soong, Y and Heges, S W, 2005. Modelling carbon dioxide sequestration in saline aquifers: significance of elevated pressures and salinities, *Fuel Processing Technology*, 86:1569-1580.

Bachu, S, 2000. Sequestration of CO_2 in geological media: criteria and approach for site selection in response to climate change, *Energy Conversion and Management*, 41(9):953-970.

Bachu, S, 2003. Screening and ranking of sedimentary basins for sequestration of CO_2 in geological media in response to climate change, *Environmental Geology*, 44:277-289.

Bachu, S, Gunter, W D and Perkins, E H, 1994. Aquifer disposal of CO_2: hydrodynamic and mineral trapping, *Energy Conversion and Management*, 35(4):269-279.

Brennan, S T and Burruss, R C, 2003. Specific sequestration volumes: a useful tool for CO_2 storage capacity assessment, in *Proceedings 2nd annual conference on Carbon Sequestration,* pp 1-12 (National Energy Technology Laboratory, USA).

Busch, A, Gensterblum, Y and Krooss, B M, 2003. Methane and CO_2 sorption and desorption measurements on dry Argonne premium coals: pure components and mixtures, *International Journal of Coal Geology*, 55:205-224.

Charrière, D, Pokryszka, Z and Behra, P, 2010. Effect of pressure and temperature on diffusion of CO_2 and CH_4 into coal from the Lorraine basin (France), *International Journal of Coal Geology*, 81:373-380.

Day, S, Fry, R, Sakurovs, R and Weir, S, 2010. Swelling of coals by supercritical gases and its relationship to sorption, *Energy Fuels*, 24:2777-2783.

Fitzgerald, J E, Zhejun, P, Sudibandriyo, M, Robinson Jr, R L, Gasem, K A M and Reeves, S, 2005. Adsorption of methane, nitrogen, carbon dioxide and their mixtures on wet Tiffany coal, *Fuel*, 85:2351-2363.

Florentin, R, Aziz, N, Black, D and Nghiem, L, 2009. Sorption characteristics of coal, particle size, gas type and time, in *Proceedings Underground Coal Operators Conference COAL2009,* pp 208-216 (The Australasian Institute of Mining and Metallurgy: Melbourne). http://ro.uow.edu.au/coal/102/.

Gaucher, E C, Défossez, P D C, Bizi, M, Bonijoly, D, Disnar, J R, Laggoun-Défarge, F, Garnier, C, Finqueneisel, G, Zimny, T, Grgic, D, Pokryszka, Z, Lafortune, S and Vidal Gilbert, S, 2010. Coal laboratory characterisation for CO_2 geological storage. *Energy Procedia*, 4:3147-3154.

Holloway, S and Savage, D, 1993. The potential for aquifer disposal of carbon dioxide in the UK, *Energy Conversion and Management*, 34(9-11):925-932.

Holloway, S, 1997. Safety of the underground disposal of carbon dioxide, *Energy Conversion and Management*, 38(Supplement):S241-S245.

International Energy Agency, 2004. Prospects for CO_2 capture and storage, (online). Available from: <http://www.oecd-ilibrary.org/docserver/download/6104281e.pdf> [Accessed: 19 December, 2012].

Jastrow, J D, Amonette, J E and Bailey, E L, 2007. Mechanisms controlling soil carbon turnover and their potential applications for enhancing carbon sequestration, *Climate Change*, 80(1-2):5-23.

Korbol, R and Kaddour, A, 1995. Sleipner vest CO_2 disposal - injection of removed CO_2 in the Utsira Formation, *Energy Conversion & Management*, 36(6-9):509-512.

Krull, E, 2010. Biochar, (online). Available from: <www.csiro.au/files/files/pnzp.pdf> [Accessed: 19 December, 2012].

Larsen, J W, 2004. The effects of dissolved CO_2 on coal structures and properties, *Coal Geology*, 57:63-70.

Lehmann, J, 2007. A handful of carbon, *Nature,* 447:143-144.

Lehmann, J, Skjemstad, J, Saran, S, Carter, J, Barson, B, Falloon, P, Coleman, K, Woodbury, P and Krull, E, 2008. Australian climate - carbon cycle feedback reduced by soil black carbon, *Nature Geoscience*, 1:832-835.

Marchetti, C, 1977. On geoengineering and the CO_2 problem, *Climatic Change*, 1(1):59-68.

McCarl, B A, Metting, F B and Rice, C, 2007. Soil carbon sequestration, *Climatic Change*, 80(1-2):1-3.

Metz, B, Davidson, O, de Coninck, H, Loos, M and Meyer, L, 2005. *IPCC special report on carbon dioxide capture and storage*, 431 p (Cambridge University Press, New York.)

Midwest Regional Carbon Sequestration Partnership, 2005. Phase 1 Final Report, (online). Available from:< http://216.109.210.162/userdata/Phase%20I%20Report/MRCSP_Phase_I_Final.pdf.> [Accessed: 19 December, 2012].

Normile, D, 2009. Round and round: a guide to the carbon cycle, *Science*, 325:1642-1643.

Nowak, 2007. Biggest carbon burial test will hunt for leaks, (online). Available from: <www.newscientist.com/article/dn11197?DCMP=Matt.Sparkes&nsref=carbon-burial> [Accessed: 19 December, 2012].

Nuttall, B C, Drahovzal, J A, Eble, C F, and Bustin, R M, 2005. CO_2 sequestration in gas shales of Kentucky, In *Abstracts Volume AAPG 2005 Annual Convention,* pp A101-A102 (American Association of Petroleum Geologists: Tulsa).

Orr Jr, F M, 2009. Onshore geologic storage of CO_2, *Science*, 325: 1656-1658.

Parliamentary Library, 2011. Carbon Sequestration, (online). Available from: <http://www.aph.gov.au/library/pubs/ClimateChange/responses/mitigation/carbon.htm> [Accessed: 19 December, 2012].

Standards Australia Limited, 2010. AS1210- 2010 Pressure Vessels, 420 p (SAI Global Limited, Sydney).

Shackley, S and Gough, C (eds), 2006. Carbon capture and its storage: an integrated approach, Ashgate Publishing Limited, Hampshire.

Singh, T, 2010. Carbon sequestration- is burying carbon dioxide a realistic option? (online). Available from: <http://oilprice.com/Environment/Global-Warming/> [Accessed: 19 December, 2012].

Victoria Parliament, 2010. Inquiry into soil sequestration in Victoria, Parliamentary Paper 362, (online). Available from: <http://www.parliament.vic.gov.au/images/stories/committees/enrc/20100902.enrc.scsv.FINREP.pdf > [Accessed: 19 December, 2012].

Zhang, D F, Cui, Y J, Liu, B, Li, S G, Song, W L and Lin, W G, 2011. Supercritical pure methane and CO_2 adsorption on various rank coals of China: experiments and modelling, *Energy Fuels,* 25:1891-1899.

COMPARISON OF PHOTOGRAMMETRY AND SURVEY LASER SCANNING OUTPUT DATA FOR USE IN MAPPING JOINTS IN OPEN CUT HIGHWALLS

Alison McQuillan

ABSTRACT: The Anglo American open-cut coal mines in Australia routinely obtain structural data from exposed highwalls to determine the potential for instability caused by joint orientation, joint dip, and joint persistence. Three methods are currently available to obtain this data: direct in-pit measurements with a geological compass, photogrammetry, and laser scanning. Direct measurements are often very time-consuming and can lack the precision of other methods due to the inability to perform proper line surveys where mandatory safety stand-off distances are enforced at the toe of each highwall. For this reason, photogrammetry has been the method of choice for many years, where stereo pairs are used to create a 3D image of the highwall. In recent years however, laser scanners now appear to be the preferred method of data acquisition due to their faster capturing and processing time, as well as their user-friendly CAD processing functionality. Concerns however have been raised over the accuracy of laser scanner data as examples to date have lacked the point cloud density necessary for picking representative joint planes. To resolve this issue, both methods were applied on the same highwall and the outputs compared. From this comparison, it was concluded that accuracy is not compromised with laser scanner acquisition methods as long as the correct intensity is selected prior to capturing the scan. Discrepancies were however identified between the joint orientation outputs of Sirovision and I-site mapping technologies. These discrepancies are attributed to the different algorithms each program uses, as well as the survey control and density of data points produced and required by each method.

INTRODUCTION

The identification and mapping of structural features such as joints, fractures, and faults is an important responsibility of the geologist/geotechnical engineer in any open-cut coal mine, where the persistence and orientation of these features can have a significant influence on the stability of an exposed hard wall (i.e. highwall or endwall). The failure to identify adverse structures ahead of mining can lead to injury to personnel, and damage to equipment, as well as significant delays and/or coal losses to mining operations in extreme conditions. Regular highwall mapping is therefore integral to assessing the geotechnical stability of future strips so coal can be uncovered as efficiently and safely as possible.

At Anglo American Metallurgical Coal (Met Coal), CSIRO/CAE's Sirovision has been the preferred software package for photogrammetry, and Maptek's I-site scanner is the most popular laser scanner utilised throughout Met Coal's five open-cut operations in Australia. Both methods produce similar results in the form of a spatially orientated 3D model of the wall under analysis, onto which the direction of joints, fractures, and faults can be traced. The methods of obtaining these results, however, vary significantly in terms of workload and user friendliness for essentially the same data.

With the advent of this technology, in-pit line surveys are now seldom used to collect mass volumes of data due to the increased exposure of personnel to "no-go" or "drop-zones" at the toe of a hardwall. Nonetheless, line surveys are still important to 'ground-truth' joint planes mapped by photogrammetry and laser scan technology.

The impetus for this paper is to present a direct comparison of laser scanner (using Maptek's I-Site 8800 laser scanner version 3.86x, Maptek, 2012) and photogrammetry (CAE's Sirovision version 4.2, CAE, 2012) data, obtained from the same highwall, to show the similarities and differences in output data of these two methods, so a comprehensive understanding of their capabilities for highwall mapping can be obtained. This comparison will ensure the most appropriate method is selected so subsequent slope stability analyses can be undertaken as efficiently, accurately, and safely as possible to suit the end user's needs.

Geotechnical Engineer, Anglo American Metallurgical Coal, Brisbane QLD 4000, alison.mcquillan@angloamerican.com, M: +61 (4) 19 748 622

OVERVIEW OF METHODS

The following section provides a brief overview of the acquisition and data processing requirements of both Sirovision and the I-site scanner. A more comprehensive description of each method is available on each of the company's websites. Both methods require both a field acquisition and an office processing component.

Sirovision

Field process

Personnel (generally site geologist/geotech) identify the area/extent of the hard wall requiring analysis and based on this area select the number of sections to be photographed. A minimum of three surveyed control points (generally in the form of high visibility marker cones) are then placed at the crest/toe of the hard wall as well as from the positions where the first set of stereo pair images are taken so that the images can be georeferenced back in the office. This process of photographing stereo pairs (i.e. near-identical photos of the same area taken at pre-determined distances apart) is continued along the desired length of the wall in a horizontally progressing fashion, ensuring adequate overlap is incorporated into adjacent images at each location so that a mosaic of sequential 3D images can be stitched during office processing.

Data processing

Several different programs and processes are required to create a 3D image suitable for joint/structure delineation once the field data is acquired. Photographs taken in the field are in the form of .RAW files that need to be converted to .TIFF files for further processing using software such as Canon's Digital Photo Professional or similar. Sirovision's Siro3D is then used to convert the original 2D images to spatially referenced 3D images so joint data can then be picked in 3D space. Within Siro3D images need to be corrected for lens distortion, spatially referenced to surveyed control points, then aligned and matched to their stereo pair using task set-ups to create a 3D image. 3D images are then imported into a third program, Sirovision's SiroJoint, where structural features such as joints, fractures, and faults can be automatically or manually mapped, digitised, and projected onto stereonets and rosette plots. Digitised planes and traces can further be exported into additional highwall analysis programs such as Rocscience's DIPS (DIPS 2012) so further analyses on the likelihood of failure may be assessed.

I-site scanner

Field process

Personnel (generally site surveyors) asses the size and features of the pit and decide on the location of the scan. An ideal location should avoid data 'shadows' and ensure the scanner is set up close enough to low reflectivity materials such as coal (to receive an adequate return signal) as well as close enough to the wall to ensure adequate resolution is acquired during the scan. For geotechnical scans, the scanner must be tripod mounted, rather than vehicle mounted. This is to avoid a reduction in accuracy which results from vehicle vibrations if it is left running when the scan is being acquired. A GPS/XYZ receiver is placed atop the scanner and the XYZ co-ordinates are recorded and confirmed with a backsight GPS system generally mounted to the surveyors light vehicle. The scanner then captures a 360° image of the area. The operator selects from this image the area to be scanned and the required resolution. For geotechnical scans, based on site trials, the minimum resolution setting the 8800 should be set at an 8-bit intensity. The laser scan is then acquired. On completion of the scan the data may be examined in the field for any errors. If errors are evident, a second scan can be performed with the necessary adjustments, before the scanner and tripod are relocated to complete another scan of the wall in a horizontally progressing fashion.

Data processing

Upon returning from the field, the scanner hardware is simply plugged into a PC and Maptek's I-site Studio software converts the point data into a spatially-referenced 3D depiction of the physical landscape. A digital image captured by the built-in 70 megapixel camera can be overlain onto this point data to produce a spatially-referenced 3D image of the scanned area. Planes and traces may then be inserted along joints, fractures, and faults and projected onto stereonets and rosette plots, similar to those produced in Sirovision's SiroJoint. However, unlike planes mapped in SiroJoint, planes mapped in

I-site Studio may be directly analysed for planar and toppling failure within I-site Studio software, significantly reducing the processing time to complete a kinematic analysis. Nevertheless, I-site Studio data may similarly be imported into additional highwall analysis programs such as DIPS so further analyses on the likelihood of failure may be analysed.

DIRECT COMPARISON OF METHODS

Sirovision and an I-site laser scan of Anglo American's Foxleigh WC highwall was undertaken in autumn 2012. This hard wall was selected based on its moderate structural complexity, ease of access, and prolonged exposure for the purpose of this comparison. To ensure the outputs were comparable, the laser scan was acquired approximately one month after the digital images were taken for Sirovision analysis. Ideally a survey scan would have been completed within a week of Sirovision, however due to end of month survey requirements the laser scanner was not available until this time. Wall conditions were not observed to change significantly during this period, as no mining activities had occurred in the study areas ensuring the trial essentially compared "apples with apples".

RESULTS

Spatially referenced 3D images of the WC highwall were successfully produced using both Sirovision and the 8800 scanner. Joint sets were then successfully mapped from these 3D images using their pertinent parent processing software (i.e. Sirovision's SiroJoint software for photogrammetry produced 3D images and Maptek's I-site Studio software for laser scan produced 3D images) - see Figures 1 and 2. In Figure 1, the distortion above the crest of the mainpass highwall is a result of Sirovision's processing of data 'black-spots'. This distortion does not have any impact on accuracy as the focus area is in the mainpass highwall. In Figure 2, the black spots that are observed above the crest of the mainpass highwall area a result of data 'shadows'. Similar to Figure 1, these shadows do not have any impact on mapping accuracy.

Figure 1 - Sirovision 3D image of the WC highwall displaying the orientation of joints mapped using Sirovision's SiroJoint

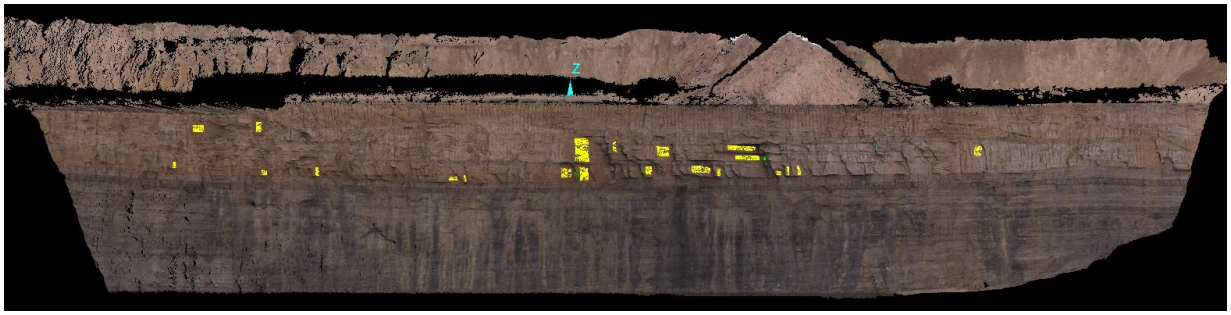

Figure 2 - I-site scan of WC highwall displaying joints mapped using Maptek's I-site Studio

Based on the CAD functionality built in to I-site Studio, joint planes were much easier to identify using Maptek's processing software, when compared to the more cumbersome SiroJoint in which the 3D image

is not able to be rotated, only zoomed in and out. This rotating feature in I-site Studio was particularly advantageous for mapping joint sets orientated at oblique angles to the highwall face. These joint sets were often not as readily identifiable when viewing the 3D image in a fixed plane view as in SiroJoint - see Figures 3 and 4 noting the significant increase in the number of joints mapped in I-site Studio compared to the number of joints mapped in SiroJoint.

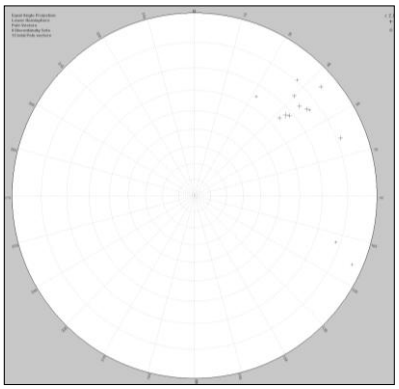

Figure 3 - Equal angle stereonet projection of SiroJoint mapped joints as displayed in Figure 1

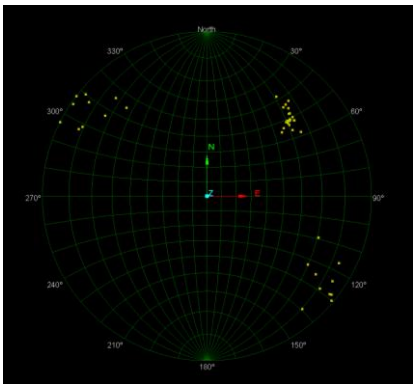

Figure 4 - Equal angle stereonet projection of I-site mapped joints as displayed in Figure 2

To directly compare the outputs of both methods, six of the larger and more readily-discernible joint planes were mapped using both SiroJoint and I-site Studio - see Figures 5 and 6. When these planes were plotted on a stereonet, appreciable discrepancies in joint dip were readily identified - see Figures 7 and 8.

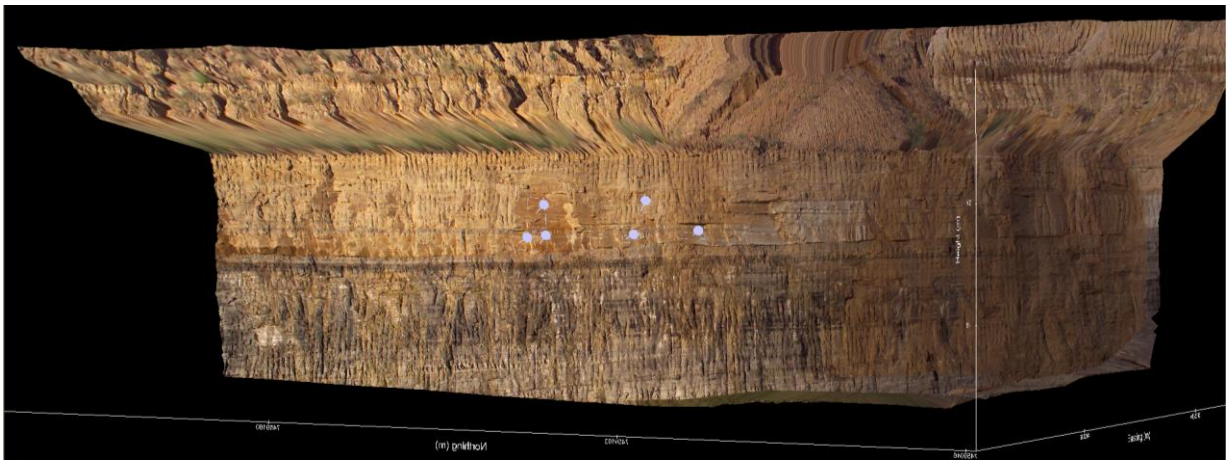

Figure 5 - SiroJoint mapped joints for direct comparison between Sirovision output and I-site Studio output

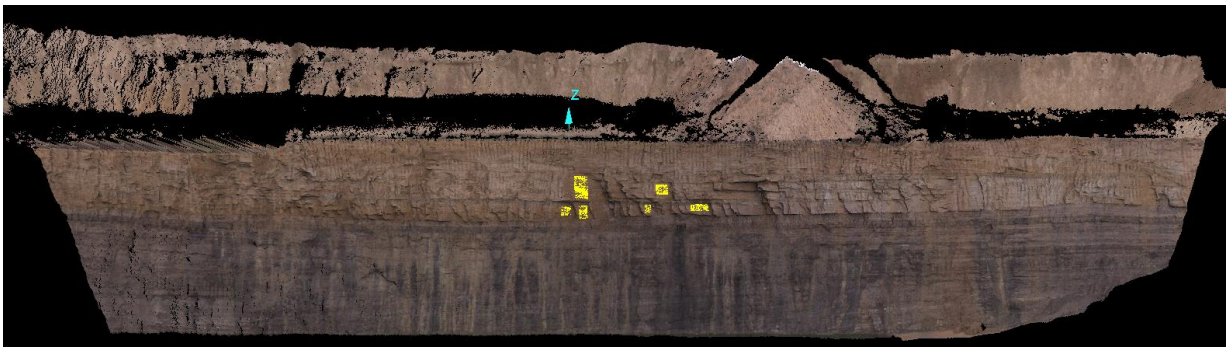

Figure 6 - I-site Studio mapped joints for direct comparison between Sirovision output and I-site Studio output

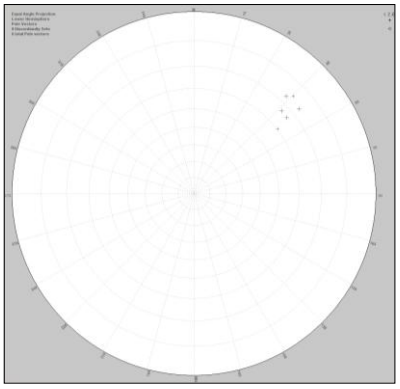

Figure 7 - Equal angle stereonet projection of SiroJoint selected joints

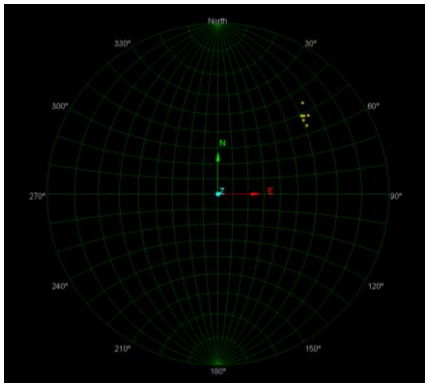

Figure 8 - Equal angle stereonet projection of I-site Studio selected joints

To investigate the joint dip orientation discrepancies, the two 3D images were overlain to compare their georeferenced position. From this comparison it was found that the images spatially correlated well to the left (north) of the highwall image, however deviated in spatial orientation to the right (south) of the highwall image - refer to Figure 9. Deviations of nearly one metre were observed when viewing the images in cross-section view - see Figures 10 and 11 (I-site scan is displayed in grey; Sirovision 3D image surface is displayed in pink).

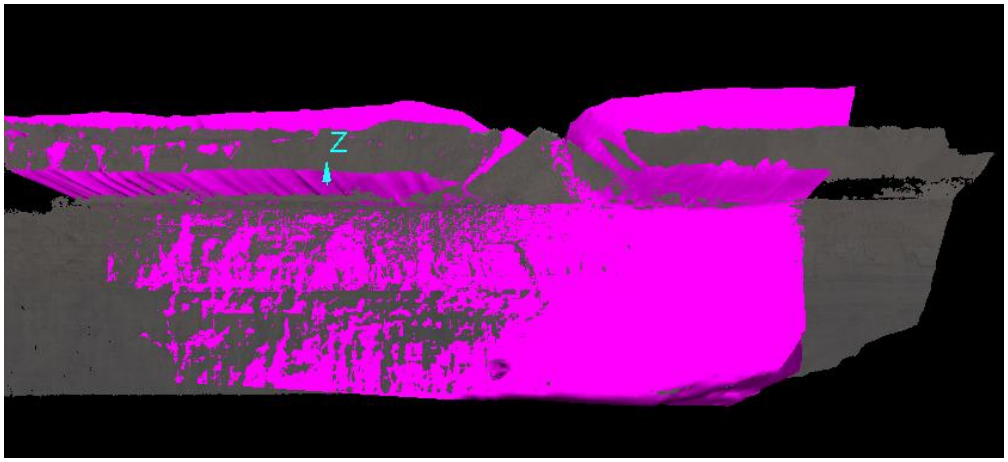

Figure 9 - Overlay of I-site scan (grey) and Sirovision 3D image surface (pink) showing the variation in spatial location of the mapped surfaces

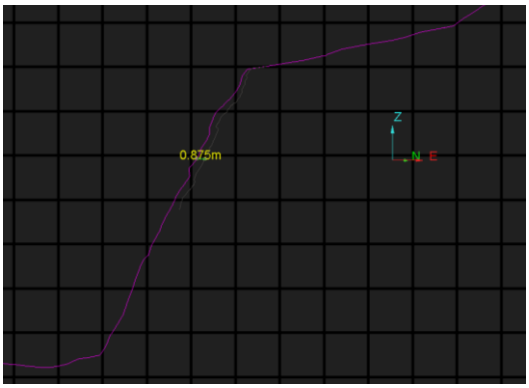

Figure 10 - Spatial variation between I-site scan 3D image/surface and Sirovision 3D image

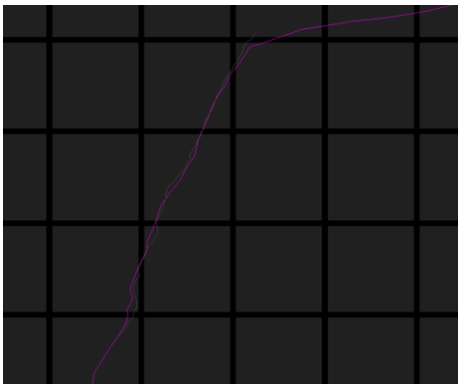

Figure 11 - Variation in surface resolution between I-site scan 3D image/surface and Sirovision 3D image

Appreciable deviations in joint dip were also observed when comparing SiroJoint manually-selected joint plane orientations with SiroJoint auto-searched joint plane orientations, where two planes were auto-mapped by SiroJoint for the one plane manually identified and traced - see Figure 12.

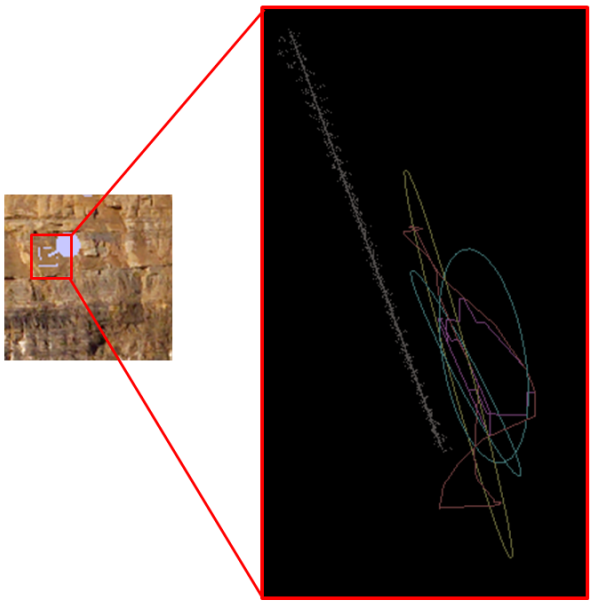

Figure 12 - Variation in mapped joint strike and joint dip using manual versus automatic joint surface delineation
Yellow dots = I-site selected data points on identified joint surface;
Grey polygon = I-site fitted plane to user-selected data points
Red polygon shell = SiroJoint manually traced joint surface (node);
Yellow circle = SiroJoint auto-fitted disc to manually selected plane
Magenta polygon shell = SiroJoint auto-search joint surface (node);
Blue circles = SiroJoint auto-fitted disc to auto-selected plane.

DISCUSSIONS

Both Sirovision (photogrammetry) and the I-site (laser) scanner provide the geologist/geotechnical engineer the necessary data to map highwall joints, fractures, and faults, however there are several differences in the acquisition and processing requirements of each method. These are summarised below:

- The acquisition time for Sirovision and an I-site scan data are very similar. However, despite taking approximately the same time to photograph/scan the same area, the acquisition process of taking digital photographs for use in Sirovision is much more physical than that required by the use of a laser scanner;
- Integrity of laser scan data can be reviewed in the field. This is unlike Sirovision data where errors are generally not identified until back in the office during the processing stage;
- Impact on production is reduced when acquiring data by laser scanners, as this method can be completed from the LW bench and generally does not require access into the base of the pit to place (and survey) control points as required by Sirovision. For this reason also, the acquisition of structural data by laser scanners may be argued as safer as there is less potential for interaction with an active pit with this process than with Sirovision;
- Processing of laser scan data is much quicker and less cumbersome than the Sirovision v4.2 process (i.e. requires only one program to process the data unlike the three required for processing Sirovision 4.2 data); and
- Sirovision has the attraction of a significantly lower initial hardware and software set up cost. However, the higher price associated with the versatility of the I-site scanner as a multi-purpose survey tool can often be justified by mine sites as it will not be used solely for highwall mapping.

In terms of output data, several differences can also be identified between the two methods. The most appreciable differences are found in the following areas:

- Mapped joint orientation;
- Spatial Referencing;
- 3D image surface resolution;
- Joint delineation in mapping software;
- 3D image clarity.

Mapped joint orientation / spatial referencing / 3D image surface resolution

Prior to this study it was believed that despite the differences in the acquisition and processing requirements between the two methods the output data from both programs was comparable. This study however identified variations of up to 5° in joint strike and 15° in joint dip between the two methods for the same joint surfaces mapped (refer to Figures 7-8). For kinematic analysis, ±5° deviations in joint orientations are considered an acceptable deviation to the true strike direction, however a ±15° deviation in dip is considered intolerable for both safety and economic considerations. These variations were discussed in detail with representatives from both CSIRO/CAE and Maptek, with both companies asserting the robustness of the algorithms built into their respective programs to delineate joint strike and joint dip. It is suggested that these variations are attributed to survey control, density of data points produced by each method, as well as the algorithms built in to the software for fitting a plane to an identified joint surface.

In terms of survey control contributing to differences in joint dip, when the laser scan surface was overlayed against the georeferenced Sirovision 3D image, deviations in spatial orientation were readily identified - see Figure 9. To measure the extent of the variation, the two 3D images were viewed in cross-section where the difference in spatial location was deemed the largest. The two 3D images were measured to be offset from each other by nearly one metre - see Figure 10. If multiple stereo pairs were joined together, a possible explanation for this discrepancy is 'data wandering', if only one end of the mosaic was georeferenced using the minimum three control points. However, as only one set of 3D images were captured for this comparison, this explanation has been ruled. Instead, based on the dual survey control and survey acquisition methods involved with the laser scanner, it is considered that the laser scan is the more accurate of the two methods. In addition to dual survey control required by the 8800, this conclusion is also based on a comparison of the two 3D images in cross-section view where 'good' spatial correlation between the georeferenced images was observed (i.e. on the left (northern) side of the highwall images). This comparison revealed greater 'definition' of the highwall face in the I-site produced 3D image, compared to a 'smoother', less-detailed surface produced by the Siro3D 3D image - see Figure 11. This increase in detail is attributed to the spatial resolution (approximately 5 mm point cloud spacing) able to be captured by the 8800 scanner. The observed increase in 'detail' in the I-site scan is perceived to reduce spatial deviations to the true joint orientation, whereby the more data points the program has to fit a plane, the less divergence from the true orientation of an *in situ* joint plane to the orientation of a fitted plane is observed, when in-built software 'averaging' algorithms are applied.

The hypothesis that the software algorithms may also be the source of joint orientation variance is based on direct comparisons of SiroJoint manually-mapped joints to SiroJoint automatically-searched mapped joints, whereby the orientation of planes fitted by an auto-search of joint planes differed appreciably from those planes that were manually selected - see Figure 12.

Joint delineation

The mapping of joint planes oblique to the exposed highwall were more readily discernible using the CAD-processing functionality of I-site Studio, compared to the more restrictive view functions in SiroJoint. Based on this study, it is perceived the cumbersomeness of SiroJoint to prohibit the centre of rotation to vary from the centre of the 3D image may lead to the oversight and/or omission of joint planes oblique to the exposed highwall being accurately mapped in spacing and persistence, as was identified in this study (see Figures 1-4).

3D Image clarity

In terms of 3D image clarity, Sirovision produced a superior quality image compared to the I-site scan (compare Figures 1-2). This difference is attributed to Sirovision's use of a digital SLR camera to obtain a photographic image, compared the use of a rotating vertical camera by I-site. Although still not as sharp as the Sirovision image, I-site's ability to overlay the photographic surface onto scanned data points mitigated any shortcoming of a lower-resolution image.

CONCLUSIONS

From in-house, on-site trials, it was concluded that laser scanner (Maptek 8800 I-Site Scanner v3.86x) methods of highwall mapping for delineating joints, fractures, and faults, for use in slope stability analysis is superior in terms of data accuracy when compared to photogrammetry (Sirovision v4.2).

Where the methods differ markedly in acquisition and processing requirements, it was found that the laser scanner had the fastest processing and least physical demands when compared to Sirovision, and was furthermore found to be the more accurate of the methods where deviations of up to 15° in joint dip were observed between the two methods. Joint planes, oblique to the exposed highwall, were also more readily discernible using the CAD-processing functionality of I-site Studio, where the same joint planes were less distinguishable using the more cumbersome SiroJoint interface.

Where there were initial apprehensions about the ability of the I-site scan to capture the necessary point cloud density to accurately map joint planes, these concerns were quickly alleviated be selecting a minimum 8-intensity setting on the scanner. At this setting, the returned point cloud spacing was less than 0.005 m providing a more than sufficient point cloud density for the purpose of mapping joints and faults in the exposed wall. It is therefore recommended that all laser scans acquired for the purpose of highwall mapping be set to a minimum of 8-intensity when the scanner is set-up on the lowwall side (i.e. approximately 50-80 m away from the scanned highwall). Where the scan is to be obtained from a distance greater than 80 m, the scan should be set to 16-intensity to ensure sufficient point cloud density for accurate joint mapping.

Although, the 3D image created by Sirovision was found to be of superior quality and resolution to the 3D photo taken by I-site and overlain on the laser scan, this study has concluded the preference of laser scanners for highwall mapping purposes. Photogrammetry should not however be disregarded as means of structural data acquisition, as there may exist pit conditions where laser scanners are not able to be set up, leaving photogrammetry as the only other acquisition method available for collecting mass joint data quickly and safely.

At all times however, any data acquired by photogrammetry or laser scanner methods should be 'ground-truthed' using a compass in order to confirm the accuracy of digitally acquired data.

Future comparisons between the Maptek I-site 8800 laser scanner and photogrammetry (using Sirovision 5) are planned when PC specifications and camera limitations are resolved. Line-survey measurements will also be included in future comparisons to provide the 'ground-truthing' discussed above.

REFERENCES

CAE Sirovision, 2012, CAEMining, Perth, accessed October 23 2012, <http://sirovision.com/>.

Canon Digital Photo Professional 2011, Middlesex, accessed October 23 2012, <http://www.canon-europe.com/support/software/dpp/>.

DIPS 2012, Rocscience inc, Toronto, accessed October 23 2012, <http://www.rocscience.com/products/1/Dips>.

Maptek, 2012, Maptek Pty Ltd, Adelaide, accessed October 23 2012, <http://www.lc.unsw.edu.au/onlib/ref_elec1.html#elec1>.

THE ECONOMICS OF EXTENDED PRE-STRIP STRIPPING

Retief Nel and Mehmet S Kizil

ABSTRACT: Waste stripping involves the most costly processes for any given open cut coal mining operation, As such, it is fundamentally important to optimise material scheduling and the sequences involved in excavating and hauling waste material. In situations constrained by fleet capacity and productivity. The only viable option to potentially yield further cost gains is to modify current mining methods. In the case of many Australian coal mines, truck-shovel systems excavate the initial overlying waste, known as pre-strip, down to a predetermined level known as the pre-strip horizon. This paper provides and analyses a simulation model to derive the optimal strip width for pre-strip activities. Case study data obtained from an established leading coal producer in the Bowen Basin was implemented into a pit simulation model to assess the effect of pre-strip width on the overall pit economics. Pre-strip widths of 60 to 120 m in 10 m increments were assessed whilst keeping dragline and coal stripping widths constant at 60 m. The simulation revealed the potential for cost reductions to be significant when a 90 m pre-strip case is adopted as opposed to the base case of 60 m. The paper presents the simulation findings for each case and discusses the key drivers behind the cost variations for each case.

INTRODUCTION

A major operation in the recovery of any coal seam by surface mining methods is the removal of the overburden (Fidler, 1979). Of the available surface mining methods, strip mining is arguably the most common method used to mine coal in Australia. Pre-strip by definition is the removal of any waste material not considered to be valuable. In surface coal mines, pre-strip often refers to the initial material that is removed to facilitate another digging process and is distinctly different from subsequent overburden removal as a continuous process in the recovery of coal (Commissioner of Taxation, 1994). Current practice involves a pre-strip pass by a truck-shovel fleet, which exposes a 60 m wide interburden bench suited for dragline excavation (Figure 1).

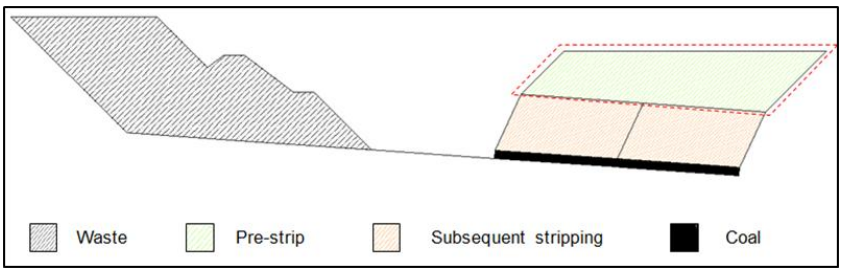

Figure 1 - Pre-strip compared to subsequent dragline stripping (After Commissioner of Taxation, 1994)

In some cases, extended pre-strip passes have been taken up to 120 m in width. Extended pre-stripping allows truck-shovel operations to use double-side loading, which is known to be more productive. Taking an extended pre-strip pass increases the interburden bench width, which provides more room for drill and blast activities, including on-bench loading of explosives. The downside to extended pre-strip passes is the cost associated with additional material movement. More waste material is moved in the short term with little or no increase in coal recovery and associated revenue.

Aside from the known productivity increase realised with wider pre-strip passes, there is a fundamental lack of understanding of the net economical effect these extended passes have on an operation's bottom-line. A Net Present Cost (NPC) evaluation was conducted on a range of pre-strip widths to derive this net economical effect for a typical pit at a multiple seam surface coal mine. In completing the evaluation, data was obtained from an established surface coal mine within the Bowen Basin in Queensland to derive a generic pit model and pit design. The pit model simulated each pre-strip production case using volumes generated for the study pit.

School of Mechanical and Mining Engineering, The University of Queensland, Brisbane, QLD, Australia, m.kizil@uq.edu.au, Tel: 07 3365 4499

PRE-STRIP MINING

Dragline stripping

Draglines are large single-bucket stripping machines and are extensively used for direct side casting of waste material (Atkinson, 1992). The most common form of dragline is the walking dragline which has emerged as the dominant overburden removal machine in surface mining operations in Australia (Mirabediny and Baafi, 1998).

Although used almost exclusively for overburden and interburden removal at established surface mines, draglines have been used in initial boxcut excavation and pre-stripping scenarios. The reason being that draglines can be used for a wide variety of rock types and strengths however rely on blasting to fragment competent rock. In addition to their ability to dig multiple rock types, a number of digging sequences can be employed depending on the seam dip, overburden depth and economic constraints of the operation.

Truck-shovel stripping

Truck-shovel systems are better suited to more complex geological conditions than its stripping counterparts with the ability to remove overburden in deeper, uneven and multiple seam situations (Holfeltz and Kunz, 1983). Being one of the preferred methods of overburden removal for most deposits, truck-shovel systems excavate a number of passes establishing benches whenever a certain depth of cut is achieved. The conventional method of stripping overburden with shovels or excavators is through exposing the coal seam in narrow strips similar to that of dragline methods (Porterfield, 1973). Truck-shovel systems are usually also employed in excavating the initial box cut to initiate mining.

Scott, *et al*., (2010) suggested the main advantages of truck-shovel systems are:

- Less capital outlay then dragline systems;
- Suitable for shorter term projects;
- Better flexibility and mobility; and
- Suitable in complex geological situations.

Truck-shovel systems however, have lower production rates, higher operating costs and require more ancillary equipment than draglines (Scott, *et al*., 2010). The term truck-shovel system refers to any one of the following equipment setups:

- Trucks and electric rope shovels;
- Trucks and hydraulic excavators/shovels; and
- Trucks and front-end loaders.

Double-side loading

Double-side loading of trucks is known to be more productive in opencast mining methods. The technique involves loading a truck on either side of the shovel leading to reductions in cycle times and increases in loading productivity. Figure 2 illustrates a typical double sided loading scenario.

Double-side loading substantially improves production per shift by improving truck productivity and has been proven to reduce individual truck spotting time by 30 s (Tasman Asia Pacific, 1998).

STRIPPING CONFIGURATION

Introduction

Strip mining requires careful consideration of the pit configuration to ensure waste movement can occur on schedule and at minimum cost. Stacked and offset pit configurations are commonly used in surface coal mines across Queensland. The study assumes an offset pit configuration to ensure some parallels can be drawn between the case study operation and the study pit.

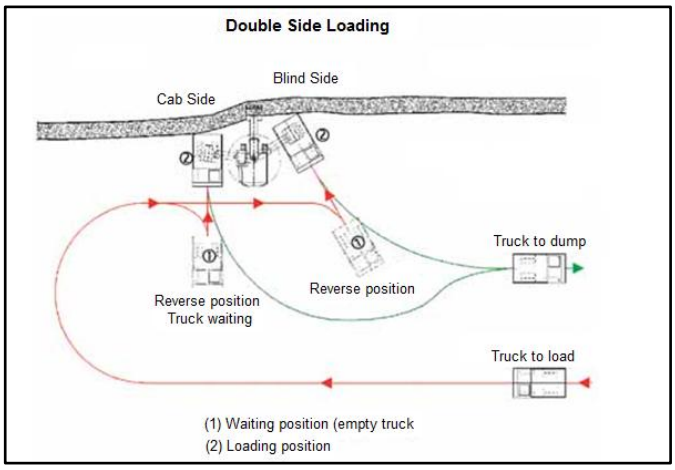

Figure 2 - Double-side truck loading (Fiscor, 2007)

Double dragline pass offset

Due to their operating cost efficiency, draglines commonly excavate the waste passes immediately overlying the valuable coal seams. As such, deep pits containing two coal seams are usually mined using a pre-strip pass and two dragline passes. The first dragline pass excavates the overburden overlying the upper coal seam with the second dragline pass excavating the interburden and exposing the lower coal seam. These two passes require some form of offset to ensure operational safety and flexibility. The offset applied to these passes most commonly amounts to a full dragline strip width plus an additional distance to allow for efficient drilling and blasting of the bench. Figure 3 illustrates the indicative dragline bench offsets applied in the study pit.

Pre-strip pass offset

A pre-strip pass offset is also required in many open cut strip mines. The pre-strip offset performs a similar role as the dragline pass offset in that it facilitates the efficient drilling and blasting of the subsequent bench. The offset also allows for safe pre-strip digging away from the free dragline bench highwall. Figure 4 shows the typical pre-strip offset applied in the study pit design.

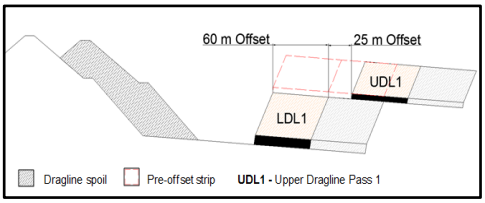

Figure 3 - Indicative dragline pass offset for the study pit

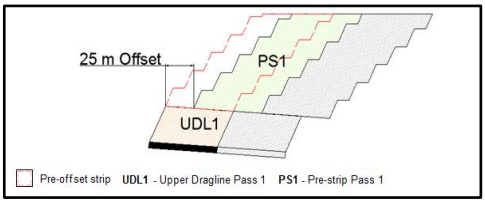

Figure 4 - Indicative pre-strip pass offset for the study pit

Study pit final strip configuration

Combining the two offsets together results in the final pit configuration which was adopted for the study pit. Figure 5 illustrates the final pit configuration which was used in designing the study pit.

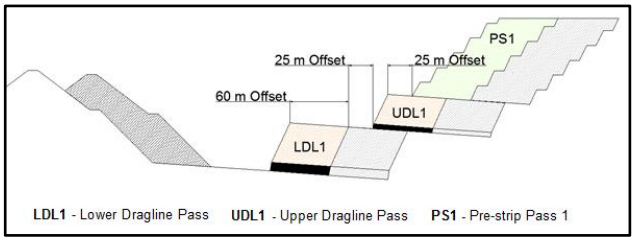

Figure 5 - Indicative final strip configuration

GENERIC PIT MODEL

A generic pit design and model was created to facilitate the evaluation of each pre-strip production case. A key driving force behind the use of a generic model over the actual pit layout and design of the case study mine was the need to generate results applicable to various mining situations. The established case study mine has a very unique pit setup and as such the evaluation implemented only the generic strata attributes, mining methods, machine productivity and costs currently in use at the site. In completing the generic pit model, data was generated using a Microsoft Excel™ pit configuration tool which generated accurate strip volumes based on user input of the basic pit layout and geotechnical considerations. It was deemed necessary to also design the pit and validate the results generated through the use of the Microsoft Excel™ tool. The study evaluated 20 future strips and relied on historical productivity and cost data from the case study mine. Table 1 outlines the key design variables used in designing the study pit (Figure 6).

Table 1 - Study pit design variables

Item	Unit	Value
Dragline strip width	(m)	60
Pre-strip width	(m)	60 - 120
Lower dragline bench height	(m)	40
Upper dragline bench height	(m)	30
Dragline highwall angle	(˚)	65
Pre-strip bench height	(m)	15
Pre-strip bench angle	(˚)	65
Upper coal seam thickness	(m)	5
Lower coal seam thickness	(m)	9
Coal seam dip	(˚)	4
Coal seam highwall angle	(˚)	80
Strip length	(m)	1000
Initial strip depth (Topography to lower seam)	(m)	130
Dragline dig depth (In-pit bench elevation)	(m)	45
Dragline dump height	(m)	40
Spoil lift 1 repose	(˚)	45
Spoil lift 2 repose	(˚)	37
Spoil berm	(m)	10
Max. pre-strip dump height above topography	(m)	60
Max. ramp grade	(%)	10

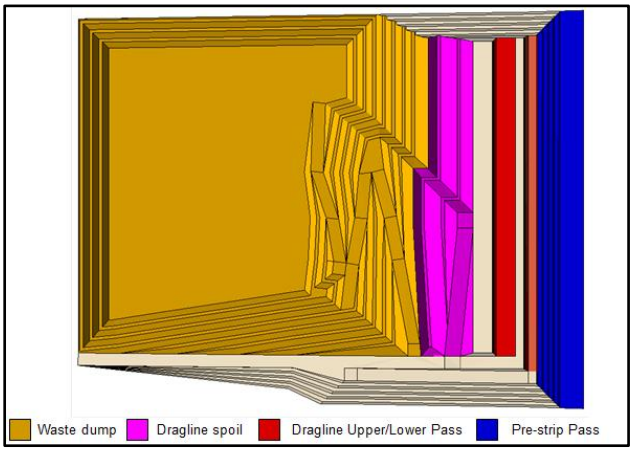

Figure 6 - Study pit design and layout

With the focus of the study being on the cost attributable to pre-strip activities, all subsequent mining activities were held constant for each pre-strip production case. This ensured that any variance in NPC

was directly related to the increase in material moved and changes in productivity realised in the truck-shovel system.

One key assumption made in completing this project was that the operation had multiple active mining areas or pits. As such, truck-shovel fleets were able to relocate to different pits when a certain pass was completed ahead of schedule. With any operation, it is preferred to defer costs as far as feasibly possible into the future whilst receiving the maximum revenue in the current period. This is facilitated through the relocation of the truck-shovel fleets. Taking an extended pre-strip pass effectively exposes a free dragline strip in the future at which point further pre-strip stripping becomes unnecessary at that point in time to sustain the current dragline path.

In essence, if the truck-shovel fleet were to continuously excavate its strips until it completes its final strip, the amount of dragline bench exposure would far exceed the required amount, thus increasing unnecessary upfront cost. Hence, as the fleets relocate to another pit, a gap in the pre-strip schedule for the focus pit is created which occurs when a free dragline strip is exposed. This free-strip essentially equates to the benefit perceived from extended stripping with the cost equating to the additional upfront waste stripping.

Pre-strip production cases

The base pre-strip production case of 60 m was extended in 10 m increments to form six additional extended cases. Figure 7 outlines the pre-strip configurations for each of the production cases evaluated in the study.

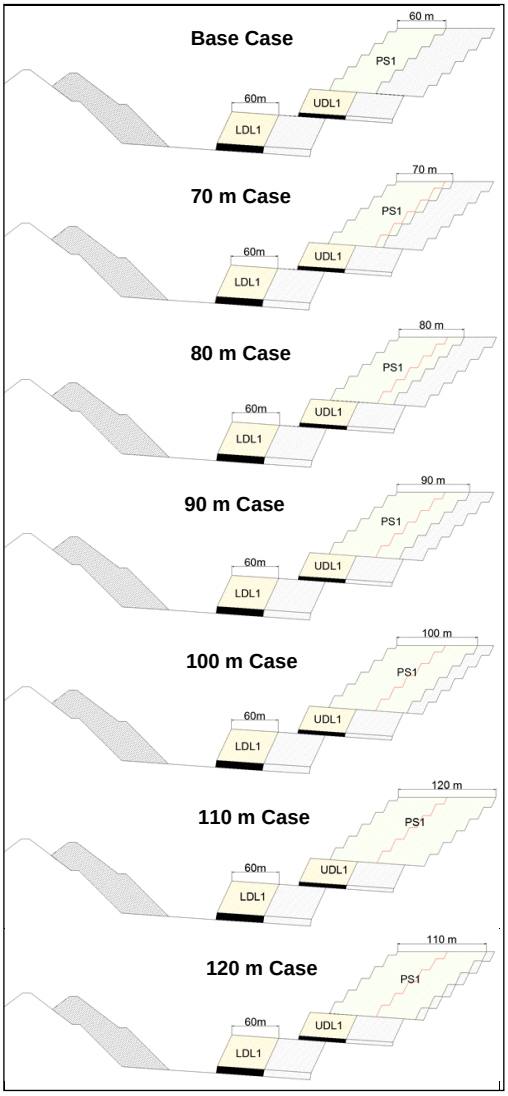

Figure 7 - Pre-strip production cases

Free-strip benefit

Summarising the number and timing of each free-strip was essential in accurately assigning delays in the scheduling and to ultimately capture the intrinsic discounted value of the pre-strip production gaps. Table 2 summarises the frequency and timing of free-strips under each of the production cases.

Table 2 - Free-strip distribution

UDL Strip Number	Pre-strip Production Case (m)						
	60	70	80	90	100	110	120
1							
2							■
3				■	■	■	
4			■				■
5					■	■	
6				■			■
7		■				■	
8			■		■		■
9				■		■	
10					■		■
11						■	
12			■	■			■
13					■		
14		■				■	■
15				■	■		
16			■			■	■
17							
18				■	■	■	■
19							
20			■		■	■	■
Number of free strips	0	2	5	6	8	9	10
■ Free-strip		UDL	Upper Dragline Pass				

PRODUCTIVITY AND COST CONSIDERATIONS

Case study fleet benchmarking and cost

Productivity and cost estimates were obtained from an established leading coal producer in the Bowen Basin. Data was collected for the year commencing January 1st, 2011 and involved both individual machine and fleet productivities. Dragline stripping productivity was estimated to be 2000 BCM/h after assigning applicable delays and a rehandle factor of 65.5 % which was determined from dragline section analysis. Dragline cost was estimated to be A$1.7/Prime BCM.

The study assumed a constant mining fleet for each production case over the nominal 20-strip mine life. For this reason, pre-strip and coal mining fleet productivity was constrained by the loading unit productivity. Figure 8 illustrates the loading unit productivity assigned to each digging unit with EXD, SHD and SHE referring to excavator, hydraulic shovel and rope shovel respectively.

Drill and blast rates and costs were estimated to closely match the case study operation with a constant A$0.7/Prime BCM being applied to all clearing, drilling and blasting activities. On-bench loading of explosives and blast preparation activities were assigned a nominal duration which was held constant for each production case.

Coal mining was assigned a productivity level of 1100 BCM/h and a unit cost of A$6.8/t hauled. Truck-shovel stripping was determined for the base production case. Excavator stripping used in excavating the initial tertiary material and the final wedge exposing a level dragline bench was assigned a productivity of 1200 BCM/h. The base production case involved a shovel productivity of 2000 BCM/h. The total truck-shovel system stripping cost for the base case was estimated to be A$3.1/Prime BCM.

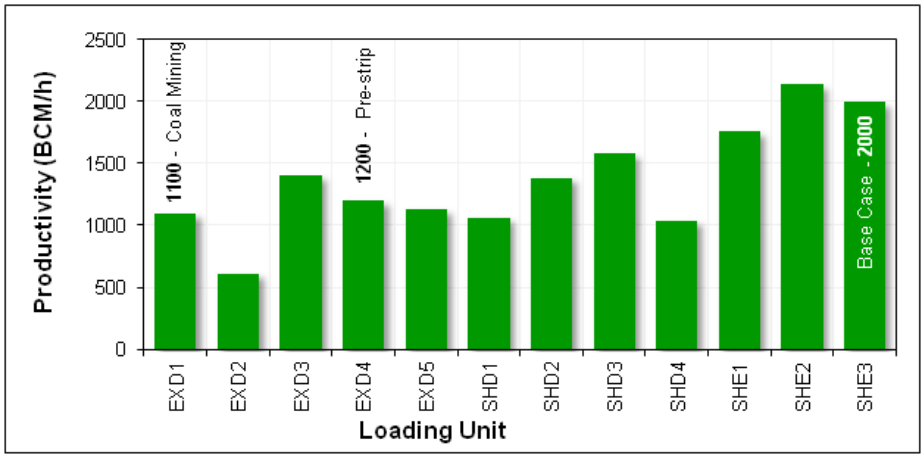

Figure 8 - Loading unit productivity analysis

Productivity and cost escalation

Indicatively, increasing the pre-strip width yielded different shovel productivities and unit costs. Productivity increases for the shovel were attributed to the transition from single-side to double-side loading and the increase in manoeuvrability and flexibility seen in wider pre-strip benches. It was assumed that unit cost was negatively correlated with productivity. This was due to constant trucking numbers for each pre-strip production case and the elimination of machine modifications.

All other unit costs applied in the base case were held constant for each pre-strip production case. Although truck-shovel unit costs reduced incrementally with increases in pre-strip width, an escalation factor was required for ancillary activities cost.

A preliminary haulage analysis yielded marginal incremental increases in cost and as such was excluded from the study. The net result of the decreasing shovel cost and increasing ancillary cost yielded an overall increase in truck-shovel system cost when pre-strip width was increased (Figure 9).

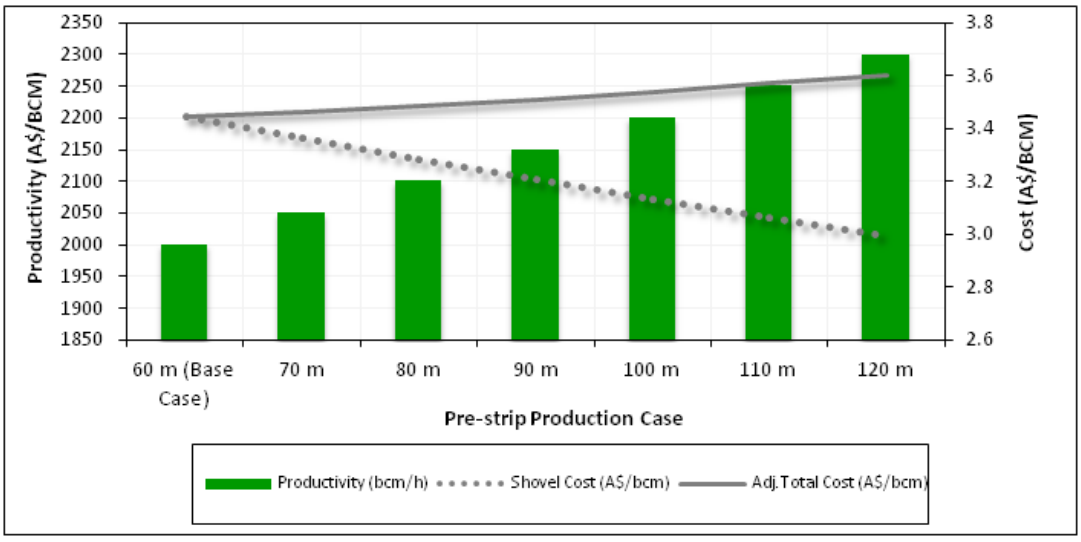

Figure 9 - Shovel unit productivity and cost escalation

SIMULATION MODEL

Pit configuration tool

A suitable Microsoft Excel™ tool was created to efficiently generate waste and coal volumes for each of the production cases. The model generated accurate volumes based on user inputs and complex trigonometry and allowed for a large number of scenarios being tested in a relatively timely manner.

Valuation model

The final stage in the project involved the economic modelling of the material movements for each production case. As such, a NPC valuation model was created in Microsoft Excel™ to accurately capture the cost-benefit of each production case. The model utilised the material movements scheduled using Microsoft Project™.

Material scheduling

The cost evaluation involved the use of Microsoft Project™ to schedule all material movements for the study pit. The scheduling strategy involved breaking the pit into equally spaced segments known as blocklines. These blocklines were spaced 100 m apart and facilitated the accurate scheduling of each activity from initial tertiary excavation to the mining of the lower seam coal (Figure 10).

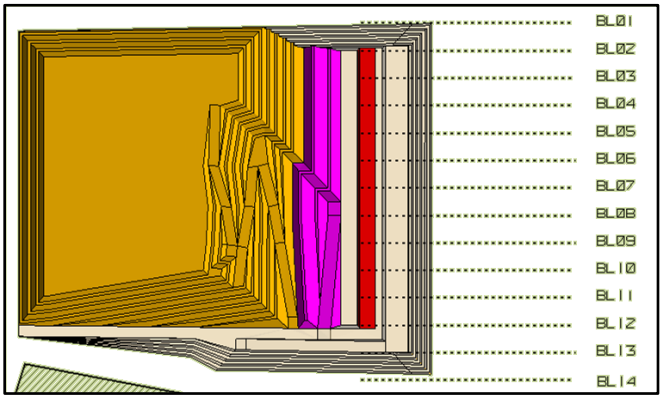

Figure 10 - Study pit blocklines

To create manageable schedules, the holistic mining operation was grouped into a number of key tasks or activities. These activities were chosen on the basis of their criticality to the overall mining process and are shown in Table 3. Each of the key activities was assigned the total number of strips required as sub-tasks which in turn were assigned blocklines as sub-tasks.

Table 3 - Scheduling tasks

Scheduling Task Hierarchy	Machine/Fleet	Reason
Upper pre-strip	Truck-excavator	Remove initial 10 m tertiary material
Middle pre-strip drill and blast	Drill and blast	Fragment shovel material
Middle pre-strip	Truck-shovel	Remove blasted material
Lower pre-strip	Truck-excavator	Remove wedge above upper dragline pass
Upper dragline drill and blast	Drill and blast	Fragment upper dragline pass material
Upper dragline	Dragline	Remove blasted material
Upper coal drill and blast	Drill and blast	Fragment coal prior to removal
Upper coal mining	Truck-excavator	Removal of fragment coal
Lower dragline drill and blast	Drill and blast	Fragment coal prior to removal
Lower dragline	Dragline	Remove blasted material
Lower coal drill and blast	Drill and blast	Fragment coal prior to removal
Lower coal mining	Truck-excavator	Removal of fragment coal

Importing the scheduled tasks into the Microsoft Excel™ models allowed for intensive data modelling and analysis. The first area of focus was the overall pre-strip material movement for each case. Figure 11 shows an example of the cumulative pre-strip waste production of the 90 m production case (the Best Case) compared to the base case.

The drill and blast material movement formed a key component of the study since additional pre-strip stripping is directly related to the amount of blasting required for efficient digging of the shovel.

The dragline material movement, although necessary to effectively schedule the pre-strip activities, falls outside of the study scope and as such has been excluded. Similarly, coal movements were constant for each production case and have not been included in this paper.

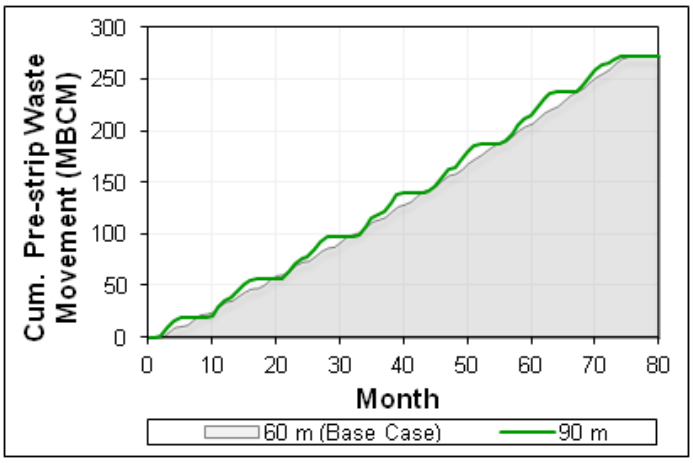

Figure 11 - Cumulative pre-strip production of 90 m production case compared to the base case

ECONOMIC EVALUATION

Cost benefit

The main aim of the project was achieved through the determination of the cost-benefit of extended pre-strip stripping. The different pre-strip production cases yielded variable NPCs with two cases yielding a lower cost than the base production case. Figure 12 illustrates the final outcomes of the evaluation models generated for each production case.

Setting the base case NPC to zero yielded the present cost variance of each case (Figure 13). The results suggest that a net saving of A$8.4 million is achievable through modifying the pre-strip width to 90 m for the life of the schedule. Marginal savings were also potentially available when a 110 m pre-strip width is adopted. The remaining extended pre-strip production cases yielded a NPC higher than that of the base production case.

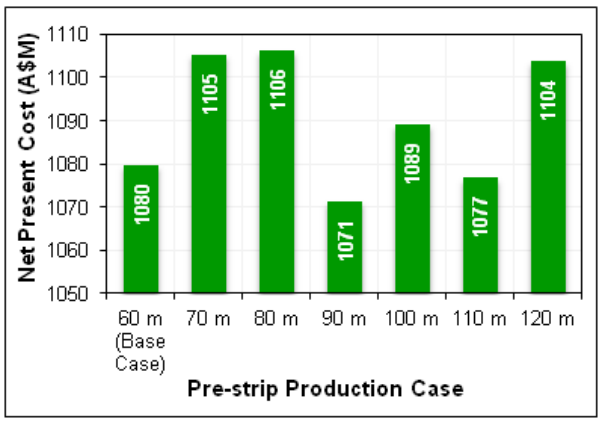

Figure 12 - Total net present cost per production case

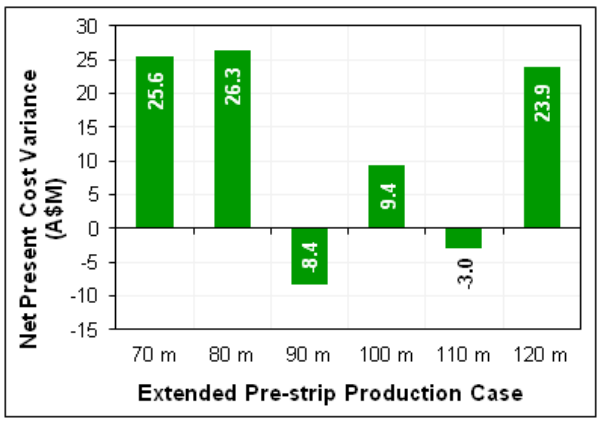

Figure 13 - Net present cost variance to base case

Annual cost variance

Discounted cash flow analysis yielding a single NPC was insufficient in explaining the implied benefit or cost associated with extended waste stripping. As such, an analysis was conducted targeting annual cost implications associated with the additional waste stripping seen in the extended pre-strip production cases. Figure 14 illustrates the annual cost variance to the base case when a 70 m pre-strip production case was adopted.

Cost variance for a 70 m production case appeared sporadic in nature with cost reductions seen in years two, five and seven. Similarly, Figure 15 illustrates the annual cost variance to the base case when an 80 m pre-strip width was adopted. An 80 m production case yielded a large increase in cost in year two with a diminishing cost saving from year three onwards. Figure 16 shows the annual cost variance to the base case when a 90 m pre-strip strip was implemented. Implementing a 90 m pre-strip strip width resulted in an incremental increase in cost over the base case for the first three years. Year four onwards realised significant cost reductions. Figure 17 shows the annual cost variance to the base case of a 100 m pre-strip production case.

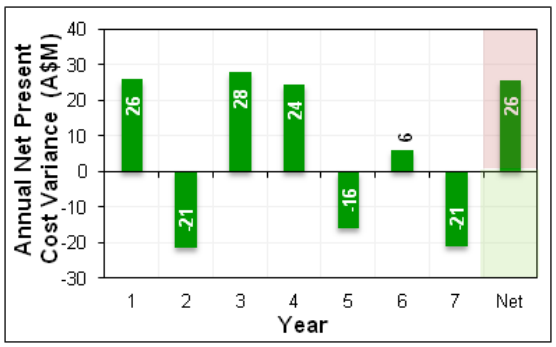

Figure 14 - 70 m production case annual cost variance

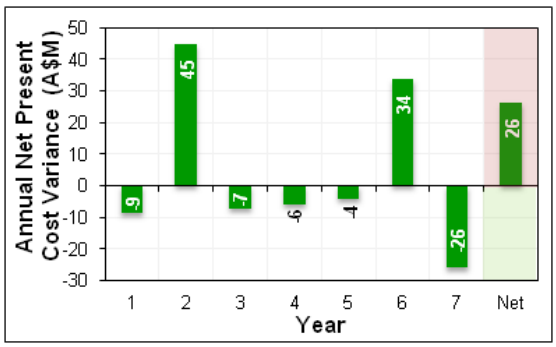

Figure 15 - 80 m production case annual cost variance

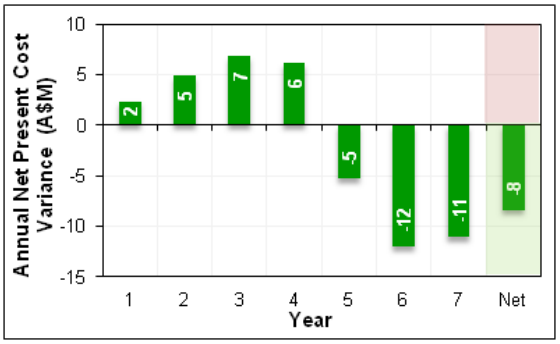

Figure 16 - 90 m production case annual cost variance

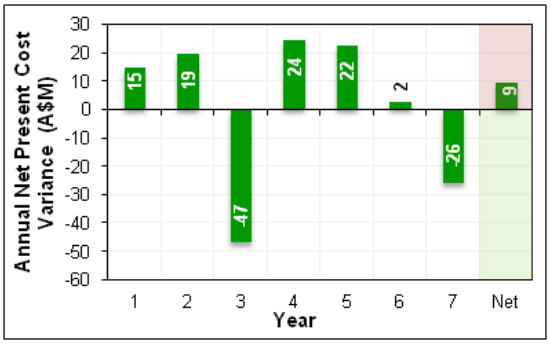

Figure 17 - 100 m production case annual cost variance

Under a 100 m pre-strip production case, a large cost reduction was evident in year three when compared to the base case. When considering the 110 m pre-strip production case, cost reductions were possible in years two, five and seven resulting in a net cost saving of A$3 million over the life of the schedule (Figure 18). Similarly, Figure 19 illustrates the cost variance per year when adopting the 120 m pre-strip production case. The cost variance under this production case followed a regular pattern of positive-negative fluctuation. Notably, this production case yielded the greatest magnitude in variance with an additional A$52 million of cost experienced in year three.

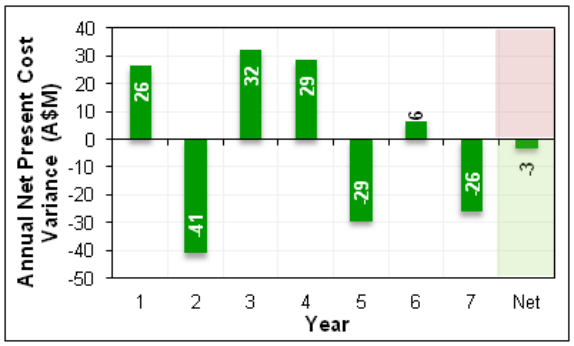

Figure 18 - 110 m production case annual cost variance

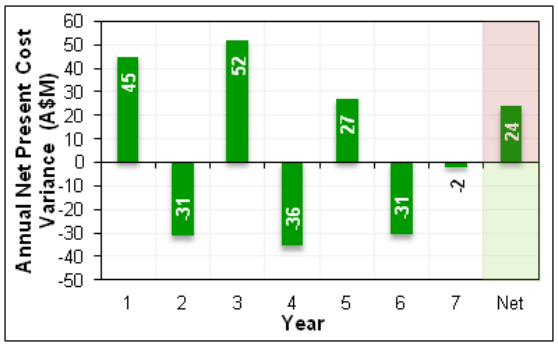

Figure 19 - 120 m production case annual cost variance

EVALUATION DRIVERS

Productivity effect

In order to evaluate the net effect that the change in productivity had on each production case NPC, the productivity effects were removed from the schedules and models to yield the NPC values in Table 4.

Table 4 - Productivity effect on net present cost

Pre-strip Production Case	NPC (A$M)	Adjusted NPC (A$M)	Productivity Effect (A$M)
60 m (Base Case)	1079.7	1079.7	0.0
70 m	1105.2	1118.9	(13.7)
80 m	1106.0	1102.5	3.5
90 m	1071.2	1055.4	15.8
100 m	1089.0	1072.8	16.3
110 m	1076.6	1071.4	5.2
120 m	1103.6	1111.5	(7.9)

The change in productivity from the base case to the 70 m and the 120 m case had an overall reducing effect on final NPC. In terms of the 70 m case, only two free-strips are realised over the life of the pit with waste production continuously exceeding that of the base case. Considering that the increased productivity led to the free-strip being exposed slightly earlier in the schedule, it is clear that the reduction in NPC through increased productivity is a result of a higher weighting being applied to the free-strip benefit under the time value of money assumption. The same understanding can be applied to the 120 m production case whereby an increased productivity yields an earlier and higher weighted free-strip benefit. This concept can be easily explained through plotting the cumulative pre-strip waste variance of each case to the base case (Figure 20).

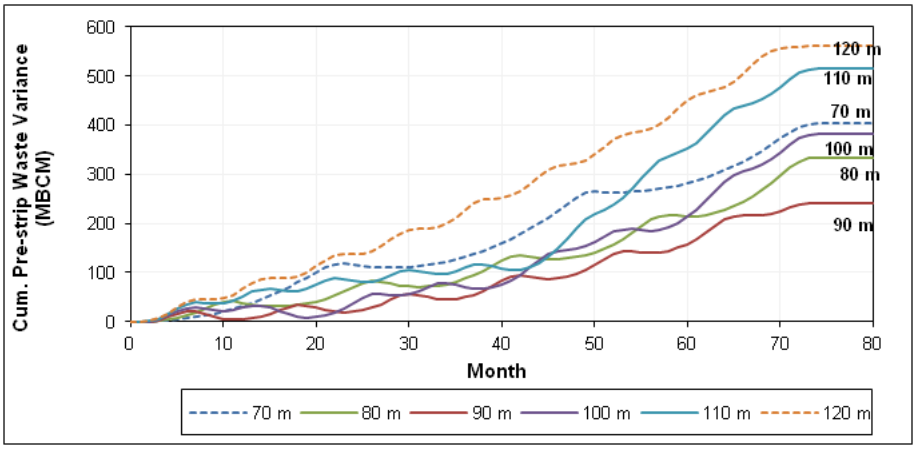

Figure 20 - Cumulative pre-strip waste variance to base case

In essence, any additional pre-strip waste moved in the extended production cases resulted in positive waste variance. Comparatively, exposing a free-strip at some point in the schedule would yield negative waste variance in that the base case would continue pre-strip stripping and the extended case will relocate and leave a gap in production for the schedule. In the case of the 70 and 120 m production cases, a large amount of positive waste variance is seen earlier in the schedule, attracting a higher discount factor and leading to an increase in NPC.

Timing effect

The timing effect on the value of money was evaluated by removing the discount factor applied to future cash flows or more simply, by setting the annual discount rate to zero. By doing this, the adjusted NPCs revealed large cost reductions when discount factors were applied (Table 5).

It is evident that the inclusion of a discount rate in the economic modelling yielded a lower NPC. This is due to the discount rate assigning a lower weighting to future cashflows, which by definition, reduces NPC. Figure 21 illustrates the timing effect compared with the productivity effect for each production case.

Table 5- Timing effect on net present cost

Pre-strip Production Case	NPC (A$M)	Adjusted NPC (A$M)	Timing Effect (A$M)
60 m (Base Case)	1079.7	1396.9	(317.2)
70 m	1105.2	1497.1	(391.9)
80 m	1106.0	1385.2	(279.2)
90 m	1071.2	1337.1	(265.8)
100 m	1089.0	1359.7	(270.7)
110 m	1076.6	1339.1	(262.5)
120 m	1103.6	1301.0	(197.4)

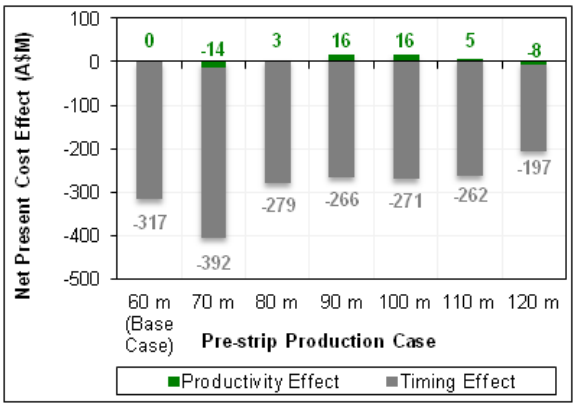

Figure 21 - Productivity and timing effects

When the base case is ignored, the timing effect trend shown in Figure 22 suggests that the amount of discounting applied in the model reduces with pre-strip width. This can be directly attributed to the increasing number of free-strips per production case. It follows that with wider pre-strip passes; more free-strips will be exposed, the time increment involved in realising those free-strips will be shorter and more weight will be applied to both additional upfront waste and subsequent free-strip production gaps.

Best production case

The 90 m pre-strip production case yielded the lowest NPC out of all of the cases in the study. Understanding why and how this result was generated formed a key component of this project. The 90 m pre-strip pass yielded a total of six free-strips over the 20-strip life with the strips being exposed in regular time intervals. Figure 22 illustrates the monthly cashflow variance for the 90 m production case when compared to the base case of 60 m.

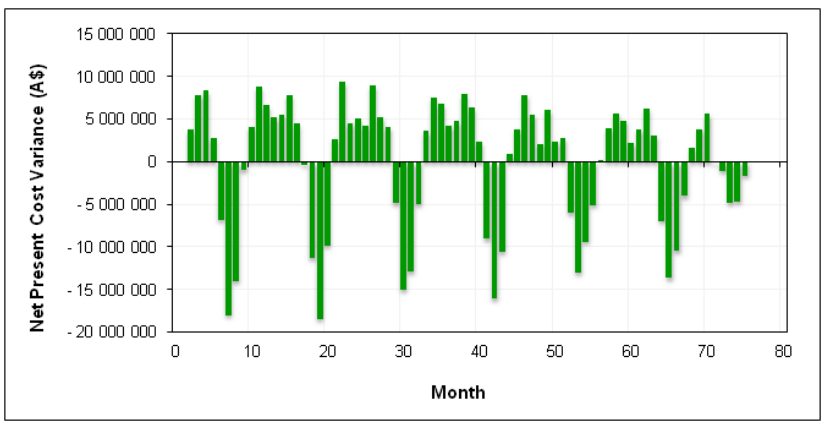

Figure 22 - Monthly cost variance for 90 m production case

The magnitude of the negative cost variance outweighs the magnitude of the positive cost variances thus leading to a reduction in NPC. The 90 m production case strikes a balance between the timing of free-strips and the additional upfront waste stripping that the other cases cannot achieve. The regularity and size of the production gap brought on by the free-strip's exposure and fleet relocation ultimately lead to significant cost reductions over the long term.

CONCLUSIONS

The evaluation suggested that a significant cost saving can be achieved when a pre-strip width of 90 m is selected. A total saving of A$8.4 million was achieved over 20 strips of minimal length. Marginal savings are also achievable when a 110 m pre-strip width is adopted.

The cost savings generated through the implementation of a 90 m pre-strip width instead of the base case was directly related to the number of free dragline strips exposed in time and the annual discount applied to cashflows. The results suggest that there is an economic trade-off point or width where the benefit of fleet relocation, through free-strip exposure, outweighs the additional costs generated in stripping waste in advance. This width has been identified as 90 m.

The project has the potential to be re-examined on a higher level with actual case study pit designs and scheduling to yield more probabilistic and specific results. Similar research has been conducted into optimum dragline strip widths however no previous economic studies have been published to evaluate different pre-strip stripping widths. Although theoretically accurate, the results presented should not be implemented at any operation without further analysis that incorporates site-specific constraints and variables.

REFERENCES

Atkinson, T, 1992. Selection and sizing of excavating equipment, in *SME Mining Engineering Handbook*, *Volume 2* (eds: H L Hartman, S G, Britton and J M Mutmansky), pp 1311-1333 (Society for Mining, Metallurgy and Exploration: Colorado).

Commissioner of Taxation, 1994. Income tax: the treatment of expenditure incurred by a mining company on the removal of overburden in open cut mining [online]. Available from: < www.law.ato.gov.au > [Accessed: 12 May 2012].

Fidler, E L, 1979. Overburden removal methods and costs associated with the recovery of western thin coal seams by surface mining, EP33144 (unpublished), Montana College of Mineral Science and Technology, Montana).

Fiscor, S, 2007. Productivity considerations for shovels and excavators, *World of Mining Professionals*, 7(1):11-12.

Holfeltz, M B and Kunz, D J, 1983. Equipment selection for burden removal associated with deep seated, thick seam coals, paper presented to SME-AIME Annual Meeting, Littleton, 19-21 October [online]. Available from: < www.onemine.org > [Accessed: 5 April 2012].

Mirabediny, H and Baafi, E Y, 1998. Dragline digging methods in Australian strip mines - a survey, in *Proceedings COAL 98 Coal Operators Conference*, University of Wollongong, 18-20 February, (eds:Baafi, Cram, Gibson, Hanna) pp 313-324 (The Australian Institute of Mining and Metallurgy). http://ro.uow.edu.au/coal/278/.

Porterfield, C W, 1973. Modern mining methods - surface, in *Elements of Practical Coal Mining* (ed: D F Crickmer), pp 514-568 (American Institute of Mining, Metallurgical and Petroleum Engineers: California).

Scott, B, Ranjith, P G, Choi, S K and Khandelwal, M, 2010. A review of existing opencast coal mining methods in Australia, *Journal of Mining Science*, 46(3):280-297.

Tasman Asia Pacific, 1998. Benchmarking the productivity of Australia's black coal industry [online]. Available from: < www.pc.gov.au > [Accessed: 6 May 2012].

IMPROVEMENTS IN TRUCK REQUIREMENT ESTIMATIONS USING DETAILED HAULAGE ANALYSIS

Patrick Doig and Mehmet S Kizil

ABSTRACT: Accuracy in haulage analysis is fundamental for reliable cost and productivity estimation. The level of detail to which haulage analysis is conducted can significantly influence these estimations. The recent advancement of computer processing has enabled a range of software to manage large datasets and run multiple and complex haulage scenarios, thus increasing the level of detail. Substantial evidence is available to affirm the benefits of detail in haulage analysis through the scope of truck cycle time and truck prediction methods. However, due to the novelty of advanced software, no literature that documents the level of detail and frequency of haul roads required for haulage analysis was found. It was therefore, the objective of ongoing work for this research project to quantify the value added through additional detail in haulage analysis, specifically, the benefit of frequently changing haul roads. To facilitate this process, nineteen haulage scenarios were analysed with varying detail. In addition, a geological model and topography was created. From the analysis conducted, a clear relationship was identified between decreasing haul road calculation frequency and inverse variance error from the mean cycle time. The research showed that performing two as opposed to a single haulage analyses for a strip can affect the calculated truck cycle times from 6% to 14%. Additionally, it was found that changes in horizontal distance from the endwall were more significant than the vertical change for the analysed strip.

INTRODUCTION

The capital and operating costs associated with truck haulage contribute heavily to the overall expenditure of a surface mine (Blackwell, 1999). The costs of truck and shovel operations alone comprise 50 to 60 per cent of the total surface mining operation costs (Nel, *et al.*, 2011). A truck can be considered as the lifeline to a loading unit. The capital cost of a truck ranges from A$1.8 to A$4.7 million for size ranges between 100 to 240 t respectively (R2Mining, 2012). Without the required number of trucks, production can be significantly impacted; a surplus of trucks however, comes at a high cost and reduces profit. Thus, truck haulage modelling is an important and complex problem for mining operations. The impacts of over or under trucked fleets can significantly influence costs, capital intensity and productivity of mining operations.

Traditionally, trucking numbers are calculated using Talpac© or other similar programs from the truck manufacturers. These methods require intense manual input and thus substantially limit the number of haul roads analysed which leads to a subsequent reduction in detail for the analysis. Increased processing capacity of computers and software development in recent years has enabled haulage models to become more detailed. Software programs such as Deswik® have automated the calculation of trucking routes. This has enabled the potential for mining and dump locations to be cut into smaller portions i.e., block and bench. From this, multiple options for haulage routes and destinations can be calculated to best achieve a predefined objective.

The benefit of additional detail in a haulage model has not been quantified. With a greater understanding of the downstream effects of detail, mining engineers can quantify the value added through detailed dump and haulage designs and make adjustments as required. This has the potential to significantly change the outputs of many mine designs and the time and cost of haulage projects. Although detail is beneficial to most projects, engineers are restricted with time and costs. Current mining practices therefore, use simple models in order to make them more transparent and auditable. Mining companies however are focusing to better align actual and maximum potential truck and shovel productive capacity (Nel, *et al.*, 2011).

This paper aims to determine the value added through more detailed haulage analysis. The primary metric was the truck cycle time and difference in excavation rate. Varying detail was assessed with mining locations, dump destinations and haul roads. The desired outcome was that additional detail in

School of Mechanical and Mining Engineering, The University of Queensland, Brisbane, Qld, 4072, Australia, m.kizil@uq.edu.au, Tel: 07 3365 4499

haulage analysis, specifically frequently changing haul roads, significantly adds value to a mining operation and thus greatly impacts on accuracy of budgets and productivity.

TRUCK CYCLE TIME PREDICTION METHODS

There are many products and methods currently available for the prediction of truck cycle times which utilise a combination of empirical or calculated data to formulate results. All of these methods appear to provide results that are acceptable within industry standards. The methods presented can be divided into three subgroups dependant on the level of manual input required, historical data and degree of automation. The three subgroups include:

- Talpac©, Arena® and FPC®;
- Multiple Regression and Artificial Neural Networks; and
- Deswik and MineSchedTM.

Chanda and Gardiner (2010) presented a comparative study of truck cycle time prediction methods for open-pit mining. This study evaluated three methods which included computer simulation, in this case Talpac©, artificial neural networks and multiple regressions with an aim to determine the best method for predicting truck requirements. Through this study, Chanda and Gardiner (2010) found that computer simulation methods both under and overestimate the truck cycle times for short and long hauls respectively. Evidence suggests that artificial neural networks and regression models are superior to computer simulations in their predictive ability (Chanda and Gardiner, 2010; Blackwell, 1999). Artificial neural networks and multiple regression methods however require detailed historical data for the calculation of their formulas. These methods therefore cannot be transferred between mining operations due to the nature and complexity of creating these systems.

The Talpac©, FPC®, Arena®, artificial neural networks and multiple regression methods typically utilise static haul roads in a single point in time. In these methods, judgment is usually made for the centroid of the dig and dump locations for the haulage analysis. Although the mining schedule usually does not significantly change in sequence, the dump schedule can vary considerably. Often mining engineers have detailed dump designs with simple spread sheets and running balances. This can lead to a large margin of error when creating a haulage analysis.

Although it can be critical in knowing the precise performance of a haulage fleet and the possible variations, longer term data is sometimes required. Most mines are much more complex with progressively changing dig and dump locations. Within these changes, large variations can be seen in the gradients and total distance travelled significantly affecting the truck performance. It is therefore beneficial that simulations or time studies are used for the calculation of truck cycle times using predetermined dig and dump strategies such as Gemcom's MineSchedTM and Deswik's Dump Scheduler software. Many mining companies have adopted Deswik software to assist in creating more accurate mine plans and cost estimations (Johnson, 2012).

The Deswik Dump Scheduler utilises a detailed method, for the calculation of truck requirements and cycle times, through the use of dynamic haul roads. The dump scheduler utilises mining solids and a mining schedule which can be created in either the Deswik Scheduler or through another scheduling package. A series of dump designs and solids are required whereby they are connected with the mining solids using haul strings. The dump schedule can then be created using a variety of different haulage objectives such as shortest haul, minimum relative level and minimum cycle time.

The truck cycle times and truck requirements are calculated using individual haulage calculating the uphill and downhill components through the use of rimpull and retard curves, stop signs and speed limiting factors. In addition to this, average utilisation, availability factors and load and dump times are used. This analysis considers hundreds of thousands of options for haulage routes and destinations within minutes. On completion of the dump analysis, 3D animations and reports can be produced. The Deswik Dump Scheduler method can help the mine planner identify errors within the analysis easily allowing for adjustments to be made and reruns of the analysis to be completed within a matter of minutes. This can result in significant time and costs savings for haulage analysis.

METHODOLOGY

Model creation

In order to uphold confidentiality agreements, actual geological and topographic mine data was not utilised in this project. Instead, a training dataset was created for the research project. The created topography and geological features replicate typical open-cut dragline and truck and shovel mining operations in the Bowen Basin coal fields. They were however created to simulate as many mines as possible.

A detailed mine design was created for four pits, R02N, R02S, R01N and R01S. These designs were completed to a short term planning level of detail which incorporated ramps to the coal floor for ten progressive strips. A total of seven coal seams of varying seam and interburden thickness were created in Excel® dipping North-East between 6% to 8%.

Five main haul roads were designed for the pits. Dragline spoil piles were designed for each of the four pits and ten strips equating to a total of 40 progressive pit designs. Each of these designs incorporated a low wall ramp that toed out at the coal floor. Upon completion of the dragline spoil designs, a spoil balance was conducted. From this spoil balance, the entire Seam I overburden material was allocated to the dragline. In addition to this, approximately half of the R01S and R01N, Seam W overburden was allocated to the dragline material due to the Seam I overburden being reduced dramatically by a roll in the coal seam.

Prestrip dump designs were completed for each progressive strip of the four ramps. The prestrip designs incorporated dump heights of 15 m with variable bench widths ranging from 15 to 50 m. Each prestrip dump design also included an offset of two dragline spoil piles for geotechnical stability reasons. Figure 1 shows an isometric view of R02N prestrip design.

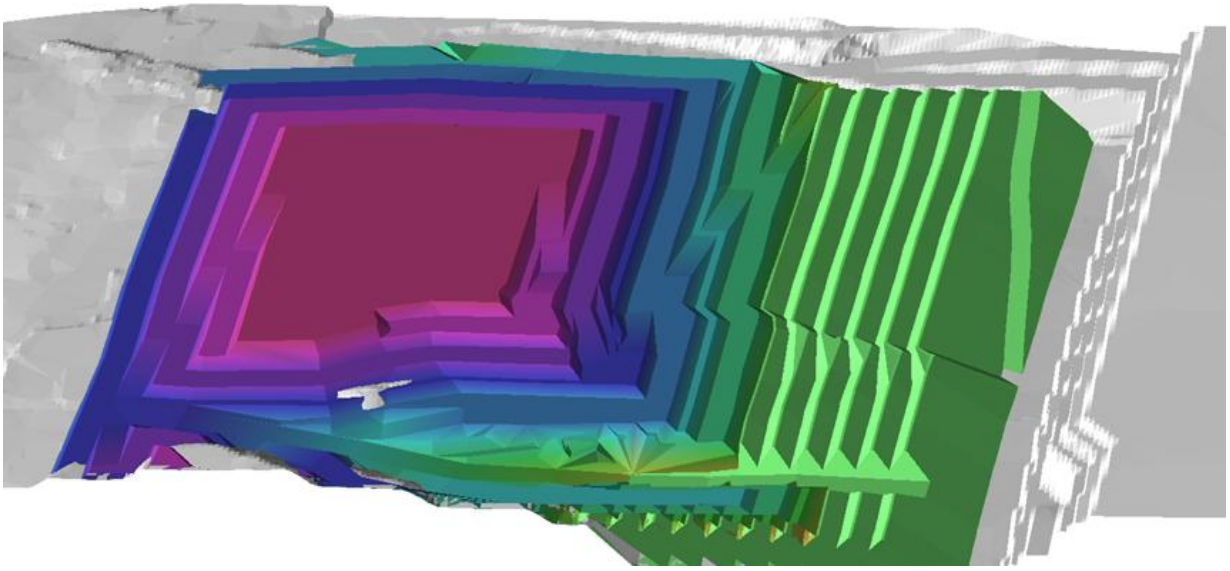

Figure 1 - Ramp RO2N isometric view

Two Caterpillar 8200-124 draglines were selected for the mine designs and schedule and two excavator fleet sizes were used in order to replicate the common practice for coal mines in the Bowen Basin. The primary overburden excavators used were RH340 Caterpillar backhoe configuration excavators with an average rate of 1750 BCM/h. The partings and coal were removed using a smaller RH120 Caterpillar backhoe configuration excavator with an average production rate of 900 t/h. It was presumed that the truck size had been optimised for this operation and Caterpillar 785B coal body trucks were selected for transport of coal. Caterpillar 785B class trucks were selected for overburden removal. The required truck numbers and cycle times were calculated in the haulage analysis.

A detailed mining schedule was created for the four ramps. Resources were then divided and allocated to the northern and southern ramps and included, coal excavators, Caterpillar 8200 draglines, and two prestrip excavators. A resource levelling algorithm was then completed using strip ascending and seam

number ascending priorities. Within this process, start and finish dates were allocated to each of the mining blocks using the assigned mining resources.

Data acquisition

A haulage analysis was conducted using a ".trux" file for a Caterpillar 785B in which a minimum cycle time scenario was run. The haulage analysis provided a variety of routes and cycle times for the dig and dump locations of the individual mining blocks. In order to remove the variable of multiple cycle times per individual mining block, a weighted average cycle time was assigned to haulage from each mining block. The resultant weighted average cycle times were subsequently imported onto the mining solid attributes which were then exported to Excel® for data analysis.

Following inspection and categorization of the exported cycle time data, it was apparent that too many variables existed between individual seam horizons to elicit trends. Consequently, a single seam horizon with the largest quantity of overburden, the S horizon, was chosen for data collection. The original haulage cycle time calculations were performed on a 25 m block size with 5 m vertical bench heights. This scenario was completed to the greatest level of detail and formed the base case. To compare the effect of the level of detail on cycle times, analysis was also completed on the following block sizes: 50 m, 100 m, 200 m, 400 m, 700 m blocks and total strip with 5 m benches, 400 m and 700 m blocks with 10 m, 15 m and 20 m benches and total vertical horizon and finally total strip with 10 m, 15 m and 20 m benches and with total vertical horizon.

RESULTS

The cycle times from the haulage scenarios were calculated to three decimal places. However, to facilitate comparison of the data results, haul cycles were pooled into 0.1 min intervals. A simplified plot of the cumulative dump volume against the pooled cycle time can be seen in Figure 2 for three scenarios. The graph clearly demonstrates that with progressively less detail, the distribution narrows, drawing closer to the mean cycle time. The weighted average cycle time of each scenario was consistent as the mining and dump block locations and their respective destinations are unchanged. There was however significant variation within the weighted average of each scenario. To ascertain the effect that increased horizontal distance from the endwall had upon the cycle time, a graph was plotted for each strip as shown in Figure 3. As expected, the cycle time progressively increased as the horizontal distance from the endwall increased. It should however be noted that there were a few exceptions to this trend. These occurred when extra ramping was required for the first few blocks mined from the endwall and, where new dumps were progressively becoming available. A similar trend was also found when analysing the weighted average effect of increased depth on cycle time.

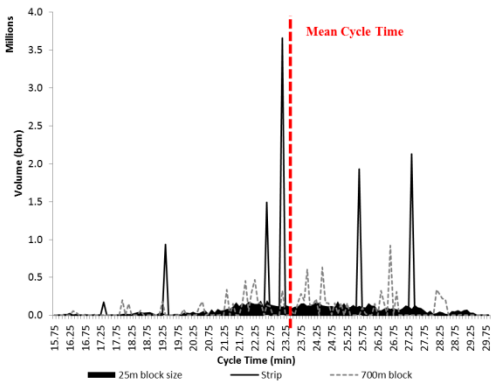

Figure 2 - RO2N S seam cycle time distribution

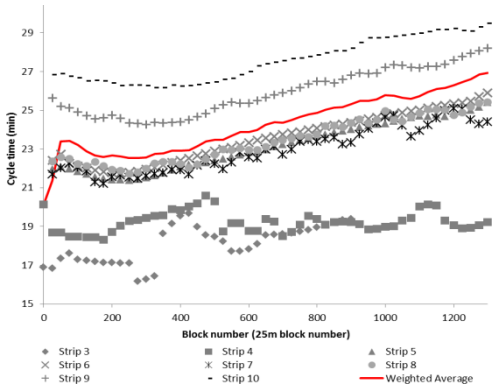

Figure 3 - Cycle time and increasing block number correlation

Figure 4, shows the increase in cycle time against the horizontal distance from the endwall for strips seven and ten. The shaded area around the weighted average cycle times for strip seven and ten shows the minimum and maximum cycle times for varying depths at a particular horizontal position. This represents the variance or error caused by changes in elevation. Figure 5, shows the weighted average cycle time for strips seven and ten against the vertical bench height. The shaded areas represent the error created by minimum and maximum horizontal distance from the endwall at a particular vertical bench height. As can be seen in this graph, a much larger variation is evident compared to that shown in

Figure 4. This shows that the horizontal distance from the endwall effects the haul cycle time to a greater extent than the vertical distance. This however could vary depending on ramping structure.

DISCUSSIONS

To assess the differences between the data, the standard deviation was calculated for each set of block ID's. To account for the fact that each cycle time pool had variable volume, the standard deviation and the variance was volume weighted. A standard deviation curve of the total S horizon overburden for horizontal block size increases can be seen in Figure 6. There was a noticeable difference in the standard deviations between the detailed haulage analysis to 700 m, and the whole strip horizon.

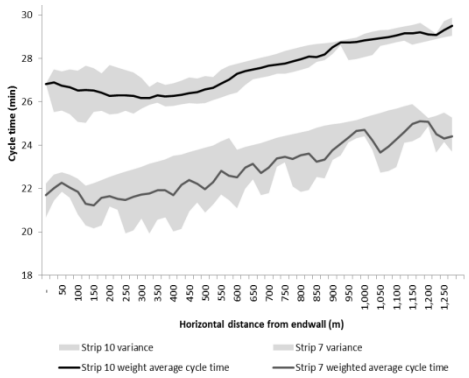

Figure 4 - Strips seven and ten distance against cycle time

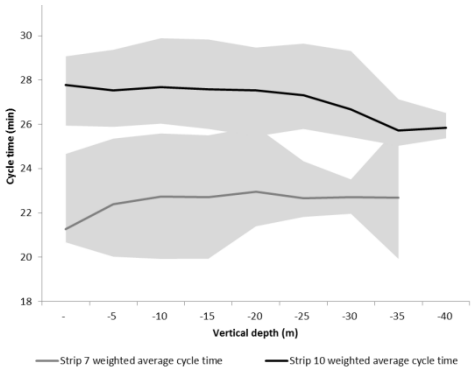

Figure 5 - Strips seven and ten bench depths against cycle time

In order to further quantify the differences, the total error was calculated for each of the detailed scenarios. This total error was calculated as two times the variance. To make the error more transparent within the scenarios, the error was translated to a percentage of the mean cycle time. Then, in order to present the 25 m block size as the base line, the error percentage was inversed as seen in Figure 7. As the detail decreased, the inverse error increased from the initial base case as the individual data points come closer to the mean cycle time.

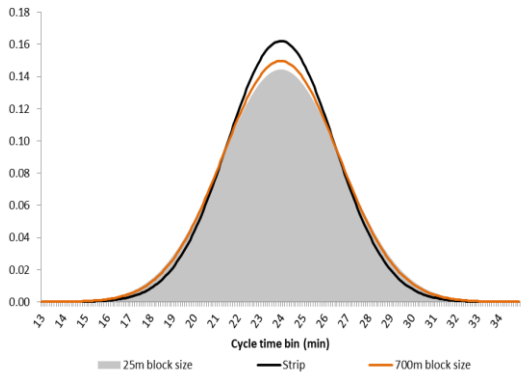

Figure 6 - S horizon overburden standard deviation for horizontal block size increase

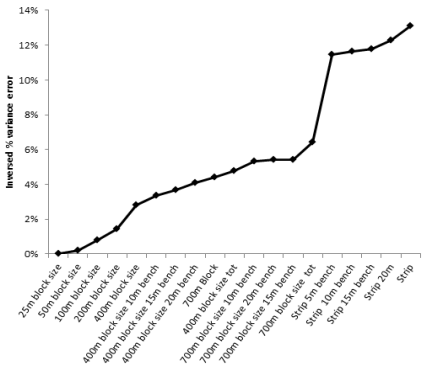

Figure 7 - Inversed percentage variance error for S horizon overburden

In order to ensure the data within the whole strip horizon followed similar trends to individual strips, an analysis was completed for strips six and seven. Due to the variability of the cycle time created from varying bench depth, only the increased horizontal block length was considered for this analysis. As can be seen in Figure 8 and Figure 9, the standard deviation graphs for strips six and seven followed a similar trend to that of the whole strip horizon with all block sizes up to half the size of the total strip producing relatively small differences within the standard deviation. The total strip standard deviation curve had a significant spike compared to that of the 700 m block size or less. This was due to the relatively small number of calculated cycle times and the effect of the variation of cycle time generated from the relative distance from the endwall. Therefore if only one data point is used for an individual bench height in the total strip, the variance of the combined benches is zero.

The inverse error percentage of strips six and seven followed a similar relationship to that of the total strips as seen in Figure 10, thus indicating that this trend was not an anomaly.

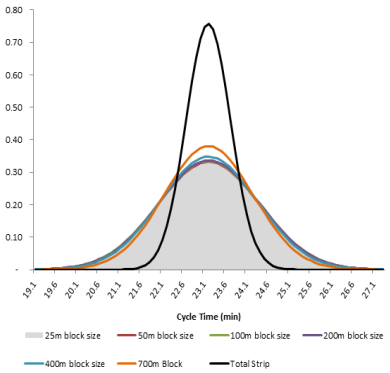

Figure 8 - Strip six horizon standard deviation for horizontal block size increase

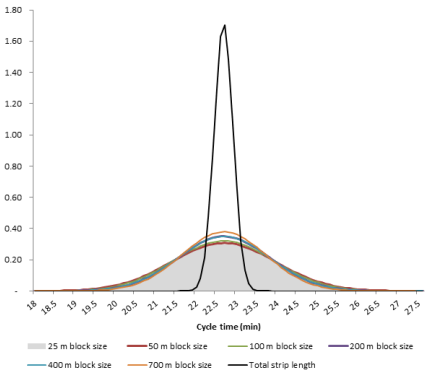

Figure 9 - Strip seven horizon standard deviation for horizontal block size increase

The variance error from the base case was then assessed for both the horizontal and vertical block sizes and plotted on a graph as seen in Figure 11. There was a noticeable difference between the varying horizontal block sizes and the varying vertical block sizes for the seam horizon. From the results presented in Figure 11, it can be assumed that it is more important to at least halve the horizontal block size for a given haulage calculation than to modify the vertical block size. This statement however is dependent upon the total seam horizon depth and the ramping structure. If there was a great variation in the cycle time between the vertical benches, it could be more beneficial to halve the block vertically than horizontally.

To present the effect block size used in a number of haulage scenarios, the variance error was calculated for the haulage cycle time. This analysis, depicted in Figure 12, showed a similar relationship to that presented by varying block sizes. In both instances, the total strip cycle time inverse error differences were significantly higher and did not appear to conform to the other detailed haulage analysis for block sizes 700 m and less. It was determined that this significant change was due to the fact that only one cycle time value was being generated for the total strip.

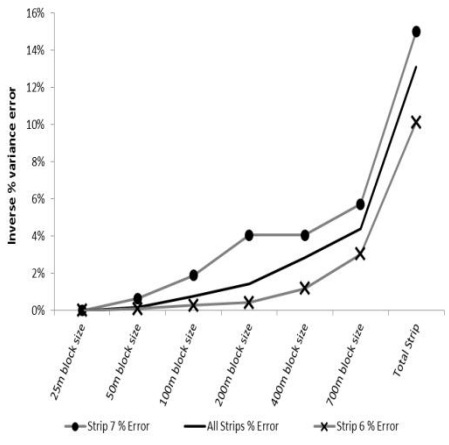

Figure 10 - Percentage variance difference for 5m bench height

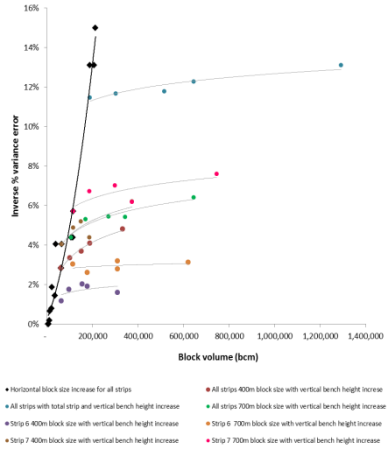

Figure 11 - Horizontal and vertical error comparison

A final analysis was completed to determine the influence of haul road calculation frequency on the mining schedule and mining rate. For this purpose an example case was generated, where the mean cycle time was utilised to calculate the overall truck requirements. In this case, six trucks were scheduled. As shown in Table 1, the average excavation rate, which is limited by the excavator mining rate, is 1270 BCM/hr. In mining the first half of the strip, where the cycle time is below the mean cycle time of 22.68 min per cycle, the excavator can maintain its maximum rate at 1270 BCM/hr. As the cycle time increases above the mean, the mining rate will be limited. This limitation is due to the fact that the excavator will no longer be loading at its maximum rate as it will be awaiting trucks for loading. Figure 13, illustrates the

varying excavator rates within one strip depending on the increased cycle time throughout the strip. This example shows that due to incorrect truck allocation the mining rate can be reduced by 12%.

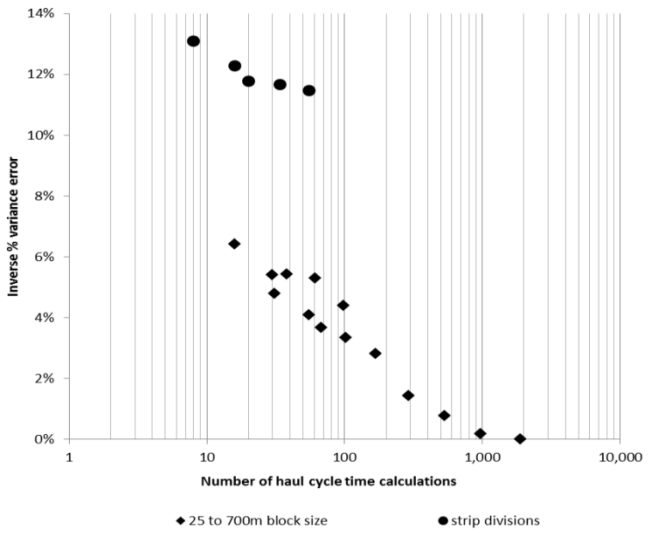

Figure 12 - Cycle time calculation frequency

Table 1 - Excavation rate variations

Parameter	Average	Min	Max
Cycle Time	22.68	25.90	19.92
bcm/load	80	80	80
Cycles/hr	2.6	2.3	2.8
bcm/hr	212	185	241
No Trucks	6	6	6
Mining Rate	1270	1112	1445
Difference		12%	14%

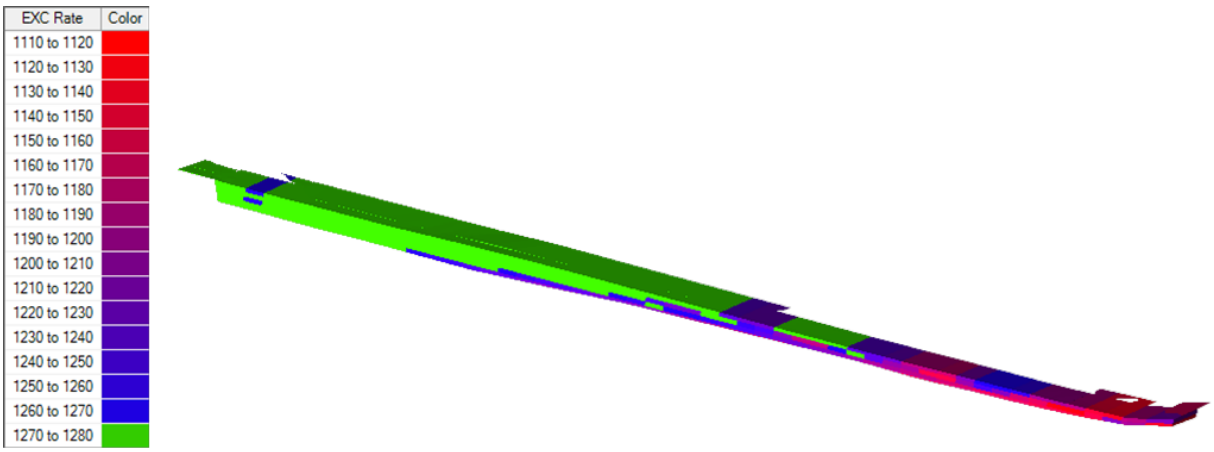

Figure 13 - Excavation rate variations

CONCLUSIONS AND RECOMMENDATIONS

Haulage is a major component of the overall cost of a surface mining operation. It is therefore imperative that adequate time, effort and resources be committed to ensuring accuracy in haulage analysis. Increasing the frequency of haul roads routes has become possible with advanced software such as Deswik.CAD®. The actual benefits of this additional detail in haulage analysis have not been quantified in the past. Many mining companies however have experienced the benefits of this software allowing them

to account for required trucks, identify areas of limited dump room, minimise cycle times and create strategic dumping strategies.

The aim of this study was to identify the value drivers for haulage analysis. The primary objective was to quantify the value added through additional detail in haulage analysis. From the haulage analysis conducted throughout this project, a correlation was identified between the size of a mining block within a strip and the change in variance error from the mean cycle time for a particular strip. The study found that the estimated cycle time can be significantly affected by the sampling frequency by up to 14%. The study also demonstrated the potential use of this result to calculate the percentage reduction of the mining rate due to under allocation of trucks. Therefore, the most significant result of the study was that sampling frequency can change truck requirement estimates. In practical terms, insufficient number of haul road routes can potentially push out mining schedules, reduce mining rates, decrease utilisation of truck fleets and decrease mine productivity and profits.

The data analysis conducted was limited to one seam horizon within a mining operation utilising one ramping and dumping system. It is therefore recommended that additional analysis be conducted to determine the effects on other ramping and dumping methods. Additionally, an analysis should be completed to determine the influence that fluctuation of truck cycle times has upon the performance and schedule of the entire site. Finally, a financial analysis should be conducted to determine the monetary value added through this additional detail.

REFERENCES

Blackwell, G H, 1999. Estimation of large open pit haulage truck requirements, *CIM Bulletin*:143-149.

Chanda, E and Gardiner, S, 2010. A comparative study of truck cycle time prediction methods in open-pit mining, *Engineering-Civil Engineering*, 17(5):446-460.

Johnson, M, 2012. Personal cummunication, Mining Consultant, Deswik Pty Ltd, 26 March 2012.

Nel, S, Kizil, M S and Knights, P, 2011. Improving truck-shovel matching, *35th APCOM Symposium*, *Ed (E Y Baafi, R J Kininmonth and I Porter),* Wollongong NSW, pp 381-392, published by The Australasian Institute of Mining and Metallurgy, Carlton Victoria, ISBN 978 1 921522 51 2, September 2011.

R2Mining, 2012. Trucks, bottom dump, coal haulers, mechanical cost calculator [online], Available from: <http://calc2011.au.costs.infomine.com/projects/equipment.aspx? sectionID=1&typeid=49> [Accessed: 11 May 2012].

ISSUES RELATED TO STABILITY DESIGN OF VERY HIGH SPOIL DUMPS

Leonie Bradfield[1], John Simmons[2] and Stephen Fityus[3]

ABSTRACT: As spoil dumps get higher, particularly in strip mining where most overburden is placed in-pit, consequences of slope failure become disproportionately greater.

Current understanding of the shearing behaviour of spoil for stability design has involved a combination of laboratory-scale diagnostic testing and engineering judgment. This is a relatively empirical approach that provides a linear shear strength envelope for materials known to exhibit non-linear behaviour, particularly under high confining stresses. A shortcoming to the diagnostic testing is that oversize particles are usually scalped to accommodate the device capacity. The influence of prototype-size particles on the geomechanical behaviour of mine spoil is not truly captured.

In response to concerns about overestimating the shear strength and stability of high spoil dumps, and current plans for coal mine dumps to exceed 400 m in height, there is a need to rationally define the stress-strain behaviour of more characteristic spoil masses under representative compressive and shearing loads.

A Large Direct Shear Machine (LDSM) has been designed at The University of Newcastle to generate reliable stress-strain data on large samples of coal measures spoil (0.72 m x 0.72 m x 0.6 m) subjected to loads representative of very high dumps (~3.5 MPa). This paper reviews current methods for predicting shear strength parameters in the context of very high spoil dumps, and presents an overview of the design considerations of the DSM.

INTRODUCTION

Following the global economic crisis in 2009, the Australian economy sustained growth as a consequence of continued coal exports. Over the next decade or so, the demand for Australia's coal is expected to increase significantly in response to the projected needs of China and India.

The aim of any open pit coal mine design is to provide the steepest possible excavation configuration that is commensurate with stability, safety and financial requirements. The economic depth for open cut coal mining, expressed as the 'strip ratio', is based on the unit revenue of the coal and the cost to recover it. The increased demand for Australia's largest export is seeing the nation's coal producers secure significant price rises for the commodity. The flow-on effect is that deeper coal reserves previously regarded unprofitable due to high stripping ratios are now being developed, with mine owners relying on experience-based models to establish stability design criteria for pit slopes.

For high-value commodities such as coking-coal, economic depths in excess of 275 m are currently underway in Australian coal mines, with plans to progress to 350 m or more. This translates to mine spoil dumps potentially reaching heights of up to 450 m. Current experience-based understanding of mine spoil stability behaviour falls well short of this, by about 330 m. Furthermore, civil engineering experience with rockfill dams is that current experience-based models overestimate strength under higher stress regimes.

Mine owners have relied on geotechnical practitioners for advice on geotechnical risks that could impact on the success of long-term mine plans. Since current methods are believed to overestimate the stability of very high spoil dumps to an unknown degree, and the consequences are potentially catastrophic, risks to mine owners cannot be evaluated and due diligence reviews may find that legal, financial and operational risks to the business are unacceptable.

[1] *University of Newcastle and Thiess Pty Ltd, Leonie.Bradfield@uon.edu.au, M: 04 8776 5555*
[2] *Sherwood Geotechnical and Research Services*
[3] *University of Newcastle*

In the context of very high spoil dumps, the uncertainty associated with current strength models can only be reduced by simulating field-scale conditions in the laboratory.

LIMITATIONS WITH CURRENT DESIGN STRENGTHS

Empirical shear strength envelopes

Linear envelope - BMA Coal strength framework

The Australian coal mining geotechnical community currently uses either totally empirical strength models or simple models based on extremely small test specimens. The BMA Coal strength framework was described in 2004 by Simmons and McManus, and represents almost two decades of extensive in-house research and collaboration with CSIRO on dragline-scale dumps. It is based on laboratory tests with empirical adjustments using back analyses of several large spoil dump failures.

The framework provides a visual-tactile method for identifying any type of spoil into one of four categories. Spoil category identification is based on the assessment of five geological attributes, comprising predominant particle size, consistency, structure, plasticity and age.

Table 1 - Spoil Categories and Attributes (after Simmons and McManus, 2004)

CATEGORY		1	2	3	4
Description Attributes	**Weighting** *(excl. Age)*	Fine-grained clay-rich high plasticity	Fine-grained low plasticity with larger clasts	Larger clasts with fine matrix, low plasticity	Large blocks, minor fines, minor slaking
Predominant Particle Size	3/31=**9.7%** *(11.6%)*	Clay	Sand	Gravel	Cobbles
Consistency: cohesive cohesionless	7/31=**22.6%** *(26.9%)*	Soft to Firm Loose	Stiff Med. Dense	Hard Dense	XLS+ rock Very Dense
Structure	7/31=**22.6%** *(26.9%)*	Matrix only	Matrix supported	Framework supported	Framework only
Liquid Limit	9/31=**29.0%** *(34.6%)*	High (>50)	Intermediate (35 – 50)	Low (20 – 35)	Not Plastic (<20)
Age	5/31=**16.1%**	0 - 2y	2 - 10y	10 - 30y	>30y

The 'structure' attribute is a fabric-related parameter, where larger particles represent the 'framework', and finer particles the 'matrix' (Figure 1). Simmons and McManus (2004) describe the framework as the larger sized fraction that is relatively stiff and transmits most of the forces within the spoil mass when in particle-to-particle contact. Comparably, they describe the matrix as the finer-sized component that fills the void spaces between framework particles. Framework-abundant spoils are said to be stronger and less compressible than matrix-abundant spoils.

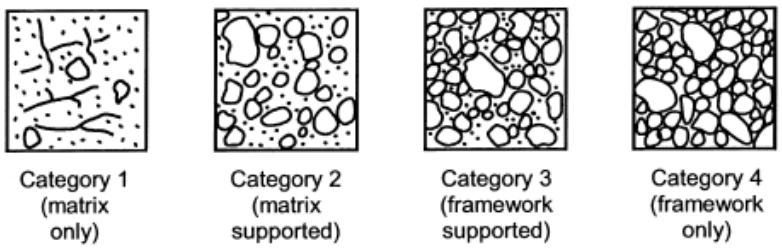

Figure 1 - Spoil structure attribute to be used with Table 1 (after Simmons and McManus, 2004)

For each category of spoil, shear strength parameters for three potential strength mobilization modes are provided, including unsaturated, saturated and remoulded conditions.

Table 2 - Shear Strength Parameters for Categories and Mobilisation Modes (after Simmons and McManus, 2004)

(Parameter standard deviations in italicised parentheses)

Category	Unsaturated			Saturated			Remoulded
	γ (kN/m³)	c' (kPa)	ϕ' (deg)	γ (kN/m³)	c' (kPa)	ϕ' (deg)	c'=0 kPa, ϕ' (deg)
1	18 *(1)*	20 *(10)*	25 *(2.5)*	20 *(1)*	0 *(0)*	18 *(3)*	18 *(1.5)*
2	18 *(1)*	30 *(15)*	28 *(3)*	20 *(1)*	15 *(7.5)*	23 *(2.5)*	18 *(1.5)*
3	18 *(1)*	50 *(15)*	30 *(2)*	20 *(1)*	20 *(10)*	25 *(2.5)*	18 *(1.5)*
4	18 *(1)*	50 *(15)*	35 *(2.5)*	20 *(1)*	0 *(0)*	30 *(1.5)*	28 *(2)*

The peak strength parameters cohesion c' and friction angle ϕ' are based on a linear fit to data obtained from laboratory tests simulating stresses experienced in 60-90 m high spoil dumps (Figure 2). The method has been validated in practice by back-analysis of instability and successful design of spoil dumps up to 120 m high. The linear Mohr-Coulomb shear strength envelope is expressed as:

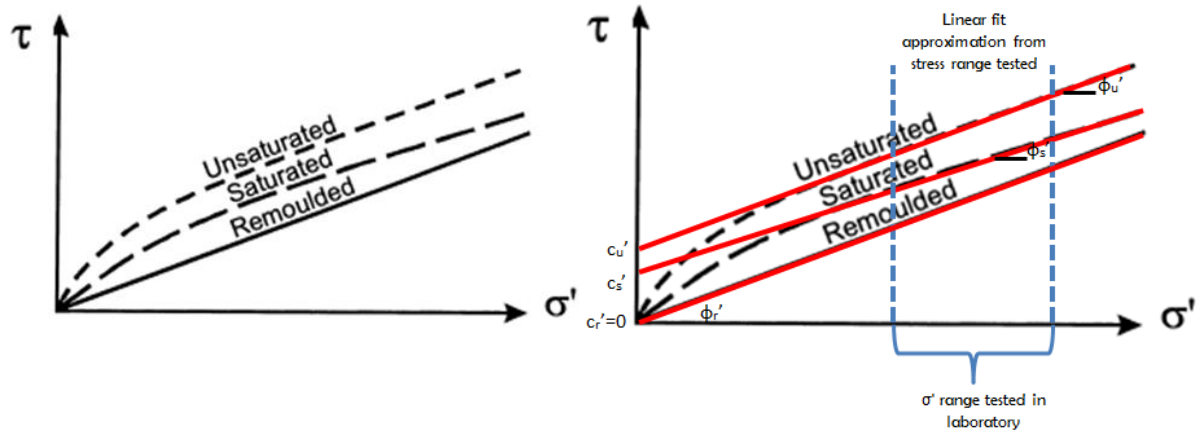

(a) (b)

Figure 2 - (a) Three conceptual strength modes for spoil as described by Simmons and McManus (2004); and (b) modified to explain the linear shear strength approximation adopted in the framework

It is generally accepted that the frictional strength of mine spoil is strongly dependent on the magnitude of confining stress. A fundamental shortcoming of the BMA strength framework is that it cannot be extrapolated to cover the stress states expected in very high dumps. This is because the framework is based on a Mohr-Coulomb linear fit for data within a defined stress range, and mine spoil shear strength behaviour is distinctly non-linear. Extrapolation of the framework will overestimate the stability of very high spoil dumps to an unknown degree, and with plans for coal mine spoil dumps to exceed 400 m there is a need to investigate the shearing behaviour of representative spoil masses at field stress conditions.

Similarly, extrapolation of the framework to the low stress range will significantly underestimate the frictional strength for low spoil slopes (<30 m high), with the actual available shear strength considerably less than that estimated (Figure 3). It is a common occurrence for the lower excavated slope within a dragline spoil dump to sit at batters steeper than repose angle for short periods of time. Simmons and McManus (2004) suggest that, in addition to the effects of matric suction, the non-linear shear strength envelope helps explain this phenomenon.

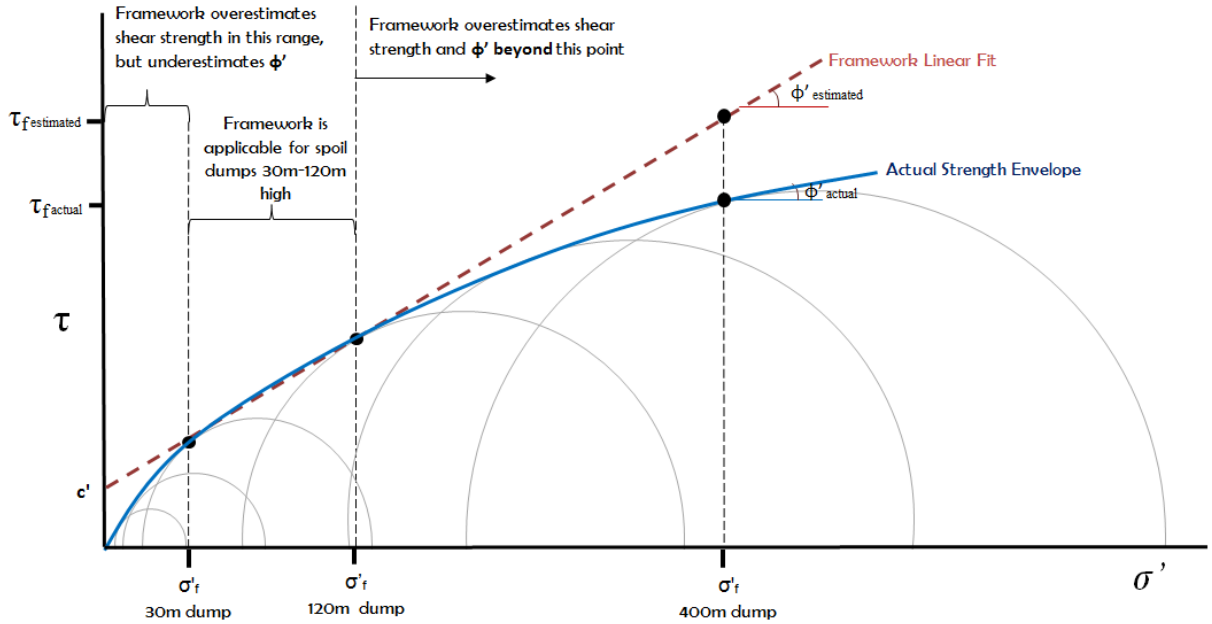

Figure 3 - Mohr diagram showing framework linear fit with respect to actual strength envelope (not to scale)

Non-linear failure envelopes

For decades, civil engineers have used non-linear failure envelopes to define the shearing behaviour of granular materials, particularly in relation to rock fill dam design. A number of studies have used power-law relationships to explain the dilatant behaviour of compacted rock fills at low effective stress, and reduced dilation due to particle crushing as stress increases.

Leps (1970) examined rock fill triaxial data obtained from over 20 dam construction projects and demonstrated a marked increase in friction angle ϕ' with decreasing confining pressure. Included in the data were test results from large apparatus capable of handling 1m diameter samples with a maximum particle size of 200 mm, at confining stresses up to 3.9 MPa. Barton and Kjaernsli (1981) developed a power-law criterion to model this data, and established a number of simple index tests that could be used to estimate the peak drained friction angle ϕ' of rock fill. Recommendations from the Barton and Kjaernsli study have strong merit for rock-fill projects using the types of rock-fills tested in the study; i.e. predominantly rocks with high to very high substance strength. However, its applicability to coal measures spoil of comparatively low substance strength is not well founded.

Charles and Watts (1980) modelled a power-law relationship to describe triaxial data obtained for rock fills of igneous, sedimentary and metamorphic origin, with varied substance strength and shape. In contrast to the aforementioned large-sample-high-stress studies, Charles and Watts placed a much higher importance on the stability of rock fill at comparatively low stresses. Samples with a maximum particle size of 38mm and specimen diameter of 230 mm were tested over the low stress range considered critical for lower-slope stability. It was proposed that over a limited stress range (40 kPa to 400 kPa) the shear strength of rock fill is given below, where constants A and b are dependent on rock type (Figure 4).

$$\tau = A\,(\sigma')^{b} \qquad (1)$$

The Charles and Watts study is applicable to rock fill embankments up to 50 m high, and covers the majority of rock types considered suitable for dam embankments. However, a number of limitations exist in the context of very high mine spoil dump design. The first is the stress range; 400 kPa is equivalent to a small spoil dump; and the equation cannot be extrapolated out to cover the higher stress range. The second is that the rock fills tested are heavily compacted well-graded samples; in contrast to mine spoil dumps that are placed in a loose state, with highly variable gradation as a result of parent rock type and mining processes. The third is that the samples were scalped to meet apparatus constraints; the deficiencies of which will be discussed later.

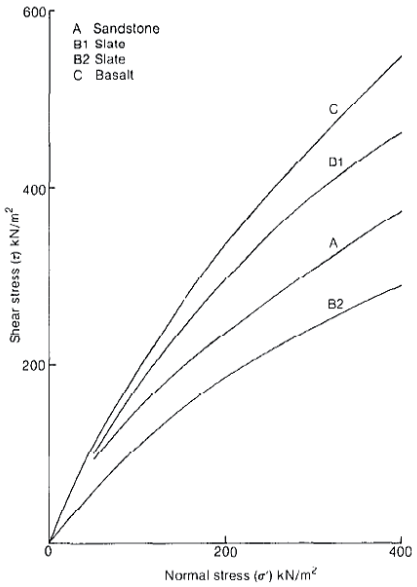

Rock type	*A*	*b*
A. Sandstone	6·8	0·67
B1. Slate	5·3	0·75
B2. Slate	3·0	0·77
C. Basalt	4·4	0·81

Figure 4 - Shear strength for rock fills at low confining pressures, and rock fill constants (Charles and Watts, 1980)

A CSIRO study (Mallett, *et al.*, 1983) performed direct shear tests on weak pit floor material at South Blackwater coal mine, and modelled best-fit linear and non-linear relationships to describe its strength envelope (Figure 5). The material was block-sampled from a clay-filled shear zone, hence not quantitatively comparable to the shear strength of mine spoil; however it is included in this paper for a number of reasons. It demonstrates the difference in frictional strength between the models for the low stress range, as is the case for a typical spoil. In addition it shows agreement for both strength models within the stress range tested in the laboratory; and infers that accurate shear strength models can only be achieved by testing representative size samples at the stress range of interest. In the case of very high spoil dumps, this translates to testing large samples at very high confining stresses.

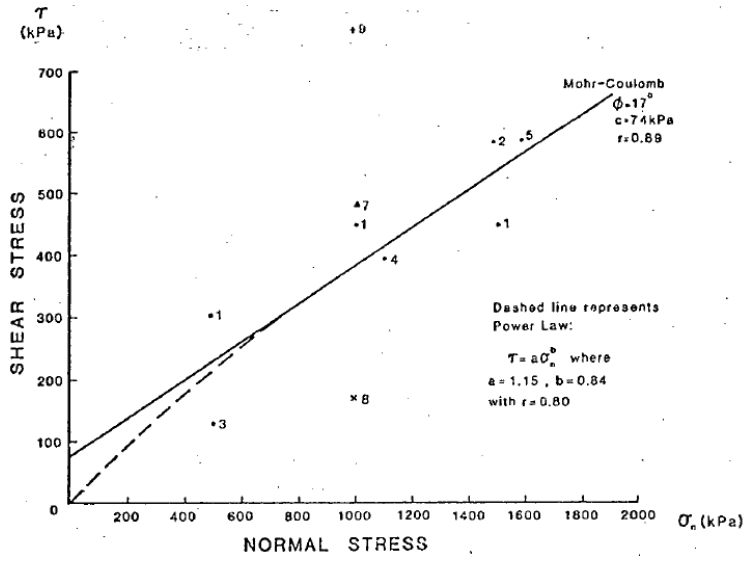

Figure 5 - Direct shear test results conducted on discontinuity material in a pit floor (Mallett, *et al.*, 1983)

Scale effects of laboratory testing

The application of laboratory data to spoil dump stability design has been used with caution for decades. This is partly attributed to the highly variable nature of mine spoil, consisting of large rocks and boulders and some fines at placement; but more so due to the inability of standard laboratory tests to account for

this variability by testing full-scale samples at as-dumped grading and porosity, and at loads representative of field conditions.

It is widely accepted that the presence of large rocks and boulders strongly influences the shearing behaviour of rock fill. A decrease in frictional strength with increasing particle size is well established, particularly at low confining stresses. Vallerga *et al.* (1957) found this relationship to be non-existent for particles less than 5 mm. Barton and Kjaernsli (1981) attribute this to the higher propensity for larger rock fragments to undergo particle crushing than are smaller particles, as they are more likely to contain planes of weakness than are sands or fine gravels. However, limitations of standard laboratory apparatus are such that the shear strength of only the finer fraction of spoil can be measured. Application of such results to slope design will result in an overestimation of shear strength and stability.

By way of explanation, a standard laboratory direct shear box can test 60 mm x 60 mm samples, of maximum particle size equivalent to fine gravel, and maximum normal stress up to 2.7 MPa. For testing coarse materials such as rock-fill, a direct shear box capable of handling larger samples (300 mm x 300 mm) is becoming common-place in geotechnical laboratories, and can test coarse gravels at normal stresses up to 1 MPa. However, this is still not of sufficient size to handle the cobble and boulder size particles typical of coal mine spoil.

The overestimation of shear strength when testing only the fine fraction of spoil is demonstrated in Figure 6. Direct shear test results conducted at the University of Newcastle for a typical category 2U spoil (according to Table 1) are compared with the geotechnical parameters implicit in the BMA Coal strength framework. A category 2 spoil predominantly consists of fine-grained low-plasticity material (sand) with larger clasts, is stiff/medium dense and matrix supported. The 'U' refers to the unsaturated strength mobilisation mode (Table 2, Figure 2). The dimension of direct shear test sample was 100 mm x 100 mm with a maximum particle size less than 4.75 mm. The BMA Coal strength framework is based on a number of shear strength investigations, including large-sample direct shear tests with size of 1 m x 0.75 m and validated by field slope performance data for dumps up to 120 m high.

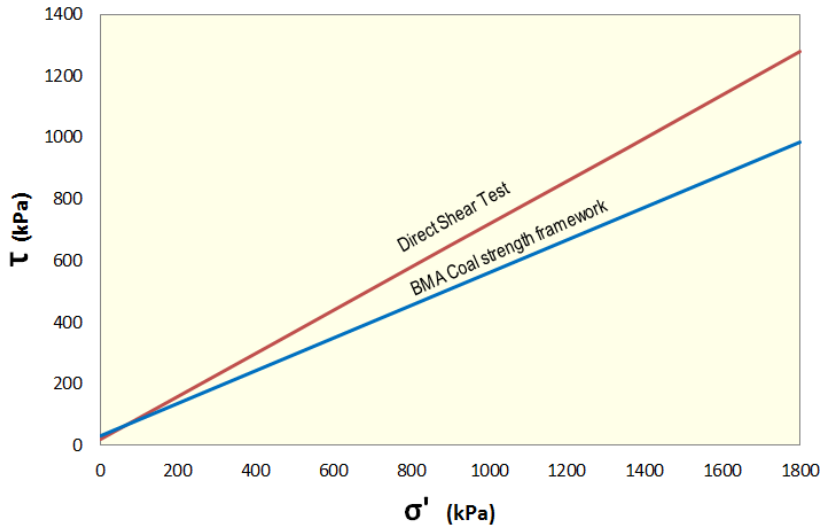

Figure 6 - Overestimation of shear strength due to scalping

Groundwater effects

The destabilizing role that water has on the soft rock spoil dumps of coal mines is widely recognized but difficult to evaluate.

Coal measures rocks are prone to physical and chemical deterioration with changes in moisture content, resulting in slaking and softening and a reduction in shear strength. Water pressure can have both positive and negative effects on slope stability; depending on the stress states within the spoil mass, the moisture content, and time-scale considered. Negative pore water pressure (suction) is usually implicit where low spoil slopes are observed to sit at batters steeper than repose angle for short periods of time. Conversely, positive water pressure reduces shear strength by pushing grains apart and reducing their intergranular friction.

It is widely accepted that water pressures must be considered in stability analysis. The civil engineering field often couples piezometer data with seepage analysis to establish the phreatic surface level and flow paths through a slope. However, water pressures are not easily ascertained in spoil materials. The logistical and practical difficulties associated with the installation of piezometers in spoil materials are many and varied, and often incur significant project costs. Voids are problematic for drilling equipment, commonly resulting in hole collapse, production disruptions and equipment damage.

Current understanding of water behaviour in strip mine spoils has not advanced far beyond the conclusions drawn by Gonano (1980, after Boyd, 1976), in that groundwater tends to occupy the basal 3 to 5 m of the spoil foundation, draining through the slope to the level at which water ponds externally. The BMA Coal strength framework employs a similar model, based on observations of spoil dumps in the Bowen Basin. It assumes that the phreatic surface is no more than 5 m above the foundation and reduces to the down-slope toe; with saturated spoil material underlying the phreatic surface.

The inherent uncertainties with groundwater behaviour in spoil dumps characterized by the strength framework are increased to an unknown degree in the context of very high spoil dumps. In particular, the extent of saturation and associated reduction in shear strength within the basal layer are significant to spoil dump stability, as large-scale deep-seated failure mechanisms commonly develop along this plane of weakness.

There is some conjecture around the potential for mine spoil to achieve effective saturation under the confining loads characteristic of very high spoil dumps. Preliminary studies at the University of Newcastle suggest that, although strongly dependent on field moisture content, this could be the case. It was found that for a typical category 2 spoil subjected to confining loads of 3.5 MPa, compression-induced saturation could develop at moisture contents greater than 11%. The field moisture content at the time of sampling ranged between 10 and 11%, following several weeks without rain. The results warrant further investigation into compression-induced saturation, which will likely be a key stability consideration for very high spoil dumps.

RESOLVING UNCERTAINTIES ASSOCIATED WITH STRENGTH FRAMEWORKS

Current knowledge of mine spoil shearing behaviour falls well short of that of soil mechanics for several reasons. The first is due to the significant costs and time associated with the design, construction and operation of equipment large enough to test characteristic spoil samples at field stress conditions. And secondly, the BMA Coal strength framework has worked well for nearly a decade, and its limitations are only starting to emerge with the prospect of deeper mines being developed.

The University of Newcastle is currently undertaking research to update and extend the BMA Coal strength framework to include very high spoil dumps. Of key importance is the ability to measure the stress-strain behaviour of characteristic spoil masses under field stress conditions.

Estimation of stress states for very high dumps

The maximum confining stress required to simulate conditions within a 400 m high spoil slope has been estimated for the two commonly observed large-scale failure mechanisms for spoil dumps; a deep seated multi-wedge mechanism, and a multi-wedge rill mechanism (Figure 7).

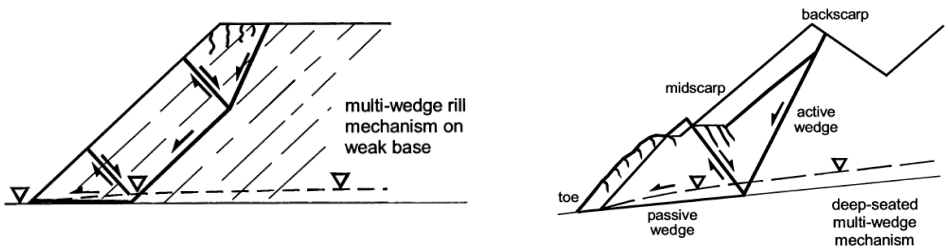

Figure 7 - Large-scale failure mechanisms for spoil dumps (Simmons and McManus 2004)

The slope geometry was simplified to rill angle (37°) for a total slope height of 400 m; the base of which was assumed saturated to a maximum of 5 m above the foundation floor. A weak remoulded basal layer

occupying the lower 2 m was also assumed. Limit equilibrium analyses explored the effects that foundation inclination and back-scarp location had on the stress distributions through the spoil mass and associated Factor of Safety. The Sarma method for non-vertical slices was used to divide the failure surface into boundaries considered most appropriate for capturing the anisotropic strength state characteristic of mine spoil (after Simmons and McManus, 2004). This method is based on the principle of limiting equilibrium and the method of slices, and calculates the critical horizontal acceleration required to bring the mass of the spoil slope bound by the failure surface to a state of limiting equilibrium (of forces and moments).

The following observations were made in the analyses:

- The deep-seated multi-wedge failure mechanism developed the highest normal stresses within the spoil mass, occurring on the base of the passive wedge.
- Enlarging the failure surface geometry by moving the backscarp away from the slope crest increased the maximum normal stress within the spoil mass. However, this also increased the Factor of Safety against failure occurring.
- Increasing the foundation inclination had the opposite effect, reducing the Factor of Safety and the maximum normal stress within the dump.

The analyses suggested that, for a marginally stable 400 m high spoil dump, the maximum normal stress acting on the base of the passive wedge could range between 3.1 and 3.4 MPa, depending on foundation inclination. Figure 8 shows an example 2D limit equilibrium analysis for a 400 m spoil dump of simplified geometry. This analysis was performed using the Galena code software (Clover Technology, 2012) and the Sarma method for non-vertical slices.

Furthermore, Mohr analysis using the BMA Coal strength framework parameters, and extrapolating to confining stresses equivalent to 400 m of spoil weight, suggests normal and shear stresses at failure are unlikely to exceed 3.5 and 2.1 MPa respectively. It is recognized that extrapolation will overestimate the shear strength to an unknown degree; however is useful in establishing the upper-bound of stress required for discussion.

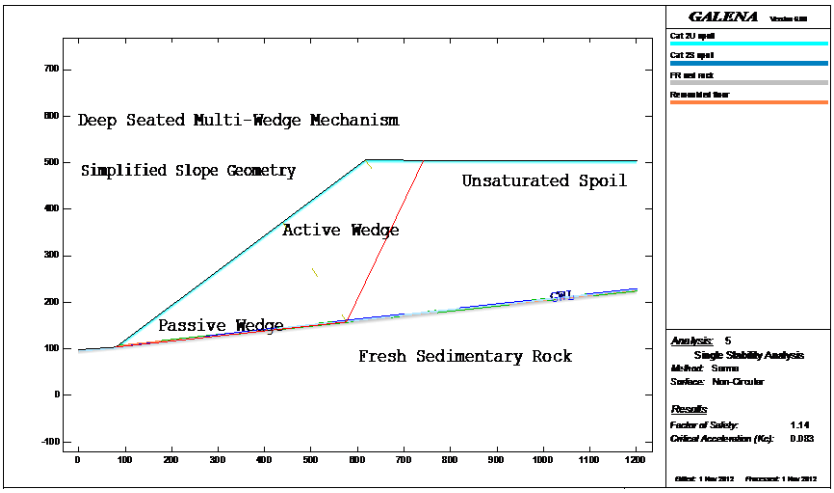

Figure 8 - Example 2D limit equilibrium analysis of a simplified geometry for a 400 m spoil dump

Field-scale test apparatus

To the authors' knowledge, few testing machines exist worldwide that can meet the large-sample-high-stress requirements for shear strength testing of representative spoil masses at field stress conditions.

A large direct shear test frame was constructed to test then-representative spoil masses as part of a CSIRO study into the stability of spoil piles (Mallett, *et al.*, 1983). At the time of the study, spoil dumps rarely surpassed 90 m in height. The apparatus could handle large samples (1 m x 0.75 m x 0.67 m) and test at consolidating and shearing loads of 1.3 MPa.

It is understood that a large-scale-high-stress triaxial device exists at the IDIEM Laboratory of the Universidad de Chile in Santiago. The apparatus can test samples 2 m x 1 m in diameter, with maximum particle size of 203 mm at confining pressures up to 2.5 MPa. The apparatus has been used to characterize the geotechnical properties of very high waste dumps in the copper mines of Codelco, Andina Division (CAD) in Chile. The waste rock tested by Linero *et al.* (2006) is classified as 'hard-rock', consisting of porphyry and granodiorite of high substance strength. To the author's knowledge, the apparatus has not been used to perform shear strength studies on the 'soft-rock' coal mine spoils.

In comparison, it is evident that the CSIRO apparatus falls short of the required design stress of 3.5 MPa for very high dumps. Furthermore, logistical limitations prevent the use of the IDIEM Laboratory device for shear strength investigations into coal measures spoil at the University of Newcastle.

Large direct shear machine

Overview

A large direct shear machine (LDSM) has been designed at the University of Newcastle as part of a postgraduate research project. Construction of the LDSM commenced in mid-2012, and is expected to be fully operational by 2013. The design criteria for the LDSM were:

- To be capable of handling large (full-scale) spoil samples;
- To have sufficient hydraulic capacity to simulate field loading conditions estimated for very high spoil dumps (minimum of 3.5 MPa and 2.1 MPa for normal and shearing loads respectively);
- To maintain constant normal load whilst also minimising tilt of the top plate;
- To apply a constant rate of horizontal displacement;
- To be as rigid as possible to prevent sample rotation and minimise side-wall deflection, whilst also minimising friction losses;
- To be able to conduct wet (inundated) and dry tests.

Figure 9 shows the schematic of large direct shear machine.

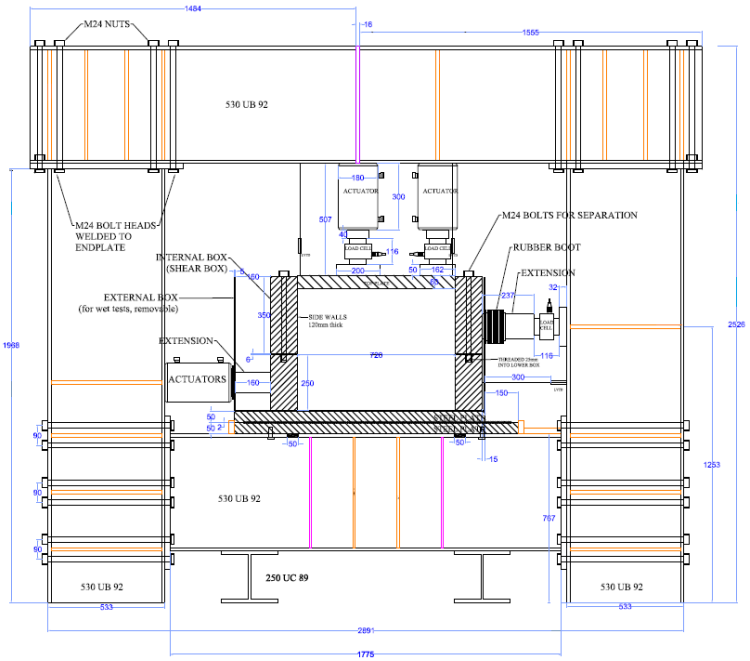

Figure 9 - Large direct shear machine

The dimensions of the internal shear box are as large as possible within budget constraints such that 3.5 MPa confining pressure can be imposed on the shear plane. The initial research proposal indicated

that a 1 m x 1 m shear box would suitably handle the large samples required. However, budget limitations have restricted the size to 0.72 m x 0.72 m.

The internal shear box consists of a 350 mm-high upper box, and a 250 mm-high lower box. The sidewalls consist of 120 mm thick solid steel (250 grade); designed to minimise deflection and associated volume changes under the very-high expected loads. High-tensile strength (Grade 8.8) 30 mm-diameter threaded rods join the sidewalls such that the boxes can be disassembled between tests if required. Removable water-proof walls (external box) encase the internal box, and enable inundated or 'wet' tests to be conducted.

The internal shear box is mounted in a large self-reacting stand-alone frame, fabricated from over 26 lineal metres of 530 mm-deep universal beams. The frame is window-shaped and has the dimensions of 3 m x 1.2 m x 2.5 m (l x w x h), and reinforced with over 100 steel plates up to 16 mm thick. During testing, the LDSM will weigh more than 8 t.

Some scalping will be necessary to accommodate the sample size. With a maximum sample height of 600 mm, and likely to reduce to 450-500 mm following the application of confining load, a maximum particle size between 65 mm and 100 mm is anticipated. Note that this is based on the recommendations from test methods developed for smaller apparatus. A new test method will be devised for the LDSM, which will set out the nominal maximum particle size, subject to machine trials.

The confining and shearing forces will be applied via a number of 100 t double-acting hydraulic actuators. Considerations to controlling tilt of the top-plate led to the strategic placement of three actuators such that corrections for displacement could be individually applied during consolidation, whilst still maintaining a common constant load between them. The three cylinders can deliver a maximum consolidating stress of up to 5.7 MPa to the shear plane; however will be restricted to 3.5 MPa in initial stages of testing. Two cylinders acting in the horizontal direction can transfer up to 3.7 MPa stress to the shear plane, however it is anticipated that the peak shear stress is unlikely to exceed 2.1 MPa.

Loads will be measured via five load cells; three positioned in series with the actuators applying the confining loads; and two opposing the horizontal actuators. Horizontal and vertical displacements will be measured via transducers located as close to the shear plane as possible.

The LDSM allows for 150 mm of horizontal travel; equivalent to approximately 21% horizontal strain. Small scale direct shear tests on the spoil intended to be tested in the LDSM indicated that a peak shear stress was generally reached between 10 and 15% horizontal strain. The available 21% allows for any potential scale effects, and for post-peak stress-strain behaviour to be observed. The nominal rates of displacement will vary for the category of spoil tested and the saturation condition; and will be determined from full-scale consolidation tests on the LDSM.

For comparison purposes, Figure 10 shows the internal shear box of large direct shear machine and a standard size shear box inset.

Figure 10 - Scale comparison: Internal shear box of large direct shear machine, with a standard size shear box inset

LDSM outputs

It is anticipated that the proposed LDSM will provide peak shear strength data for coal mine spoils subjected to a wide range of confining loads, particularly those representative of very high dumps. The

widest possible range of coal measures spoil types will be tested at various moisture contents in keeping with the strength mobilisation modes outlined in the BMA Coal strength framework.

The framework is used with confidence to characterize coal measures spoil dumps up to 120 m high. The LDSM data will be used to generate the full-scale stress-strain data required to extend the BMA Coal strength framework to reliably assess the stability for spoil dumps up to 400 m high.

Additionally, the LDSM will allow for scale effects to be measured. Although some scalping will be necessary to accommodate its capacity, it is expected that the stress-strain data can be calibrated by back-analysis of existing very-high coal mine spoil dumps.

CONCLUSIONS

The uncertainties associated with the application of current shear strength models to very high coal measures spoil dumps have been presented, and scale-effects inherent to standard laboratory testing of mine spoils have been discussed. These shortcomings can only be overcome by the construction of a purpose built machine capable of simulating field-scale conditions; however access limitations prevent the use of existing large-sample-high-stress machines for testing Australian coal measures spoils. A large direct shear machine (LDSM) has been designed at the University of Newcastle as part of a postgraduate research project. It is anticipated that the LDSM will provide reliable stress-strain data for full-scale samples of spoil subjected to loads representative of very high dumps. The data will be used to update and extend the BMA Coal strength framework to cover these higher stress ranges.

ACKNOWLEDGEMENTS

This paper describes aspects of the first author's postgraduate research, funded by Australian Coal Association Research Program as Project C20019 based at the University of Newcastle. In-kind support from Thiess Pty Ltd, particularly for provision of the hydraulic components vital to the operation of the LDSM, is gratefully acknowledged.

REFERENCES

Barton, N and Kjaernsli B, 1981. Shear strength of rockfill, *Journal of the Geotechnical Engineering Division*, ASCE, 107(GT7):873-891.

Boyd, G, 1976. Spoil pile stabilization - report on conditions for failure and minimum pit preparation for stability. *Utah Development Company Report*.

Charles, J A and Watts, K S, 1980. The influence of confining pressure on the shear strength of compacted rockfill, *Géotechnique,* 30(4):353-367.

Clover Technology, 2012. GALENA Slope stability analysis system, version 6.00 [online]. Available from: www.GalenaSoftware.com.

Gonano, L P, 1980. An integrated report on slope failure mechanisms at Goonyella. Technical Report Number 114, Division of Applied Mechanics, Institute of Earth Resources, Commonwealth Scientific and Industrial Research Organisation, Victoria.

Leps, T M, 1970. Review of Shearing Strength of Rockfill, *Journal of the Soil Mechanics and Foundations Division*, ASCE, 96(SM4):1159-1170.

Linero, S, Palma, C and Apablaza, R, 2006. Geotechnical Characterisation of Waste Material in Very High Dumps with Large Scale Triaxial Testing. *Proceedings International Symposium on Rock Slope Stability in Open Pit Mining and Civil Engineering 2007* (ed:Y Potvin). pp 59-75 (Australian Centre for Geomechanics: Perth).

Mallett, C W, Dunbavan, M, Seedsman, R W and Ross, D J, 1983. Stability of spoil piles and highwalls in deep surface mines. End of Grant Report Number 150, National Energy Research Development and Demonstration Program, Australian Government, Canberra.

Simmons, J, and McManus, D, 2004. Shear strength framework for design of dumped spoil slopes for open pit coal mines, in *Proceedings Advances in Geotechnical Engineering: The Skempton Conference* (ed: RJ Jardine, DM Potts & KG Higgins) Vol 2, pp 981-991 (Thomas Telford).

Vallerga, B A, Seed, H B, Monismith, C L and Cooper, R S, 1957. Effect of shape, size, and surface roughness of aggregate particles on the strength of granular materials, *Special Technical Publications*, American Society for Testing and Materials, 212:63-74.

EVALUATION OF STRUCTURAL COMPONENT DESIGN IN LIFE-OF-MINE PLANNING

Greg Kay[1] and Michael Salu[2]

ABSTRACT: Industry practice around structural component design has progressed significantly in recent years with a key result being the application of known engineering principles to the design of ventilation control devices and bulkheads. The properties of shot blast products are now well understood with computer modelling and full-scale live blast test analysis having aided the selection of the most effective type of device for specific site conditions. However, as underground mines increasingly focus on life-of-mine planning, understanding the long-term behaviour of installations plays an increasingly important role in structural system design. As many structural components found in underground mines have been designed and certified at time of installation, the review of these installations, specifically the impact of environmental and other factors, provides the opportunity for continued learning and development in this area. Studies conducted at underground mines where structural components have undergone long term testing and monitoring are discussed. The impact of key environmental conditions on the behaviour of structural components in underground mines is described. The limitations of current testing and monitoring processes as well as opportunities for long term mine planning are assessed.

INTRODUCTION

While rigorous assessment is conducted at the time of mine planning to minimise safety risk and maximise production capabilities, the impact of unpredictable natural events such as severe weather, geological changes and seismic activity, can impact on the long term effectiveness of mine planning. Structural devices are used extensively in underground coal mines to segregate and stabilise mined-out areas as well as to isolate underground areas that are susceptible to fire, gas, water or unstable geological conditions. Stoppings are typically designed for differential air pressures up to 35 kPa (5 psi) while seals are typically designed to resist blast pressures of 140 to 345 kPa (20-50 psi). Other structural devices, including water-retaining bulkheads and dam walls play a critical role in storing and retaining water, often in areas where high heads and volumes of water are prevalent. In designing bulkheads and dam walls, the erosion capacity of water, combined with an analysis of the surrounding strata conditions, play a significant role in determining the factor of safety. Structural components have traditionally been constructed using a variety of materials and methods to address specific mine site conditions. However, as many installations have been temporary in nature, specific research into the construction requirements and performance measurement of devices has been limited.

As coal mines age and become more developed, greater attention needs to be placed on the long term integrity of structural devices. The risk of a device failure has the potential to be catastrophic and while sound engineering principles can be applied in the design stages, substantive measurement and monitoring of installed structural components is of critical importance.

In addition to reviewing the various factors influencing long term structural integrity, this paper highlights structural components installed at Australian mine sites as an assessment model. With the benefit of having engineered and constructed a range of structural devices at the site more than five years ago, as well as having implemented an ongoing site audit and assessment regime over a number of years, this paper assesses the design and construction of structural devices and reviews key environmental factors that have impacted on the devices' long term integrity.

STRUCTURAL COMPONENT DESIGN BACKGROUND

The long-term effectiveness of a structural device relies on many factors including geology, sitting, design, materials, construction and maintenance. While mine planning relies on comprehensive models to simulate the various scenarios of flow distributions, gas capture designs, inertisation strategies, head of water and geological and seismic activity, predicting the performance of underground structures has

[1] *Aquacrete, Newcastle, NSW, Australia, gregk@aquacrete.com.au, M: 04 3866 8051*
[2] *Parsons Brinckerhoff, Brisbane, QLD, Australia*

posed a significant challenge for underground mines. In 1998, Aquacrete worked with Parsons Brinckerhoff (PB) to develop an engineering basis for the design of shotblasted seals, stoppings and other structural components for underground mines.

With data obtained from live underground testing of structural devices, explosion dynamics and structural responses of full-size stoppings were analysed to establish precise device specifications. While limited testing had been conducted at purpose-built facilities such as the Londonderry testing facility in New South Wales, Aquacrete selected an underground mine in Western Australia which allowed the use of higher blast pressures due to full underground confinement of explosive testing. This enabled a wider range of tests to be completed and the results could be confidently extrapolated to ensure closer relevance to operational mines.

The blast test results were analysed and used to calibrate a 3-dimensional finite-element computer model of a seal subjected to blast loading. This calibration began by transferring actual pressure distribution contours from the testing and then compared axial, bending and shear stresses as well as total loading and deflection between various configurations. The results were then used to develop a design tool that is now widely used to assess the required thickness of a structure for any combination of height, width, over pressure, head of water and factor of safety for individual site location. Following the successful application of this model over a number of years, Aquacrete again worked with PB to conduct trials on its water-resistant product to determine an engineering model for the construction of water-retaining bulkheads and dam walls. Compressive strength and water permeability were tested on full-size structural devices at varying time intervals from two days up to three months to gain a full understanding of material behaviour, which would be vital to accurately predict structural performance.

In developing the engineering parameters for bulkheads and dam walls to withstand sustained water pressure, certain key differences to blast pressure were relevant:

- Water pressure is not constant, with maximum pressure exhibited at the base of the bulkhead or dam and varying pressure elsewhere;
- Sustained water pressure over a significant period of time can lead to softening;
- Sustained water pressure poses the risk of leakage through fractures and strata surrounding the bulkhead;
- Unlike Ventilation Control Devices (VCDs) and bulkheads that are supported on four sides, dam walls are supported on three. This results in a reduction in robustness, which is addressed by use of appropriate factors of safety;
- Unpredictable roof falls can generate a pressure wave to a bulkhead or create a surface wave to over-top a dam.

DEWATERING SUMP DAM WALLS AND BULKHEAD DESIGN

Largely as a result of the high level of risk associated with the design and construction of dam walls and bulkheads, many underground mines specify large factors of safety that take into account uncertainties in construction, nature of the surrounding strata and potential for roof falls or explosions in the goaf. A significant factor in the design of dam walls is that, unlike VCDs and bulkheads that are supported on four sides, dam walls are supported on three. This results in a reduction in robustness, which is addressed by use of an appropriate factor of safety. Unpredictable roof falls that can generate a surface wave to over-top a dam need to be considered in addition to the static water pressure.

In developing the design parameters for dam walls and bulkheads at a dewatering sump installation in New South Wales (Figure 1), PB considered the mine plan that had been developed to address the faults and geological nature of the mine. These factors necessitated each device to be independently designed to address the potential life of device, based on the water head, the geological factors affecting each site as well as consideration for the duration of potential exposure of the seal to the mine workings before becoming part of the goaf.

The engineering solution encompassed the design and installation of a combination of bulkheads and dam walls (Figure 1). Due to the extensive approach, combining the use of bulkheads and dam walls to mitigate potential risks and unforeseen events, the mine requested a factor of safety of two.

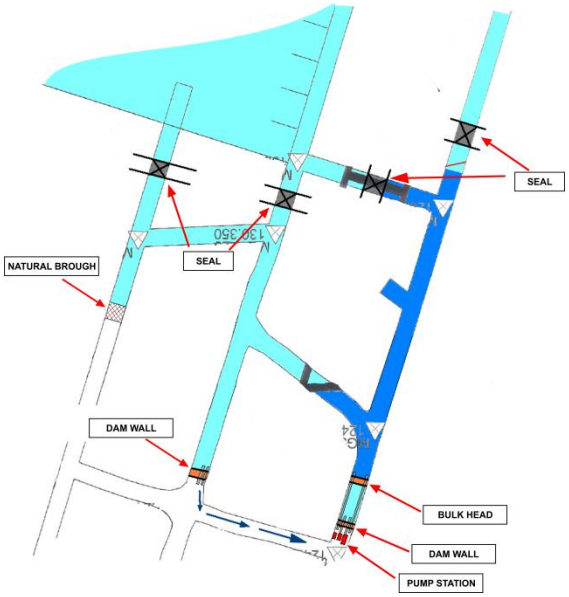

Figure 1 - Dewatering sump dam wall and bulkhead design

Dam wall 1 (Figure 2) was designed to accommodate a 5.6 m wide x 2.4 m high cavity while Dam wall 2 was designed to be 5.61 m wide x 2.0 m high. The dam walls were installed using accepted shotblast techniques, achieving a thickness of 400 mm and 350 mm respectively, and included a 200 mm key all around into the ribs and floor.

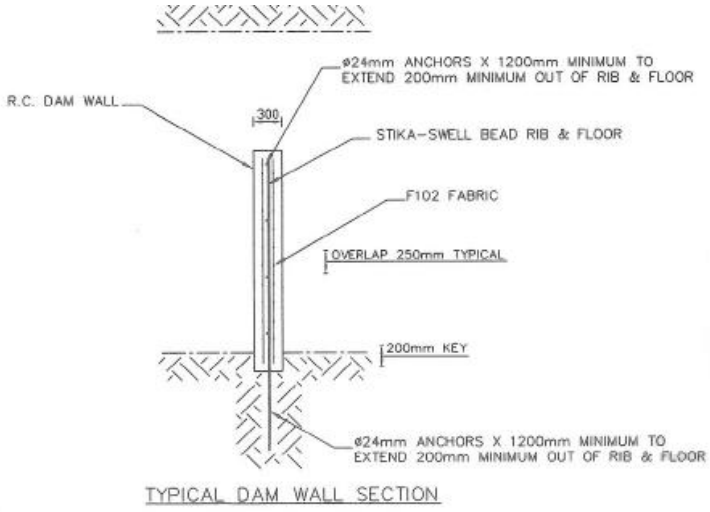

Figure 2 - Dam wall design, side view shown

INSPECTION AND MONITORING OF BULKHEADS AND DAM WALLS

Regular inspection of structural devices not only contributes significantly to their successful long-term performance, but also impacts on the safety of operational environments. Having identified the potential stress of the dam walls at the New South Wales site, PB worked with Aquacrete to establish a site audit procedure that has been implemented consistently over a period of two years.

Visual inspections

Ongoing fluctuations in water level behind the dam walls, combined with the three-sided construction of these devices provided an ideal monitoring environment where visual inspections could assess potential deterioration and stress of the dam walls and their surrounding strata.

Key areas of observation included:

- An inspection of the surrounding strata to identify water leakage;
- Potential softening of the structural device;
- Erosion and breakdown of structural integrity;
- Measurement of device thickness.

As outlined in Table 1 below, following inspections conducted over a period of two years, no visual deterioration or softening to the surface of the dam wall has been observed. An assessment of the dam walls' ability to cope with the variations in water pressures and geological activity have been monitored and reviewed by the mine staff and potential risks have been re-assessed to determine any changes in the site conditions.

Following one event on site, where an unplanned power outage prevented water from being pumped outbye, the site engineer reported that the water head reached a height of 2.5 m. The water pressure as a result of this incident was well in excess of the design specifications. While site engineers took all necessary precautions to maintain site safety during the event, inspection of the dam walls after the event confirmed that no water leakage occurred and the dam wall maintained full integrity.

Table 1 - Site inspection summary table

Site Inspection Date	Site Observations
August 2010	Inspection of 2 completed bulkheads and 1 dam wall. Inspect preparation for 2nd dam wall. Bulkheads and dam wall installed to specification. Strata bond appears good ; effective overspray carried out
December 2010	Inspection of completed works. Dam walls sprayed to 500mm thickness
October 2011	Inspection of dam walls. No deterioration or erosion of device. Wall thickness measured and still 500mm
November 2012	Inspection of dam walls. No deterioration or erosion of device. Wall thickness and velocity testing confirm structural integrity of devices

Non-destructive testing

While visual inspections of structural devices provide significant reassurance of a structure's integrity, the 'health' of a device can be verified with the use of echo impact testing. This method of testing uses sound waves to test a material for integrity and strength properties. It works by striking a surface with a hammer and then measuring the elapsed time for the sound waves to reflect off the far surface. If there are any defects within the material such as voids, the sound waves will not transmit through and the instrument will record the sound waves bouncing off an apparently thinner section.

If the thickness of a section is known, as is the case with the installed dam walls at the New South Wales mine site, then the speed of sound in the material can be measured. Following extensive trials with an echo impact tester on VCDs, PB has worked with Aquacrete to confirm the performance and suitability of this testing method as it applies to the density and material structure of Aquacrete products.

Levels of testing have included testing of cored samples (Table 2) as well as verification of installed seals both in a controlled environment (Table 3) and a live underground site (Table 4). These results have verified the effectiveness of long term monitoring of structural devices using non-destructive testing methods.

Testing of dam wall integrity at the New South Wales site has confirmed that structural integrity of the devices has been maintained, with the measured thickness being verified by the measurements shown in the echo impact testing.

Table 2 - Results from testing cored samples

Material	Average Cylinder Height (mm)	Average Velocity (m/s)
Aquacrete OPR2	199	2250
Aquacrete Wet-Repel	203	2550

Table 3 - Results from mines rescue station

Location	Material	Tested thickness	Actual thickness	Average velocity (m/s)
Stopping 1	OPR2	218	200	2200
Stopping 2	OPR2	150	155	2150
Stopping 3	Wet-Repel	216	209	2420

Table 4 - Results from underground mine testing

Location	Stopping/Rating	Tested thickness	Minimum thickness	Pass/Fail
Site 1 c/t	OPR2/2psi	86	75	Pass
Site 2 c/t	OPR2/2psi	93	75	Pass
Site 3 c/t	OPR2/5psi	162	100	Pass
Site 4 c/t	OPR2/5psi	138	100	Pass

SUMMARY AND CONCLUSIONS

Live testing and the subsequent development of engineering models have been used for many years to provide mines with the assurance that their structural devices are constructed to withstand the geological and operational conditions relevant to individual mine sites.

As the focus in underground mining continues to shift to life-of-mine planning, mines are increasingly looking for reliable tools and methods to measure and monitor the structural integrity of devices, particularly in environments where unpredictable events have the potential of affecting underground safety.

Using structural design specifications as a benchmark, and applying an audit process encompassing a combination of visual inspection and non-destructive testing processes has proved to be an effective monitoring approach for a New South Wales mine.

There is significant opportunity for the mining industry to develop new methods that will further assist in life-of-mine planning for structural devices, which in turn will provide greater assurance of underground safety and productivity.

REFERENCES

Kay, G, and Salu, M, 2009. Performance testing and certification of ventilation control devices, *Queensland Mines Inspectorate Sealing Parts of a Coal Mine Semina 2009.*

Pearson, D, Gillies, ADS, Day, R and Dux, P, 2000. Evaluation of a full scale pressure test for ventilation control devices, *ACARP Final Report C8006 December 2000.*

Oberholzer, J W, 2002. Develop in-situ test methods for ventilation structures - Phase 1 *ACARP Final Report C10014 May 2002.*

Salu, M S, 2005. Predicting the performance of underground mine seals, *Technical Excellence Committee presentation for Parsons Brinckerhoff, Brisbane, Queensland, Australia.*

Tuck, M A, 2011. Mine Ventilation, in *SME Mining Engineering Handbook.* Ch 15.3 (SME Littleton).

Kay, G and Salu, M, 2011. Advances in *in-situ* testing of ventilation control devices for underground mines, *University of New South Wales Mine Ventilation Conference 2011.*

Pearson, D, Gillies, ADS, Green, A, Day, R and Dux, P, 2000. New approaches to the design and evaluation of mine stoppings and seals *Queensland Mining Industry: A New Era in Mine Health and Safety Management Conference 2000.*

Foreman, J, 1998. Engineered structures for sealing underground mines, *West Virginia Surface Mine Drainage Task Force Symposium 1998.*

MEGA PROJECT DEVELOPMENT: OPTIMISING CURRENT PRACTICES AND STRATEGIES

Richard Wittig

ABSTRACT: The forecast capital cost for the 295 Australian projects that are in the project development phase (Evaluation) is approximately A$245 billion. With average prices for projects increasing, the project development phases have never been more critical (Australian Government, Bureau of Resources and Energy Economics 2012). Project development in the Australian mining community is generally undertaken in four separate stage-gated study phases Resource Planning, Concept, Pre-feasibility and Feasibility. Each phase further defines the level of maturity required for investment, risk and project portfolio evaluation purposes. However, even with this mature project development approach, the vast majority of mining mega projects has experienced cost and schedule overruns. Current industry practices are outlined, which suggests a vertically integrated framework for the four study phases through project development. This approach is focused on increasing the links between project development and program and project portfolio management and presents a new vertically integrated model in an optimised project development life cycle, adapted from current standard linear.

INTRODUCTION

In 2012, the Australian Government Bureau of Resources and Energy Economics (AGBREE) noted that there are 393 listed projects within Australia of which 98 are in the advanced (Implementation) category and 295 are in the less advanced (Project Development Phase) category. The total value of the proposed capital expenditure for the advanced projects is over $260 billion which is a 34 per cent increase from April 2011.The forecast capital cost for the less advanced projects currently under evaluation is approximately $245 billion. The Australian mining sector was spending at record levels in 2010-2011; mineral exploration expenditures were double the average expenditure during the previous 30 years (AGBREE, 2012).With the current market fluctuations and uncertainty, mega projects have to deal with competing projects, frequently changing context, purposes, cost constraints and ambitions (Giezen, 2012). Average prices for projects are increasing and the project development phases have never been more critical. These key study phases ensure that proposed projects align with current business strategies as well as provide confidence in long term asset viability during international downturns (Smith, 2006; AGBREE, 2012).

The Project Management institute (2008) describes a "project" as a temporary endeavour undertaken to create a unique product, service or result. Development, on the other hand is defined in the Oxford Dictionary (2012) as a specified state of growth or advancement. In this paper, the term "project development" refers to a staged approach which increases the maturity and definition of a proposed mine as a temporary endeavour. Project development in the Australian mining and metals industry generally comprises four separate stage gated study phases Resource Planning, Concept, Pre-feasibility and Feasibility (Anglo American, 2009). Each phase(see Figure 1) further defines the level of maturity required for engineering and construction, investment, risk and project portfolio evaluation purposes at relevant stages of the project development(Yescombe, 2002; Nethery, 2003; Madic, 2011). The study phases are generally depicted as a linear approach moving from one phase to the next via stage gate approval processes. In each phase, the owner develops a detailed definition of the scope and engineering requirements for a capital project to meet business objectives (Independent Project Analysis, 2004). The level of maturity and cost of the project scope is further refined as it progresses from one phase to the next through the development of standard deliverables and the estimating process.

The maximum ability to influence value for the project occurs in the Concept and the first half of Pre-feasibility study phases of the project development cycle. As the project progresses through the subsequent project development phases, the implementation of change has a disproportionate effect on cost (Van Der Weijde, 2008).

QISB Pty Ltd, rwittig@hotmail.com, M: 04 0182 0263

Figure 1 - Linear project development cycle (Anglo American, 2009)

THE STAGE-GATE PROCESS

The stage-gate process is a review of the project based on the developed deliverables in each project development phase. This review is generally provided by specialists who assess the project against its objectives and measure the project's potential to provide continuing value in the next phase of development (Cooper, *et al.*, 2002). If the project does not align with the expected benefits or strategic objectives, or it does not provide business confidence at any stage of the project review cycle, the study may return to the start of the phase, or be returned to the key value-adding phases of Concept and Pre-feasibility (Mackenzie and Cusworth, 2007). The objective of the stage-gate process is to validate the project maturity and benefit alignment, as well as identify implementation issues in a later phase (Magnussen and Samset, 2005). The stage-gate process also allows program and project portfolio input into the long term project strategy. As a point to note, according to Anglo American (2009), approximately 12.5% of mega projects in the minerals industry actually deliver on the benefits that were originally anticipated.

PROGRAMS AND PROJECT PORTFOLIOS

Organisations are increasingly using projects as a means to achieve their business objectives economically which increases the number of projects and therefore creates the need for program and portfolio management (Blomquist and Muller, 2006). According to Ataya (2007), programs are a structured group of interdependent projects that are both necessary and sufficient to achieve the desired business outcome and deliver value. A project portfolio is a grouping of programs, projects, services or assets which are selected, managed and monitored to optimise value (Ataya, 2007). Similarly, Koh (2010) has described portfolio management as a tool for optimising the organisational returns from project investments by improving the alignment of projects with strategy and ensuring resource efficiency. The key differentiator is that, unlike projects or programs, portfolios do not have a finite life. Portfolio management is a continuous process and requires regular tending to ensure the portfolio remains in balance and consistent with the organisation's strategic objectives (AIPM, 2011).

RESOURCE PLANNING PHASE

The purpose of the Resource Planning Phase is to identify deficiencies and gain confidence in the geological data from existing assets as a basis for the project pipeline development (Anglo American, 2008). This phase also identifies all value adding business alternatives and outlines a preferred approach to develop a potentially viable asset (Anglo American, 2009).At this initial stage of the project development cycle, uncertainty about the future is high and tolerance of project uncertainty is required (Atkinson, *et al.*, 2006).

The project pipeline developed in the resource planning phase provides internal competiveness between projects and strategies which ensure the focus remains on higher value projects (Anglo American, 2009). This focus on delivering corporate strategy is a key component of organisational success and long term growth (Aitken and Crawford, 2012).This body of work is generally a high level assessment based on current resource assets overlayed with project costs based on benchmarking data or factored project pipeline costs from recently estimated or executed projects (Golding, 2009). If the resource planning opportunity gains approval through the stage-gate process, it will then proceed to the Concept Study Phase. If not, the opportunity will be re-assessed in the resource planning phase and recycled as required.

CONCEPT STUDY PHASE

The purpose of a concept study is to define the future potential of a project, reduce sub optimal alternatives and determine if there is sufficient justification to continue to the next phase of development

(Noort and C, 2006).This work involves understanding and leveraging off the optionality generated in the Resource Planning Phase.

The concept study report should outline clear objectives, identify how the project fits into the program and project portfolio and is portrayed in a business perspective (Anglo American, 2009). It also outlines the project risk profile and its potential impact on development. Generally the concept study is a mix of benchmark, production or capacity factored top down cost estimates based on typical industry processing technology (Golding, 2009).At the relevant time the concept study is reviewed through a stage-gate process. It is assessed against the maturity of optionality, alignment with the business strategy and risk profile. If the project can demonstrate it has the capacity to deliver strategic objectives and has an acceptable risk profile, it will generally progress to the pre-feasibility study phase. If the project does not gain support through the stage-gate process it can be recycled back to the resource planning phase or return to the start of the concept phase (Mackenzie and Cusworth, 2007).

PRE-FEASIBILITY PHASE

The pre-feasibility study phase has two stages. The initial stage is primarily focused on assessing all valid options and identifying the best value case. The valid options are generally permutations of those developed in the concept study phase. The permutations are developed through an opportunity framing process in which operational and business unit stakeholders identify the potential development options in a workshop environment (Da, *et al.*, 2012). The valid options are scoped, estimated (capital and operating costs), risk assessed and financially modelled to ensure the best long term value option is selected. This process also identifies the key drivers and risks associated with each option and the organisation's risk appetite for the development of the preferred option.

At this stage of the project development market conditions and short to mid-term supply forecasts have emergent strategy impacts and may introduce additional or reduced optionality into the assessment process which was not identified or taken forward from the Concept study (Mintzberg, 1987). This is primarily due to the time duration of the studies to get to this stage. The preferred option is subjected to a mid-point stage gating process where the optionality is assessed against the business strategy and objectives.

The second stage of the pre-feasibility study involves validating that the selected case will retain value as the project maturity increases and the level of contingency decreases. At this point the majority of the deliverables change from a factored or top down methodology to a more quantifiable bottom up basis. This change from a top down factored estimate to a bottom up basis has a considerable impact on the resource project workload. At the end of the options assessment, the best value case is audited via the stage gate process to ensure it has the potential to deliver the benefits identified in the first stage of the Pre-feasibility Study Phase. If the project submission is not successful in the stage gate review, it may be recycled to the initial optionality framing stage of the Pre-feasibility Phase or even recycled to the start of the Concept Phase. Overall this is the most complex of the four study phases because of the dynamic nature of optionality refinement, assessment and selection (Collyer and Warren, 2009).This complexity is compounded by the integration alignment of key stakeholders from business, project, program and portfolio management. This alignment and agreement to project success then transfers into corporate success (Cook-Davies, 2002).

FEASIBILITY PHASE

The main objective of the feasibility study phase is to validate all previous design, economic assumptions as well as ensure the project aligns with both internal and external benefits (Bruzelius, *et al.*, 2002). This is the longest and most detailed of the four phases. The feasibility study provides a complete analysis of the project and its risk profile, justifies the project implementation, provides investment or funding basis for the project and supplies a detailed framework for monitoring cost control (Anglo American, 2008). This phase includes considerable value improvement processes which, according to Independent Project Analysis (2004), are out-of-the-ordinary practices used to improve cost, schedule, and/or reliability of capital projects. At the end of this phase, the study is subjected to the final stage-gate process in the project development cycle. If the project is successful in showing it can deliver the benefits and long term value originally forecasted, and provide confidence to the portfolio management team, it will progress to the execution phase. However there may be approval challenges even if the benefits cannot be realised. These challenges may result from higher performing projects receiving funding preference or changes in the strategic direction of the organisation, as seen in the mining and metals industry in the recent past.

AN INTEGRATED LIFECYCLE APPROACH

In the optimised approach, each study phase is not only linearly integrated with subsequent study phases in the project development lifecycle but has the added dimension of vertical integration with business strategy, program and portfolio management. This increases the project's exposure to major decisions which link deliberate and corporate strategy earlier in the study phase cycle (Mintzberg, 1987; Bowman, 2001).

The resource planning phase is primarily supported by data developed from concept, pre feasibility and feasibility studies for projects currently in execution within the organisation. Linking the start of the resource planning and the end of the typical linear feasibility study ensures the Resource Planning Phase has access to current project estimates and data. The cost benefit of this is seen immediately if the pipeline projects are similar to those being studied or executed as the estimates are considerably more mature than would be expected at this early stage of the development (Van Der Weijde, 2008). Resource planning is developed directly from the business strategy which becomes the core of the radial project development lifecycle. (Refer to Figure 6.) In this case, business strategy is primarily focused on how the business competes in a particular industry or market (Bowman and Helfat, 2001). As the business strategy area is encapsulated by the four phases of the project development cycle it creates axis point for vertical integration through each study phase.

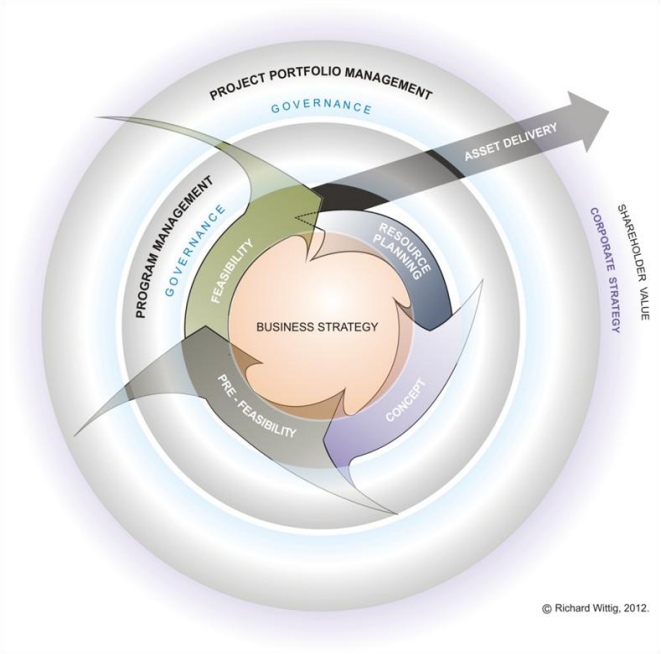

Figure 2 - Radial project development lifecycle

As Ataya (2007) has described, program management is a structured group of interdependent projects that are both necessary and sufficient to achieve the desired business outcome and deliver value. With that in mind, a program management and governance layer was added to the radial project development lifecycle.

As outlined earlier project portfolio is a grouping of programs, projects or assets, selected, managed and monitored to optimise value (Ataya, 2007). Considering the value management requirement of programs, project portfolio management and governance was added to the radial project development lifecycle. This provides the tool for optimising the business organisational returns from project investments by improving the alignment of project portfolios with corporate strategy (Koh, 2010; Bowman, 2001). The radial project development lifecycle includes a time aspect. This is in a clockwise motion based on the development timeframes associated with each study phase. The stage gate recycling process (non-approval) is in the form of anticlockwise movement. The project lifecycle phase can be reset so that the time impact can be clearly seen and further approval process understood. Once the project is approved at the end of the Feasibility phase it then moves into the asset delivery lifecycle. This asset delivery section outlines the transformation from project development cycle to execution phase and shows the value increase to the asset over time.

From a phased project approach, the utilisation of the radial lifecycle appears to offer the following vertical integration benefits:

- Resource Planning
  - A clear link with business strategy during initial idea generation
- Concept Phase
  - Ongoing integration with business strategy and project pipeline optionality
  - Project optionality supported by business strategy area
  - Early integration to program management and governance requirements
  - Early project exposure to program management approvals
- Pre-Feasibility Phase
  - Embedded business strategy and practices within the project
  - Project optionality supported by program management and governance and business strategy areas
  - Embedded program management approvals and governance requirements
  - Early integration with project portfolio governance requirements
  - Early exposure to project portfolio management approvals
- Feasibility Phase
  - Project "option" supported by program, project portfolio and business strategy areas
  - Embedded program, portfolio management and governance practices within the project
  - Integrated with board level approvals and governance requirements
  - Provides ongoing integration with business strategy and project pipeline optionality via supply of real time pricing for resource planning optionality planning.

As can be seen in Figure 2, project, program and project portfolio management can be linked to the business strategy axis point at any stage of the project. This also defines the current level of integration and forecasts the level of engagement required to ensure all stakeholders are aligned with the project requirements. This strategic alignment is critical to enable optimum resource utilisation whilst working inside the mandated strategic boundaries and identified constraints (Smith, *et al.*, 2006)

CONCLUSIONS

The success of any mining company is primarily due to its ability to effectively manage its capital investment in a strategic context to ensure acceptable stakeholder returns (Smith, *et al.*, 2006). The objective of the resource planning study phase is to provide a pipeline of projects to be evaluated to ensure growth from business strategy and existing assets. The concept study focus is to validate the business opportunity and identify the scope alternatives that will be the subject of a trade-off evaluation in the next phase (Anglo American, 2009). The objective of the Pre feasibility study is to assess all valid options, narrow the project to one scope and confirm project economics and the role of the fourth study phase, feasibility, is to validate all previous design and economic assumptions and ensure the project aligns with both internal and external benefits(Mackenzie, 2007; Bruzelius, *et al*., 2002).

By utilising the vertically integrated optimised model, each study phase is linearly integrated with the added value of vertical integration within the project development lifecycle. This vertical integration with business strategy, program and portfolio management increases the project's exposure to governance which links deliberate and corporate strategy earlier in the study phase lifecycle, thereby increasing the chance of project success (Mintzberg, 1987; Bowman, 2001).

A summary of benefits, as outcomes from the project development phases, is, improved cost predictability, enhanced cost effectiveness, better schedule predictability, faster project delivery (schedule effectiveness), optimised scope, and better operability and safety performance (Van Der Weijde, 2008).
The realisation of the project development phases is easily quantified once the project becomes operational. The focus then turns from project development to operational efficiency and long term optimisation where the long term value is extracted from the asset (Mackenzie and Cusworth, 2007).

In summary, project development plays a crucial role in corporate strategy via the delivery of benefits through portfolio, program and project management to enable long term business growth delivered through the operating facilities we extract value from today (Aitken and Crawford, 2012).

REFERENCES

AIPM, 2011. AIPM professional competency standards - Part F certified practising portfolio executive, AIPM, Sydney.

Aitken, A and Crawford, L, 2012. Delivering on strategy - Benchmarking your way to better performance, Human Systems Asia Pacific Pty Ltd, Bond University Master of Project Management Class Material.

Anglo American, 2008. Project managers handbook, Anglo American, viewed 1st August 2012, https://technical.angloamerican.com/.

Anglo American, 2009. Group Asset development standard rev, viewed 1st August 2012, www.anglotechnical.co.za/AA_STD_000002.PDF.

AIPM, 2011. AIPM professional competency standards - Part F certified practising portfolio executive, AIPM, Sydney.

Aitken, A and Crawford, L, 2012. Delivering on strategy - Benchmarking your way to better performance, Human Systems Asia Pacific Pty Ltd, Bond University Master of Project Management Class Material.

Anglo American, 2008, Project managers handbook, Anglo American, viewed 1st August 2012, https://technical.angloamerican.com/.

Anglo American, 2009. Group asset development standard rev, viewed 1st August 2012, www.anglotechnical.co.za/AA_STD_000002.PDF.

Ataya, 2007. Portfolio management - Unlocking the value of IT investments, *Information Systems Control Journal*, 4:1-2.

Atkinson, R, Crawford, L and Ward, S, 2006. Fundamental uncertainties in projects and the scope and the scope of project management, *International Journal of Project Management*, 24:687-698, doi:10.1016/j.ijproman.2006.09.011.

Australian Government, Bureau of Resources and Energy Economics 2012, http://www.bree.gov.au/publications, viewed 20 August 2012.

Blomquist, T and Muller, R, 2006. Practices, roles, and responsibilities of middle managers in program and portfolio management, *Project Management Journal*, 52-66.

Bowman, E and Helfat, C, 2001. Does corporate strategy matter? *Strategic Management Journal*, 22:1-23.

Bruzelius, N, Flyvbjerg, B and Rothengatter, W, 2002. Big decisions, big risks. improving accountability in mega projects, *Transport Policy 9*, 9:143-154.

Collyer, S and Warren, C, 2009. Project management approaches for dynamic environments, *International Journal of Project Management*, 27:355-364,doi:10.1016/j.ijproman.2008.04.004.

Cook-Davies, T, 2002. The "real" success factors on projects, *International Journal of Project Management*, 20:185-190.

Cooper, R, Edgett, S and Kleinschmidt, E, 2002. Optimising the stage gate process, *Industrial Research Institute*, 45(5):1-14.

Da Siva, P, Gillespie, B and and Buckeridge, F, 2012. Investment appraisal of mining capital projects, Brisbane, viewed 1st September 2012, http://www.pwc.com.au/industry/energy-utilities-mining/publications/index.htm.

Giezen, M, 2012. Keeping it simple? A case study into the advantages and disadvantages of reducing complexity in a mega project planning, *International Journal of Project Management*, vol JPMA-01379, In Press.

Golding, T, 2009. Financial evaluation, in PG Newlings (ed.), Advanced Coal Preparation Monograph Series, Operation Management, 2nd edn, Australian Coal Preparation Society, Sydney, NSW, Australia.

Independent Project Analysis, 2004. Northwest Construction Consumer Council, viewed 29th August 2012, http://www.nwccc.org/past-presentations.cfm#pres79.

Koh, A, 2010. Investigating the roles, responsibilities and practices of portfolio managers in Australia; A literary review and research outline, PMOZ, Bond University, Bisbane.

Mackenzie, W and Cusworth, N, 2007. The use and abuse of feasibility studies, Project Evaluation Conference, Melbourne.

Madic, B, Trujic, V and Mihajlovic, I, 2011. Project portfolio management implementation review, *African Journal of Business Management*, 5(2):240-248.

Magnussen, M and Samset, K, 2005. Successful megaprojects: ensuring quality at entry, EURAM 2005 Responsible Management in an Uncertain World, TUM Business School, Munich.

Mintzberg, H F, 1987. The strategy concept: five p's for strategy, Calafornia Management Review, pp. 11-24.

Nethery, B, 2003. The role of feasibility studies in mining ventures, Conference Board of Canada, Structuring More Effective Mining Ventures, AMEC Mining and Metals, Vancouver.

Noort, D and C, A, 2006. Effective mining project management systems, International Mine Management Conference, Melbourne.

Oxford Dictionaries, 2012. Dictionary, viewed 1st October 2012, http://oxforddictionaries.com/definition/english/development?q=development.

Price Waterhouse Coopers, 2012. Investment appraisal of mining projects, Brisbane, viewed 1st September 2012, http://www.pwc.com.au/industry/energy-utilities-mining/publications/index.htm.

Project Management Institute, 2008. Glossary, definitions, in A guide to the Project Management Body of Knowledge, 4th edn, Project Management Institute, Newtown Square, PA, USA.

Smith, G, Anderson, D and Pearson-Taylor, J, 2006. Project valuation, capital investment and strategic alignment - tools and techniques at Anglo Platinum, *The Journal of Southern African Institute of Mining and Metallurgy*, 195-203.

Van Der Weijde, G, 2008. Front end loading in the oil and gas industry, towards a fit front-end development phase, Delft University of Technology.

Xstrata, 2012. Xstrata, viewed 02 September 2012, http://www.xstrata.com/investors/speechesandpresentations/2012/.

Yescombe, ER, 2002. Project development and management, in Principles of Project Finance, Elsevier, London, United Kingdom.

CHANGES IN ROCK PROPERTIES FOLLOWING IMMERSION IN VARIOUS CHEMICAL SOLUTIONS

Luke Summersby[1], Paul Hagan[1], Serkan Saydam[1] and Shu Ren Wang[2]

ABSTRACT: Many clay-bearing rocks will undergo changes in material properties after immersion in water. This is often accompanied by a reduction in strength and cuttability properties associated with increased degradation. In extreme cases such as with water active shales, it can lead to complete collapse or sloughing of the material. This can have important implications for Australian coal mining operations in terms of maintaining ground stability where clay-bearing rocks are in close proximity to coal formations.

Previous research has examined whether chemical solutions containing potassium chloride and copper sulphate could arrest these changes in rock properties. While they provided encouraging results, they did not fully explore the effects of altering the exposure times or concentrations of chemical solutions. The purpose of this paper is to outline the effect of changes in the concentration and exposure times of potassium chloride, magnesium chloride and copper sulphate solutions on clay-bearing rock.

The Slake Durability Index Test was used to examine the degradation of a claystone after immersion in a range of chemical solutions at different concentrations. There was little quantitative change due in part to the low permeability of the rock. Qualitatively it was found however that degradation was exacerbated following immersion in a copper sulphate solution and to a lesser extent with magnesium chloride. Conversely, potassium chloride at all concentrations was found to reduce the degradation effects of water.

Immersion of the test specimen in each of the solutions of potassium chloride, magnesium chloride and copper sulphate improved rock cuttability relative to dry, untreated rock.

INTRODUCTION

Clay minerals are found in most of the sedimentary rocks that make up the strata in coal formations (Hall, 1987). When clay comes into contact with water, it undergoes changes including swelling or dispersion (Ghazali, 2012). Certain clay minerals are more susceptible to swelling including smectitie, illite, kaolinite and chlorite. Such changes can lead to wall instability due to internal stresses generated by the swelling (Morkel, 2006). Moist clay-bearing materials will also experience lower strength, elastic modulus, cutting forces and pick wear (Mammen, *et al.*, 2007).

This phenomenon has posed particular problems in the oil and gas drilling industry where various chemical agents have been developed to mitigate the problems. In the case of mining, it can be particularly detrimental to the performance of machinery that uses drag picks such as roadheaders, longwall shearers and continuous miners. It has been reported for example that clay swelling can decrease the net cutting rate of these types of machines by up to 50% due to "sticky"faces (Bilgin, *et al.*, 2004).

Potassium cations in the form of potassium chloride were found to reduce the severity of this effect in rocks containing the clay mineral smectite (Morkel and Saydam, 2008; Nasr-El-Din, Al-Mulhem and Lynn, 1998). Research undertaken into another clay mineral, nacrite, showed similar results following immersion for 24 hours in potassium chloride. Interestingly immersion for only 6 h seemed to have magnified the degradation effects compared to the longer immersion time (Hagan, *et al.*, 2011).

These findings prompted further investigation into whether a treatment regimen could be optimized in terms of chemical selection, immersion time and solution concentration. The key parameters measured

[1] *University of New South Wales, Sydney, corresponding author: p.hagan@unsw.edu.au. Tel:+61 (0) 9385 5998*
[2] *School of Civil Engineering and Mechanics, Yanshan University, Qinhuangdao, China*

in the study were changes in degradation of the sample, forces of cutting, specific energy, yield, abrasivity and coarseness index.

EXPERIMENTAL PROCEDURE

Slake durability index test

Degradation of a rock sample following immersion in a chemical solution were assessed using the slake durability index test. This particular test is a measure of the resistance to degradation by subjecting material to four cycles of wetting, agitation and drying.

The solutions used in the test program included:

- pure water;
- KCl at concentrations of 0.5, 1.5 and 3 Molar;
- $MgCl_2$ at 1.5 M; and
- $CuSO_4$ at 1.5 M.

The 1.5 M solution was selected as the standard concentration in order to allow comparison with previously reported results by Deramore Denver (2010). These solutions were used as the slaking fluid in the test. The 0.5 M and 3.0 M solutions were selected to examine whether if there exists some critical salt concentration and whether changes in concentration have any effect on the extent of degradation.

A claystone sample from Ulan Coal Mine was used in the test. The main clay-bearing mineral in the sample is kaolinite. This mineral has a similar composition and clay chemistry to nacrite (Ghazali, 2012). Test specimens were prepared by crushing a sample into fragment sizes each weighting within the range of 40 to 60 g with the rough edges and corners removed to create rounded lumps of rock as per the suggested method of the ISRM (1981). Ten lumps having a combined mass of between 480 and 500 g were then placed into a steel mesh drum and oven dried at 105 °C to remove all inherent moisture before being weighed. The drum containing the rock fragments was placed within a tank and filled with the test solution as shown in Figure 1.

Figure 1 - Slake durability index test apparatus

The drum was rotated within the solution at 20 rpm for 10 min afterwhich the drum and its contents were removed and oven dried for 16 h before again being weighed. This set of processes comprise one slaking cycle. The results were calculated according to Equation 1:

$$I_{d2} = \frac{C - D}{A - D} \times 100\% \quad (1)$$

where:

I_{d2}: Slake durability index value;

C: mass of the drum plus retained sample portion after slake cycle;

A: initial mass of the sample;

D: mass of steel mesh drum.

The cycle was repeated four times and the results graphed.

Diffusion test

To determine the rate of diffusion of a solution within rock, a test was devised where 30 mm diameter specimens of rock core were submerged in a tank containing a solution of water and disodium a-[4-(N-ethyl-3-sulfonato benzyl amino) phenyl]-a-[4-N-ethyl-3-sulfonato benzyl amino) cyclohexa-2,5-dienylidene] toulene-2-sulfonate, a commonly found blue-coloured food dye. The methodology was modelled after experiments conducted by Mammen, *et al.* (2007). The test is based on the assumption that a chemical solution will diffuse into a rock mass at approximately the same rate as the dye molecules.

The test involved cores immersed in the dye solution at time intervals of 1, 2, 4, 8, 16 and 24 h. After a specimen had been immersed for the nominated time, it was cut open and the depth of dye penetration measured.

Core cuttability index test

The core cutting tests utilised a tri-axial dynamometer rock cutting rig as shown in Figure 2.

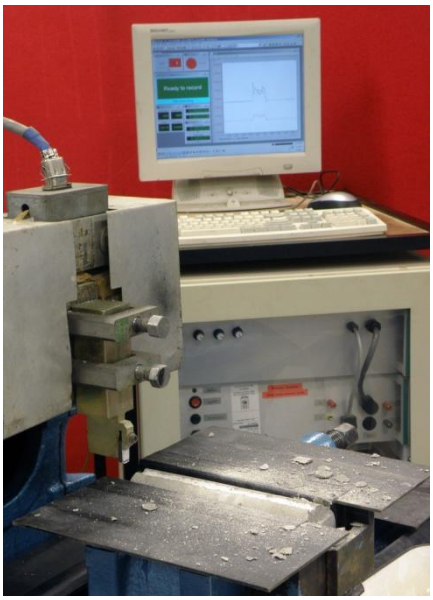

Figure 2 - Instrumentation used in the core cuttability test procedure at UNSW

The diffusion test revealed a treatment time of 24 h was required to obtain a penetration equivalent to the cutting depth of 5 mm.

In this test, diamond cored specimens of Hawkesbury Sandstone were used. The cores were first oven dried at 105 °C before being treated with a chemical solution.

Seven test scenarios were examined with solutions of different chemical composition and immersion times. The results were compared against dry untreated rock, the control specimen. The test solutions included pure water, KCl, $MgCl_2$, $CuSO_4$ where the test specimens were immersed for 24 h. A further three tests were conducted using a solution of KCl where the immersion times were 5 min, 1 h and 8 h. The concentration of each solution was held constant at 1.5 M.

In addition to measuring cutting forces and specific energy, the particle size distribution of the cutting debris was determined. This was based on the coarseness index procedure using sieve sizes of 4.75, 1.70, 0.50 and 0.125 mm.

RESULTS

Slake durability index test

The results for the slake durability index test are shown in Table 1.

Table 1 - Results of slake durability index test

slaking fluid	slake durability			
	I_{d-1} (%)	I_{d-2} (%)	I_{d-3} (%)	I_{d-4} (%)
water	100.0	100.0	98.7	98.7
KCl (0.5 M)	100.0	100.0	99.6	99.2
KCl (1.5 M)	100.0	100.0	100.0	98.8
KCl (3.0 M)	100.0	100.0	100.0	98.8
$MgCl_2$ (1.5 M)	99.6	99.2	98.3	97.9
$CuSO_4$ (1.5 M)	99.7	99.3	98.3	95.1

The magnitude of the mass change relative to the mass of the steel drum was small thus limiting quantitative analysis. However, the results indicated the degree of degradation was greatest using the $CuSO_4$ and $MgCl_2$ solutions while it was more limited with the KCl solution.

Diffusion test results

It was found that the penetration of solutions into the Hawkesbury Sandstone specimens could be modelled by a linear relationship for exposure times up to 24 h. This relationship is shown in Equation 2.

$$y = 0.117x + 1.45 \quad (2)$$

where:

y: penetration (mm);

x: exposure time (h).

With respect to the claystone, due to its very low permeability only surface staining was observed for all treatment times.

Cuttability index test

The results of the cutting tests are summarised in Table 2. They indicate there was a significant reduction in the cutting parameters of the test specimens that had been immersed in a solution whether it was pure water or any of the chemical solutions as compared to the dry, untreated rock specimen.

When considering immersed for 24 h, the reduction in forces and specific energy were all greater with the three chemical solutions than pure water. The greatest reductions of 56.5% and 25.2% was attained with the magnesium chloride solution compared to the dry and the water-only treated specimens respectively.

Unexpectedly, the abrasivity of the specimens was found to have increased substantially with all chemical solutions in comparison to the dry sample having more than doubled after immersion in the copper sulphate solution.

With respect to the series of tests that examined immersion times in a potassium chloride solution, there was a significant reduction in forces and specific energy even after the shortest immersion time of 5 min. This is consistent with the results reported by Mammen *et al.* (2007).

Interestingly the greatest reduction in cutting parameters was obtained with the potassium chloride solution after immersion for 8 h. This is consistent with the results reported by Hagan *et al.* (2011). As noted earlier, immersion for 8 h was unlikely to have allowed sufficient time for the solution to diffuse into the rock to a distance equivalent to the full cutting depth. The reductions in cutting parameters were of a similar magnitude to that achieved with the magnesium chloride solution after 24 h immersion.
A possible mechanism to explain this is that despite the immersion times being of relative short duration, it nevertheless allowed for sufficient penetration of the solution causing rupture of the clay sheets thus

improving cuttability. By contrast, an immersion time of 24 h would allow for penetration to the full depth of cut thus strengthening the rock within the entire cutting zone.

All treatments reduced the coarseness index by a small amount indicating only a minor decrease in cutting efficiency. Overall, the results achieved with an immersion time of 24 h are consistent with the results observed in smectite with a less exaggerated result for KCl (Morkel, 2006).

Table 2 - Results of core cuttability index test

solution & immersion time	force		specific energy (MJ/m^3)	impact abrasivity (mg/m)
	cutting (kN)	normal (kN)		
dry untreated	1.19	0.94	17.7	1.8
water (24 h)	0.74	0.59	10.3	2.2
KCl (24 h)	0.72	0.61	8.9	2.7
$CuSO_4$ (24 h)	0.62	0.37	8.4	4.2
$MgCl_2$ (24 h)	0.57	0.39	7.7	3.1
KCl (5 min)	0.79	0.63	11.2	6.8
KCl (1 h)	0.76	0.62	11.4	5.3
KCl (8 h)	0.55	0.38	7.9	3.2
KCl (24 h)	0.72	0.61	8.9	2.7

CONCLUSIONS

The results from the Slake Durability Index tests using Ulan claystone indicate the cations have a strong effect on durability of rock with the strength of the effect following the order: $Cu^{2+} > Mg^{2+} > H2O > K^+$.

It was found that the penetration rate of chemical solutions could be modelled using a linear relationship for exposure times up to 24 h for the Hawkesbury Sandstone. Furthermore, it was found that Hawkesbury Sandstone underwent a minor decrease in density following all treatment regimens with the exception of $MgCl_2$ where a slight increase was measured.

The results showed that treatments in solutions of KCl, $MgCl_2$ and $CuSO_4$ for 24 h improved cuttability relative to pure water and even more so when compared against dry, untreated rock (the control specimen). Prolonged immersion in KCl tended to stabilise the material to a level where the results similar to that achieved with pure water. When considering the results of Deramore Denver (2010), the optimum immersion time seems to be between 6 h and 8 h.

A possible mechanism behind these results is that while the shorter immersion times only allows for limited diffusion into the rock, it can cause rupture of the clay sheets which thereby improves cuttability. By contrast, a treatment time of 24 h allows penetration equivalent to the full depth of cut, strengthening the rock within the cutting zone. The results achieved from the 5 min and 1 h immersion intervals with KCl were likely attributable to the low level of diffusion resulting in values nearer that of the control. None of the chemical solutions improved stability to an extent comparable to the control specimen. Higher impact abrasivity was seen with all treatments. Overall, the 24 h results conform to the reactions observed in rocks containing smectite with a less exaggerated result for KCl (Morkel, 2006).

These findings will assist in the development of treatment regimens both for improving stability in excavations and improving cuttability in specific mining operations that contain kaolinitic clays.

REFERENCES

Bilgin, N, Dincer, T, Copur, H and Erdogan, M, 2004. Some geological and geotechnical factors affecting the performance of a roadheader in an inclined tunnel, *Tunnelling and Underground Space Technology,* 19: 629-639.

Deramore Denver, L, 2010. Enhancing the cuttability of rock using chemical solutions, Honours thesis (unpublished), University of New South Wales, Sydney.

Ghazali, 2012. Clay Chemistry [online]. Available from: <http://www.scribd.com/doc/56573987/Clay-Chemistry> [Accessed: 22 April 2012].

Hagan P, Saydam S, Elias E, Deramore Denver L and Hebblewhite B, 2011. The effect of certain chemical solutions on some material properties of clay bearing rocks, in *Harmonising Rock Engineering and the Environment - Proceedings of 12th ISRM International Congress on Rock Mechanics*, Beijing, 18-21 October, (Taylor and Francis Inc., United States).

Hall, P L, 1987. Clays: their significance, properties, origins and uses, *A Handbook of Determinative Methods in Clay Mineralogy*, pp 1-26 (Chapman and Hall: New York).

ISRM, 1981. Rock characterization, testing and monitoring: ISRM suggested methods, pp 92-121 (Pergamon Press: Oxford).

Mammen, J M, Saydam, S and Hagan, P, 2007. The study of the effect of moisture content on rock cutting performance, in *Proceedings 2009 Coal Operators' Conference*, Wollongong, Australia, pp 340-347 (The AusIMM Illawarra Branch).

Morkel, J, 2006. Kimberlite Weathering: Mineralogy and Mechanism, PhD thesis (unpublished), University of Pretoria, Pretoria.

Morkel, J and Saydam, S, 2008. The influence of potassium on the weathering properties of kimberlite and the information provided by different testing methods, *International Journal of Rock Mechanics and Mining Sciences,* 45:1187-1194.

Nasr-El-Din, H A, Al-Mulhem, A A and Lynn, J D, 1998. Evaluation of clay stabilizers for a sandstone field in central Saudi Arabia, in *Proceedings International Symposium on Formation Damage Control*, Lafayette, United States of America, pp 613-629 (Society of Petroleum Engineers).

NUMERICAL MODELLING OF CYLCIC SHEAR BEHAVIOUR OF ROCK JOINTS UNDER CANS CONDITION

Ali Mirzaghorbanali and Jan Nemcik

ABSTRACT: The cyclic shear behaviour of rock joints was investigated in the laboratory under constant normal stiffness condition for low and high values of initial normal stress and asperity angle. The Universal Distinct Element Code was applied (UDEC) to simulate the laboratory behaviour using two available models. The predicted shear stress, normal stress, and dilation with shear displacement were compared with experimental results. It was observed that the change in the shear strength and recovery of dilation upon load reversal are simulated using the Coulomb Slip model for low values of initial normal stress and asperity angle when the shearing mechanism was sliding over asperities. However, the Continuously Yielding model replicated better cyclic shear behaviour of rock joints under breaking mechanism (i.e. high levels of initial normal stress and asperity angle), as this model represents progressive damage of asperities during shearing and approaching to the residual friction angle when asperities are fully degraded.

INTRODUCTION

Designing of open cast and underground mining, construction of dams, and slope movements can be strongly influenced by the presence of joints within a rock mass. In this sense, a correct evaluation of the mechanical behaviour of joints and discontinuities including the stress-displacement relationship is imperative to simulate behaviour of a rock mass.

Patton (1966) was among the first researchers to systematically study the effect of joint asperity on the shear behaviour of rock joints and proposed a bilinear shear strength criterion. Jaeger (1971) replaced the bilinear form of Patton's with a non-linear function and introduced a new failure criterion. Barton (1973) performed an extensive number of laboratory tests on three dimensional joints and introduced a peak shear strength criterion incorporating the concept of joint roughness coefficient.

Barton (1976) modified the concept of joint roughness coefficient and introduced the mobilized roughness coefficient to capture the effect of asperity damage as a function of the normalized shear displacement. The continuously yielding model was proposed by Itasca Consulting Group (Cundall and Hart, 1984) to provide a coherent and unified discontinuity deformation and strength model for joints undergoing both elastic and plastic deformations. An effective mechanical model was introduced by Plesha (1987) who assumed sliding occurs along an inclined asperity angle degraded exponentially due to the plastic shear work. Gens *et al*. (1990) developed an elasto-plastic constitutive model for rock joints considering a hyperbolic yield function. In another study of shear behaviour of rock joints, Roosta *et al*. (2006) introduced an elasto-plastic constitutive model in a multi laminate framework.

Johnston and Lam (1989) presented an analytical model to determine the average shear resistance of concrete/rock interface under Constant Normal Stiffness (CNS) condition followed by Seidel and Haberfield (1995) who introduced a new shear strength criterion for rock joints based on the idealized asperity geometry. Indrarata (2000) extended the shear strength model proposed by Seidel and Haberfield (1995) by applying the Fourier series concept to represent the dilation of undulated joints in relation to shear displacement under a CNS condition. Finally, Oliveira and Indraratna (2010) revised Indraratna's model to better represent the post peak shear strength of rock joints.

Among the above mentioned models, the Continuously Yielding (CY) model along with the conventional Coulomb Slip (CS) criterion are extensively applied to simulate the shear behaviour of rock joints within the rock mass due to their simplicity and availability in Universal Distinct Element Code (UDEC). This study is an attempt to investigate the capabilities of CS and CY models in simulating the cyclic shear behaviour of rock joints under CNS conditions. Firstly, the results of large scale cyclic direct shear tests conducted on artificial rock joints for low and high values of initial normal stress and asperity angle under

University of Wollongong, Wollongong, NSW, Australia, 2500. am001@uowmail.edu.au, contact: Jan Nemcik, Tel:04 0871 1280

constant normal stiffness condition are presented. Subsequently, the UDEC code is applied to model the observed laboratory behaviour using CS and CY constitutive models.

SPECIMENS, TEST APPARATUS, AND EXPERIMENTAL PLAN

The joint surface was prepared based on a regular triangular saw tooth shape with inclination angles equal to 9.5° and 26.5°. The joint surface area for the prepared samples was 187.45 cm^2 (250 x 75 mm) with a total of 8 asperities (30 mm long) in the direction of shearing. A close view of the prepared sample with initial asperity angle equals to 26.5° is shown in Figure 1.

In this study, high strength Gypsum plaster ($CaSo_4.H_2O$ hemihydrates, fraction of $CaSo_4$ to H_2O = 3.5:1) was used to mould the artificial rock joints. This material can take any desired shape when mixed with water and the long term strength is independent of time once the chemical hydration is complete. The initial setting time of plaster is about 25 min. Furthermore, the cured plaster mix shows a repeatable uniaxial compressive strength in the range of 60 MPa which is comparable to many sedimentary rocks. Testing on planar joints with the Gypsum Plaster showed a basic friction angle of approximately 35°.

The large scale cyclic direct shear tests were conducted at the rock mechanics laboratory of University of Wollongong. The CNS direct shear apparatus (Figure 2) consists of two boxes, one of size of 250 mm in length, 75 mm in width and 150 mm in height, at the top and the other of size 250×75×100 mm, at the bottom. The bottom box is fixed on a rigid base by bearings and can only move horizontally. The top box can only move in the vertical direction along which the stiffness is kept constant by a set of springs simulating the normal stiffness of surrounding rocks. The desired initial normal stress is applied via a hydraulic jack located at the top of the apparatus where the applied load is measured via a calibrated load cell. The cyclic shear load is applied via a hydraulic actuator which is connected to the controller unit. The applied cyclic shear load is recorded via strain meters fitted to a load cell. Finally, the desired rate of cyclic displacement can be set by the controller unit.

Low and high values of initial normal stress (0.56 and 2.4 MPa) were applied to the samples. The specimens were sheared cyclically at a constant rate of 0.5 mm/min and under a constant normal stiffness of approximately 8 kN/mm. The values of shear load, normal load, and normal displacement were recorded upon the applied shear displacement during each cyclic shear test.

RESULTS OF EXPERIMENTS

Results of cyclic shear tests performed on the prepared samples for low and high values of initial normal stress and asperity angle are shown in Figures 3 (a) and (b). It is observed that for low levels of initial normal stress and asperity angle, the shearing mechanism is sliding over asperities with higher shear strength in forward loading rather than the reverse one. Asperity degradation is evident by reduction of dilation and appeared to be a function of loading cycle and shearing direction such that less damage was observed in reverse loading and further cycles. The shearing mechanism for high values of initial normal stress and asperity angle is breaking of asperities. The shear strength after the initial rapid degradation approaches the residual value and there is no difference in the shear strength between forward and reverse loading (i.e. no contribution of roughness in friction angle). After asperity breaking in first forward loading cycle, contraction may be observed rather than dilation. This might be related to the loss of damaged material from the shearing box when asperities are broken up from the base.

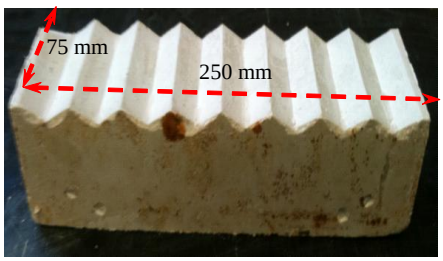

Figure 1 - A close view of artificial joint prepared for testing

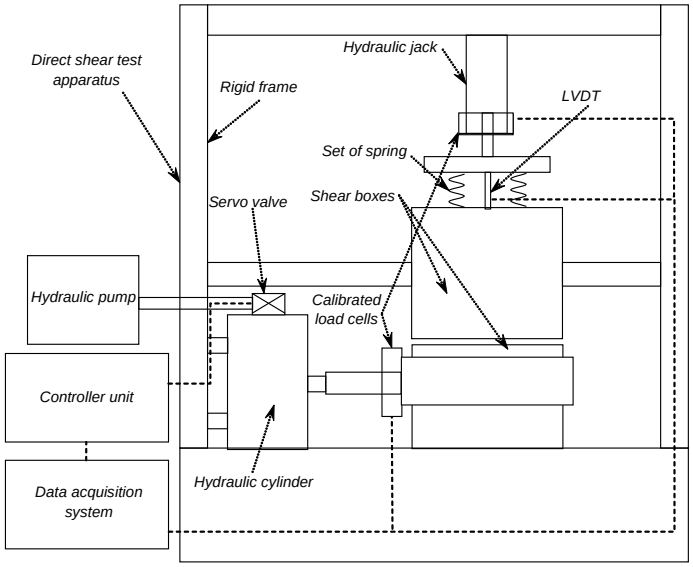

Figure 2 - Schematic diagram of the CNS cyclic shear apparatus

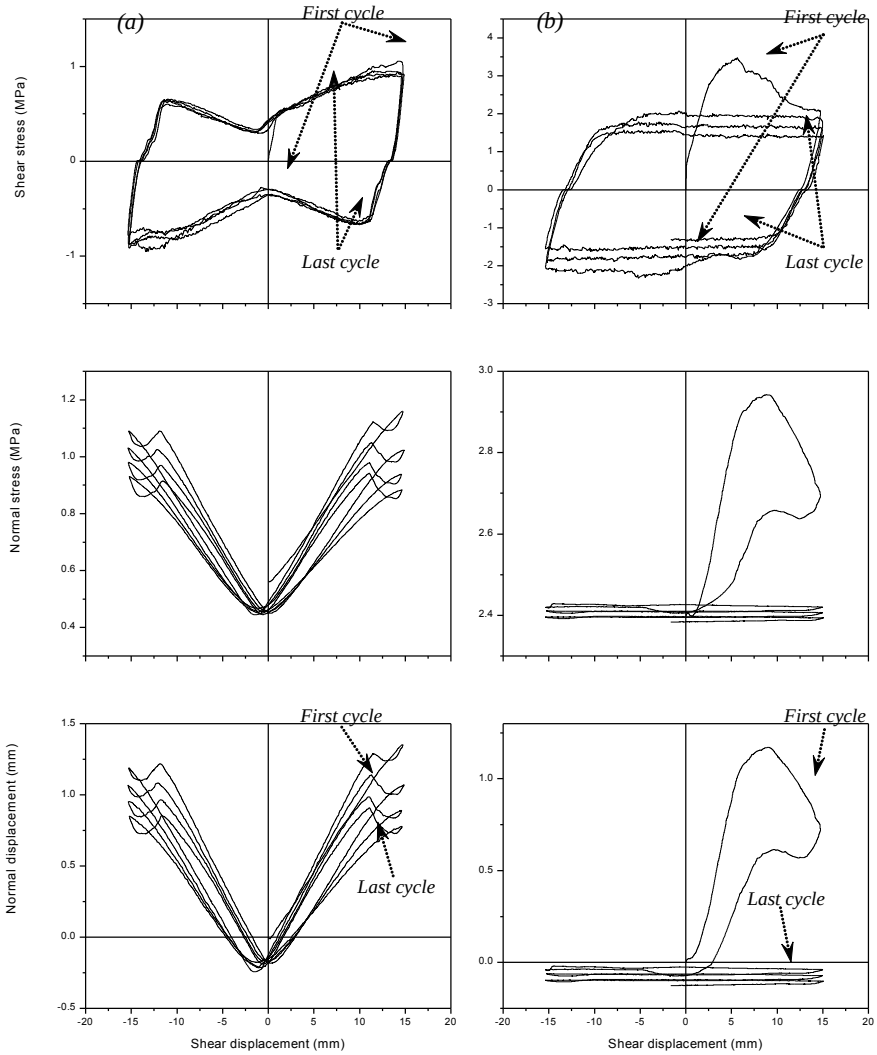

Figure 3 - Cyclic shear test on idealized asperity angle (a) asperity angle = 9.5° and normal stress = 0.56 MPa (b) asperity angle = 26.5° and normal stress = 2.4 MPa

THEORY AND BACKGROUND

The theory and background of applied joint models are concisely described in this section for completeness in discussion of the analysis.

CS model

This criterion provides only a limiting shear strength value for the joint without considering the progressive damage exerted on asperities upon shear displacement:

$$\tau_\circ = \sigma_n \tan(\varphi) + c \quad (1)$$

where, $\tau_\circ$ is the shear strength along the joint, σ_n is the applied normal stress, c is the cohesion, and φ is the friction angle.

The dilation starts with a constant angle ($\psi_\circ$) when the joint begins to slip (i.e. plastic deformation) and can be restricted after attaining a critical shear displacement:

If $\tau < \tau_\circ$ then $\psi = 0$ (2)
If $\tau > \tau_\circ$ and $u < u_{cs}$ then $\psi = \psi_\circ$ (2*a*)
If $\tau > \tau_\circ$ and $u \geq u_{cs}$ then $\psi = 0$ (2*b*)

where, u is the shear displacement, u_{cs} is the critical shear displacement, and ψ is the dilation angle. The effective friction angle is obtained by adding the assigned dilation angle to the friction angle and the shear strength becomes equal to the residual value when the critical shear displacement is reached (i.e. no dilation).

CY model

This model is more realistic than the CS model and takes into account the progressive damage of the joint surface during shearing observed in physical tests. In shear, the model considers irreversible, non-linear behaviour from the onset of shearing:

$$\tau = \sigma_n \tan(\varphi_m)\, sign\Delta u \quad (3)$$

where, φ_m is the friction angle prior to any damage of asperity and Δu is the increment of shear displacement.

As damage accumulates, the friction angle continuously reduces according to the following equation:

$$\varphi_m = (\varphi_m^i - \varphi_b)\exp(\frac{-u^p}{R}) + \varphi_b \quad (4)$$

where, φ^i_m is the initial friction angle, φ_b is the basic friction angle, R is a parameter with the dimension of length and related to joint roughness, and u^p is the plastic shear displacement.

The effective dilation angle in the CY model is obtained by reducing the friction angle from the basic friction angle upon each increment of shear displacement.

$$i = tan^{-1}\left(\frac{|\tau|}{\sigma_n}\right) - \varphi_b \quad (5)$$

UDEC SHEAR MODELING AND SIMPLIFICATION

The CNS cyclic direct shear test was simulated in UDEC as shown in Figure 4. The material properties of block (a) were prescribed as bulk module = 21.3 MPa and shear module = 31.95 MPa in a way to precisely simulate the stiffness of surrounding media (8 kN/mm). The blocks (b) and (c) were discretised according to the laboratory specimen size and assigned properties (bulk module = 1400 MPa and shear module = 792 MPa) of the material prospected.

Firstly, the desired normal stress was subjected to the joint and the model was allowed to reach equilibrium. A periodic horizontal velocity was applied to the block (c) to produce the required cyclic shear displacement. The average normal and shear stresses along the joint were calculated using a FISH function. The associated dilation and shear displacement were also determined via FISH functions.

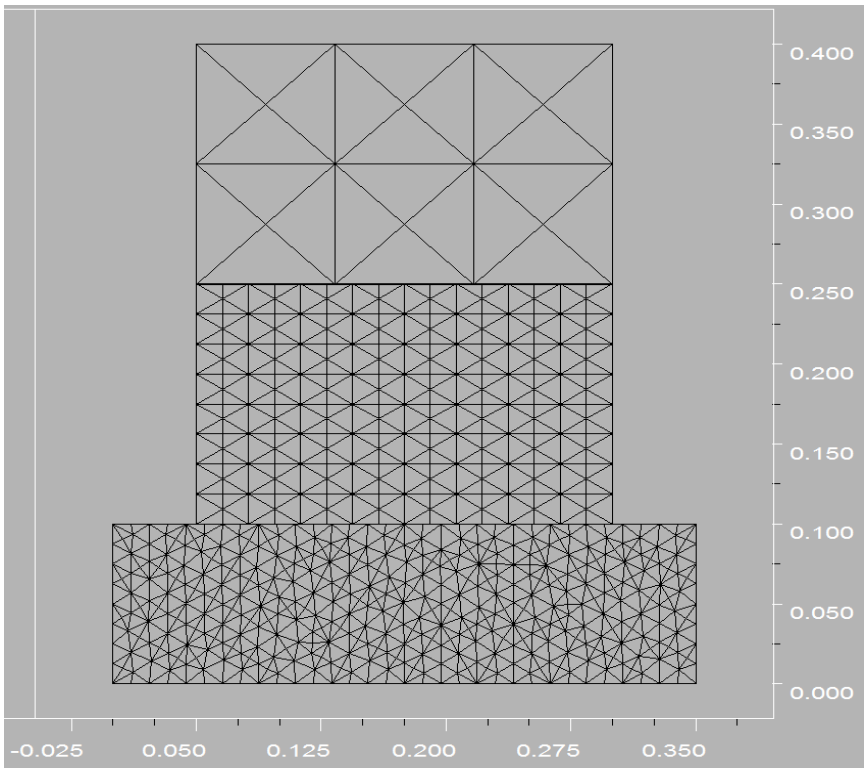

Figure 4 - The simulated CNS direct shear test (dimensions in Meters)

RESULTS OF NUMERICAL MODELING AND DISCUSSIONS

The CS and CY models were applied separately to replicate the observed experimental behaviour using the simulated CNS direct shear test in UDEC. The relevant model parameters used in the analysis for different conditions are listed in Table 1.

Table 1 - Model parameters for CS and CY

Model	Normal stress = 0.56 (MPa)	Normal stress = 2.4 (MPa)
CS	$\Psi = 5.2°$	$\Psi = 4.1°$
CY	$\varphi'_m = 44.5°$ and R =0.012 (mm)	$\varphi'_m = 40.7°$ and R = 0.005 (mm)

The application of the CS model in simulation of rock joints shear behaviour under cyclic loading for low and high values of applied normal stress and asperity angle is shown in Figures 5 (a) and (b). It is observed that for low levels of initial normal stress and asperity angle when shearing mechanism is sliding over asperities, the CS model can simulate different frictional resistance for forward and backward shearing and recovery of dilation behaviour upon load reversal. However, for the breaking mechanism when asperity is highly degraded at the first forward shear cycle; the CS model cannot represent approaching to the residual shear strength (i.e. no contribution of roughness in shear strength) and the effect of asperity damage in dilation.

The results of cyclic numerical analysis conducted using a CY model for asperity sliding and breaking mechanisms are shown in Figures 6 (a) and (b). In contrast with CS, the CY model cannot represent different frictional behaviour and recovery of dilation upon load reversal (Figure 6a) under sliding mechanism.

As shown in Figure 6 (b), for high values of initial normal stress and roughness, appearance of residual shear strength (i.e. the same shear strength in forward and backward shearing) is reasonably captured by the CY model. Nevertheless, the predicted peak shear strength is underestimated since the additional shear strength provided by asperity breaking is neglected in this model. In addition, the simulated normal displacement shows excessive dilation when shear strength becomes equal to the residual shear strength.

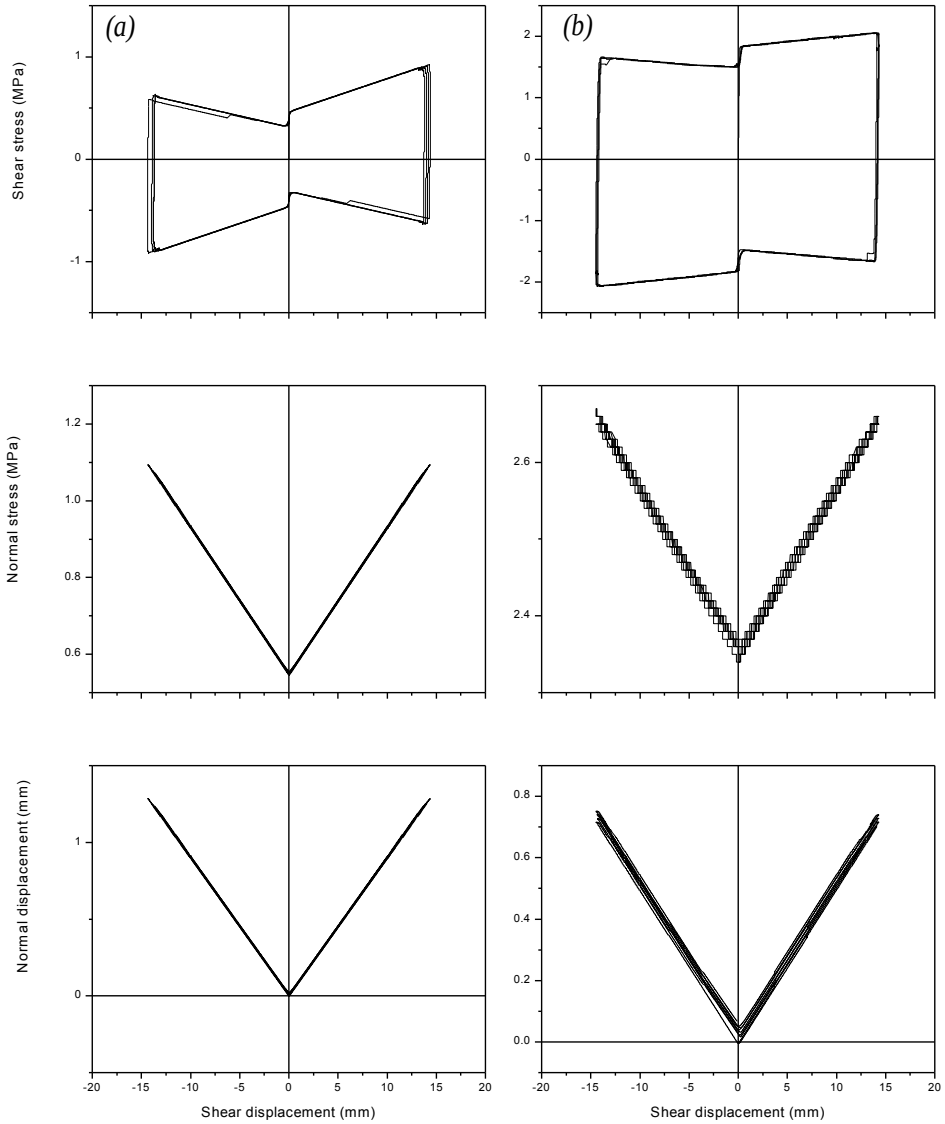

Figure 5 - CS model predicted results (a) asperity angle = 9.5° and normal stress = 0.56 MPa (b) asperity angle = 26.5° and normal stress = 2.4 MPa

CONCLUSIONS

The cyclic shear behaviour of rock joints was simulated in a simplified manner using two available constitutive models in UDEC under CNS conditions. For a given set of data, the variation of cyclic average shear stress, average normal stress, and dilation with shear displacement were studied and simulated using CS and CY models.

The results indicate that the capabilities of CS and CY models in simulating cyclic shear behaviour of rock joints under CNS condition depends on the governing shearing mechanism. For sliding mechanism observed in low levels of applied normal stress and asperity angle, the CS model can simulate different frictional behaviour and recovery of dilation during load reversal. However, for asperity breaking mechanism, this model excludes the effect of asperity damage on shear resistance and dilation angle. In this condition, the CY model can better represent cyclic shear behaviour of rock joints by considering progressive damage of asperities upon plastic shear displacement.

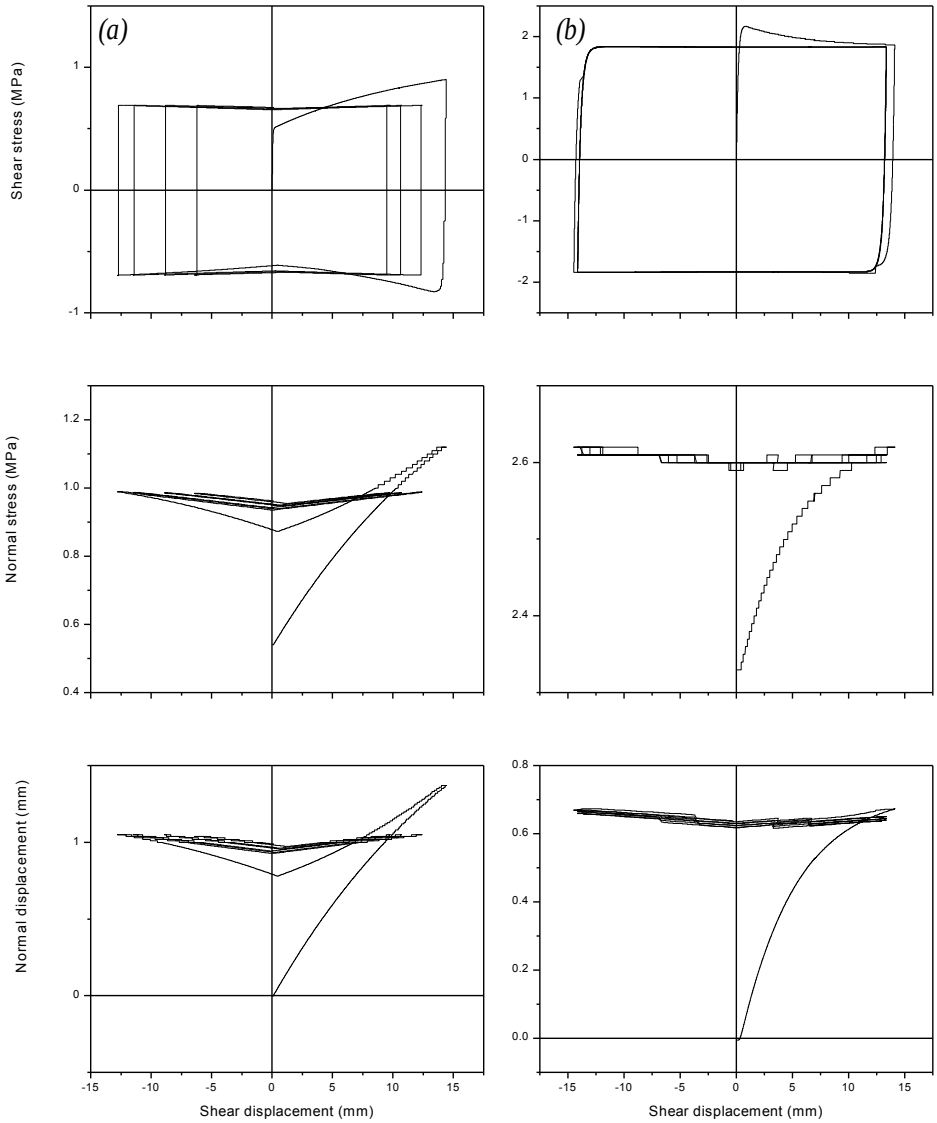

Figure 6 - CY model predicted results (a) asperity angle = 9.5° and normal stress = 0.56 MPa (b) asperity angle = 26.5° and normal stress = 2.4 MPa

REFRENCES

Barton, N, 1973. Review of a new shear-strength criterion for rock joints, *Engineering Geology,* 7: 287-332.

Barton, N, 1976. The shear strength of rock and rock joints, *International Journal of Rock Mechanics and Mining Sciences,* 13:255-279.

Cundall, P A and Hart, R D, 1984. *Analysis of block test No.1- Inelastic Rock Mass Behaviour: Phase 3- A characterisation of joint behaviour (Final Report).* Itasca Consulting Group Report, Rockwell Handford Operations, Subcontact SA-957 (cited from UDEC manual).

Gens, A, Carol, I and Alonso, E E, 1990. A constitutive model for rock joints formulation and numerical implementation, *Computers and Geotechnics,* 9: 3-20.

Indraratna, B A and Haque, A, 2000. Shear behaviour of rock joints*,* Rotterdam, Netherlands, A.A. Balkema.

Jaeger, J C, 1971. Friction of rocks and stability of rock slopes, *Geotechnique,* 21:97-134.

Johnston, I W and Lam, T S K, 1989. Shear behaviour of regular triangular concrete/rock joints analysis, *Journal of Geotechnical Engineering,* 115:711-727.

Oliveira, D A F and Iindraratna, B, 2010. Comparison between models of rock discontinuity strength and deformation, *Journal of Geotechnical and Geoenvironmental Engineering,* 136:864-874.

Patton, F D, 1966. Multiple modes of shear failure in rocks. *In: 1st Cong. ISRM*, 1966 Lisbon. 509-513.

Plesha, M E, 1987. Constitutive models for rock discontinuities with dilatancy and surface degradation, *International Journal for Numerical and Analytical Methods in Geomechanics,* 11:345-362.

Roosta, R M, Sadaghiani, M H, Pak, A and Saleh, Y, 2006. Rock joint modeling using a visco-plastic multilaminate model at constant normal load condition, *Geotechnical and Geological Engineering,* 24:1449-1468.

Seidel, J P and Haberfield, C M, 1995. The application of energy principles to the determination of the sliding resistance of rock joints, *Rock Mechanics and Rock Engineering,* 28:211-226.

EFFECT OF DYNAMIC ELASTIC PROPERTIES OF ROCK ON FRAGMENTATION IN CHOGHART IRONORE MINE, CENTRAL IRAN

Mohammad Farouq Hossaini[1], Rostam Ghafoori[2], Alireza Yarahmadi[3] and Mehdi Pourghasemi[4]

ABSTRACT: Blast fragmentation is a measure of efficiency in an open cast blast operation. Specific Charge (SC) plays an influential role on the fragmentation distribution, the quality of product and the production cost. Dynamic properties of rocks can be used for estimation of rock fragmentation and specific charge. Fragmentation analysis by digital image processing is a low cost and quick method. In this paper, the results of the seismic refraction technique are presented for Choghart Iron ore mine in central Iran. The P-wave velocity of the ore body has been measured at the site. The source of vibration generation was by hammering. The fragmentation resulting from blasting was monitored using a digital camera. Split Desktop software was used to quantify fragmentation size distribution. The mean fragmentation size of P50 was obtained as representative of the average fragmentation size. SC of ANFO was calculated. The relationship between SC with P50, Vp and Dynamic Elasticity Modulus (Edyn) were obtained. It was found that P50 and SC are increased with increased Vp and Edyn. P50, increases with increase of SC. These results can be utilised in blasting design in order to optimise fragmentation and SC for improvement in t the blast operation efficiency.

INTRODUCTION

Proper evaluation of rock fragmentationin blasting is a crucial aspect in mining. A desirable fragmentation enhances the production quality and efficiency. Many investigations have been carried out in order to quantify the effect of influential factors on blasting fragmentation. Amongst these factors are the dynamic properties of blasted rocks, which have been found to be a factor in fragmentation. Rakishev (1981), Latham (1999), Han, *et al.,* (2000) and Ramulu, *et al.,* (2012) are among those who have investigated the influence of dynamic rock properties on fragmentation, specific charge and explosive specifications.

In this research, the SC has been calculated as the amount of ANFO in kg per cubic meter of ore. The fragmentation due to blasting has been figured out through analysing the digital photos by Split Desktop (SD) software. The amount of P50 has been selected as the base for fragmentation assessment. P50 is the representative of the size, for which 50% of the blasted particles are smaller than it. P-wave Velocity (Vp) has been measured and analysed and Dynamic Elasticity Modulus (Edyn) of the rock has been calculated. The relationships between Sc and P50 with Vp and Edyn have been calculated, which can be used for rock fragmentation and SCplanning.

SITE DESCRIPTION

The experiments were conducted at 2nd largest Iron ore mine, Choghart, which is located at 12 km from Bafq town and 125 km from Yazd city, the capital city of Yazd province, central Iran (Figure 1). Estimated deposit of Choghart mine is more than 200 mt of which around 3.5 mt are mined each year. Magnetite is the main mineral of the deposit, together with hematite, goethite, hydro-goethite and ologist. The overall average density of orebody is in the order of 4.1 t/m^3. The total blasted rocks, including overburden, mounts to 11 Mtpa. The main explosive used is ANFO with absolute energy of 2745 J/kg. Emulite with absolute energy of 3495 J/kg is used as booster or as the main charge in boreholes containing water. Staggered blast patterns are mostly applied in drilling and blasting.

[1] *Associate Professor, School of Mining Engineering, University College of Engineering, the University of Tehran, mfarogh@ut.ac.ir*
[2] *MSc graduate, School of Mining Engineering, University College of Engineering, the University of Tehran*
[3] *Assistant Professor, Department of Mining and Metallurgical Engineering, Yazd University*
[4] *PhD student, School of Mining Engineering, University College of Engineering, the University of Tehran*

Figure 1 - Location of the mine

DYNAMIC PARAMETERS

The seismic refraction method was applied at iron ore benches. The source of vibration generation was by hammering. The instrumentation used for acquiring the data of seismic profiling was Terraloc MK8 along with 12 geophones of 10 Hz frequency. The seismic data collected in the field was analysed by software called REFLEXW. The statistical output from this analysis is presented in Table 1.

Table 1 - Statistical results of blocks dynamic parameters

	V_P (m/s)	E_{dyn} (GPa)
Maximum	2380.74	12.55
Minimum	1212.00	4.72
Mean	295.25	1.99
Standard deviation	1678.35	7.61
Variance	87 170.54	3.96

FRAGMENTATION ASSESMENT

Size distribution measurement

Size distribution of blasted rock was measured using the digital image processing software "Split-Desktop system". Recent fragmentation assessment techniques using digital image processing program allowed rapid and accurate blast fragmentation size distribution assessments. The fragmentation analysis by digital image processing was a low cost and quick method. Split system is one of the digital image processing software developed to compute the size distribution of fragmented rock from digital images. The digital image software was developed through the 1990s and at present is an accepted tool worldwide in the mining and mineral processing industries. Its main advantage is that it can

be used on a continuous basis without affecting the production cycle, which makes it the only practical tool for evaluating fragmentation of the run of mine (Siddiqui, *et al.*, 2009).

Image preparation

There are two sampling methods available for image preparation, random and systematic. The systematic method has been used for this investigation to get the image of all portions of blasted rock muckp using a digital camera. To provide a scale of the images, two football size balls of 18 cm in diameter were used. The distance between the two ballswas kept as 2 m in all the cases. The images were taken by a camera of 16 Mega Pixcl resolution. Best efforts were made to observe all image taking rules recommended by the Split-Desktop manual (Split Engineering, LLC, 2010). Figure 2 shows typical image presented by Split-Desktop software. The images have been manually edited, where needed, and the divided large pieces are reintegrated so that the particle edges are clearly outlined in lines (Figure 3).

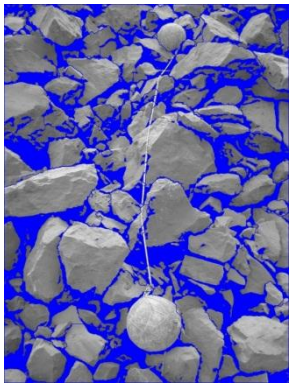

Figure 2 - An image recorded by the software

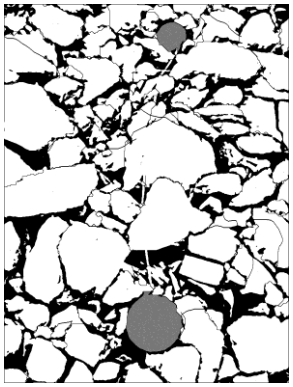

Figure 3 - An edited image saved for software analysis

Size distribution computation

Computation of size distribution is the last step and the most crucial part of the fragmentation assessment. The distribution of fine particles in each image has been figured out using the Rosin-Rambler distribution approach. Statistical detail of P50 size is presented in Table 2. The calculated size distribution curve and related table are shown in Figure 4.

Table 2 - Statistical parameters of P50 and specific charge

	P50 (mm)	Specific charge (kg ANFO/m^3)
Maximum	623.70	1.63
Minimum	88.89	0.49
Mean	154.00	0.31
Standard deviation	291.29	0.93
Variance	23716.11	0.10

RELATIONSHIPS BETWEEN THE SPECIFIC CHARGE WITH FRAGMENTATION AND DYNAMICS PARAMETERS

Analysing the data produced and monitored for the purpose of finding relationships between the rock specifications and the blasting results leads to the dependency of the SC and fragmentation on dynamic properties. As SC is increased the P50 size is increased as shown in Figure 5. This might look somehow against the expectations. But it can be due to the discrepancy between the way of increasing SC and the properties of blasted rock. This discrepancy might be considered as a problem for which a solution has to be searched. In practice, various amounts of specific charges are used in various portions of Ghoghart mine. This is because the properties of the blasted mineral are not the same everywhere in the mine.

The increase of SC with increase in Vp and Edyn are shown in Figures 5 and 6. The coefficients of determination (R^2) for these correlations are 0.6711 and 0.9523 respectively. Figure 7 shows the relationship between SC and Edyn.

Correlation has been found between fragmentation with (Vp) and Edyn of the blasted mineral for which the coefficients of determination (R^2) are 0.6042 and 0.9312 respectively as shown in Figures 8 and 9.

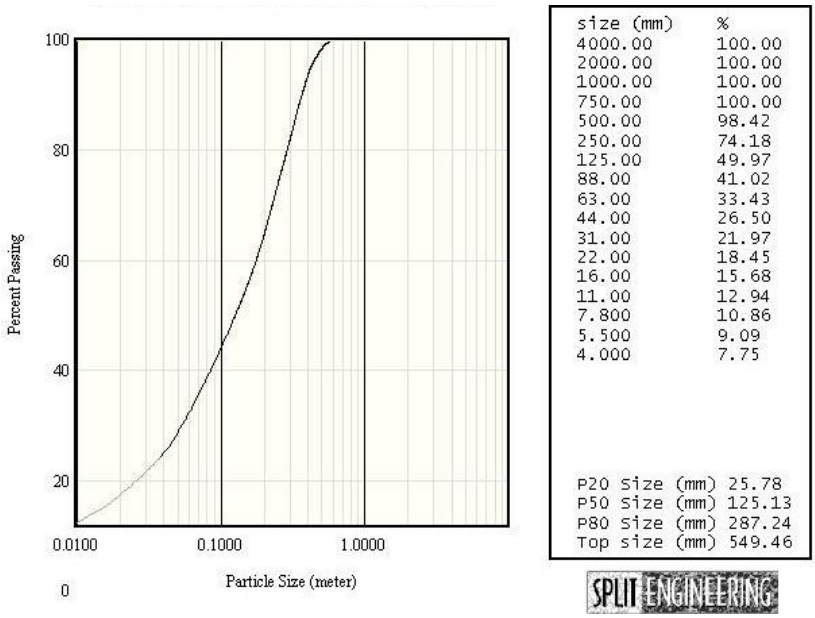

Figure 4 - Size distribution results of fragmentation

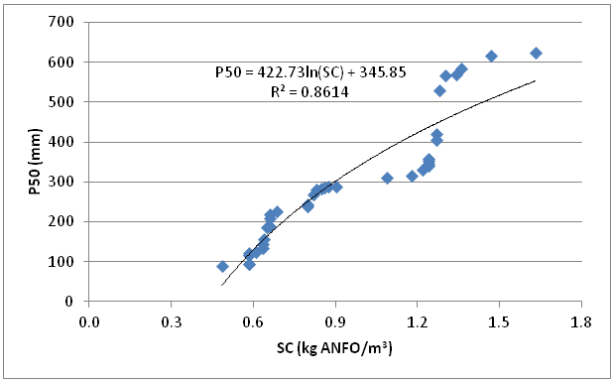

Figure 5 - Fragmentation versus specific charge

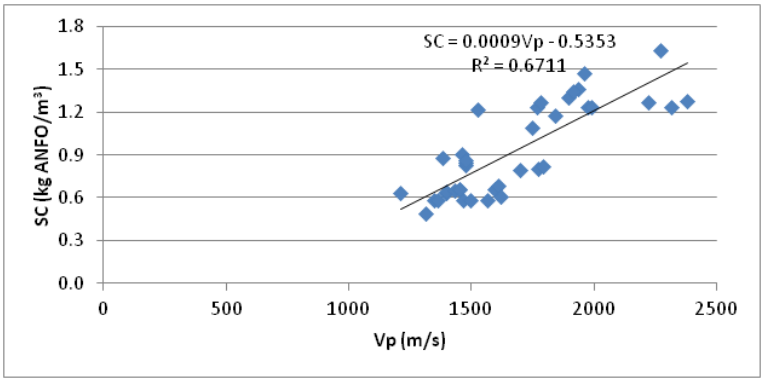

Figure 6 - Specific charge versus P-wave velocity

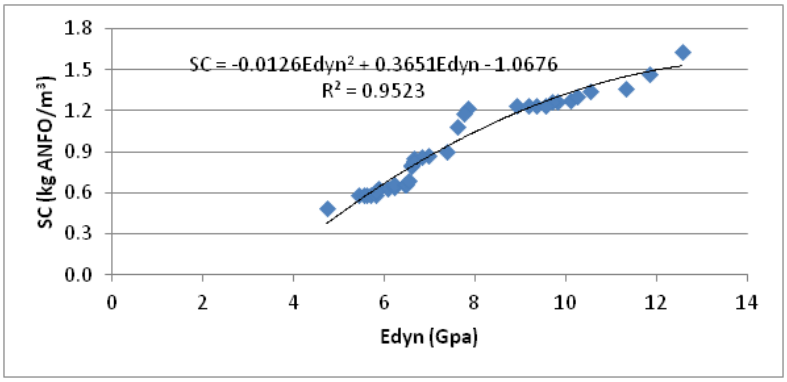

Figure 7 - Specific charge versus dynamic elasticity modulus

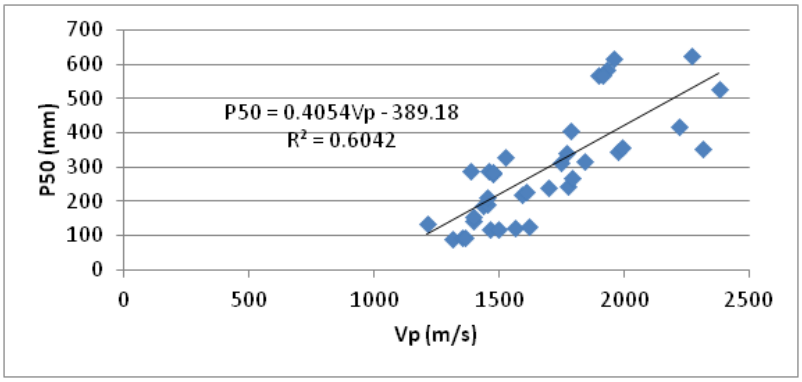

Figure 8 - Fragmentation versus P wave velocity

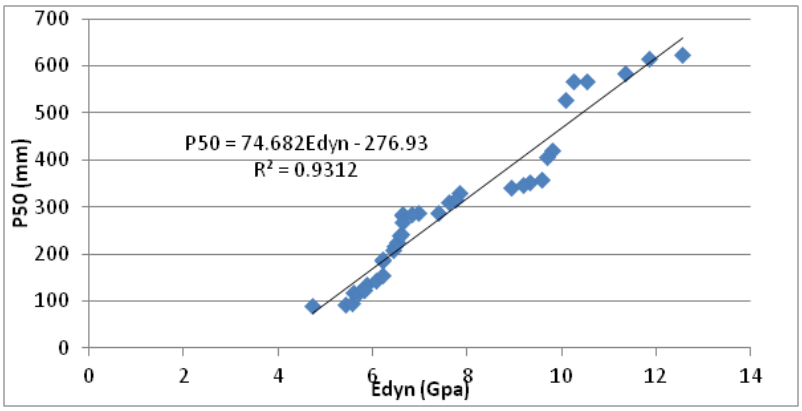

Figure 9 - Fragmentation versus dynamic elasticity modulus

CONCLUSIONS

Blast fragmentation of Ghoghart iron mine has been analysed and fragmentation distribution has been defined through muckpile images using Split-Desktop. The value of P_{50} obtained were in the range of 88.89 to390.8.

Relationship between $P_{50}$and specific charge has been defined for which a coefficient of determination was 0.95. This correlation shows that in Ghoghart mine the amount of $P_{50}$is increased with increasing SC

Both SC and P_{50} depend on dynamic properties of rock and increased with increase in P wave velocity and Edyn. The relationships between these factors have been introduced for the mine blasting practice.

The results of this investigation can be used in blast design and fragmentation arrangement in accordance with the properties of the rock in Choghart mine.

REFERENCES

Han, J, Weiya, X and Shouyi, W, 2000. Artificial Neural Network Method of Rock Mass Blastability Classification. *Geocpmptation*.

Latham, J P and Lu, P, 1999. Development of an assessment system for the blastability of rock masses. *International Journal of Rock Mechanics and Mining Sciences*, 36:41-55.

Rakishev, B R, 1981. A new characteristic of the blastability of rock in quarries. *Fiziko-Tekhnicheskie Problemy Razrabotki Poleznykh Is Kopaemykh*, 3:77-80.

Ramulu, M, Sangode, A G and Siha, A, 2012. Blast optimisation with *in situ* rock mass characterization by seismic profiling at an opencast coal mine in India. In *Proceedings of 2012 Coal Operators' Conf*erence. University of Wollongong, Australia, 16-17 Feb, pp 387-396. http://ro.uow.edu.au/coal/430/.

Siddiqui, F I; Ali Shah, S M and Behan, M Y. 2009. Measurement of size distribution of blasted rock using digital image processing. *JKAU: Eng. Sci.,* 20(2):81-93.

Split Engineering, LLC, 2010. Split-Desktop Software Manual, Tucson, Arizona, USA.

MODELLING AND DESIGN OF PENTICE PROTECTIVE STRUCTURES TO RESIST HIGH-SPEED PROJECTILE IMPACTS

Alex Remennikov[1] and Ryan Norton[2]

ABSTRACT: This paper presents the results of a research study carried out to investigate the performance of the mine pentice at an underground mine in NSW during the extension and equipping of a haulage shaft by Macmahon under high-speed impact loading caused by the potential projectiles falling from the surface. This assessment will allow the structure to comply with AS 3785.5 for "Headframes" (Australian Standard, 1998).

The pentice structure is installed 1000 m below the surface in a 4.268 m diameter shaft at the considered underground mine. The objective of the pentice is to allow Macmahon construction and shaft sinking crews to work in the shaft without any risk to their safety. The pentice structure includes a number of steel boxes 1-m high that are filled with high yielding foaming grout Tekseal from Minova Australia Pty Ltd. The major aim of this investigation is to evaluate the capacity of the existing pentice to resist high-velocity impacts and to develop a high-performance protective system which is capable of absorbing energy and terminating large projectiles falling from a height of 1000 m.

High-fidelity physics based finite element models for the mine pentice were developed to find a satisfactory solution to protect workers 1000 m below the surface from potential falling projectiles. It is established that the existing level 11 pentice structure is not capable of stopping the projectiles dropping from a height of 1000 m. Several high-performance protective solutions for strengthening the pentice against impact loads were proposed and evaluated numerically. As the final design, two-level protection is designed that includes the 9 level and 11 level pentice protective structures. The models of the 9 level pentice and the 11 level pentice are evaluated for the relevant impact loads.

It is found that the new 9 level pentice requires an additional layer of the railway concrete sleepers along with the high-strength steel cover plate to provide adequate protection and terminate the falling projectiles. The supporting frames for the 9 level and 11 level pentice structures are designed using the dynamic reaction forces transferred from the pentice boxes. The developed two-level pentice protective system has proven to provide high level of protection against high-speed falling projectiles for workers performing shaft sinking duties in the shaft below.

INTRODUCTION

The mine pentice is a device used to protect workers performing shaft sinking duties to extend the existing shaft below. Macmahon are in the process of extending and equipping an existing shaft from 1000 m to 1500 m deep to become the main haulage shaft at an underground mine as part of the materials handling system designed and installed by Macmahon. This requires construction crews to work in the existing upper shaft to install service pipes and fixed guides while shaft sinking crews work below to extend the shaft depth using a blind sink method. The relevant design Code used for designing this pentice structure is AS 3785.5 (Australian Standard, 1998). The protective structures shall be designed to withstand the design impact loads without significant damage or collapse. The modelling techniques developed for protecting civil infrastructure against severe impact loads (Remennikov (2007), Remennikov and Carolan (2008)) are extended in this paper to the protective structures installed inside the mine shaft.

Foam-filled steel boxes form the basis of protection structure of the pentice at this underground mine. A typical overhead protection box is shown in Figure 1. One-metre thick layer of Tekseal foaming grout is cast into the overhead boxes to act a protective energy absorption layer. The protective boxes typically have 10-mm thick steel bottom plates designed to prevent penetrations by the falling objects.

Three design impact events are considered in this study:

[1] *Centre for Infrastructure Protection and Mining Safety, University of Wollongong, alex_rememmikov@uow.edu.au Tel: 02 42 215 574*
[2] *MacMahon Engineering, Perth, WA, Australia*

- The falling guide of 200 x 200 x 9 SHS with a weight of approximately 475 kg.
- The falling slick line pipe of 150NB sch80 with table E flanges with a weight of approximately 530 kg.
- The falling shaft bracket with a total weight of approximately 85 kg.

All objects may potentially fall from a maximum height of 1000 m. Calculating the velocity reached from falling 1000 m (ignoring air resistance), it will be 140 m/s.

In this paper, the modelling results for a falling slick line pipe and a shaft bracket are discussed. The purpose of this investigation is to develop an effective protective design solution to protect workers working below the pentice structure against potentially lethal threat from high-speed falling projectiles.

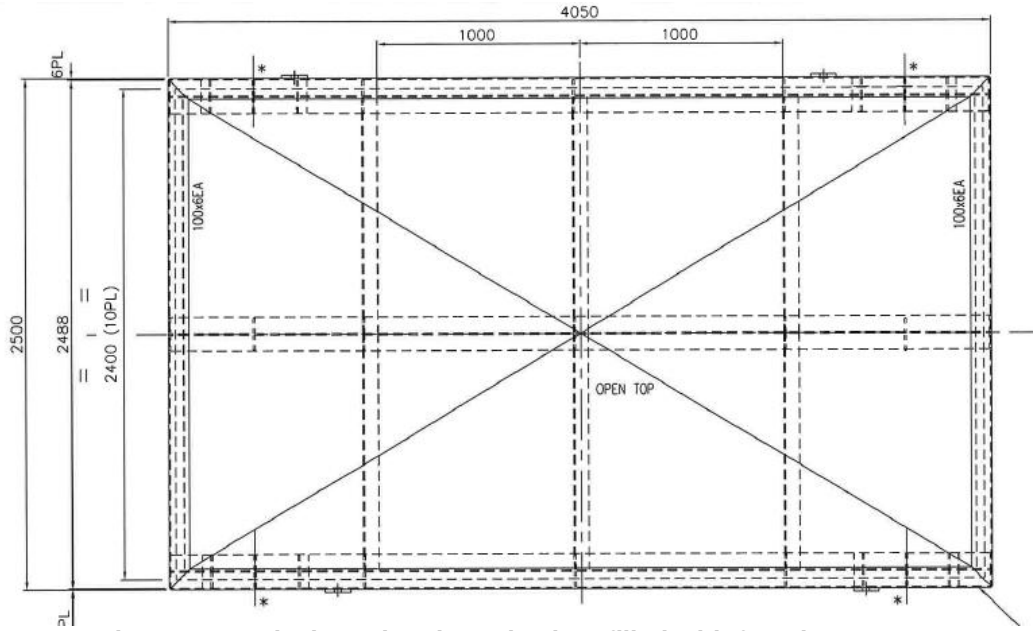

Figure 1 - Typical overhead pentice box filled with foaming grout

METHODOLOGY

Description of impact loading cases

Three typical large objects that could fall onto the pentice are considered in this study:

- **The guide** - 200x200x9 SHS with a total weight of 475 kg falling 1000 m to the pentice;
- **The slick line pipe** – 150 NB slick line pipe with flanges and with a total weight of 530 kg falling 1000 m to the pentice; and
- **The shaft bracket** - total weight of 85 kg falling 1000 m to the pentice.

Table 1 presents the details of impact events considered in this investigation. It can be seen from Table 1 that the impact event 2 (the slick line pipe) is the worst impact case with the highest energy of impact. Therefore, the slick line pipe is used in this investigation as the design load case to evaluate the effectiveness of the pentice structure for the considered underground mine in NSW. Impact event 3 is also considered and numerically modelled for cases where a reduced impact protection could be afforded.

A two-level protective pentice structure is also investigated as an alternative design involving the existing 11 level pentice and a new 9 level pentice. For this pentice design, the 9 level pentice is subjected to significantly reduced impact loading, which allows the development of a more efficient impact resisting system.

Table 1 - Parameters of potentials impact events

Impact Event	Impact Mass, kg	Drop Height, m	Impact Velocity, m/s	Energy of Impact (kJ)
1	475	1000	140	4,655
2	530	1000	140	5,194
3	52.0	1000	140	509.6

Numerical simulations using FEA models

A general purpose transient dynamic finite element software LS-DYNA (LS-DYNA, 2008) is used in this study to develop the finite element models. LS-DYNA is used to solve multi-physics problems including solid mechanics, heat transfer, and fluid dynamics either as separate phenomena or as coupled physics, e.g., thermal stress or fluid structure interaction. LS-DYNA is an industry accepted dynamic first-principle based code for analysis of structures under extreme loads generated by blast and impact events with the ability to compute large deformations due to flexure, shear, and material failures.

Since the pentice overhead boxes filled with foaming grout form the basis for protection of workers in the mine, the numerical model includes a steel box with the 6-mm thick vertical walls and 10-mm thick floor plate. The steel box is filled with 1-m thick Tekseal foaming grout as shown in Figure 1. In order to simulate an impact event, a projectile is modelled in close proximity to the slab of foaming grout and is given an initial velocity as per Table 1.

Table 2 presents a summary of finite element models developed for this study and brief description and purpose for each model.

Table 2 - Summary of FE models developed in this study

Model #	Design Concept	Models developed	Model description and purpose
1	Single Level Pentice Protective Structure (11 level pentice is to resist full design impact load)	Model of existing pentice box protected with additional 1.5 m layer of sand	Evaluates the effectiveness of sand cushion to prevent penetration of the pentice box by falling pipe.
2		Model of existing pentice box protected with additional single layer of concrete sleepers	Evaluates the effectiveness of railway sleepers to prevent penetration of the pentice box by falling pipe.
3		Model of existing pentice box protected with additional two layers of concrete sleepers	Evaluates the effectiveness of two layers of sleepers to prevent penetration of the pentice box by falling pipe.
4		Model of existing pentice box protected with additional two layers of concrete sleepers plus cover steel plate	Evaluates the effectiveness of steel cover plate in addition to two layers of concrete sleepers to stop impacting pipe.
5	Two-Level Pentice Protective Structures (9 level pentice is to resist reduced impact load and protect 11 level pentice)	Model of the 11 level pentice box impacted by a 1-ton steel section	Evaluates the performance of the existing pentice box to stop impacting projectile falling from a height of 191 m.
6		Model of supporting frame for the 11 level pentice	Evaluates the performance of the 11 level supporting structure to resist the reaction forces provided by Model #5.
7		Model of the 9 level pentice box with single layer of sleepers and steel plate on top	Evaluates the performance of the 9 level pentice box to stop a projectile falling from a height of 810 m.
8		Model of the 9 level pentice supporting structure	Evaluates the performance of the 9 level supporting structure to resist the reaction forces provided by Model #7.

Discussion of finite element models

The finite element models used in this study are shown in Figures 2 through 9. Solid elements with a single integration point are used to model the steel box walls and floor and the grouting foam infill. Overall model dimensions and the sizes of finite elements are determined from a mesh convergence study. The mesh convergence study included a number of runs of the model with variable model dimensions and increasing levels of mesh refinement. In the final model, the steel box and grout are modelled with 50-mm by 50-mm solid elements, and the areas being directly affected by the impact are modelled with 25-mm by 25-mm solid elements. Interaction between the grout material and steel box is simulated using surface to surface contact algorithms.

Several protection schemes are evaluated initially for the existing 11 level pentice. This includes adding protective layers of sand and railway concrete sleepers to enhance impact resistance of the existing pentice. Figure 2 shows the model of the existing pentice box with a 1.5-m layer of sand added over the steel cover plate. The falling 150 NB pipe impacts the sand with a velocity of 140 m/s. The sand is modelled using a hybrid modelling technique where the Lagrangian finite element mesh is combined with SPH (Smooth Particle Hydrodynamics) mesh for the sand experiencing severe deformations due to a high-speed impact.

Figure 3 shows the model of the existing pentice box with an addition of a layer of railway concrete sleepers. The model of concrete sleepers is developed based on the drawings of Austrak Heavy Duty prestressed concrete sleepers. The falling 150 NB pipe is modelled to impact the concrete sleepers with a velocity of 140 m/s. The concrete sleepers are modelled using the advanced concrete material model in LS-DYNA that allows simulation of non-linear concrete characteristics such as cracking, strength softening and damage.

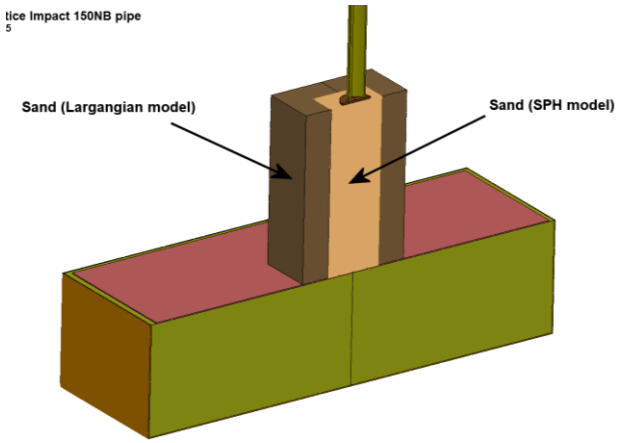

Figure 2 - Modelling sand layer protection

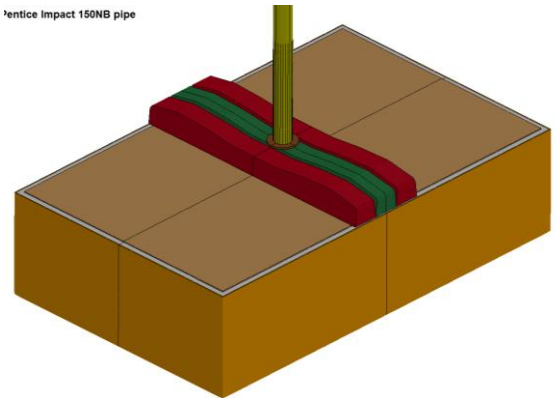

Figure 3 - Concrete sleepers layer protection

Figure 4 shows the model of the existing pentice box with additional two layers of railway concrete sleepers. The top layer of sleepers is subjected to the impact load from a falling 150 NB pipe with a velocity of 140 m/s. The concrete sleepers are modelled using the advanced concrete material model in LS-DYNA that allows simulation of non-linear concrete characteristics such as cracking, strength softening and damage. In Figure 5, the protective structure is enhanced with an additional 10 mm high-strength steel plate on top of the sleepers.

Model No 5 in Figure 6 is developed following the decision to provide two levels of protection by installing the 9 level pentice and the 11 level pentice to reduce the impact load demand on the pentice. Figure 7 shows the model of the 11 level pentice box filled with foaming grout with the 8-mm high-strength steel cover plate on the top. Since the 11 level pentice is located 191 m below the 9 level pentice, there is the potential for a heavy object falling from that height with a velocity of 61.2 m/s. Model No 5 simulates an impact event when a 1-ton steel section is dropped from the 9 level pentice, which represents the worst case scenario.

Model No 6 in Figure 7 is a three-dimensional steel frame that is developed to evaluate the performance of the supporting frame for the 11 level pentice. The model is developed using Strand7 computer program utilising standard beam elements. The dynamic reaction forces generated by Model 5 are applied as uniformly distributed dynamic loads to the beams supporting the pentice boxes.

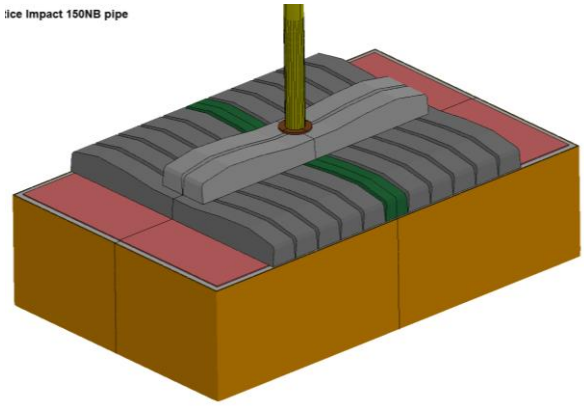

Figure 4 - Two layers of sleepers protection

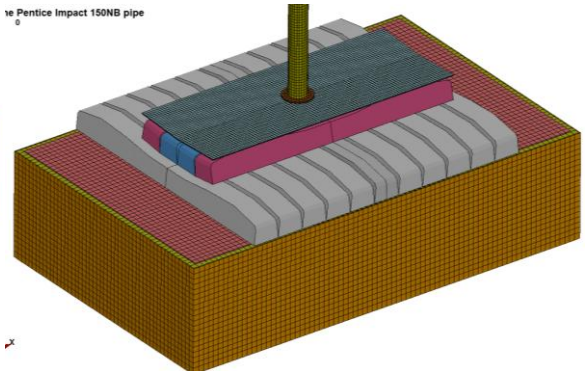

Figure 5 - Concrete sleepers and steel plate

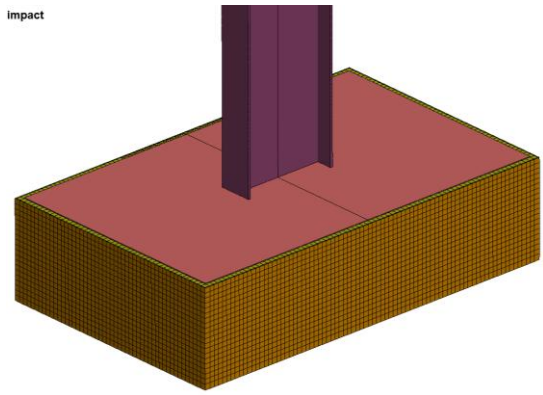

Figure 6 - 11 level pentice impact model

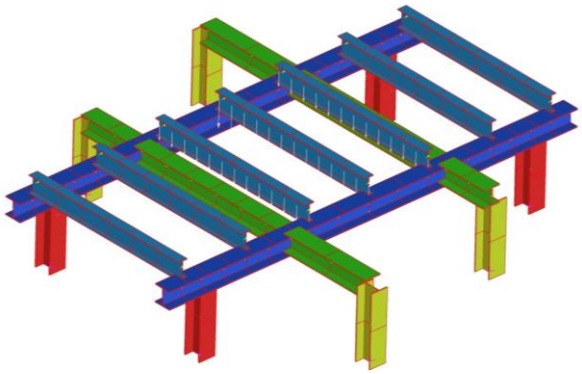

Figure 7 - 11 level support frame model

Model No 7 in Figure 8 is developed for the two-level protective system consisting of the 9 level pentice and the 11 level pentice. Figure 9 shows the model of the 9 level pentice box filled with foaming grout with the 8-mm high-strength steel cover plate and one layer of concrete sleepers on top and then the 10-mm high-strength plate on top of the sleepers. The 9 level pentice is located 810 m below the surface, therefore it is subjected to impact by the slick line pipe 150 NB falling from a height of 810 m with a velocity of 126 m/s, which is expected to deliver reduced energy of impact and thus simpler design for the pentice.

Four main steel beams spaning across the shaft and five beams supporting the pentice boxes at the 9 level are represented in Model No 8 shown in Figure 9. The model is developed using Strand7 computer program utilising standard beam elements. The dynamic reaction forces generated by Model No 7 are transferred into the Strand7 model and applied as uniformly distributed dynamic loads to the beams supporting the pentice box.

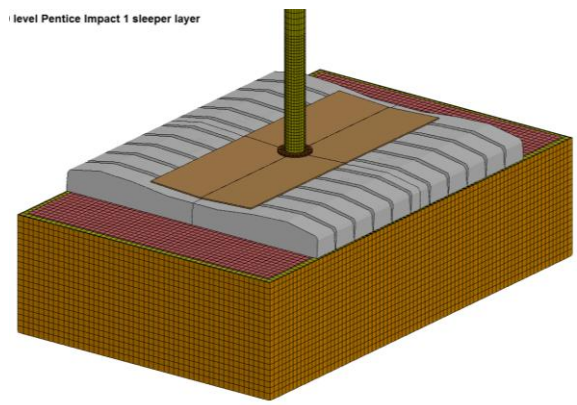

Figure 8 - 9 level pentice impact model

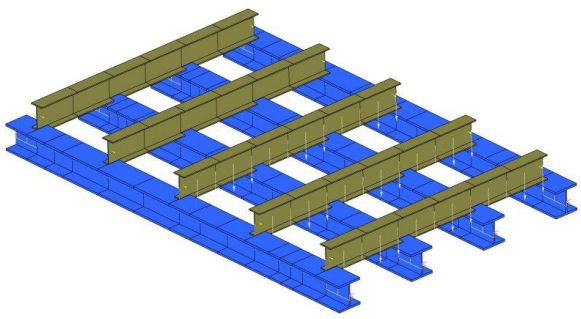

Figure 9 - 9 level support frame model

MATERIAL MODELS

Foaming grout Tekseal is modelled using Material Type 173 based on Mohr-Coulomb criterion in LS-DYNA. The material has a Mohr Coulomb yield surface, given by $\tau_{max} = C + \sigma_n \tan(phi)$, where τ_{max} = maximum shear stress on any plane, σ_n = normal stress on that plane, C = cohesion, *phi* = friction angle. The tensile strength is given by $\sigma_{max} = C / \tan(phi)$. After the material reaches its tensile strength, further tensile straining leads to volumetric voiding.

The appropriate material modelling parameters for the Tekseal foaming grout are summarised in Table 3.

Table 3 - Material properties for 200 psi Tekseal

Material	Young's Modulus (MPa)	Poisson's Ratio	Friction Angle (deg)	Cohesion (MPa)	Compressive Strength (MPa)	Tensile Strength (MPa)
200 psi Tekseal	200	0.43	19	0.6	1.4	0.3

Steel plates of the pentice box are modelled using Material Type 3 in LS-DYNA representing elasto-plastic behaviour of the steel material. The steel is assumed to be Grade 300 with a yield stress of 300 MPa. The projectile is modelled using Material Type 20 representing absolutely rigid steel material.

High-strength steel plates placed on top of foaming grout infill and on top of concrete sleepers are placed in contact with the surfaces of the grout and sleepers and simulated using the penalty contact algorithm *CONTACT_SURFACE_TO_SURFACE in LS-DYNA. The plates are given the material properties based on the information provided by Bisalloy Steel Group Limited for Bisalloy 80. The mechanical properties of Bisalloy 80 used in the model are summarised in Table 4.

Table 4 - Material properties for Bisalloy 80

Material	0.2% Proof Stress	Tensile Strength	Elongation in 50mm GL	Hardness
Bisalloy 80	750 MPa	830 MPa	20%	255 HB

RESULTS OF NUMERICAL MODELLING

Based on the FE models shown in Figures 2 through 9 and the loading and material properties described in the previous sections, non-linear dynamic analyses are carried out for the pentice boxes and their supporting structures. All models are analysed so as to investigate an emergency impact load condition based on a 150 NB slick line pipe falling from the top surface of the mine. The results of non-linear dynamic analyses are presented and discussed below.

Response of the 11 level pentice with a layer of sand or concrete sleepers

Figure 10 demonstrates the outcome of the impact analysis of the existing 11 level pentice box subjected to impact by the 150 NB pipe with an impact velocity of 140 m/s. It can be seen that the steel pipe penetrates the layer of sand and the slab of foaming grout and perforates the 10-mm floor plate of the pentice. The analysis results indicate that a 1.5-m thick sand cushion is able to slow down the impacting pipe by only 5 m/s, thus subjecting the pentice structure to the impact velocity of 135 m/s. This results in perforation of the existing cover steel plate, penetration of the foam infill and finally in perforation of the bottom plate of the box, as shown in Figure 10. This solution is found to be ineffective for stopping the falling pipe with a velocity of 140 m/s.

A separate model of the pentice is developed to investigate the effectiveness of railway concrete sleepers to prevent penetration of the pentice by the high-speed falling pipe. The concrete sleepers are placed on top of the existing pentice and subjected to the impact load generated by the falling pipe. The results of numerical simulation are shown in Figure 11. It can be seen that the impacted sleeper is fully disintegrated and the falling pipe penetrates the 1-m deep grout and the bottom plate of the box. The sleepers contribute to slowing down the impacting pipe to 80 m/s velocity from an initial velocity of 140 m/s. This solution is found to be ineffective for stopping the falling pipe with a velocity of 140 m/s.

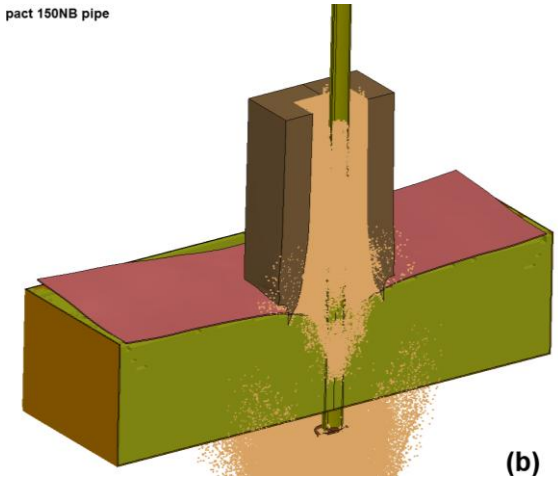

Figure 10 - Penetration through sand layer

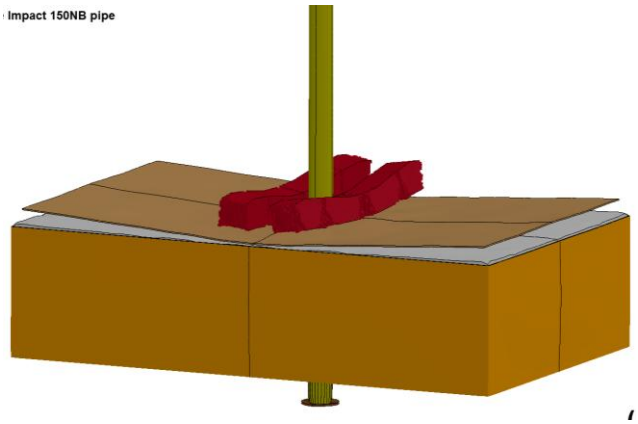

Figure 11 - Effect of single layer of sleepers

Response of the pentice with two layers of concrete sleepers

Since single layer of concrete sleepers is not effective for protecting the pentice against penetration, a model of the pentice with two layers of concrete sleepers is developed. The results of numerical simulation are shown in Figure 12. It can be seen that the pipe projectile crashed the top and bottom sleepers and penetrated the pentice box, as shown in Figure 12. Therefore, this solution is also found to be not adequate for protecting the pentice box against penetration by the projectile.

A protective system based on two layers of concrete sleepers and the cover 10 mm high-strength steel plate on top is further evaluated. The results of numerical simulation are shown in Figure 13. It is established that the sleepers directly impacted by the pipe would be severely damaged and the cover steel plate would come in contact with the existing steel plate on top of the pentice. The energy absorbed by crushing concrete sleepers is sufficient for reducing the pipe velocity to about 55 m/s, and the two plates with the foam infill stopped the projectile and prevented penetration damage of the pentice structure within about 25 msec after the impact. Therefore, this solution may be considered effective for stopping the falling pipe projectile with an impact velocity of 140 m/s.

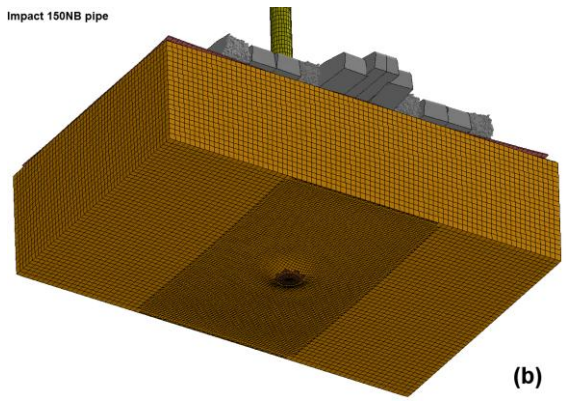

Figure 12 - Effect of two layers of sleepers

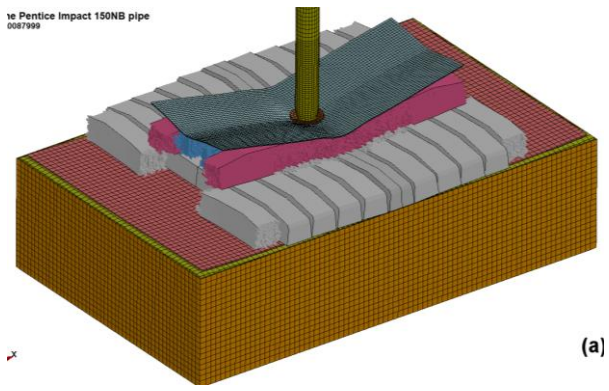

Figure 13 - Effect of sleepers and steel plate

Given that the 11 level pentice is installed more than 1000 m below ground level and there is no crane access in the shaft, development and design of the enhanced impact resistant 11 level pentice structure is not economically and technically viable. To optimise the protective structure, a two-level pentice solution is adopted and investigated next.

Response of the 11 level pentice to a 1-tonne falling section

The 11 level pentice is located 190 m below the 9 level pentice. Therefore, the protective performance of the 11 level pentice is investigated for an accidental fall of a large steel section from a height of 191 m and an impact velocity of 61.2 m/s. The results of simulation of the 11 level pentice subject to impact by a 1-tonne falling steel section are presented in Figure 14. It is established that in the final state the projectile

penetrates through the grouting foam to the depth of 950 mm. The velocity graph in Figure 14 confirms that the projectile velocity is reduced to zero from the initial value of 61.2 m/s implying that the projectile is terminated by the existing 11 level pentice. Based on these results, it is concluded that the existing 11 level pentice can provide sufficient protection against large projectiles falling from the level of the 9 pentice.

The 11 level pentice supporting frame model is analysed using the dynamic reaction forces determined from the impact analysis of the pentice box. The graph of vertical beam displacements in Figure 15 shows the peak beam deformation of about 1.5 mm, which is deemed satisfactory.

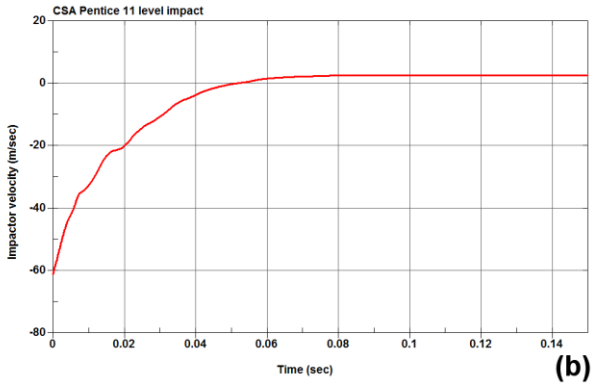

Figure 14 - Response of 11 level pentice

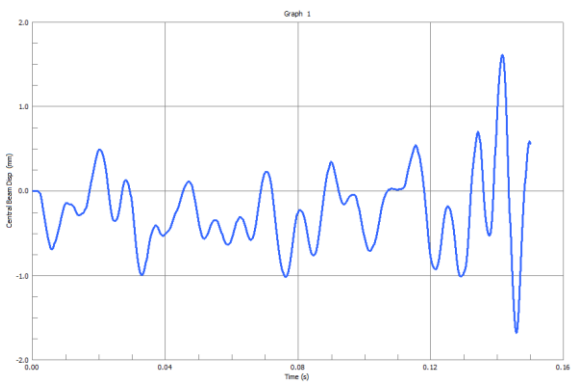

Figure 15 - Response of 11 pentice frame

Response of the 9 level pentice to impact by a slick line pipe

The 9 level pentice with one layer of concrete sleepers and the 10-mm Bisalloy plate on top is analysed for the impact loads due to a falling 150 NB pipe from a height of 810 m (126 m/s velocity). Figure 16 shows the response of this protective system. It is established that the sleepers directly impacted by the pipe would be severely damaged and the cover steel plate would come in contact with the existing steel plate on top of the pentice. As can be seen from the graph in Figure 17 the projectile velocity will be brought to zero in about 25 msec by the proposed 9 level pentice design. Therefore, this solution may be considered effective for stopping the falling possible projectiles with an impact velocity of 126 m/s.

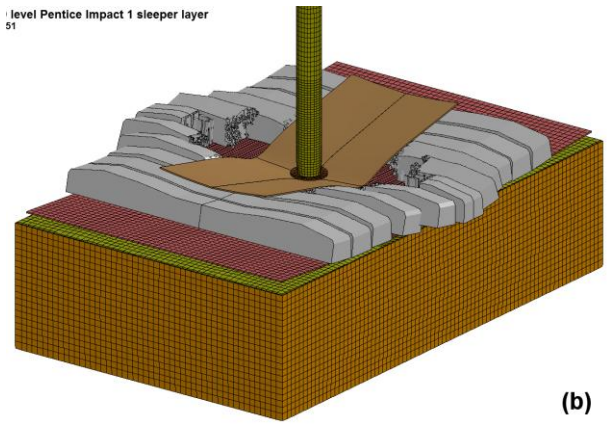

Figure 16 - Response of 9 level pentice

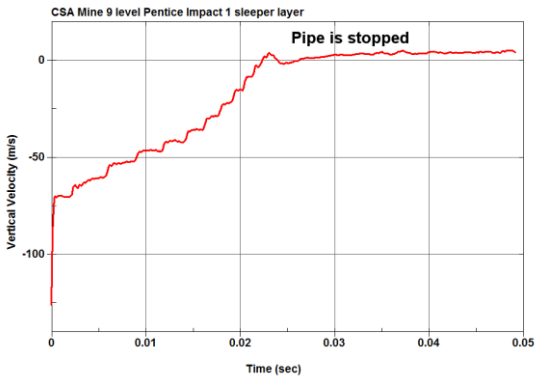

Figure 17 - Projectile velocity time history

PENTICE IMPACT ANALYSIS FOR A FALLING WALL BRACKET

The final part of this investigation is concerned with modelling the consequences of not utilising the 9 level pentice discussed above during operations of installing wall brackets. These operations require mounting the wall brackets to the wall of the mine shaft which could become high-speed projectiles if one of the brackets falls into the shaft from a maximum height of 1000 m. Considerable time and labour resources could be saved by not requiring installation of the 9 level pentice. This requires evaluation of the dynamic response of the 11 level pentice protective structures to absorb energy and terminate a falling wall bracket from a height of 1000 m.

Figure 18 shows the model of the 11 level pentice box with the 8-mm steel cover plate and the assumed orientation of the wall bracket just prior to impact. The falling wall bracket impacts the top steel plate with a velocity of 140 m/s.

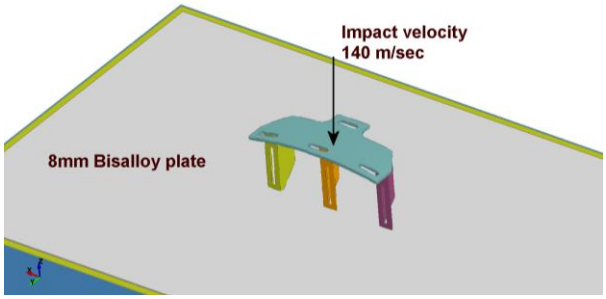

Figure 18 - Model of wall bracket impacting pentice structure

Figure 19 demonstrates the outcomes of the impact analysis of the level 11 pentice box subjected to impact by the wall bracket with an impact velocity of 140 m/s. It is seen that the steel wall bracket experiences severe plastic deformations upon impact with the top steel plate as shown in Figure 19. The wall bracket penetrates the 8-mm high-strength steel plate as demonstrated in Figure 20. From Figure 21, the wall bracket is fully stopped by the pentice protective structures within about 10-15 msec after coming into contact with the steel cover plate.

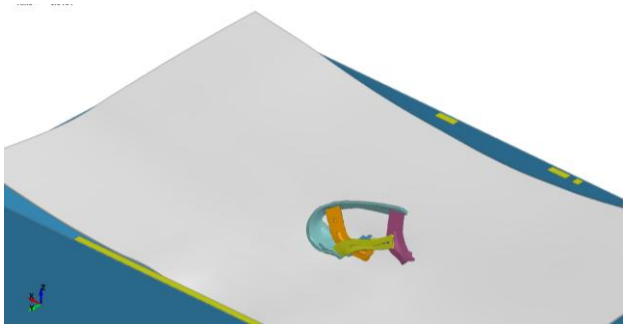

Figure 19 - Large deformations of wall bracket

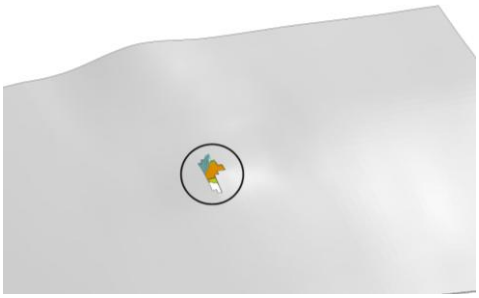

Figure 20 - Perforation of steel cover plate

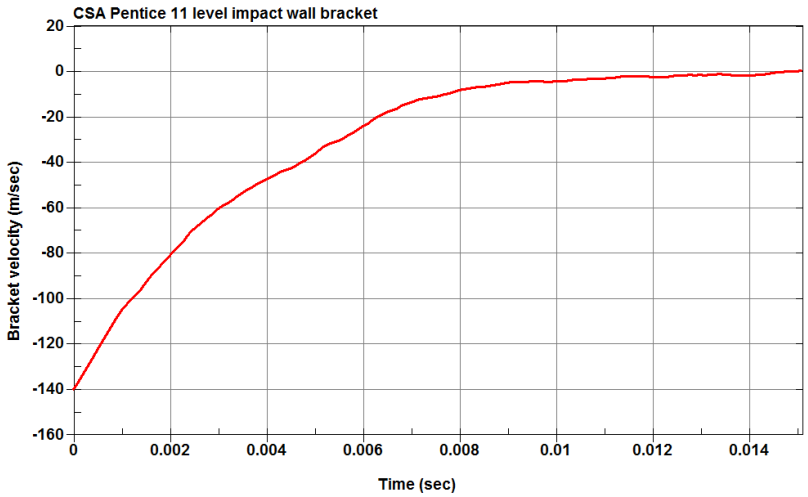

Figure 21 - Time history of wall bracket velocity

It is established that the pentice boxes filled with foaming grout and protected with a 8-mm high-strength steel cover plate provide sufficient resistance to terminate a falling 52-kg wall bracket projectile. The support frame for the 11 level pentice is also verified to resist the dynamic forces transferred from the pentice boxes during the high-speed impact.

CONCLUSIONS

In this paper, high-fidelity physics based finite element models for the underground mine 11 level pentice and 9 level pentice are developed to find a satisfactory solution to protect workers 1000 m below the surface from falling projectiles during maintenance operations. The impact velocity of a projectile falling from the surface is about 140 m/s, which requires very high level of protection to be afforded by the pentice protective structures.

Several high-performance protective solutions were proposed and evaluated for strengthening the pentice against impact loads. Given that the pentice is installed more than 1000 m below ground and the shaft area cannot be accessed with a crane, it was required to develop a protective system that would be easy to manhandle. The final design of the impact-resistant protective system includes two levels of pentice structures. The first level, the 9 level pentice, is designed to terminate the projectiles falling from the ground level. It includes a combination of railway concrete sleepers and high-strength steel cover plate to provide additional energy absorbing capacity to the pentice. The second level of protection, the 11 level pentice, does not require strengthening as it has sufficient capacity to resist impacting projectiles falling from the 9 level pentice.

The supporting frames for the 9 level pentice and the 11 level pentice were also verified and designed to have sufficient stiffness and capacity to resist the dynamic loads transferred from the pentice boxes subjected to impact. The high effectiveness of the developed protective structures is ensured by high-fidelity physics-bases numerical modelling utilising three-dimensional non-linear dynamic analysis techniques in this study which can be extended to providing effective protection against the "emergency" impact events in other mining applications.

REFERENCES

Australian Standard AS 3785.5, 1998. Underground mining - Shaft equipment - Headframes.

LS-DYNA Version 971, 2008. Livermore Software Technology Corp., Livermore, CA, May 2008.

Remennikov, A, 2007. Behaviour of high performance steel sections subjected to impact loads. *Proceedings of the 5th International Conference on Advances in Steel Structures,* December 2007, Singapore, pp 929-934.

Remennikov, A M and Carolan, D, 2008. High-performance protection technologies for blast and impact retrofitting of building facades, *Australasian Structural Engineering Conference (ASEC),* 26-27 June 2008, Melbourne [paper No.82 on CD-ROM].

HYBRID DOUBLE-SKIN TUBULAR MEMBERS FOR SUSTAINABLE MINING INFRASTRUCTURE

Tao Yu and Alex Remennikov

ABSTRACT: Hybrid FRP-concrete-steel double-skin tubular members (hybrid DSTMs) are a new form of hybrid structural members. A hybrid DSTM consists of an outer tube made of fibre reinforced polymer (FRP) and an inner tube made of steel, with the space between filled with concrete. The two tubes may be concentrically placed to produce a section form more suitable for compression members, or eccentrically placed to produce a section form more suitable for flexural members. In hybrid DSTMs, the three constituent materials are optimally combined to achieve several advantages not available with existing structural members, including their excellent corrosion resistance and energy-dissipation capacity. Hybrid DSTMs are therefore a sustainable alternative to existing structural components, especially for use in structures which are likely to be exposed to a harsh environment. This paper explains the rationale and advantages of this new form of structural members, presents an overview of existing and ongoing research on their structural behaviour and design, and discusses their potential applications in mining infrastructure.

INTRODUCTION

Hybrid FRP-concrete-steel double-skin tubular members (referred to as hybrid DSTMs) (Figure 1) are a new form of hybrid members (Teng, *et al.*, 2007). A hybrid DSTM consists of an outer tube made of fiber-reinforced polymer (FRP) and an inner tube made of steel, with the space between filled with concrete. The two tubes may be concentrically placed (Figures 1a and 1b) to produce a section form more suitable for columns, or eccentrically placed to produce a section form more suitable for beams (Figures 1c and 1d). In hybrid DSTMs, the FRP tube offers mechanical resistance primarily in the hoop direction to confine the concrete and to enhance the shear resistance of the member. Hybrid DSTMs may be constructed in-situ or precast, with the two tubes acting as the stay-in-place form. The sections of the two tubes may be both circular (Figures 1a and 1c), rectangular (Figure 1d), or in another shape; they may also have shapes different from each other (Figure 1b). Shear connectors need to be provided between the steel tube and the concrete, particularly in beams, but are generally not needed for the FRP tube which is normally designed to have only a small longitudinal stiffness.

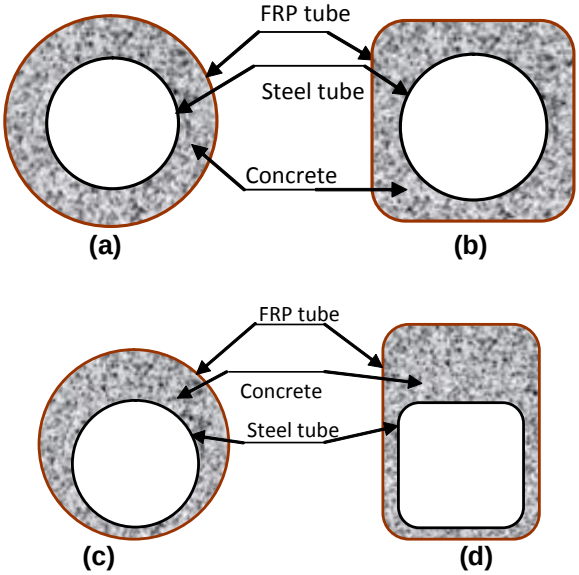

Figure 1 - Typical sections of hybrid DSTMs

School of Civil, Mining and Environmental Engineering, Faculty of Engineering, University of Wollongong, NSW, Australia, Email: taoy@uow.edu.au, Tel: 4221 3786

The most important advantage of hybrid DSTMs is their excellent corrosion resistance, as the FRP tube is highly resistant to corrosion while the steel tube is protected by the FRP tube and the concrete. The other main advantages of hybrid DSTMs include (1) excellent ductility, as the concrete is well confined by the two tubes and outward local buckling of the steel tube is constrained by the concrete; (2) a high strength/stiffness-to-weight ratio as the inner void largely eliminates the redundant concrete; (3) ease for construction, as the two tubes act as a permanent form for casting concrete, and the presence of the inner steel tube and the concrete allows easy connection to other members. More discussions of the rationale and advantages of hybrid DSTMs are available in Teng, *et al*. (2007).

COMPARISON WITH EXISTING COLUMNS

Comparison with hollow RC columns

Among the existing forms of columns which may be replaced by hybrid DSTMs, hollow reinforced concrete (RC) columns are the most cost-effective. Hollow RC columns have been widely used (Priestley, *et al.*, 1996; Pinto, *et al.*, 2003) because of their high bending resistance coupled with reduced weight (Priestley, *et al.*, 1996). A direct comparison of the construction cost of a hybrid DSTM and that of a hollow RC column, undertaken in 2006 and reported in Teng, *et al*., (2009), is therefore presented below to demonstrate the cost effectiveness of hybrid DSTMs. The materials and design strengths follow the specifications given by relevant Chinese codes, and particularly the Chinese Code for the Design of Concrete Structures (2002) and the Chinese Technical Code for Infrastructure Application of FRP Composites (2011) (a draft version was referred to at the time of comparison but the relevant provision remained unchanged during the remaining period of preparation). The stress-strain curve for the confined concrete in the DSTM is that proposed in Yu, *et al*. (2010c). The prices of materials adopted in the comparison were the prevailing market rates in mainland China in 2006 when this comparison was conducted and included labour costs. The prices of concrete, steel rebars, steel tubes, and formwork were the prevailing market rates in Guangzhou, China, while the price of RMB20 per kilogram for GFRP tubes was the commercial rate available in mainland China for large orders as normally required by real construction projects. The formwork cost varies with column height and the present comparison was based on the assumption that the column height is 5 m.

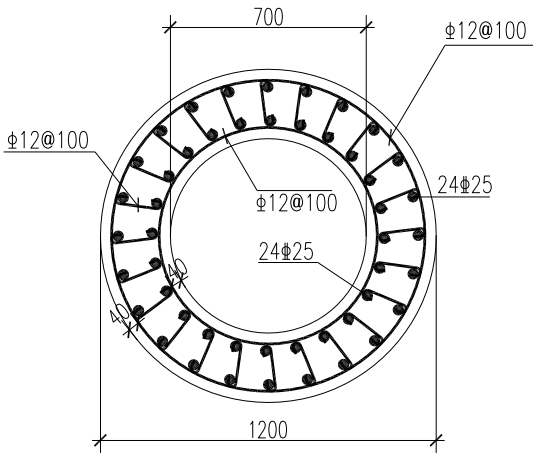

Figure 2 - Cross-section of hollow RC column

Both columns have an outer diameter of 1200 mm and are constructed with grade 40 concrete (i.e. with a design compressive strength of 19.1 MPa according to GB-50010 (2002)). The hollow RC column (Figure 2) is reinforced with 48 ϕ 25 longitudinal steel bars evenly distributed around the circumference and ϕ 12 hoops/ties at 100 mm centres (both with a design strength of 300 MPa) and provided with a concrete cover of 40 mm. The hybrid DSTM has a steel inner tube with an outer diameter *D* of 700 mm, a thickness *t* of 10 mm and a design strength of 300 MPa, and an FRP outer tube with a thickness of 4 mm, an elastic modulus of 47.8 GPa in the hoop direction, and a design rupture strain of 0.0114 (an environmental reduction factor was included).

Tables 1 and 2 provide the comparison of costs per meter, which indicates that the hybrid DSTM is a little cheaper. It can thus be concluded that in general, the two types of columns have similar initial construction costs. The axial force-bending moment interaction diagrams of these two columns are compared in Figure 3, which shows that the hybrid DSTM has a larger section capacity than the hollow

RC column when the axial force is reasonably high but the two sections have similar section capacities when bending dominates the behaviour. The curve for the hollow RC column shown in Figure 3 was obtained without considering the confining effect of the steel hoops. However, even if this effect is considered based on the model of Mander, *et al.* (1988) and assuming that the concrete is as effectively confined as in a solid section, the axial load capacity is still below 24 000 kN, which is considerably smaller than that of the hybrid DSTM. This means that the corresponding interaction curve also stays considerably below that of the hybrid DSTM. Besides the load capacity, it should also be noted that hybrid DSTMs possess two important advantages over hollow RC columns: excellent corrosion resistance and excellent seismic resistance.

Table 1 - Construction cost of a hollow RC column per metre

Item	Description	Quantity per metre	Unit Price (RMB)	Cost (RMB)
Concrete	C40	0.75 m^3	327.8 / m^3	245.9
Longitudinal steel bars	48 ϕ 25	183.69 kg	3.8 / kg	698.0
Transverse steel bars	ϕ 12 @100	149.22 kg	3.7 / kg	552.1
Formwork	3-5.8 meters high	5.97 m^2	29.4 / m^2	175.4
Total				1671.4

Table 2 - Construction cost of a hybrid DSTM per metre

Item	Description	Quantity per metre	Unit Price (RMB)	Cost (RMB)
Concrete	C40	0.75 m^3	327.8 / m^3	245.9
Steel tube	D = 700 mm, t = 10 mm	170.22 kg	4.2 / kg	714.9
FRP tube	D = 1200 mm, t = 4 mm	30.09 kg	20 / kg	601.8
Total				1562.6

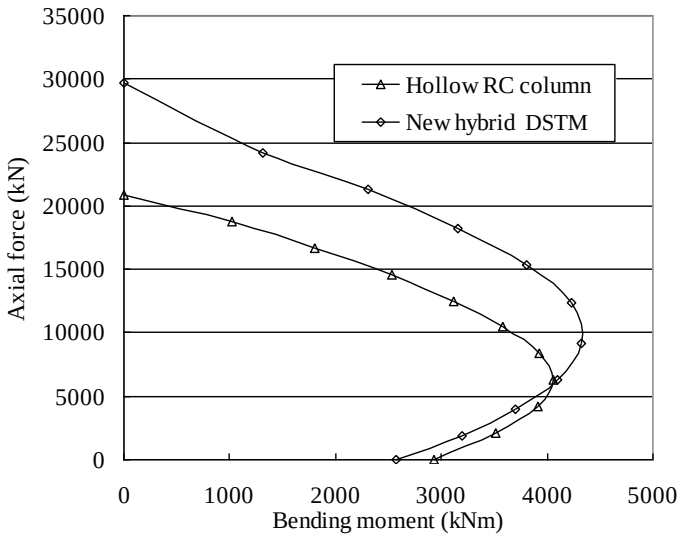

Figure 3 - Axial force-bending moment interaction diagram

Comparison with other columns

Steel-concrete DSTMs with both skins made of steel have been used in construction and have been intensively researched (Zhao and Han, 2006). Such columns have a higher initial construction cost than hollow RC columns for the same structural performance, similar to the well-known fact that concrete-filled steel tubes are more expensive than RC columns (Webb and Peyton, 1990). FRP-concrete DSTMs with two FRP tubes have also been explored (Fam and Rizkalla, 2001) but the use of FRP instead of steel for the inner tube does not lead to any significant advantage but a number of significant disadvantages (e.g. higher cost, reduced stiffness to confine concrete, brittle failure in tension).

Intensive recent research has been conducted on concrete-filled FRP tubes (CFFTs) (i.e. with a solid concrete core) as columns and piles (e.g. Mirmiran and Shahawy, 1997; Fam and Rizkalla, 2001; Yu and Teng, 2011). There have also been some field applications of CFFTs. If excellent durability is the overriding criterion, CFFTs are a possible choice but they are significantly more expensive than RC columns because the FRP tube needs to be thick and to be provided with both longitudinal and hoop fibres. If the FRP tube is not sufficiently thick, premature buckling under compression will considerably compromise its confinement of the concrete core. Even if buckling does not occur, adverse interaction exists between axial compression and hoop tension in such a tube. A hybrid DSTM may be seen as a CFFT with its FRP tube split into an outer FRP tube containing the hoop fibres and an inner FRP tube containing the axial fibres which is then replaced by a much stiffer and much more ductile steel tube. The inner void can also be used for the passing of service ducts. It needs to be emphasised that the FRP tube in a DSTM should generally be quite thin, as its main purpose is to enhance the ductility of the column. Hybrid DSTMs offer many advantages over CFFTs: (a) better confinement of concrete by the FRP tube which contains fibres predominately oriented in the hoop direction; such a tube is mainly subjected to hoop tension and does not buckle under axial straining as has been observed in numerous existing tests of FRP-confined concrete columns; (b) ductile failure in bending as the steel inner tube acts as the longitudinal reinforcement; and (c) savings in cost as the FRP tube is used as a confining device for ductile column response and does not need to be thick.

EXISTING RESEARCH

A large amount of research has been conducted on hybrid DSTMs by the first author and his colleagues. Most of the work undertaken prior to 2007 can be found in Teng, *et al.,* (2007), Yu, *et al*., (2006), Wong, *et al*., (2008), and Yu, *et al.*, (2010a, 2010b, 2010c, 2010d). Teng, *et al*., (2007) explained in detail the rationale for the new member form together with its expected advantages, and presented preliminary experimental results to demonstrate some of the advantages of this new member form, such as excellent ductility and shear resistance. Yu, *et al*., (2006) presented the results of a systematic experimental study on the flexural behavior of hybrid DSTMs as well as results from a corresponding theoretical model based on the fiber element approach. Yu, *et al*., (2006) showed that the flexural response of hybrid DSTMs, including their flexural stiffness, cracking load and ultimate load, can be substantially improved by shifting the inner steel tube towards the tension zone or by providing FRP bars as additional longitudinal reinforcement. Wong, *et al.*, (2008) presented a systematic experimental study on the compressive behavior of hybrid DSTMs and compared the performance of hybrid DSTMs with that of FRP-confined solid cylinder/column (FCSC) specimens and FRP-confined hollow cylinder/column (FCHC) specimens; a good understanding of the behaviour of concrete in hybrid DSTMs resulted from this study. Yu*, et al*., (2010a, b) developed a new plastic-damage model for FRP-confined concrete based on a critical review of the previous D-P type plasticity models. A finite element model incorporating the new plastic-damage model was shown to provide close predictions of the test results of hybrid DSTMs (Yu, *et al*., 2010b). Based on the available experimental observations and the results from the finite element model, Yu, *et al*., (2010c) proposed a design-oriented stress-strain model for the confined concrete in hybrid DSTMs subjected to axial compression. Yu, *et al*., (2010d) presented experimental results on the behaviour of hybrid DSTMs subjected to eccentric compression as well as a so-called "variable confinement model" for the confined concrete to account for the effect of strain gradient on confinement effectiveness. These studies have led to a simple design approach for hybrid DSTMs as columns, and this design approach has recently been adopted by the Chinese Technical Code for Infrastructure Application of FRP Composites (GB50608 2011).

Intensive research on the behaviour and design of hybrid DSTMs is continuing at UoW, in collaboaration with The Hong Kong Polytechnic University. The research at UoW has been particularly on the dynamic response of hybrid DSTMs. Preliminary results from a recent experimental study at UoW are briefly presented in the next section.

LATERAL IMPACT TESTS

A total of three hybrid DSTMs were tested under dynamic three-point bending. All specimens had an outer diameter of 152.4 mm, and a clear span of 1300 mm. The steel inner tube all had an outer diameter of 76.1 mm and a thickness of 3.2 mm. The test variables included the thickness of the FRP tube and the end constraint of the beam. These tests were performed using an instrumented drop hammer facility at the High Bay Lab of University of Wollongong (Figure 4). In the tests, a 592 kg mass was released from a height of 1300 mm to directly impact the specimens at the mid-span. A dynamic load cell was mounted on the drop hammer to measure the contact force between the specimen and the drop hammer; a

high-speed camera was used to capture the deflection during the impact process. Figure 5 shows a specimen after test.

Figure 4 - instrumented drop hammer facility **Figure 5 - A specimen after test**

A typical impact load-time curve is shown in Figure 6 while a typical mid-span delfection-time curve is shown in Figure 7. The test results showed that hybrid DSTMs possess excellent ductility and are able to sustain very large inelastic rotation without significant reduction in the load capacity. The maximum end rotation was found to be over 10 degrees, which is significantly higher than normally expected for reinforced concrete flexural members (i.e. 4-5 degrees). Hybrid DSTMs therefore has very good potential for resisting large blast and impact loads.

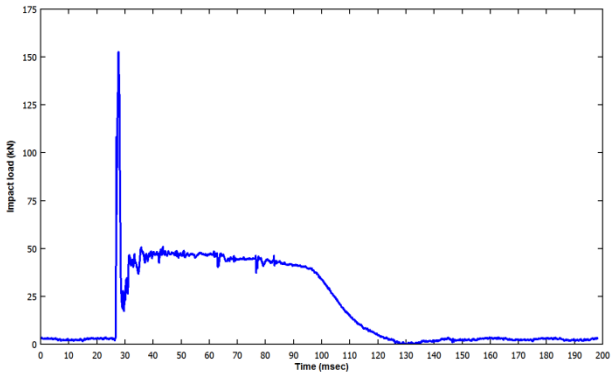

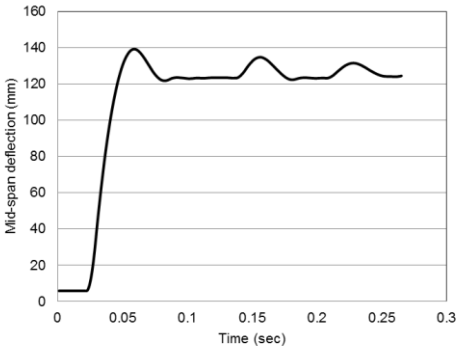

Figure 6 - Typical impact load-time curve **Figure 7 - Typical mid-span deflection-time curve**

POTENTIAL PRACTICAL APPLICATION

Because of their excellent corrosion resistance, hybrid DSTMs is most suitable for use in structures which are likely to be exposed to a harsh environment (e.g. coastal structures and underground structures). Hybrid DSTMs can be used as compression members, such as piles, various towers (e.g. wind turbine towers and electricity transmission towers) and other similar structures. In longwall mining, hybrid DSTMs can be used in a roof support system for maingates and/or tailgates. The presence of an inner void in hybrid DSTMs is also an important advantage which can be exploited in mining applications. The inner void can be used for the passing of service ducts or for ventilation, so that hybrid DSTMs serve not only as structural components, but also as functional components.

In practical applications, when the length of DSTMs becomes very large, they can be constructed using a segmental method, which involves the segmental construction of the outer FRP tube and the inner steel tube and the use of the two tubes as the permanent formwork for the in-situ casting of concrete as schematically illustrated in Figure 8. The flanges of the steel tubular segments and the FRP profiles inside the FRP tubular segments serve not only as longitudinal connectors between the segments, but

also as (1) shear connectors between the concrete and the tubes; and (2) stiffeners to both tubes, thus improving the structural performance of hybrid DSTMs.

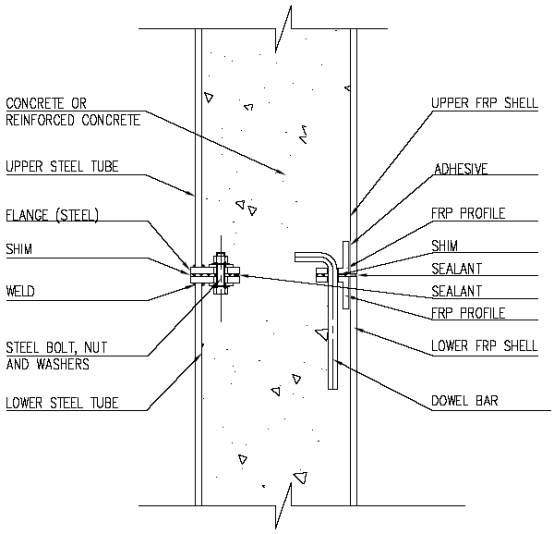

Figure 8 - Segmental construction of hybrid DSTMs

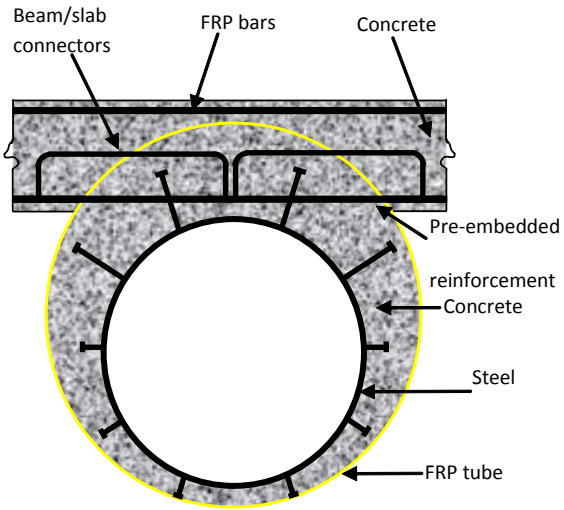

Figure 9 - Hybrid DSTMs/slab units

Hybrid DSTMs can also be used as flexural members in structures exposed to a harsh environment (e.g. underground structures). Hybrid DSTMs can be used alone or be integrated into a concrete slab reinforced with FRP bars to form a durable floor system (Figure 9). In such cases, pre-embedded steel (stainless steel may be used here) reinforcement in the DSTM can be spliced with the bottom layer of FRP bars in the deck using mechanical couplers for beam-slab connection (Figure 9). Additional shear connectors in the form of U-shaped dowels (or other appropriate forms) passing through the FRP tube may also be used to ensure the longitudinal composite action between the beam and the deck (Figure 9). As the fibres in the FRP tube are close to the hoop direction, the passing of steel bars through the tube is expected to affect little its overall performance.

CONCLUDING REMARKS

This paper has discussed the rationale and advantages of hybrid FRP-concrete-steel double-skin tubular members (i.e. hybrid DSTMs), provided a brief summary of existing and ongoing research on hybrid DSTMs, and discussed their potential applications in mining infrastructure. Hybrid DSTMs have a great potential for use in a roof support system for maingates and/or tailgates in longwall mining. The presence of an inner void in hybrid DSTMs is also an important advantage which can be exploited in mining applications. While existing and current research is mainly concerned with structural behaviour of hybrid

DSTMs, exciting opportunities exist for the exploration of real practical applications of such novel structural members in mining infrastructure.

ACKNOWLEDGEMENTS

The authors are grateful to their colleagues Drs. Ting Ren and Jan Nemcik for their valuable discussions in the preparation of this paper.

REFERENCES

Fam, A Z and Rizkalla, S H, 2001. Behaviour of axially loaded concrete-filled circular fibre-reinforced polymer tubes, *ACI Structural Journal*, 98(3):280-289.

GB 50010, 2002. *Code for design of concrete structures* (China Architecture and Building Press, China).

GB 50608, 2011. *Technical Code for Infrastructure Application of FRP Composites* (China Planning Press, China).

Mander, J B, Priestley, M J N and Park, R, 1988. Theoretical stress-strain model for confined concrete, *Journal of Structural Engineering*, ASCE, 114(8):1804-1826.

Mirmiran, A and Shahawy, M, 1997. Behaviour of concrete columns confined by fibre composites, *Journal of Structural Engineering*, ASCE, 123(5):583-590.

Pinto, A V, Molina, J and Tsionis, G, 2003. Cyclic tests on large scale models of existing bridge piers with rectangular hollow cross-section, *Earthquake Engineering and Structural Mechanics*, 32:1995-2012.

Priestley, M J N, Seible, F, and Calvi, G M, 1996. *Seismic Design and Retrofit of Bridges* (John Wiley and Sons, Inc).

Teng, J G, Yu, T, Wong, Y L and Dong, S L, 2007. Hybrid FRP-concrete-steel tubular columns: concept and behaviour, *Construction and Building Materials*, 21(4):846-854.

Teng J G, Yu, T and Fernando, D, 2009. FRP composites in steel structures, in *Proceedings, the Third International Forum on Advances in Structural Engineering 2009*.

Wong, Y L, Yu, T, Teng, J G and Dong, S L, 2008. Behaviour of FRP-confined concrete in annular section columns, *Composites: Part B-Engineering,* 39:451-466.

Webb, J and Peyton, J J, 1990. Composite concrete filled steel tube columns, *Proceedings of the Structural Engineering Conference 1990*, pp 181-185.

Yu, T, Wong, Y L, Teng, J G, Dong, S L and Lam, S S, 2006. Flexural behaviour of hybrid FRP-concrete-steel double skin tubular members, *Journal of Composites for Construction*, ASCE, 10 (5):443-452.

Yu, T, Teng, J G, Wong, Y L and Dong, S L, 2010a. Finite element modelling of confined concrete-I: Drucker-Prager type plasticity model, *Engineering Structures,* 32(3):665-679.

Yu, T, Teng, J G, Wong, Y L and Dong, S L, 2010b. Finite element modelling of confined concrete-II: plastic-damage model, *Engineering Structures,* 32(3):680-691.

Yu, T, Teng, J G and Wong, Y L, 2010c. Stress-strain behaviour of concrete in hybrid double-skin tubular columns, *Journal of Structural Engineering*, ASCE, 136(4):379-389.

Yu, T, Wong, Y L and Teng, J G, 2010d. Behaviour of hybrid FRP-concrete-steel double-skin tubular columns subjected to eccentric compression, *Advances in Structural Engineering*, 13(5):961-974.

Yu, T and Teng, J G, 2011. Design of concrete-filled FRP tubular columns: Provisions in the Chinese technical code for infrastructure application of FRP composites, *Journal of Composites for Construction*, ASCE, 15(3):451-461.

Zhao, X L and Han, L H, 2006. Double skin composite construction, *Progress in Structural Engineering and Materials*, 8:93-102.

INDEX TO AUTHORS